4. Method 4

Given: The same configuration as in Sample Problems 1, 2, and 3.

Additional Characteristics:

$$\alpha = 50^{o} \qquad R_{\ell} = 10^{6}$$

Compute:

$$\alpha' = \alpha = 50^{o}$$

$C_f = 0.0042$ (Figure 4.2.3.2-27)

$$\ell_B/d = \frac{5.04}{0.510} = 9.88 \qquad \frac{d_b}{d} = \frac{0.376}{0.510} = 0.737 \quad \text{(Sample Problem 1)}$$

$$\frac{S_S}{S_b} = 28.7 \quad \text{(Figure 2.3-3)}$$

$$(C_{D_f})_b = C_f \left[1 + \frac{60}{(\ell_B/d)^3} + 0.0025\left(\frac{\ell_B}{d}\right)\right] \frac{S_S}{S_B} \quad \text{(first term in Equation 4.2.3.1-a)}$$

$$= 0.0042 \left[1 + \frac{60}{(5.04/0.510)^3} + 0.0025\left(\frac{5.04}{0.510}\right)\right] 28.7$$

$$= 0.131$$

$$C_{D_b} = 0.029\left(\frac{d_b}{d}\right)^3 \Big/ \sqrt{(C_{D_f})_b} \quad \text{(Equation 4.2.3.1-b}$$

$$= (0.029)\left(\frac{0.376}{0.510}\right)^3 \Big/ \sqrt{0.131}$$

$$= 0.0321$$

Solution:

$$C_{X_{\alpha=0}} = -(C_f + C_{D_b}) \quad \text{(Equation 4.2.3.2-g)}$$

$$= -(0.0042 + 0.0321)$$

$$= -0.0363$$

$$C_X = C_{X_{\alpha=0}} \cos^2\alpha' \quad \text{(Equation 4.2.3.2-e)}$$

$$= -(0.0363)(0.6428)^2$$

$$= -0.0150 \text{ (based on body base area)}$$

No test data are available for a comparison.

B. TRANSONIC

Slender-body theory may be applied for a rapid but approximate estimate of body drag at angle of attack.

DATCOM METHOD

The drag coefficient due to angle of attack from slender-body theory is

$$C_D(\alpha) = \alpha^2 \text{ (based on } S_b) \qquad 4.2.3.2\text{-i}$$

where the drag coefficient is referred to body base area and α is the body angle of attack in radians.

C. SUPERSONIC

Three methods are given for estimating body drag due to angle of attack at supersonic speeds. The first two methods correspond to the first two methods of estimating body lift in Section 4.2.1.2. The general discussion of the methods used in Section 4.2.1.2 will not be repeated here. In addition, a third method is given for estimating the body axial-force coefficient (based on Reference 4 and similar to Method 4 of Paragraph A of this section). This method is applicable up to an angle of attack of 180^0 and is limited to bodies of revolution with blunt, conical, ogive, and 3/4-power noses.

DATCOM METHODS

Method 1

The supersonic body drag due to angle of attack, determined by the method of Reference 9 for moderate angles of attack, is

$$C_D(\alpha) = C_L\alpha \qquad 4.2.3.2\text{-j}$$

where C_L is given by Equation 4.2.1.2-g or Equation 4.2.1.2-h, depending on whether the body cross section is circular or elliptical, and α is the angle of attack in radians.

The supersonic drag due to angle of attack of a body of revolution, based on body base area, is then

$$C_D(\alpha) = 2\alpha^2 + c_{d_c}\frac{S_p}{S_b}\alpha^3 \qquad 4.2.3.2\text{-k}$$

where all the parameters are defined under Method 2 of Paragraph A.

The supersonic drag due to angle of attack of a body having an elliptical cross section, based on body base area, is

$$[C_D(\alpha)]_{a/b} = \left[\frac{a}{b}\cos^2\phi + \frac{b}{a}\sin^2\phi\right] C_D(\alpha) \qquad 4.2.3.2\text{-}\ell$$

where

a is the major axis of the elliptical cross section.

b is the minor axis of the elliptical cross section.

ϕ is the angle of bank of the body about its longitudinal axis; $\phi = 0$ with the major axis horizontal and $\phi = 90^o$ with the minor axis horizontal.

$C_D(\alpha)$ is the drag due to angle of attack of a body of revolution having the the same cross-sectional area distribution along its axis as the elliptical-cross-section body of interest. It is given by Equation 4.2.3.2-k.

Calculated results using this method have been compared with test data in Reference 9. The comparison included bodies of revolution and bodies of elliptical cross section, both having the same axial distribution of cross-sectional area. The tests included bodies of fineness ratios 6 and 10 at M = 1.98 and bodies of fineness ratio 6 at M = 3.88. The angle-of-attack range was from zero to approximately 20^o. For the cases considered, there is good agreement between results calculated by this method and test values.

Method 2

A method for predicting the normal force of bodies of revolution at supersonic speeds is given in Section 4.2.1.2. The drag due to angle of attack of a body of revolution can be expressed as

$$C_D(\alpha) = C_N \sin\alpha - C_X \cos\alpha \qquad 4.2.3.2\text{-m}$$

where C_N and C_X are defined in Sketch (a). For small angles of attack the resultant force vector is nearly normal to the body surface and the chordwise force component is neglected. Equation 4.2.3.2-m can then be approximated at small angles of attack as

$$C_D(\alpha) = C_N\alpha \qquad 4.2.3.2\text{-n}$$

where

α is the body angle of attack in radians.

C_N is the body normal-force coefficient at angle of attack, based on body base area, obtained from Figure 4.2.1.2-38.

The normal-force data of Figure 4.2.1.2-38 are for cone-cylinder configurations, but may be used for general pointed bodies without great loss of accuracy.

Method 3

The following method (Reference 4) predicts the axial-force coefficient C_X in the angle-of-attack range of 0 to 180°. The method is limited to bodies of revolution with blunt, conical, ogive, and 3/4-power nose shapes. Due to the complexity of calculating drag for bodies with noncircular cross sections, the Datcom method is limited to bodies with circular cross sections. For noncircular cross-section bodies, the user is referred to the treatment presented in References 4 and 5. This C_X term may be used in conjunction with the C_N calculated in Section 4.2.1.2 to obtain C_D; i.e., $C_D = C_N \sin\alpha - C_X \cos\alpha$.

The axial-force C_X of a circular-cross-section body at an angle of attack is given by

$$C_X = C_{X_{\alpha=0}} \cos^2\alpha' \quad (\text{for } 0 \leqslant \alpha \leqslant 90^\circ) \qquad 4.2.3.2\text{-o}$$

$$C_X = C_{X_{\alpha=180^\circ}} \cos^2\alpha' \quad (\text{for } 90^\circ \leqslant \alpha \leqslant 180^\circ) \qquad 4.2.3.2\text{-p}$$

and

$$C_{X_{\alpha=0}} = -(C_f + C_{D_b} + C_{D_w}) \qquad 4.2.3.2\text{-q}$$

$$C_{X_{\alpha=180^\circ}} = C_f + C_{D_b} + C_{D_w} \qquad 4.2.3.2\text{-r}$$

where

C_{D_b} is the base-drag coefficient for bodies of revolution, from Figure 4.2.3.1-60.

C_{D_w} is the wave-drag coefficient determined from Figure 4.2.3.2-28a for blunt nose or blunt base forward, or Figure 4.2.3.2-28b for other nose shapes.

The remaining terms are defined in Paragraph A of Section 4.2.3.2.

A comparison of test data taken from References 7 and 8 with results calculated by this method is presented in Table 4.2.3.2-A. It should be noted that very little reliable test data at high angles of attack were available, and much of that used to substantiate the method is suspected of being affected by model support interference. The method generally predicts a lower absolute value of C_X than evidenced by available test data; however, the user should be cautious in view of the uncertainty of the test data.

It is recommended that other Datcom methods be used whenever possible, especially at low angles of attack.

The method is applicable to $0 \leqslant M \leqslant 7$; however, caution should be used in the hypersonic range because of the lack of substantiating data.

Sample Problems

1. Method 1

Given: Three bodies of Reference 11, each having the same longitudinal area distribution.

Body 1. Ogive-cylinder

ℓ_B = 42.0 in. ℓ_N = 14.0 in. ℓ_A = 28.0 in. $d_b = d_{max}$ = 4.0 in.

f = 10.5 S_b = 12.57 sq in. S_p = 154.0 sq in.

Body 2. Horizontal ellipse

Same longitudinal area distribution as ogive-cylinder body.

a = 4.90 in. b = 3.26 in. $\phi = 0$

Body 3. Vertical ellipse

Same longitudinal area distribution as ogive-cylinder body.

a = 4.90 in. b = 3.26 in. $\phi = 90^o$

Additional Characteristics:

M = 2.01; β = 1.744 $0 \leq \alpha \leq 10^o$

Body 1. Ogive-cylinder

Compute:

S_p/S_b = 154.0/12.57 = 12.25

M_c = M sin α

c_{d_c} (Figure 4.2.1.2-35b)

(See calculation table below.)

Solution:

$$C_D(\alpha) = 2\alpha^2 + c_{d_c} \frac{S_p}{S_b} \alpha^3$$ (Equation 4.2.3.2-k)

①	②	③	④	⑤	⑥	⑦	⑧
α (deg)	α (rad)	α^2 (rad^2)	α^3 (rad^3)	M_c M sin α	c_{d_c} (Fig. 4.2.1.2-35b)	$c_{d_c} \frac{S_p}{S_b}$ ⑥ 12.25	$C_D(\alpha)$ (Eq. 4.2.3.2-k) 2 ③ + ⑦ ④
0	0	0	0	0	1.20	14.70	0
2	0.0349	0.00122	0.00004	0.0701	1.20	14.70	0.00303
4	0.0698	0.00487	0.00034	0.1402	1.20	14.70	0.01474
6	0.1047	0.01096	0.00115	0.2101	1.20	14.70	0.03882
8	0.1396	0.01949	0.00272	0.2797	1.21	14.82	0.07929
10	0.1745	0.03045	0.00531	0.3489	1.233	15.10	0.1411

Bodies 2 and 3

Compute:

Horizontal ellipse

$$\left[\frac{a}{b}\cos^2\phi + \frac{b}{a}\sin^2\phi\right] = \left[1.5\cos^2(0) + 0.667\sin^2(0)\right] = 1.50$$

Vertical ellipse

$$\left[\frac{a}{b}\cos^2\phi + \frac{b}{a}\sin^2\phi\right] = \left[1.5\cos^2(90^o) + 0.667\sin^2(90^o)\right] = 0.667$$

Solution:

$$\left[C_D(\alpha)\right]_{a/b} = \left[\frac{a}{b}\cos^2\phi + \frac{b}{a}\sin^2\phi\right] C_D(\alpha) \quad \text{(Equation 4.2.3.2-}\ell\text{)}$$

$$= 1.50\, C_D(\alpha) \quad \text{Horizontal ellipse}$$

$$= 0.667\, C_D(\alpha) \quad \text{Vertical ellipse}$$

①	②	③	④
α (deg)	$C_D(\alpha)$ Ogive-Cyl.	$\left[C_D(\alpha)\right]_{a/b}$ Horiz. Ellipse 1.50 ②	$\left[C_D(\alpha)\right]_{a/b}$ Vert. Ellipse 0.667 ②
0	0	0	0
2	0.00303	0.00454	0.00202
4	0.01474	0.02211	0.00983
6	0.03882	0.05823	0.02589
8	0.07929	0.1189	0.0529
10	0.1411	0.2116	0.0941

The calculated results for the three bodies are compared with test values from Reference 11 in Sketch (c).

2. Method 2

Given: The ogive-cylinder body of Sample Problem 1.

Compute:

$$f_N = \frac{\ell_N}{d_{max}} = \frac{14.0}{4.0} = 3.50$$

$$f_A = \frac{\ell_A}{d_{max}} = \frac{28.0}{4.0} = 7.0$$

$$f_A/f_N = 7.0/3.50 = 2.0$$

$$\beta/f_N = 1.744/3.50 = 0.498$$

βC_N (Figure 4.2.1.2-38b) (See calculation table below.)

$C_N = \beta C_N/\beta$ (based on body base area) (See calculation table below.)

Solution:

$C_D(\alpha) = C_N \alpha$ (Equation 4.2.3.2-*n*)

①	②	③	④	⑤	⑥
α (deg)	α (rad)	$\beta\alpha$ (deg)	βC_N (Fig. 4.2.1.2-38b)	C_N ④ /β	$C_D(\alpha)$ (Eq. 4.2.3.2-n) ⑤②
0	0	0	0	0	0
2	0.0349	3.488	0.15	0.086	0.0030
4	0.0698	6.976	0.30	0.172	0.0120
6	0.1047	10.464	0.52	0.298	0.0312
8	0.1396	13.952	0.80	0.459	0.0641
10	0.1745	17.44	1.20	0.688	0.1201

The calculated results are compared with test values from Reference 11 in Sketch (c).

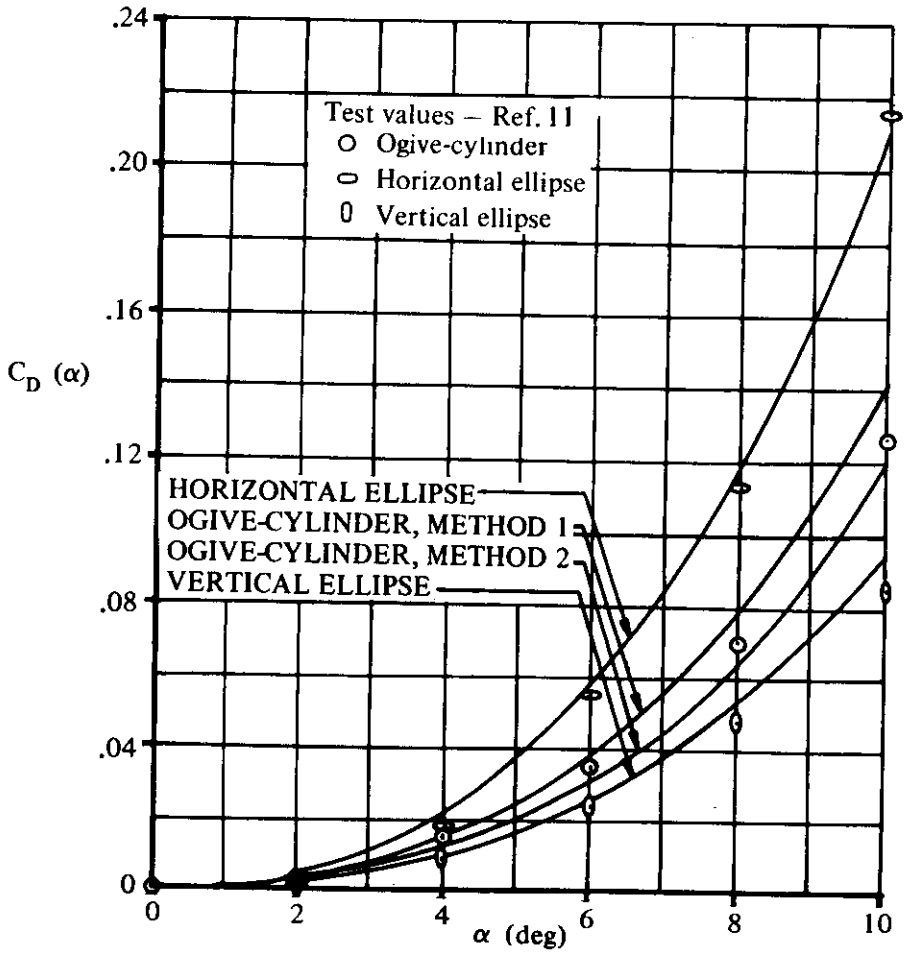

SKETCH (c)

3. Method 3

Given: An ogive-cylinder body of Reference 7.

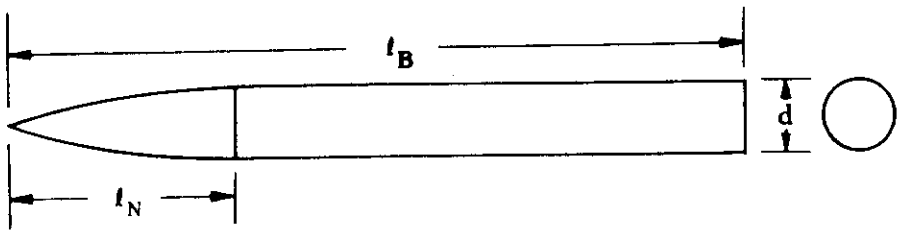

Body Characteristics:

$$\frac{\ell_B}{d} = 11 \qquad \frac{\ell_N}{d} = 5$$

Additional Characteristics:

$$\alpha = 40^o, 120^o \qquad M = 2.86 \qquad R_\ell = 1.375 \times 10^6$$

Compute:

C_X at $\alpha = 40^o$

$$\alpha' = \alpha = 40^o$$

$$C_f = 0.00287 \text{ (Figure 4.2.3.2-27)}$$

$$C_{D_b} = 0.103 \text{ (Figure 4.2.3.1-60)}$$

$$M\frac{d}{\ell_N} = (2.86)\left(\frac{1}{5}\right) = 0.572$$

$$0.7M^2 C_{D_w} = 0.215 \text{ (Figure 4.2.3.2-28b)}$$

$$C_{D_w} = \frac{0.215}{0.7M^2} = \frac{0.215}{0.7(2.86)^2} = 0.0375$$

$$C_{X_{\alpha=0}} = -(C_f + C_{D_b} + C_{D_w}) \text{ (Equation 4.2.3.2-q)}$$

$$= -(0.00287 + 0.103 + 0.0375)$$

$$= -0.143$$

$$C_X = C_{X_{\alpha=0}} \cos^2\alpha' \quad \text{(Equation 4.2.3.2-o)}$$

$$= -(0.143)(0.587)$$

$$= -0.084 \text{ (based on body base area)}$$

C_X at $\alpha = 120^o$

$$\alpha' = 180^o - \alpha = 60^o$$

$$C_f = 0.00287 \text{ (Figure 4.2.3.2-27)}$$

$$C_{D_b} = 0.103 \text{ (Figure 4.2.3.1-60)}$$

$$C_{D_w} = 1.747 \text{ (Figure 4.2.3.2-28a for blunt base forward)}$$

$$C_{X_{\alpha=180^o}} = C_f + C_{D_b} + C_{D_w} \quad \text{(Equation 4.2.3.2-r)}$$

$$= 0.00287 + 0.103 + 1.747$$

$$= 1.85$$

$$C_X = C_{X_{\alpha=180^o}} \cos^2\alpha' \quad \text{(Equation 4.2.3.2-p)}$$

$$= (1.85)(0.25)$$

$$= 0.46 \text{ (based on body base area)}$$

Additional values have been calculated below:

M	α (deg)	C_X
2.86	0	−0.14
2.86	20	−0.126
2.86	40	−0.084
2.86	60	−0.036
2.86	80	−0.004
2.86	100	0.006
2.86	120	0.46
2.86	140	1.08
2.86	160	1.63
2.86	180	1.84

The calculated results of the sample problem are compared to test values from Reference 7 in Sketch (d).

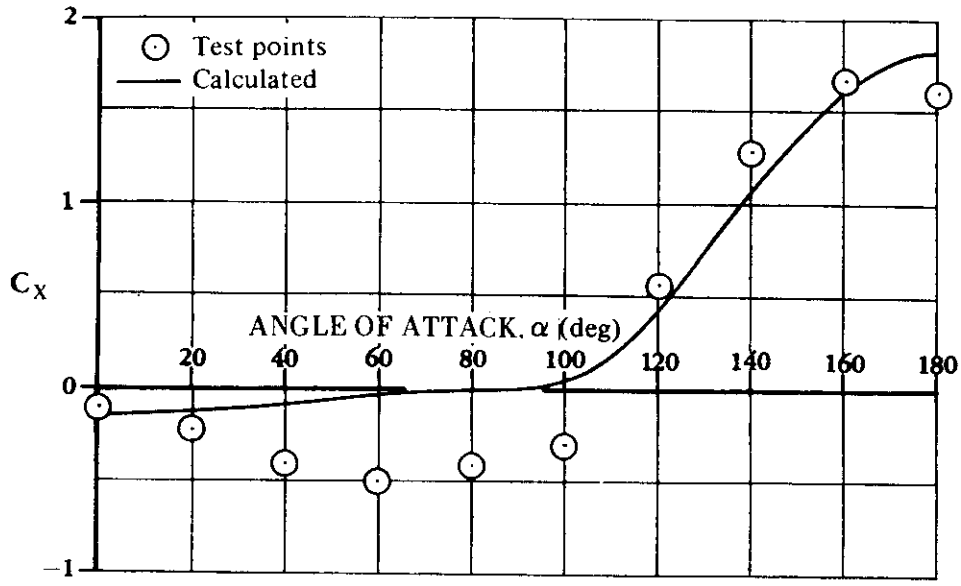

SKETCH (d)

D. HYPERSONIC

For small or moderate angles of attack the hypersonic drag of a body is given by Method 2 of Paragraph C. For large angles of attack the method of Reference 4 presented as Method 3 of Paragraph C of this section may be used.

DATCOM METHODS

Method 1

At small to moderate angles of attack, body drag due to angle of attack, based on base area, is given by Equation 4.2.3.2-n; i.e.,

$$C_D(\alpha) = C_N \alpha$$

where C_N is obtained from Paragraph D of Section 4.2.1.2 and α is the body angle of attack in radians. The design charts of Section 4.2.1.2 can be used to determine the normal-force coefficient at angles of attack for cone-cylinder-flare, cone-cylinder, or cone-flare bodies with pointed or spherically blunted noses, or for spherically blunted or pointed cones.

An approximate value of $C_D(\alpha)$ at small angles of attack for a spherically blunted ogive can be determined by

$$C_D(\alpha) = C_{N_\alpha} \alpha^2 \qquad 4.2.3.2\text{-s}$$

where C_{N_α} is obtained from Figure 4.2.1.1-25 and α is the body angle of attack in radians.

Method 2

This method is identical to Method 3 presented in Paragraph C of this section. The method is applicable to angles of attack from 0 to 180° and Mach numbers up to 7. Substantiating test data taken from Reference 8 for $\alpha \leq 25^{\circ}$ are presented in Table 4.2.3.2-A. The method has not been substantiated at higher angles of attack. It is recommended that the method be used cautiously and only when Method 1 cannot be used.

Sample Problems

1. Method 1

Given: A cone-cylinder body ofReference 12.

$\ell_B = 8.0$ in. $\quad \ell_A = 4.68$ in. $\quad \ell_N = 3.32$ in. $\quad d = 1.17$ in.

$M = 6.86$; $\beta = 6.79$ $\quad 0 \leq \alpha \leq 24^{\circ}$

Compute:

$$f_A = \frac{\ell_A}{d} = \frac{4.68}{1.17} = 4.0; \quad f_N = \frac{\ell_N}{d} = \frac{3.32}{1.17} = 2.84$$

$f_A/f_N = 4.0/2.84 = 1.41$

$\beta/f_N = 6.79/2.84 = 2.39$

βC_N (Figure 4.2.1.2-40a through -40d, interpolated) (See calculation table.)

$C_N = \beta C_N/\beta$ (based on body base area) (See calculation table.)

Solution:

$C_D(\alpha) = C_N \alpha$ (based on S_b) (Equation 4.2.3.2-n)

①	②	③	④	⑤	⑥
α (deg)	$\beta\alpha$ (deg)	βC_N (Fig. 4.2.1.2-40)	C_N ③ /6.79	α (rad)	$C_D(\alpha)$ (Eq. 4.2.3.2-n) ④⑤
0	0	0	0	0	0
4	27.2	1.4	0.206	0.0698	0.0144
8	54.3	3.0	0.442	0.1396	0.0617
12	81.5	5.2	0.766	0.2094	0.1604
16	108.6	7.7	1.134	0.2792	0.3166
20	135.8	10.4	1.53[illegible]	0.3490	0.5347
24	163.0	13.3	1.959	0.4188	0.8204

The calculated results are compared with test values from Reference 12 in Sketch (e)

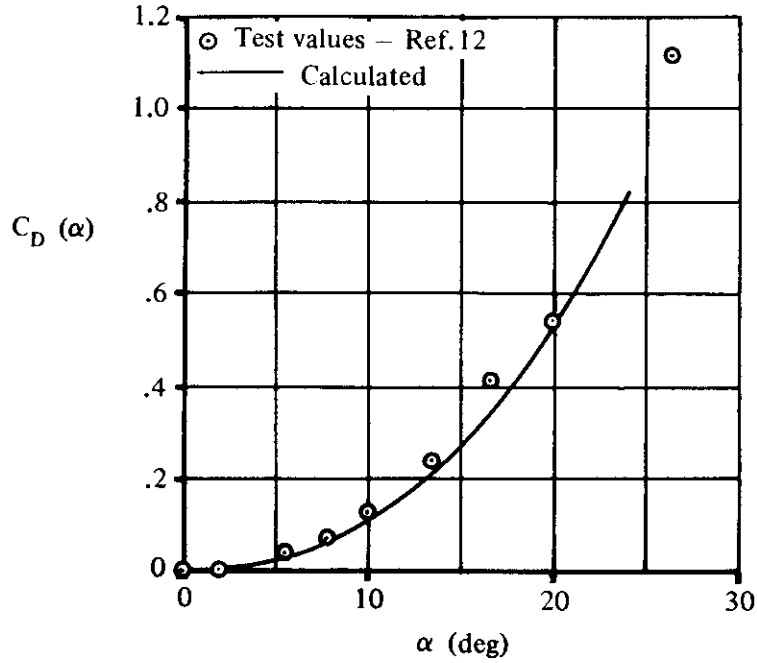

SKETCH (e)

2. Method 1

Given: A cone-cylinder-flare body of Reference 13.

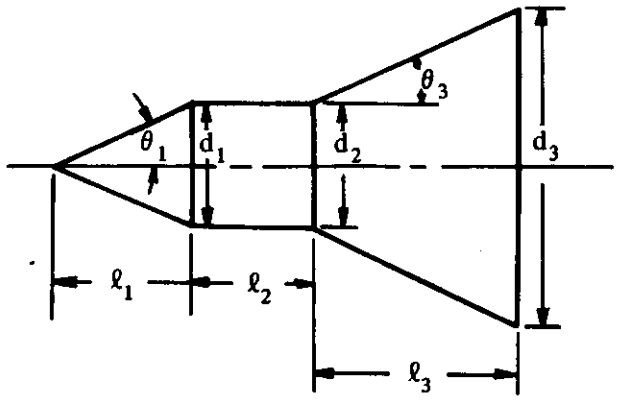

Cone:

$\ell_1 = \ell_N = 2.414$ in.

$d_1 = d_2 = 2.0$ in. $\theta_1 = 22.5^o$

Cylinder:

$\ell_2 = \ell_C = 2.0$ in. $d_2 = 2.0$ in.

Flare:

$\ell_3 = \ell_F = 3.29$ in.

$d_3 = 5.80$ in. $\theta_3 = 30^o$

Additional Characteristics:

$M = 6.0$; $\beta = 5.92$ $0 \leq \alpha \leq 16^o$

Compute:

In accordance with the method of Section 4.2.1.2, the increment of normal force due to the flare is added to the normal force of the cone-cylinder body.

$(C_N)_{cone\text{-}cylinder}$

$f_N = \ell_N/d = 2.414/2.0 = 1.207$

$f_A = f_C = \ell_C/d = 2.0/2.0 = 1.0$

$f_A/f_N = 1.0/1.207 = 0.829$

$\beta/f_N = 5.92/1.207 = 4.90$

βC_N (Figure 4.2.1.2-40d and -40e, interpolated) (See calculation table.)

$C_N = \beta C_N/\beta$ (based on cone-cylinder maximum frontal area) (See calculation table.)

$(C_N)_{flare}$

$$1 - \left(\frac{d_2}{d_3}\right)^2 = 1 - \left(\frac{2.0}{5.80}\right)^2 = 1 - 0.119 = 0.881$$

$$\frac{\left(\Delta C_N\right)_F}{1 - \left(\frac{d_2}{d_3}\right)^2}$$ (Figure 4.2.1.2-42b) (See calculation table.)

$$(\Delta C_N)_F = \frac{(\Delta C_N)_F}{1 - \left(\frac{d_2}{d_3}\right)^2}\left[1 - \left(\frac{d_2}{d_3}\right)^2\right] = 0.881 \frac{(\Delta C_N)_F}{1 - \left(\frac{d_2}{d_3}\right)^2}$$ (based on flare base area) (See calculation table.)

$(C_N)_{cone\text{-}cylinder\text{-}flare}$

$$C_N = (C_N)_{cone\text{-}cyl.} + (\Delta C_N)_F \left(\frac{d_3}{d_2}\right)^2$$ (based on cone-cylinder maximum frontal area) (See calculation table.)

Solution:

$C_D(\alpha) = C_N \alpha$ (Equation 4.2.3.2-n)

① α (deg)	② $\beta\alpha$ (deg)	③ $\beta C_{N_{cone\text{-}cyl.}}$ (Fig. 4.2.1.2-40)	④ $C_{N_{cone\text{-}cyl.}}$ ③ /5.92	⑤ $\frac{(\Delta C_N)_F}{1-\left(\frac{d_2}{d_3}\right)^2}$ (Fig. 4.2.1.2-42b)	⑥ $(\Delta C_N)_F$ ⑤ 0.881	⑦ $(\Delta C_N)_F \left(\frac{d_3}{d_2}\right)^2$ 8.41 ⑥	⑧ C_N ④ + ⑦	⑨ α (rad)	⑩ $C_D(\alpha)$ (Eq. 4.2.3.2-n) ⑧⑨
0	0	0	0	0	0	0	0	0	0
4	23.7	0.86	0.145	0.09	0.08	0.673	0.818	0.0698	0.0571
8	47.4	1.75	0.296	0.18	0.16	1.346	1.642	0.1396	0.2292
12	71.0	2.62	0.443	0.275	0.24	2.018	2.461	0.2094	0.5153
16	94.7	3.50	0.591	0.35	0.31	2.607	3.198	0.2792	0.8929

The calculated results are compared with test values from Reference 13 in Sketch (f).

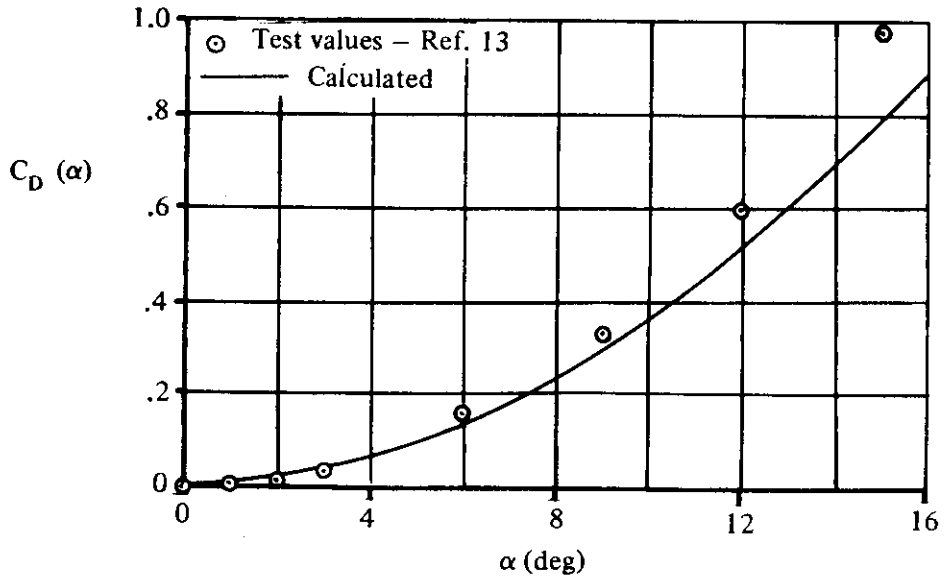

SKETCH (f)

3. Method 2

Refer to Sample Problem 3 in Paragraph C of this section for an example of the application of the method.

REFERENCES

1. Hopkins, E. J.: A Semiempirical Method for Calculating the Pitching Moment of Bodies of Revolution at Low Mach Number. NACA RM A51C14, 1951. (U)

2. Allen, H. J., and Perkins, E. W.: Characteristics of Flow Over Inclined Bodies of Revolution. NACA RM A50L07, 1951. (U)

3. Kelly, H. R.: The Estimation of Normal-Force, Drag, and Pitching-Moment Coefficients for Blunt-Based Bodies of Revolution at Large Angles of Attack. Jour. Aero. Sci., Aug. 1954. (U)

4. Jorgensen, L. H.: Prediction of Static Aerodynamic Characteristics for Space-Shuttle-Like and Other Bodies at Angles of Attack from 0^{o} to 180^{o}. NASA TN D-6996, 1973. (U)

5. Jorgensen, L. H.: A Method for Estimating Static Aerodynamic Characteristics for Slender Bodies of Circular and Noncircular Cross Section Alone and with Lifting Surfaces at Angles of Attack from 0^{o} to 90^{o}. NASA TN D-7228, 1973. (U)

6. Hopkins, E. J.: Charts for Predicting Turbulent Skin Friction from the Van Driest Method (II). NASA TN D-6945, 1972. (U)

7. Jernell, L. S.: Aerodynamic Characteristics of Bodies of Revolution at Mach Numbers from 1.50 to 2.86 and Angles of Attack to 180^{o}. NASA TM X-1658, 1968. (U)

8. Dennis, D. H., and Cunningham, B. E.: Forces and Moments on Inclined Bodies at Mach Numbers from 3.0 to 6.3. NACA RM A54E03, 1954. (U)

9. Jorgensen, L. H.: Inclined Bodies of Various Cross Sections at Supersonic Speeds. NASA Memo 12-3-58A, 1958. (U)

10. Jones, J. L., and Demele, F. A.: Aerodynamic Study of a Wing-Fuselage Combination Employing a Wing Swept Back 63^{o} – Characteristics Throughout the Subsonic Speed Range with the Wing Cambered and Twisted for a Uniform Load at a Lift Coefficient of 0.25. NACA RM A9D25, 1949. (U)

11. Carlson, H. W., and Gapcynski, J. P.: An Experimental Investigation at a Mach Number of 2.01 of the Effects of Body Cross-Section Shape on the Aerodynamic Characteristics of Bodies and Wing-Body Combinations. NACA RM L55E23, 1955. (U)

12. Cooper, R. D., and Robinson, R. A.: An Investigation of the Aerodynamic Characteristics of a Series of Cone-Cylinder Configurations at a Mach Number of 6.86. NACA RM L51J09, 1951. (U)

13. Ashby, G. C., Jr., and Cary, A. M., Jr.: A Parametric Study of the Aerodynamic Characteristics of Nose-Cylinder-Flare Bodies at a Mach Number of 6.0 NASA TN D-2854, 1965. (U)

TABLE 4.2.3.2-A
SUPERSONIC AXIAL FORCE COEFFICIENT FOR
CYLINDER-BODIES WITH VARIOUS NOSE SHAPES
METHOD 3
DATA SUMMARY AND SUBSTANTIATION

Ref	M	R_ℓ (based on diam)	$\frac{\ell_B}{d}$	$\frac{\ell_N}{d}$	Nose Shape	α (deg)	$C_{X_{calc}}$	$C_{X_{test}}$	ΔC_X
7	2.86	1.25×10^5	6	0	Blunt	0	−1.84	−1.70	−0.14
						20	−1.63	−1.69	0.06
						40	−1.08	−1.46	0.38
						60	−0.46	−0.84	0.38
						80	−0.56	−0.27	−0.29
						100	0.56	0	0.56
				3	Cone	0	−0.18	−0.22	0.04
						20	−0.16	−0.33	0.17
						40	−0.11	−0.44	0.33
						60	−0.05	−0.52	0.47
						80	−0.005	−0.50	0.49
						100	0.06	−0.21	0.27
						120	0.46	0.57	−0.11
						140	1.08	1.32	−0.24
						160	1.63	1.63	0
						180	1.84	1.64	0.20
				5	Ogive	0	−0.14	−0.11	−0.03
						20	−0.12	−0.22	0.10
						40	−0.08	−0.40	0.32
						60	−0.03	−0.50	0.47
						80	−0.004	−0.42	0.42
						100	0.06	−0.30	0.36
						120	0.46	0.57	−0.11
						140	1.08	1.30	−0.22
						160	1.63	1.68	−0.05
						180	1.84	1.62	0.22
8	4.24	5.4×10^5	7	3	Cone	0	−0.137	−0.105	−0.032
						5	−0.136	−0.096	−0.040
						10	−0.132	−0.107	−0.025
						15	−0.128	−0.121	−0.007
						20	−0.121	−0.171	0.050
						25	−0.112	−0.213	0.101
			10			0	−0.137	−0.125	−0.012
						5	−0.136	−0.128	−0.008
						10	−0.133	−0.124	−0.009
						15	−0.128	−0.120	−0.008
						20	−0.121	−0.122	0.001
						25	−0.113	−0.124	0.011
	5.04	2.6×10^5				0	−0.119	−0.151	0.032
						5	−0.118	−0.160	0.042

TABLE 4.2.3.2-A (CONTD)

Ref	M	R_ℓ (based on diam)	$\frac{\ell_B}{d}$	$\frac{\ell_N}{d}$	Nose Shape	α (deg)	$C_{X_{calc}}$	$C_{X_{test}}$	ΔC_X
8	5.04	2.6×10^5	10	3	Cone	10	−0.115	−0.177	0.062
						15	−0.111	−0.159	0.048
						20	−0.105	−0.159	0.054
						25	−0.098	−0.216	0.118
			7	5	Ogive	0	−0.082	−0.076	−0.006
						5	−0.081	−0.068	−0.013
						10	−0.0795	−0.0895	0.010
						15	−0.076	−0.120	0.044
	6.28	1.1×10^5		3	Cone	0	−0.096	−0.208	0.112
						5	−0.095	−0.195	0.100
						10	−0.093	−0.202	0.109
						15	−0.089	−0.236	0.147
						20	−0.084	−0.288	0.204
						25	−0.079	−0.320	0.241

Average Error = $\sum \frac{|\Delta C_x|}{n} = 0.149$

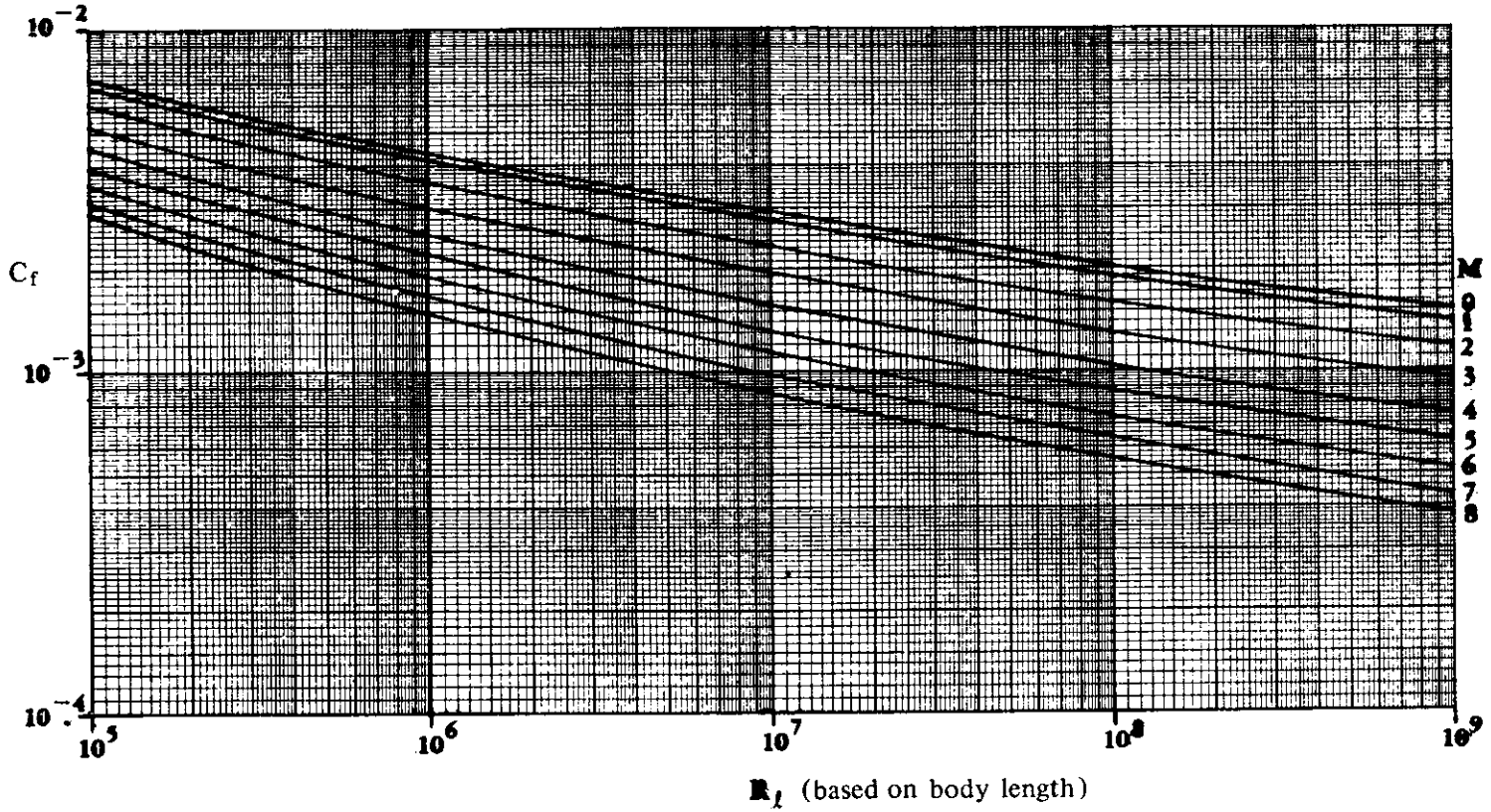

FIGURE 4.2.3.2 -27 TURBULENT FLAT-PLATE SKIN-FRICTION COEFFICIENT

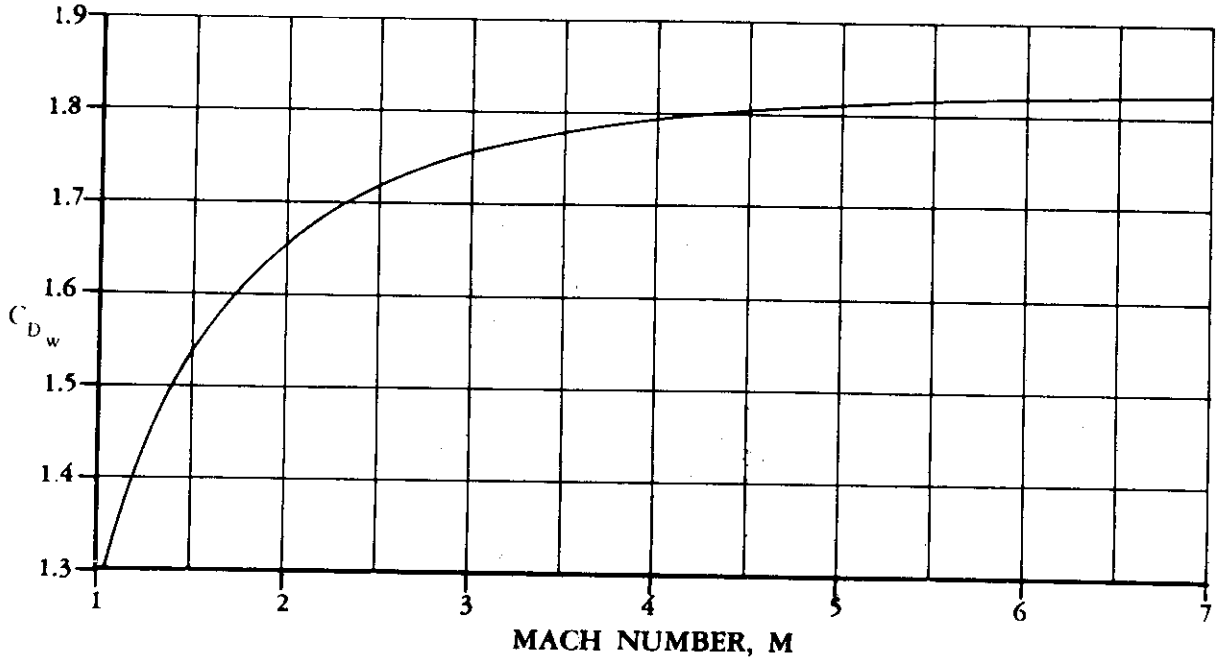

FIGURE 4.2.3.2 -28a BODY WAVE-DRAG COEFFICIENT FOR BLUNT NOSE

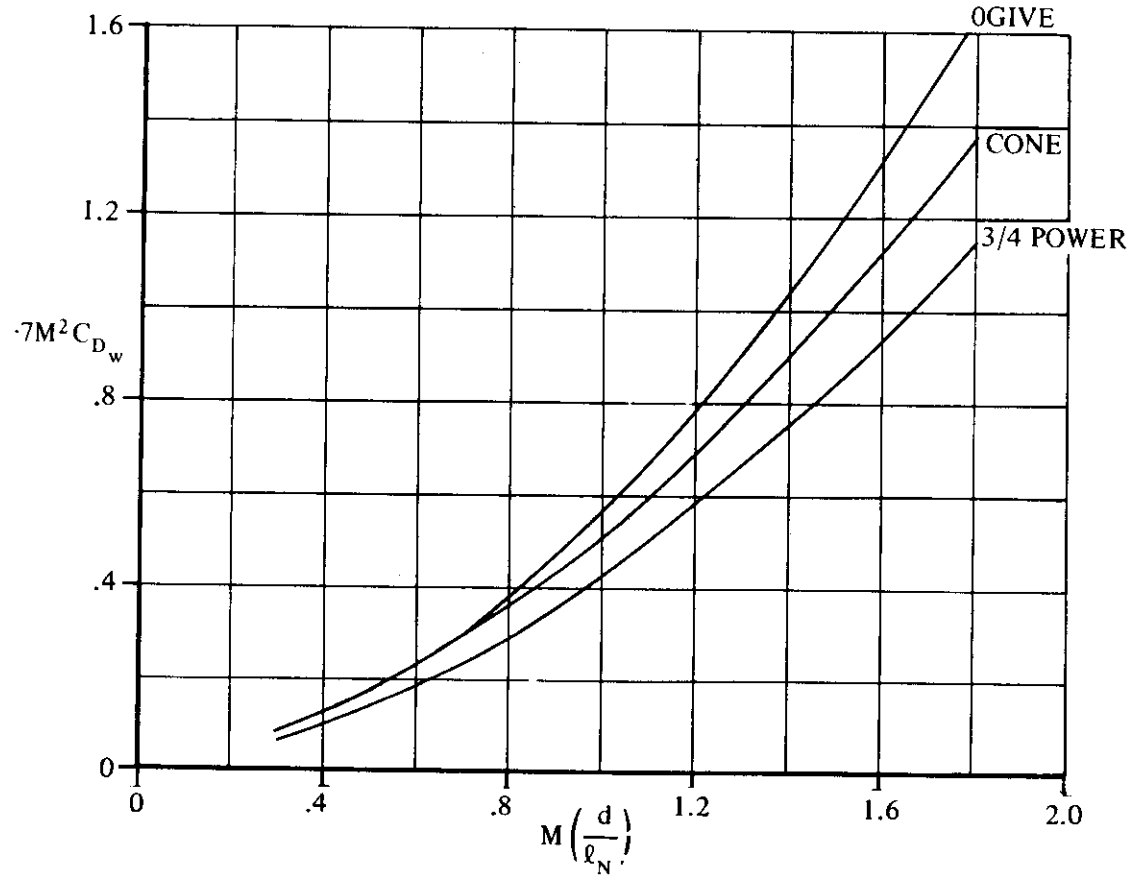

FIGURE 4.2.3.2 -28b VARIATION OF WAVE-DRAG COEFFICIENT WITH HYPERSONIC SIMILARITY PARAMETER FOR VARIOUS NOSE SHAPES

4.3 WING-BODY, TAIL-BODY COMBINATIONS AT ANGLE OF ATTACK

4.3.1 WING-BODY LIFT

4.3.1.2 WING-BODY LIFT-CURVE SLOPE

When a lifting panel is added to a body at low angles of attack, certain mutual interference effects may arise between the components. These can be classified as (a) the effect of body upwash or cross flow on the local angle of attack of the lifting panel, (b) the effect of local body-flow properties such as Mach number and dynamic pressure on the panel characteristics, (c) the effect of the lift carryover from the panel onto the body, (d) the effect of panel upwash on the body ahead of the panel (at subsonic speeds only), and (e) the effect of the panel lifting vortices on the body behind the wing. These interferences are generally small for configurations with large panel-span-to-body-diameter ratios typified by conventional, long-range subsonic aircraft. For these configurations the lift-curve slope of the combination is essentially the sum of the lift-curve slopes of the components. For configurations in which the panel-span-to-body-diameter ratio is small, such as conventional missiles or canard surfaces, these interference effects must usually be considered.

A. SUBSONIC

At subsonic speeds the wing-body (tail-body) interference effects are particularly difficult to estimate. Each of the interference effects discussed in the introduction is discussed below for this speed regime.

Body Upwash (Cross Flow)

In potential flow, a cylinder with the axis normal to the flow has a maximum velocity at the ends of the diameters normal to the flow equal to twice the free-stream velocity. An inclined cylinder can be treated by considering the cylinder to be in a combined axial and cross flow. The cross-flow velocity is thus equal to $2V\sin\alpha$ and serves to increase the local angle of attack of the lifting panel. In practice only about 40 percent of the full potential velocity is attained (see reference 1).

Body Flow Field (Axial Flow)

The perturbations in the potential flow field about a three-dimensional body are less than those for a corresponding two-dimensional body. For example, the local velocity about a three-dimensional body varies as $1/r^2$ and about a two-dimensional body as $1/r$, where r is the distance from the body centerline. Nevertheless, the effects of these perturbations can become significant and have sometimes been used in refined design analysis. However, for purposes of the Datcom, these effects are considered to be outside the scope of the book. Reference 2 contains a theoretical development that uses a distributed source-sink and doublet representation for elongated bodies. This method is best suited to machine computation.

Panel Lift Carryover

The carryover of the panel loading onto the body is calculated in reference 3 by means of a conformal mapping procedure. The lift that includes this carryover effect is always less than the lift of the gross panel. No method is included in the Datcom at the present time for estimating this effect.

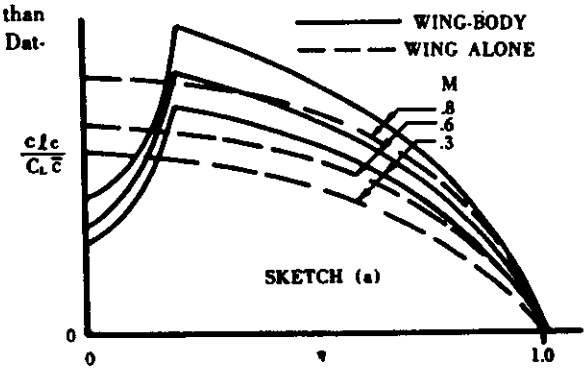

The combined effect of the lift carryover and the body upwash is shown for several Mach numbers in sketch (a) above. The comparison of the isolated panel and the combination indicates that these two effects tend to compensate for each other. The increment in lift-curve slope due to these effects is shown in sketch (b) as a function of body size and Mach number. The smaller bodies tend to increase the lift-curve slope and the larger bodies tend to decrease it.

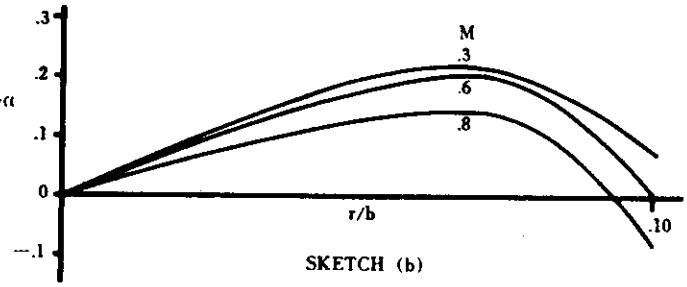

SKETCH (b)

Panel Upwash

The induced effects of the bound and trailing vortices of the panel are such as to cause an upwash ahead of the panel. The upwash is a maximum at the panel leading edge and rapidly decays with distance forward. These effects are more important for pitching-moment considerations than for lift.

Panel Vortices

The downwash behind the panel due to the bound and trailing vortices reduces the effective angle of attack on the aft portion of the body and hence reduces the body lift. Again the effect on the lift of the combination is invariably small; whereas the effect on pitching moment is more significant. These latter two effects have been successfully treated by Multhopp (reference 4).

A simple, yet relatively accurate, approach to the problem of wing-body interference is given in reference 5. In this reference a method based primarily on slender-body theory is presented for calculating the ratio of the lift of the wing-body combination to that of the wing alone. The derivation of the interference effects in terms of these ratios permits the extension of the method to nonslender configurations. The reason for this is that in certain instances slender-body theory accurately predicts the ratio of the wing-body lift to wing lift, even though it does not accurately predict the magnitudes of the individual lift-curve slopes.

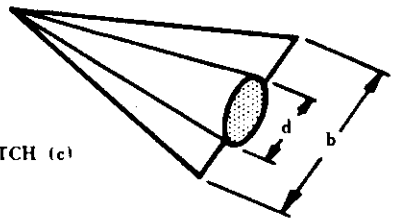

SKETCH (c)

The specific case of a conical body mounted on a delta wing (sketch (c)) has been solved by Spreiter in reference 6. Slender-body theory is used to obtain the ratio of the wing-body lift to that of the wing alone. Correlation with experimental data by this method is good throughout the speed range. In this Section, charts are presented for the determination of the appropriate wing-body interference ratios by means of the methods of references 5 and 6.

The methods are applicable to axisymmetric bodies in combination with straight-taper wings and are restricted to unbanked wings (zero roll angle). According to the limitations of slender-body theory, the methods of references 5 and 6 are not applicable to wings with sweptback trailing edges. Nevertheless, experimental data (see sample problems) indicate that good correlations can be obtained for these configurations.

The definition of exposed wing area depends upon the geometry of the wing-body combination. Two cases are illustrated in sketch (d) below. For a wing mounted on a cylindrical portion of a body the exposed wing is defined as the exposed half-wings joined together. For a wing mounted on an expanding section of a body the exposed wing is defined as the parts of the wing outboard of the largest body diameter at the wing-body intersection.

When the wing is mounted on a cylindrical body section, the nose of the body is defined as the section of the body ahead of the wing. When the wing is mounted on an expanding portion of the body, the nose is defined as the expanding portion of the body.

The latter definition is recommended in reference 5 for the case of a configuration with a small body-diameter-to-wing-

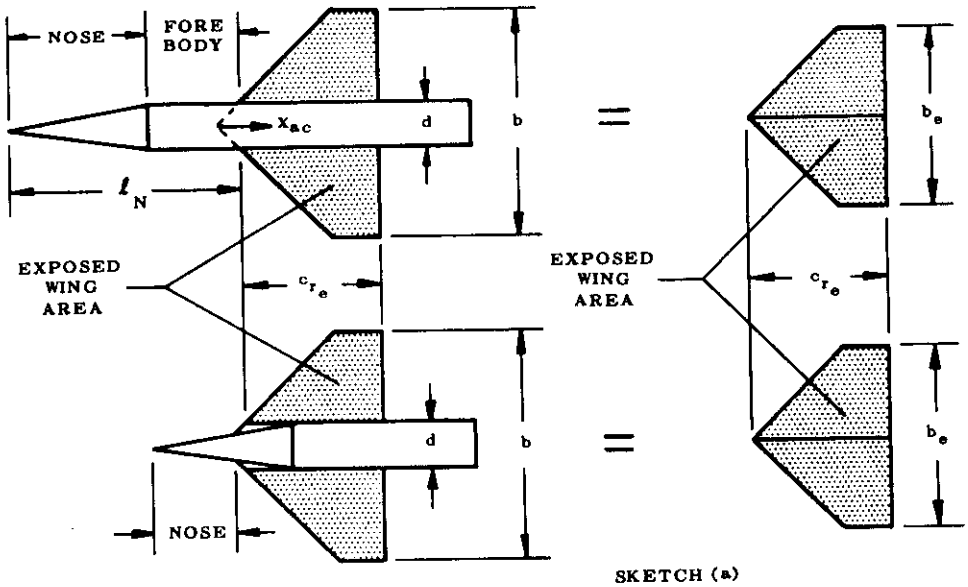

SKETCH (a)

span ratio; but for the case of a relatively large body-diameter-to-wing-span ratio with the wing extending the entire length of the body (see sketch (c)), the use of this definition can lead to substantial error.

DATCOM METHODS

Method 1 (reference 5)

This method is applicable to configurations such as those in sketch (d). The lift on a wing-body combination is taken to be the sum of three principal components:

1. Lift on nose including forebody (see sketch (d), upper configuration)
2. Lift on wing in presence of body
3. Lift on body due to the wing

Two cases of wing-body interference are considered. The first case is that in which the wing incidence is fixed relative to the body and the angle of attack is varied for the wing-body combination as a unit. The second case is that in which the body angle of attack remains fixed and the wing incidence varies relative to the body.

For the first case — wing fixed at zero incidence — the equation for wing-body lift-curve slope based on the total projected wing area, including that intercepted by the fuselage, is:

$$(C_{L_\alpha})_{WB} = \left[K_N + K_{W(B)} + K_{B(W)}\right](C_{L_\alpha})_e \frac{S_e}{S_W} \qquad 4.3.1.2\text{-a}$$

The quantities K_N, $K_{W(B)}$, and $K_{B(W)}$ represent the ratios of the nose lift, the wing lift in the presence of the body, and the body lift in the presence of the wing, respectively, to the wing-alone lift. For wings mounted on expanding bodies, the same procedure, with application of the definitions of sketch (d) in the discussion, usually yields satisfactory results. Configurations similar to that of sketch (c) are treated separately, in later paragraphs.

For the second case — fuselage fixed at zero angle of attack and wing incidence varying — the equation is:

$$(C_{L_i})_{WB} = \left[k_{W(B)} + k_{B(W)}\right](C_{L_\alpha})_e \frac{S_e}{S_W} \qquad 4.3.1.2\text{-b}$$

For both equations above, the best results are obtained for configurations in which the body radii do not exceed 80 percent of the total wing semispan. For larger ratios, the aerodynamic characteristics of the combination tend to be determined more by the body than by the wing.

The parameters common to equations 4.3.1.2-a and 4.3.1.2-b are determined as follows:

S_W = total projected wing area

S_e = exposed wing area. Exposed wing is defined as the exposed half-wings joined together for configurations in which the wing is mounted on a cylindrical section of the body (see sketch (d), upper configuration). For wings on expanding portions of bodies, the exposed wing area is the area outside of the maximum body diameter (see sketch (d), lower configuration).

$(C_{L_\alpha})_e$ = lift-curve slope of exposed wing based on exposed wing area and exposed aspect ratio. Determine from Section 4.1.3.2.

$$K_N = \frac{(C_{L_\alpha})_N S_{N_{ref}}}{(C_{L_\alpha})_e S_e}$$

$(C_{L_\alpha})_N$ = nose lift-curve slope. In most cases a value of 2 per radian (based on body frontal area) is sufficiently accurate. For cases where a higher degree of accuracy is required, use Section 4.2.1.1.

$S_{N_{ref}}$ = reference area for nose lift-curve slope, usually πr^2

$K_{W(B)}^*$ is obtained from figure 4.3.1.2-10

$K_{B(W)}^*$ is obtained from figure 4.3.1.2-10

$k_{W(B)}$ is obtained from figure 4.3.1.2-12a

$k_{B(W)}$ is obtained from figure 4.3.1.2-12a

Method 2 (reference 6)

This method is applicable to configurations similar to that of sketch (c).

The wing-body lift-curve slope is given by the following equation:

$$(C_{L_\alpha})_{WB} = K_{(WB)} (C_{L_\alpha})_W \qquad 4.3.1.2\text{-c}$$

where

$(C_{L_\alpha})_W$ is the wing lift-curve slope from section 4.1.3.2 (based on total wing area)

$K_{(WB)}$ is obtained from figure 4.3.1.2-12c

Comparison between experimental and calculated wing-body characteristics for a large number of cases (reference 5) shows that the lift of the wing-body combination is generally estimated by these methods to within ±10 percent.

Sample Problem

Given:

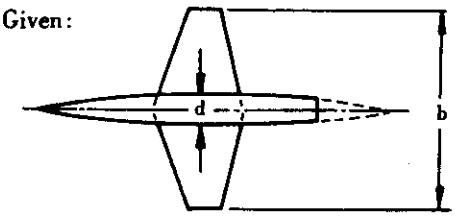

$A = 3$

$\Lambda_{LE} = 19.1°$

$\lambda = 0.4$

$\frac{d}{b} = 0.145$

Compute:

$\lambda_e = 0.438$

$A_e = 2.74$

$\frac{S_e}{S_w} = 0.802$

$\frac{S_{N_{ref}}}{S_e} = 0.0617$

$\Lambda_{c/2} = 0$

$(C_{L_\alpha})_e = 3.23$ (figure 4.1.3.2-49)

$K_N = \frac{(C_{L_\alpha})_N S_{N_{ref}}}{(C_{L_\alpha})_e S_e} = \frac{2}{3.23}(.0617) = 0.037$

*The calculation (Reference 10) of the sum of $K_{W(B)}$ and $K_{B(W)}$ can be expressed in terms of the planform geometry as follows

$$K_{W(B)} + K_{B(W)} = \left(\frac{d}{b} + 1\right)^2.$$

$M = .25$ $K_{W(B)} = 1.12$ (figure 4.3.1.2-10)

$R_\ell = 2 \times 10^6$ to 8×10^6 (based on wing MAC) $K_{B(W)} = 0.20$ (figure 4.3.1.2-10)

Note: This is configuration 4 of reference 7

Solution:

$$(C_{L_\alpha})_{WB} = \left[K_N + K_{W(B)} + K_{B(W)} \right] (C_{L_\alpha})_e \frac{S_e}{S_w} = 3.51 \text{ per radian (equation 4.3.1.2-a)}$$

This compares with an experimental value of $(C_{N_\alpha})_{WB} = 3.33$ (figures 6 and 21 of reference 7).

B. TRANSONIC

For slender wing-body configurations, the aerodynamic interference effects are relatively insensitive to Mach number, and slender wing-body theory gives reasonable results. For nonslender configurations transonic interference effects can become quite large and sensitive to minor changes in local contour. At present, these effects cannot be predicted with any accuracy.

DATCOM METHOD

The method, which is based on slender-body theory, presented in Paragraph C below should be applied at transonic speeds.

C. SUPERSONIC

The mutual aerodynamic interference between a panel and a body at supersonic speeds at low angles of attack is due primarily to the upwash of the body and the lift carryover of the panel onto the body. The body upwash appears similar to its subsonic counterpart, that is, the upwash is a maximum at the body surface and decays with increasing distance from the surface. The integrated effect over the span of the panel at positive angles of attack increases the lift-curve slope of the panel.

The lift carryover on the body is displaced downstream parallel to the Mach lines, as illustrated in sketch (e) below. Important lift and moment differences can therefore exist between configurations in which the fuselage terminates at the wing trailing edge and those in which the fuselage extends beyond the wing trailing edge.

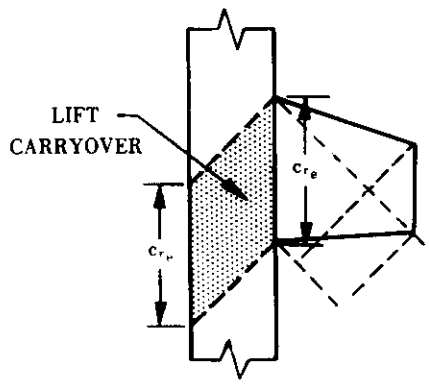

SKETCH (e)

These effects have been adequately predicted by slender-body theory in references 5 and 6 (see paragraph A above).

The local Mach-number and dynamic-pressure-ratio perturbations due to the axial flow component can also cause significant changes in the characteristics of the panels when the local body slopes in the vicinity of the panel become large. These perturbations decay with increasing distance from the body surface. This decay is more rapid than that in the corresponding two-dimensional case, because of the three-dimensional aspect of the body flow field. Sudden changes

in contour like flare or boattail corners, cause a two-dimensional Mach-number and dynamic-pressure-ratio change at the surface that then decays in a three-dimensional manner. Two-dimensional compression values for dynamic pressure and Mach number are given by equations 4.4.1-z and 4.4.1-aa, respectively, and corresponding expansion values are given in figure 4.4.1-74. The average values of these parameters acting on a panel are always less than the two-dimensional values.

DATCOM METHODS

Two methods are presented for estimating the lift-curve slope of wing-body or tail-body combinations. These methods, which are based on slender wing-body theory, are the same as those used in the subsonic paragraph.

Method 1:

Two cases are presented: (a) panel fixed at zero incidence to the body and angle of attack of the combination varied and (b) body kept at zero angle of attack and wing incidence varied. The lift is given by the following equations:

$$(a) \qquad (C_{L_\alpha})_{WB} = \left[K_N + K_{W(B)} + K_{B(W)}\right](C_{L_\alpha})_e \frac{S_e}{S_W} \qquad (4.3.1.2\text{-a})$$

$$(b) \qquad (C_{L_1})_{WB} = \left[k_{W(B)} + k_{B(W)}\right](C_{L_\alpha})_e \frac{S_e}{S_W} \qquad (4.3.1.2\text{-b})$$

The basic definitions and limitations for these equations are the same as those discussed in paragraph A above. However, special care must be used in specifying the "k" factors. These are summarized for the supersonic speed regime below.

$$K_N = \frac{(C_{L_\alpha})_N S_{N_{ref}}}{(C_{L_\alpha})_e \; S_e}$$

$K_{W(B)}$ all planforms use figure 4.3.1.2-10

$K_{B(W)}$:

- triangular-type planforms:
  - If $\beta A_e \leq 1$, use figure 4.3.1.2-10
  - If $\beta A_e > 1$,
    - and the fuselage extends beyond wing trailing edge, use figure 4.3.1.2-11a
    - and the fuselage does not extend beyond the wing trailing edge, use figure 4.3.1.2-11b
- nontriangular planforms:
  - If $\beta A_e(1 + \lambda_e)\left(\frac{\tan \Lambda_{LE}}{\beta} + 1\right) \leq 4$, use figure 4.3.1.2-10
  - If $\beta A_e(1 + \lambda_e)\left(\frac{\tan \Lambda_{LE}}{\beta} + 1\right) > 4$,
    - and fuselage extends beyond wing trailing edge, use figure 4.3.1.2-11a
    - and fuselage does not extend beyond wing trailing edge, use figure 4.3.1.2-11b

$k_{W(B)}$ is obtained from figure 4.3.1.2-12b

$k_{B(W)}$ is obtained from figure 4.3.1.2-12a

Method 2:

This method is applicable to configurations similar ot that of sketch (c) and is identical to that presented as Method 2 of paragraph A.

Sample Problems

1. Supersonic Lift-Curve Slope of Wing-Body Combination

Given:

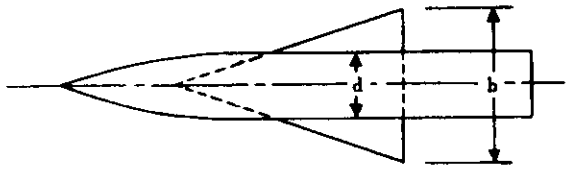

$A = 1.34$

$\Lambda_{LE} = 71.6°$

$\lambda = 0$

Airfoil: 8-percent-thick double wedge (free-stream direction)

$\frac{d}{b} = 0.428$

$M = 2.02$

$R = 2.6 \times 10^6$ (based on root chord)

Note: This is configuration 2 of reference 8.

Compute:

$\lambda_e = 0$

$A_e = 1.34$

$\frac{S_e}{S_w} = 0.328$

$\frac{S_{N\,ref}}{S_e} = 0.590$

$\beta = 1.75$

$A_e \tan \Lambda_{LE} = 4$

$\frac{\beta}{\tan \Lambda_{LE}} = 0.584$

$[(C_{N_\alpha})_e]_{theory} = 1.65$ (Section 4.1.3.2)

$\frac{(C_{N_\alpha})_e}{[(C_{N_\alpha})_e]_{theory}} = 0.94$ (Section 4.1.3.2) based on $\delta_\perp = 14.5°$

$(C_{N_\alpha})_e = 1.55$

$\frac{\beta}{f_N} = 0.526$

$(C_{N_\alpha})_N = 2.47$ (Section 4.2.1.1)

$K_{W(B)} = 1.38$ (figure 4.3.1.2-10)

$\frac{\beta d}{c_{r_e}} = 0.875$

$K_{B(W)}\,\beta\,(C_{L_\alpha})_e\,(\lambda_e + 1)\left(\frac{b}{d} - 1\right) = 2.1$ (figure 4.3.1.2-11a)

$\beta\,(\lambda_e + 1)\left(\frac{b}{d} - 1\right) = 2.35$

$K_{B(W)} = 0.576$

$K_N = \frac{(C_{N_\alpha})_N}{(C_{N_\alpha})_e}\ \frac{S_{N\,ref}}{S_e} = 0.936$

Solution:

$$(C_{L_\alpha})_{WB} = [K_N + K_{W(B)} + K_{B(W)}](C_{L_\alpha})_e \frac{S_e}{S_w} = 1.47 \text{ (equation 4.3.1.2-a)}$$

This compares with an experimental value of $(C_{L_\alpha})_{WB} = 1.57$ from reference 8.

2. Supersonic Lift-Curve Slope — Wing in Presence of Body

Case One: Wing incidence fixed at $i_w = 0$, fuselage rotating with wing

Given:

$A = 2.31$

$\Lambda_{LE} = 60°$

$\lambda = 0$

Airfoil: 9-percent-thick biconvex (free-stream direction)

$\frac{d}{b} = 0.23$

$M = 1.9$

$R_l = 1.9 \times 10^6$ (based on root chord)

Note: This is the delta-wing configuration in reference 9.

Compute:

$\lambda_e = 0$

$A_e = 2.31$

$\beta = 1.62$

$A_e \tan \Lambda_{LE} = 4$

$\frac{\beta}{\tan \Lambda_{LE}} = .935$

$[(C_{N_\alpha})_e]_{theory} = 2.38$ (Section 4.1.3.2)

$\frac{(C_{N_\alpha})_e}{[(C_{N_\alpha})_e]_{theory}} = .75$ (Section 4.1.3.2) based on $\delta_\perp = 20.7°$

$(C_{N_\alpha})_e = 1.79$

$K_{W(B)} = 1.2$ (figure 4.3.1.2-10)

Solution:

Since only the lift on the wing is of interest, the reference area is the exposed wing area, and equation 4.3.1.2-a reduces to

$$(C_{L_\alpha})_{w_e(B)} = K_{W(B)} (C_{L_\alpha})_e$$

Thus the wing lift in the presence of the body is $(C_{L_\alpha})_{w_e(B)} = 2.15$

The experimental value from reference 9 is $(C_{L_\alpha})_{w_e(B)} = 2.22$

Case Two: Body fixed at $\alpha = 0$, wing incidence variable

Given:

Same as Case One

Compute:

$k_{W(B)} = 0.96$ (figure 4.3.1.2-12b)
Other coefficients same as in Case One

Solution:

Again only the wing lift is of interest. Equation 4.3.1.2-b becomes

$$(C_{L_\alpha})_{w_e(B)} = k_{W(B)} (C_{L_\alpha})_e$$
$$= 1.72$$

The experimental value from reference 9 is 1.67.

REFERENCES

1. Zahm, A. F.: Flow and Drag Formulas for Simple Quadrics. NACA TR 253, 1926. (U)

2. Kaplan, C.: Potential Flow About Elongated Bodies of Revolution. NACA TR 516, 1935. (U)

3. Donovan, A. F., and Lawrence, H. R.: Aerodynamic Components of Aircraft at High Speeds. Princeton University Press, 1957. (U)

4. Multhopp, H.: Zur Aerodynamik des Flugzeugrumpfes (On the Aerodynamics of the Fuselage). Luftfahrtforschung 18, 52-66, 1941. (U)

5. Pitts, W., Nielsen, J., and Kaattari, G.: Lift and Center of Pressure of Wing-Body-Tail Combinations at Subsonic, Transonic, and Supersonic Speeds. NACA TR 1307, 1957. (U)

6. Spreiter, J.: The Aerodynamic Forces on Slender Plane and Cruciform-Wing and Body Combinations. NACA TR 962, 1950. (U)

7. Smith, D., Shibata, H., and Selan, R.: Lift, Drag, and Pitching Moment of Low-Aspect Ratio Wings at Subsonic and Supersonic Speeds – An Investigation at Large Reynolds Numbers of the Low-Speed Characteristics of Several Wing-Body Combinations. NACA RM A51K28, 1952. (U)

8. Nielsen, J., Katzen, E., and Tang, K.: Lift and Pitching-Moment Interference Between a Pointed Cylindrical Body and Triangular Wings of Various Aspect Ratios at Mach Numbers of 1.50 and 2.02. NACA TN 3795, 1956. (U)

9. Conner, D.: Aerodynamic Characteristics of Two All-Movable Wings Tested in the Presence of a Fuselage at a Mach Number of 1.9. NACA RM L8H04, 1948. (U)

10. Graham, R. E., and McDowell, J. L.: Simplification of the Wing-Body Interference Problem. Jour. of Aircraft Vol. 9 No. 10, Oct 1972. (U)

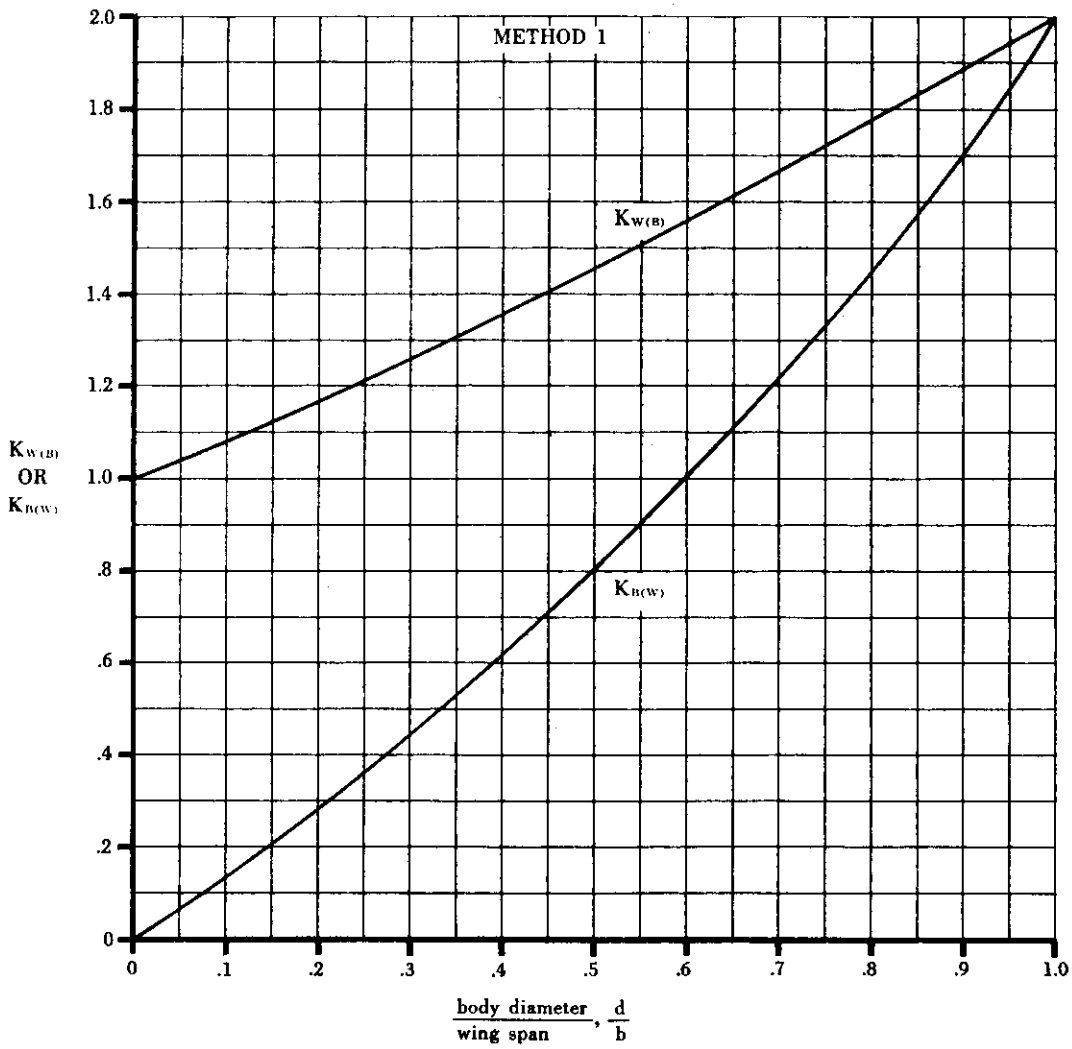

FIGURE 4.3.1.2-14 LIFT RATIOS $K_{W(B)}$ AND $K_{B(W)}$ —SLENDER-BODY THEORY— FIXED INCIDENCE—ALL SPEEDS

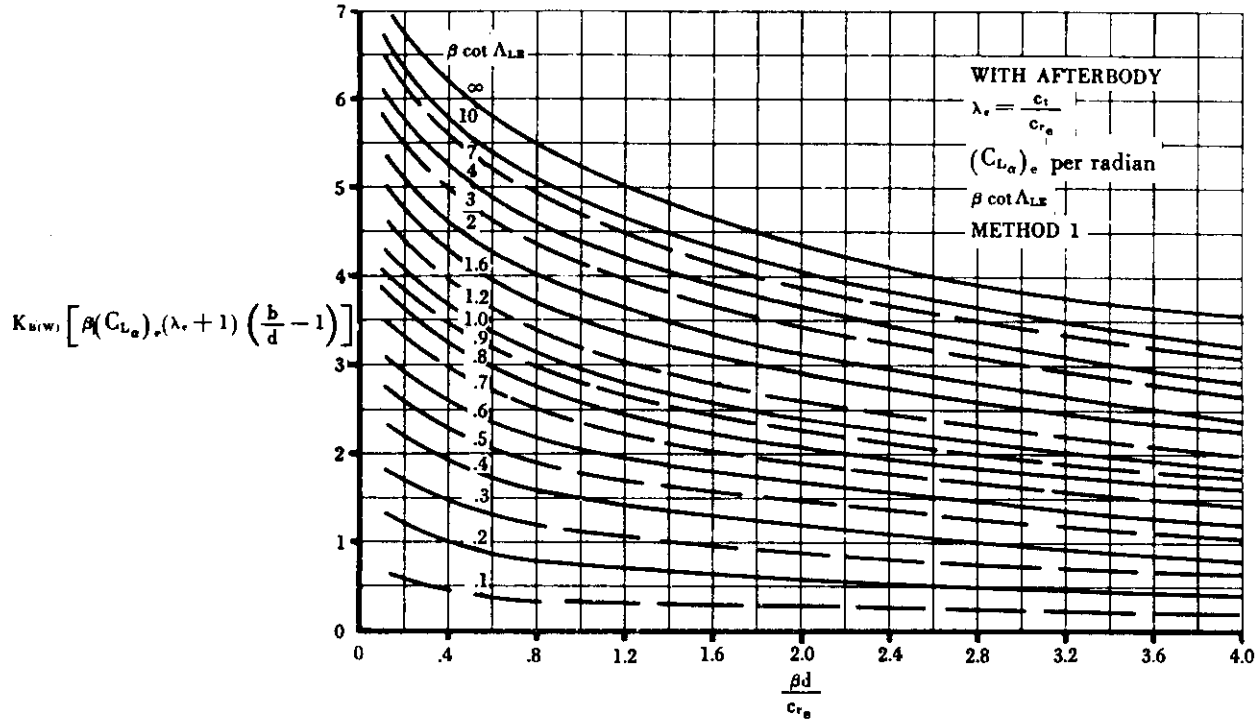

FIGURE 4.3.1.2-11a LIFT ON BODY IN PRESENCE OF WING—WITH AFTERBODY—FIXED WING INCIDENCE—SUPERSONIC SPEEDS

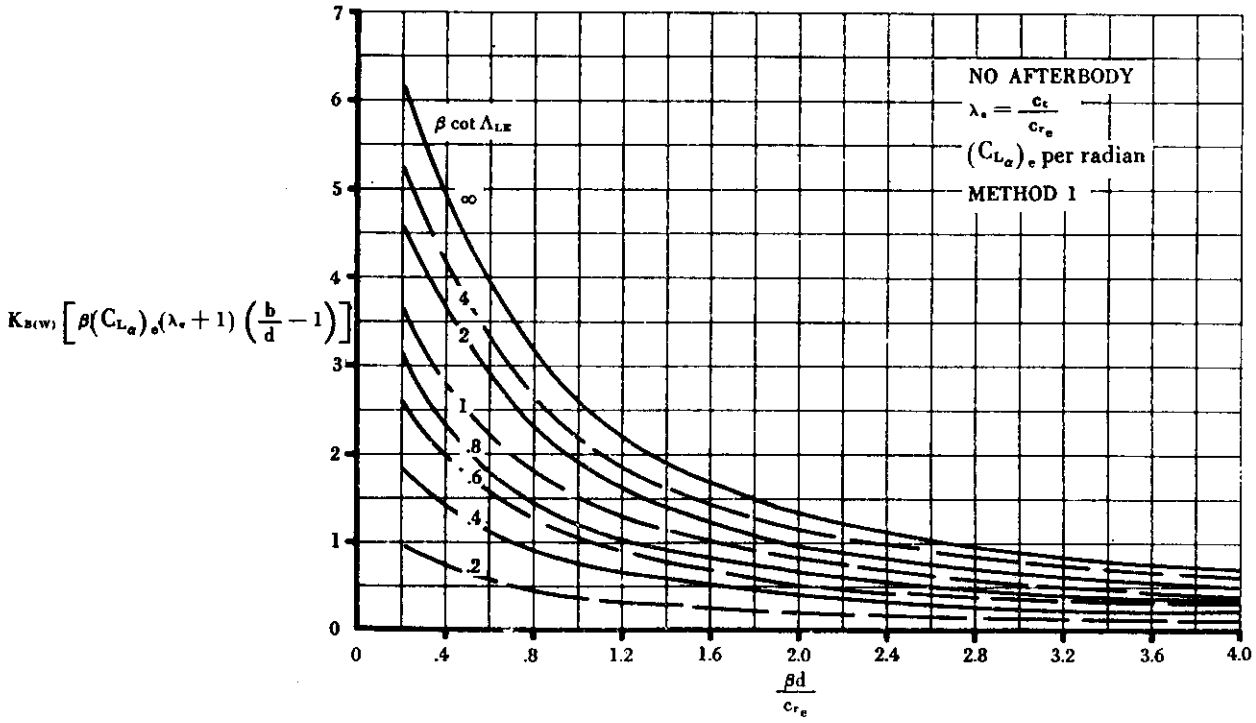

FIGURE 4.3.1.2-11b LIFT ON BODY IN PRESENCE OF WING—NO AFTERBODY—FIXED WING INCIDENCE—SUPERSONIC SPEEDS

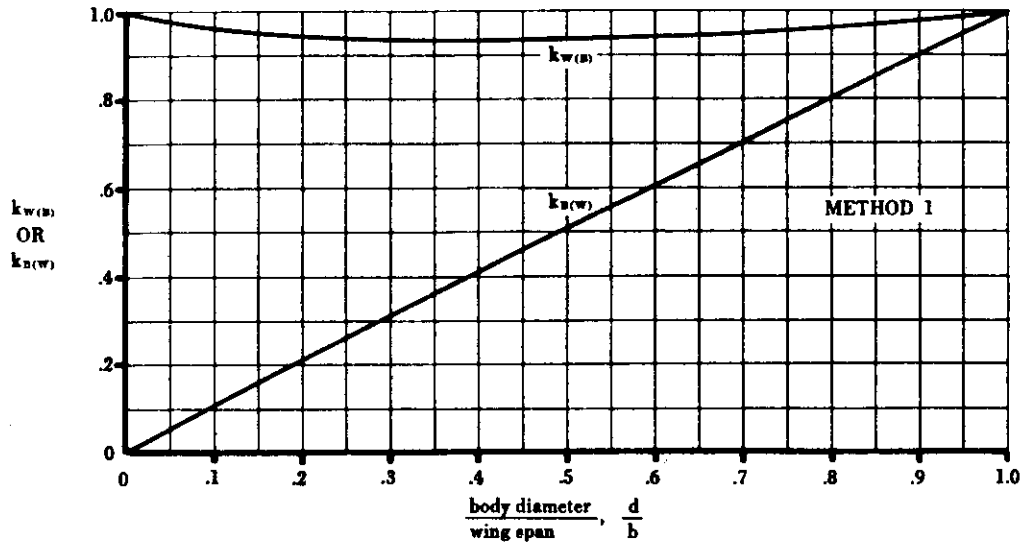

FIGURE 4.3.1.2-12a LIFT RATIOS $k_{w(B)}$ AND $k_{B(W)}$—SLENDER-BODY THEORY VARIABLE INCIDENCE—ALL SPEEDS

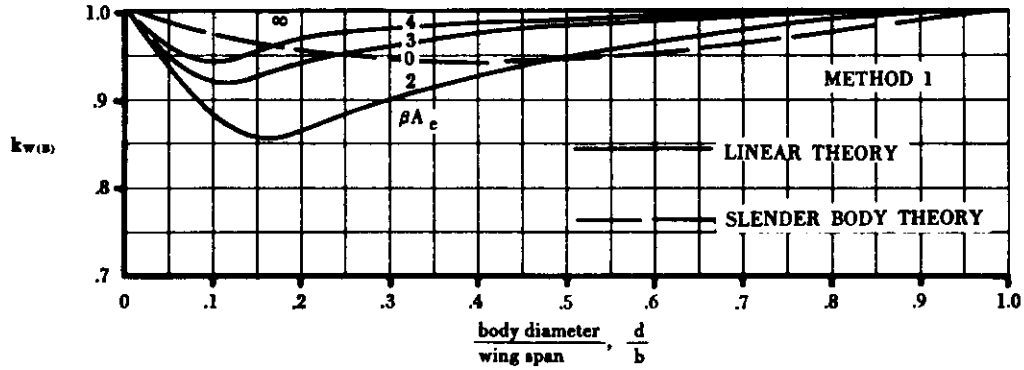

FIGURE 4.3.1.2-12b LIFT ON BODY IN PRESENCE OF WING—VARIABLE INCIDENCE SUPERSONIC SPEEDS

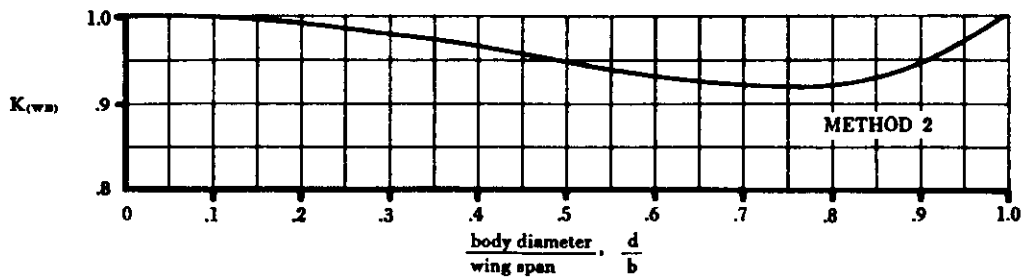

FIGURE 4.3.1.2-12c LIFT RATIO FOR METHOD 2

4.3.1.3 WING-BODY LIFT IN THE NONLINEAR ANGLE-OF-ATTACK RANGE

The mutual interference factors that influence the lift of a wing-body or a tail-body combination at low angles of attack (see Section 4.3.1.2) are also present at higher angles of attack. These include the nonlinear characteristics of the basic wing and body components (see Sections 4.1.3.3 and 4.2.1.2, respectively).

In addition, at angles of attack of approximately six degrees body vortices appear that can have strong influences on the loading on the lifting panels. The flow separates just behind or above the area of minimum pressure along the side of the body near the nose and wraps up into a pair of symmetrical vortices that proceed downstream in a nearly free-stream direction. The point at which separation first takes place depends upon the angle of attack (the higher the angle of attack, the nearer the nose separation occurs), the nose profile shape (the blunter the nose, the nearer the nose separation occurs), and body cross-sectional shape (sharply curving lateral contours promote early separation). The vortices increase in size and strength with increasing downstream distance. Since their strength also increases as the square of the angle of attack, they become quite significant at the higher angles of attack.

Quantitatively, these vortices do not change significantly between subsonic and supersonic speeds. This fact is substantiated by reference 1, which derives from supersonic data a method of estimating the cross-flow lift that gives equally reliable answers at subsonic and supersonic speeds. This is the method presented by the Datcom for handling the effects of these vortices on lifting surfaces at both subsonic and supersonic speeds.

A. SUBSONIC

Two methods of estimating the lift of wing-body configurations in the nonlinear angle-of-attack range are presented. The first uses the estimated nonlinear lift characteristics of isolated wings and bodies corrected by the slender-body interference factors used in Section 4.3.1.2. The effects of the body vortices are then added. This method is valid up to high angles of attack and is the more accurate of the two methods, though more laborious to use.

The second method simply uses the linear methods of Section 4.3.1.2 and adds the effects due to the body vortices. This method can be used with a minimum of effort but is less accurate than the first method because it does not include the nonlinearities of the basic components.

DATCOM METHODS

Method 1

The variation of lift with angle of attack is determined by the equation

$$C_N = \left\{(C_N)_N \frac{S_{N_{ref}}}{S_e} + \left[K_{W(B)} + K_{B(W)}\right](C_N)_e\right\}\frac{S_e}{S_W} + I_{V_{B(W)}}\left(\frac{\Gamma}{2\pi\,a\,Vr}\right)\frac{r}{b_W/2}\,\frac{q}{q_\infty}\,a\left(C_{L_a}\right)_W \qquad 4.3.1.3\text{-a}$$

where

$(C_N)_N$ is the nose normal-force coefficient at a given angle of attack based on body frontal area $S_{N_{ref}}$ from Section 4.2.1.2

$K_{W(B)}$ and $K_{B(W)}$ are the mutual linear-theory interference values from figure 4.3.1.2-10

$(C_N)_e$ is the normal-force coefficient, at any given angle of attack, for the exposed wing (calculated by the method of Section 4.1.3.3 and based on exposed wing area)

$I_{V_{B(W)}}$ is the vortex interference factor for a lifting surface mounted on the body center line. This factor is given in figures 4.3.1.3-7a through 4.3.1.3-7ℓ for various wing taper ratios, relative wing sizes, and vortex-center line positions. In using these figures a possible problem can develop when interpolation must be made with respect to λ and $r/(b_W/2)$. For positions of the vortex near the body, the interpolation in $r/(b_W/2)$ can carry the vortex inside the body. Under these circumstances, it is recommended that the interpolation be made using $(y_o - r)/(b_W/2 - r)$ for the vortex lateral position in place of $y_o/(b_W/2)$, to avoid vortex positions inside the body. These figures are derived by means of strip theory in reference 2.

The vertical and lateral vortex positions at any given longitudinal station x can be determined from figures 4.3.1.3-13b and 4.3.1.3-14, respectively. These figures are based on the data of references 3, 4, and 5, for an ogive-cylinder, a cone-cylinder, and a modified cone-cylinder, respectively. The longitudinal position of vortex separation used in these figures is obtained from figure 4.3.1.3-13a, which is based on the ogive-cylinder test at a Mach number of 1.98 from reference 3.

$\frac{\Gamma}{2\pi a Vr}$ is the nondimensional vortex strength from figure 4.3.1.3-15. which is also based on the data of references 3, 4, and 5.

$\frac{r}{b_W/2}$ is the ratio of the radius of the body at the midpoint of the exposed root chord of the lifting panel to the semispan of the panel.

q/q_∞ is the dynamic pressure ratio acting on the panel. This value can either be assumed to be unity or can be estimated, with the information in Section 4.4.1 as a guide.

$(C_{L_\alpha})_W$ is the lift-curve slope of the isolated gross panel from Section 4.1.3.2.

Method 2

The variation of lift with angle of attack is given by the equation

$$C_L = \left[K_N + K_{W(B)} + K_{B(W)} \right] (C_{L_\alpha})_e \, a \frac{S_e}{S_W} + I_{v_{B(W)}} \left(\frac{\Gamma}{2\pi a Vr} \right) \frac{r}{b_W/2} \frac{q}{q_\infty} \, a \left(C_{L_\alpha} \right)_W \qquad 4.3.1.3\text{-b}$$

where the first term on the right-hand side is given by the method presented in Section 4.3.1.2 and the second term is determined as in Method 1.

The last terms of equations 4.3.1.3-a and -b, respectively, which represent the contributions of the body vortices, can normally be ignored for normal airplane-type wing-body combinations. For conventional missile configurations, these effects may become sizable.

Sample Problems

1. Method 1

Given:

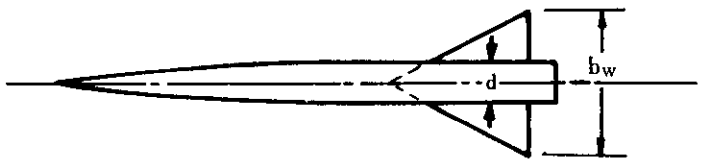

$A_W = A_e = 2$

$\Lambda_{c/2} = 45°$

$\lambda_W = \lambda_e = 0$

$\frac{S_e}{S_W} = 0.518$

$\frac{d}{b_W} = 0.280$

Airfoil: NACA 0005

$M = 0.2$

$q/q_\infty = 1.0$

$\frac{S_{N_{ref}}}{S_e} = 0.238$

$\frac{r}{b_W/2} = 0.280$

$\frac{x}{r} = 21.10$

where

x = distance from nose to c/4-point of the MAC of the exposed wing panel.

The following lift variation with angle of attack (from test data)

α(deg)	$(C_N)_N$	$(C_N)_e$
0	−.010	0
4	.035	.150
8	.175	.300
12	.430	.430
16	.810	.700

$(C_N)_N$ is based on $S_{N_{ref}}$

$(C_N)_e$ is based on S_e

The following lift-curve slopes

$(C_{L_\alpha})_e$ = 2.12 per radian (test data)

$(C_{L_\alpha})_W$ = 2.34 per radian (methods of Section 4.1.3.2)

$(C_{L_\alpha})_N$ = 2 per radian (slender-body theory)

$(C_{L_\alpha})_e$ based on S_e

$(C_{L_\alpha})_W$ based on S_W

$(C_{L_\alpha})_N$ based on $S_{N_{ref}}$

Compute:

$K_{W(B)} = 1.240$
$K_{B(W)} = 0.420$ } (figure 4.3.1.2-10)

The lift variation with angle of attack for the wing-body configuration, excluding the effect of body vortices, is calculated as follows:

$$\frac{C_L}{\cos\alpha} \approx C_N = \left\{(C_N)_N \frac{S_{N_{ref}}}{S_e} + \left[K_{W(B)} + K_{B(W)}\right](C_N)_e\right\}\frac{S_e}{S_W} \quad \text{(equation 4.3.1.3-a)}$$

α deg	C_N without vortices effect	$C_L = C_N \cos\alpha$
0	−.001	−.001
4	.133	.133
8	.280	.277
12	.423	.414
16	.701	.674

The calculation procedure for the effect of body vortices on lift variation with angle of attack is shown below.

$\frac{x_s}{r}$ (figure 4.3.1.3-13a)

$\frac{x}{r} - \frac{x_s}{r} = 21.10 - \frac{x_s}{r}$

$\alpha\left(\frac{x}{r} - \frac{x_s}{r}\right)$ (α in radians)

$\frac{z_o}{r}$ (figure 4.3.1.3-13b)

$\frac{y_o}{r}$ (figure 4.3.1.3-14)

$\frac{\Gamma}{2\pi a V_r}$ (figure 4.3.1.3-15)

$\frac{y_o}{b_w/2} = \frac{y_o}{r}\frac{r}{b_w/2}$

$\frac{z_o}{b_w/2} = \frac{z_o}{r}\frac{r}{b_w/2}$

$I_{v_{B(W)}}$ (figures 4.3.1.3-7a, 4.3.1.3-7b, and 4.3.1.3-7c, interpolated for $\frac{r}{b_w/2} = 0.280$)

$\frac{r}{b_w/2}\frac{q}{q_\infty}(C_{L_\alpha})_W \alpha = 0.280\ (1.0)\ (.0408)\ \alpha^\circ = 0.0114\alpha^O$

The solution for the vortices effect is

$$I_{v_{B(W)}}\left(\frac{\Gamma}{2\pi a V_r}\right)\frac{r}{b_w/2}\frac{q}{q_\infty}\alpha\left(C_{L_\alpha}\right)_W \quad (\alpha \text{ in degrees})$$

The details of the calculation for vortices effect are shown below.

① α deg	② $\frac{x_a}{r}$	③ $\alpha\left(\frac{x}{r}-\frac{x_a}{r}\right)$	④ $\frac{y_o}{r}$	⑤ $\frac{z_o}{r}$	⑥ $\frac{\Gamma}{2\pi a V_r}$
0	—	—	—	—	—
4	—	—	—	—	—
8	16.90	.58	.58	1.06	.51
12	11.25	2.05	.69	1.54	.82
16	8.55	3.50	.74	1.84	1.13

① α deg	⑦ $\frac{y_o}{b_w/2}$	⑧ $\frac{z_o}{b_w/2}$	⑨ $I_{v_{B(W)}}$	⑩ lift due to body vortices = 0.0114 ① ⑥ ⑨
0	—	—	—	—
4	—	—	—	—
8	.162	.297	−.22	−.0102
12	.193	.431	−.31	−.0348
16	.207	.515	−.38	−.0783

The solution for the lift variation with angle of attack of the wing-body configuration, including effect of body vortices, is shown below.

α deg	① C_L without vortices effect	② C_L due to body vortices	③ C_L = ① + ②
0	−.001	—	−.001
4	.133	—	.133
8	.277	−.0102	.267
12	.414	−.0348	.379
16	.674	−.0783	.596

2. Method 2

Given:

The same configuration and characteristics as in Method 1 above.

Compute:

$$K_N = \frac{(C_{L_\alpha})_N}{(C_{L_\alpha})_e} \frac{S_{N_{ref}}}{S_e} \quad \text{(Section 4.3.1.2)}$$

$$= \frac{2}{2.12} (.238)$$

$$= 0.225$$

$$\left.\begin{aligned} K_{W(B)} &= 1.240 \\ K_{B(W)} &= 0.420 \end{aligned}\right\} \text{ see Method 1 above}$$

The lift variation with angle of attack for the wing-body configuration, excluding the effect of body vortices, is calculated as follows:

$$C_L = [K_N + K_{W(B)} + K_{B(W)}] \frac{S_e}{S_w} (C_{L_\alpha})_e \alpha \ (\alpha \text{ in degrees})$$

$$= [.225 + 1.240 + .420] \ (.518) \ (.0370) \ \alpha$$

$$= 0.03613 \ \alpha \ (\alpha \text{ in degrees})$$

The lift due to body vortices is the same as that calculated in Method 1 above. The total lift variation is shown below.

α deg	① C_L without vortices effect	② C_L due to body vortices	③ C_L = ① + ②
0	0	—	0
4	.144	—	.144
8	.289	−.0102	.279
12	.434	−.0348	.399
16	.578	−.0783	.500

B. TRANSONIC

At transonic speeds compression and expansion waves interact at much greater distances from the body than at supersonic speeds. The disturbances in the flow field extend to greater distances from the body surface than at subsonic or supersonic speeds. With a knowledge of conditions at the surface of a body, the characteristics of a lifting surface mounted on the body can be approximated by assuming that the flow disturbances propagate undiminished in a direction normal to the free stream. An excellent discussion of methods of calculating surface pressures on bodies of revolution at zero angle of attack is given in reference 6. However, the corresponding problem at angle of attack is not well covered in the literature.

At angle of attack, the appearance of body vortices due to viscous separation effects is exactly analogous to that which occurs at subsonic or supersonic speeds.

DATCOM METHOD

No explicit method is presented in the Datcom at the present time, because of the complexity and uncertainty of estimating nonviscous transonic flow properties. It is recommended that the methods detailed in paragraph C be used at transonic speeds.

C. SUPERSONIC

The discussion of the potential flow field about a body at angle of attack, given in Section 4.2.1.2 is directly applicable to this Section, and therefore no new information is presented. Body vortices are also present at angles of attack in excess of approximately 6°. The physical mechanism of these vortices and their effect upon lifting panels are the same as at subsonic speeds; they are discussed in some detail in paragraph A.

DATCOM METHOD

Two methods are available for estimating the lift of wing-body configurations at supersonic speeds. These can be represented by equations 4.3.1.3-a and -b, respectively, of paragraph A. Because of the similarity of the application of these methods, the sample problem of paragraph A suffices to illustrate these methods.

REFERENCES

1. Kelly, H. R.: The Estimation of Normal-Force, Drag, and Pitching-Moment Coefficients for Blunt-Based Bodies of Revolution at Large Angles of Attack. Jour. Aero. Sci., Vol. 21, No. 8, August 1954. (U)
2. Pitts, W. C., Nielsen, J. N., and Kaattari, G. E.: Lift and Center of Pressure of Wing-Body-Tail Combinations at Subsonic, Transonic, and Supersonic Speeds. NACA TR 1307, 1959. (U)
3. Jorgensen, L. H. and Perkins, E. W.: Investigation of Some Wake Vortex Characteristics of an Inclined Ogive-Cylinder Body at Mach Number 1.98. NACA RM A55E31, August 1955. (U)
4. Mello, J. F.: Investigation of Normal-Force Distributions and Wake Vortex Characteristics of Bodies of Revolution at Supersonic Speeds. APL/JHU Rep. CM 867, Johns Hopkins Univ., April 1956. (U)
5. Raney, D. J.: Measurement of the Cross Flow Around an Inclined Body at a Mach Number of 1.91. British Report RAE TN Aero 2357 (ASTIA AD 82 343), January 1955. (U)
6. Spreiter, J. R.: Aerodynamics of Wings and Bodies at Transonic Speeds. Jour. Aero. Sci., Vol. 26, No. 8, August 1959. (U)

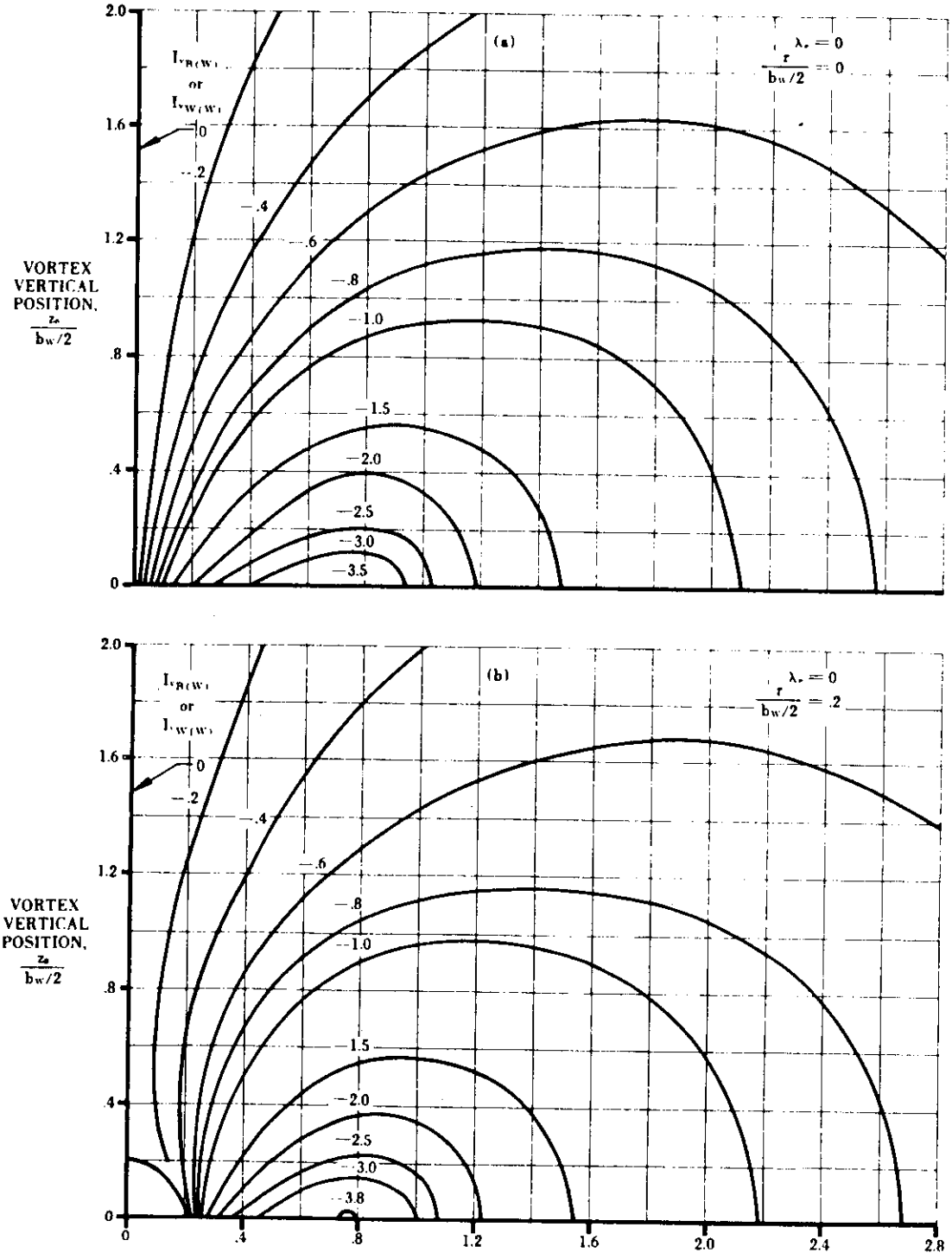

FIGURE 4.3.1.3-7 VORTEX INTERFERENCE FACTOR

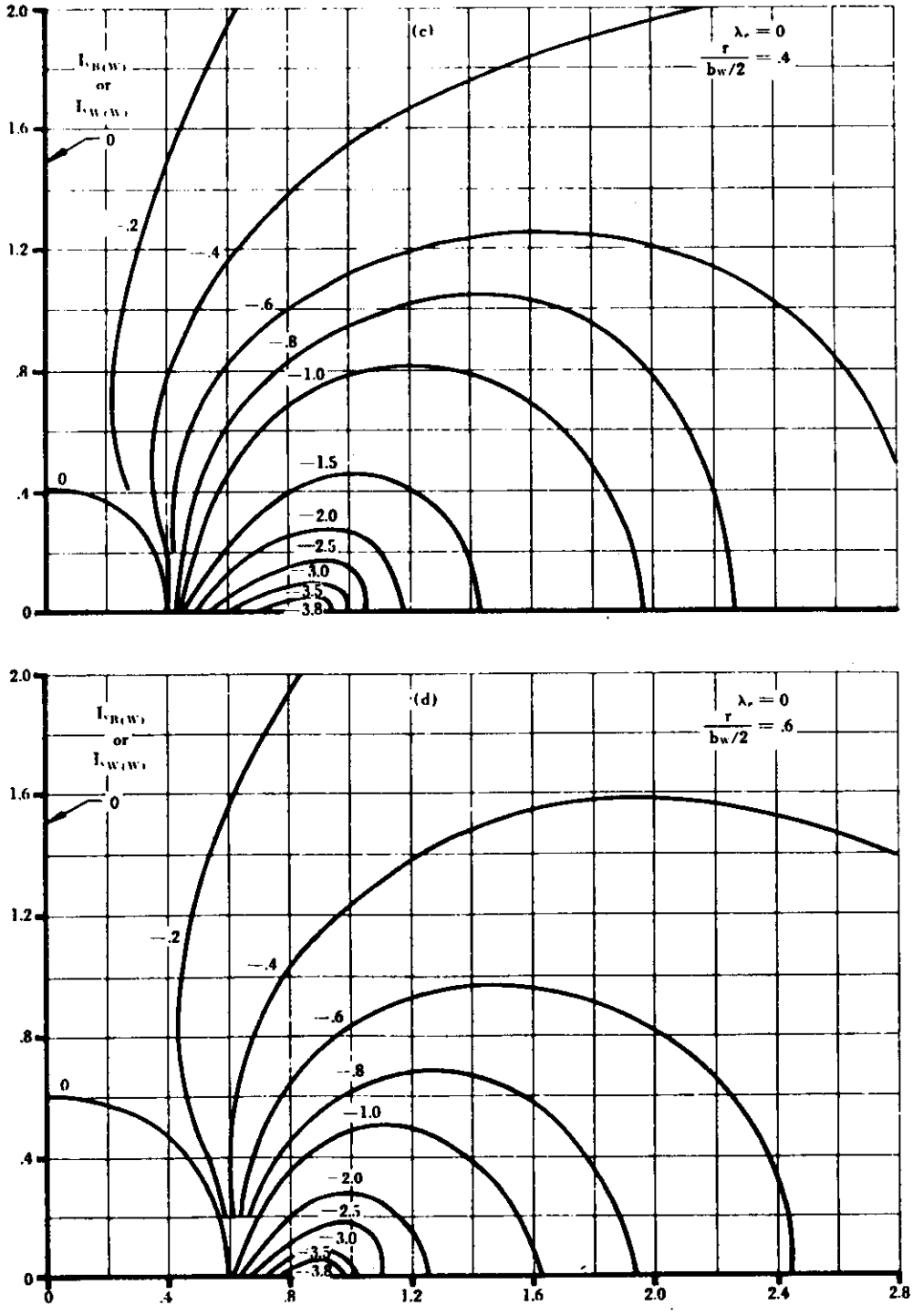

FIGURE 4.3.1.3-7 VORTEX INTERFERENCE FACTOR (CONT'D)

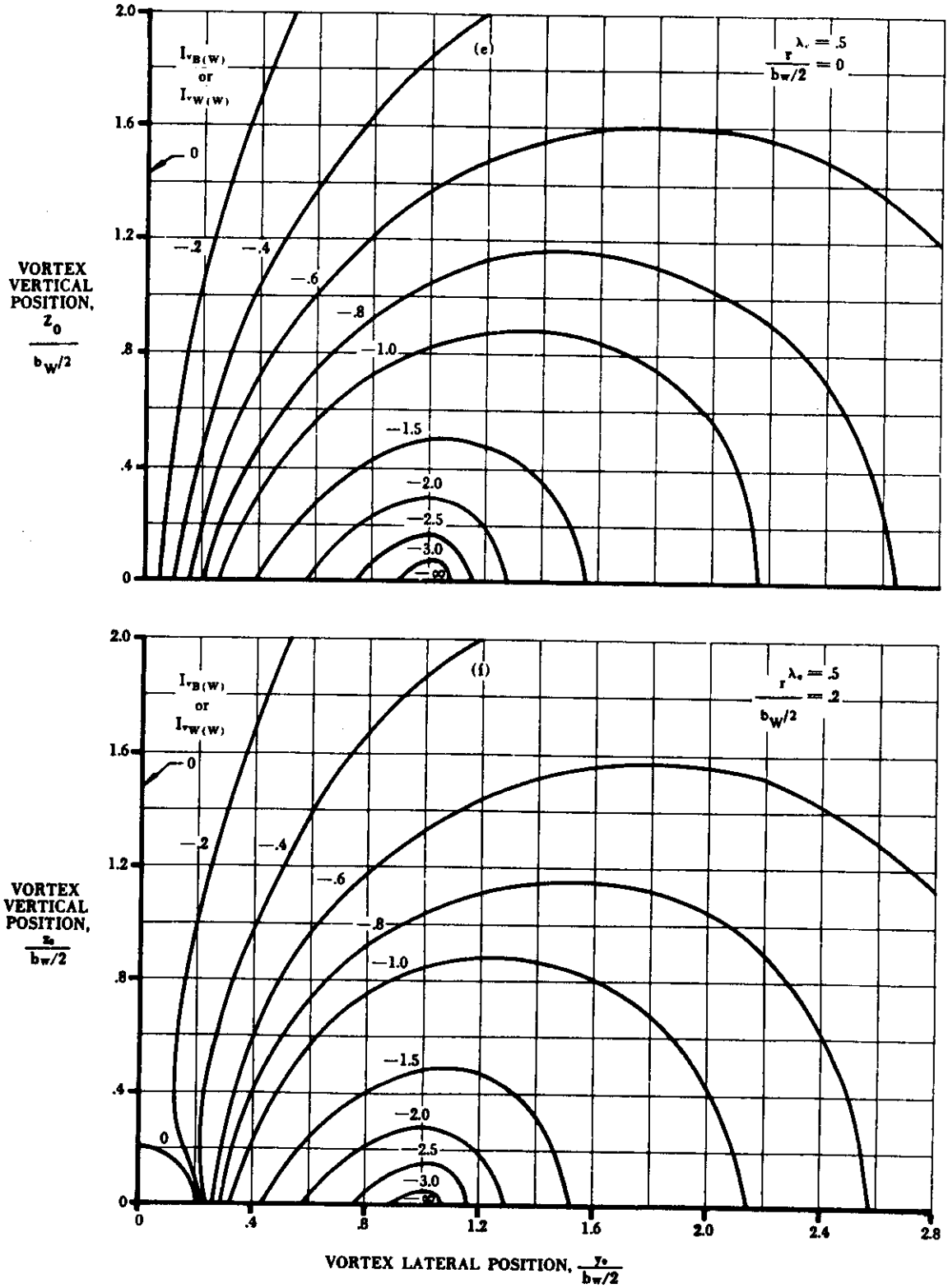

FIGURE 4.3.1.3-7 VORTEX INTERFERENCE FACTOR (CONT'D)

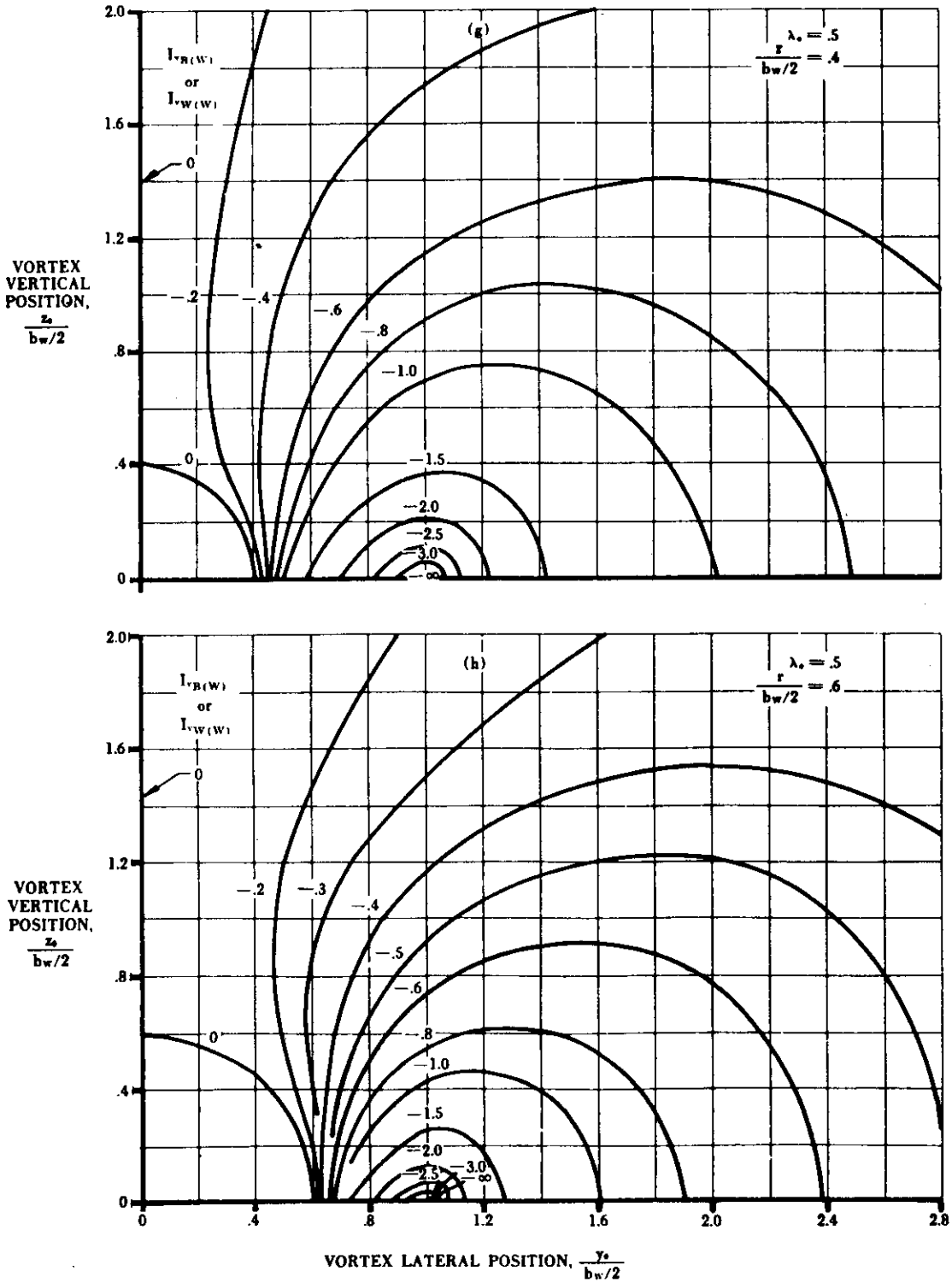

FIGURE 4.3.1.3-7 VORTEX INTERFERENCE FACTOR (CONT'D)

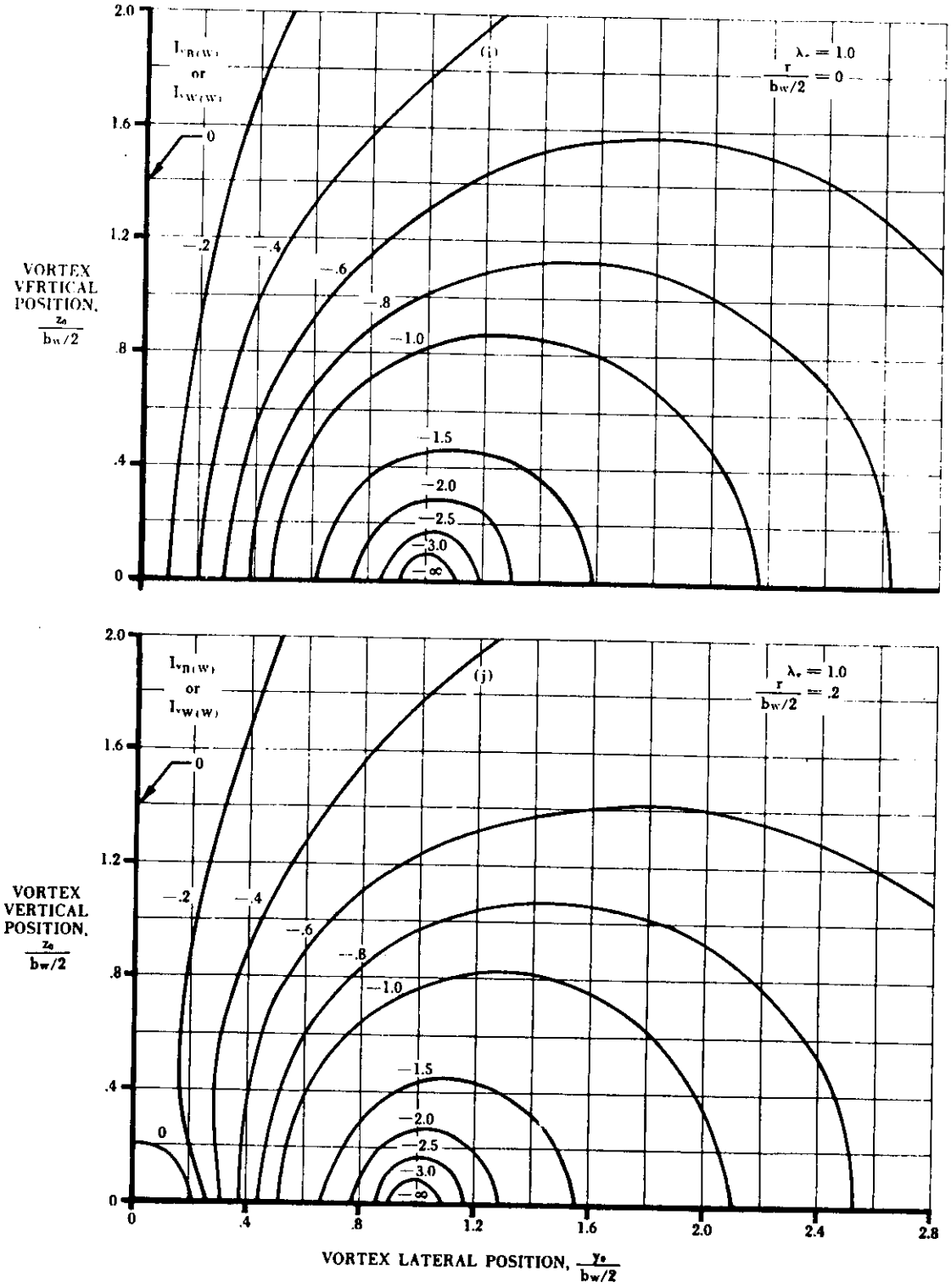

FIGURE 4.3.1.3-7 VORTEX INTERFERENCE FACTOR (CONT'D)

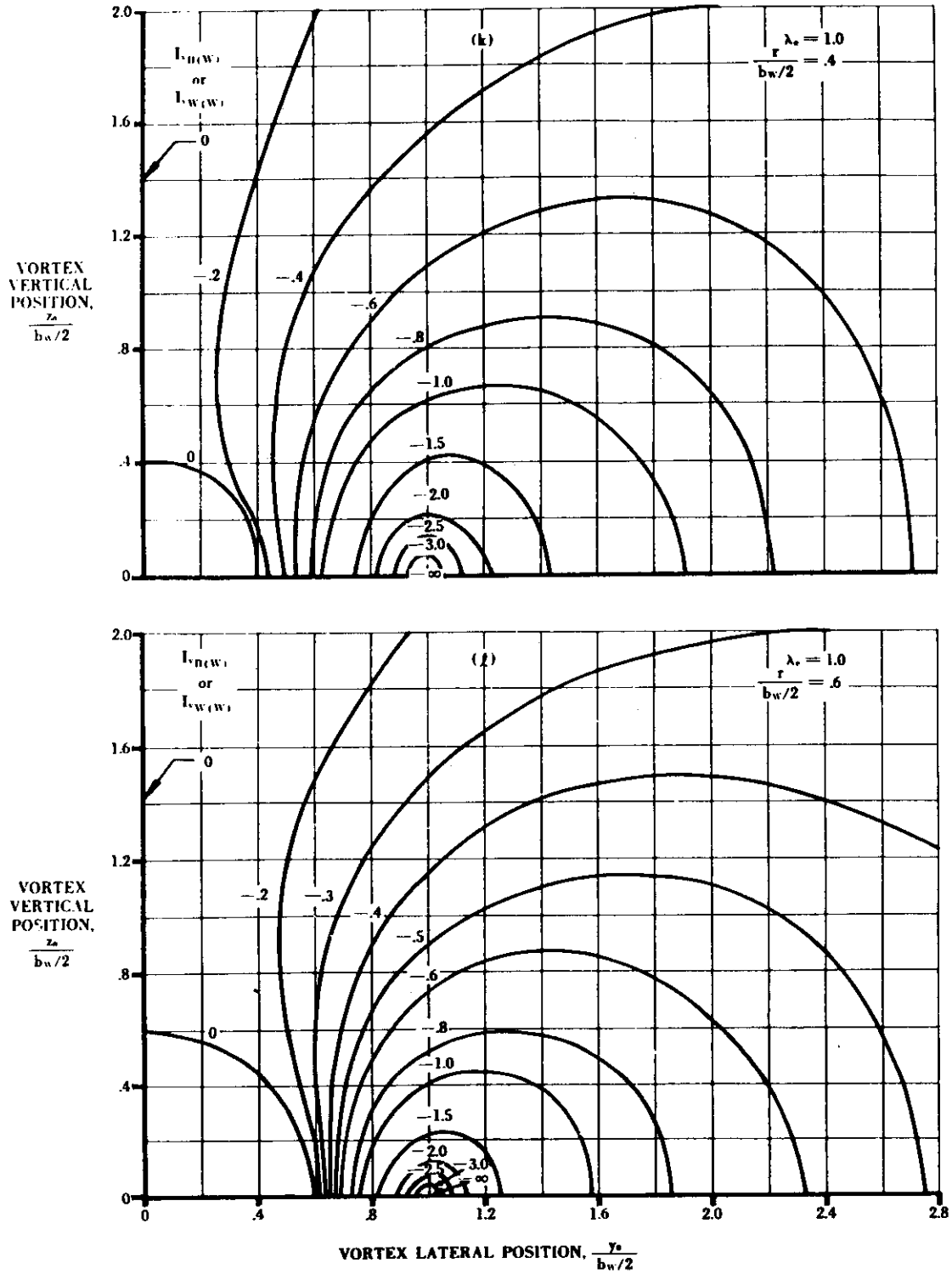

FIGURE 4.3.1.3-7 VORTEX INTERFERENCE FACTOR (CONT'D)

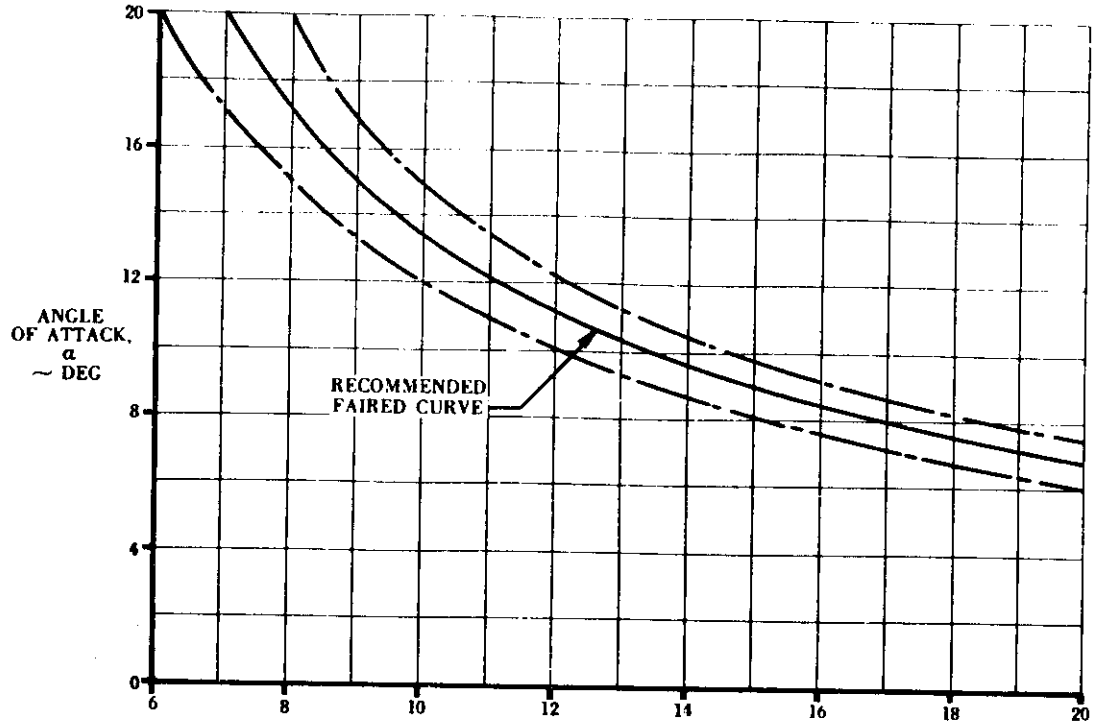

FIGURE 4.3.1.3-13a LONGITUDINAL POSITION OF VORTEX SEPARATION

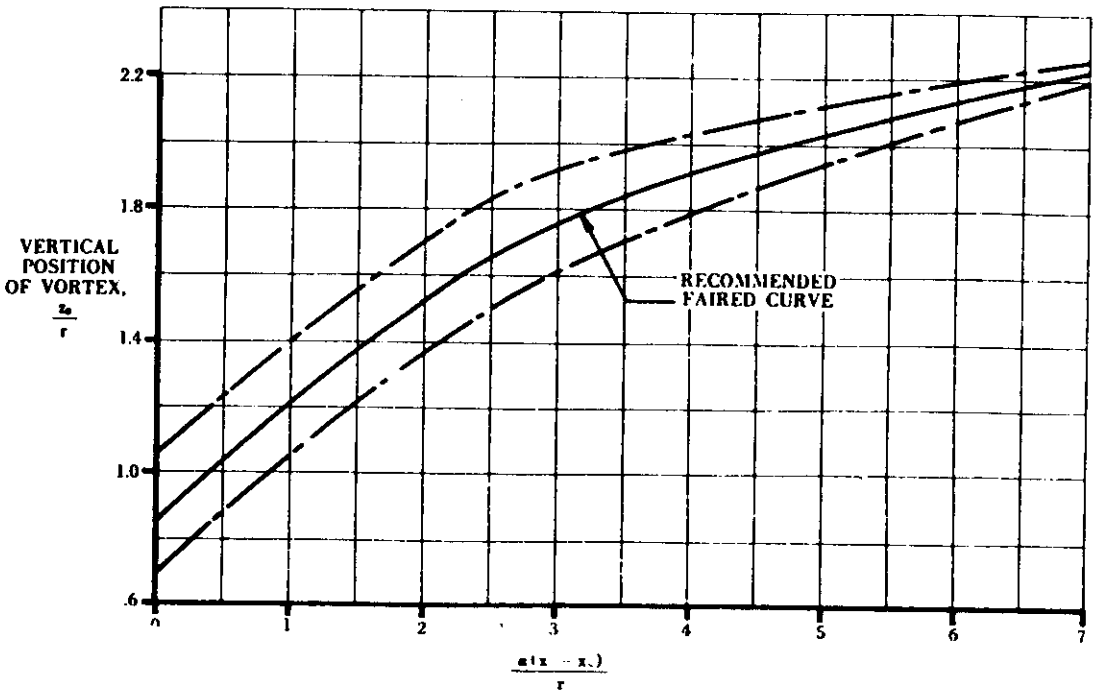

FIGURE 4.3.1.3-13b VERTICAL POSITION OF VORTEX

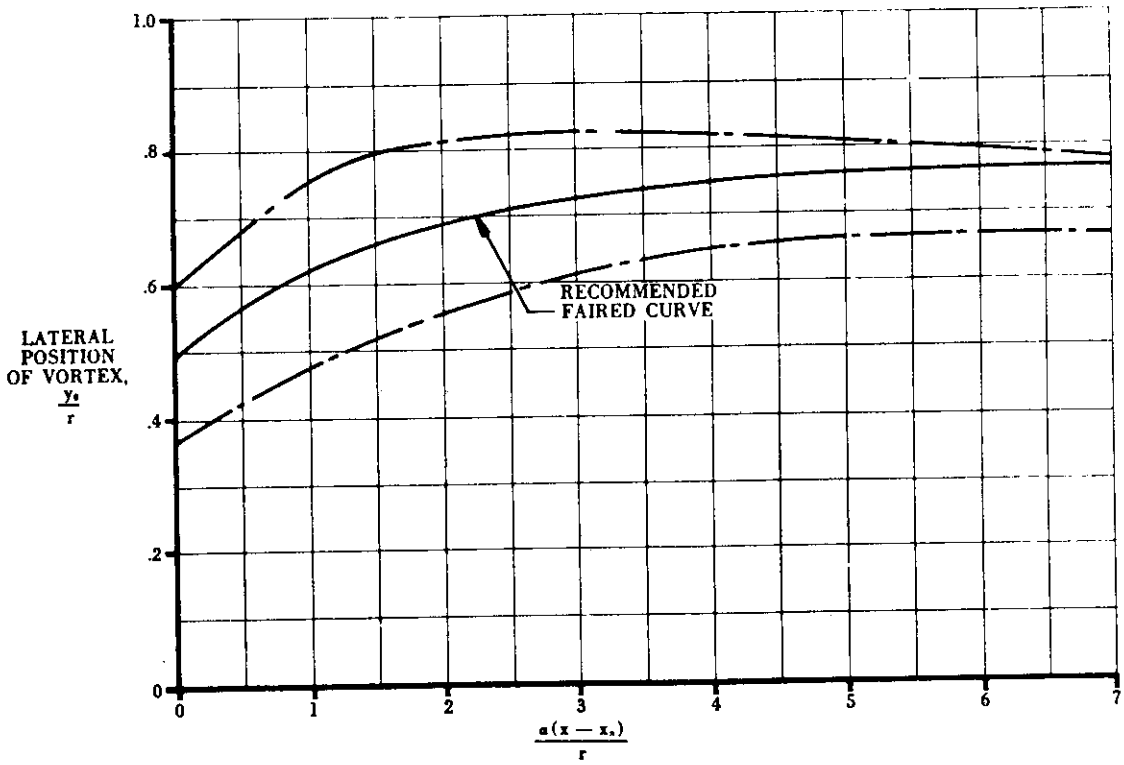

FIGURE 4.3.1.3-14 LATERAL POSITION OF VORTEX

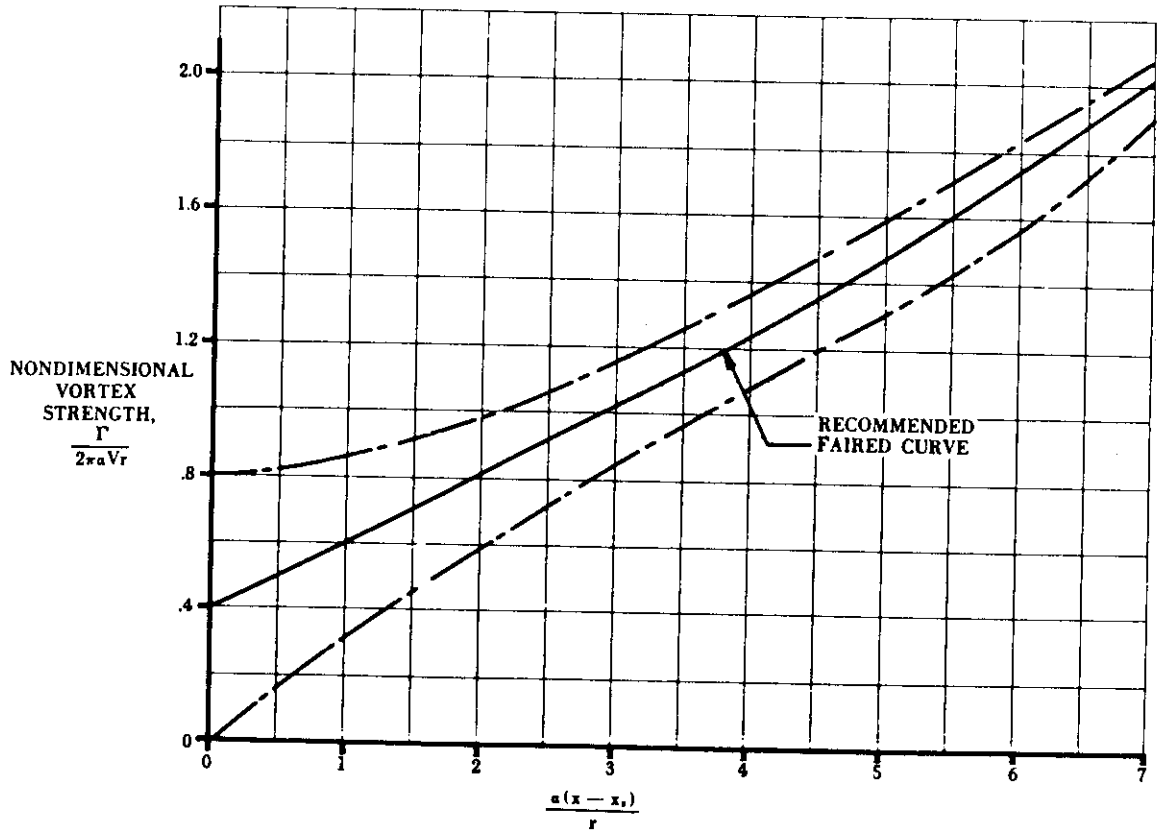

FIGURE 4.3.1.3-15 VORTEX STRENGTH

4.3.1.4 WING-BODY MAXIMUM LIFT

A. SUBSONIC

The addition of a body of revolution to a wing at high angles of attack increases the wing-induced angle of attack at all spanwise stations. The increase is greatest at the root and falls off in an exponential manner with increasing distance from the body.

This effective increase in angle of attack tends to make the wing in the presence of the body stall at a lower geometric angle of attack than that corresponding to the wing alone. However, this tendency to stall at a lower angle of attack may be modified or counteracted by changes in the wing stalling pattern. These changes are the result of the nonlinear spanwise variation of body-induced flow and also of the partial blanketing of the wing by the body. The relative magnitudes of these latter two effects are largely dependent on specific wing planform shape. This means that wing planform shape is a primary parameter in considering wing-body maximum lift.

Varying the wing height on the body, the body cross-section shape, or the body local area distribution (area rule) changes the body-induced effects on the wing and hence the maximum lift of the combination. Experimental data on variations of this type show small but generally consistent differences (see References 1, 2, 3, and 4).

The first method presented below is essentially that of Section 4.1.3.4, in that it requires the user to employ the most accurate wing-body spanwise-loading computer program available. In case no such program is available to the user, an alternate empirical method is presented as Method 2.

DATCOM METHODS

Method 1

This method requires that the user have at his disposal an accurate wing-body spanwise-loading computer program, e.g., a lifting-surface-theory computer program. Specific instructions for application of the program to obtain the wing-body maximum lift are identical to Steps 1 through 4 of Paragraph A in Section 4.1.3.4, which pertain to the wing-alone case.

No substantiation of this method is presented because of the variety of spanwise-loading programs that are available to different Datcom users.

Method 2

This method is based on empirical correlations and the wing-alone method of Section 4.1.3.4, and should be restricted to Mach numbers equal to or less than 0.60. The wing-body maximum lift coefficient and angle of attack at maximum lift are obtained using

$$\left(C_{L_{max}}\right)_{WB} = \frac{\left(C_{L_{max}}\right)_{WB}}{\left(C_{L_{max}}\right)_{W}} \left(C_{L_{max}}\right)_{W} \qquad 4.3.1.4\text{-a}$$

$$(\alpha_{C_{L_{max}}})_{WB} = \frac{(\alpha_{C_{L_{max}}})_{WB}}{(\alpha_{C_{L_{max}}})_{W}} (\alpha_{C_{L_{max}}})_{W} \qquad 4.3.1.4\text{-b}$$

where

$\frac{(C_{L_{max}})_{WB}}{(C_{L_{max}})_{W}}$ is the ratio of the wing-body maximum lift to wing maximum lift, obtained from Figure 4.3.1.4-12b as a function of wing-body geometry.

$(C_{L_{max}})_{W}$ is the wing maximum lift obtained from the appropriate method of Paragraph A in Section 4.1.3.4. The wing-alone value is based on the total wing, including that part covered by the body.

$\frac{(\alpha_{C_{L_{max}}})_{WB}}{(\alpha_{C_{L_{max}}})_{W}}$ is the ratio of the wing-body angle of attack at maximum lift to the wing angle of attack at maximum lift. This value is obtained from Figure 4.3.1.4-12c as a function of wing-body geometry.

$(\alpha_{C_{L_{max}}})_{W}$ is the wing-alone angle of attack at maximum lift obtained from the appropriate method of Paragraph A in Section 4.1.3.4. The wing-alone value is based on the total wing, including that part covered by the body.

A comparison of test data from References 5 through 17 with results calculated by this method is presented in Table 4.3.1.4-A.

Sample Problem

Given: Configuration 4 of Reference 14.

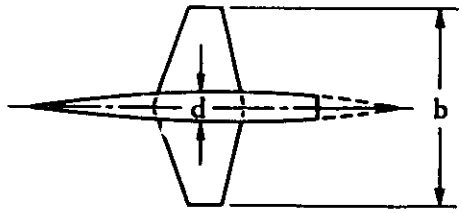

$A = 3.0$ $\Lambda_{LE} = 19.1^{o}$ $\lambda = 0.4$

Airfoil: 3-percent biconvex (free-stream direction)

$\frac{d}{b} = 0.145$ $M = 0.25$ $R_{\ell} = 8.8 \times 10^{6}$

$(C_{L_{max}})_{W} = 0.77$

$(\alpha_{C_{L_{max}}})_{W} = 15.9^{o}$

} Obtained using Section 4.1.3.4

Compute:

$C_2 = 1.10$ (Figure 4.3.1.4-12a)

$$(C_2 + 1) A \tan \Lambda_{LE} = (1.10 + 1)(3)(0.3463) = 2.18$$

$$\frac{\left(C_{L_{max}}\right)_{WB}}{\left(C_{L_{max}}\right)_{W}} = 0.98 \qquad \text{(Figure 4.3.1.4-12b)}$$

$$\frac{(\alpha_{C_{L_{max}}})_{WB}}{(\alpha_{C_{L_{max}}})_{W}} = 0.99 \qquad \text{(Figure 4.3.1.4-12c)}$$

Solution:

$$\left(C_{L_{max}}\right)_{WB} = \frac{\left(C_{L_{max}}\right)_{WB}}{\left(C_{L_{max}}\right)_{W}} \left(C_{L_{max}}\right)_{W} \qquad \text{(Equation 4.3.1.4-a)}$$

$$= (0.98)(0.77)$$

$$= 0.75$$

$$(\alpha_{C_{L_{max}}})_{WB} = \frac{(\alpha_{C_{L_{max}}})_{WB}}{(\alpha_{C_{L_{max}}})_{W}} (\alpha_{C_{L_{max}}})_{W} \qquad \text{(Equation 4.3.1.4-b)}$$

$$= (0.99)(15.9)$$

$$= 15.7^{o}$$

These compare with test-data values from Reference 14 of $\left(C_{L_{max}}\right)_{WB} = 0.71$ and $\left(\alpha_{C_{L_{max}}}\right)_{WB} = 14.3^{o}$

B. TRANSONIC

No method is presented in this speed regime. The lack of sufficient experimental data prevents the presentation of any empirical method. However, the trend of the limited data available (Reference 5) indicates that the wing-body maximum lift converges to the wing-alone value as the Mach number is increased above M = 0.6.

C. SUPERSONIC

Two separate methods are presented in this section for estimating the wing-body maximum lift at supersonic speeds. The first method is somewhat easier to apply than the second method. Both methods yield approximately the same degree of accuracy, based on the limited available test data (References 18, 19, and 20). Attempts to substantiate these methods completely have been impaired by lack of test data in the stall regime.

The first method is based on the application of the wing-body interference coefficients of Section 4.3.1.2 to the exposed-wing-alone maximum lift of Section 4.1.3.4. This approach is justified, since at supersonic and hypersonic speeds the wing lift is limited by geometric considerations rather than by flow separation on the wing. That is, maximum lift is reached when the component of the normal force in the lift direction ceases to increase with angle of attack. Therefore, the body-induced effects are felt mainly through their influence on the lift-curve slope, rather than on wing separation. This implies that the supersonic maximum lift of the wing-body combination may be obtained by applying wing-body interference coefficients to the wing-alone maximum lift value.

The second method uses the method of Section 4.3.1.3 to calculate the complete normal-force curve, from which the lift curve can easily be calculated.

Both methods assume that the angle of attack at wing-body maximum lift is the same as the angle of attack for wing maximum lift.

DATCOM METHODS

Method 1

This method applies the wing-body interference factors from Paragraph C of Section 4.3.1.2 to the wing-alone maximum lift coefficient. The limitations of the sections used in this method will also apply to this method. The wing-body maximum lift, based on S_W, is found by

$$\left(C_{L_{max}}\right)_{WB} = \left(C_{L_{max}}\right)_e \left[K_N + K_{W(B)} + K_{B(W)}\right] \frac{S_e}{S_W} \qquad 4.3.1.4\text{-a}$$

where

$\left(C_{L_{max}}\right)_e$ is the exposed-wing-alone maximum lift coefficient determined by Paragraph C of Section 4.1.3.4. (For the definition of exposed wing, see Section 4.3.1.2)

K_N, $K_{W(B)}$, and $K_{B(W)}$ are the wing-body interference factors from Method 1 of Paragraph C of Section 4.3.1.2.

$\frac{S_e}{S_W}$ is the ratio of the exposed wing area to the total wing area.

No substantiation of this method is presented; however, application of the method is illustrated in Sample Problem 1.

Method 2

Application of this method is restricted to straight-tapered planforms. The wing-body maximum lift is determined by using Equation 4.3.1.3-a to obtain the normal force C_N as a function of angle of attack. Then the lift curve is constructed by using the approximation $C_L \cong C_N \cos\alpha$, from which the $C_{L_{max}}$ value is obtained. The determination of the nose contribution term $(C_N)_N$ of Equation 4.3.1-3-a may present somewhat of a problem, since the supersonic design curves (Section 4.2.1.2) are inadequate at the higher angles of attack. Consequently, it is suggested that Method 2 of Paragraph D of Section 4.2.1.2 be used for determining $(C_N)_N$ in the high angle-of-attack regime.

No substantiation of this method is presented; however, application of the method is illustrated in Sample Problem 2.

Sample Problems

1. Method 1

Given: The wing-body configuration of Reference 19.

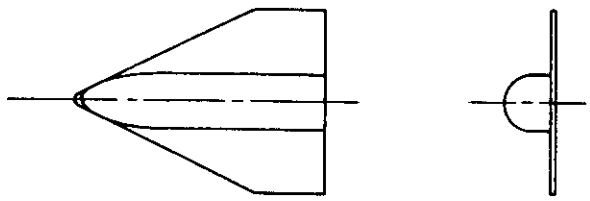

Total Wing:

$A = 1.15$ $\lambda = 0.3$ $b = 8.26$ in. $c_r = 11.0$ in.

$c_t = 3.30$ in. $\Lambda_{LE} = 63^o$ $S_W = 0.409$ sq ft Airfoil: flat plate

Exposed Wing:

$A_e = 0.97$ $\lambda_e = 0.354$ $b_e = 6.13$ in. $c_{r_e} = 9.31$ in.

$S_e = 0.268$ sq ft

Additional Characteristics:

$\ell_B = 10.65$ in. $d = 2.13$ in. LER = 0.125 in. $M = 1.97; \beta = 1.70$

Compute:

$\left(C_{L_{max}}\right)_e$

$A_e \tan \Lambda_{LE} = (0.97)(1.963) = 1.904$

$$\frac{\beta}{\tan \Lambda_{LE}} = \frac{1.70}{1.963} = 0.866$$

$\tan \Lambda_{LE} \left(C_{N_\alpha}\right)_{theory} = 3.175$ (Figure 4.1.3.2-56 interpolated)

$$\left(C_{N_\alpha}\right)_{theory} = \frac{3.175}{1.963} = 1.617 \text{ per rad}$$

$$\frac{C_{N_\alpha}}{\left(C_{N_\alpha}\right)_{theory}} = 1.0 \text{ for a flat plate} \qquad \text{(Figure 4.1.3.2-60)}$$

$$C_{N_\alpha} = 1.617 \text{ per rad}$$

$$\frac{\beta C_{N_\alpha}}{4} = \frac{(1.70)(1.617)}{4} = 0.687$$

$$\frac{1}{M} = \frac{1}{1.97} = 0.5076$$

$$\left(C_{L_{max}}\right)_e = 0.985 \qquad \text{(Figure 4.1.3.4-27a)}$$

K_N = 0, since nose does not extend ahead of wing apex

$K_{W(B)}$

$$\frac{d}{b} = \frac{2.13}{8.26} = 0.258$$

$K_{W(B)}$ = 1.22 (Figure 4.3.1.2-10)

$K_{B(W)}$

$$\frac{\beta d}{c_{r_e}} = \frac{(1.70)(2.13)}{9.31} = 0.389$$

$$\beta \cot \Lambda_{LE} = (1.70)(0.5095) = 0.866$$

$$K_{B(W)}\left[\beta\left(C_{L_\alpha}\right)_e\left(\lambda_e + 1\right)\left(\frac{b}{d} - 1\right)\right] = 2.5 \qquad \text{(Figure 4.3.1.2-11b)}$$

$$K_{B(W)} = \frac{2.5}{(1.70)(1.617)(1.354)\left(\frac{8.26}{2.13} - 1\right)} = \frac{2.5}{10.71} = 0.233$$

Solution:

$$\left(C_{L_{max}}\right)_{WB} = \left(C_{L_{max}}\right)_e\left[K_N + K_{W(B)} + K_{B(W)}\right]\frac{S_e}{S_W} \qquad \text{(Equation 4.3.1.4-a)}$$

$$= (0.985)(0 + 1.22 + 0.233)\left(\frac{0.268}{0.409}\right) = 0.937$$

$\alpha_{C_{L_{max}}} = 44.2^{o}$ (Figure 4.1.3.4-27b)

This compares with a test value of $C_{L_{max}} = 0.94$ and $\alpha_{C_{L_{max}}} = 42^{o}$

2. Method 2

Given: Same configuration as Sample Problem 1.

$A = 1.15$ $\lambda = 0.3$ $\Lambda_{LE} = 63^{o}$ $S_W = 0.409$ sq ft

$S_e = 0.268$ sq ft Airfoil: flat plate

$K_{W(B)} = 1.22$

$K_{B(W)} = 0.233$ } (Sample Problem 1, above)

$\left(C_{N_\alpha}\right)_e = 1.617$ per rad

$M = 1.97$; $\beta = 1.70$

Compute:

$\left(C_N\right)_N = 0$, since nose does not extend ahead of wing apex

$\left(C_N\right)_e$

$$\frac{\beta}{\tan \Lambda_{LE}} = \frac{1.70}{1.963} < 1$$ (subsonic leading edge)

Step 1. $\left(C_{N_\alpha}\right)_e = 1.617$

Step 2. Empirical Parameter E (see Paragraph C of Section 4.1.3.3)

$$\frac{\tan \Lambda_{LE}}{1.92} = \frac{1.963}{1.92} > 1$$, therefore use equation:

$$E = \left(C_{N_\alpha}\right)_e \left[\frac{\tan \Lambda_{LE}}{1.92} + C\left(\frac{\tan \Lambda_{LE}}{1.92} - 1\right)\right]$$

$$\delta_\perp = \tan^{-1} \frac{\Delta y_\perp}{5.85} = 0 \text{ for flat plate} \qquad \text{(see sketch on Figure 2.2.1-8)}$$

$$C = 0 \qquad \text{(Figure 4.1.3.3-59a)}$$

$$E = (1.617)\left[\frac{1.963}{1.92} + (0)\left(\frac{1.963}{1.92} - 1\right)\right]$$

$$= 1.653 \text{ per rad}$$

Step 3.

$$E\,\frac{\beta}{\tan \Lambda_{LE}} = 1.653\,\frac{1.70}{1.963} = 1.432$$

$$\frac{C_{N_\alpha}}{\left(C_{N_\alpha}\right)_{theory}} = 1.0 \text{ for a flat plate} \qquad \text{(Figure 4.1.3.2-60)}$$

$$\frac{\left(C_{N_\alpha}\right)_{theory}}{C_{N_\alpha}}\,\beta \tan \alpha = \beta \tan \alpha; \quad \frac{C_{N_\alpha}}{\left(C_{N_\alpha}\right)_{theory}}\,\frac{1}{\beta \tan \alpha} = \frac{1}{\beta \tan \alpha}$$

Step 4.

$$\left(C_N\right)_e = C_{N_\alpha}\,\frac{\sin 2\alpha}{2} + C_{N_{\alpha\alpha}} \sin \alpha |\sin \alpha| \qquad \text{(Equation 4.1.3.3-a)}$$

①	②	③	④	⑤	⑥	⑦	⑧	⑨	⑩
α (deg)	$\beta \tan \alpha$	$\frac{1}{\beta \tan \alpha}$	$C_{N_{\alpha\alpha}}$ (Fig. 4.1.3.3-59b)	$\sin \alpha$	$\sin^2 \alpha$ ⑤^2	$\sin 2\alpha$	$\left(C_{N_\alpha}\right)_e \frac{\sin 2\alpha}{2}$ (1.617)⑦/2	$C_{N_{\alpha\alpha}} \sin^2 \alpha$ ④⑥	$\left(C_N\right)_e$ ⑧ + ⑨
16	0.4874		1.58	0.2756	0.0760	0.5299	0.4284	0.1201	0.5485
20	0.6188		1.50	0.3420	0.1170	0.6428	0.5197	0.1755	0.6952
24	0.7568		1.42	0.4067	0.1654	0.7431	0.6008	0.2349	0.8357
28	0.9039		1.35	0.4695	0.2204	0.8290	0.6702	0.2975	0.9677
32		0.9413	1.29	0.5299	0.2808	0.8988	0.7267	0.3622	1.0889
36		0.8097	1.26	0.5878	0.3455	0.9511	0.7690	0.4353	1.2043
40		0.7010	1.25	0.6428	0.4132	0.9848	0.7962	0.5165	1.3127
44		0.6091	1.26	0.6947	0.4826	0.9994	0.8080	0.6081	1.4161
48		0.5297	1.27	0.7431	0.5522	0.9945	0.8041	0.7013	1.5054
52		0.4696	1.30	0.7880	0.6209	0.9703	0.7845	0.8072	1.5917

The contribution of body vortices (last term of Equation 4.3.1.3-a) can be neglected, since the configuration is more typical of an airplane configuration than of a missile.

Solution:

$$C_N = \left\{ \left(C_N\right)_N \frac{S_{N_{ref}}}{S_e} + \left[K_{W(B)} + K_{B(W)}\right] \left(C_N\right)_e \right\} \frac{S_e}{S_W} + I_{v_{B(W)}} \frac{\Gamma}{2\pi\alpha V r} \frac{r}{b_W/2} \frac{q}{q_\infty} \alpha \left(C_{L_\alpha}\right)_W$$

(Equation 4.3.1.3-a)

$$= \left\{ 0 + \left[1.22 + 0.233\right] \left(C_N\right)_e \right\} \left(\frac{0.268}{0.409}\right) + 0$$

$$= 0.952 \left(C_N\right)_e$$

① α (deg)	② $\left(C_N\right)_e$	③ C_N 0.952 ②	④ C_L cos α ③
16	0.5485	0.5222	0.502
20	0.6952	0.6618	0.622
24	0.8357	0.7956	0.727
28	0.9677	0.9213	0.813
32	1.0889	1.0366	0.879
36	1.2043	1.1465	0.928
40	1.3127	1.2497	0.957
44	1.4161	1.3481	0.970
48	1.5054	1.4331	0.959
52	1.5917	1.5153	0.933

These data are plotted in Sketch (a), where $C_{L_{max}} = 0.970$ and $\alpha_{C_{L_{max}}} = 44^o$. These compare with test values of $C_{L_{max}} = 0.94$ and $\alpha_{C_{L_{max}}} = 42^o$.

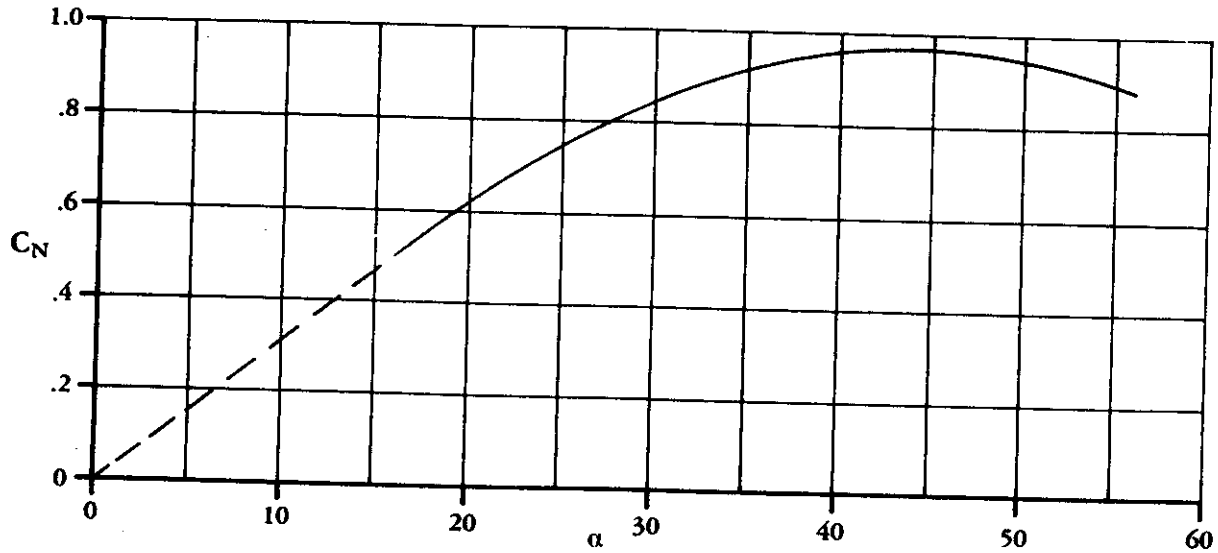

SKETCH (a)

REFERENCES

1. Letko, W., and Williams, J.: Experimental Investigation at Low Speed of Effects of Fuselage Cross Section on Static Longitudinal and Lateral Stability Characteristics of Models Having 0° and 45° Sweptback Surfaces. NACA TN 3551, 1955. (U)

2. Goodman, A., and Thomas, D.: Effects of Wing Position and Fuselage Size on the Low-Speed Static and Rolling Stability Characteristics of a Delta-Wing Model. NACA TR 1224, 1955. (U)

3. Fischetti, T.: Investigation of Mach Numbers from 0.80 to 1.43 of Pressure and Load Distributions over a Thin 45° Sweptback Highly Tapered Wing in Combination With Basic and Indented Bodies. NACA RM L57D29a, 1957. (U)

4. Sutton, F., and Lautenberger, W.: The Effect of Body Contouring on the Longitudinal Characteristics at Mach Numbers up to 0.92 of a Wing-Fuselage-Tail and Several Wing-Fuselage Combinations Having Sweptback Wings of Relatively High Aspect Ratio. NACA RM A56J08, 1957. (U)

5. Wiley, H.: Aerodynamic Characteristics Extended to High Angles of Attack at Transonic Speeds of Small-Scale 0° Sweep Wing, 45° Sweptback Wing, and 60° Delta Wing. NACA RM L52I30. (U)

6. Fischel, J., and Schneiter, L.: An Investigation at Low Speed of a 51.3° Sweptback Semispan Wing Equipped With 16.7-Percent-Chord Plain Flaps and Ailerons Having Various Spans and Three Trailing-Edge Angles. NACA RM L8H20, 1948. (U)

7. Foster, G., and Fitzpatrick, J.: Longitudinal-Stability Investigation of High-Lift and Stall-Control Devices on a 52° Sweptback Wing With and Without Fuselage and Horizontal Tail at a Reynolds Number of 6.8×10^{6}. NACA RM L8I08, 1948. (U)

8. Anderson, A.: An Investigation at Low Speed of a Large-Scale Triangular Wing of Aspect Ratio Two — III Characteristics of Wing With Body and Vertical Tail. NACA RM A9H04, 1949. (U)

9. Johnson, B., and Rollins, F.: Investigation of a Thin Wing of Aspect Ratio 4 in the Ames 12-Foot Pressure Wind Tunnel. V — Static Longitudinal Stability and Control Throughout the Subsonic Speed Range of a Semispan Model of a Supersonic Airplane. NACA RM A9I01, 1949. (U)

10. Griner, R., and Foster, G.: Low-Speed Longitudinal and Wake Air-Flow Characteristics at Reynolds Number of 6×10^{6} of a 52° Sweptback Wing Equipped With Various Spans of Leading-Edge and Trailing-Edge Flaps, a Fuselage, and a Horizontal Tail at Various Vertical Positions. NACA RM L50K29, 1951. (U)

11. Jaquet, B., and Queijo, M.: Low-Speed Static Longitudinal Stability and Control Characteristics of a 60° Triangular-Wing Model Having Half-Delta Tip Controls. NACA RM L51D20a, 1951. (U)

12. Johnson, B., and Shibata, H.: Characteristics Throughout the Subsonic Speed Range of a Plane Wing and of a Cambered and Twisted Wing, Both Having 45° of Sweepback. NACA RM A51D27, 1951. (U)

13. Hopkins, E., and Carel, H.: Experimental and Theoretical Study of the Effects of Body Size on the Aerodynamic Characteristics of an Aspect Ratio 3.0 Wing-Body Combination. NACA RM A51G24, 1951. (U)

14. Smith, D., Shibata, H., and Selan, R.: Lift, Drag, and Pitching Moment of Low-Aspect-Ratio Wings at Subsonic and Supersonic Speeds — An Investigation at Large Reynolds Numbers of the Low-Speed Characteristics of Several Wing-Body Combinations. NACA RM A51K28, 1952. (U)

15. Johnson, H.: Wind-Tunnel Investigation at Low Speed of the Effect of Varying the Ratio of Body Diameter to Wing Span From 0.1 to 0.8 on the Aerodynamic Characteristics in Pitch of a 45° Sweptback-Wing-Body Combination. NACA RM L53J09a, 1953. (U)

16. Wolhart, W., and Thomas, D., Jr.: Static Longitudinal and Lateral Stability Characteristics at Low Speed of Unswept-Midwing Models Having Wings With an Aspect Ratio of 2, 4, or 6. NACA TN 3649, 1956. (U)

17. Thomas, D., Jr., and Wolhart, W.: Static Longitudinal and Lateral Stability Characteristics at Low Speed of 45° Sweptback-Midwing Models Having Wings With an Aspect Ratio of 2, 4, or 6. NACA TN 4077, 1957. (U)

18. Foster, G. V.: Exploratory Investigation at Mach Number of 2.01 of the Longitudinal Stability and Control Characteristics of a Winged Reentry Configuration. NASA TM X-178, 1959. (U)

19. Foster, G. V.: Longitudinal Aerodynamic Characteristics at a Mach Number of 1.97 of a Series of Related Winged Reentry Configurations for Angles of Attack from 0° to 90°. NASA TM X-461, 1961. (U)

20. Stone, D. R.: Aerodynamic Characteristics of a Fixed-Wing Manned Space Shuttle Concept at a Mach Number of 6.0 NASA TM X-2049, 1970. (U)

TABLE 4.3.1.4-A
METHOD 2
SUBSONIC MAXIMUM LIFT COEFFICIENTS OF WING-BODY COMBINATIONS
DATA SUMMARY AND SUBSTANTIATION

Ref.	A	Λ_{LE} (deg)	$\frac{d}{b}$	Airfoil*	M	$\alpha_{C_{L_{max}}}$ Calc.	$\alpha_{C_{L_{max}}}$ Calc.	$C_{L_{max}}$ Test	$\alpha C_{L_{max}}$ Test	Percent Error, e	
										$C_{L_{max}}$	$\alpha_{C_{L_{max}}}$
5	2.31	60	.18	65-006	.60	1.02	27.2°	.99	28°	3.0	−2.9
6	3.43	51.3	.065	65-012 (⊥ to .5c)	.12	1.04	26.8°	1.05	27°	−1.0	−0.7
7	2.88	52	.15	64_1-112 (⊥ to .25c)	.13	1.15	26.8°	1.17	26°	−1.7	3.1
8	2.04	63	.18	Double Wedge 5%	.13	1.32	31.5°	1.32	31.5°	0	0
9	4	10	.12	Double Wedge 4.2%	.20	.71	12.8°	.715	13.2°	−0.7	−3.0
10	2.88	52	.15	64_1-112 (⊥ to.28c)	.12	1.15	26.8°	1.18	30°	−2.5	−10.7
11	2.31	60	.18	65-006.5	.17	1.08	29.9°	1.08	33.2°	0	−10.0
12	5	46	.10	64A-010 (⊥ to.25c)	.25	1.09	22.9°	.955	23°	14.1	−0.4
						.925	20.9°	.955	22°	−3.1	−5.0
13	3	23	.196	4.5% Hex.	.25	.795	15.1°	.82	14°	−3.0	7.9
			.259			.76	14.7°	.74	12.8°	2.7	14.8
			.343			.72	13.2°	.72	12.5°	0	5.6
14	3	19	.145	3% Bi-Convex	.25	.75	15.6[b]	.71	14.3°	+5.6	9.1
					.60	.75	14.9°	.70	15°	7.1	−0.7
	4	45	.127			.845	21.1°	.85	22°	−0.6	−4.1
					.25	.875	22.1°	.883	23°	−0.9	−3.9
	3	53.1				1.00	25°	1.04	26°	−3.8	−3.8
15	3	45	.10	65A-006	.29	.93	24.8°	.94	22°	−1.1	12.7
			.20			.91	20°	.98	18.2°	−7.1	9.9
			.30			.95	16.4°	.96	16.6°	−1.0	−1.2
			.40			1.03	16.3°	1.00	16.0°	3.0	1.9
			.60			1.25	19.5°	1.24	18.3°	0.8	6.6
			.80			–	32°	2.24	31°	–	3.2
16	2	7.2	.23	65A-008	.13	.73	24°	.75	19°	−2.7	26.3
	4	3.6	.15			.75	14.4°	.76	16°	1.3	−10.0
	6	2.4	.135			.75	12.3°	.78	12°	−3.8	2.5
17	2	48	.23	65A-008	.13	.93	22.2°	.96	22.3°	−3.1	−0.4
	4	47	.15			.89	20.5°	.96	20°	−7.3	2.5
	6	46	.135			.89	18°	.96	20.4°	−7.3	−11.8

*Airfoil defined parallel to free stream unless stated otherwise.

Average Error in $C_{L_{max}} = \frac{\Sigma \mid e \mid}{n} = 3.2\%$

Average Error in $\alpha_{C_{L_{max}}} = \frac{\Sigma \mid e \mid}{n} = 6.0\%$

SUBSONIC SPEEDS

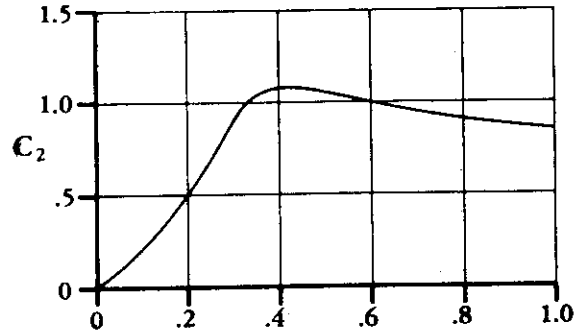

FIGURE 4.3.1.4-12a TAPER-RATIO CORRECTION FACTOR

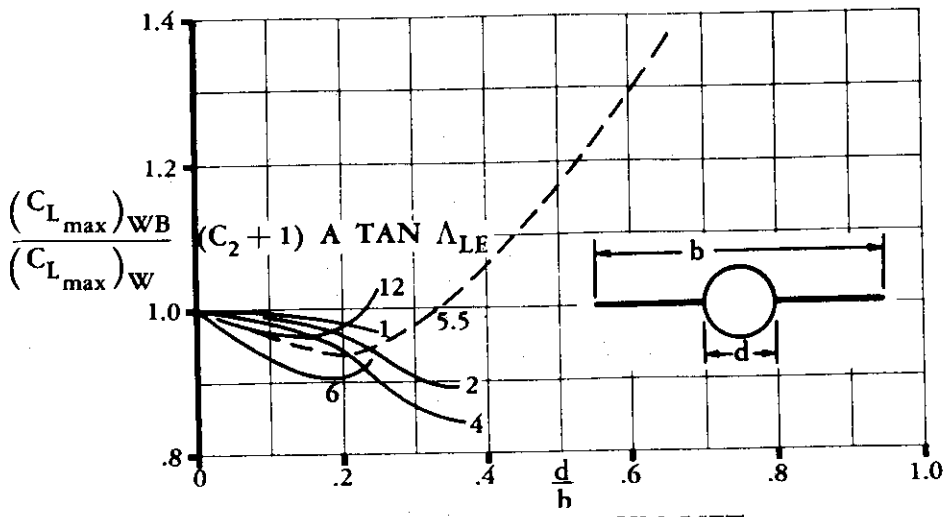

FIGURE 4.3.1.4-12b WING-BODY MAXIMUM LIFT

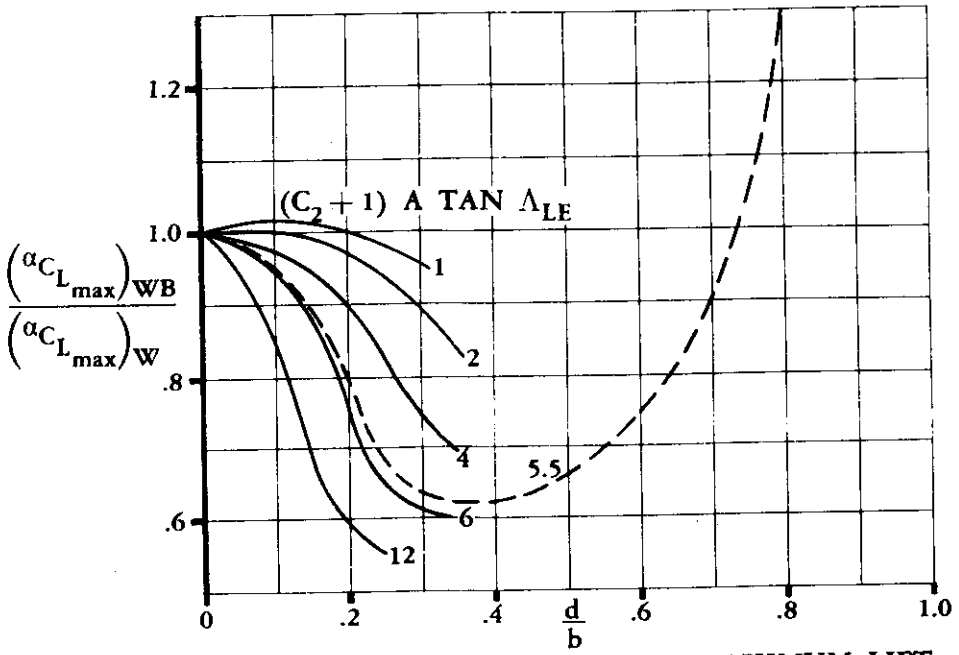

FIGURE 4.3.1.4-12c ANGLE OF ATTACK FOR MAXIMUM LIFT

4.3.2.1 WING-BODY ZERO-LIFT PITCHING MOMENT

Methods are presented for determining the wing-body zero-lift pitching-moment coefficient in the subsonic, transonic, and supersonic speed regimes. It is advisable to use experimental data whenever possible in each speed regime.

A. SUBSONIC

Two methods are presented for estimating the subsonic wing-body zero-lift pitching-moment coefficient for straight-tapered wings. Method 1 (Reference 1) was derived using the momentum considerations of H. Multhopp (Reference 2). Method 2 (Reference 3) has been empirically derived from fighter-type test data. Method 1 is considered to be more accurate than Method 2 because it includes the effects of fuselage width and fuselage camber distribution. Neither method is limited to bodies of revolution; however, only Method 1 accounts explicitly for noncircular bodies. If it becomes necessary to analyze a noncircular body in combination with a wing, the results of Method 2 should be used with caution.

DATCOM METHODS

Method 1

The wing-body zero-lift pitching-moment coefficient for straight-tapered wings* may be approximated by

$$\left(C_{m_0}\right)_{WB} = \left[\left(C_{m_0}\right)_W + \left(C_{m_0}\right)_B\right] \frac{\left(C_{m_0}\right)_M}{\left(C_{m_0}\right)_{M=0}} \qquad 4.3.2.1\text{-a}$$

where

$\left(C_{m_0}\right)_W$ is the wing zero-lift pitching-moment coefficient uncorrected for Mach-number effects, obtained from Section 4.1.4.1.

$\frac{\left(C_{m_0}\right)_M}{\left(C_{m_0}\right)_{M=0}}$ is the Mach-number correction factor obtained from Figure 4.1.4.1-6 as a function of Mach number. This chart gives the ratio of wing-body zero-lift pitching-moment coefficient in compressible flow to that in incompressible flow, based on test data.

$\left(C_{m_0}\right)_B$ is the body zero-lift pitching-moment coefficient, uncorrected for Mach-number effects. This parameter is approximated by using

$$\left(C_{m_0}\right)_B = \frac{(k_2 - k_1)}{36.5\, S_W \bar{c}} \sum_{x=0}^{x=\ell_B} w_f^{\,2}\, [(\alpha_0)_W + (i_{CL})_B]\, \Delta x \qquad 4.3.2.1\text{-b}$$

*Method 1 should apply to non-straight-tapered planforms. However, the lack of a method for predicting the wing zero-lift pitching-moment contribution has prevented any substantiation of this method for non-straight-tapered planforms.

where

$(k_2 - k_1)$ is the apparent mass factor developed by Munk, obtained from Figure 4.2.1.1-20a as a function of the body fineness ratio

S_W is the wing reference area

$\bar{c}$ is the wing mean aerodynamic chord

w_f is the average width of a body increment (see Sketch (a))

$(\alpha_0)_W$ is the wing zero-lift angle relative to the fuselage reference plane, obtained from test data or estimated by using the wing zero-lift angle-of-attack method of Section 4.1.3.1 (the effects of wing incidence must be considered when using the method of this section).

$(i_{CL})_B$ is the incidence angle of the fuselage camber line relative to the fuselage reference plane at the increment center. The sign convention of $(i_{CL})_B$ is identical to that of horizontal-tail incidence, and is negative for both nose droop and upsweep as shown in Sketch (a). The fuselage camber line is defined by the vertical location of the fuselage-maximum-width line or the body mean line where the maximum-width line is not clearly defined (see Sketch (b)).

Δx is the length of the body increment (see Sketch (a)). Fuselage increment length should be chosen so that neither the change in average width nor the change in camber line incidence is too large between successive increments. The increments need not be of equal length.

ℓ_B is the body length.

Equation 4.3.2.1-b may be evaluated by dividing the fuselage into increments (see Sketch (a)), computing the value of each increment, and adding them up.

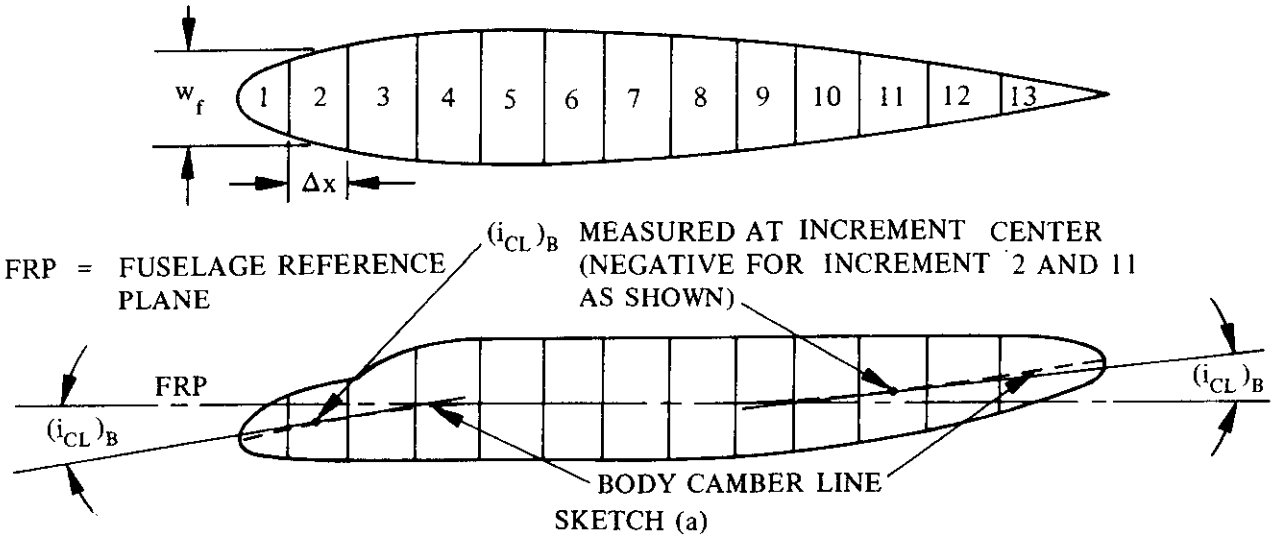

SKETCH (a)

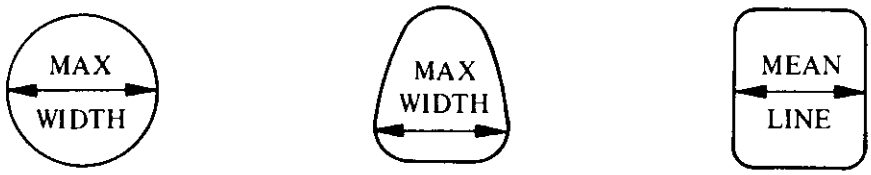

SEVERAL FUSELAGE CROSS-SECTIONS
SHOWING CAMBER LINE VERTICAL LOCATION

SKETCH (b)

A comparison of test data with results calculated by this method is presented in Table 4.3.2.1-A. It should be noted that the test data are for configurations having cambered airfoils. For most configurations with symmetrical wings with no twist, the predicted values are zero or very small.

Method 2

This method was developed in Reference 3 for fighter-type aircraft by using the linear regression analysis of mathematical statistics. In general, a regression analysis involves the study of a group of variables to determine their effect on a given parameter. Because of the empirical nature of this method (values for the regression coefficients), exact solutions are available only at the following Mach numbers: 0.4, 0.6, 0.7, 0.8, 0.9, 0.95, 1.0, 1.1, 1.2, 1.3, 1.4, 1.5, 2.0, and 2.5. At other Mach numbers interpolation is necessary.

It is advisable to restrict the applicability of this method to the range of geometric parameters of the test data used in the formulation of the regression coefficients. The test data used in the formulation of the regression coefficients have geometric parameters within the following limits:

aspect ratio, A	1.6 to 6.0
taper ratio, λ	0 to 1
twist, θ	0 to -9.4^{o}
leading-edge radius, LER/$\bar{c}$	0 to 0.015
thickness, t/$\bar{c}$	0.025 to 0.10
NACA camber, $(y_c)_{max}/\bar{c}$	0 to 0.0263
conical-camber design lift coefficient, C_{L_d}	0 to 0.45
forebody fineness ratio, ℓ_N/d	2.2 to 8.4
afterbody fineness ratio, ℓ_A/d	0.3 to 5.6
leading-edge sweep, Λ_{LE}	0 to 70^{o}
Reynolds number, R_ℓ	0.8×10^6 to 8×10^6

This method is not limited to bodies of revolution; however, no attempt is made to account for the effects of noncircular bodies. If it becomes necessary to analyze a noncircular body in combination with a wing, it is suggested that an equivalent body of revolution be used, i.e., a body of revolution with the same cross-sectional area.

The wing-body zero-lift pitching-moment coefficient, based on the product of the wing area and mean aerodynamic chord $S_W \bar{c}_W$, is given at a specific Mach number by

$$\left(C_{m_0}\right)_{WB} = C_0 + C_1\left(\frac{1}{A}\right) + C_2\, A + C_3 \tan \Lambda_{LE} + C_4\left(\frac{t}{\bar{c}}\right) + C_5\left(\frac{\ell_N}{d}\right) + C_6\left(\frac{\ell_A}{d}\right) + C_7\, \lambda$$

$$+ C_8\, \lambda^2 + C_9\, (T_R) + C_{10}\left(\frac{LER}{\bar{c}}\right) + C_{11}\, \theta + C_{12}\left[\frac{\left(y_c\right)_{max}}{\bar{c}}\right] + C_{13}\, C_{L_d}$$

$$+ C_{14}\, W_L + C_{15}\, V_T + C_{16}\left(\frac{h}{d}\right) + C_{17}\left(\frac{u}{b}\right) + C_{18}\, R_\ell \qquad \text{4.3.2.1-c}$$

where

$C_0, C_1, \ldots C_{18}$ are the regression coefficients as a function of Mach number, obtained from Table 4.3.2.1-B.

A is the total wing aspect ratio.

Λ_{LE} is the sweep of the leading edge.

$\frac{t}{\bar{c}}$ is the wing thickness ratio at the mean aerodynamic chord.

$\frac{\ell_N}{d}$ is the nose and forebody fineness ratio (see Sketch (b)).

$\frac{\ell_A}{d}$ is the afterbody fineness ratio taken at the afterbody wing-body juncture (see Sketch (b)).

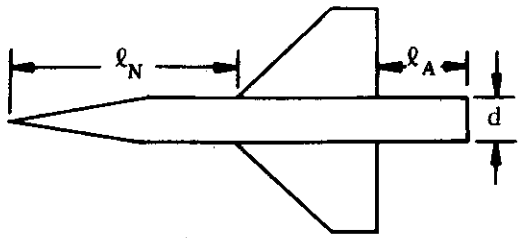

SKETCH (c)

λ is the wing taper ratio.

T_R is the transition indicator; 0 for no transition strips and 1 for transition strips or flight test.

$\frac{LER}{\bar{c}}$ is the ratio of the leading-edge radius to the mean aerodynamic chord taken at the mean aerodynamic chord.

θ is the wing twist between the root and tip sections in radians, negative for washout (see Figure 5.1.2.1-30b).

$\frac{(y_c)_{max}}{\bar{c}}$ is the NACA camber in the form of a ratio of the maximum ordinate of the mean line to the airfoil chord taken at the mean aerodynamic chord.

C_{L_d} is the conical-camber design lift coefficient for a M = 1.0 design with the designated camber ray line intersecting the wing trailing edge at 0.8 b/2. (For more details see Reference 4.) If the wing does not have a conical-camber design, the value of C_{L_d} is zero.

W_L is the wing location index, with W_L = 1.0 for a high wing, W_L = 0.5 for a midwing, and W_L = 0 for a low wing.

V_T is the vertical-tail indicator, with V_T = 1.0 for a vertical tail, and V_T = 0 for no vertical tail.

$\frac{h}{d}$ is the ratio of the maximum canopy height measured from the body center line to the body height at the point of maximum canopy height.

$\frac{d}{b}$ is the ratio of the maximum body width to wing span.

R_ℓ is the Reynolds number based on the mean aerodynamic chord. For Reynolds numbers in excess of 8×10^6, the value of 8×10^6 should be used.

Sample Problems

1. Method 1

Given: The wing-body configuration of Reference 5 (Sketch (d))

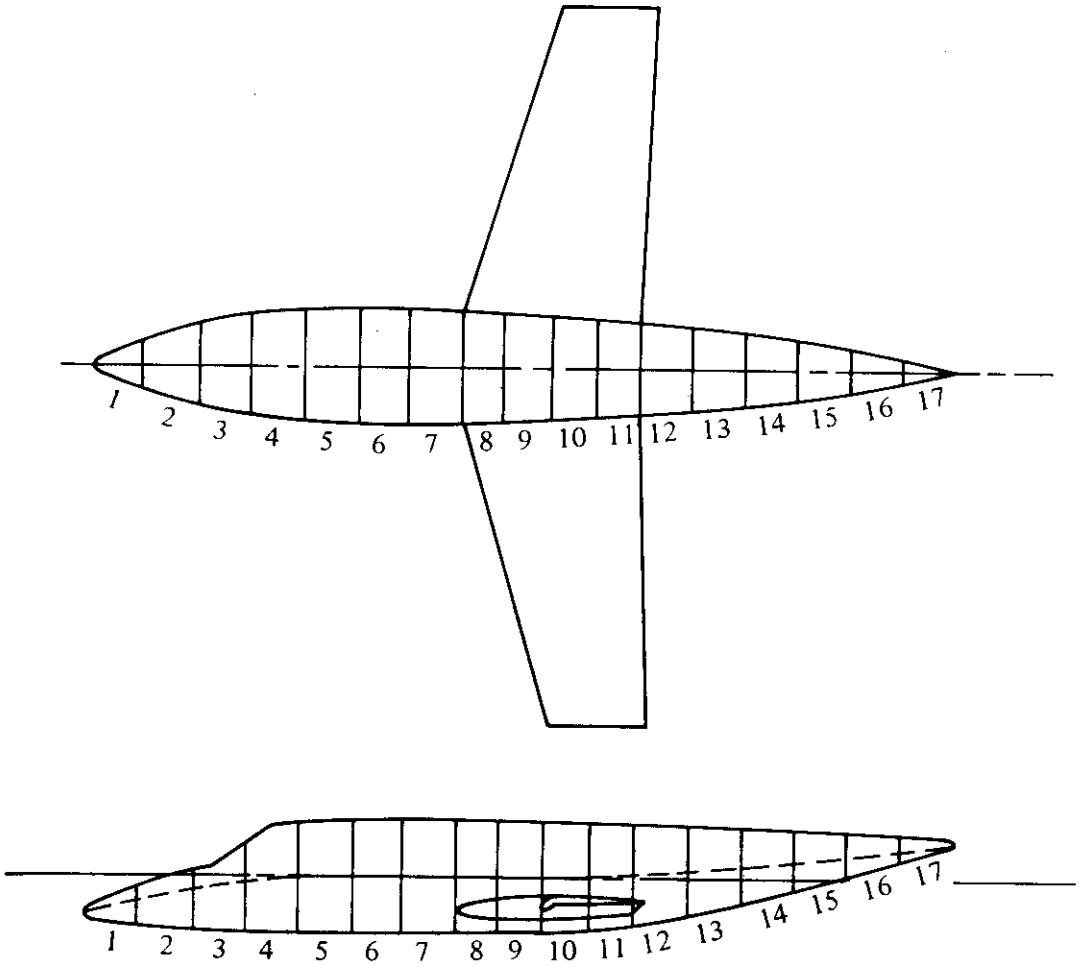

SKETCH (d)

Wing Characteristics:

$S_W = 21.51\ m^2$ $\quad \bar{c} = 2.14\ m$ $\quad \theta = 0^o$

$A = 5.02$ $\quad \lambda = 0.507$ $\quad \Lambda_{c/4} = 13^o$

$(\alpha_0)_W = -1.2^o$ (test data) $\quad M = 0.17$

Root section airfoil is a NACA 64A-109

Tip section airfoil is a NACA 64A-109 modified by drooping the leading edge (Sketch (e)).

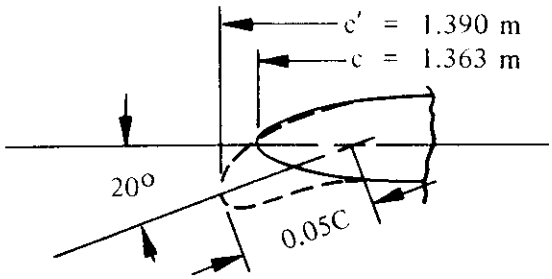

SKETCH (e)

For the Tip Section

$c' = 1.390$ m $\quad c = 1.363$ m $\quad \delta_{f_{LE}} = 20^{o}$ $c_{f_{LE}} = 0.05c$

The drooped leading edge varies linearly across the span from the tip section as shown in Sketch (e), to zero extension and deflection at the root section.

Fuselage Characteristics:

$\ell_B = 12.50$ m $\quad d_{max} = 1.62$ m

Other fuselage dimensions are measured from the three view drawings in Reference 5 and are listed in tabular form when used.

Compute:

Determine wing section c_{m_0}

Root Section (64A-109) c_{m_0} is determined through use of data from Table 4.1.1-B

SECTION	c_{m_0}
64A-010	0
64A-210	-0.040
64-108	-0.015
64-110	-0.020

Note that the variation in c_{m_0} due to camber is identical for the "64" and "64A" series airfoils, i.e., the 64A-210 airfoil has twice the camber of the 64-110 airfoil and twice the c_{m_0}. Therefore, the "64" series airfoil c_{m_0} values can be used to determine the thickness effects.

$$c_{m_{0_{64A\text{-}109}}} = \frac{c_{m_{0\,64\text{-}108}} + c_{m_{0_{64\text{-}110}}}}{2} = \frac{-0.015 - 0.020}{2} = -0.0175$$

Tip section c_{m_0} can be determined by the method of Section 6.1.2.1.

$$\frac{c_{f_{LE}}}{c'} = \left(\frac{c_{f_{LE}}}{c}\right)\frac{c}{c'} = 0.05\ \frac{(1.363)}{(1.390)} = 0.049$$

$$c'_{m_{\delta_{LE}}} = -0.00024 \qquad \text{(Figure 6.1.2.1-36)}$$

Since the wing is assumed to be at zero-lift, and drooped leading edges contribute essentially zero incremental lift at constant angle of attack, assume: $\Delta c_\ell = c_\ell = 0$.

$$\Delta c_{m_{LE}} = c'_{m_{\delta_{LE}}}\left(\frac{c'}{c}\right)\delta_{f_{LE}} + \left(\frac{x_{ref}}{c} + \frac{c' - c}{c}\right)\Delta c_\ell + c_m\left[\left(\frac{c'}{c}\right)^2 - 1\right]$$

$$+ 0.075\, c_\ell \left(\frac{c'}{c}\right)\left(\frac{c'}{c} - 1\right) \qquad \text{(Equation 6.1.2.1-b)}$$

$$= -0.00024\left(\frac{1.390}{1.363}\right)20 + 0 - 0.0175\left[\left(\frac{1.390}{1.363}\right)^2 - 1\right] + 0$$

$$\Delta c_{m_{LE}} = -0.0056$$

$$c_{m_{0_{TIP}}} = c_{m_{0_{\substack{\text{BASIC}\\\text{AIRFOIL}}}}} + \Delta c_{m_{LE}}$$

$$= -0.0175 - 0.0056$$

$$= -0.0231$$

Determine wing zero-lift pitching-moment coefficient using Section 4.1.4.1.

$$\left(C_{m_0}\right)_{\theta=0} = \frac{A\cos^2\Lambda_{c/4}}{A + 2\cos\Lambda_{c/4}}\left(\frac{c_{m_{0_{ROOT}}} + c_{m_{0_{TIP}}}}{2}\right) \qquad \text{(Equation 4.1.4.1-b)}$$

$$= \frac{5.02\cos^2(13^o)}{5.02 + 2\cos(13^o)}\left(\frac{-0.0175 - 0.0231}{2}\right)$$

$$= -0.0139$$

Determine the fuselage $(C_{m_0})_B$ using Equation 4.3.2.1-b and the three-view drawing in Reference 5. Divide the fuselage into incremental parts and compute the value under the summation sign for each increment (Sketch (d)).

INCREMENT	w_f (m)	$(\alpha_0)_W$ (DEG)	$(i_{CL})_B$ (DEG)	Δx (m)	$w_f^2 [(\alpha_0)_W + (i_{CL})_B] \Delta x$
1	0.41	−1.2	−13.5	0.759	−1.876
2	0.95		−10.75		−8.186
3	1.32		−8.00		−12.167
4	1.50		−5.25		−11.015
5	1.58		−2.75		−7.484
6	1.61		−0.75		−3.836
7	1.59		0.0		−2.303
8	1.535		0.0	0.635	−1.795
9	1.460		0.0		−1.624
10	1.340		−0.500		−1.938
11	1.255		−2.000		−3.200
12	1.190		−3.750	0.758	−5.313
13	1.100		−4.750		−5.457
14	0.950		−5.375		−4.498
15	0.735		−6.250		−3.051
16	0.485		−6.875		−1.440
17	0.175		−7.000		−0.190

$$\sum_{x=0}^{\ell_B} w_f^2 [(\alpha_0)_W + (i_{CL})_B] \Delta x = -75.373$$

Determine the apparent mass factor

$$\frac{\ell_B}{d_{max}} = \frac{12.50}{1.62} = 7.72$$

$(k_2 - k_1) = 0.905$ (Figure 4.2.1.1-20a)

Determine $(C_{m_0})_B$

$$\left(C_{m_0}\right)_B = \frac{(k_2 - k_1)}{36.5\, S_W \bar{c}} \sum_{x=0}^{x=\ell_B} w_f^2 [(\alpha_0)_W + (i_{CL})_B] \Delta x \qquad \text{(Equation 4.3.2.1-b)}$$

$$= \frac{0.905}{(36.5)(21.51)(2.14)} = (-75.373)$$

$$= -0.0406$$

$$\frac{\left(C_{m_0}\right)_M}{\left(C_{m_0}\right)_{M=0}} = 1.0 \text{ at } M = 0.17 \qquad \text{(Figure 4.1.4.1-6)}$$

Solution:

$$\left(C_{m_0}\right)_{WB} = \left[\left(C_{m_0}\right)_W + \left(C_{m_0}\right)_B\right] \frac{\left(C_{m_0}\right)_M}{\left(C_{m_0}\right)_{M=0}} \qquad \text{(Equation 4.3.2.1-a)}$$

$$= (-0.0139 - 0.0406)\ 1.0$$

$$= -0.0545 \qquad \text{(based on } S_W \bar{c}\text{)}$$

This compares to a test value of −0.05 from Reference 5.

2. Method 2

Given: A wing-body configuration similar to that of Sample Problem 1 (See Sketch (f)).

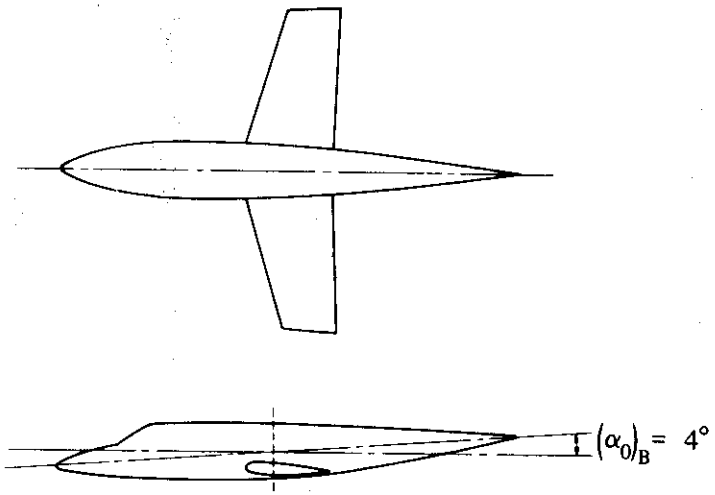

SKETCH (f)

Wing Characteristics:

A = 5.0 $\quad \Lambda_{LE} = 15.6^o \quad \lambda = 0.5 \quad \theta = 0$

NACA 65-209 airfoil $\quad \frac{LER}{\bar{c}} = 0.00552$

$\frac{(y_c)_{max}}{\bar{c}} = 0.01071 \quad C_{L_d} = 0 \quad$ Low wing

Body Characteristics:

$\frac{\ell_N}{d} = 3.32 \quad \frac{\ell_A}{d} = 2.99 \quad \frac{h}{d} = 0.50 \quad \frac{d}{b} = 0.152$

Additional Characteristics:

M = 0.4 $\quad R_\ell = 6 \times 10^6 \quad$ No vertical tail $\quad T_R = 1$

Compute:

The regression coefficients below are obtained from Table 4.3.2.1-B at M = 0.4.

Regression Coefficient	Value Table 4.3.2.1-B
C_0	−0.61496
C_1	0.034113
C_2	−0.0043111
C_3	−0.0067607
C_4	0.58626
C_5	−0.0021631
C_6	−0.0029718
C_7	−0.0013161
C_8	0.0034451
C_9	−0.0097535
C_{10}	−3.9389
C_{11}	−0.52560
C_{12}	−4.3982
C_{13}	0.036116
C_{14}	0.034068
C_{15}	−0.073114
C_{16}	1.2683
C_{17}	−0.16503
C_{18}	$-0.00077192 \times 10^{-6}$

Solution:

$$\left(C_{m_0}\right)_{WB} = C_0 + C_1\left(\frac{l}{A}\right) + C_2\ A + C_3\ \tan\Lambda_{LE} + C_4\left(\frac{t}{\bar{c}}\right) + C_5\left(\frac{\ell_N}{d}\right) + C_6\left(\frac{\ell_A}{d}\right)$$

$$+ C_7\ \lambda + C_8\ \lambda^2 + C_9\ (T_R) + C_{10}\left(\frac{LER}{\bar{c}}\right) + C_{11}\ \theta + C_{12}\left[\frac{\left(y_c\right)_{max}}{\bar{c}}\right]$$

$$+ C_{13}\ C_{L_d} + C_{14}\ W_L + C_{15}\ V_T + C_{16}\left(\frac{h}{d}\right) + C_{17}\left(\frac{d}{b}\right) + C_{18}\ R_\ell$$

(Equation 4.3.2.1-c)

$$\left(C_{m_0}\right)_{WB} = -0.61496 + \frac{0.034113}{5} - 0.0043111\,(5) - 0.0067607\,(0.2793)$$

$$+ 0.58626\,(0.09) - 0.0021631\,(3.32) - 0.0029718\,(2.99)$$

$$- 0.0013161\,(0.5) + 0.0034451\,(0.25) - 0.0097535\,(1)$$

$$- 3.9389\,(0.00552) - 0.5256\,(0) - 4.3982\,(0.01071) + 0.036116\,(0)$$

$$+ 0.034068\,(0) - 0.073114\,(0) + (1.2683)\,(0.5) - 0.16503\,(0.152)$$

$$- 0.00077192 \times 10^{-6}\,(6 \times 10^{6})$$

$$= -0.61496 + 0.0068226 - 0.021555 - 0.00188826 + 0.052763$$

$$- 0.0071815 - 0.0088857 - 0.00065805 + 0.00086128 - 0.0097535$$

$$- 0.021743 - 0.047105 + 0.63415 - 0.0250846 - 0.0046315$$

$$= -0.0688 \text{ (based on } S_W \bar{c}\ )$$

B. TRANSONIC

The comments and methods of Paragraph A are applicable here. It should be noted that at near-sonic conditions or whenever shocks begin appearing on the wing, the value of $(C_{m_0})_{WB}$ may begin to change abruptly. For this reason Method 1 should not be used above M = 0.9 and should be used judiciously for $0.8 \leqslant M \leqslant 0.9$. Likewise, Method 2 should be applied with caution at near-sonic conditions.

DATCOM METHODS

At transonic speeds the methods described in Paragraph A may be applied. (It should be noted for Method 1 that the subsonic method of Section 4.1.4.1 must be used to evaluate the wing zero-lift pitching-moment contribution.) Both methods are restricted to straight-tapered-wing configurations.

Sample Problems

No sample problems are presented here because their solutions would be obtained in the same manner as in the subsonic speed regime.

C. SUPERSONIC

In the supersonic speed regime Method 2 of Paragraph A of this section may be used to estimate $(C_{m_0})_{WB}$ for fighter-type aircraft. The comments in Paragraph A pertaining to Method 2 are applicable here.

DATCOM METHOD

At supersonic speeds Method 2 described in Paragraph A may be applied to fighter-type straight-tapered-wing configurations.

Sample Problem

No sample problem is presented here because its solution would be obtained in the same manner as in the subsonic speed regime.

REFERENCES

1. Anderson, A. K., Jr.: Douglas Aircraft Company Memorandum C1-250-Aero-77-178, 7 March 1977. (U)
2. Multhopp, H.: Aerodynamics of the Fuselage. NACA TM-1036, 1942. (U)
3. Simon, W. E., et al.: Prediction of Aircraft Drag Due to Lift. AFFDL-TR-71-84, 1971. (U)
4. Boyd, J. W., Migotsky, E., and Wetzel, B. E.: A Study of Conical Camber for Triangular and Sweptback Wings. NACA RM A55G19, 1955. (U)
5. Soderman, P.T., and Aiken, T. N.: Full-Scale Wind-Tunnel Tests of a Small Unpowered Jet Aircraft with a T-Tail. NASA TN D-6573, 1971. (U)
6. Burrows, D. L., and Palmer, W. E.: A Transonic Wind-Tunnel Investigation of the Longitudinal Force and Moment Characteristics of a Plane and a Cambered 3-Percent-Thick Delta Wing of Aspect Ratio 3 on a Slender Body. NACA RM L54H25, 1954. (U)
7. Bielat, R. P.: A Transonic Wind-Tunnel Investigation of the Aerodynamic Characteristics of Three 4-Percent-Thick Wings of Sweepback Angles 10.8°, 35°, and 47°, Aspect Ratio 3.5, and Taper Ratio 0.2 in Combination with a Body. NACA RM L52B08, 1952. (U)
8. Bielat, R. P., Harrison, D. E., and Coppolino, D. A.: An Investigation at Transonic Speeds of the Effects of Thickness Ratio and of Thickened Root Sections on the Aerodynamic Characteristics of Wings with 47° Sweepback, Aspect Ratio 3.5, and Taper Ratio 0.2 in the Slotted Test Section of the Langley 8-Foot High-Speed Tunnel. NACA RM L51I04a, 1951. (U)
9. Loving, D. L.: A Transonic Investigation of Changing Indentation Design Mach Number on the Aerodynamic Characteristics of a 45° Sweptback-Wing-Body Combination Designed for High Performance. NACA RM L55J07, 1956. (U)
10. Munk, M. M.: The Aerodynamic Forces on Airship Hulls. NACA TR 184, 1924. (U)

TABLE 4.3.2.1-A

METHOD 1
DATA SUMMARY AND SUBSTANTIATION

Ref.	A	λ	$\Lambda_{c/4}$ (deg)	θ (deg)	M	$(C_{m_0})_{WB}$ Calc	$(C_{m_0})_{WB}$ Test	$\Delta\,(C_{m_0})_{WB}$ Calc-Test
5	5.02	0.507	13	0	0.08	−0.0543	−0.04	−0.0143
↓	↓	↓	↓	↓	0.17	−0.0545	−0.05	−0.0045
6	3	0	45	0	0.67	−0.00496	−0.008	+0.0030
↓	↓	↓	↓	↓	0.76	−0.00526	−0.005	−0.0003
↓	↓	↓	↓	↓	0.89	−0.00602	−0.004	−0.0020
7	3.5	0.20	10.8	0	0.7	−0.0234	−0.018	−0.0054
↓	↓	↓	↓	↓	0.85	−0.0266	−0.024	−0.0026
↓	↓	↓	↓	↓	0.9	−0.0282	−0.027	−0.0012
↓	↓	↓	35	↓	0.7	−0.0183	−0.018	−0.0003
↓	↓	↓	↓	↓	0.85	−0.0207	−0.022	0.0013
↓	↓	↓	↓	↓	0.9	−0.0220	−0.024	0.0020
↓	↓	↓	47	↓	0.696	−0.0137	−0.019	0.0053
↓	↓	↓	↓	↓	0.843	−0.0154	−0.023	0.0076
↓	↓	↓	↓	↓	0.892	−0.0164	−0.024	0.0076
8	3.5	0.20	47	0	0.696	−0.0137	−0.019	0.0053
↓	↓	↓	↓	↓	0.892	−0.0165	−0.024	0.0075
↓	↓	↓	↓	↓	0.7	−0.0149	−0.018	0.0031
↓	↓	↓	↓	↓	0.9	−0.0180	−0.022	0.0040
↓	↓	↓	↓	↓	0.696	−0.0139	−0.014	0.0001
↓	↓	↓	↓	↓	0.892	−0.0168	−0.019	0.0022
↓	↓	↓	↓	↓	0.7	−0.0145	−0.016	0.0015
↓	↓	↓	↓	↓	0.9	−0.0175	−0.017	−0.0005
9	4	0.15	45	0	0.8	−0.0219	−0.031	0.0091
↓	↓	↓	↓	↓	0.85	−0.0231	−0.033	0.0099
↓	↓	↓	↓	↓	0.9	−0.0246	−0.036	0.0114

TABLE 4.3.2.1-A (CONTD)

Ref.	A	λ	$\Lambda_{c/4}$ (deg)	θ (deg)	M	$(C_{m_0})_{WB}$ Calc	$(C_{m_0})_{WB}$ Test	$\Delta (C_{m_0})_{WB}$ Calc-Test
Unpub. data	7.028	0.230	30.61	−4.05	0.2	−0.0329	−0.040	0.0071
					0.4	−0.0339	−0.040	0.0061
					0.6	−0.0372	−0.040	0.0028
					0.7	−0.0393	−0.042	0.0027
					0.8	−0.0423	−0.046	0.0037
					0.825	−0.0436	−0.0455	0.0019
					0.85	−0.0444	−0.043	−0.0014
	8.71	0.2036	24.5	−4.7	0.2	−0.0760	−0.0830	0.0070
					0.3	−0.0761	−0.0830	0.0069
					0.4	−0.0783	−0.0835	0.0052
					0.5	−0.0813	−0.0845	0.0032
					0.6	−0.0859	−0.0860	0.0001
					0.7	−0.0908	−0.0890	−0.0018
					0.8	−0.0973	−0.0935	−0.0038
					0.85	−0.1026	−0.0950	−0.0076
	6.8	0.30	35	−7.1	0.2	−0.0223	−0.0220	−0.0003
					0.4	−0.0230	−0.0220	−0.0010
					0.6	−0.0252	−0.0245	−0.0007
					0.7	−0.0266	−0.0270	0.0004
					0.8	−0.0285	−0.0288	0.0003
					0.825	−0.0295	−0.0292	−0.0003
					0.85	−0.0302	−0.0300	−0.0002
					0.875	−0.0312	−0.0308	−0.0004
					0.9	−0.0321	−0.0315	−0.0006

Average $\Delta (C_{m_0})_{WB} = \dfrac{\Sigma |\Delta (C_{m_0})_{WB}|}{n} = 0.0036$

TABLE 4.3.2.1-8

METHOD 2
REGRESSION COEFFICIENTS

MACH NUMBER	C_0	C_1	C_2	C_3	C_4	C_5	C_6	C_7	C_8	C_9
0.4	−0.61496	0.034113	−0.0043111	−0.0067607	0.58626	−0.0021631	−0.0029718	−0.0013161	0.0034451	−0.0097535
0.6	0.030521	−0.026482	−0.0031117	0.00040854	0.043533	0.00010412	−0.0023971	0.010412	−0.0049864	−0.0023881
0.7	0.010449	0.0019975	−0.0011029	0.00019192	0.028208	0.00079415	−0.0012200	0.0051328	−0.0029594	0.00074312
0.8	0.024846	−0.0055509	−0.0024707	−0.0014904	0.031764	0.00036833	0.00037272	−0.0035006	0.00073299	0.0012306
0.9	0.023233	−0.00054868	−0.0027806	−0.0014790	0.024266	0.00040862	−0.00092113	0.00091995	−0.0010519	0.0021653
0.95	−0.029503	0.056041	0.0052306	−0.0021117	0.024656	0.00082755	−0.0016469	−0.0085456	0.0092825	0.0037542
1.0	−0.072508	0.11805	0.0091112	−0.0055601	0.016164	−0.0019504	0.0043904	−0.050916	0.039982	0.00011703
1.1	−0.047882	0.087861	0.012725	0.00058939	0.049004	−0.00018951	−0.0014263	−0.0073144	0.0025290	−0.00011616
1.2	−0.0077024	0.067409	0.0037585	−0.0020553	−0.013639	−0.00084471	−0.0027075	−0.00035333	−0.00030929	0.0017132
1.3	−0.0090333	0.081884	0.0029019	−0.0035078	−0.027873	−0.0016508	−0.00070990	−0.010550	0.0032408	0.00057507
1.4	−0.064029	0.11973	0.012987	0.0014900	−0.029892	−0.0013285	−0.0019031	0.0093873	−0.0049618	0.0011079
1.5	0.014988	0.066427	0.0007897	−0.0065439	−0.022854	−0.00098949	−0.0024785	−0.011328	0.0026880	−0.00002373
2.0	−0.10257	0.17653	0.022724	−0.0065667	0.0026084	−0.00036847	0.0015647	−0.026630	0.010089	−0.0018213
2.5	−0.097877	0.16776	0.028670	0.0043908	0.0020467	−0.0013417	−0.00077258	−0.023909	0.0094275	0.00057215

MACH NUMBER	C_{10}	C_{11}	C_{12}	C_{13}	C_{14}	C_{15}	C_{16}	C_{17}	C_{18} x 10^{+6}	
0.4	−3.9389	−0.52560	−4.3982	0.036116	0.034068	−0.073114	1.2683	−0.16503	−0.00077192	
0.6	0.56516	−0.51829	−4.0930	−0.0069271	0.011685	−0.0010598	−0.017713	−0.052268	0.00025439	
0.7	0.12045	−0.53503	−4.2059	−0.0013549	0.0053796	0.0020454	−0.0039115	−0.043905	−0.0012391	
0.8	−0.10408	−0.49728	−3.9283	0.0048901	0.0014643	0.0027298	−0.0092493	−0.051001	−0.0011483	
0.9	0.098669	−0.62200	−4.8034	0.0018263	0.0028848	0.00025683	0.0065923	−0.10221	−0.00078181	
0.95	−0.82906	−0.31518	−3.1686	0.0075362	−0.0038225	−0.0035619	0.0074832	−0.019949	−0.0010290	
1.0	1.0256	−0.39402	−3.4999	0.0035393	0.030079	0.0016422	0.025312	−0.053897	−0.0013250	
1.1	−0.62097	−0.36576	−3.1159	0.010248	0.0047945	−0.00065869	−0.037542	0.0063401	−0.00051180	
1.2	−1.5639	−0.21108	−2.5628	0.011013	0.0016835	0.0016923	0.017427	−0.13287	−0.0013416	
1.3	−0.43130	−0.10254	−2.0192	0.0067985	0.0083637	0.0013512	0.020635	−0.13673	−0.0023095	
1.4	−0.83720	−0.029314	−1.7911	0.0017144	0.0034691	0.0011693	0.018158	−0.080305	−0.0022940	
1.5	−0.16698	0.45021	0.13537	0.0022793	0.0040738	0.0032272	0.016570	−0.18294	−0.0014919	
2.0	0.97612	−4.7537	−15.553	−0.0010677	−0.0042213	0.0045941	−0.00063330	−0.11299	0.00094537	
2.5	1.3090	−5.3830	−16.996	0.014219	−0.0091883	0.0026961	−0.016885	−0.068530	−0.00099505	

4.3.2.2 WING-BODY PITCHING-MOMENT-CURVE SLOPE (AERODYNAMIC CENTER)

For wing-body configurations in which the body radii are large relative to the wing semispan, there exist mutual aerodynamic interferences between wing and body that can appreciably affect the aerodynamic center of the wing-body combination.

The body influences the wing lift primarily by inducing a change in the local angle of attack along the span. The wing influences the body by a lift carryover from the wing onto the body. For supersonic speeds the wing lift carryover on the body is displaced downstream parallel to the Mach lines, as illustrated in sketch (e) on page 4.3.1.2-5. Important moment differences can therefore exist between configurations in which the fuselage terminates at the wing trailing edge and those in which the fuselage extends beyond the wing trailing edge.

The aerodynamic-center location of a wing-body configuration is given in reference 1 as

$$\frac{x'_{a.c.}}{c_{r_e}} = \frac{\left(\frac{x'_{a.c.}}{c_{r_e}}\right)_N C_{L_{a_N}} + \left(\frac{x'_{a.c.}}{c_{r_e}}\right)_{W(B)} C_{L_{a_{W(B)}}} + \left(\frac{x'_{a.c.}}{c_{r_e}}\right)_{B(W)} C_{L_{a_{B(W)}}}}{C_{L_{a_N}} + C_{L_{a_{W(B)}}} + C_{L_{a_{B(W)}}}} \qquad 4.3.2.2\text{-a}$$

where the $x'_{a.c.}/c_{r_e}$ terms are the chordwise distances measured in exposed wing root chords from the apex of the exposed wing to the aerodynamic center, positive aft. The methods for calculating these terms are presented in this section and are based on exposed-wing geometry. The exposed wing is defined as the parts of the wing outboard of the largest body diameter at the wing-body intersection. Two cases are illustrated in sketch (a).

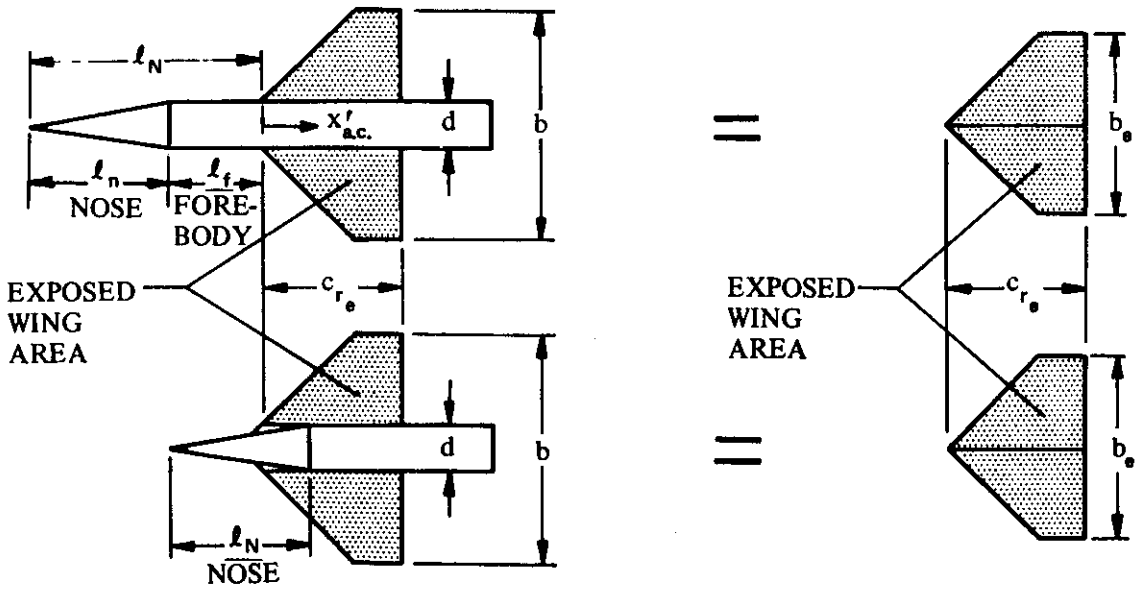

SKETCH (a)

The lift-curve slopes used in Equation 4.3.2.2-a are referred to the total wing area.

The aerodynamic-center location measured in wing root chords aft of the wing apex is given by

$$\frac{x_{a.c.}}{c_r} = \left(\frac{x'_{a.c.}}{c_{r_e}}\right) \frac{c_{r_e}}{c_r} + \frac{d}{2c_r} \tan \Lambda_{LE} \qquad 4.3.2.2\text{-b}$$

where $x'_{a.c.}/c_{r_e}$ is given by Equation 4.3.2.2-a.

The nose of the body is defined as the expanding portion of the body ahead of the wing. The forebody is the cylindrical portion of the body ahead of the wing. The base of the forebody is defined as the cross section at the wing-leading-edge – body intersection.

If the wing is at incidence relative to the body, the a.c. can be approximated by using the lift coefficient of each component – in the linear or near-linear range only – instead of the lift-curve slope. The angle of attack of the body relative to the free stream is used to calculate the body lift, and the angle of attack of the wing relative to the free stream is used to calculate the wing lift and lift carryover on the body.

The specific case of a conical body mounted on a delta wing (Sketch (c) on Page 4.3.1.2-2) has been solved by Spreiter in Reference 2. Slender-body theory is used to obtain the ratio of the wing-body lift to that of the wing alone. Correlation with experimental data by this method is good throughout the speed range. The method predicts that the aerodynamic center of the wing-body combination is the same as that of the wing alone.

Methods are presented in this section that are applicable to axisymmetric bodies in combination with straight-tapered wings throughout the subsonic, transonic, and supersonic speed ranges, and in combination with non-straight-tapered wings at subsonic and supersonic speeds. The methods are applicable only in the linear-lift range.

The effects of body cross-section shape and wing vertical position on wing-body lift-curve slope are not considered. (Some test data on these variables are given in References 3 and 4.) Therefore, the methods should not be construed as pertaining to generalized wing-body combinations with arbitrary body shapes.

The results of this section apply to single-wing-body configurations only; for cruciform and other multi-panel arrangements, interference effects may exist between the various panels.

The following general categories of non-straight-tapered wings are considered at subsonic and supersonic speeds:

Double-delta wings
Cranked wings
Curved (Gothic and ogee) wings

These wings are illustrated in Sketch (a) of Section 4.1.3.2. Their wing-geometry parameters are presented in Section 2.2.2.

A. SUBSONIC

DATCOM METHODS

Straight-Tapered Wing-Body Configurations

The subsonic aerodynamic-center location near zero lift of a wing-body configuration with a straight-tapered wing is obtained from the procedure outlined in the following steps:

Step 1. Divide the wing-body configuration into three components as follows and determine their pertinent geometric parameters (see Sketch (a)).

(1) The exposed wing in the presence of the body, denoted by the subscript W(B).

(2) The body in the presence of the wing, denoted by the subscript B(W).

(3) The body nose and forebody ahead of the wing-body juncture, denoted by the subscript N.

Step 2. Determine the lift-curve slope of the exposed wing $\left(C_{L_\alpha}\right)_e$ from the straight-tapered wing method of Paragraph A of Section 4.1.3.2, based on its exposed area S_e.

Step 3. Determine the lift-curve slope of the body nose by the method of paragraph A of Section 4.2.1.1. In most cases the slender-body-theory value of $\left(C_{N_\alpha}\right)_B = 2$ per radian (based on the nose frontal area) is sufficiently accurate.

Step 4. Using the lift-curve slopes determined in Steps 2 and 3, calculate $C_{L_{\alpha_{W(B)}}}$, $C_{L_{\alpha_{B(W)}}}$, and $C_{L_{\alpha_N}}$, referred to the total wing area, by

$$C_{L_{\alpha_{W(B)}}} = K_{W(B)} \left(C_{L_\alpha}\right)_e \frac{S_e}{S_W}$$

$$C_{L_{\alpha_{B(W)}}} = K_{B(W)} \left(C_{L_\alpha}\right)_e \frac{S_e}{S_W}$$

$$\left(C_{N_\alpha}\right)_N^* = \left(C_{N_\alpha}\right)_B \frac{\pi d^2}{4 S_W}$$

where $K_{W(B)}$ and $K_{B(W)}$ are interference factors obtained from Figure 4.3.1.2-10.

Step 5. Determine the a.c. location of the exposed wing as a fraction of the root chord of the exposed wing $\frac{x'_{a.c.}}{c_{r_e}}$ from Figure 4.1.4.2-26. The interference effect of the body lift in the presence of the wing is neglected, and the a.c. location of the body-lift carryover on the wing is taken as the a.c. location for the exposed wing, i.e.,

$$\left(\frac{x'_{a.c.}}{c_{r_e}}\right)_{W(B)} = \frac{x'_{a.c.}}{c_{r_e}}$$

---

*The equation given for $\left(C_{N_\alpha}\right)_N$ is based on the slender-body-theory value for $\left(C_{N_\alpha}\right)_B$. If Equation 4.2.1.1-a is used to obtain $\left(C_{N_\alpha}\right)_B$, then $C_{N_{\alpha_N}} = \left(C_{N_\alpha}\right)_B \frac{(V_B)^{2/3}}{S_W}$

Step 6. Determine the a.c. location of the wing-lift carryover on the body $\left(\frac{x'_{a.c.}}{c_{r_e}}\right)_{B(W)}$

For $\beta A_e \geq 4.0$, the a.c. contribution due to the lift carryover of the wing on the body is obtained from the equation

$$\left(\frac{x'_{a.c.}}{c_{r_e}}\right)_{B(W)} = \frac{1}{4} + \frac{b-d}{2c_{r_e}} \tan \Lambda_{c/4} \left[- \frac{k}{1-k} + \frac{\sqrt{1-2k}\ \log_e\left(\frac{1-k}{k} + \frac{1}{k}\sqrt{1-2k}\right) - (1-k) + \frac{\pi}{2}\ k}{\frac{k(1-k)}{\sqrt{1-2k}}\ \log_e\left(\frac{1-k}{k} + \frac{1}{k}\sqrt{1-2k}\right) + \frac{(1-k)^2}{k} - \frac{\pi}{2}\ (1-k)} \right] \qquad 4.3.2.2\text{-c}$$

where $k = d/b$ and the term inside the brackets is plotted for various values of k in Figure 4.3.2.2-35.

Equation 4.3.2.2-c is developed from lifting-line theory applied to the portion of a fictitious wing inside the body, defined by the image of the actual wing at the intersection of the wing quarter-chord line with the body. Equation 4.3.2.2-c is mathematically limited to $\frac{d}{b} \leq 0.5$, but extrapolation to $\frac{d}{b} = 0.8$ gives accurate results.

For $\beta A_e < 4.0$ an interpolation procedure is required. The a.c. location at $\beta A_e = 0$, derived from slender-body theory, is given in Figure 4.3.2.2-36b. For βA_e between 0 and 4.0, the a.c. of the wing-lift carryover on the body is obtained by fairing values between those obtained from Figure 4.3.2.2-36b and Equation 4.3.2.2-c for $\beta A_e = 0$ and $\beta A_e \geq 4.0$, respectively. It is recommended in Reference 1 that the interpolation procedure for $\beta A_e < 4.0$ be performed using the calculated wing-alone values $\left(\frac{d}{b} = 0\right)$ as a guide. However, for the purpose of the Datcom this calculation is omitted, and the fairing is performed between $\beta A_e = 0$ and $\beta A_e = 4.0$ by a curve through the value at $\beta A_e = 0$ and tangent to the calculated line for $\beta A_e \geq 4$.

Step 7. Determine the a.c. location of the body nose and forebody as a fraction of the root chord of the exposed wing $\left(\frac{x'_{a.c.}}{c_{r_e}}\right)_N$, and referred to the exposed-wing apex.

Two methods are presented here for estimating the aerodynamic center of the nose and forebody (see Sketch (a)).

The first, which is based on the methods of Sections 4.2.1.1 and 4.2.2.1, is the more accurate of the two. It should be used when the nose lift is a significant fraction of the total lift of the vehicle. In Equation 4.2.2.1-b, ℓ_N should be substituted for x_m and dC_m/dC_L should be multiplied by the negative cube root of the nose volume and divided by c_{r_e}. This refers the moments to the apex of the exposed wing, i.e.,

$$\left(\frac{x'_{a.c.}}{c_{r_e}}\right)_N = \left(C_{m_\alpha}\right)_{4.2.2.1} \left[- \frac{V_B^{1/3}}{c_{r_e}\left(C_{L_\alpha}\right)_{4.2.1.1}} \right]$$

The second method presented in this section gives more approximate answers than the first method. Figure 4.3.2.2-36a gives the aerodynamic-center location for cones, ogives, and ellipsoids without forebodies. For ogives with forebodies an approximation can be made by defining an equivalent ogive to replace the actual ogive and forebody. Thus

$$(f)_{equiv} = (f)_{nose} + 1.6\,(f)_{forebody} \qquad 4.3.2.2\text{-d}$$

where $(f)_{nose}$, $(f)_{forebody}$, and $(f)_{equiv}$ are the fineness ratios of the actual nose, the forebody, and the equivalent nose, respectively. Figure 4.3.2.2-36a is entered with the actual nose fineness ratio to obtain the a.c. of the equivalent nose, referred to the apex of the exposed wing. Then

$$\left(\frac{x'_{a.c.}}{c_{r_e}}\right)_N = \left(\frac{x_{a.c.}}{\ell_{equiv}}\right)_N \left(\frac{\ell_{equiv}}{c_{r_e}}\right)$$

where ℓ_{equiv} is the length of the equivalent nose ($\ell_{equiv} = f_{equiv}\, d$).

Step 8. Using the results calculated in Steps 4 through 7, Equation 4.3.2.2-a gives the a.c. location of the wing-body configuration measured in exposed-wing root chords aft of the apex of the exposed wing. The a.c. location measured in wing root chords aft of the wing apex is given by Equation 4.3.2.2-b.

Application of this method is illustrated by the sample problem on Pages 4.3.2.2-7 through 4.3.2.2-10.

A comparison of test data with results calculated by using this method is presented as Table 4.3.2.2-A. The ranges of planform and flow parameters of the test data are:

$$2.88 \leqslant A \leqslant 4.0$$

$$7^o \leqslant \Lambda_{LE} \leqslant 60^o$$

$$0.143 \leqslant \lambda \leqslant 1.0$$

$$0.14 \leqslant d/b \leqslant 0.80$$

$$0.13 \leqslant M \leqslant 0.91$$

$$0.9 \times 10^6 \leqslant R\ell_{MAC} \leqslant 6.8 \times 10^6$$

Although ranges of planform and flow parameters of the test data are in most cases quite broad, the limited number of test points makes it rather difficult to draw general conclusions regarding parameters not specifically noted in the prediction method. Within the linear-lift range, profile parameters such as camber, twist, and airfoil shape would be expected to have only a minor influence on the wing-body aerodynamic-center location. There are not enough data to allow a quantitative prediction of Reynolds-number effect, but it is reasonable to expect that Reynolds number will influence the wing-body aerodynamic-center location.

Non-Straight-Tapered Wing-Body Configuration

The method for determining the subsonic aerodynamic-center location near zero lift of wing-body configura-

tions with non-straight-tapered wings is taken fromReference 5. During the course of the study conducted in connection withReference 5, it was validated that the subsonic wing-body aerodynamic-center location of configurations with non-straight-tapered wings can be determined by using the wing-alone approach and neglecting the exposed-wing and body lift carryover and body-nose effects. Therefore, the method presented in paragraph A of Section 4.1.4.2 for determining the aerodynamic-center location of non-straight-tapered wings is directly applicable to the case of a body in combination with a non-straight-tapered wing.

Essentially, the method consists of dividing the complete theoretical wing planform (extended to the plane of symmetry) into two panels with each panel having conventional, straight-tapered geometry. Then for each of the constructed panels, the individual lift-curve slope and aerodynamic-center location are estimated by treating each constructed panel as a complete wing. The individual lift and aerodynamic-center location determined for each constructed panel are then mutually combined in accordance with an "inboard-outboard" weighted-area relationship to estimate the aerodynamic-center location for the basic wing-body configuration.

The sample problem of Paragraph A of Section 4.1.4.2 illustrates the use of the method.

Comparisons of test data with results calculated by using this wing-alone approach are presented as Tables 4.3.2.2-B and 4.3.2.2-C (both taken fromReference 5) for wing-body combinations with double-delta and cranked wings, respectively. Although the technique is applicable to wing-body combinations with curved wings, test data on such configurations are not available for substantiation purposes. Only two wing-body combinations with curved wings have been investigated. Since both of these configurations have very small bodies and the wing planform projection effectively blankets nearly all the body, they have been included in the curved wing-alone substantiation of Section 4.1.4.2 (Table 4.1.4.2-B). The ranges of planform parameters of the double-delta and cranked-wing configuration test data are:

Double-Delta Configurations			Cranked Configurations		
$1.3 \leq$	A	≤ 3.0	$1.68 \leq$	A	≤ 6.93
$60^o \leq$	Λ_{LE_i}	$\leq 82.9^o$	$25^o \leq$	Λ_{LE_i}	$\leq 75^o$
$38.1^o \leq$	Λ_{LE_o}	$\leq 60^o$	$12^o \leq$	Λ_{LE_o}	$\leq 75^o$
$0.217 \leq$	η_B	≤ 0.654	$0.224 \leq$	η_B	≤ 0.654
$0 \leq$	ℓ_N/ℓ_B	≤ 0.7	$0 \leq$	ℓ_N/ℓ_B	≤ 0.7

The Mach-number range of the test data for the above configurations is $0.1 \leq M \leq 0.9$.

The test results indicate that airfoil shape, camber, and twist have only a minor influence on the wing-body aerodynamic-center location within the linear-lift range. There are not enough data to allow a quantitative prediction of Reynolds-number effect, but it is reasonable to expect that Reynolds number will influence the wing-body aerodynamic-center location.

Many double-delta and cranked wings have non-straight trailing edges with the trailing-edge break at a different span station from the leading-edge break. For such wings the irregular trailing-edge sweep angles of the subdivided panels are modified by using straight trailing-edge sweep angles for each panel, constructed so that the area moment about the respective wing-panel apex remains approximately the same.

All the configurations listed inTables 4.3.2.2-B and 4.3.2.2-C have only one break in the wing leading edge. In certain cases, more than one wing leading-edge break can be handled provided the wing can be approximated by an equivalent two-panel planform. Such an approximation has been made for two cranked-wing

planforms included in the cranked-wing-alone data summary of Section 4.1.4.2 (Table 4.1.4.2-A). In both cases the inboard panel remains unchanged, and an outboard panel is approximated which has the same area moment about the wing-root apex as the original outer panels by adjusting and constructing straight leading and trailing edges.

Sample Problem

Straight-Tapered Wing Configuration

Given: A wing-body configuration ofReference 9.

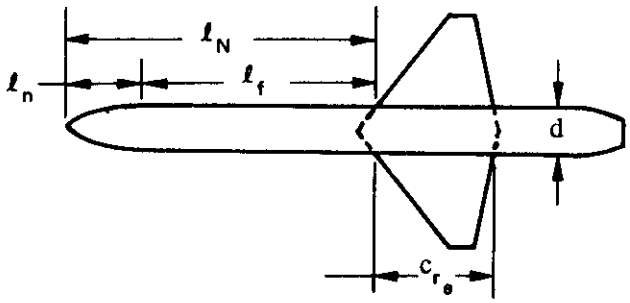

Total-Wing Characteristics:

$A_W = 3.0 \quad S_W = 250.56$ sq in. $\quad \lambda_W = 0.143$

$\Lambda_{LE_W} = 38.7^o \qquad \Lambda_{c/4_W} = 28.8^o$

$b_W = 27.4$ in. $\qquad c_{r_W} = 16.0$ in.

Exposed-Wing Characteristics:

$$A_e = 2.84 \quad \lambda_e = 0.169 \quad \Lambda_{LE_e} = \Lambda_{LE_W} = 38.7^o \quad \Lambda_{c/2_e} = 16.7^o$$

$$c_{r_e} = 13.5 \text{ in.} \quad \frac{S_e}{S_W} = 0.705$$

Body-Nose Characteristics:

$$\text{Ogive-cylinder} \quad d = 5.0 \text{ in.} \quad \frac{d}{b_W} = 0.183$$

$$\ell_n = 8.75 \text{ in.} \quad f_{nose} = \frac{\ell_n}{d} = 1.75$$

$$\ell_f = \ell_{forebody} = 26.65 \text{ in.} \quad f_{forebody} = \frac{\ell_f}{d} = 5.33$$

Additional Characteristics:

$M = 0.60$; $\beta = 0.80 \quad \kappa = 1.0$ (assumed)

Compute:

$\left(C_{L_\alpha}\right)_e$ (Section 4.1.3.2)

$$\frac{A_e}{\kappa}\left[\beta^2 + \tan^2 \Lambda_{c/2_e}\right]^{1/2} = 2.43$$

$$\left(\frac{C_{L_\alpha}}{A}\right)_e = 1.22 \text{ per rad} \quad \text{(Figure 4.1.3.2-49)}$$

$$\left(C_{L_\alpha}\right)_e = 3.46 \text{ per rad}$$

$\left(C_{N_\alpha}\right)_B$

$$\left(C_{N_\alpha}\right)_B = 2 \text{ per rad (based on nose frontal area) (slender-body theory)}$$

Interference factors (Section 4.3.1.2)

$$\left.\begin{aligned} K_{W(B)} &= 1.153 \\ K_{B(W)} &= 0.255 \end{aligned}\right\} \quad \text{(Figure 4.3.1.2-10 at } \frac{d}{b_W} = 0.183\text{)}$$

Component lift-curve slopes, referred to S_W

$$C_{L_{\alpha_{W(B)}}} = K_{W(B)} \left(C_{L_\alpha}\right)_e \frac{S_e}{S_W} = (1.153)(3.46)(0.705) = 2.81 \text{ per rad}$$

$$C_{L_{\alpha_{B(W)}}} = K_{B(W)} \left(C_{L_\alpha}\right)_e \frac{S_e}{S_W} = (0.255)(3.46)(0.705) = 0.622 \text{ per rad}$$

$$C_{L_{\alpha_N}} = \left(C_{N_\alpha}\right)_B \frac{\pi d^2}{4S_W} = (2.0) \frac{\pi (5.0)^2}{(4)(250.56)} = 0.1567 \text{ per rad}$$

$\left(\frac{x'_{a.c.}}{c_{r_e}}\right)_{W(B)}$ (Section 4.1.4.2)

$$\frac{\beta}{\tan \Lambda_{LE_e}} = \frac{0.80}{\tan 38.7^\circ} = 1.00$$

$$(A \tan \Lambda_{LE})_e = (2.84)(\tan 38.7^\circ) = 2.28$$

$$\frac{x'_{a.c.}}{c_{r_e}} = 0.440 \text{ (Figure 4.1.4.2-26a through -26c, interpolated for } \lambda_e\text{)}$$

$$\left(\frac{x'_{a.c.}}{c_{r_e}}\right)_{W(B)} = \frac{x'_{a.c.}}{c_{r_e}} = 0.440$$

$\left(\frac{x'_{a.c.}}{c_{r_e}}\right)_{B(W)}$

$\beta A_e = (0.80)(2.84) = 2.28$. Since $\beta A_e < 4.0$, an interpolation between values of $\left(\frac{x'_{a.c.}}{c_{r_e}}\right)_{B(W)}$ at $\beta A_e = 0$ and $\beta A_e \geq 4.0$ must be performed. (See Step 6 of Datcom method.)

$\left(\frac{x'_{a.c.}}{c_{r_e}}\right)_{B(W)}$ at $\beta A_e = 0$

$$\frac{1}{4} A_e (1 + \lambda_e) \tan\Lambda_{LE} = \frac{1}{4} (2.84)(1.169)(\tan 38.7^{o}) = 0.665$$

$$\left(\frac{x'_{a.c.}}{c_{r_e}}\right)_{B(W)} = 0.330 \text{ (Figure 4.3.2.2-36b)}$$

$\left(\frac{x'_{a.c}}{c_{r_e}}\right)_{B(W)}$ at $\beta A_e \geq 4.0$

$$k = \frac{d}{b_W} = 0.183;\ 1 - k = 0.817;\ \sqrt{1 - 2k} = 0.796$$

$$\log_e \left(\frac{1 - k}{k} + \frac{1}{k}\sqrt{1 - 2k}\right) = 2.176$$

Evaluate the term in brackets of Equation 4.3.2.2-c

$$\left[- \frac{k}{1-k} + \frac{\frac{b}{2}\sqrt{1-2k}\log_e\left(\frac{1-k}{k} + \frac{1}{k}\sqrt{1-2k}\right) - \frac{b}{2}(1-k) + \frac{\pi b}{4} k}{\frac{b}{2}\frac{k(1-k)}{\sqrt{1-2k}}\log_e\left(\frac{1-k}{k} + \frac{1}{k}\sqrt{1-2k}\right) + \frac{b}{2}\frac{(1-k)^2}{k} - \frac{\pi b}{4}(1-k)} \right] =$$

$$\left[- \frac{0.183}{0.817} + \frac{13.7\ (0.796)\ (2.176) - 13.7\ (0.817) + \frac{\pi}{2}(13.7)(0.183)}{\frac{13.7\ (0.183)\ (0.817)\ (2.176)}{0.796} + 13.7\ \frac{(0.817)^2}{0.183} - \frac{\pi}{2}(13.7)(0.817)} \right] = 0.210$$

$$\left(\frac{x'_{a.c.}}{c_{r_e}}\right)_{B(W)} = \frac{1}{4} + \frac{b - d}{2 c_{r_e}} \tan \Lambda_{c/4} \ [0.210] \text{ (Equation 4.3.2.2-c)}$$

$$= \frac{1}{4} + \frac{27.4 - 5}{2(13.5)} (0.5498)\ [0.210]$$

$$= 0.346$$

$$\left(\frac{x'_{a.c.}}{c_{r_e}}\right)_{B(W)} = 0.345 \text{ (interpolated using values at } \beta A_e = 0 \text{ and } \beta A_e \geq 4.0)$$

(See Step 6 of the Datcom method for the interpolation procedure.)

$$\left(\frac{x'_{a.c.}}{c_{r_e}}\right)_N$$

$(f)_{equiv} = (f)_{nose} + 1.6\,(f)_{forebody}$ (Equation 4.3.2.2-d)

$= 1.75 + 1.6\,(5.33) = 10.28$

$\ell_{equiv} = (f_{equiv})\,(d) = (10.28)\,(5) = 51.4$

$\left(\frac{x_{a.c.}}{\ell_{equiv}}\right)_N = -0.545$ (Figure 4.3.2.2-36a at f_{nose})

$$\left(\frac{x'_{a.c.}}{c_{r_e}}\right)_N = \left(\frac{x_{a.c.}}{\ell_{equiv}}\right)\left(\frac{\ell_{equiv}}{c_{r_e}}\right) = (-0.545)\ \frac{51.4}{13.5} = -2.075$$

Solution:

$$\frac{x'_{a.c.}}{c_{r_e}} = \frac{\left(\frac{x'_{a.c.}}{c_{r_e}}\right)_N C_{L_{a_N}} + \left(\frac{x'_{a.c.}}{c_{r_e}}\right)_{W(B)} C_{L_{a_{W(B)}}} + \left(\frac{x'_{a.c.}}{c_{r_e}}\right)_{B(W)} C_{L_{a_{B(W)}}}}{C_{L_{a_N}} + C_{L_{a_{W(B)}}} + C_{L_{a_{B(W)}}}} \quad \text{(Equation 4.3.2.2-a)}$$

$$= \frac{(-2.075)\,(0.1567) + (0.440)\,(2.81) + (0.345)\,(0.622)}{0.1567 + 2.81 + 0.622}$$

$= 0.313$

$$\frac{x_{a.c.}}{c_r} = \left(\frac{x'_{a.c.}}{c_{r_e}}\right)\frac{c_{r_e}}{c_r} + \frac{d}{2\,c_r}\tan\Lambda_{LE} \quad \text{(Equation 4.3.2.2-b)}$$

$$= (0.313)\ \frac{13.5}{16.0} + \frac{5}{2\,(16)}\,(0.8012)$$

$= 0.389$

The calculated result compares with a test value of $\frac{x_{a.c.}}{c_r} = 0.35$ from Reference 9.

B. TRANSONIC

DATCOM METHOD

The transonic aerodynamic-center location near zero lift of a wing-body configuration with a straight-tapered wing may be approximated by the wing-body-combination approach presented in Paragraph A. In using this method at transonic speeds, care must be taken to evaluate the parameters by using the transonic methods presented in the applicable Datcom sections. The estimation of both the lift-curve slope and the aerodynamic-center location of the exposed wing at transonic speeds requires the use of data-fairing techniques outlined in Paragraphs B of Sections 4.1.3.2 and 4.1.4.2, respectively. It is suggested that the aerodynamic-center location of the wing lift carryover on the body $\left(x'_{a.c.}/c_{r_e}\right)_{B(W)}$ be estimated by the methods of Paragraphs A and C of this section, and any differences in the subsonic and supersonic values should be faired out smoothly in the transonic range. The two methods presented for estimating the aerodynamic-center location of the nose and forebody $\left(x'_{a.c.}/c_{r_e}\right)_N$ in Paragraph A of this section may be applied at transonic speeds.

The relatively simple application of the body effects on the aerodynamic-center location at transonic speeds is based on slender-body theory, which states that body force and moment characteristics are not functions of Mach number. On the other hand, the aerodynamic characteristics of wings in the transonic speed range are quite complex, and theoretical solutions are available for only a few specific planforms. Wing lift and pitching-moment characteristics at transonic speeds are discussed in Sections 4.1.3.2 and 4.1.4.2, respectively, and are not repeated here. The transonic methods of Sections 4.1.3.2 and 4.1.4.2 are applicable only to wings having symmetrical airfoils of conventional thickness distribution at low angles of attack.

C. SUPERSONIC

DATCOM METHODS

Straight-Tapered Wing-Body Configuration

The supersonic aerodynamic-center location near zero lift of a wing-body configuration with a straight-tapered wing is obtained by the wing-body-combination approach presented in Paragraph A. The procedure, applied at supersonic speeds, is outlined in the following steps:

Step 1. Divide the wing-body configuration into three components as in Step 1 of Paragraph A.

Step 2. Determine the normal-force-curve slope of the exposed wing $\left(C_{N_\alpha}\right)_e$ from the straight-tapered-wing method of Paragraph C of Section 4.1.3.2, based on its exposed area S_e.

Step 3. Determine the normal-force-curve slope of the body nose $\left(C_{N_\alpha}\right)_B$ by the method of Paragraph C of Section 4.2.1.1, based on the nose frontal area.

Step 4. Using the normal-force-curve slopes determined in Steps 2 and 3, calculate $C_{N_{\alpha_{W(B)}}}$, $C_{N_{\alpha_{B(W)}}}$, and $C_{N_{\alpha_N}}$, referred to the total wing area, by

$$C_{N_{\alpha_{W(B)}}} = K_{W(B)} \left(C_{N_\alpha}\right)_e \frac{S_e}{S_W}$$

$$C_{N_{\alpha_{B(W)}}} = K_{B(W)} \left(C_{N_\alpha}\right)_e \frac{S_e}{S_W}$$

$$C_{N_{a_N}} = \left(C_{N_a}\right)_B \frac{\pi d^2}{4S_W}$$

where $K_{W(B)}$ and $K_{B(W)}$ are interference factors obtained from Paragraph C of Section 4.3.1.2.

Step 5. Determine the a.c. location of the exposed wing as a fraction of the root chord of the exposed wing $\frac{x'_{a.c.}}{c_{r_e}}$ from Figure 4.1.4.2-26. The interference effect of the body-lift in the presence of the wing is neglected and the a.c. location of the body-lift carryover on the wing is taken as the a.c. location for the exposed wing, i.e.,

$$\left(\frac{x'_{a.c.}}{c_{r_e}}\right)_{W(B)} = \frac{x'_{a.c.}}{c_{r_e}}$$

Step 6. Determine the a.c. location of the wing-lift carryover on the body $\left(\frac{x'_{a.c.}}{c_{r_e}}\right)_{B(W)}$

Figure 4.3.2.2-37 is presented for estimating the a.c. of the lift carryover of the wing onto the body. The result is referred to the leading edge of the root chord of the exposed wing. Figure 4.3.2.2-37 is valid for

$$\beta A_e \ (1 + \lambda_e) \left(1 + \frac{1}{\beta \cot \Lambda_{LE}}\right) \geq 4.0$$

Figure 4.3.2.2-37 can be used for an approximation to $\left(\frac{x'_{a.c.}}{c_{r_e}}\right)_{B(W)}$ for the low-aspect-ratio range. However, if a more accurate result is desired, the low-aspect-ratio values may be found by cross-plotting these charts and extrapolating them to the slender-body-theory values at $\beta A_e = 0$ from Figure 4.3.2.2-36b.

Step 7. Determine the a.c. location of the body nose and forebody as a fraction of the root chord of the exposed wing $\left(\frac{x'_{a.c.}}{c_{r_e}}\right)_N$, and referred to the exposed-wing apex.

The center of pressure of the body nose and forebody as a fraction of body-nose length $\frac{x_{c.p.}}{\ell_N}$, and referred to the nose apex is obtained from Paragraph C of Section 4.2.2.1. Then

$$\left(\frac{x'_{a.c.}}{c_{r_e}}\right)_N = \frac{\ell_N}{c_{r_e}} \left(\frac{x_{c.p.}}{\ell_N} - 1\right)$$

Step 8. Using the results calculated in Steps 4 through 7, Equation 4.3.2.2-a gives the a.c. location of the wing-body configuration measured in exposed wing root chords and aft of the exposed wing apex. The a.c. location measured in wing root chords aft of the wing apex is given by Equation 4.3.2.2-b.

Sample Problem 1 on Pages 4.3.2.2-18 through 4.3.2.2-21 illustrates the use of this method.

A comparison of test data with results calculated by using this method is presented as Table 4.3.2.2-D. The limited number of test points presented precludes substantiation of this method over other than very limited ranges of planform and flow parameters. Within the linear-lift range, profile parameters such as camber, twist, and airfoil shape would be expected to have only a minor influence on the wing-body aerodynamic-center location.

It should be noted that the Datcom method for configurations with non-straight-tapered wings, which follows, uses essentially the same approach as that presented for configurations with straight-tapered wings. Therefore, substantiation of the method for non-straight-tapered wings serves to validate the method for straight-tapered wings.

Non-Straight-Tapered Wing-Body Configurations

The method for determining the supersonic aerodynamic-center location near zero lift of wing-body configurations with non-straight-tapered wings is taken from Reference 5. Both the wing-alone and the wing-body a.c.-prediction approaches are applied at supersonic speeds. Criteria have been established, during the course of the study conducted in connection with Reference 5, for determining which prediction approach is applicable to a given configuration.

The wing-body combinations are treated as wing-alone cases when the theoretical wing planform practically blankets the body. For such cases, the Datcom method for predicting the aerodynamic-center location of non-straight-tapered wings presented in Paragraph C of Section 4.1.4.2 is directly applicable. The method consists of dividing the complete theoretical planform (extended to the plane of symmetry) into two panels with each panel having conventional, straight-tapered geometry. Then for each of the constructed panels, the individual normal-force-curve slope and aerodynamic-center location are estimated by treating each constructed panel as a complete wing. The individual normal-force-curve slope and aerodynamic-center location determined for each constructed panel are then mutually combined in accordance with an "inboard-outboard" weighted-area relationship to estimate the aerodynamic-center location for the basic wing-body configuration.

The sample problem at the conclusion of Paragraph C of Section 4.1.4.2 illustrates the wing-alone approach.

The majority of the wing-body combinations investigated in Reference 5 required application of the wing-body approach to predict the linear aerodynamic-center location. This approach, introduced in this section, consists of breaking down the wing-body configuration into components and evaluating the exposed-wing lift in the presence of the body, the wing-lift carryover on the body, and the body nose effects. The basic approach is then essentially that presented for predicting the aerodynamic-center location of straight-tapered wing-body configurations at supersonic speeds. However, the method is more complex, since the exposed composite wing must be subdivided in order to estimate its normal-force-curve slope and aerodynamic-center location.

The procedure to be followed in using the wing-body approach to predict the supersonic linear aerodynamic-center location of a non-straight-tapered wing-body combination is outlined in the following steps:

Step 1. Divide the wing-body configuration into three components as follows (see Sketch (a)):

(1) The exposed composite wing in the presence of the body, denoted by the subscript W(B).

(2) The body in the presence of the wing, denoted by the subscript B(W).

(3) The body nose and forebody ahead of the wing-body juncture, denoted by the subscript N.

Step 2. Subdivide the exposed composite wing into inboard and outboard panels and determine their pertinent geometric parameters. The exposed wing is subdivided as discussed and illustrated in Paragraph A of Section 4.1.4.2 (see Pages 4.1.4.2-4 through 4.1.4.2-6). Application of that technique applied to a typical wing-body configuration is illustrated in Sketch (b).

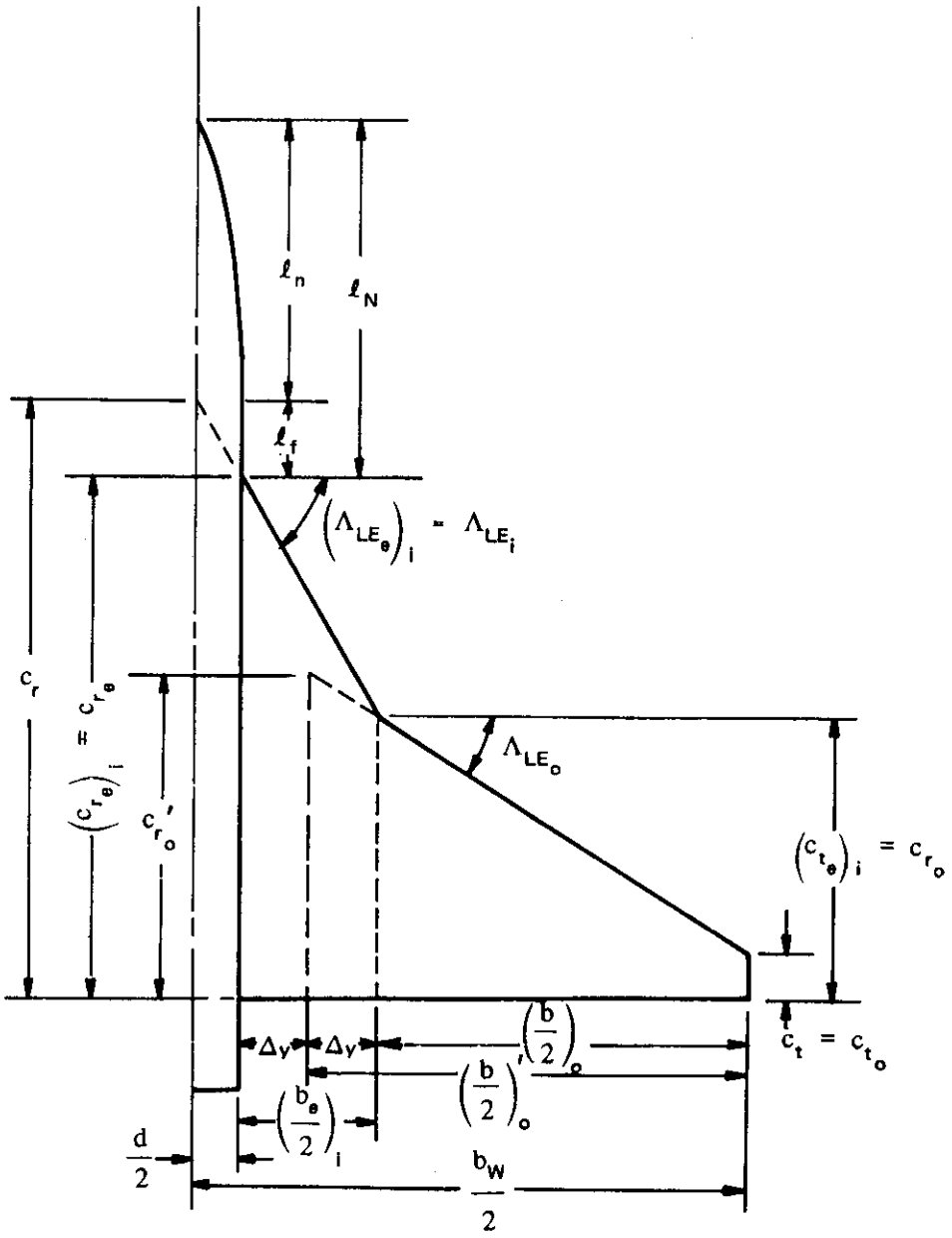

SKETCH (b)

Step 3. Determine the normal-force-curve slope $\left[\left(C_{N_\alpha}\right)_e\right]_i$ of the constructed inboard panel using the method for straight-tapered wings of Paragraph C, Section 4.1.3.2, based on the area $(S_e)_i$.

Step 4. Determine the a.c. location of the constructed inboard panel $\left(\frac{x'_{a.c.}}{c_{r_e}}\right)_i$ as a fraction of its root chord from Figure 4.1.4.2-26. This a.c. location is aft of the apex of the exposed constructed inboard panel.

Step 5. Determine the normal-force-curve slope $\left(C_{N_\alpha}\right)_o'$ of the constructed outboard panel using the method for the straight-tapered wings of Paragraph C of Section 4.1.3.2, based on the area S_o'.

Step 6. Determine the a.c. location of the constructed outboard panel $\left(\frac{x_{a.c.}}{c_r}\right)_o'$ as a fraction of its root chord from Figure 4.1.4.2-26. This a.c. location is aft of the apex of the constructed outboard panel.

Step 7. Convert the a.c. location determined in Step 6 to a fraction of the root chord of the exposed constructed inboard panel and aft of the apex of the exposed constructed inboard panel by

$$\frac{(x'_{a.c.})'_o}{\left(c_{r_e}\right)_i} = \left(\frac{x_{a.c.}}{c_r}\right)_o' \frac{c_{r_o}'}{\left(c_{r_e}\right)_i} - \frac{\Delta y}{\left(c_{r_e}\right)_i} \tan \Lambda_{LE_o} + \frac{(b_e)_i}{2\left(c_{r_e}\right)_i} \tan \Lambda_{LE_i} \qquad 4.3.2.2\text{-e}$$

Step 8. Calculate the a.c. location for the exposed composite wing, measured in root chords of the exposed inboard panel, aft of the exposed composite-wing apex by

$$\frac{x'_{a.c.}}{c_{r_e}} = \frac{\left[\left(C_{N_\alpha}\right)_e\right]_i (S_e)_i \left(\frac{x'_{a.c.}}{c_{r_e}}\right)_i + \left(C_{N_\alpha}\right)_o' S_o' \frac{(x'_{a.c.})'_o}{\left(c_{r_e}\right)_i}}{\left[\left(C_{N_\alpha}\right)_e\right]_i (S_e)_i + \left(C_{N_\alpha}\right)_o' S_o'} \qquad 4.3.2.2\text{-f}$$

Step 9. Calculate the normal-force-curve slope for the exposed composite wing, based on the exposed wing area, by

$$\left(C_{N_\alpha}\right)_e = \frac{\left[\left(C_{N_\alpha}\right)_e\right]_i (S_e)_i + \left(C_{N_\alpha}\right)_o' S_o'}{(S_e)_i + S_o'} \qquad 4.3.2.2\text{-g}$$

Step 10. Determine the normal-force-curve slope of the body nose $\left(C_{N_\alpha}\right)_B$ by the method of Paragraph C of Section 4.2.1.1, based on the nose frontal area.

Step 11. Using the normal-force-curve slopes determined in Steps 9 and 10, calculate $C_{N_{\alpha_{W(B)}}}$, $C_{N_{\alpha_{B(W)}}}$, and $C_{N_{\alpha_N}}$, referred to the total wing area, by

$$C_{N_{a_{W(B)}}} = K_{W(B)} \left(C_{N_a}\right)_e \frac{(S_e)_i + S'_o}{S_W}$$

$$C_{N_{a_{B(W)}}} = K_{B(W)} \left(C_{N_a}\right)_e \frac{(S_e)_i + S'_o}{S_W}$$

$$C_{N_{a_N}} = \left(C_{N_a}\right)_B \frac{\pi d^2}{4S_W}$$

where $K_{W(B)}$ and $K_{B(W)}$ are interference factors obtained from Paragraph C of Section 4.3.1.2. The design charts of Section 4.3.1.2 are entered with the following geometric parameters:

A_e is the aspect ratio of the exposed composite wing.

λ_e is the taper ratio of the exposed composite wing $c_t/\left(c_{r_e}\right)_i$

Λ_{LE} is replaced by Λ_{LE_i}.

b is the total wing span (to body center line).

c_{r_e} is replaced by $\left(c_{r_e}\right)_i$.

Step 12. Determine the a.c. location of the exposed wing in the presence of the body $\left(\frac{x'_{a.c.}}{c_{r_e}}\right)_{W(B)}$. Th interference effect of the body lift in the presence of the wing is neglected and

$$\left(\frac{x'_{a.c.}}{c_{r_e}}\right)_{W(B)} = \frac{x'_{a.c.}}{c_{r_e}} \text{ (from Step 8)}$$

Step 13. Determine the a.c. location of the wing-lift carryover on the body $\left(\frac{x'_{a.c.}}{c_{r_e}}\right)_{B(W)}$ by the procedure outlined in Step 6 of the supersonic Datcom method for determining $\left(\frac{x'_{a.c.}}{c_{r_e}}\right)_{B(W)}$ for a straight-tapered wing-body configuration (Page 4.3.2.2-12). In applying that procedure the geometric parameters to be used are those defined in Step 11 of this method (see above).

Step 14. Determine the a.c. location of the body nose as a fraction of the root chord of the exposed wing $\left(\frac{x'_{a.c.}}{c_{r_e}}\right)_N$, and referred to the exposed-wing apex,by the procedure outlined in Step 7 of the Datcom method for a straight-tapered wing-body configuration (Page 4.3.2.2-12).

Step 15. Using the results calculated in Steps 11 through 14, Equation 4.3.2.2-a gives the a.c. location of the wing-body configuration measured in root chords of the exposed composite wing and aft of the apex of the exposed composite wing. The a.c. location, measured in root chords of the composite wing and aft of the wing apex, is given by Equation 4.3.2.2-b. In applying Equation 4.3.2.2-b the leading-edge sweep angle is that of the inboard panel Λ_{LE_i}.

This method is illustrated by Sample Problem 2 on Pages 4.3.2.2-21 through 4.3.2.2-26.

Comparisons of test data with results calculated by using this method are presented in Tables 4.3.2.2-E and 4.3.2.2-F (both taken from Reference 5) for configurations with double-delta and cranked wings, respectively The test data indicate that within the linear-lift range, profile parameters such as camber, twist, and airfoil shape have only a minor effect on the wing-body aerodynamic-center location. The ranges of planform parameters of the test data are:

Double-Delta Configurations	Cranked Configurations
$1.3 \leqslant A \leqslant 3.0$	$1.88 \leqslant A \leqslant 4.60$
$0 \leqslant \lambda \leqslant 0.143$	$0.086 \leqslant \lambda \leqslant 0.333$
$0.217 \leqslant \eta_B \leqslant 0.710$	$0.400 \leqslant \eta_B \leqslant 0.700$
$60^o \leqslant \Lambda_{LE_i} \leqslant 82.9^o$	$60^o \leqslant \Lambda_{LE_i} \leqslant 70.7^o$
$35^o \leqslant \Lambda_{LE_o} \leqslant 60^o$	$35^o \leqslant \Lambda_{LE_o} \leqslant 75^o$

The range of Mach number for both of these configurations is $1.0 \leqslant M \leqslant 3.0$.

The test configurations investigated have only one break in the leading-edge sweep, and for those configurations with both leading- and trailing-edge breaks, both breaks occur at the same span station.

Three double-delta configurations of Table 4.3.2.2-E meet the criteria established for the wing-alone prediction technique. Satisfactory results were obtained for each of these configurations by using the wing-alone approach. These cases are noted in Table 4.3.2.2-E. All the cranked-wing test configurations of Table 4.3.2.2-F were analyzed by using the wing-body approach.

It should be noted that several configurations which meet the prediction criteria for the wing-body approach have been evaluated by using the wing-alone approach, in which the wing-lift carryover and body-nose effects are neglected. The wing-alone approach did not yield satisfactory predictions for any of those configurations.

Although the techniques are applicable to wing-body combinations with curved wings, test data are not available for substantiation purposes. Only one wing-body combination with a curved wing has been investigated at supersonic speeds. Since this configuration has a very small body and the planform projection effectively blankets nearly all the body, it has been included in the curved wing-alone substantiation of Section 4.1.4.2 (Table 4.1.4.2-C).

Sample Problems

1. Straight-Tapered Wing-Body Configuration

Given: A wing-body configuration of Reference 26.

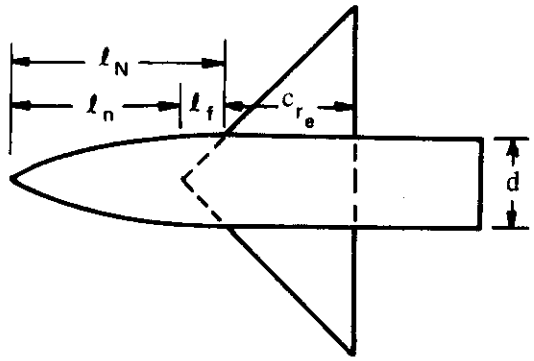

Total-Wing Characteristics:

$A_W = 4.0 \quad S_W = 13.99$ sq in. $\quad \lambda_W = 0$

$\Lambda_{LE_W} = 45^o \quad b_W = 7.48$ in.

$c_{r_W} = 3.74$ in.

Airfoil: 8-percent-thick double wedge (free-stream direction)

Exposed-Wing Characteristics:

$$A_e = 4.0 \quad \lambda_e = 0 \quad \Lambda_{LE_e} = \Lambda_{LE_W} = 45^o$$

$$c_{r_e} = 3.0 \text{ in.} \quad \frac{S_e}{S_W} = 0.64$$

Body-Nose Characteristics:

Ogive-cylinder $\quad d = 1.50$in. $\quad \dfrac{d}{b_W} = 0.20 \quad \ell_N = 5.0$ in.

$$\ell_n = 4.25 \text{ in.} \quad f_{nose} = \frac{\ell_n}{d} = 2.83$$

$$\ell_f = \ell_{forebody} = 0.75 \text{ in.} \quad f_{forebody} = \frac{\ell_f}{d} = 0.50$$

Additional Characteristics:

$M = 1.50$; $\beta = 1.12$

Compute:

$\left(C_{N_\alpha}\right)_e$ (Section 4.1.3.2)

$$\frac{\tan \Lambda_{LE}}{\beta} = \frac{1.00}{1.12} = 0.893 \text{ ; } A_e \tan \Lambda_{LE} = (4.0)(1.00) = 4.00$$

$$\beta \left[\left(C_{N_\alpha}\right)_{theory}\right]_e = 4.0 \text{ per rad (Figure 4.1.3.2-56a)}$$

$$\left[\left(C_{N_\alpha}\right)_{\text{theory}}\right]_e = 4.0/1.12 = 3.57 \text{ per rad}$$

$$\delta_\perp = \frac{\tan^{-1}\ \frac{0.04}{0.50}}{\cos \Lambda_{LE}} = 6.48^o$$

$$\left[\frac{C_{N_\alpha}}{\left(C_{N_\alpha}\right)_{\text{theory}}}\right]_e = 0.884 \text{ (Figure 4.1.3.2-60)}$$

$$\left(C_{N_\alpha}\right)_e = \left[\frac{C_{N_\alpha}}{\left(C_{N_\alpha}\right)_{\text{theory}}}\right]_e \left[\left(C_{N_\alpha}\right)_{\text{theory}}\right]_e = 0.884\ (3.57) = 3.16 \text{ per rad}$$

$\left(C_{N_\alpha}\right)_B$ (Section 4.2.1.1)

$$\frac{\beta}{f_n} = \frac{1.12}{2.83} = 0.396\ ;\ \frac{f_f}{f_n} = \frac{0.50}{2.83} = 0.177$$

$\left(C_{N_\alpha}\right)_B = 2.60$ per rad (based on nose frontal area) (Figure 4.2.1.1-21a)

Interference factors (Section 4.3.1.2)

$K_{W(B)} = 1.17$ (Figure 4.3.1.2-10 at $\frac{d}{b_W} = 0.20$)

$K_{B(W)}$ (Figure 4.3.1.2-11a)

$$\frac{\beta d}{c_{r_e}} = \frac{(1.12)\ (1.50)}{3.0} = 0.560\ ;\ \beta \cot \Lambda_{LE} = (1.12)\ (1.00) = 1.12$$

$$\left[\beta \left(C_{N_\alpha}\right)_e\ (\lambda_e + 1)\left(\frac{b}{d} - 1\right)\right] = 1.12\ (3.16)\ (1.0)\ (4.0) = 14.16$$

$$K_{B(W)}\left[\beta \left(C_{N_\alpha}\right)_e\ (\lambda_e + 1)\left(\frac{b}{d} - 1\right)\right] = 3.60 \text{ (Figure 4.3.1.2-11a)}$$

$K_{B(W)} = 3.60/14.16 = 0.254$

Component normal-force-curve slopes, referred to S_W

$$C_{N_{\alpha_{W(B)}}} = K_{W(B)}\ \left(C_{N_\alpha}\right)_e \frac{S_e}{S_W} = 1.17\ (3.16)\ (0.64) = 2.37 \text{ per rad}$$

$$C_{N_{\alpha_{B(W)}}} = K_{B(W)} \left(C_{N_\alpha}\right)_e \frac{S_e}{S_W} = 0.254 \ (3.16)\,(0.64) = 0.514 \text{ per rad}$$

$$C_{N_{\alpha_N}} = \left(C_{N_\alpha}\right)_B \frac{\pi d^2}{4S_W} = 2.60 \ \frac{\pi(1.5)^2}{4(13.99)} = 0.328 \text{ per rad}$$

$\left(\frac{x'_{a.c.}}{c_{r_e}}\right)_{W(B)}$ (Section 4.1.4.2)

$\frac{x'_{a.c.}}{c_{r_e}} = 0.670$ (Figure 4.1.4.2-26a)

$$\left(\frac{x'_{a.c.}}{c_{r_e}}\right)_{W(B)} = \frac{x'_{a.c.}}{c_{r_e}} = 0.670$$

$\left(\frac{x'_{a.c.}}{c_{r_e}}\right)_{B(W)}$

$$\beta A_e \ (1 + \lambda_e) \left(1 + \frac{1}{\beta \cot \Lambda_{LE}}\right) = (1.12)\,(4.0)\,(1.0) \left(1 + \frac{1}{1.12}\right) = 8.48; > 4.0.$$

$\left(\frac{x'_{a.c.}}{c_{r_e}}\right)_{B(W)} = 0.800$ (Figure 4.3.2.2-37a)

$\left(\frac{x'_{a.c.}}{c_{r_e}}\right)_N$

$\frac{x_{c.p.}}{\ell_N} = 0.488$ (Figure 4.2.2.1-18a)

$$\left(\frac{x'_{a.c.}}{c_{r_e}}\right)_N = \frac{\ell_N}{c_{r_e}} \left(\frac{x_{c.p.}}{\ell_N} - 1\right) = \frac{5}{3} \ (0.488 - 1) = -0.853$$

Solution:

$$\frac{x'_{a.c.}}{c_{r_e}} = \frac{\left(\frac{x'_{a.c.}}{c_{r_e}}\right)_N C_{N_{\alpha_N}} + \left(\frac{x'_{a.c.}}{c_{r_e}}\right)_{W(B)} C_{N_{\alpha_{W(B)}}} + \left(\frac{x'_{a.c.}}{c_{r_e}}\right)_{B(W)} C_{N_{\alpha_{B(W)}}}}{C_{N_{\alpha_N}} + C_{N_{\alpha_{W(B)}}} + C_{N_{\alpha_{B(W)}}}}$$ (Equation 4.3.2.2-a)

$$= \frac{-0.853\,(0.328) + 0.670\,(2.37) + 0.800\,(0.514)}{0.328 + 2.37 + 0.514}$$

$$= 0.535$$

$$\frac{x_{a.c.}}{c_r} = \left(\frac{x'_{a.c.}}{c_{r_e}}\right)\left(\frac{c_{r_e}}{c_r}\right) + \frac{d}{2c_r}\tan\Lambda_{LE} \quad \text{(Equation 4.3.2.2-b)}$$

$$= 0.535\left(\frac{3}{3.74}\right) + \frac{1.5\,(1.0)}{2(3.74)} = 0.630$$

The calculated result compares with a test value of $\frac{x_{a.c.}}{c_r} = 0.62$ from Reference 26.

2. Non-Straight-Tapered Wing-Body Combination

Given: The wing-body combination of Reference 32 designated 6-67-67.

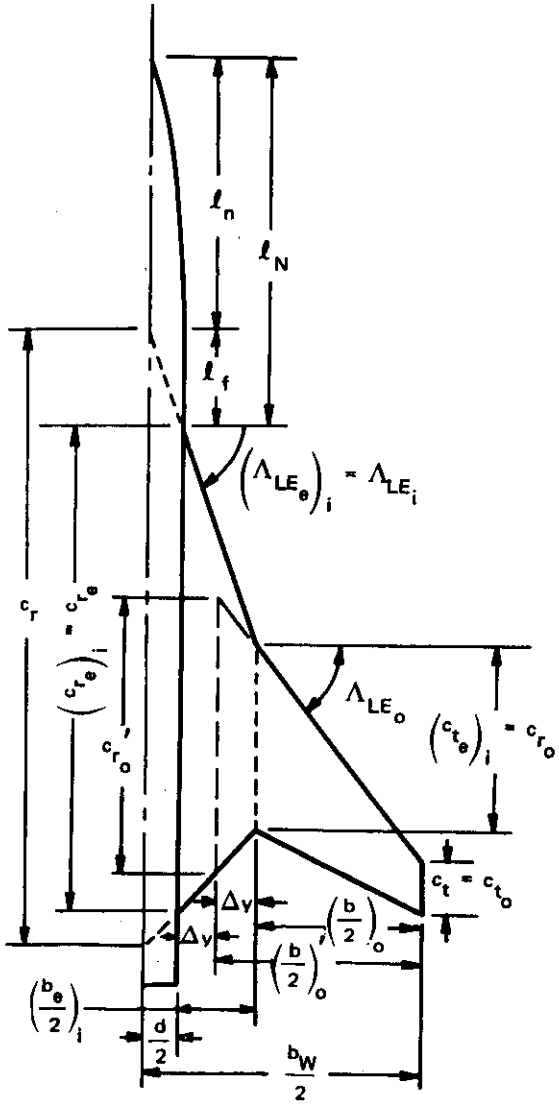

Total-Wing Characteristics:

$A_W = 2.42$ $S_W = 238.0$ sq in. $\lambda_W = 0.086$

$\Lambda_{LE_i} = 70.67^o$ $\Lambda_{LE_o} = 51.63^o$ $\eta_B = 0.40$

$\Lambda_{TE_i} = -47.37^o$ $\Lambda_{TE_o} = 26.62^o$ $c_t = 2.29$ in.

$c_r = 26.63$ in. $b_W = 24.0$ in.

Airfoil: 6% hexagonal with maximum thickness at c/3 (streamwise)

Exposed-Wing Characteristics:

$A_e = 1.82$ $\lambda_e = 0.110$ $c_{r_e} = 20.76$ in.

$b_e = 21.0$ in.

Body-Nose Characteristics:

Ogive-cylinder $d = 3.0$ in. $\frac{d}{b_W} = 0.125$

$\ell_n = 10.5$ in. $f_n = 3.50$

$\ell_f = \ell_{forebody} = 5.33$ in. $f_f = 1.78$

$\ell_N = 15.83$ in.

Constructed-Exposed-Inboard-Panel Characteristics:

$(A_e)_i = 0.463 \quad (\lambda_e)_i = 0.374 \quad \left(c_{r_e}\right)_i = 20.76 \text{ in.} \quad \left(\Lambda_{LE_e}\right)_i = \Lambda_{LE_i} = 70.67^o$

$\left(\frac{b_e}{2}\right)_i = 3.30 \text{ in.} \quad \Delta y = 1.65 \text{ in.} \quad (S_e)_i = 94.15 \text{ sq in.}$

Constructed-Exposed-Outboard-Panel Characteristics:

$A_o' = 3.13 \quad \lambda_o' = 0.254 \quad c_{r_o}' = 9.03 \text{ in.} \quad \Lambda_{LE_o}' = \Lambda_{LE_o} = 51.63^o$

$\left(\frac{b}{2}\right)_o' = 8.85 \text{ in.} \quad S_o' = 100.2 \text{ sq in.}$

Additional Characteristics:

$M = 2.01 \; ; \; \beta = 1.744$

Compute:

$\left[\left(C_{N_\alpha}\right)_e\right]_i$ (Section 4.1.3.2)

$\frac{\beta}{\tan \Lambda_{LE_i}} = \frac{1.744}{\tan 70.67^o} = 0.6117; \; \left[(A \tan \Lambda_{LE})_e\right]_i = (0.463)(\tan 70.67^o) = 1.32$

$\tan \Lambda_{LE_i} \left[\left(C_{N_\alpha}\right)_{e_{theory}}\right]_i = 2.30 \text{ per rad}$ (Figures 4.1.3.2-56c through -56e, interpolated)

$\left[\left(C_{N_\alpha}\right)_{e_{theory}}\right]_i = 0.807 \text{ per rad}$

$\delta_\perp = \frac{\tan^{-1} \frac{0.03}{0.333}}{\cos \Lambda_{LE_i}} = 15.63^o \; ; \; \Delta y_\perp = 5.85 \tan \delta_\perp = 1.638$

$\left[\frac{\left(C_{N_\alpha}\right)_e}{\left(C_{N_\alpha}\right)_{e_{theory}}}\right]_i = 0.920$ (Figure 4.1.3.2-60)

$\left[\left(C_{N_\alpha}\right)_e\right]_i = \left[\frac{\left(C_{N_\alpha}\right)_e}{\left(C_{N_\alpha}\right)_{e_{theory}}}\right]_i \left[\left(C_{N_\alpha}\right)_{e_{theory}}\right]_i = 0.742 \text{ per rad}$

$\left(\frac{x'_{a.c.}}{c_{r_e}}\right)_i$ (Section 4.1.4.2)

$\left(\frac{x'_{a.c.}}{c_{r_e}}\right)_i = 0.430$ (Figures 4.1.4.2-26c through -26e, interpolated)

$\left(C_{N_\alpha}\right)'_o$ (Section 4.1.3.2)

$\frac{\tan \Lambda_{LE_o}}{\beta} = \frac{\tan 51.63^o}{1.744} = 0.724$; $(A \tan \Lambda_{LE})'_o \doteq (3.13)(\tan 51.63^o) = 3.95$

$\beta \left[\left(C_{N_\alpha}\right)_{theory}\right]'_o = 4.18$ per rad (Figures 4.1.3.2-56b through -56d, interpolated)

$\left[\left(C_{N_\alpha}\right)_{theory}\right]'_o \doteq 2.40$ per rad

$\delta_\perp = \frac{\tan^{-1} \frac{0.03}{0.333}}{\cos \Lambda_{LE_o}} = 8.30^o$

$\left[\frac{C_{N_\alpha}}{\left(C_{N_\alpha}\right)_{theory}}\right]'_o = 0.896$ (Figure 4.1.3.2-60)

$\left(C_{N_\alpha}\right)'_o = \left[\frac{C_{N_\alpha}}{\left(C_{N_\alpha}\right)_{theory}}\right]'_o \left[\left(C_{N_\alpha}\right)_{theory}\right]'_o \doteq 2.15$ per rad

$\left(\frac{x_{a.c.}}{c_r}\right)'_o$ (Section 4.1.4.2)

$\left(\frac{x_{a.c.}}{c_r}\right)'_o = 0.863$ (Figures 4.1.4.2-26b through -26d, interpolated)

$\frac{(x'_{a.c.})'_o}{\left(c_{r_e}\right)_i} = \left(\frac{x_{a.c.}}{c_r}\right)'_o \frac{c_{r_o}}{\left(c_{r_e}\right)_i} - \frac{\Delta y}{\left(c_{r_e}\right)_i} \tan \Lambda_{LE_o} + \frac{(b_e)_i}{2\left(c_{r_e}\right)_i} \tan \Lambda_{LE_i}$ (Equation 4.3.2.2-e)

$= 0.863 \frac{9.03}{20.76} - \frac{1.65}{20.76}(1.2631) + \frac{3.30}{20.76}(2.851) = 0.728$

Determine the a.c. location of the exposed composite wing $\frac{x'_{a.c.}}{c_{r_e}}$

$$\frac{x'_{a.c.}}{c_{r_e}} = \frac{\left[\left(C_{N_\alpha}\right)_e\right]_i (S_e)_i \left(\frac{x'_{a.c.}}{c_{r_e}}\right)_i + \left(C_{N_\alpha}\right)'_o S'_o \frac{(x'_{a.c.})'_o}{\left(c_{r_e}\right)_i}}{\left[\left(C_{N_\alpha}\right)_e\right]_i (S_e)_i + \left(C_{N_\alpha}\right)'_o S'_o} \quad \text{(Equation 4.3.2.2-f)}$$

$$= \frac{0.742\,(94.15)\,(0.430) + 2.15\,(100.2)\,(0.728)}{0.742\,(94.15) + 2.15\,(100.2)}$$

$$= 0.655$$

Determine the normal-force-curve slope of the exposed composite wing $\left(C_{N_\alpha}\right)_e$

$$\left(C_{N_\alpha}\right)_e = \frac{\left[\left(C_{N_\alpha}\right)_e\right]_i (S_e)_i + \left(C_{N_\alpha}\right)'_o S'_o}{(S_e)_i + S'_o} \quad \text{(Equation 4.3.2.2-g)}$$

$$= \frac{0.742\,(94.15) + 2.15\,(100.2)}{94.15 + 100.2}$$

$$= 1.468 \text{ per rad}$$

$\left(C_{N_\alpha}\right)_B$ (Section 4.2.1.1)

$$\frac{\beta}{f_n} = \frac{1.744}{3.50} = 0.50 \; ; \frac{f_f}{f_n} = \frac{1.78}{3.50} = 0.51$$

$\left(C_{N_\alpha}\right)_B = 2.78$ per rad (Figure 4.2.1.1-21a)

Interference factors (Section 4.3.1.2) (See Step 11 of Datcom method for correct geometric parameters, Page 4.3.2.2-16.)

$K_{W(B)} = 1.10$ (figure 4.3.1.2-10 at $\frac{d}{b_W} = 0.125$)

$K_{B(W)}$

$$\beta A_e (1 + \lambda_e) \left(\frac{\tan \Lambda_{LE_i}}{\beta} + 1\right) = (1.744)(1.82)(1.110)\left(\frac{2.851}{1.744} + 1\right) = 9.28;$$

therefore, use Figure 4.3.1.2-11a.

$$\left[\beta \left(C_{N_\alpha}\right)_e (\lambda_e + 1)\left(\frac{b}{d} - 1\right)\right] = 1.744\,(1.468)\,(1.110)\,(7.0) = 19.89$$

$$\beta \cot \Lambda_{LE_i} = (1.744)(0.3508) = 0.612; \quad \frac{\beta d}{(c_{r_e})_i} = \frac{(1.744)(3.0)}{20.76} = 0.252$$

$$K_{B(W)} \left[\beta (C_{N_\alpha})_e \ (\lambda_e + 1) \left(\frac{b}{d} - 1 \right) \right] = 2.90 \quad \text{(Figure 4.3.1.2-11a)}$$

$$K_{B(W)} = 0.147$$

Component normal-force-curve slopes, referred to S_W

$$C_{N_{\alpha_{W(B)}}} = K_{W(B)} (C_{N_\alpha})_e \frac{(S_e)_i + S'_o}{S_W} = 1.10\,(1.468) \frac{94.15 + 100.2}{238.0} = 1.32 \text{ per rad}$$

$$C_{N_{\alpha_{B(W)}}} = K_{B(W)} (C_{N_\alpha})_e \frac{(S_e)_i + S'_o}{S_W} = 0.147\,(1.468) \frac{94.15 + 100.2}{238.0} = 0.176 \text{ per rad}$$

$$C_{N_{\alpha_N}} = (C_{N_\alpha})_B \frac{\pi d^2}{4 S_W} = (2.78) \frac{\pi 9}{4(238)} = 0.0826 \text{ per rad}$$

$\left(\frac{x'_{a.c.}}{c_{r_e}} \right)_{W(B)}$ The interference effect of the body is neglected.

$$\left(\frac{x'_{a.c.}}{c_{r_e}} \right)_{W(B)} = \frac{x'_{a.c.}}{c_{r_e}} = 0.655 \text{ (calculated on Page 4.3.2.2-24)}$$

$\left(\frac{x'_{a.c.}}{c_{r_e}} \right)_{B(W)}$ (See Step 11 of Datcom method for correct geometric parameters, Page 4.3.2.2-16.)

$$\left(\frac{x'_{a.c.}}{c_{r_e}} \right)_{B(W)} = 0.640 \text{ (Figure 4.3.2.2-37a)}$$

$\left(\frac{x'_{a.c.}}{c_{r_e}} \right)_N$

$$\frac{x_{c.p.}}{\ell_N} = 0.405 \text{ (Figure 4.2.2.1-18a)}$$

$$\left(\frac{x'_{a.c.}}{c_{r_e}} \right)_N = \frac{\ell_N}{c_{r_e}} \left(\frac{x_{c.p.}}{\ell_N} - 1 \right) = \frac{15.83}{20.76} (0.405 - 1) = -0.454$$

Solution:

$$\frac{x'_{a.c.}}{c_{r_e}} = \frac{\left(\frac{x'_{a.c.}}{c_{r_e}}\right)_N C_{N_{a_N}} + \left(\frac{x'_{a.c.}}{c_{r_e}}\right)_{W(B)} C_{N_{a_{W(B)}}} + \left(\frac{x'_{a.c.}}{c_{r_e}}\right)_{B(W)} C_{N_{a_{B(W)}}}}{C_{N_{a_N}} + C_{N_{a_{W(B)}}} + C_{N_{a_{B(W)}}}} \quad \text{(Equation 4.3.2.2-a)}$$

$$= \frac{-0.454\,(0.0826) + 0.655\,(1.32) + 0.640\,(0.176)}{0.0826 + 1.32 + 0.176}$$

$$= 0.595$$

$$\frac{x_{a.c.}}{c_r} = \left(\frac{x'_{a.c.}}{c_{r_e}}\right)\left(\frac{c_{r_e}}{c_r}\right) + \frac{d}{2c_r} \tan \Lambda_{LE_i} \quad \text{(Equation 4.3.2.2-b)}$$

$$= 0.595 \quad \frac{20.76}{26.63} + \frac{3}{2(26.63)} \quad (2.851)$$

$$= 0.624$$

The calculated result compares with a test value of $\frac{x_{a.c.}}{c_r} = 0.626$ from Reference 32.

REFERENCES

1. Pitts, W., Nielsen, J., and Kaattari, G.: Lift and Center of Pressure of Wing-Body-Tail Combinations at Subsonic, Transonic, and Supersonic Speeds. NACA TR 1307, 1957. (U)

2. Spreiter, J.: The Aerodynamic Forces on Slender Plane- and Cruciform-Wing and Body Combinations. NACA TR 962, 1950. (U)

3. Letko, W., and Williams, J.: Experimental Investigation at Low Speed of Effects of Fuselage Cross Section on Static Longitudinal and Lateral Stability Characteristics of Models Having 0^o and 45^o Sweptback Surfaces. NACA TN 3551, 1955. (U)

4. Spearman, L.: Investigation of the Aerodynamic Characteristics in Pitch and Sideslip of a 45^o Sweptback-Wing Airplane Model With Various Vertical Locations of the Wing and Horizontal Tail. NACA RM L55B18, 1955. (U)

5. Benepe, D. B., Kouri, B. G., Webb, J. B., et al: Aerodynamic Characteristics of Non-Straight-Taper Wings. AFFDL-TR-66-73, 1966. (U)

6. Foster, G., and Fitzpatrick, J.: Longitudinal-Stability Investigation of High-Lift and Stall-Control Devices on a 52^o Sweptback Wing with and Without Fuselage and Horizontal Tail at a Reynolds Number of 6.8×10^6. NACA RM L8I08, 1948. (U)

7. Wiggins, J., and Kuhn, R. E.: Wind-Tunnel Investigation of the Aerodynamic Characteristics in Pitch of Wing-Fuselage Combinations at High-Subsonic Speeds – Sweep Series. NACA RM L52D18, 1952. (U)

8. Johnson, H.: Wind-Tunnel Investigation at Low Speed of the Effect of Varying the Ratio of Body Diameter to Wing Span from 0.1 to 0.8 on the Aerodynamic Characteristics in Pitch of a 45^o Sweptback-Wing-Body Combination. NACA RM L53J09a, 1953. (U)

9. Goodson, K.: Effect of Nose Length, Fuselage Length, and Nose Fineness Ratio on the Longitudinal Aerodynamic Characteristics of Two Complete Models at High Subsonic Speeds. NASA Memo 10-10-58L, 1958. (U)

10. Anon: Small-Scale Wing-Body Planform Investigation at Mach Numbers from 0.40 to 2.94. Unpublished Data. (U)

11. Kuhns, R. M.: HSWT-083-0 Analysis Report, Supersonic Transport Lifting Fuselage Investigation. Convair, General Dynamics, San Diego Report AD-SST-012, 1961. (U)

12. Anon: Large-Scale Double-Delta Wing-Body Planform Investigation at Low Speed. Unpublished Data. (U)

13. Kuhns, R. M.: LSWT-322 Analysis Report, Supersonic Transport Low-Speed Investigation. Convair, General Dynamics, San Diego Report AD-SST-016, 1961. (U)

14. Anon: System 125A, Convair Model 25, Summary Data Report, Subsonic Tests of a Preliminary 1/27-Scale Force Model (CVAL 201). Convair, General Dynamics, F/W Report FZT-25-004, 1956. (C) Title Unclassified

15. Anon: System 125A, Convair Model 25 Preliminary Design Proposal, Summary of Wind-Tunnel Results on Wing-Tip Configurations. Convair, General Dynamics, F/W Report FZA-25-017, 1956. (C) Title Unclassified

16. Koenig, D. G., and Corsiglia, V. R.: Large-Scale Low-Speed Wind-Tunnel Tests of a Delta-Wing Supersonic-Transport Model With Various Canard, Horizontal-Tail, and Wing Modifications. NASA TM X-857, 1964. (C) Title Unclassified

17. Grant, F. C., and Sevier, J. R., Jr.: Transonic and Supersonic Wind-Tunnel Tests of Wing-Body Combinations Designed for High Efficiency at a Mach Number of 1.41. NASA TN D-435, 1960. (U)

18. Mansell, C. J.: Low-Speed Wind-Tunnel Tests on Two Thin Cranked Wings With 60-Degree Sweepback Inboard. ARC R&M 2995, 1957. (U)

19. Jernell, L. S.: The Effects of Conical Camber on the Longitudinal Aerodynamic Characteristics of a Variable-Sweep Wing-Fuselage Configuration at Mach Numbers From 0.50 to 3.50. NASA TM X-804, 1964. (C) Title Unclassified

20. Trescot, C. D., and Spencer, B., Jr.: Effect of Reynolds Number on the Low-Speed Longitudinal Aerodynamic Characteristics of Two Variable-Wing-Sweep Airplane Configurations. NASA TM X-434, 1961. (C) Title Unclassified

21. Spencer, B., Jr.: Low-Speed Longitudinal Aerodynamic Characteristics Associated With Variations in the Geometry of the Fixed Portion of a Variable-Wing-Sweep Airplane Configuration Having an Outboard Pivot. NASA TM X-625, 1962. (C) Title Unclassified

22. Spencer, B., Jr.: Stability and Control Characteristics at Low Subsonic Speeds of an Airplane Configuration Having Two Types of Variable-Sweep Wings. NASA TM X-303, 1960. (U)

23. Spearman, M. L.: Longitudinal and Lateral Aerodynamic Characteristics at Mach Numbers From 0.60 to 2.20 of a Variable-Sweep Fighter Model With Sweep Angles From 25° to 75°. NASA TM X-710, 1962. (C) Title Unclassified

24. Sleeman, W. C., Jr., and Robins, A. W.: Low-Speed Investigation of the Aerodynamic Characteristics of a Variable-Sweep Supersonic Transport Configuration Having a Blended Wing and Body. NASA TM X-619, 1961. (C) Title Unclassified

25. Henderson, W. P.: Low-Speed Longitudinal Stability Characteristics of a Supersonic Transport Configuration With Variable-Sweep Wings Employing a Double Inboard Pivot. NASA TM X-744, 1963. (C) Title Unclassified

26. Nielsen, J., Katzen, E., and Tang, K.: Lift and Pitching-Moment Interference Between a Pointed Cylindrical Body and Triangular Wings of Various Aspect Ratios at Mach Numbers of 1.50 and 2.02. NACA TN 3795, 1956. (U)

27. Robinson, R.: Aerodynamic Characteristics at Supersonic Speeds of a Series of Wing-Body Combinations Having Cambered Wings With an Aspect Ratio of 3.5 and a Taper Ratio of 0.2. Effects of Sweep Angle and Thickness Ratio on the Aerodynamic Characteristics in Pitch at M = 2.01. NACA RM L52E09, 1952. (U)

28. Sevier, J. R., Jr.: Aerodynamic Characteristics at Mach Numbers of 1.41 and 2.01 of a Series of Cranked Wings Ranging in Aspect Ratio From 4.0 to 1.74 in Combination With a Body. NASA TM X-172, 1960. (U)

29. Bryson, R. B.: Project MX-1964, Summary Data Report of Force Tests of B-58 Airplane Models With a Linearizer. CVAL 269, ARC 9 x 7 Test 43. Convair, General Dynamics, F/W Report FZT-4-206, 1959. (U)

30. Foster, G. V.: Exploratory Investigation at Mach Number of 2.01 of the Longitudinal Stability and Control Characteristics of a Winged Reentry Configuration. NASA TM X-178, 1959. (U)

31. Pierce, S. R.: System 126A, Convair Model 25 Summary Data Report, Wind-Tunnel Tests of a 1/125-Scale Model. JPL 20-202, Convair, General Dynamics, F/W Report FZT-25-006, 1956. (C) Title Unclassified

32. Cooper, M. and Sevier, J. R., Jr.: Effects of a Series of Inboard Plan-Form Modifications on the Longitudinal Characteristics of Two 47° Sweptback Wings of Aspect Ratio 3.5, Taper Ratio 0.2, and Different Thickness Distributions at Mach Numbers of 1.61 and 2.01. NACA RM L53E07a, 1953. (U)

33. Sevier, J. R., Jr.: Investigation of the Effects of Body Indentation and Wing-Plan-Form Modification on the Longitudinal Characteristics of a 60° Swept-Wing-Body Combination at Mach Numbers of 1.41, 1.61, and 2.01. NACA RM L55E17, 1955. (U)

34. Foster, G. V.: Stability and Control Characteristics at Mach Numbers of 2.50, 3.00, and 3.71 of a Variable-Wing-Sweep Configuration With Outboard Wing Panels Swept Back 75°. NASA TM X-267, 1960. (U)

35. Alford, W. J., Jr., Luoma, A. A., and Henderson, W. P.: Wind-Tunnel Studies at Subsonic and Transonic Speeds of a Multiple-Mission Variable-Wing-Sweep Airplane Configuration. NASA TM X-206, 1959. (U)

36. Jones, R. T.: Properties of Low-Aspect-Ratio Pointed Wings at Speeds Below and Above the Speed of Sound. NACA TR 835, 1946. (U)

37. Lawrence, H. R.: The Lift Distribution on Low Aspect Ratio Wings at Subsonic Speeds. Jour. Aero. Sci., Vol. 18, No. 10, October, 1951. (U)

TABLE 4.3.2.2-A

SUBSONIC AERODYNAMIC-CENTER LOCATIONS OF WING-BODY COMBINATIONS WITH STRAIGHT-TAPERED WINGS

DATA SUMMARY AND SUBSTANTIATION

Ref.	$\frac{d}{b}$	λ_e	$\frac{S_e}{S_W}$	A_e	Λ_{LE} (deg)	f_N	f_f	M	$R\ell_{MAC} \times 10^{-6}$	$\frac{x_{a.c.}}{c_r}$ Calc.	$\frac{x_{a.c.}}{c_r}$ Test	e Percent Error
6	.15	.67	.82	2.54	52	2.75	.80	.13	6.8	.910	.900	1.1
7	.14	.62	.83	3.58	60	4.00	0	.40	2.0	1.510	1.520	-0.7
								.70	3.1	1.520	1.520	0
								.91	3.5	1.530	1.540	-0.6
	.14	.62	.83	3.58	35	5.00	0	.40	2.0	.690	.690	0
								.70	3.1	.690	.690	0
								.91	3.5	.750	.770	-2.6
	.14	.62	.83	3.58	7	5.50	0	.40	2.0	.220	.230	-4.3
								.70	3.1	.220	.230	-4.3
								.91	3.5	.300	.330	-9.1
8	.20	1.00	.80	2.40	45	1.50	1.0	.29	.9	.960	.950	1.1
	.40		.60	1.80						.640	.650	-1.5
	.80		.20	.60						-2.180	-2.200	-0.9
9	.18	.17	.70	2.84	38.7	1.75	5.33	.60	3.0	.389	.350	11.1

Average Error = $\frac{\Sigma |e|}{n}$ = 2.7%

TABLE 4.3.2.2-B

SUBSONIC AERODYNAMIC-CENTER LOCATIONS OF WING-BODY COMBINATIONS WITH DOUBLE-DELTA WINGS

DATA SUMMARY AND SUBSTANTIATION

Ref.	Config.	A	λ	η_B	Λ_{LE_i} (deg)	Λ_{LE_o} (deg)	M	$\frac{x_{a.c.}}{c_r}$ Calc.	$\frac{x_{a.c.}}{c_r}$ Test	e Percent Error
10	WB	2.01	0.067	0.313	78.0	53.3	0.40	0.689	0.714	− 3.5
							0.70	0.697	0.724	− 3.7
							0.90	0.705	0.738	− 4.5
		1.96	0.062	0.405		48.5	0.40	0.702	0.728	− 3.6
							0.70	0.710	0.738	− 3.8
							0.90	0.722	0.756	− 4.5
		1.93	0.059	0.498		38.1	0.40	0.714	0.738	− 3.3
							0.70	0.726	0.746	− 2.7
							0.90	0.739	0.772	− 4.3
		1.30	0	0.500	82.0	60.0	0.40	0.737	0.777	− 5.1
							0.70	0.750	0.785	− 4.5
							0.90	0.765	0.798	− 4.1
		1.33	0.049	0.403			0.40	0.737	0.770	− 4.3
							0.70	0.741	0.744	− 0.4
							0.90	0.749	0.788	− 4.9
		1.55	0	0.400		59.0	0.40	0.730	0.743	− 1.7
							0.70	0.737	0.755	− 2.4
							0.90	0.748	0.768	− 2.6
		1.72		0.414	77.4		0.40	0.668	0.700	− 4.6
							0.70	0.676	0.707	− 4.4
							0.90	0.688	0.727	− 5.4
11	WB	2.39	0	0.217	82.9	50.0	0.70	0.757	0.748	1.2
							0.90	0.764	0.761	0.4
12	WB	1.87	0	0.424	72.6	59.0	0.10	0.685	0.710	− 3.5
		1.73		0.551	73.0			0.681	0.721	− 5.5
				0.414	77.4			0.663	0.676	− 1.9

TABLE 4.3.2.2-B (CONTD)

Ref.	Config.	A	λ	η_B	Λ_{LE_i} (deg)	Λ_{LE_o} (deg)	M	$\frac{x_{a.c.}}{c_r}$ Calc.	$\frac{x_{a.c.}}{c_r}$ Test	e Percent Error
12	WB	1.87	0	0.332	77.2	59.0	0.10	0.662	0.660	0.3
		1.46	0.091	0.484	72.6			0.644	0.683	– 5.7
		1.34	0.083	0.628	73.0			0.643	0.706	– 8.9
			0.075	0.473	77.4			0.633	0.666	– 5.0
		1.46	0.082	0.379	77.2			0.628	0.659	– 4.7
13	WB	2.39	0	0.217	82.9	50.0	0.30	0.753	0.750	0.4
14	WBV	3.00	0	0.654	60.0	42.1	0.20	0.576	(a)	
15	WB	3.00	0	0.654	60.0	42.1	0.70	0.589		
							0.80	0.595		
							0.90	0.604		
16	WBV	1.89	0	0.400	73.4	59.0	0.10	0.624		

(a) This information is classified CONFIDENTIAL.

Average Error = $\frac{\Sigma |e|}{n}$ = 3.4%

TABLE 4.3.2.2-C

SUBSONIC AERODYNAMIC-CENTER LOCATIONS OF WING-BODY COMBINATIONS WITH CRANKED WINGS

DATA SUMMARY AND SUBSTANTIATION

Ref.	Config.	A	λ	η_B	Λ_{LE_i} (deg)	Λ_{LE_o} (deg)	M	$\frac{x_{a.c.}}{c_r}$ Calc.	$\frac{x_{a.c.}}{c_r}$ Test	e Percent Error
17	WB	2.91	.167	.500	67.0	61.7	.60	.770	.797	– 3.4
							.30	.780	.802	– 2.7
							.90	.784	.804	– 2.5
18	WB	3.00	.455	.584	59.0	48.5	.18	1.038	.997	4.1
19	WB	6.18	.136	.308	65.0	12.0	.50	.739	(a)	
							.80	.750		
							.90	.757		

TABLE 4.3.2.2-C (CONTD)

Ref.	Config.	A	λ	η_B	Λ_{LE_i} (deg)	Λ_{LE_o} (deg)	M	$\frac{x_{a.c.}}{c_r}$ Calc.	$\frac{x_{a.c.}}{c_r}$ Test	e Percent Error
19	WB	4.60	Raked	.404		45.0	.50	.928		
							.80	.943		
							.90	.954		
20	WBV	5.95	0	.345	60.0	25.0	.30	.771		
		5.15	.090	.379				.689	(a)	
21	WBV	2.49	.280	.654	25.0	75.0	.25	.610		
		2.18	.187		45.0			.672		
		1.86	.129		60.0			.707		
		1.68	.104		66.3			.726		
22	WBVN	5.15	.089	.371	60.0	25.0	.23	.679	.683	– 0.6
		1.89	Raked	.640		75.0		.845	.900	– 6.1
		4.49	.129	.269		30.0	.21	.654	.660	– 0.9
		4.00	.152	.302		43.0		.714	.725	– 1.5
		1.75	Raked	.463		70.5		.690	.749	– 7.9
23	WBVN	5.15	.090	.379	60.0	25.0	.60	.693		
							.80	.704		
							.90	.716		
		3.44	Raked	.475		55.0	.60	.802		
							.80	.814		
							.90	.832	(a)	
23	WBVN	1.88	Raked	.654	60.0	75.0	.60	.831		
							.80	.835		
							.90	.833		
24	WBV	3.63	.075	.413	72.0	25.0	.19	.720		
25	WB	6.93	.116	.224	75.0	35.0	.27	.964		
		6.40	.102	.270				.823		

(a) This information is classified CONFIDENTIAL.

Average Error = $\frac{\Sigma |e|}{n}$ = 3.0%

TABLE 4.3.2.2-D

SUPERSONIC AERODYNAMIC-CENTER LOCATIONS OF WING-BODY COMBINATIONS WITH STRAIGHT-TAPERED WINGS

DATA SUMMARY

Ref.	$\frac{d}{b}$	λ_e	$\frac{S_e}{S_W}$	A_e	Λ_{LE} (deg)	f_N	f_f	M	$R_{\ell_{MAC}} \times 10^{-6}$	$\frac{x_{a.c.}}{c_r}$ Calc.	$\frac{x_{a.c.}}{c_r}$ Test	e Percent Error
26	.60	0	.16	.67	80.4	2.85	.50	1.50	5.5	.570	.580	−1.7
								2.02		.580	.560	3.6
	.20	0	.64	4.0	45.0	2.85	.50	1.50	5.5	.630	.620	1.6
								2.02		.620	.620	0
27	.09	.21	.85	3.4	51.5	2.9	1.6	2.01	2.2	.860	.848	1.4
										.860	.844	1.9
										.850	.828	2.7
	.09	.21	.85	3.4	21.5	2.9	3.3	1.60	2.2	.460	.463	−0.6
								2.01		.470	.450	4.4

Average Error = $\frac{\Sigma |e|}{n}$ = 2.0%

TABLE 4.3.2.2-E

SUPERSONIC AERODYNAMIC-CENTER LOCATIONS OF WING-BODY COMBINATIONS WITH DOUBLE-DELTA WINGS

DATA SUMMARY AND SUBSTANTIATION

Ref.	Config.	A	λ	η_B	Λ_{LE_i} (deg)	Λ_{LE_o} (deg)	M	$\frac{x_{a.c.}}{c_r}$ Calc.	$\frac{x_{a.c.}}{c_r}$ Test	e Percent Error
10	WB	1.30	0	.500	82.0	60.0	1.00	.795	.821	− 3.2
							1.10	.790	.821	− 3.8
							1.40	.787	.805	− 2.2
							1.98	.775	.785	− 1.3
							2.94	.754	.760	− 0.8
	WB	1.33	.049	.403	82.0	60.0	1.00	.766	.861	− 11.0
							1.10	.790	.813	− 2.8
							1.40	.786	.808	− 2.7
							1.98	.775	.791	− 2.0
							2.94	.762	.771	−1.2

TABLE 4.3.2.2-E (CONTD)

Ref.	Config.	A	λ	η_B	Λ_{LE_i} (deg)	Λ_{LE_o} (deg)	M	$\frac{x_{a.c.}}{c_r}$ Calc.	$\frac{x_{a.c.}}{c_r}$ Test	e Percent Error
10	WB[a]	1.55	0	.400	82.0	59.0	1.00	.769	.790	− 2.7
							1.10	.774	.790	− 2.0
							1.40	.765	.781	− 2.0
							1.98	.753	.768	− 2.0
							2.94	.738	.749	− 1.5
	WB	1.72	0	.414	82.0	59.0	1.00	.725	.751	−3.5
							1.10	.737	.750	− 1.7
							1.39	.732	.748	− 2.1
11	WB[a]	2.39	0	.217	82.9	50.0	1.20	.800	.800	0
							2.00	.785	.790	− 0.6
							3.00	.700	.778	− 1.0
							4.00	.759	.771	− 1.6
28	WB	2.35	.143	.700	61.7	35.0	1.41	.670	.680	− 1.5
							2.01	.660	.640	3.1
		1.95	.111				1.41	.544	.569	− 4.4
							2.01	.546	.531	2.8
29	WBVN	1.95	0	.215	74.7	60.0	1.70	.669	.697	− 4.0
							2.00	.671	.694	− 3.3
							2.20	.673	.688	− 2.2
30	WB[a]	1.79	.104	.556	73.0	47.2	2.01	.724	.705	2.7
15	WB	3.00	0	.654	60.0	42.1	1.00	.656	(b)	
							1.05	.654		
							1.25	.655		
							1.30	.656		
31	WB	2.60	0	.710	60.0	49.3	1.80	.645		
							2.16	.647		
							2.56	.650		
							3.07	.652		

(a) Predicted using wing-alone approach

(b) This information is classified CONFIDENTIAL.

Average Error = $\frac{\Sigma\ |e|}{n}$ = 2.6%

TABLE 4.3.2.2-F

SUPERSONIC AERODYNAMIC-CENTER LOCATIONS OF WING-BODY COMBINATIONS WITH CRANKED WINGS

DATA SUMMARY AND SUBSTANTIATION

Ref.	Config.	A	λ	η_B	Λ_{LE_i} (deg)	Λ_{LE_o} (deg)	M	$\frac{x_{a.c.}}{c_r}$ Calc	$\frac{x_{a.c.}}{c_r}$ Test	e Percent Error
32	WB	3.15	.150	.400	64.1	51.6	1.61	.845	.845	0
		2.86	.120					.691	.688	0.4
		2.62	.100					.584	.586	− 0.3
		2.86	.120		70.7	51.6		.859	.863	− 0.5
		2.62	.100					.724	.727	− 0.4
		2.42	.086					.631	.635	− 0.6
		2.86	.120				2.01	.853	.846	0.8
		2.42	.086					.624	.626	− 0.3
28	WB	4.00	.333	.700	61.7	35.0	1.41	1.433	1.420	0.9
							2.01	1.391	1.364	2.0
		2.97	.200	.700	61.7	35.0	1.41	.891	.903	− 1.3
							2.01	.876	.864	1.4
17	WB	2.91	.167	.500	67.0	61.7	1.41	.843	.872	− 3.3
							2.01	.853	.863	− 1.2
33	WB	2.91	.167	.500	67.0	61.7	1.41	.859	.899	− 4.4
							1.61	.865	.899	− 3.8
							2.01	.852	.879	− 3.1
34	WBV	1.88	.130	.654	60.0	75.0	2.50	.896	.875	2.4
							3.00	.903	.862	4.8
35							1.00	.776	.790	− 1.8
							1.13	.810	.821	− 1.3
							1.20	.821	.824	− 0.4
							1.30	.828	.827	0.1
19	WB	4.60	Raked tip	.404	65.0	45.0	1.03	1.008	.990	1.8
							1.20	1.012	1.010	0.2
							2.30	.977	.946	3.3
							2.60	.970	.926	4.8
							3.00	.962	.910	5.7

TABLE 4.3.2.2-F (CONTD)

Ref.	Config.	A	λ	η_B	Λ_{LE_i} (deg)	Λ_{LE_o} (deg)	M	$\frac{x_{a.c.}}{c_r}$ Calc.	$\frac{x_{a.c.}}{c_r}$ Test	e Percent Error
23	WBVN	3.44	Raked tip	.475	60.0	55.0	1.00	.935	(a)	
							1.20	.956		
							1.40	.962		
							2.20	.979		
		1.88	Raked tip	.675	60.0	75.0	1.00	.949		
							1.20	1.004		
							1.40	1.002		
							2.20	1.100		

(a) This information is classified CONFIDENTIAL.

Average Error $= \frac{\Sigma\ |e|}{n} = 2.6\%$

$$\left[\frac{k}{1-k} + \frac{\sqrt{1-2k}\log_e\left(\frac{1-k}{k}+\frac{1}{k}\sqrt{1-2k}\right) - (1-k) + \frac{\pi}{2}k}{\frac{k(1-k)}{\sqrt{1-2k}}\log_e\left(\frac{1-k}{k}+\frac{1}{k}\sqrt{1-2k}\right) + \frac{(1-k)^2}{k} - \frac{\pi}{2}(1-k)}\right]$$

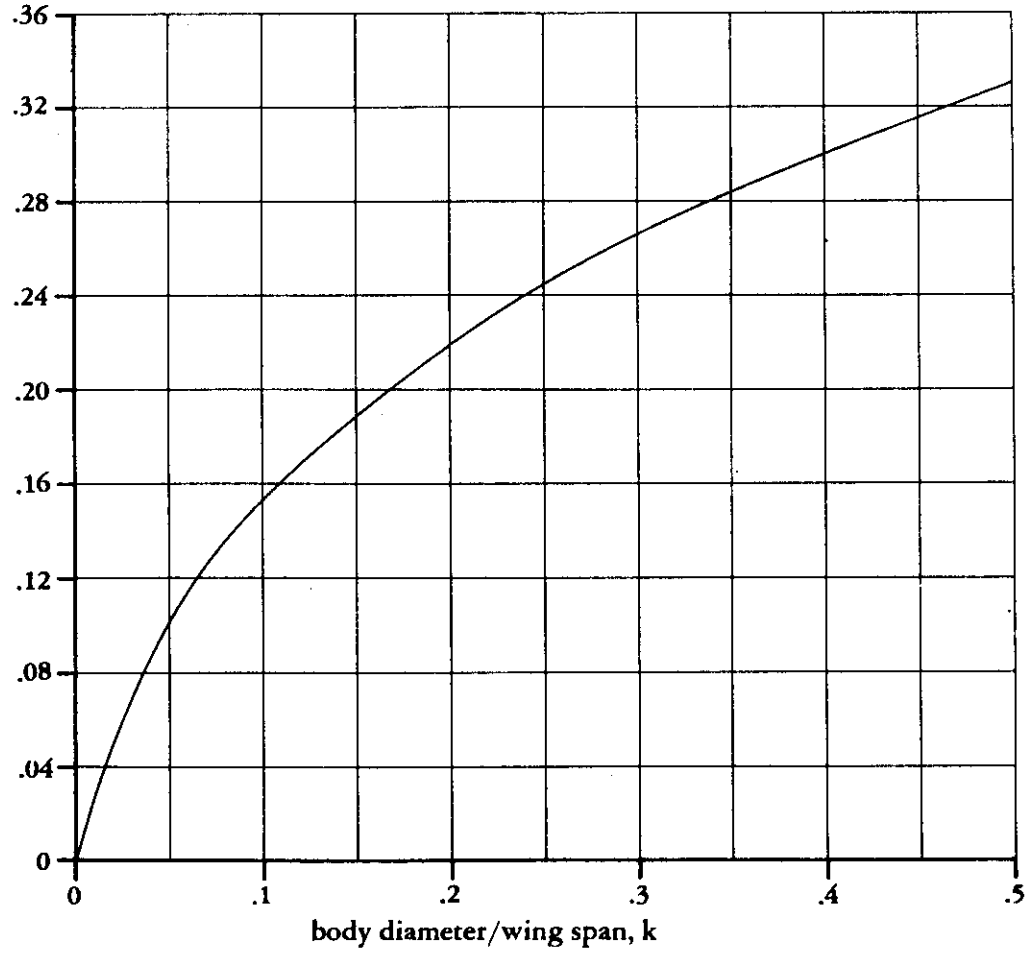

FIGURE 4.3.2.2-35 PARAMETER USED IN ACCOUNTING FOR WING-LIFT CARRYOVER ON THE BODY

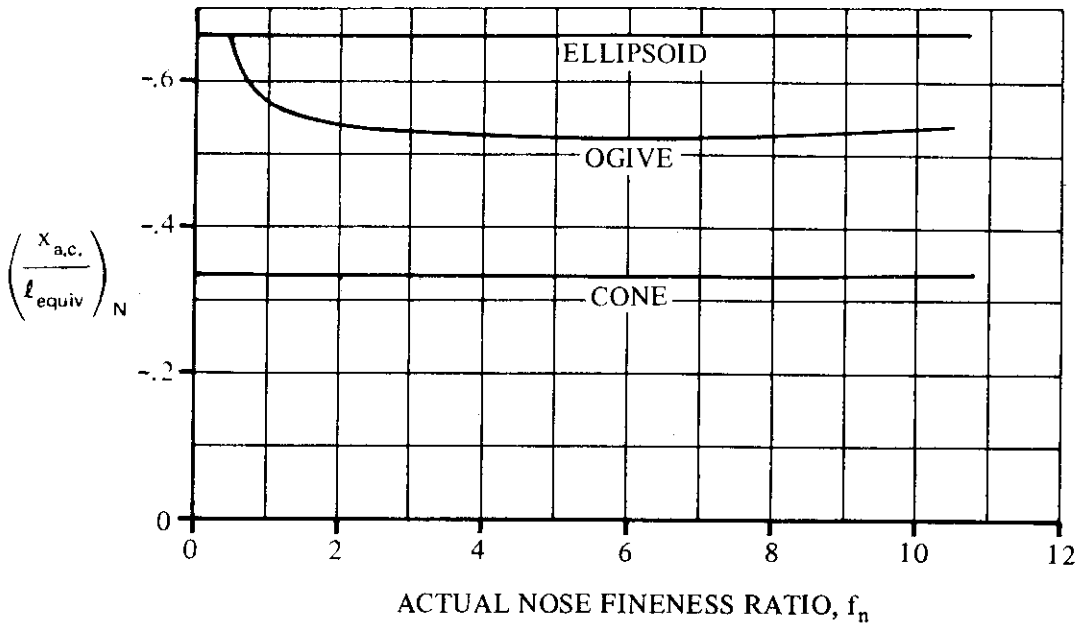

FIGURE 4.3.2.2-36a AERODYNAMIC-CENTER LOCATIONS OF VARIOUS NOSES (SLENDER-BODY THEORY)

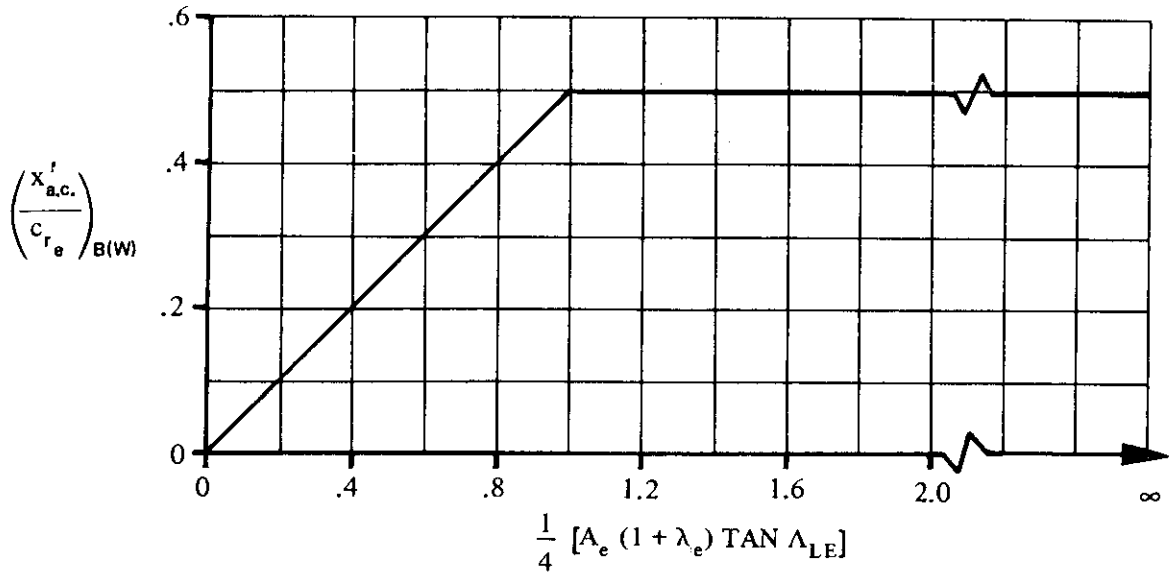

FIGURE 4.3.2.2-36b THEORETICAL AERODYNAMIC-CENTER LOCATIONS FOR βA_e =

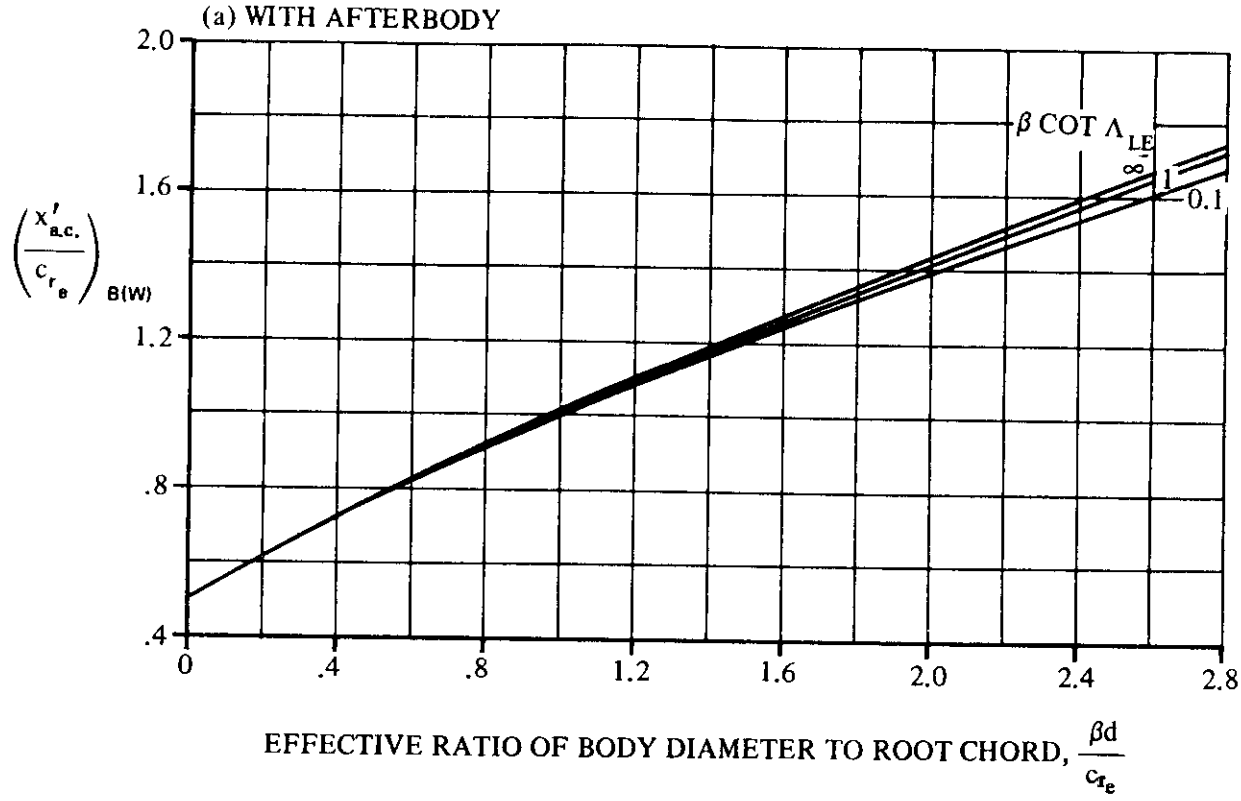

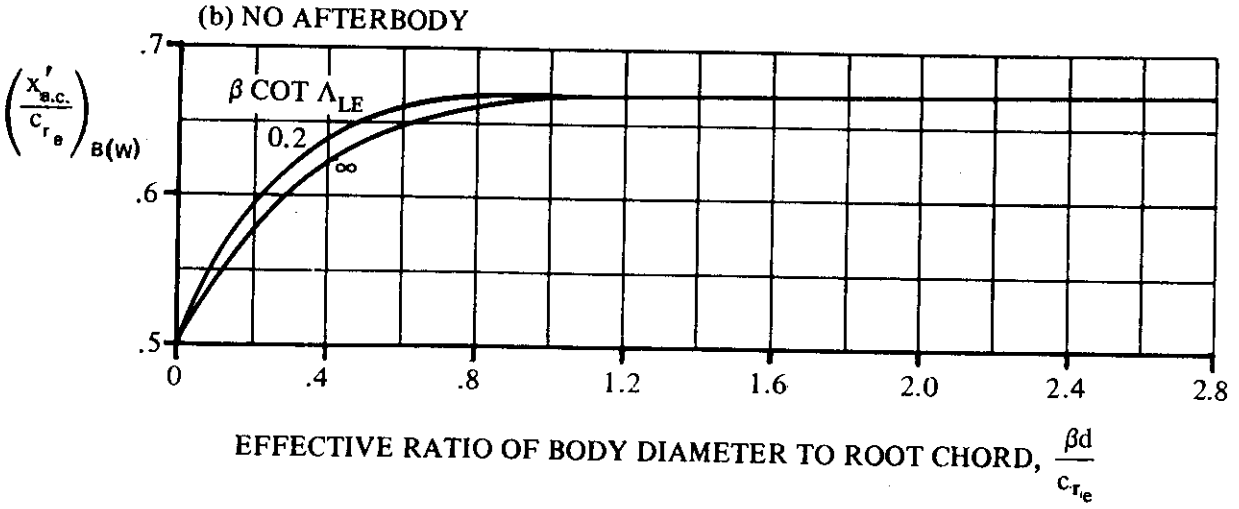

FIGURE 4.3.2.2-37 AERODYNAMIC-CENTER LOCATIONS FOR LIFT CARRYOVER OF WING ONTO BODY AT SUPERSONIC SPEEDS WHEN $\beta A_e (1 + \lambda_e) \left(1 + \frac{1}{\beta \text{ COT } \Lambda_{LE}}\right) \geq 4.0$

4.3.3 WING-BODY DRAG

4.3.3.1 WING-BODY ZERO-LIFT DRAG

The problem of estimating the zero-lift drag of a wing-body combination is one of properly accounting for the mutual interferences that exist between its components. There are two principal approaches to the problem. One attempts to isolate the individual interferences, and the other combines the drag of components with the interference drag and analyzes the total configuration. The Datcom method for subsonic speeds consists of applying an interference correction factor to the skin-friction and pressure-drag contributions of the exposed components. The method presented for transonic speeds treats the configuration as a unit by simply adding the drag contributions of the gross components. At supersonic speeds the wing-body zero-lift drag is obtained by summing the drag contributions of the exposed wing and the isolated body. The methods presented for the subsonic-, transonic-, and supersonic-speed regimes are for a fully turbulent boundary layer over the body and the wing.

A. SUBSONIC

Subsonic wing-body interference is caused by several phenomena, of which two are especially important. First, the wing and body produce supervelocities due to thickness that increase the skin friction in the vicinity of the wing-body junction. Second, the confluence of boundary layers at the junction can cause premature boundary-layer separation, which, however, can sometimes be prevented or at least postponed by proper fillet design. It has not been possible to establish a general method for estimating interference drag. Although the Datcom method uses interference correction factors based on experimental results for wing-body combinations, it should be pointed out that most of the bodies were conventional, ogive-cylinder combinations of high fineness ratio, and no detailed investigation has been made to evaluate body effects. Therefore, the method should not be construed as pertaining to generalized wing-body combinations with arbitrary body shapes.

The Datcom method is that of reference 1 and is applicable to wing-body configurations consisting of a body of revolution in combination with the following two classes of wing planforms:

Straight-Tapered Wings (conventional, trapezoidal planforms)

Non-Straight-Tapered Wings

- Double-delta wings
- Cranked wings
- Curved (Gothic and ogee) wings

DATCOM METHOD

The subsonic zero-lift drag coefficient of a wing-body combination, based on the reference area, is determined by adding the drag coefficients of the exposed components and applying an interference correction factor to the skin-friction and pressure-drag contributions. The component contributions of the wing and body are determined by the methods of Sections 4.1.5.1 and 4.2.3.1, respectively. This approach is summarized by

$$\left(C_{D_0}\right)_{WB} = \left\{ C_{f_W} \left[1 + L\left(\frac{t}{c}\right) + 100\left(\frac{t}{c}\right)^4 \right] R_{L.S.} \frac{(S_{wet})_e}{S_{ref}} + C_{f_B} \left[1 + \frac{60}{(\ell_B/d)^3} + 0.0025\frac{\ell_B}{d} \right] \frac{(S_S)_e}{S_{ref}} \right\} R_{WB} + C_{D_b} \frac{S_B}{S_{ref}} \qquad 4.3.3.1\text{-a}$$

where

C_{f_W} is the turbulent flat-plate skin-friction coefficient of the wing (or wing panel in the case of composite wings), including roughness effects, as a function of Mach number and the Reynolds number based on the reference length ℓ. This value is determined as discussed in paragraph A of Section 4.1.5.1. The reference length ℓ is the mean aerodynamic chord $\overline{c}_e$ of the exposed wing (or exposed wing panels in the case of composite wings).

C_{f_B} is the turbulent flat-plate skin-friction coefficient of the body, including roughness effects, as a function of Mach number and the Reynolds number based on the reference length ℓ. This value is determined as discussed in paragraph A of Section 4.1.5.1. The reference length ℓ is the actual body length ℓ_B.

$(S_{wet})_e$ is the wetted area of the exposed wing (or exposed wing panels in the case of composite wings).

$(S_S)_e$ is the exposed wetted area of the body (the wetted area of the isolated body minus the surface area covered by the wing at the wing-body juncture).

S_{ref} is the reference area.

R_{WB} is the wing-body interference correlation factor obtained from figure 4.3.3.1-37 as a function of Mach number and the fuselage Reynolds number based on the actual body length ℓ_B.

The remaining parameters in equation 4.3.3.1-a are presented in either Section 4.1.5.1 or Section 4.2.3.1.

In treating non-straight-tapered wings the wing zero-lift drag contribution is obtained for the exposed inboard and the outboard panels separately (based on the reference area) and then added. Curved planforms are approximated by combinations of trapezoidal panels, in which case two such panels are usually sufficient to give a satisfactory result. An ogee planform has been chosen for the sample problem to illustrate how the method is applied to curved planforms, as well as to show the general application of the method to double-delta and cranked planforms.

Non-straight-tapered wing geometric parameters are presented in Section 2.2.2.

The wing-body interference correlation factor R_{WB} was developed in reference 1 by determining the ratio of test values of C_{D_0} to values predicted on the basis of $R_{WB} = 1.0$ for several wing-body combinations. Both conventional, trapezoidal planforms and composite planforms have been used in the correlation; however, most of the bodies were conventional ogive-cylinders of high fineness ratio. Composite planform data are limited to values of fuselage Reynolds number below 2.4×10^7. The curves for values of $R_{\ell_{fus}} > 2.4 \times 10^7$ were generated using the basic prediction method of reference 2, which has been correlated with flight-test data. It should also be noted that the correlation does not include data below $M = 0.25$.

A comparison of test data for 15 configurations with $\left(C_{D_0}\right)_{WB}$ calculated by this method is presented as table 4.3.3.1-A (taken from reference 1). The results are indicative of the accuracy that can be expected when applying the method to configurations with $R_{\ell_{fus}} \leq 2.4 \times 10^7$. The validity of the method for configurations with non-straight-tapered wings has not been verified above $R_{\ell_{fus}} > 2.4 \times 10^7$; however, the accuracy of the basic prediction method as applied to configurations consisting of conventional, trapezoidal wings mounted on ogive-cylinders of high fineness ratio indicates that accuracy to within ±10 percent can be expected. It should be noted that the test values in table 4.3.3.1-A have been corrected to remove base drag and that the calculated values do not include the base-drag term of equation 4.3.3.1-a.

Sample Problem

Given: A wing-body configuration of reference 14. The ogee planform is approximated by a double-delta planform with a streamwise tip. The inboard and outboard panels of the double-delta wing have been selected to have leading and trailing edges which closely approximate the sweeps of the curved edges. The sweeps of the maximum thickness lines of the inboard and outboard panels closely approximate the sweep of the maximum thickness line of the ogee planform within the boundaries of each panel.

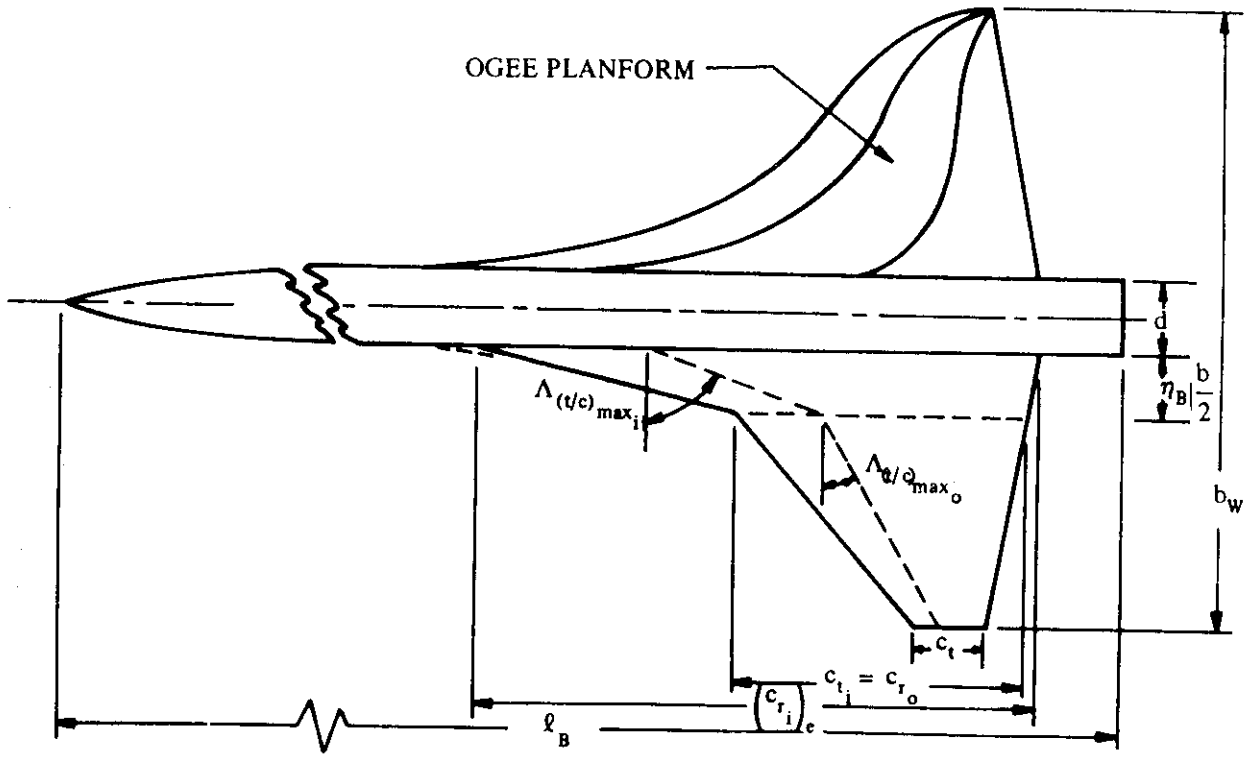

SKETCH (a)

Ogee Planform:

$S_W = S_{ref} = 21.75$ sq in. $\quad S_{W_e} = 16.57$ sq in. $\quad t/c = 0.02$

Airfoil section: Hexagonal with ridge lines at 0.30c and 0.70c (x_t @ 0.30c)

Body:

Ogive-cylinder $\quad \ell_B = 14.216$ in. $\quad d = 0.875$ in. $\quad f_{fus} = 16.25$

$(S_S)_e = 33.70$ sq in. (fuselage area covered by wing at wing-body juncture is removed from isolated body wetted area).

$\frac{(S_S)_e}{S_{ref}} = 1.550 \quad \frac{d_b}{d} = 1.0 \quad \frac{S_B}{S_{ref}} = 0.0276 \quad \frac{(S_S)_e}{S_B} = 56.04$

Double-Delta Approximation:

Inboard panel:

$(S_i)_e$ = 7.21 sq in. $\left(S_{wet_i}\right)_e$ = 14.42 sq in. $\left(S_{wet_i}\right)_e / S_{ref}$ = 0.663

$(\bar{c}_i)_e$ = 5.11 in. $\Lambda_{(t/c)_{max_i}} = 70^o$ $(t/c)_i$ = 0.02

Outboard panel:

$(S_o)_e$ = 9.67 sq in. $\left(S_{wet_o}\right)_e$ = 19.34 sq in. $\left(S_{wet_o}\right)_e / S_{ref}$ = 0.889

$(\bar{c}_o)_e$ = 2.375 in. $\Lambda_{(t/c)_{max_o}} = 31^o$ $(t/c)_o$ = 0.02

Additional Characteristics:

M = 0.70 $R_\ell = 2.5 \times 10^6$ per ft

Polished metal surface (assume k = 0.03×10^{-3} in.)

Compute:

Determine C_f for each component (Section 4.1.5.1)

Body

$R_\ell = (2.50 \times 10^6)(\ell_B) = (2.5 \times 10^6)(14.216/12) = 2.96 \times 10^6$

$\ell/k = 14.216/(.03 \times 10^{-3}) = 4.74 \times 10^5$; cutoff $R_\ell \simeq 4.5 \times 10^7$ (figure 4.1.5.1-27)

Since cutoff R_ℓ > calculated R_ℓ, read C_{f_B} at calculated R_ℓ.

C_{f_B} = 0.00354 (figure 4.1.5.1-26)

Inboard Panel

$R_\ell = (2.5 \times 10^6)(\bar{c}_i)_e = (2.5 \times 10^6)(5.11/12) = 1.065 \times 10^6$

$\ell/k = 5.11/(.03 \times 10^{-3}) = 1.70 \times 10^5$; cutoff $R_\ell \simeq 1.4 \times 10^7$ (figure 4.1.5.1-27)

Since cutoff $R_\ell \simeq$ calculated R_ℓ, read $\left(C_{f_W}\right)_i$ at calculated R_ℓ.

$\left(C_{f_W}\right)_i$ = 0.00425 (figure 4.1.5.1-26)

Outboard Panel

$R_\ell = (2.5 \times 10^6)(\bar{c}_o)_e = (2.5 \times 10^6)(2.375/12) = 4.95 \times 10^5$

$\ell/k = 2.375/(.03 \times 10^{-3}) = 7.92 \times 10^4$; cutoff $R_\ell \simeq 6.5 \times 10^6$ (figure 4.1.5.1-27)

Since cutoff R_ℓ > calculated R_ℓ, read $\left(C_{f_W}\right)_o$ at calculated R_ℓ.

$\left(C_{f_W}\right)_o = 0.00488$ (figure 4.1.5.1-26)

Determine the zero-lift drag contribution of the exposed inboard and outboard panels (Section 4.1.5.1).

Inboard panel

$\left[1 + L\left(\frac{t}{c}\right) + 100\left(\frac{t}{c}\right)^4\right] = 1.021$ (figure 4.1.5.1-28a, for L = 1.2)

$\cos \Lambda_{(t/c)_{max_i}} = \cos 70^o = 0.342$

$(R_{L.S.})_i = 1.055$ (figure 4.1.5.1-28b, interpolated using dashed lines)

$$\left(C_{D_0}\right)_i = \left(C_{f_W}\right)_i \left[1 + L\left(\frac{t}{c}\right) + 100\left(\frac{t}{c}\right)^4\right] R_{L.S.} \frac{\left(S_{wet_i}\right)_e}{S_{ref}} = (0.00425)(1.021)(1.055)(0.663)$$

$= 0.003035$ (based on S_{ref})

Outboard panel

$\left[1 + L\left(\frac{t}{c}\right) + 100\left(\frac{t}{c}\right)^4\right] = 1.021$ (figure 4.1.5.1-28a, for L = 1.2)

$\cos \Lambda_{(t/c)_{max_o}} = \cos 31^o = 0.8572$

$(R_{L.S.})_o = 1.180$ (figure 4.1.5.1-28b, interpolated using solid lines)

$$\left(C_{D_0}\right)_o = \left(C_{f_W}\right)_o \left[1 + L\left(\frac{t}{c}\right) + 100\left(\frac{t}{c}\right)^4\right] R_{L.S.} \frac{\left(S_{wet_o}\right)_e}{S_{ref}}$$

$= (0.00488)(1.021)(1.180)(0.889) = 0.00523$ (based on S_{ref})

Determine the zero-lift drag contribution of the isolated body (Section 4.2.3.1)

Zero-lift drag exclusive of base drag

$$\left[1 + \frac{60}{(\ell_B/d)^3} + 0.0025\,\frac{\ell_B}{d}\right] = 1.054$$

$$C_{f_B}\left[1 + \frac{60}{(\ell_B/d)^3} + 0.0025\,\frac{\ell_B}{d}\right]\frac{(S_S)_e}{S_{ref}} = (0.00354)\,(1.054)\,(1.550) = 0.00578 \text{ (based on } S_{ref})$$

Base-drag coefficient

$$C_{D_b} = 0.029\left(\frac{d_b}{d}\right)^3 \Big/ \sqrt{\left(C_{D_f}\right)_b} \quad \text{(equation 4.2.3.1-b)}$$

where $\left(C_{D_f}\right)_b$ is the zero-lift drag coefficient exclusive of the base drag,

based on body base area; i.e.,

$$\left(C_{D_f}\right)_b = C_{f_B}\left[1 + \frac{60}{(\ell_B/d)^3} + 0.0025\,\frac{\ell_B}{d}\right]\frac{(S_S)_e}{S_B}$$

$$= (0.00354)\,(1.054)\,(56.04) = 0.209$$

$$C_{D_b} = (0.029)\,(1.0)^3 / \sqrt{0.209} = 0.0634 \quad \text{(based on } S_B)$$

Determine the wing-body correlation factor R_{WB}

R_{WB} = 0.955 (figure 4.3.3.1-37)

Solution:

$$\left(C_{D_0}\right)_{WB} = \left\{C_{f_W}\left[1 + L\left(\frac{t}{c}\right) + 100\left(\frac{t}{c}\right)^4\right] R_{L.S.}\,\frac{(S_{wet})_e}{S_{ref}} + C_{f_B}\left[1 + \frac{60}{(\ell_B/d)^3} + 0.0025\,\frac{\ell_B}{d}\right]\frac{(S_S)_e}{S_{ref}}\right\} R_{WB}$$

$$+ C_{D_b}\,\frac{S_B}{S_{ref}} \quad \text{(equation 4.3.3.1-a)}$$

$$= \left\{\left[(0.003035) + (0.00523)\right] + (0.00578)\right\}(0.955) + (0.0634)\,(0.0276)$$

$$= 0.0152 \text{ (based on } S_{ref})$$

The test value from reference 14, corrected to remove base drag, is 0.0131. The corresponding calculated value is 0.0152 - 0.00175 = 0.01345

B. TRANSONIC

Interference effects in the transonic range are generally greater than those in the subsonic region, because of the higher local velocities of the individual components and the greater propagation of these perturbations from their source. There often exist large supersonic regions that contribute substantially to the wave drag Many theoretical attempts have been made to correlate these effects in the transonic range, but until the advent of the area-rule concept, none of them proved very satisfactory.

The area-rule method is based on supersonic linear theory, which assumes that pressure disturbances are propagated in the direction of the Mach lines and do not diminish with distance. If it is assumed that these concepts can be applied in a limiting case at a Mach number of one, where Mach lines are normal to the flow direction, it can also be assumed that at large distances from the body the disturbances are independent of the arrangement of the components and only a function of the cross-sectional-area distribution. This means that the drag of a wing-body combination can be calculated as though the combination were a body of revolution with equivalent-area cross sections.

In addition to affording a means of estimating drag by calculation or by testing a simplified model (body of revolution) in the transonic range, the area rule is extremely useful as a design tool, since it indicates the most desirable way to arrange the vehicle components for minimum wave drag. The most common example of this is to indent, or "coke-bottle," a fuselage enough to permit the wing to be added without a marked increase in the over-all area distribution. As is obvious from the body-of-revolution wave-drag curves, it is always desirable from the wave-drag point of view to have a body of as high a fineness ratio as possible. However, it should be remembered that "coke-bottling" should be used judiciously, to avoid undesirable local effects.

The linear-theory wave drag of a smooth, pointed, closed body of revolution was first given by von Kármán (reference 3) as

$$C_D = \frac{1}{2\pi S_{ref}} \int_0^{\ell_B} \int_0^{\ell_B} \frac{d^2S}{dx^2} \frac{d^2S}{d\xi^2} \ell n\,(x - \xi)\, dx d\xi \qquad 4.3.3.1\text{-b}$$

where

ℓ_B is the body length.

x is any point on the longitudinal axis; $x = 0$ at the nose and $x = \ell_B$ at the aft end.

ξ is any point on the longitudinal axis; $\xi = 0$ at the nose and $\xi = \ell_B$ at the aft end (not necessarily the same point as x).

S is the cross-sectional area of the body at any point x.

$\frac{d^2S}{dx^2}$ and $\frac{d^2S}{d\xi^2}$ are obtained from the area distribution determined in step 1 of paragraph C below.

S_{ref} is the reference area, usually the total wing area.

This equation is subject to the conditions:

1. $\left(\frac{dS}{dx}\right)_{x=0} = \left(\frac{dS}{dx}\right)_{x=\ell_B} = 0$

2. The body is slender, in accordance with the usual slender-body restrictions (reference 3).

3. No discontinuities in dS/dx occur anywhere along the body.

Additional terms have been derived that account for the condition $(dS/dx)_{x=\ell_B} \neq 0$ and for finite discontinuities in dS/dx along the body. References 3, 4, 5, and 6 pertain to these conditions.

References 7 and 8 contain numerical methods of evaluating equation 4.3.3.1-b. However, the solution of this equation by hand is tedious, and automatic computing equipment is invariably used. The preparation of the area-distribution plot for a given configuration is usually performed manually.

The accuracy of this method varies with the smoothness and fineness ratio of the equivalent body. Studies of the accuracy of the area rule are given in references 8, 9, 10, and 11.

The Datcom method is at best approximate and consists of simply adding the zero-lift drag coefficients of the individual isolated components. Since the exposed wetted area of a wing-body combination is less than the sum of the wing-alone and body-alone wetted areas, this amounts to adding an increment to the wing-body drag of the combination to account for interference effects.

The interference drag is usually positive for configurations not specifically contoured to reduce this drag component. However, for area-ruled configurations, this interference drag can become negative.

The Datcom method is applicable only to configurations with conventional, trapezoidal wings.

DATCOM METHOD

At the present it is recommended that the transonic zero-lift drag coefficient of a wing-body combination be approximated by adding the drag coefficients based on the total wetted area of each individual component and referred to a common reference area. This approach is summarized by

$$\left(C_{D_0}\right)_{WB} = \left(C_{D_0}\right)_W + \left(C_{D_0}\right)_B \frac{S_B}{S_{ref}} \qquad 4.3.3.1\text{-c}$$

where

$\left(C_{D_0}\right)_W$ is the zero-lift drag coefficient of the wing, based on the reference area, obtained from paragraph B of Section 4.1.5.1; i.e.,

$$\left(C_{D_0}\right)_W = \left(C_{D_f} + C_{D_w}\right)_W \quad \text{(equation 4.1.5.1-g)}$$

$\left(C_{D_0}\right)_B$ is the zero-lift drag coefficient of the body, based on body base area, obtained from paragraph B of Section 4.2.3.1; i.e.,

$$\left(C_{D_0}\right)_B = \left(C_{D_f}\right)_B + C_{D_p} + C_{D_b} + \left(C_{D_w}\right)_B \quad \text{(equation 4.2.3.1-e)}$$

S_B/S_{ref} is the ratio of the body base area to the reference area.

Sample Problem

Given: The swept-wing cylindrical-body configuration of reference 19.

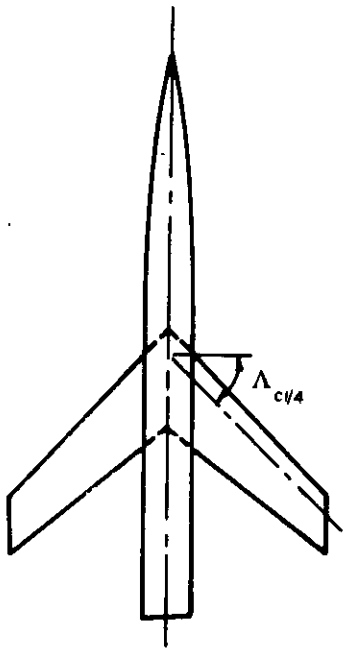

Body Characteristics:

Ogive-cylinder $\ell_B = 43.0$ in. $d_{max} = d_b = 3.75$ in.

$\ell_B/d = 11.47$ $S_B = 11.05$ sq in. $\frac{S_S}{S_B} = 40.19$

Wing Characteristics:

$A = 4.0$ $\Lambda_{c/4} = 45^o$ $\lambda = 0.60$ $\bar{c} = 6.125$ in.

$S_W = S_{ref} = 144$ sq in. $S_{wet} = 288$ sq in.

NACA 65A006 airfoil (x_t @ 0.50c) t/c = 0.06

Additional Characteristics:

$R_{\ell_{M=0.6}} = 2.50 \times 10^5$ per in. $0.80 \le M \le 1.2$

Polished metal surface (assume $k = 0.03 \times 10^{-3}$ in.)

Compute:

The final calculations are presented in table form on page 4.3.3.1-13. Many of the quantities listed below appear as columns in the table.

Wing zero-lift drag coefficient $\left(C_{D_0}\right)_W$ (Section 4.1.5.1)

Determine the skin-friction drag coefficient.

$R_\ell = (2.50 \times 10^5)(\bar{c}) = (2.50 \times 10^5)(6.125) = 1.53 \times 10^6$

$\ell/k = 6.125/(0.03 \times 10^{-3}) = 2.04 \times 10^5$; cutoff $R_{\ell_{M=0.6}} \simeq 1.6 \times 10^7$ (figure 4.1.5.1-27)

Since cutoff $R_\ell >$ calculated R_ℓ, read $(C_f)_W$ at calculated R_ℓ.

$(C_f)_W = 0.0040$ (figure 4.1.5.1-26 @ M = 0.60)

$$\left(C_{D_f}\right)_W = (C_f)_W \left[1 + L\left(\frac{t}{c}\right)\right]\frac{S_{wet}}{S_{ref}} \quad \text{(equation 4.1.5.1-c)}$$

$$= (0.0040)[1 + 1.2(0.06)]\frac{288}{144} \quad (L = 1.2 \text{ for } x_t > 0.30c) = 0.00858$$

Determine and construct the variation of $\left(C_{D_w}\right)_W$ with Mach number for an unswept wing.

$$A\left(\frac{t}{c}\right)^{1/3} = (4.0)(0.392) = 1.568$$

① M	② $\frac{\sqrt{\lvert M^2-1\rvert}}{(t/c)^{1/3}}$	③ $\frac{\left(C_{D_w}\right)_W}{(t/c)^{5/3}}$ fig 4.1.5.1-29	④ $\left(C_{D_w}\right)_W$ ③ (0.0092)
0.80	1.53	0	0
0.85	1.34	0.10	0.0009
0.90	1.11	0.58	0.0053
0.95	0.80	1.95	0.0179
1.00	0	3.02	0.0278
1.025	0.57	3.08	0.0283
1.05	0.82	3.10	0.0285
1.10	1.17	3.12	0.0287
1.15	1.45	3.13	0.0288

Plot $\left(C_{D_w}\right)_W$ vs M for the unswept wing (sketch (a))

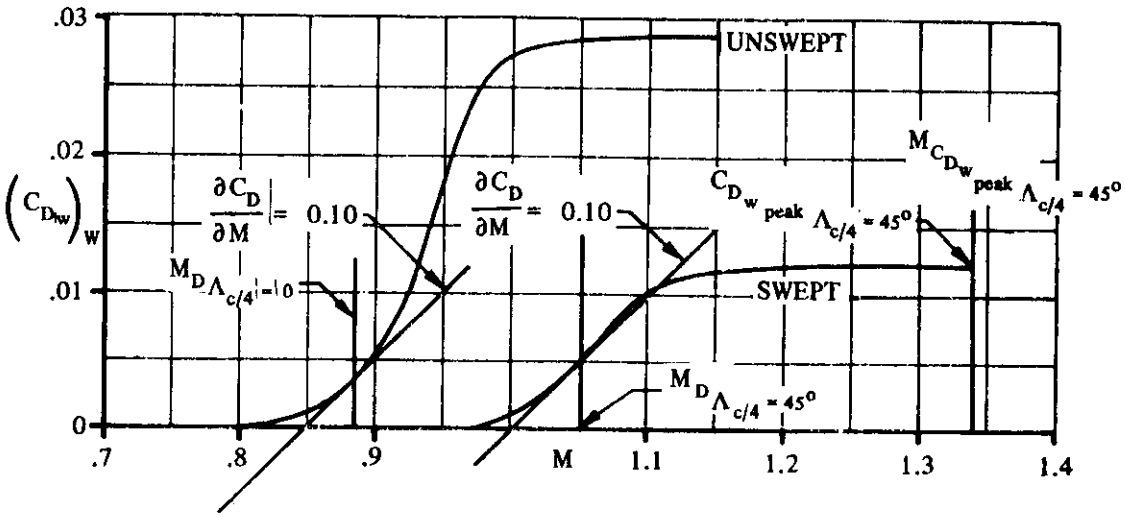

SKETCH (a)

Read the following values from the curve of $\left(C_{D_w}\right)_W$ vs M for the unswept wing:

$$M_{D_{\Lambda_{c/4}=0}} = 0.885$$

$$C_{D_{w_{peak}\Lambda_{c/4}=0}} = 0.0288$$

$$M_{C_{D_{w_{peak}\Lambda_{c/4}=0}}} = 1.125$$

Apply sweep corrections:

$$M_{D_{\Lambda_{c/4}=45^\circ}} = \frac{M_{D_{\Lambda_{c/4}=0}}}{(\cos 45^\circ)^{1/2}} = 1.05 \quad \text{(equation 4.1.5.1-d)}$$

$$C_{D_{w_{peak}\Lambda_{c/4}=45^\circ}} = C_{D_{w_{peak}\Lambda_{c/4}=0}} (\cos 45^\circ)^{2.5} = 0.0121 \quad \text{(equation 4.1.5.1-e)}$$

$$M_{C_{D_{w_{peak}\Lambda_{c/4}=45^\circ}}} = \frac{M_{C_{D_{w_{peak}\Lambda_{c/4}=0}}}}{(\cos 45^\circ)^{1/2}} = 1.34 \quad \text{(equation 4.1.5.1-f)}$$

Construct the curve of $\left(C_{D_w}\right)_W$ vs M for the swept wing using the straight-wing curve to aid in fairing (see sketch (a)). List the swept-wing values in column (3) of the calculation table on page 4.3.3.1-13.

The wing zero-lift drag coefficient is tabulated in column (4) of the calculation table on page 4.3.3.1-13 as

$$\left(C_{D_0}\right)_W = \left(C_{D_f} + C_{D_w}\right)_W \quad \text{(equation 4.1.5.1-g)}$$

Body zero-lift drag coefficient $\left(C_{D_0}\right)_B$ (Section 4.2.3.1)

Determine the skin-friction drag coefficient.

$$R_\ell = (2.50 \times 10^5)(\ell_B) = (2.50 \times 10^5)(43.0) = 1.075 \times 10^7$$

$$\ell/k = 43.0/(0.03 \times 10^{-3}) = 1.433 \times 10^6; \text{ cutoff } R_{\ell_{M=0.6}} = 1.3 \times 10^8 \quad \text{(figure 4.1.5.1-27)}$$

Since cutoff R_ℓ > calculated R_ℓ, read $(C_f)_B$ at calculated R_ℓ.

$(C_f)_B = 0.00288$ (figure 4.1.5.1-26 @ M = 0.60)

$$\left(C_{D_f}\right)_B = (C_f)_B \frac{S_S}{S_B} \quad \text{(equation 4.2.3.1-c)}$$

$$= (0.00288)(40.19) = 0.1157$$

Determine the pressure-drag coefficient.

$$C_{D_P} = (C_f)_{B_{M=0.6}} \left[\frac{60}{(\ell_B/d)^3} + 0.0025 \frac{\ell_B}{d} \right] \frac{S_S}{S_B} \quad \text{(equation 4.2.3.1-d)}$$

$$= 0.00288 \left[\frac{60}{(11.47)^3} + 0.0025 (11.47) \right] 40.19$$

$$= 0.00792 \text{ (based on } S_B)$$

This value of C_{D_P} is taken to be constant for $0 < M < 1.0$, then reduced linearly to zero at M = 1.2 (see column (6) of calculation table, page 4.3.3.1-13).

Determine the base-drag coefficient.

$$C_{D_b} = 0.029 \left(\frac{d_b}{d}\right)^3 \Big/ \sqrt{\left(\overline{C_{D_f}}\right)_b} \quad \text{(equation 4.2.3.1-b)}$$

$$\left(C_{D_f}\right)_b = (C_f)_{B_{M=0.6}} \left[1 + \frac{60}{(\ell_B/d)^3} + 0.0025 \frac{\ell_B}{d} \right] \frac{S_S}{S_B} \quad \text{(first term, eq. 4.2.3.1-a)}$$

$$= (C_f)_{B_{M=0.6}} \frac{S_S}{S_B} + C_{D_P} = (0.00288)(40.19) + 0.00792$$

$$= 0.124$$

$$C_{D_b} = (0.029)(1.0)^3 / \sqrt{0.124} = 0.0824 \text{ (at M = 0.6)}$$

$$\left[\frac{C_{D_b}}{\left(\frac{d_b}{d}\right)^2} \right]_{M=0.6} = \frac{0.0824}{(1)^2} = 0.0824$$

With this value and by using the curves of figure 4.2.3.1-24 as guide lines, obtain values of $C_{D_b}/(d_b/d)^2$ for $0.8 < M < 1.2$.

Then $C_{D_b} = \left[C_{D_b}/(d_b/d)^2\right]_{M=0.6}(d_b/d)^2$ (see column ⑦ of calculation table, page 4.3.3.1-13).

Determine the drag-divergence Mach number.

M_D = 0.98 (figure 4.2.3.1-25)

Determine the wave-drag coefficient.

The wave-drag coefficient as a f(M) is obtained from figure 4.2.3.1-26 (see column ⑧ of the calculation table, page 4.3.3.1-13).

The body zero-lift drag coefficient is tabulated in column ⑨ of the calculation table on page 4.3.3.1-13 as

$$\left(C_{D_0}\right)_B = \left(C_{D_f}\right)_B + C_{D_P} + C_{D_b} + \left(C_{D_w}\right)_B \quad \text{(equation 4.2.3.1-e)}$$

Solution:

$$\left(C_{D_0}\right)_{WB} = \left(C_{D_0}\right)_W + \left(C_{D_0}\right)_B \frac{S_B}{S_{ref}} \quad \text{(equation 4.3.3.1-c)}$$

$$= \left(C_{D_f} + C_{D_w}\right)_W + \left(C_{D_f} + C_{D_P} + C_{D_b} + C_{D_w}\right)_B \frac{S_B}{S_{ref}}$$

Zero-Lift Drag-Coefficient Calculation Table

	Wing C_{D_0}			Body C_{D_0}						
①	②	③	④	⑤	⑥	⑦	⑧	⑨	⑩	⑪
M	$\left(C_{D_f}\right)_W$ eq. 4.1.5.1-c	$\left(C_{D_w}\right)_W$ sketch (a)	$\left(C_{D_0}\right)_W$ eq. 4.1.5.1-g ② + ③	$\left(C_{D_f}\right)_B$ eq. 4.2.3.1-c	C_{D_P} eq. 4.2.3.1-d	C_{D_b} fig. 4.2.3.1-24	$\left(C_{D_w}\right)_B$ fig. 4.2.3.1-26	$\left(C_{D_0}\right)_B$ eq. 4.2.3.1-e ⑤ + ⑥ + ⑦ + ⑧	$\left(C_{D_0}\right)_B S_B/S_{ref}$ ⑨ S_B/S_{ref}	$\left(C_{D_0}\right)_{WB}$ eq. 4.3.3.1-c ④ + ⑩
0.80	0.00858	---	0.00858	0.1157	0.00792	0.083	---	0.2066	0.01585	0.0244
0.90	↓	---	0.00858	↓	0.00792	0.096	---	0.2186	0.01677	0.0254
0.95	↓	---	0.00858	↓	0.00792	0.112	---	0.2356	0.01808	0.0267
1.00	↓	0.0010	0.00958	↓	0.00792	0.160	0.031	0.3146	0.02414	0.0337
1.025	↓	0.0025	0.01108	↓	0.00893	0.163	0.046	0.3316	0.02544	0.0366
1.05	↓	0.00475	0.01333	↓	0.00894	0.1026	0.054	0.2781	0.02134	0.0347
1.10	↓	0.0101	0.01868	↓	0.00398	0.077	0.061	0.2677	0.01977	0.0385
1.20	↓	0.0121	0.02068	↓	0	0.081	0.064	0.2407	0.01847	0.0382

The calculated values of the wing-body zero-lift drag coefficient are compared with modified test results from reference 19 in sketch (b). The drag-divergence Mach number of the isolated body has been used to aid in fairing the curve through the calculated points. The test results presented in reference 19 were corrected to a condition at which the base pressure is equal to the stream static pressure. The test points plotted on sketch (b) have been modified by addition of the calculated base-drag coefficient.

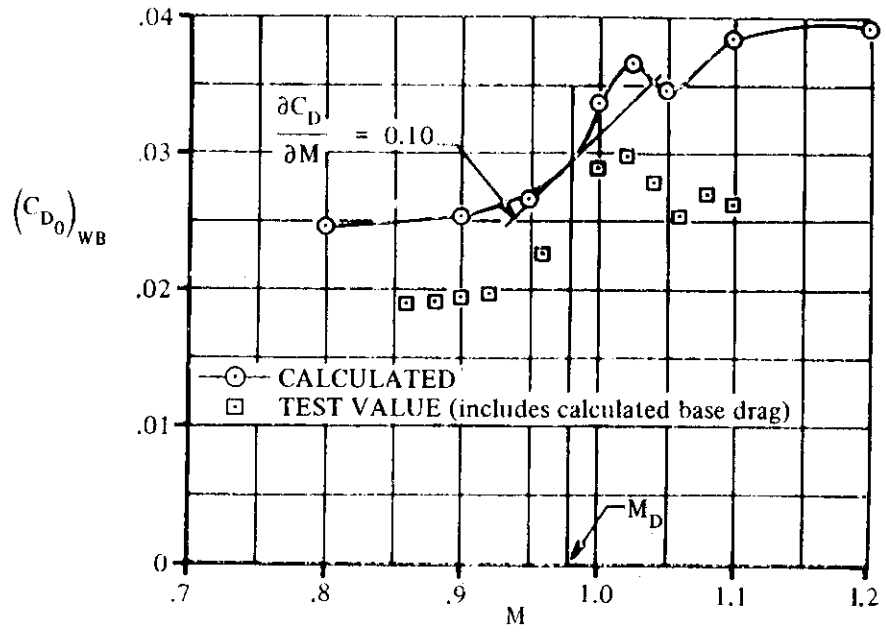

SKETCH (b)

C. SUPERSONIC

The estimation of wing-body drag at supersonic speeds also involves the calculation of interference effects. It is possible by using linear or higher-order theories to calculate some of these effects. However, the calculations require considerable effort and must be tailored carefully to the geometry of the configuration. The equivalent-body technique discussed in paragraph B above has been adapted to supersonic speeds, but with considerable complication. The resulting method, termed the "supersonic area-rule," gives the wave drag, including aerodynamic interferences, at a given Mach number.

Application of the supersonic area-rule requires automatic computing equipment. If such a computer is to be used, the following steps are required to prepare the machine input information and to interpret the computed drag values obtained.

Step 1. At a series of longitudinal stations compute the cross-sectional area intercepted by planes inclined at the angle $\mu = \sin^{-1}(1/M)$ to the x-axis (see sketch (c)). The areas so determined at each station are then projected on the plane normal to the longitudinal axis. The values of these projected areas are plotted at the intersection of the inclined plane and the longitudinal axis. This plot is the area distribution of the equivalent body of revolution.

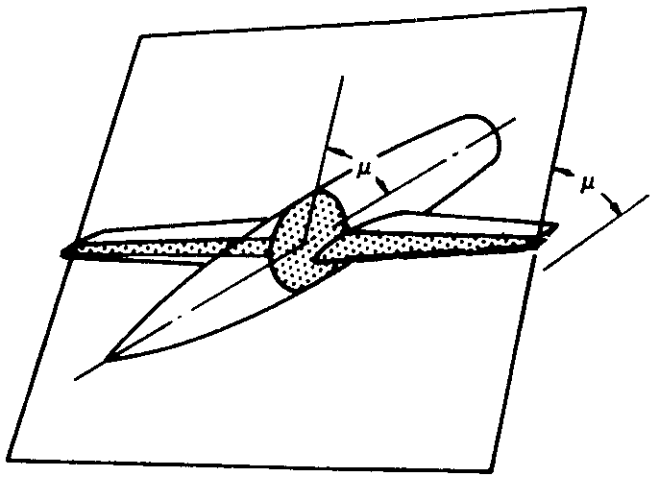

SKETCH (c)

This step can be simplified by using the following graphical procedure. First, construct cross sections normal to the longitudinal axis at an evenly-spaced number of longitudinal stations, say, spaced at Δx. Prepare a set of parallel lines on transparent paper with a spacing equal to $\Delta x \tan \mu$. Each one of these lines corresponds to one of the downstream stations intercepted by the inclined plane. The required projected cross section at a given station x is then determined by overlaying the transparent paper on the given normal cross sections and plotting the intersection of each of the parallel lines with its corresponding given normal-cross-section contour. The curve formed on the transparent paper by connecting the above intersections encloses the required projected area that when integrated is to be plotted at station x. This procedure is illustrated in sketch (d).

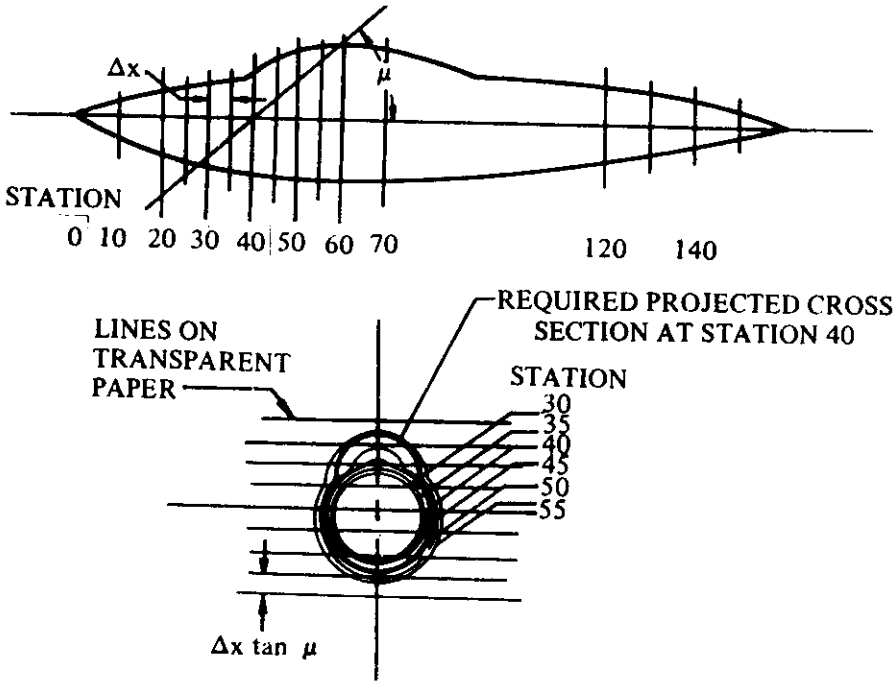

SKETCH (d)

Step 2. The procedure of step 1 is repeated for additional cases, where the inclined plane is fixed and the vehicle is rolled at a specified number of roll angles, as shown in sketch (e). For a configuration with four planes of symmetry, such as a symmetrical cruciform missile, only roll angles between 0 and 45^{o} must be considered. For cruciform configurations with two planes of symmetry, roll angles between 0 and 90^{o} should be considered. If there is just one plane of symmetry, roll angles between 0 and 180^{o} need to be considered.

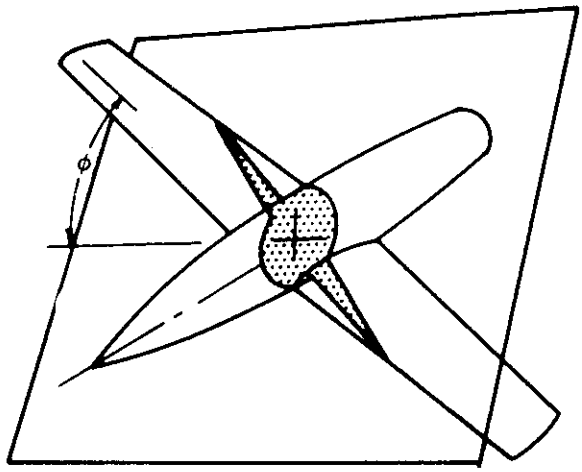

SKETCH (e)

Step 3. The drag for the equivalent body of revolution at each roll angle is then calculated by means of equation 4.3.3.1-b, or by the equation given in, for example, reference 4. These drag values are plotted as a function of roll angle and integrated to determine an average value of C_D. This average drag coefficient is taken to be the wave drag of the configuration at the chosen Mach number.

The number of roll angles required to achieve an accurate value of C_D varies with the configuration. If the C_D vs ϕ plot can be constructed without ambiguity with the number of roll angles chosen, then that number is sufficient. One should be particularly careful of conditions where the Mach angle lies along or very close to the leading edge of a wing, since this condition causes "spikes" in the C_D vs ϕ plot.

If automatic computing equipment is available, the supersonic-area-rule method should be used. Otherwise the Datcom method outlined below may be used.

The Datcom method is taken from reference 1 and is applicable to the following two classes of wing planforms:

Straight-Tapered Wings (conventional, trapezoidal planforms)

Non-Straight-Tapered Wings

- Double-delta wings
- Cranked wings
- Curved (Gothic and ogee) wings

DATCOM METHOD

The supersonic zero-lift drag coefficient of a wing-body combination, based on the reference area, is determined by adding the drag coefficients of the exposed components. The component contributions of the wing and body are determined by the methods of Sections 4.1.5.1 and 4.2.3.1, respectively. This approach is summarized by

$$\left(C_{D_0}\right)_{WB} = \left(C_{D_0}\right)_W + \left(C_{D_0}\right)_B \frac{S_B}{S_{ref}} \qquad 4.3.3.1\text{-d}$$

where

$\left(C_{D_0}\right)_W$ is the wing zero-lift drag coefficient at supersonic speeds determined as outlined below.

$\left(C_{D_0}\right)_B$ is the body zero-lift drag coefficient at supersonic speeds based on the body base area. This value is obtained from paragraph C of Section 4.2.3.1.

$\frac{S_B}{S_{ref}}$ is the ratio of the body base area to the reference area.

The method of determining the wing zero-lift drag coefficient is essentially that of paragraph C of Section 4.1.5.1, but with the parameters of the exposed wing (or wing panels in the case of composite wings) used to determine the skin-friction and wave-drag contributions. In order to present a more comprehensive method, the procedure of Section 4.1.5.1 as applied to the exposed panel(s) is fully outlined below.

The wing zero-lift drag coefficient is given by

$$\left(C_{D_0}\right)_W = \left(C_{D_f} + C_{D_w}\right)_W \qquad 4.3.3.1\text{-e}$$

where C_{D_f} and C_{D_w} are the supersonic skin-friction drag coefficient and the supersonic wave-drag coefficient, respectively, both based on a common reference area and outlined in the following paragraphs.

Skin-Friction Drag Coefficient

The supersonic skin-friction drag coefficient is given by

$$\left(C_{D_f}\right)_W = \left(C_f\right)_W \frac{\left(S_{wet}\right)_e}{S_{ref}} \qquad 4.3.3.1\text{-f}$$

for a conventional, trapezoidal planform, and

$$\left(C_{D_f}\right)_W = \left(C_{f_W}\right)_i \frac{\left(S_{wet_i}\right)_e}{S_{ref}} + \left(C_{f_W}\right)_o \frac{S_{wet_o}}{S_{ref}} \qquad 4.3.3.1\text{-g}$$

for a non-straight-tapered planform;

where

C_{f_W} is the turbulent flat-plate skin-friction coefficient of the wing (or wing panel in the case of composite wings), including roughness effects, as a function of Mach number and the Reynolds number based on the reference length ℓ. This value is determined as discussed in paragraph A of Section 4.1.5.1. The reference length ℓ is the mean aerodynamic chord $\bar{c}_e$ of the expose wing (or exposed wing panel in the case of composite wings).

$\frac{(S_{wet})_e}{S_{ref}}$ is the ratio of the wetted area of the exposed wing (or exposed wing panel in the case of composite wings) to the reference area.

The subscripts i and o refer to the inboard and outboard panels, respectively, of composite planforms.

Curved planforms are approximated by combinations of trapezoidal panels, in which case two such panels are usually sufficient to give a satisfactory result.

Non-straight-tapered wing geometric parameters are presented in Section 2.2.2.

Wave-Drag Coefficient

The form of the supersonic wave-drag-coefficient equation is in accordance with the results that have been arrived at in linear supersonic theory for the two-dimensional case. The effects of changes in wing planform and variable thickness ratio are accounted for by defining an effective thickness ratio and computing the wave-drag coefficient on a basic planform shape. A distinction is made between wings with sharp-nosed airfoil sections and wings with round-nosed airfoil sections.

Wings With Sharp-Nosed Airfoil Sections

For wings with sharp-nosed airfoil sections

$$\left(C_{D_w}\right)_W = \frac{K}{\beta}\left(\frac{t}{c}\right)^2_{eff} \frac{(S_{bw})_e}{S_{ref}} \qquad 4.3.3.1\text{-h}$$

when the leading edge of the basic wing is supersonic ($\beta \cot \Lambda_{LE_{bw}} \geq 1$), and

$$\left(C_{D_w}\right)_W = K \cot \Lambda_{LE_{bw}} \left(\frac{t}{c}\right)^2_{eff} \frac{(S_{bw})_e}{S_{ref}} \qquad 4.3.3.1\text{-i}$$

when the leading edge of the basic wing is subsonic ($\beta \cot \Lambda_{LE_{bw}} < 1$). The subscript bw refers to the basic wing (straight leading and trailing edges), and

$(S_{bw})_e$ is the area of the exposed basic wing. The selection of the basic planform for composite wings is discussed and illustrated schematically in paragraph C of Section 4.1.5.1.

$\left(\frac{t}{c}\right)_{eff}$ is the effective thickness ratio (for a conventional, trapezoidal planform, use the average thickness ratio of the exposed planform $(t/c)_{av}$). For a nonstraight-tapered planform

the effective thickness ratio is defined in terms of the basic planform and is given by

$$\left(\frac{t}{c}\right)_{eff} = \left[\frac{\int_{r_b}^{b/2} \left(\frac{t}{c}\right)^2 c_{bw}\ dy}{\int_{r_b}^{b/2} c_{bw}\ dy}\right]^{1/2} \qquad 4.3.3.1\text{-j}$$

where c_{bw} is the chord of the basic wing and r_b is the average radius of the body at the wing-body juncture. Note that both the chord of the actual wing and the chord of the basic wing appear in the numerator. The denominator is one-half the planform area of the exposed basic wing, so that

$$\left(\frac{t}{c}\right)_{eff} = \frac{\left[\int_{r_b}^{b/2} \left(\frac{t}{c}\right)^2 c_{bw}\ dy\right]^{1/2}}{\left[\frac{(S_{bw})_e}{2}\right]^{1/2}} \qquad 4.3.3.1\text{-j}'$$

Numerical integration of the integrand in the numerator is illustrated in the sample problem.

$\Lambda_{LE_{bw}}$ is the leading-edge sweep of the basic wing.

K is a constant factor for a given sharp-nosed airfoil section. K factors for sharp-nosed airfoils are presented in paragraph C of Section 4.1.5.1. For basic wings with variable thickness ratios the K factor is based on the airfoil section at the average chord of the exposed planform.

Wings With Round-Nosed Airfoil Sections

Wings with round-nosed airfoil sections exhibit a detached bow wave and a stagnation point, and the pressure-drag coefficient increases as a function of Mach number in a manner similar to the stagnation pressure. Consequently, a constant value of K cannot be used for basic wings with round-nosed airfoils.

The wave-drag coefficient of wings with round-nosed airfoil sections is approximated by adding the pressure drag of a blunt leading edge to the wave drag of the basic wing with an assumed sharp leading edge. By assuming a biconvex shape aft of the leading edge, the wave drag of a wing with a round-nosed leading edge is given by

$$\left(C_{D_w}\right)_w = C_{D_{LE}} + \frac{16}{3\beta}\left(\frac{t}{c}\right)^2_{eff} \frac{(S_{bw})_e}{S_{ref}} \qquad 4.3.3.1\text{-k}$$

when the leading edge of the basic wing is supersonic ($\beta \cot \Lambda_{LE} \geq 1$), and

$$\left(C_{D_w}\right)_w = C_{D_{LE}} + \frac{16}{3}\cot \Lambda_{LE_{bw}} \left(\frac{t}{c}\right)^2_{eff} \frac{(S_{bw})_e}{S_{ref}} \qquad 4.3.3.1\text{-}\ell$$

when the leading edge of the basic wing is subsonic ($\beta \cot \Lambda_{LE_{bw}} < 1$).

The second terms on the right-hand side of equations 4.3.3.1-k and 4.3.3.1-ℓ are the wing wave-drag coefficients of the basic wing with sharp-nosed, biconvex airfoils at the appropriate leading-edge condition, and

$C_{D_{LE}}$ is the pressure-drag coefficient on a swept, cylindrical leading edge obtained as a function of the Mach number and the leading-edge sweep of the basic wing from figure 4.3.3.1-38. The term $2r_{LE_{bw}} \dfrac{b_{bw} - 2r_b}{\cos \Lambda_{LE_{bw}}}$ is the frontal area of the leading edge of the exposed planform. For basic wings with variable thickness ratios the leading-edge radius $r_{LE_{bw}}$ is the radius of the section at the average chord of the exposed planform.

The correlation of cylindrical leading-edge pressure-drag coefficients is derived in reference 12 and has been substantiated over the Mach number range from 0.5 to 8.0 and for sweep angles from 0 to 75°.

A comparison of test data for 52 configurations with $\left(C_{D_0}\right)_{WB}$ calculated by this method is presented as table 4.3.3.1-B (taken from reference 1). The test configurations consisted of conventional and composite wings with sharp-nosed airfoil sections mounted on ogive-cylinder bodies of high fineness ratio. No detailed investigation has been made to evaluate body effects; therefore, the method should not be construed as pertaining to generalized wing-body combinations with arbitrary body shapes.

Within the limitations of the body shapes investigated, the method shows good agreement with the test results of reference 15. This can be attributed largely to low-thickness-ratio airfoils and small planform modifications – the conditions for which the wing-wave drag method of reference 1 is primarily intended. Predictions for the configurations of the remaining references are generally lower than the test results. This should be expected since the supersonic linear theory used as the basis for the wave-drag prediction is expected to underpredict this contribution for the thicker wing sections and the more extensive planform modifications.

The authors of reference 1 point out that some of the error is quite possibly associated with the manner in which the test data were analyzed. The test results presented in reference 14 were obtained on wing-body configurations without boundary-layer trips and with slightly blunted leading edges. Corrections were applied by the authors of reference 1 to obtain drag values corresponding to fully turbulent flow and sharp leading edges. References 20 and 21 present test results with natural transition. The skin-friction drag for these configurations was predicted by assuming fully turbulent flow over the body and laminar flow over the wing as suggested in the references.

It should be noted that the test values in table 4.3.3.1-B have been corrected to remove base drag, and that the calculated values do not include the base-drag term.

Perhaps the greatest value of the method is that it can be used to predict the supersonic wave-drag increments due to planform modifications and thickness variations. If test data are available for a configuration, the wave drag for a similar configuration can be estimated by predicting the wave drag for both configurations using the Datcom technique, and then applying the increment between the predictions to the test data. Sketches (f) and (g), both taken from reference 1, illustrate the application of this technique to predict the wave-drag variation as a function of planform modification and thickness variation, respectively. Note that although the absolute value of wave drag is not accurately predicted, the trends due to planform modifications and thickness variations are predicted quite well, even for thick, highly modified planforms.

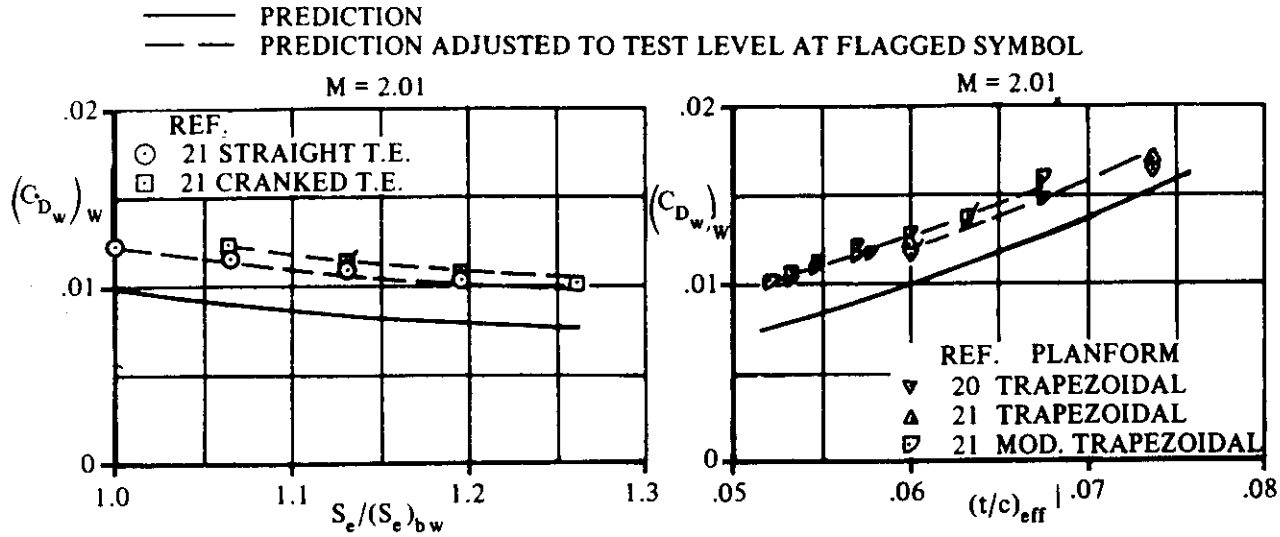

EFFECT OF PLANFORM MODIFICATIONS ON WING WAVE DRAG

SKETCH (f)

EFFECT OF THICKNESS DISTRIBUTION ON WING WAVE DRAG

SKETCH (g)

The limited availability of test data precludes substantiation of the supersonic zero-lift-drag method over wide ranges of planform and flow parameters for configurations having wings with blunt leading edges. A brief statement of an analysis conducted on the blunt-leading-edge planforms of references 23 and 24 is reported in reference 1. It is indicated therein that the method will give satisfactory results for bluntness drag for thin wings.

Sample Problem

Given: The wing-body configuration of reference 15. The configuration consists of a double-delta wing mounted on a cylindrical-ogive body.

Actual Wing Characteristics:

Double-delta planform $A = 1.25$ $\lambda = 0$ $\Lambda_{LE_i} = 83^o$ $\Lambda_{LE_o} = 70^o$

$\Lambda_{TE} = -15^o$ $b/2 = 10.0$ in. $\eta_B = 0.181$ $c_r = 40.0$ in.

$S_W = 319.32$ sq in. t/c (varies, see sketch (h))

Body Characteristics:

Ogive-cylinder $\ell_B = 40.0$ in. $d_{max} = 2.0$ in. $d_b = 2.0$ in. $\ell_B/d = 20.0$

$\ell_N = 12.0$ in. $f_N = \ell_N/d = 6.0$ $\ell_A = 28.0$ in. $f_A = \ell_A/d = 14.0$

$S_B = 3.14$ sq in. $S_S/S_B = 72.0$ $\theta_N = 8.5^o$

Basic Wing Characteristics (Wave-drag calculations):

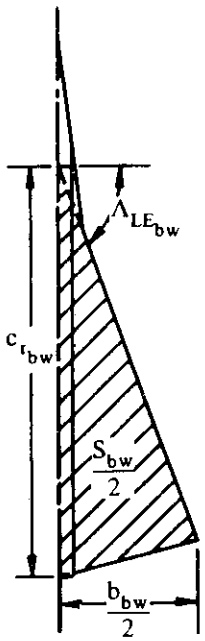

Delta planform $A_{bw} = 1.33$ $\lambda_{bw} = 0$ $\Lambda_{LE_{bw}} = 70^{o}$

$\Lambda_{TE_{bw}} = -15^{o}$ $(b/2)_{bw} = 10.0$ in. $c_{r_{bw}} = 30.16$ in.

$(S_{bw})_e = 244.26$ sq in.

Airfoil: hexagonal, sharp leading edge

$\frac{x_1}{c} = 0.4$ $\frac{x_2}{c} = 0.3$ $\frac{x_3}{c} = 0.3$ $(t/c)_{bw} = 0.02$

Inboard and Outboard Panel Characteristics (Skin-friction drag calculations):

Inboard panel (exposed)

$\left(c_{r_i}\right)_e = 31.165$ in. $(\lambda_i)_e = 0.794$

$(\bar{c}_i)_e = 28.25$ in. $(S_i)_e = 45.275$ sq in.

$\left(S_{wet_i}\right)_e = 90.55$ sq in. $(b_i/2)_e = 0.81$ in.

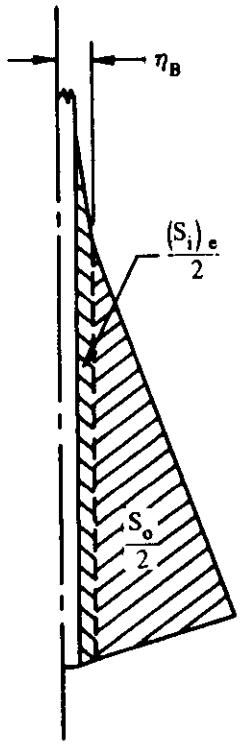

Outboard panel

$c_{r_o} = 24.73$ in. $\lambda_o = 0$ $\bar{c}_o = 16.5$ in.

$S_o = 202.52$ sq in. $(S_{wet})_o = 405.04$ sq in.

$b_o/2 = 8.19$ in.

Additional Characteristics:

$M = 2.98$; $\beta = 2.807$ Smooth surfaces (assume $k = 0$)

$S_{ref} = S_{bw} = 301.55$ sq in. $R_\ell = 1.741 \times 10^6$ per in.

Compute:

Determine the wing skin-friction-drag contribution

Inboard panel (exposed)

$$R_\ell = (1.741 \times 10^6)(\bar{c}_i)_e = (1.741 \times 10^6)(28.25) = 4.92 \times 10^7$$

$\ell/k = \infty$, read $\left(C_{f_W}\right)_i$ at calculated R_ℓ

$\left(C_{f_W}\right)_i = 0.00146$ (figure 4.1.5.1-26)

Outboard panel

$$R_\ell = (1.741 \times 10^6)(\bar{c}_o) = (1.741 \times 10^6)(16.5) = 2.87 \times 10^7$$

$\ell/k = \infty$, read $\left(C_{f_W}\right)_o$ at calculated R_ℓ

$\left(C_{f_W}\right)_o = 0.00158$ (figure 4.1.5.1-26)

$$\left(C_{D_f}\right)_W = \left(C_{f_W}\right)_i \frac{\left(S_{wet_i}\right)_e}{S_{ref}} + \left(C_{f_W}\right)_o \frac{S_{wet_o}}{S_{ref}} \quad \text{(equation 4.3.3.1-g)}$$

$$= (0.00146)\frac{90.55}{301.55} + (0.00158)\frac{405.04}{301.55}$$

$= 0.00256$ (based on S_{ref})

Determine the wing wave-drag coefficient.

$$K = \frac{c(c - x_2)}{x_1 x_3} = \frac{1\,(1 - 0.3)}{(0.4)\,(0.3)} = 5.833$$

$(t/c)_{eff}$

The thickness distribution of the actual wing and the chord distribution of the basic wing are shown in sketch (h).

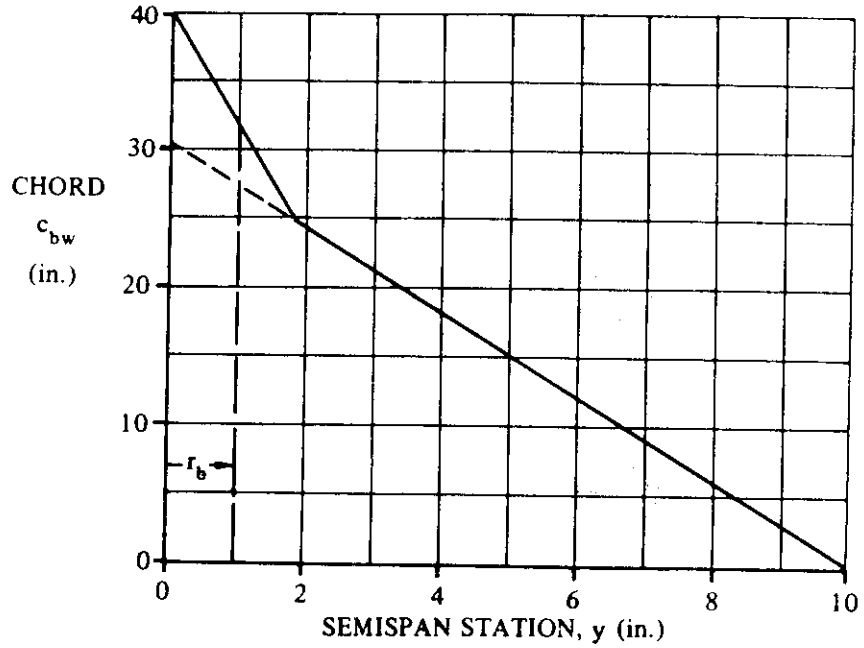

CHORD DISTRIBUTION (BASIC WING)

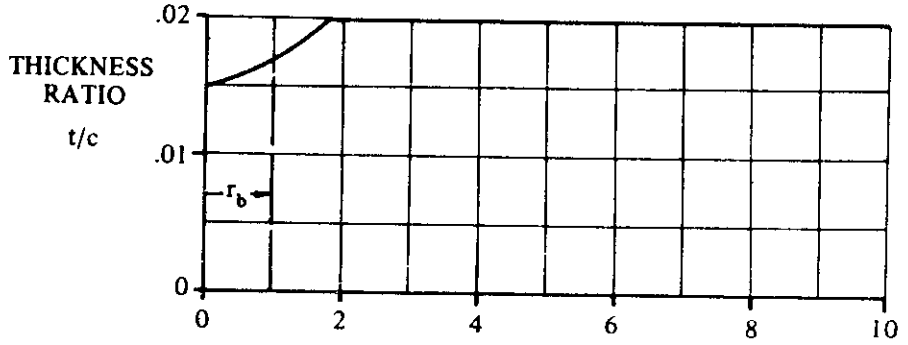

THICKNESS DISTRIBUTION (ACTUAL PLANFORM)

SKETCH (h)

Sketch (i) shows $(t/c)^2\ c_{bw}$ versus spanwise position. Graphical integration of this curve gives

$$\int_{r_b}^{b/2} \left(\frac{t}{c}\right)^2 c_{bw}\ dy = 0.0474 \text{ sq in.}$$

$$\left(\frac{t}{c}\right)^2_{eff} = \frac{\int_{r_b}^{b/2} \left(\frac{t}{c}\right)^2 c_{bw}\ dy}{1/2\ (S_{bw})_e} \quad \text{(equation 4.3.3.1-j')}$$

$$= \frac{0.0474}{1/2\,(244.26)} = 0.000388$$

$$\left(\frac{t}{c}\right)_{eff} = 0.0197$$

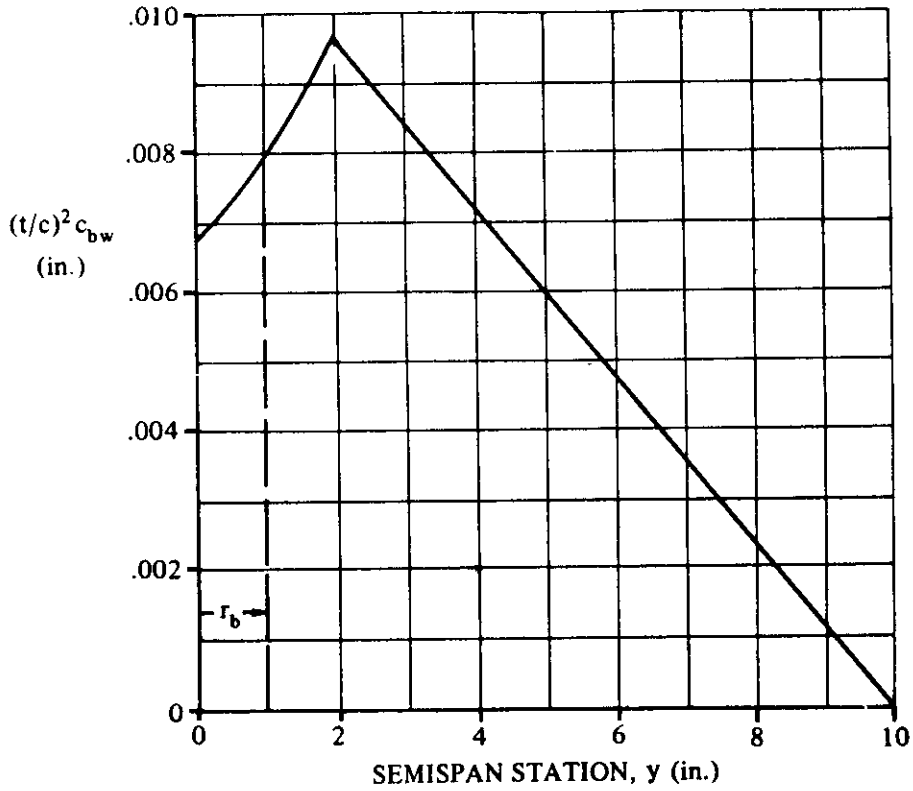

INTEGRAND FOR DETERMINING $(t/c)_{eff}$ FOR WING OF SAMPLE WAVE-DRAG CALCULATION

SKETCH (i)

$\beta \cot \Lambda_{LE} = (2.807)(\cot 70^{o}) = 1.022$ (supersonic leading edge)

$$\left(C_{D_w}\right)_W = \frac{K}{\beta}\left(\frac{t}{c}\right)^2_{eff} \frac{(S_{bw})_e}{S_{ref}} \quad \text{(equation 4.3.3.1-h)}$$

$$= \left(\frac{5.833}{2.807}\right)(0.0197)^2 \frac{244.26}{301.55}$$

$= 0.00065$ (based on S_{ref})

Determine the body contribution.

Skin-friction-drag coefficient

$R_{\ell} = (1.741 \times 10^6)(\ell_B) = (1.741 \times 10^6)(40) = 6.964 \times 10^7$

$\ell/k = \infty$, read $(C_f)_B$ at calculated R_{ℓ}

$(C_f)_B = 0.00139$ (figure 4.1.5.1-26)

Wave-drag coefficients (method 2, paragraph C, Section 4.2.3.1)

Forebody

$\beta/f_N = \frac{2.807}{6.0} = 0.468$; $K_N = 1.005$ (figure 4.2.3.1-63)

$C_{D_{N_2}} \left[f_N^2 + \frac{1}{4}\right] K_N = 0.985$ (figure 4.2.3.1-61)

$C_{D_{N_2}} = \frac{0.985}{(36 + 0.25)(1.005)} = 0.0270$ (based on S_B)

Afterbody

$\frac{d_b}{d} = 1.0$; $C_{D_A} = 0$ (figure 4.2.3.1-64)

Nose bluntness

$C_{D_{N_1}} = 0$ (no bluntness)

Afterbody interference-drag coefficient

$\frac{d_b}{d} = 1.0$; $C_{D_{A(NC)}} = 0$ (figure 4.2.3.1-44a)

Base-drag coefficient

$C_{D_b} = 0.098$ (figure 4.2.3.1-60) (based on S_B)

$\left(C_{D_0}\right)_B = (C_f)_B \frac{S_S}{S_B} + C_{D_{N_2}} + C_{D_A} + C_{D_{A(NC)}} + C_{D_{N_1}} + C_{D_b}$ (equation 4.2.3.1-h)

$= (0.00139)(72.0) + 0.0270 + 0 + 0 + 0 + 0.098$

$= 0.225$ (based on S_B)

Solution:

$$C_{D_0} = \left(C_{D_0}\right)_W + \left(C_{D_0}\right)_B \frac{S_B}{S_{ref}} \quad \text{(equation 4.3.3.1-d)}$$

$$= \left(C_{D_f} + C_{D_w}\right)_W + \left(C_{D_0}\right)_B \frac{S_B}{S_{ref}}$$

$$= 0.00256 + 0.00065 + (0.225)\frac{3.14}{301.55}$$

$$= 0.00555 \text{ (based on } S_{ref})$$

The test value from reference 15, corrected to remove base drag, is $C_{D_0} = 0.0046$. The corresponding calculated value is given by

$$C_{D_0} = 0.00555 - C_{D_b}\frac{S_B}{S_{ref}}$$

$$= 0.00555 - 0.00102$$

$$= 0.00453 \text{ (based on } S_{ref})$$

REFERENCES

1. Benepe, D.B., Kouri, B.G., Webb, J.B., et al: Aerodynamic Characteristics of Non-Straight-Taper Wings. AFFDL-TR-66-73, 1966. (U)
2. Marquardt, R.F.: A General Method for Predicting Subsonic Minimum Drag of an Arbitrary Aircraft Configuration. General Dynamics, F/W MR-A-1261, 1961. (C) Title Unclassified
3. Ward, G.N.: Supersonic Flow Past Slender Pointed Bodies. Quart. Jour. Mech. and Appl. Math., Vol. II, Pt. I, 1949. (U)
4. Fraenkel, L.E.: The Theoretical Wave Drag of Some Bodies of Revolution. RAE Aero 2420, 1951. (U)
5. Eminton, E.: On the Minimisation and Numerical Evaluation of Wave Drag. RAE Aero 2564, 1955. (U)
6. Weber, J.: Numerical Methods for Calculating the Zero-Lift Wave-Drag and the Lift-Dependent Wave-Drag of Slender Wings. RAE Aero 2629, 1959. (U)
7. Cahn, M.S., and Olstad, W.B.: A Numerical Method for Evaluating Wave Drag. NACA TN 4258, 1958. (U)
8. Holdaway, G.H.: Comparison of Theoretical and Experimental Zero-Lift Drag-Rise Characteristics of Wing-Body-Tail Combinations Near the Speed of Sound. NACA RM A53H17, 1953. (U)
9. Whitcomb, R.T.: Recent Results Pertaining to the Application of the "Area Rule." NACA RM L53I15a, 1953. (U)
10. Spreiter, J.R.: On the Range of Applicability of the Transonic Area Rule. NACA RM A54F28, 1954. (U)
11. Nelson, R.L., and Welsh, C.J.: Some Examples of the Applications of the Transonic and Supersonic Area Rules to the Prediction of Wave Drag. NASA TN D-446, 1960. (U)
12. Crosthwait, E.L.: Drag of Two-Dimensional Cylindrical Leading Edges. General Dynamics, F/W Rpt. AIM No. 50, 1966. (U)
13. Holdaway, G.H., and Mellenthin, J.A.: Evaluation of Blended Wing-Body Combinations with Curved Planforms at Mach Numbers up to 3.0. NASA TM X-379, 1960. (U)
14. Hicks, R.M., and Hopkins, E.J.: Effects of Spanwise Variation of Leading-Edge Sweep on the Lift, Drag, and Pitching Moment of a Wing-Body Combination at Mach Numbers from 0.7 to 2.94. NASA TN D-2236, 1964. (U)

15. Anon: Wind-Tunnel Tests of a Series of . . . Wing-Body Configurations for Investigation of Supersonic Lift/Drag Ratios. Unpublished Data. (U)

16. Anon: Unpublished Data on a Wing-Body-Glove Model Tested at Subsonic Speeds. (U)

17. Alford, W.J., and Ward, R.J.: Low-Speed Wind-Tunnel Investigation of the Aerodynamic Characteristics of a Hypersonic Airplane Model With Variable Wing Geometry. NASA TM X-663, 1962. (C) Title Unclassified

18. Jernell, L.S.: The Effects of Conical Camber on the Longitudinal Aerodynamic Characteristics of a Variable-Sweep Wing-Fuselage Configuration at Mach Numbers from 0.50 to 3.50. NASA TM X-804, 1963. (C) Title Unclassified

19. Whitcomb, R.T.: A Study of the Zero-Lift Drag Rise Characteristics of Wing-Body Combinations Near the Speed of Sound. NACA TR 1273, 1956. (U)

20. Cooper, M., and Sevier, J.R., Jr.: Effects of a Series of Inboard Planform Modifications on the Longitudinal Characteristics of Two 47° Sweptback Wings of Aspect Ratio 3.5, Taper Ratio 0.2, and Different Thickness Distributions at Mach Numbers of 1.61 and 2.01. NACA RM L53E07a, 1953. (U)

21. Sevier, J.R., Jr.: Effects of a Series of Inboard Plan-form Modifications on the Longitudinal Characteristics of Two Unswept Wings of Aspect Ratio 3.5, Taper Ratio 0.2, and Different Thickness Distributions at Mach Numbers of 1.61 and 2.01. NACA RM L53K11, 1954. (U)

22. Robins, A.W., Harris, R.V., Jr., and Jackson, C.M., Jr.: Characteristics at Mach Number of 2.03 of a Series of Wings Having Various Spanwise Distributions of Thickness Ratio and Chord. NASA TN D-631, 1960. (U)

23. Durgin, F.A.: A Study of Twist and Camber on Wings in Supersonic Flow. FDL-TDR-64-109, 1964. (U)

24. Anon: System 125A Design Study—Summary and Analysis of Wind-Tunnel Test Results from 1/125-Scale Model. General Dynamics, F/W Rpt. FZA-105, 1955. (C) Title Unclassified

TABLE 4.3.3.1-A

SUBSONIC WING-BODY ZERO-LIFT DRAG

DATA SUMMARY AND SUBSTANTIATION

Ref.	Config.	Planform	S_{ref} (ft^2)	ℓ_B (ft)	f_{fus}	$(S_S)_e$ (ft^2)	$\bar{c}_e$ (ft)	$\frac{t}{c}$	$\Lambda_{(t/c)_{max}}$ (deg)	$(S_{wet})_e$ (ft^2)	M	$R\ell$/ft x 10^{-6}	$(C_{D_0})_{WB}$ Calc.	$(C_{D_0})_{WB}$ Test	e Percent Error
13	WB	Ogee	5.55	5.0	18.75	3.55	$(2.58)_i$ $(1.47)_o$	$(0.060)_i$ $(0.025)_o$	$(74)_i$ $(20)_o$	$(3.28)_i$ $(6.68)_o$	0.6	3.50	0.00844	0.0083	1.7
											0.7	3.75	0.00834	0.0081	3.0
											0.8	4.00	0.00835	0.0081	3.1
											0.9		0.00811	0.0079	2.7
14	WB	Ogee	0.151	1.185	16.25	0.234	$(0.426)_i$ $(0.198)_o$	$(0.020)_i$ $(0.020)_o$	$(70)_i$ $(31)_o$	$(0.100)_i$ $(0.134)_o$	0.7	2.50	0.01345	0.0131	2.7
											0.9		0.01307	0.0128	2.1
	WB	Delta	0.151	1.185	16.25	0.234	0.231	0.020	47.5	0.230	0.7	2.50	0.01332	0.0131	1.7
											0.9		0.01279	0.0130	-1.6
	WB	Modified Trapezoidal	0.151	1.185	16.25	0.234	$(0.636)_i$ $(0.209)_o$	$(0.020)_i$ $(0.020)_o$	$(77.5)_i$ $(21.5)_o$	$(0.079)_i$ $(0.122)_o$	0.7	2.50	0.01362	0.0138	-1.3
											0.9		0.01381	0.0134	3.1
	WB	Trapezoidal	0.151	1.185	16.25	0.234	0.230	0.020	10	0.230	0.7	2.50	0.01427	0.0147	-2.9
15	WB	Double-Delta	2.44	3.465	18.9	1.788	$(2.23)_i$ $(1.13)_o$	$(0.026)_i$ $(0.027)_o$	$(75)_i$ $(47.5)_o$	$(0.803)_i$ $(2.93)_o$	0.4	6.2	0.00740	0.0074	0
											0.72	6.8	0.00699	0.0073	-4.2
											0.89	6.1	0.00694	0.0070	-0.9
			2.46	3.465	18.9	1.788	$(2.20)_i$ $(1.12)_o$	$(0.026)_i$ $(0.025)_o$	$(75)_i$ $(47.5)_o$	$(1.01)_i$ $(2.78)_o$	0.41	3.7	0.00745	0.0076	-2.0
											0.72	5.5	0.00708	0.0071	-0.3
											0.88	6.3	0.00683	0.0065	5.1

TABLE 4.3.3.1-A (CONTD)

Ref.	Config.	Planform	S_{ref} (ft^2)	ℓ_B (ft)	f_{fus}	$(S_S)_e$ (ft^2)	$\bar{c}_e$ (ft)	$\frac{t}{c}$	$\Lambda_{(t/c)_{max}}$ (deg)	$(S_{wet})_e$ (ft^2)	M	R /ft $\times 10^{-6}$	$(C_{D_0})_{WB}$ Calc.	$(C_{D_0})_{WB}$ Test	e Percent Error
16	WB	Cranked	0.913	3.33	10	2.66	$(0.615)_i$ $(0.334)_o$	$(0.118)_i$ $(0.102)_o$	$(8.5)_i$ $(12.5)_o$	$(0.326)_i$ $(1.330)_o$	0.7	7.0	0.0220	0.0210	4.8
			0.913	3.33	10	2.66	$(0.794)_i$ $(0.334)_o$	$(0.091)_i$ $(0.102)_o$	$(30.5)_i$ $(12.5)_o$	$(0.868)_i$ $(1.330)_o$	0.7	7.0	0.0254	0.0251	1.2
			0.913	3.33	10	2.66	$(0.997)_i$ $(0.334)_o$	$(0.073)_i$ $(0.102)_o$	$(41)_i$ $(12.5)_o$	$(1.520)_i$ $(1.330)_o$	0.7	7.0	0.0274	0.0282	-2.8
17	WBNHV	Cranked	4.67	5.34	17.8	2.81	$(1.69)_i$ $(0.682)_o$	$(0.0123)_i$ $(0.0372)_o$	$(70)_i$ $(25)_o$	$(4.28)_i$ $(3.58)_o$	0.25	1.31	0.0175	(a)	
			4.58	5.34	17.8	2.81	$(1.87)_i$ $(0.813)_o$	$(0.0115)_i$ $(0.0328)_o$	$(70)_i$ $(47.5)_o$	$(4.42)_i$ $(3.31)_o$	0.25	1.31	0.01695		
18	WB	Cranked	1.30	3.70	18.2	1.984	$(0.844)_i$ $(0.306)_o$	$(0.032)_i$ $(0.060)_o$	$(52)_i$ $(7.4)_o$	$(1.120)_i$ $(1.186)_o$	0.5	1.042	0.01538		
			1.30	3.70	18.2	1.984	$(0.806)_i$ $(0.367)_o$	$(0.032)_i$ $(0.040)_o$	$(54.6)_i$ $(40)_o$	$(1.508)_i$ $(0.934)_o$	0.5	1.042	0.01394		
											0.8	1.414	0.01298		
			1.30	3.70	18.2	1.984	$(1.008)_i$ $(0.378)_o$	$(0.032)_i$ $(0.021)_o$	$(64.5)_i$ $(70)_o$	$(1.412)_i$ $(0.704)_o$	0.5	1.042	0.01227		
											0.8	1.414	0.01150		
											0.9	1.498	0.01115		

(a) This information is classified CONFIDENTIAL.

Average Error = $\frac{\Sigma|e|}{n}$ = 2.8%

TABLE 4.3.3.1-8
SUPERSONIC WING-BODY ZERO-LIFT DRAG
DATA SUMMARY AND SUBSTANTIATION

Ref.	Config.	Planform	Airfoil	f_N	S_{ref} (ft^2)	A	Λ_{LE_i} (deg)	Λ_{LE_o} (deg)	η_B	$\left(\frac{t}{c}\right)_{eff}$	M	$R\ell$/ft x 10^{-6}	$\left(C_{D_0}\right)_{WB}$ Calc.	$\left(C_{D_0}\right)_{WB}$ Test	e Percent Error
20	WB	Trapezoidal	Hexagonal	3.5	1.14	3.50	—	51.6	—	0.06	1.61	4.1	0.0235	0.0238	-1.3
		↓	↓	↓	↓	↓	—	↓	—	↓	2.01	3.4	0.0194	0.0215	-9.8
		Modified Trapezoidal	Hexagonal	3.5	1.14	3.15	—	51.6	—	0.0569	1.61	4.1	0.0221	0.0235	-6.0
						2.86	—	51.6	—	0.0547	1.61	4.1	0.0211	0.0233	-9.4
						↓	—	↓	—	↓	2.01	3.4	0.0177	0.0208	-14.9
						3.15	64.1	51.6	0.40	0.0569	1.61	4.1	0.0221	0.0228	-3.1
						2.86	64.1	51.6	0.40	0.0547	1.61	4.1	0.0211	0.0225	-6.2
						2.62	64.1	51.6	0.40	0.0532	1.61	3.4	0.0207	0.0221	-6.3
						2.86	70.7	51.6	0.40	0.0547	1.61	4.1	0.0211	0.0227	-7.0
						↓	↓	↓	↓	↓	2.01	3.4	0.0177	0.0202	-12.4
						2.62	70.7	51.6	0.40	0.0532	1.61	4.1	0.0207	0.0225	-8.0
						2.42	70.7	51.6	0.40	0.0519	1.61	3.4	0.0202	0.0221	-8.6
						↓	↓	↓	↓	↓	2.01	3.4	0.0168	0.0207	-18.9
		Trapezoidal	Hexagonal	3.5	1.14	3.50	—	51.6	—	0.0737	1.61	4.1	0.0304	0.0296	2.7
		↓	↓	↓	↓	↓	—	51.6	—	↓	2.01	3.4	0.0245	0.0265	-7.5
		Modified Trapezoidal	Hexagonal	3.5	1.14	3.15	—	51.6	—	0.0674	1.61	4.1	0.0270	0.0280	-3.6
						2.86	—	51.6	—	0.0632	1.61	4.1	0.0249	0.0273	-8.8
						↓	—	↓	—	↓	2.01	3.4	0.0205	0.0252	-18.7
						3.15	64.1	51.6	0.40	0.0674	1.61	4.1	0.0270	0.0279	-3.2

TABLE 4.3.3.1-B (CONTD)

Ref.	Config.	Planform	Airfoil	f_N	S_{ref} (ft^2)	A	Λ_{LE_i} (deg)	Λ_{LE_o} (deg)	η_B	$\left(\frac{t}{c}\right)_{eff}$	M	$R\ell$/ft $\times 10^{-6}$	$\left(C_{D_0}\right)_{WB}$ Calc.	$\left(C_{D_0}\right)_{WB}$ Test	e Percent Error
20	WB	Trapezoidal	Hexagonal	3.5	1.14	2.86	64.1	51.6	0.40	0.0632	1.61	4.1	0.0249	0.0258	-3.5
						2.62	64.1	51.6	0.40	0.0600	1.61	3.4	0.0237	0.0248	-4.4
						2.86	70.7	51.6	0.40	0.0632	1.61	4.1	0.0249	0.0265	-6.0
						↓	↓	↓	↓	↓	2.01	3.4	0.0205	0.0235	-12.8
						2.62	70.7	51.6	0.40	0.0600	1.61	3.4	0.0237	0.0249	-4.8
						2.42	70.7	51.6	0.40	0.0577	1.61	3.4	0.0266	0.0238	11.8
						↓	↓	↓	↓	↓	2.01	3.4	0.0186	0.0218	-14.7
21	WB	Trapezoidal	Hexagonal	3.5	1.14	3.50	--	20.9	--	0.060	1.61	4.1	0.0235	0.0270	-13.0
		↓	↓	↓	↓	↓	--	↓	--	↓	2.01	3.4	0.0194	0.0218	-11.0
		Modified Trapezoidal	Hexagonal	3.5	1.14	3.15	49.6	20.9	0.40	0.0569	2.01	3.4	0.0184	0.0210	-12.4
						2.86	63.1	20.9	0.40	0.0547	2.01	3.4	0.0177	0.0203	-12.8
						2.62	70.1	20.9	0.40	0.0532	1.61	2.2	0.0217	0.0241	-10.0
						2.62	70.1	20.9	0.40	0.0532	2.01	2.5	0.0179	0.0204	-12.3
						3.15	--	20.9	--	0.0569	1.61	4.1	0.0221	0.0266	-16.9
						↓	--	↓	--	↓	2.01	3.4	0.0184	0.0217	-19.8
						2.86	49.6	20.9	0.40	0.0547	2.01	3.4	0.0177	0.0208	-14.9
						2.62	63.1	20.9	0.40	0.0532	2.01	3.4	0.0172	0.0201	-14.4
						2.42	70.1	20.9	0.40	0.0519	1.61	2.2	0.0213	0.0240	-11.3
						↓	↓	↓	↓	↓	2.01	2.5	0.0176	0.0202	-12.9
		Trapezoidal	Hexagonal	3.5	1.14	3.50	--	20.9	--	0.0737	1.61	4.1	0.0304	0.0323	-5.9
		↓	↓	↓	↓	↓	--	↓	--	↓	2.01	3.4	0.0245	0.0260	-5.8

TABLE 4.3.3.1-B (CONTD)

Ref.	Config.	Planform	Airfoil	f_N	S_{ref} (ft^2)	A	Λ_{LE_i} (deg)	Λ_{LE_o} (deg)	η_B	$\left(\frac{t}{c}\right)_{eff}$	M	$R\ell/ft$ x 10^{-6}	$\left(C_{D_0}\right)_{WB}$ Calc.	$\left(C_{D_0}\right)_{WB}$ Test	e Percent Error
21	WB	Modified Trapezoidal	Hexagonal	3.5	1.14	3.15	49.6	20.9	0.40	0.0674	2.01	3.4	0.0220	0.0242	-9.1
						2.86	63.1	20.9	0.40	0.0632	2.01	3.4	0.0205	0.0230	-10.9
						2.62	70.1	20.9	0.40	0.0600	1.61	2.2	0.0247	0.0272	-9.2
						↓	↓	↓	↓	↓	2.01	2.5	0.0200	0.0224	-10.7
						3.15	—	20.9	—	0.0674	1.61	4.1	0.0207	0.0311	-13.2
						↓	—	↓	—	↓	2.01	3.4	0.0220	0.0255	-13.7
						2.86	49.6	20.9	0.40	0.0632	2.01	3.4	0.0205	0.0232	-11.6
						2.62	63.1	20.9	0.40	0.0600	2.01	3.4	0.0193	0.0223	-13.5
						2.42	70.1	20.9	0.40	0.0577	1.61	2.2	0.0237	0.0266	-10.9
						↓	↓	↓	↓	↓	2.01	2.5	0.0193	0.0218	-11.5
		Delta	Hexagonal	6.0	2.09	1.33	—	70	—	0.02	2.98	10.8	0.0048	0.0046	4.3
		↓	↓	↓	↓	↓	—	↓	—	↓	↓	20.5	0.0044	0.0044	0
15	WB	Double-Delta	Hexagonal	6.0	1.94	1.57	80	60	0.322	0.0258	3.01	10.8	0.0060	0.0060	0
											2.98	20.8	0.0056	0.0048	16.7
											2.59	10.0	0.0067	0.0063	6.3
											↓	22.8	0.0061	0.0062	-1.6
			Parabolic	6.0	1.91	1.60	80	60	0.330	0.0253	2.98	10.9	0.0059	0.0068	-13.2
			↓	↓	↓	↓	↓	↓	↓	↓	↓	20.8	0.0054	0.0067	-19.4
			Hexagonal	6.0	2.09	1.25	83	70	0.181	0.0199	2.98	11.1	0.0049	0.0049	0
			↓	↓	↓	↓	↓	↓	↓	↓	↓	20.9	0.0045	0.0046	-2.2

TABLE 4.3.3.1-B (CONTD)

Ref.	Config.	Planform	Airfoil	f_N	S_{ref} (ft^2)	A	Λ_{LE_i} (deg)	Λ_{LE_o} (deg)	η_B	$\left(\frac{t}{c}\right)_{eff}$	M	Rℓ/ft x 10^{-6}	$\left(C_{D_0}\right)_{WB}$ Calc.	$\left(C_{D_0}\right)_{WB}$ Test	e Percent Error
15	WB	Double Delta	Hexagonal	6.0	2.08	1.05	83	70	0.197	0.0198	2.98	11.0	0.0051	0.0048	6.3
												20.7	0.0047	0.0045	4.4
											2.59	10.0	0.0056	0.0054	3.7
												22.8	0.0051	0.0051	0
			Hexagonal	6.0	2.02	1.64	82	60	0.215	0.0185	2.98	10.9	0.0062	0.0062	0
											2.59	9.9	0.0070	0.0071	-1.4
			Hexagonal	6.0	2.28	1.53	81	63	0.215	0.0171	2.98	11.5	0.0058	0.0058	0
											2.59	10.6	0.0063	0.0064	-1.6
					2.51	1.41	80	66	0.215	0.0155	2.98	11.0	0.0053	0.0054	-1.9
			Double-Wedge	6.2	2.16	1.52	83	62	0.215	0.0218	2.98	11.3	0.0052	0.0051	2.0
												21.9	0.0048	0.0048	0
											2.59	10.2	0.0057	0.0057	0
												22.2	0.0063	0.0054	-1.9
											2.20	10.5	0.0063	0.0064	-1.6
											1.59	10.6	0.0070	0.0070	0
			Parabolic	6.0	2.16	1.52	83	62	0.215	0.0214	2.98	11.5	0.0054	0.0051	5.9
												22.4	0.0049	0.0048	2.1
											2.81	10.8	0.0057	0.0057	0
												22.6	0.0052	0.0054	-3.7
											2.59	10.3	0.0060	0.0059	1.7
												22.3	0.0055	0.0054	1.9

TABLE 4.3.3.1-B (CONTD)

Ref.	Config.	Planform	Airfoil	f_N	S_{ref} (ft^2)	A	Λ_{LE_i} (deg)	Λ_{LE_o} (deg)	η_B	$\left(\frac{t}{c}\right)_{eff}$	M	$R\ell$/ft x 10^{-6}	$\left(C_{D_0}\right)_{WB}$ Calc.	$\left(C_{D_0}\right)_{WB}$ Test	e Percent Error
15	WB	Double-Delta	Parabolic	6.0	2.16	1.52	83	62	0.215	0.0214	2.20	10.4	0.0066	0.0062	6.5
											1.59	10.5	0.0073	0.0067	9.0
											1.08	6.6	0.0084	0.0085	-1.2
			Hexagonal	6.0	2.25	1.48	83	62	0.215	0.0168	2.98	11.8	0.0057	0.0057	0
											2.81	10.9	0.0060	0.0061	-1.6
											2.59	10.6	0.0064	0.0063	1.6
											2.20	10.6	0.0071	0.0071	0
											1.59	13.2	0.0076	0.0076	0
											1.17	6.5	0.0087	0.0096	-9.4
14	WB	Delta	Hexagonal	6.5	0.15	2.17	—	59	—	0.02	1.40	2.5	0.0131	0.0159	-17.6
							—		—		1.98	2.5	0.0118	0.0125	-5.6
							—		—		2.94	2.5	0.0095	0.0114	-16.7
		Ogee	Hexagonal	6.5	0.15	2.17	—	—	—	0.02	1.40	2.5	0.0131	0.0150	-12.7
							—	—	—		1.98	2.5	0.0118	0.0116	1.7
							—	—	—		2.94	2.5	0.0095	0.0100	-5.0
		Trapezoidal	Hexagonal	6.5	0.15	1.9	—	10	—	0.02	1.40	2.5	0.0143	0.0160	-10.6
							—		—		1.98	2.5	0.0122	0.0125	-2.4
							—		—		2.94	2.5	0.0098	0.0114	-14.0
		Modified Trapezoidal	Hexagonal	6.5	0.15	1.9	—	—	—	0.02	1.40	2.5	0.0141	0.0152	-7.2
							—	—	—		1.98	2.5	0.0119	0.0129	-7.8
							—	—	—		2.94	2.5	0.0096	0.0108	-11.1

TABLE 4.3.3.1-B (CONTD)

Ref.	Config.	Planform	Airfoil	t_N	S_{ref} (ft^2)	A	Λ_{LE_i} (deg)	Λ_{LE_o} (deg)	η_B	$\left(\frac{t}{c}\right)_{eff}$	M	R_ℓ/ft x 10^{-6}	$\left(C_{D_0}\right)_{WB}$ Calc.	$\left(C_{D_0}\right)_{WB}$ Test	e Percent Error
22	W	Trapezoidal	Biconvex	—	1.60	2.5	—	63.4	—	0.04	2.03	4.3	0.0097	0.0110	-11.8
				—			—		—			2.1	0.0104	0.0112	-7.1
				—			—		—			4.3	0.0097	0.0109	-11.0
				—			—		—			2.1	0.0104	0.0114	-8.8
				—	0.96	1.5	—	63.4	—	0.04	2.03	5.5	0.0094	0.0106	-11.3
				—			—		—			6.8	0.0101	0.0113	-10.6

Average Error = $\frac{\Sigma|e|}{n}$ = 7.5%

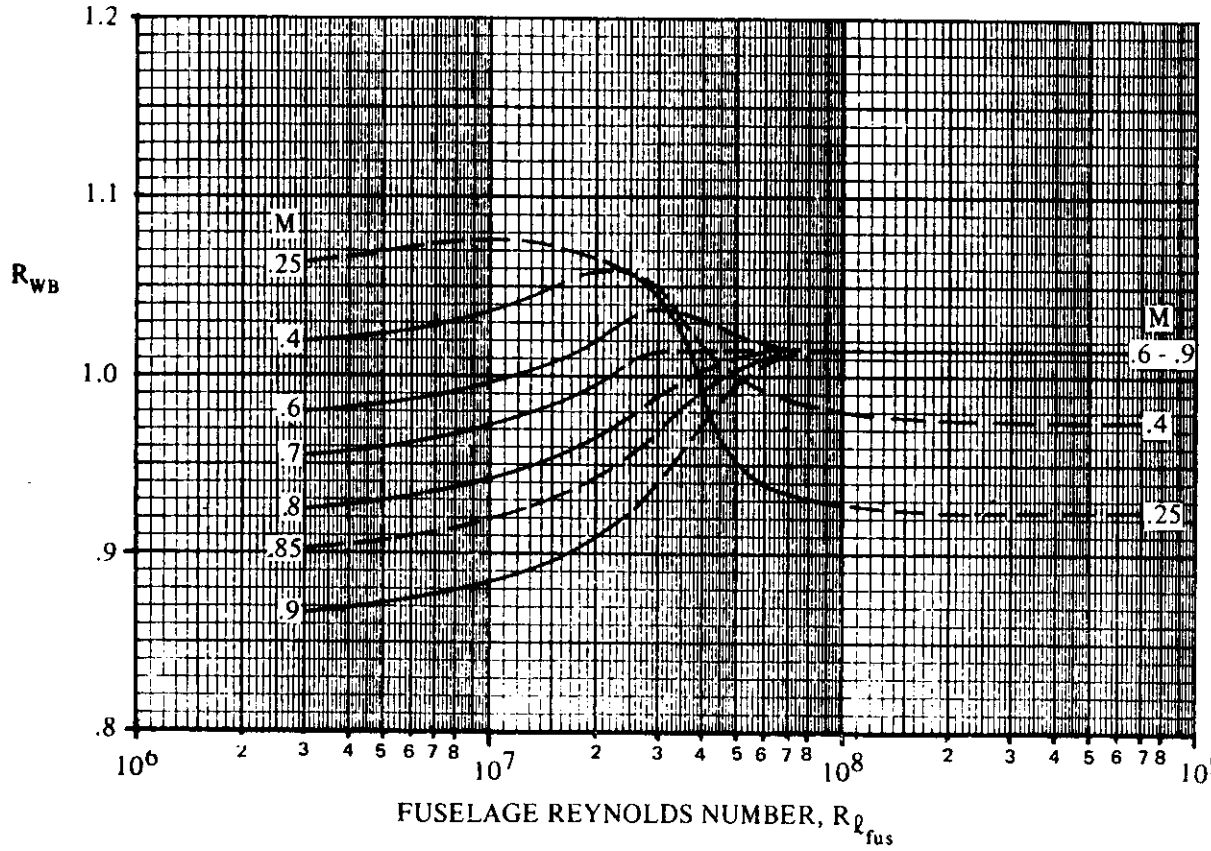

FIGURE 4.3.3.1-37 WING-BODY INTERFERENCE CORRELATION FACTOR – SUBSONIC SPEEDS

$$C_{D_{LE}}\left[\frac{S_{ref}}{2r_{LE_{bw}}\left(\frac{b_{bw}-2r_b}{\cos\Lambda_{LE_{bw}}}\right)}\right] = 1.28\,\frac{M^3\cos^6\Lambda_{LE_{bw}}}{1+M^3\cos^3\Lambda_{LE_{bw}}} \quad \text{(Ref. 12)}$$

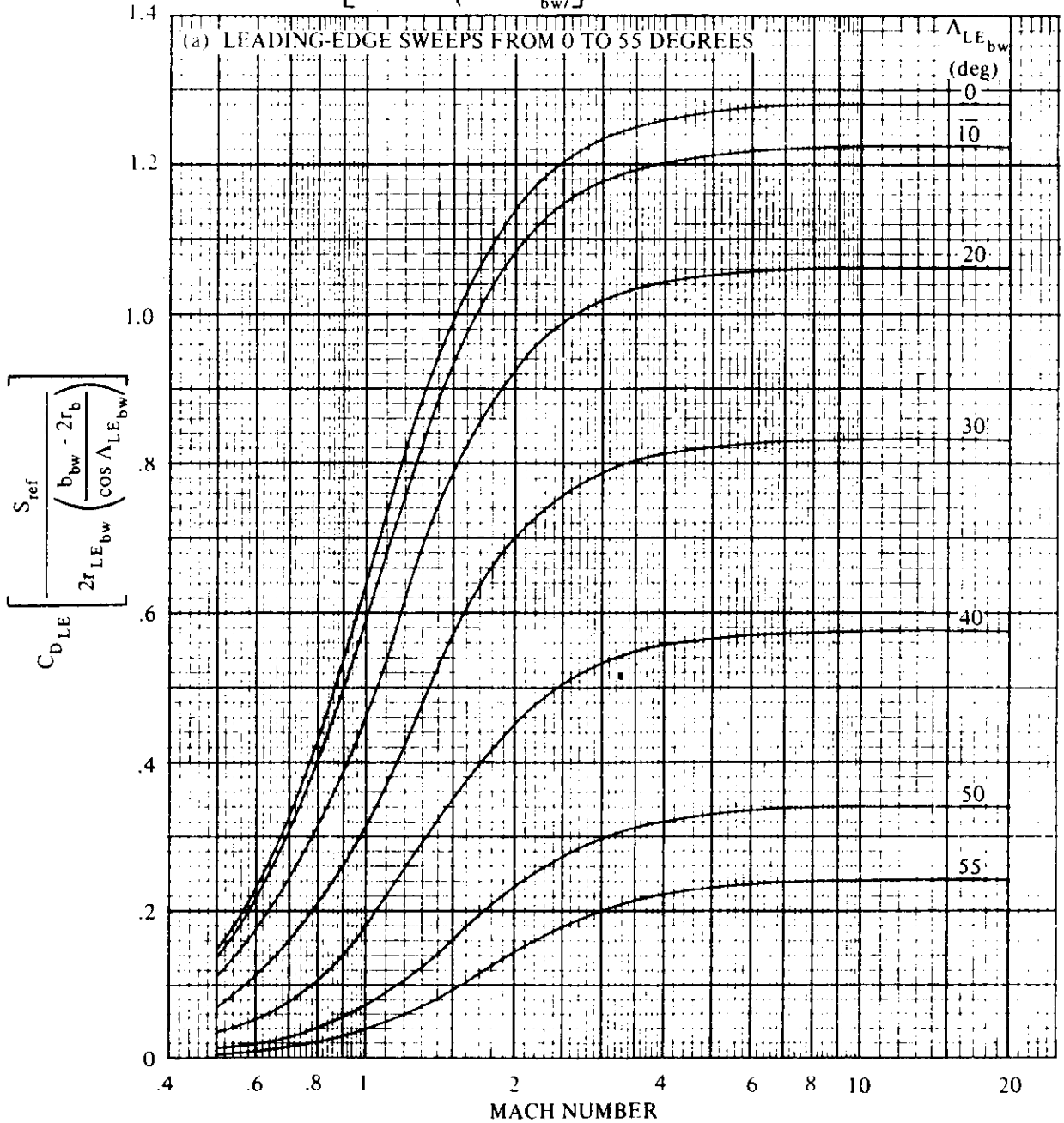

FIGURE 4.3.3.1-38 CORRELATION OF CYLINDRICAL LEADING-EDGE PRESSURE DRAG COEFFICIENTS

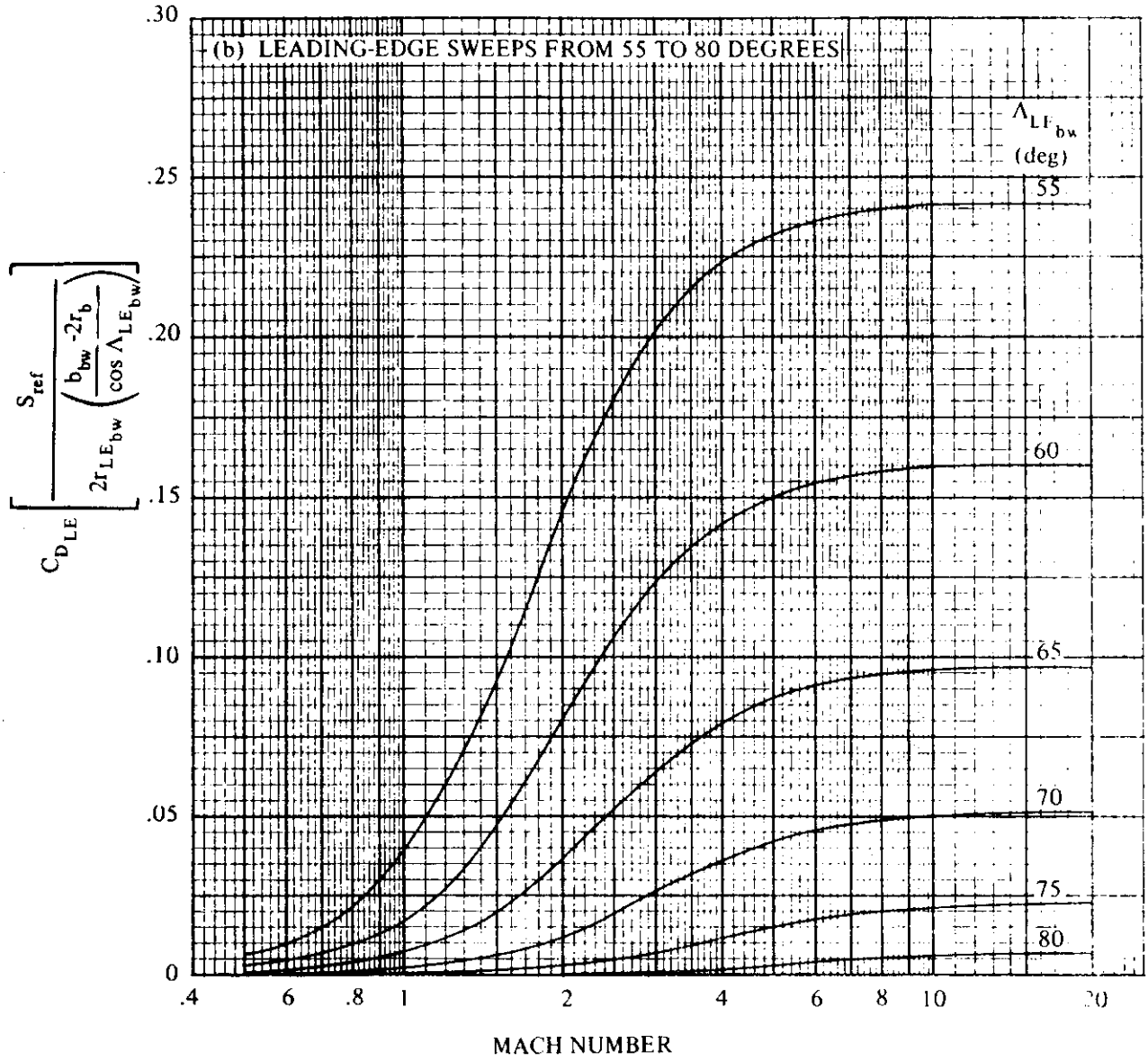

FIGURE 4.3.3.1-38 (CONTD)

4.3.3.2 WING-BODY DRAG AT ANGLE OF ATTACK

Determination of wing-body or tail-body drag at angle of attack is more an art than a science. Little is known concerning the wing-body aerodynamic interferences that occur at angle of attack. These interferences are usually significant only during the detailed design of a configuration or for a configuration especially designed for minimum interference at a particular flight condition. The total drag of a wing-body configuration at angle of attack may be expressed in the form

$$(C_D)_{WB} = (C_{D_0})_{WB} + (C_{D_L})_{WB} \qquad 4.3.3.2\text{-a}$$

where $(C_{D_0})_{WB}$ is the zero-lift drag and $(C_{D_L})_{WB}$ represents the drag due to lift. The zero-lift drag of the wing-body configuration may be obtained by using the methods of Section 4.3.3.1. The same two methods for estimating the wing-body drag-due-to-lift term are presented in each speed regime of this section. The first method, taken from Reference 1, evaluates the wing-body configuration as a unit. The second method evaluates and combines the isolated drag due to lift of the wing and of the body.

The primary advantage of Method 1 is its consideration of camber effects and its applicability to the high-lift region, i.e., beyond the parabolic drag region. However, its application is restricted to fighter-type aircraft with straight-tapered planforms.

Because of the empirical nature of Method 1 (values for the regression coefficients), exact solutions are available only at the following Mach numbers: 0.6, 0.7, 0.8, 0.9, 0.95, 1.0, 1.1, 1.2, 1.3, 1.4, 1.5, 2.0, and 2.5. At other Mach numbers interpolation is necessary. For the low-speed regime, the $M = 0.6$ values can be used, but only as an approximation. The solutions at Mach numbers 1.0 and 2.5 should be used cautiously, because of the somewhat limited amount of test data used in the determination of the regression coefficients.

A. SUBSONIC

Two different methods are presented for evaluating the total drag of a wing-body configuration. The first method is restricted to fighter-type aircraft with straight-tapered planforms. The second method is general and may be applied to both straight-tapered planforms and non-straight-tapered planforms, including double-delta, cranked, and curved wings.

The general categories of non-straight-tapered wings are illustrated in Sketch (a) of Section 4.1.3.2, while the wing-geometry parameters are presented in Section 2.2.2.

For Mach numbers less than 0.6 and values within the parabolic drag region (generally for $C_L < 0.4$ or 0.5), Method 2 should be used because of the limitation of Method 1 for Mach numbers below 0.6.

DATCOM METHOD

Method 1

This method was developed in Reference 1 for fighter-type aircraft by using the linear regression analysis of mathematical statistics. In general, a regression analysis involves the study of a group of variables to determine their effect on a given parameter. In this case, multidimensional least-squares curve fits were used to relate linearly the incremental drag due to lift of a wing-body configuration

to certain nondimensional geometric parameters. The result of this work is presented below in Equation 4.3.3.2-b, a purely empirical equation based on the various total-wing-planform geometric parameters and Reynolds number. For more detailed information regarding the analysis, the reader is referred to Reference 1.

The regression coefficients given in Table 4.3.3.2-D, as a function of Mach number and angle of attack, are not those presented in Reference 1. Those in Table 4.3.3.2-D are a more recent and improved version obtained from the authors of Reference 1.

An unfortunate feature of this method is the lack of physical appreciation of where the parabolic drag region ends; i.e., where separation effects become prominent. A second method, called the semiempirical method, which provides a physical appreciation of the flow conditions, is also presented in Reference 1. The semiempirical method is structured to consider the following various flow conditions: attached flow, initially contained separated or mixed flow, and major flow separation occurring after the initially contained separated or mixed flow. The semiempirical method is somewhat more difficult to apply, while its accuracy is approximately the same as that of Method 1 presented herein. For the details regarding the application of the semiempirical method, the reader is referred to Reference 1.

It is advisable to restrict the applicability of Method 1 to the range of geometric parameters of the test data used in the formulation of the regression coefficients. If the method is used for configurations that exceed the range of test data, the results should be applied with caution. The test data used in the formulation of the regression coefficients have geometric parameters within the following limits:

aspect ratio, A	1.6 to 6.0
taper ratio, λ	0 to 1
twist, θ	0 to -9.4^{o}
leading-edge radius, LER/$\bar{c}$	0 to 0.015
thickness, t/$\bar{c}$	0.025 to 0.10
NACA camber, $(y_c)_{max}/\bar{c}$	0 to 0.0263
conical-camber design lift coefficient, C_{L_d}	0 to 0.45
forebody fineness ratio, ℓ_N/d	2.2 to 8.4
afterbody fineness ratio, ℓ_A/d	0.3 to 5.6
leading-edge sweep, Λ_{LE}	0 to 70^{o}
Reynolds number, R_ℓ	0.8×10^6 to 8×10^6

Equation 4.3.3.2-b below enables the user to calculate the drag due to lift as a function of angle of attack and Mach number. When a series of points are calculated to define the drag due to lift versus angle of attack, it becomes necessary to use discretion and fair the best possible curve through the points. This is necessary since some values at high angles of attack do not describe a smooth continuous curve.

This method is not limited to bodies of revolution; however, no attempt is made to account for the effects of noncircular bodies. If it becomes necessary to analyze a noncircular body in combination with a wing, it is suggested that an equivalent body of revolution be used, i.e., a body of revolution with the same cross-sectional area.

The drag due to lift at a given angle of attack of a wing-body configuration, based on the area of the basic straight-tapered wing, is given by

$$(C_{D_L})_{WB} = B_0 + B_1\left(\frac{1}{A}\right) + B_2 A + B_3(\tan \Lambda_{LE})^{1/2} + B_4(t/\bar{c}) + B_5\left(\frac{\ell_N}{d}\right) + B_6\left(\frac{\ell_A}{d}\right) + B_7\lambda$$
$$+ B_8\lambda^2 + B_9\lambda^3 + B_{10}(T_R) + B_{11}\left(\frac{LER}{\bar{c}}\right) + B_{12}\theta + B_{13}\left[\frac{(y_c)_{max}}{\bar{c}}\right] + B_{14}\, C_{L_d}$$
$$+ B_{15} R_\ell \qquad \text{4.3.3.2-b}$$

where

$B_0, B_1, \ldots B_{15}$ are the regression coefficients as a function of Mach number and angle of attack obtained from Table 4.3.3.2-D.

A is the total wing aspect ratio.

Λ_{LE} is the sweep of the leading edge.

$t/\bar{c}$ is the wing thickness ratio at the mean aerodynamic chord.

$\frac{\ell_N}{d}$ is the nose and forebody fineness ratio (see Sketch (a)).

$\frac{\ell_A}{d}$ is the afterbody fineness ratio taken at the afterbody wing-body juncture (see Sketch (a)).

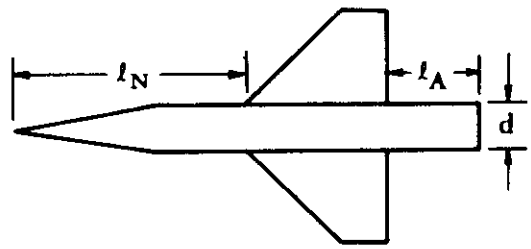

SKETCH (a)

λ is the wing taper ratio.

T_R is the transition indicator; 0 for no transition strips and 1 for transition strips or flight test.

$\frac{LER}{\bar{c}}$ is the ratio of the leading-edge radius to the mean aerodynamic chord taken at the mean aerodynamic chord.

θ is the wing twist between the root and tip sections in radians, negative for washout (see Figure 5.1.2.1-30b).

$\frac{(y_c)_{max}}{\bar{c}}$ is the NACA camber in the form of a ratio of the maximum ordinate of the mean line to the airfoil chord taken at the mean aerodynamic chord.

C_{L_d} is the conical camber design lift coefficient for a M = 1.0 design with the designated camber ray line intersecting the wing trailing edge at 0.8 b/2. (For more details see Reference 2.) If the wing does not have a conical-camber design, the value of C_{L_d} is zero.

R_ℓ is the Reynolds number based on the mean aerodynamic chord. For Reynolds numbers in excess of 8×10^6, the value of 8×10^6 should be used.

An indication of the accuracy of Method 1 can be obtained from Table 4.3.3.2-A. This table contains a comparison of test values with results calculated by using this method for wing-body configurations without camber. The test data used in this comparison are taken from Table 4.1.5.2-A and some have been used in the determination of the regression coefficients.

Method 2

This method evaluates and combines the isolated drag due to lift of the wing and of the body. The limitations of the method are those of Sections 4.1.5.2 and 4.2.3.2. The method is not applicable to generalized wing-body configurations with arbitrary body shapes. If it becomes necessary to analyze a noncircular body in combination with a wing, it is suggested that an equivalent body of revolution be used, i.e., a body of revolution with the same cross-sectional area. The method is applicable only for wing lift coefficients up to the critical lift coefficients for configurations having straight-tapered wings; whereas, for non-straight-tapered wings the method may be applied to configurations over a wide range of lift coefficients (see Paragraph A, Section 4.1.5.2).

The drag due to lift of a wing-body configuration is given by

$$(C_{D_L})_{WB} = (C_{D_L})_W + [C_D(\alpha)]_B \frac{(S_B)_{ref}}{S_W} \qquad 4.3.3.2\text{-c}$$

where

$(C_{D_L})_W$ is the drag due to lift of the wing, obtained from Paragraph A of Section 4.1.5.2 and based on the total wing area.

$[C_D(\alpha)]_B$ is the body drag due to angle of attack, obtained from Paragraph A of Section 4.2.3.2 and based on the maximum body frontal area.

$\frac{(S_B)_{ref}}{S_W}$ is the ratio of the body reference area (maximum body frontal area) to the total wing area.

No substantiation is presented for this method. However, substantiation tables for the wing contribution are presented in Section 4.1.5.2 for straight-tapered and non-straight-tapered planforms.

Sample Problems

The same wing-body configurations will be evaluated for both Methods 1 and 2 to enable a comparison of their application to be made.

1. Method 1

Given: The straight-tapered wing-body configuration of Reference 3.

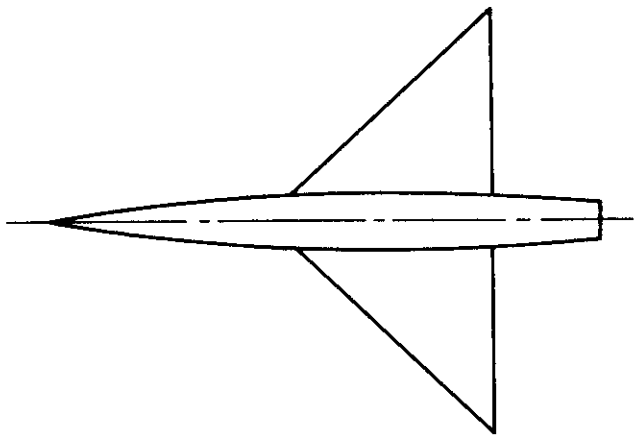

Wing Characteristics:

$A = 4.0$ $\quad \lambda = 0$ $\quad t/c = 0.03$ $\quad \Lambda_{LE} = 45^{o}$

$\theta = 0$ $\quad$ No camber, $\dfrac{(y_c)_{max}}{\bar{c}} = 0$ $\quad C_{L_d} = 0$

3-percent-thick biconvex airfoil with elliptic nose

$$\frac{LER}{\bar{c}} = 0.00045$$

Body Characteristics:

$$\frac{\ell_N}{d} = 4.28 \qquad \frac{\ell_A}{d} = 2.141$$

Additional Characteristics:

$M = 0.61$ $\quad R_\ell = 4.20 \times 10^6$ $\quad$ No transition strips, $T_R = 0$

Compute the drag due to lift for the above configuration at an angle of attack of 10^{o}.

The regression coefficients below are obtained from Table 4.3.3.2-D at M = 0.6.

Regression Coefficient	Value Table 4.3.3.2-D
B_0	0.12873
B_1	–0.05227
B_2	0.00855
B_3	–0.00826
B_4	–0.69952
B_5	–0.00295
B_6	–0.00487
B_7	0.14051
B_8	–0.28982
B_9	0.16952
B_{10}	–0.00215
B_{11}	2.27613
B_{12}	–0.34643
B_{13}	–0.52607
B_{14}	–0.09097
B_{15}	-0.00076×10^{-6}

Solution:

$$(C_{D_L})_{WB} = B_0 + B_1\left(\frac{1}{A}\right) + B_2 A + B_3(\tan \Lambda_{LE})^{1/2} + B_4(t/\bar{c}) + B_5\left(\frac{\ell_N}{d}\right) + B_6\left(\frac{\ell_A}{d}\right) + B_7\lambda$$

$$+ B_8\lambda^2 + B_9\lambda^3 + B_{10}T_R + B_{11}\left(\frac{LER}{\bar{c}}\right) + B_{12}\theta + B_{13}\left[\frac{(y_c)_{max}}{\bar{c}}\right]$$

$$+ B_{14}C_{L_d} + B_{15}R_\ell \qquad \text{(Equation 4.3.3.2-b)}$$

$$C_{D_L} = 0.12873 - 0.05227\left(\frac{1}{4}\right) + 0.00855(4) - 0.00826(1)^{1/2} - 0.69952(0.03)$$

$$- 0.00295(4.28) - 0.00487(2.141) + 0.14051(0) - 0.28982(0)^2 + 0.16952(0)^3$$

$$- 0.00215(0) + 2.27613(0.00045) - 0.34643(0) - 0.52607(0) - 0.09097(0)$$

$$0.00076 \times 10^{-6}(4.20 \times 10^6)$$

$$= 0.12873 - 0.01307 + 0.03420 - 0.00826 - 0.02099 - 0.01263 - 0.01043$$

$$+ 0.00102 - 0.00319$$

$$= 0.0954$$

The above procedure is used to generate the complete variation of C_{D_L} given below as a function of angle of attack. The comparison of test data with these predicted values and the predicted values from Method 2 are presented in Sketch (b), which follows the next sample problem.

α (deg)	$(C_{D_L})_{WB}$
0	0
1	0.00059
2	0.00196
3	0.00568
4	0.0115
6	0.0306
8	0.0598
10	0.0954
12	0.1356
14	0.1769
16	0.2196
18	0.2644

2. Method 2

Given: The same wing-body configuration used in Sample Problem 1, i.e., from Reference 3.

Wing Characteristics:

$A = 4.0$ $\quad \lambda = 0$ $\quad t/c = 0.03$ $\quad \Lambda_{LE} = 45^{O}$

$S_W = 2.425\ ft^2$ $\quad \bar{c} = 1.038\ ft$

$\theta = 0$ $\quad$ No camber $\quad \dfrac{LER}{\bar{c}} = 0.00045$

Body Characteristics:

$\ell_B = 46.93$ in. $\quad d = 4.76$ in. $\quad d_b = 2.589$ in.

$V_B = 0.2687\ ft^3$ $\quad V_B^{2/3} = 0.4164\ ft^2$

$f = \dfrac{\ell_B}{d} = 9.86$ $\quad r = 2.38\left[1 - \left(1 - \dfrac{2x}{59.5}\right)^2\right]^{3/2}$

Additional Characteristics:

$M = 0.61, \beta^2 = 0.6279$ $\quad R_{\ell_{MAC}} = 4.20 \times 10^6$ $\quad \kappa = 1.0$ (assumed)

Compute:

Wing Drag Due to Lift (Section 4.1.5.2)

$$\tan \Lambda_{c/2} = \tan \Lambda_{LE} - \frac{4}{A}\left[\frac{1}{2}\left(\frac{1-\lambda}{1+\lambda}\right)\right]$$

$$= 1.0 - \frac{4}{4}\left[\frac{1}{2}\left(\frac{1.0}{1.0}\right)\right]$$

$$= 0.5$$

$$\frac{A}{\kappa}[\beta^2 + \tan^2 \Lambda_{c/2}]^{1/2} = \frac{4}{1.0}[0.6279 + (0.5)^2]^{1/2} = 3.748$$

$$\frac{C_{L_\alpha}}{A} = 1.0 \text{ per rad} \qquad \text{(Figure 4.1.3.2-49)}$$

$$R_{\ell_{LER}} = 4.20 \times 10^6 \frac{0.00045\ \bar{c}}{\bar{c}} = 1.89 \times 10^3$$

$$R_{\ell_{LER}} \cot \Lambda_{LE} \sqrt{1 - M^2 \cos^2 \Lambda_{LE}} = (1.89 \times 10^3)(1.0)\sqrt{1 - (0.372)(0.7071)^2}$$

$$= 1.705 \times 10^3$$

$$\frac{A\lambda}{\cos \Lambda_{LE}} = \frac{(4.0)(0)}{(0.7071)} = 0$$

$R = 0.120$ (Figure 4.1.5.2-53a)

$$e = \frac{1.1\,(C_{L_\alpha}/A)}{R(C_{L_\alpha}/A) + (1 - R)\pi} \qquad \text{(Equation 4.1.5.2-i)}$$

$$= \frac{1.1(1.0)}{0.120(1.0) + (1 - 0.120)\pi}$$

$$= 0.382$$

$$(C_{D_L})_W = \frac{C_L{}^2}{\pi A e} + C_L \theta\, c_{\ell_\alpha} v + (\theta c_{\ell_\alpha})^2\, w \qquad \text{(Equation 4.1.5.2-h)}$$

$$= \frac{C_L{}^2}{\pi(4.0)(0.382)}$$

C_L	$C_{D_L} = 0.209\ C_L^2$
0	0
0.05	0.00052
0.10	0.00209
0.15	0.00470
0.20	0.00836
0.25	0.01306
0.30	0.01881
0.35	0.02560
0.40	0.03344
0.50	0.05225

Body Drag Due to Lift (Section 4.2.3.2)

$k_2 - k_1 = 0.94$ (Figure 4.2.1.1-20a)

$x_1 = 46.93$ (by inspection)

$$\frac{x_1}{\ell_B} = 1.0$$

$$\frac{x_o}{\ell_B} = 0.905 \qquad \text{(Figure 4.2.1.1-20b)}$$

$x_o = 42.47$ in.

$$(r)_{x_o} = 2.38 \left[1 - \left(1 - \frac{2(42.4)}{59.5}\right)^2\right]^{3/2} = 1.765 \text{ in.}$$

$$S_o = \pi r^2 = \pi(1.765)^2 = 9.79 \text{ in.}^2$$

$$C_{L_\alpha} = \frac{2(k_2 - k_1)\, S_o}{V_B^{2/3}} \qquad \text{(Equation 4.2.1.1-a)}$$

$$= \frac{2(0.94)(9.79)}{(0.4164)144}$$

$$= 0.307 \text{ per rad}$$

$\eta = 0.686$ (Figure 4.2.1.2-23a)

$M_c = M \sin \alpha$

The α range is approximately $0 \leq \alpha \leq 10^o$

M_c varies from 0.6(0) to 0.6(0.1736)

$0 \leq M_c \leq 0.104$

$c_{d_c} = 1.20$ (constant) (Figure 4.2.1.2-23b)

$$\int_{x_o}^{\ell_B} \eta \, r \, c_{d_c} \, dx = \int_{42.47}^{46.93} (0.686) \, r \, (1.20) \, dx$$

Assuming r varies linearly from x_o to ℓ_B

$$\int_{x_o}^{\ell_B} \eta \, r \, c_{d_c} \, dx = \int_{42.47}^{46.93} (0.686)\left(\frac{1.765 + 1.295}{2}\right)(1.20)dx$$

$$= 1.26(46.93 - 42.47)$$

$$= 5.62 \text{ sq in.} = 0.0390 \text{ sq ft}$$

$$C_D(\alpha) = \frac{k_2 - k_1}{V_B^{2/3}} 2\alpha^2 S_o + \frac{2\alpha^3}{V_B^{2/3}} \int_{x_o}^{\ell_B} \eta \, r \, c_{d_c} \, dx \qquad \text{(Equation 4.2.3.2-b)}$$

$$= 0.307\alpha^2 + \frac{2\alpha^3}{0.4164}(0.0390)$$

$$= 0.307\alpha^2 + 0.187\alpha^3$$

Equation 4.2.3.2-b becomes

$$[C_D(\alpha)]_B \frac{S_{B_{ref}}}{S_W} = (0.307\alpha^2 + 0.187\alpha^3)\frac{V_B^{2/3}}{S_W}$$

$$= (0.307\alpha^2 + 0.187\alpha^3)\frac{0.4164}{2.425}$$

$$= 0.0527\alpha^2 + 0.0321\alpha^3$$

$(C_{L_\alpha})_W = (C_{L_\alpha}/A)\,A = (1.0)(4.0) = 4.0$ per rad

(1)	(2)	(3)	(4)	(5)
C_L	$\alpha = \frac{C_L^*}{(C_{L_\alpha})_W}$ (rad)	$0.0527\,\alpha^2$	$0.0321\,\alpha^3$	$[C_D(\alpha)]_B \frac{S_{B_{ref}}}{S_W}$ (3) + (4)
0	0	0	0	0
0.05	0.0125	0.000008	0	0.000008
0.10	0.0250	0.000033	0.000001	0.000034
0.15	0.0375	0.000074	0.000002	0.000076
0.20	0.0500	0.000132	0.000004	0.000136
0.25	0.0625	0.000206	0.000008	0.000214
0.30	0.0750	0.000296	0.000014	0.000310
0.35	0.0875	0.000403	0.000022	0.000425
0.40	0.1000	0.000527	0.000032	0.000559
0.50	0.1250	0.000823	0.000063	0.000886

Solution:

$$(C_{D\,L})_{W\,B} = (C_{D\,L})_W + [C_D(\alpha)]_B \frac{S_{B\,ref}}{S_W} \qquad \text{(Equation 4.3.3.2-a)}$$

(1)	(2)	(3)	(4)
C_L	$(C_{D_L})_W$	$[C_D(\alpha)]_B \frac{S_{B_{ref}}}{S_W}$	$(C_{D_L})_{WB}$ (2) + (3)
0	0	0	0
0.05	0.00052	0.000008	0.00053
0.10	0.00209	0.000034	0.00212
0.15	0.00470	0.000076	0.00478
0.20	0.00836	0.000136	0.00850
0.25	0.01306	0.000214	0.01327
0.30	0.01881	0.000310	0.01912
0.35	0.02560	0.000425	0.02603
0.40	0.03344	0.000559	0.03400
0.50	0.05225	0.000886	0.05314

These calculated results are compared with the calculated results from Method 1 and the test values from Reference 3 in Sketch (b).

*This approximation assumes a zero lift value of zero.

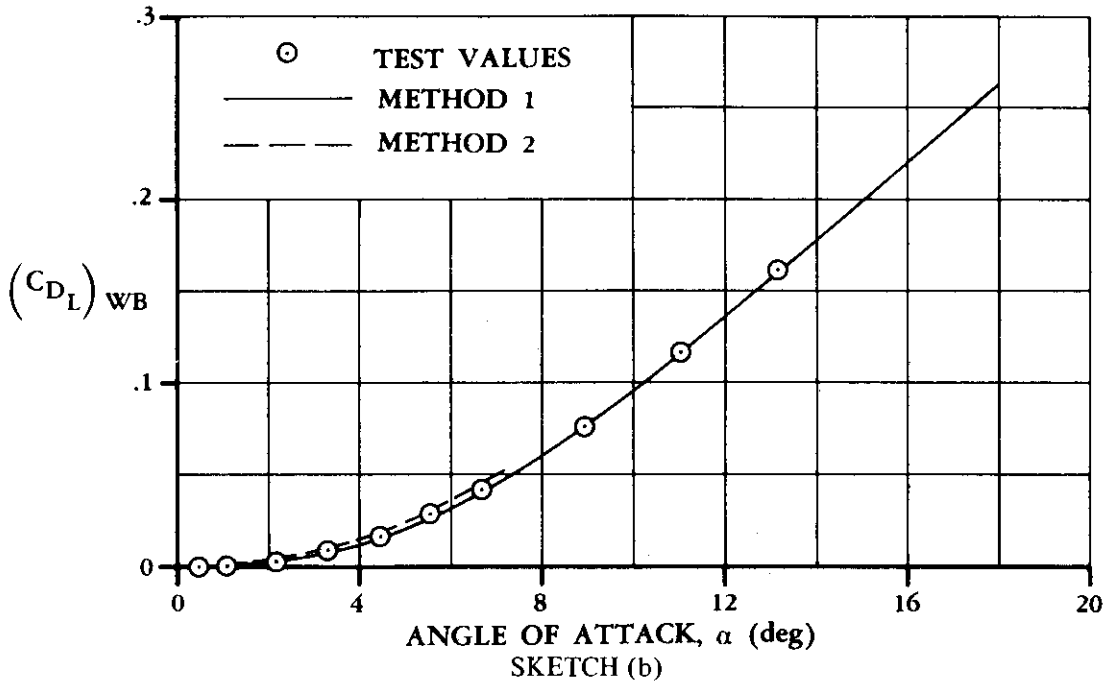

SKETCH (b)

B. TRANSONIC

The comments presented in the discussion preceding Paragraph A are applicable here.

DATCOM METHODS

At transonic speeds the methods described in Paragraph A may be applied. Both methods are restricted to straight-tapered-wing configurations. Method 1 may be applied in the high-lift region; while Method 2 is restricted to the parabolic-drag region.

An indication of the accuracy of Method 1 can be obtained from Table 4.3.3.2-B. This table contains a comparison of test values with results calculated by using this method for wing-body configurations without camber.

Sample Problem

No sample problem is presented for Method 1 because its application is identical to that in the subsonic speed regime.

Method 2

Given: A wing-body configuration of Reference 2 designated 45-series.

Wing Characteristics:

$A = 3.0$ $\quad \lambda = 0.40$ $\quad b_W = 10.8$ in. $\quad \Lambda_{LE} = 45^o$

$\Lambda_{c/2} = 35.54^o$ $\quad (t/c)_{av} = 0.045$ $\quad S_W = 38.889$ sq in. $\quad$ Round-nosed airfoil

Additional Characteristics:

$\frac{S_b}{S_W} = 0.0278$ $\quad 0 \leq C_L \leq 0.50$ $\quad M = 1.02;\ \beta = 0.20$ $\quad \kappa = 1.0$ (assumed)

Compute:

Wing Drag Due to Lift (Section 4.1.5.2)

$$\left(t/c\right)^{1/3} = 0.3557$$

$$\left(t/c\right)^{2/3} = 0.1265$$

$$A\left(t/c\right)^{1/3} = 3(0.3557) = 1.067$$

$$A \tan \Lambda_{LE} = 3.0$$

$$\frac{M^2 - 1}{(t/c)^{2/3}} = \frac{0.0404}{0.1265} = 0.319$$

$$\left(\frac{t}{c}\right)^{-1/3} \frac{C_{D_L}}{C_L{}^2} = 0.590$$ (Figure 4.1.5.2-55b, interpolated)

$$\frac{C_{D_L}}{C_L{}^2} = 0.590\,(0.3557) = 0.210$$

①	②	③
C_L	$C_L{}^2$	$\left(C_{D_L}\right)_W$ 0.210 ②
0	0	0
.05	.0025	.00053
.10	.0100	.00210
.15	.0225	.00473
.20	.0400	.00840
.25	.0625	.01313
.30	.0900	.01890
.35	.1225	.02573
.40	.1600	.03360
.45	.2025	.04253
.50	.2500	.05250

Body Drag Due to Lift (Section 4.2.3.2)

$$\left[\left(C_{L_\alpha}\right)_W\right]_{M\,=\,1.02} = 4.0 \text{ per rad}$$ (method of Paragraph B, Section 4.1.3.2)

Equation 4.2.3.2-e becomes $$\left[C_D(\alpha)\right]_B \frac{S_b}{S_W} = \alpha^2 \frac{S_b}{S_W}$$

①	②	③	④
C_L	$C_L / \left(C_{L_\alpha}\right)_W$ ① /4.0 (rad)	α^2 (rad^2)	$\left[C_D(\alpha)\right]_B \frac{S_b}{S_W}$ ③ (0.0278)
0	0	0	0
.05	.0125	.00016	0
.10	.0250	.00063	.00002
.15	.0375	.00141	.00004
.20	.0500	.00250	.00007
.25	.0625	.00391	.00011
.30	.0750	.00563	.00016
.35	.0875	.00766	.00021
.40	.1000	.01000	.00028
.45	.1125	.01266	.00035
.50	.1250	.01563	.00043

Solution:

$$\left(C_{D_L}\right)_{WB} = \left(C_{D_L}\right)_W + \left[C_D(\alpha)\right]_B \frac{S_b}{S_W} \quad \text{(Equation 4.3.3.2-a)}$$

①	②	③	④
C_L	$\left(C_{D_L}\right)_W$	$\left[C_D(\alpha)\right]_B \frac{S_b}{S_W}$	$\left(C_{D_L}\right)_{WB}$ ② + ③
0	0	0	0
.05	.00053	0	.00053
.10	.00210	.00002	.00212
.15	.00473	.00004	.00477
.20	.00840	.00007	.00847
.25	.01313	.00011	.01324
.30	.01890	.00016	.01906
.35	.02573	.00021	.02594
.40	.03360	.00028	.03388
.45	.04253	.00035	.04288
.50	.05250	.00043	.05293

The calculated results are compared with test values from Reference 4 in Sketch (c).

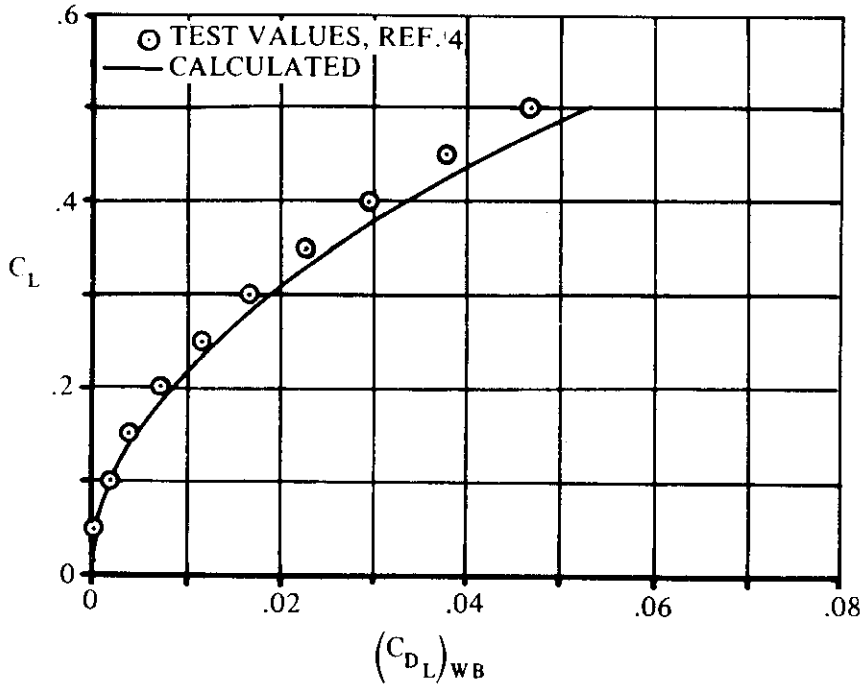

SKETCH (c)

C. SUPERSONIC

The comments presented in the discussion preceding Paragraph A are applicable here.

DATCOM METHODS

At supersonic speeds the methods described in Paragraph A may be applied. Method 1 is restricted to straight-tapered planforms; while Method 2 may be applied to either straight-tapered or non-straight-tapered wings. An indication of the accuracy of Method 1 can be obtained from Table 4.3.3.2-C. This table contains a comparison of test values with results calculated by using this method for wing-body configurations without camber.

Sample Problem

No sample problem is presented for Method 1 because its application is identical to that in the subsonic speed regime.

Method 2

Given: The wing-body configuration of Reference 5.

Wing Characteristics:

$A = 3.50$ $b_W = 24$ in. $\lambda = 0.20$ $\Lambda_{LE} = 51.6^o$

$\ell = 17.44$ in. $S_W = 164.64$ sq in. $\delta_\perp = 8.4^o$

Airfoil: 6-percent-thick hexagonal section with maximum thickness at c/3 (sharp-nosed airfoil)

Additional Characteristics:

$M = 2.01$; $\beta = 1.744$ $\qquad S_b = 12.57$ sq in.

$0 \le C_L \le 0.40$ $\qquad S_p = 154$ sq in.

Compute:

Wing Drag Due to Lift (Section 4.1.5.2)

$$\frac{\beta b_w}{2\ell} = \frac{1.744\,(24)}{2\,(17.44)} = 1.20$$

$$p = \frac{S_w}{b_w \ell} = \frac{164.64}{24\,(17.44)} = 0.393$$

$$\pi A \frac{C_{D_L}}{C_L^2} \frac{p}{1+p} = 1.29 \qquad \text{(Figure 4.1.5.2-58)}$$

$$\frac{C_{D_L}}{C_L^2} = \left[\pi A \frac{C_{D_L}}{C_L^2} \frac{p}{1+p}\right] \frac{1}{\pi A} \frac{1+p}{p} \qquad \text{(Equation 4.1.5.2-n)}$$

$$= 1.29 \left(\frac{1}{\pi(3.5)}\right)\left(\frac{1.393}{0.393}\right)$$

$$= 0.416$$

①	②	③
C_L	C_L^2	C_{D_L} 0.416 ②
0	0	0
0.05	0.0025	0.00104
0.10	0.0100	0.00416
0.15	0.0225	0.00936
0.20	0.0400	0.01664
0.25	0.0625	0.02600
0.30	0.0900	0.03744
0.35	0.1225	0.05096
0.40	0.1600	0.06656

Body Drag Due to Lift (Section 4.2.3.2)

Wing C_{N_α} (Section 4.1.3.2)

$$\frac{\tan \Lambda_{LE}}{\beta} = \frac{1.262}{1.744} = 0.724$$

$$A \tan \Lambda_{LE} = 3.5\,(1.262) = 4.42$$

$$\beta\left(C_{N_\alpha}\right)_{theory} = 4.24 \text{ per rad} \quad \text{(Figure 4.1.3.2-56b)}$$

$$\left(C_{N_\alpha}\right)_{theory} = 4.24/1.744 = 2.43 \text{ per rad}$$

$$\frac{C_{N_\alpha}}{\left(C_{N_\alpha}\right)_{theory}} = 0.895 \quad \text{(Figure 4.1.3.2-60)}$$

$$C_{N_\alpha} = (2.43)\,(0.895) = 2.17 \text{ per rad}$$

$\left[C_D(\alpha)\right]_B$ (based on body base area)

$$\left[C_D(\alpha)\right]_B = 2\alpha^2 + c_{d_c}\frac{S_p}{S_b}\alpha^3 \quad \text{(Equation 4.2.3.2-g)}$$

$$\frac{S_p}{S_b} = \frac{154}{12.57} = 12.25$$

①	②	③	④	⑤	⑥	⑦	⑧	⑨
C_L	$C_L/\left(C_{N_\alpha}\right)_W$ ①/2.17 (rad)	α^2 (rad^2)	α^3 (rad^3)	α (deg)	M_c M sin α	c_{d_c} Fig. 4.2.1.2-23b	$c_{d_c}\frac{S_p}{S_b}$ ⑦ 12.25	$\left[C_D(\alpha)\right]_B$ 2③+④⑧
0	0	0	0	0	0	1.20	14.70	0
0.05	0.0230	0.00053	0.00001	1.32	0.0463	1.20	14.70	0.00121
0.10	0.0461	0.00213	0.00010	2.64	0.0926	1.20	14.70	0.00573
0.15	0.0691	0.00477	0.00033	3.96	0.1388	1.20	14.70	0.01439
0.20	0.0922	0.00850	0.00078	5.28	0.1850	1.20	14.70	0.02847
0.25	0.1152	0.01327	0.00153	6.60	0.2310	1.20	14.70	0.04903
0.30	0.1382	0.01910	0.00264	7.92	0.2770	1.21	14.82	0.07732
0.35	0.1613	0.02602	0.00420	9.24	0.3227	1.213	14.98	0.11495
0.40	0.1843	0.03397	0.00626	10.56	0.3684	1.244	15.24	0.16334

Solution:

Equation 4.3.3.2-a becomes

$$\left(C_{D_L}\right)_{WB} = \left(C_{D_L}\right)_W + \left[C_D(\alpha)\right]_B \frac{S_b}{S_W}$$

$$\frac{S_b}{S_W} = \frac{12.57}{164.64} = 0.0763$$

(1) C_L	(2) C_{D_L}	(3) $[C_D(\alpha)]_B$ (based on S_b)	(4) $(C_{D_L})_{WB}$ (2) + 0.0763 (3)
0.05	0.00104	0.00121	0.0011
0.10	0.00416	0.00573	0.0046
0.15	0.00936	0.01439	0.0105
0.20	0.01664	0.02847	0.0188
0.25	0.02600	0.04903	0.0297
0.30	0.03744	0.07732	0.0433
0.35	0.05096	0.11495	0.0597
0.40	0.06656	0.16334	0.0790

The calculated results are compared with test values from Reference 5 in Sketch (d).

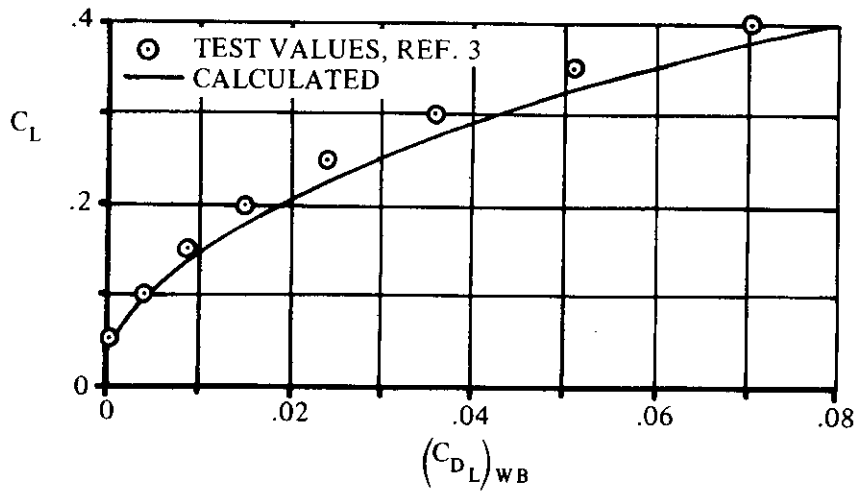

SKETCH (d)

REFERENCES

1. Simon, W. E., et al.: Prediction of Aircraft Drag Due to Lift. AFFDL-TR-71-84, 1971. (U)

2. Boyd, J. W., Migotsky, E., and Wetzel, B. E.: A Study of Conical Camber for Triangular and Sweptback Wings. NACA RM A55G19, 1955. (U)

3. Hall, C. F.: Lift, Drag, and Pitching Moment of Low-Aspect-Ratio Wings at Subsonic and Supersonic Speeds. NACA RM A53A30, 1953. (U)

4. Wakefield, R. M.: Effects of Wing-Crank, Leading-Edge Chord Extensions and Horizontal-Tail Height on the Longitudinal Stability of Swept-Wing Models at Mach Numbers from 0.6 to 1.4. NASA TM X-92, 1959. (U)

5. Carlson, H. W., and Gapcynski, J. P.: An Experimental Investigation at a Mach Number of 2.01 of the Effects of Body Cross-Section Shape on the Aerodynamic Characteristics of Bodies and Wing-Body Combinations. NACA RM L55E23, 1955. (U)

6. Kuhn, R. E., and Wiggins, J. W.: Wind-Tunnel Investigation of the Aerodynamic Characteristics in Pitch of Wing-Fuselage Combinations at High Subsonic Speeds – Aspect-Ratio Series. NACA RM L52A29, 1952. (U)

7. Tinling, B. E., and Kolk, W. R.: The Effects of Mach Number and Reynolds Number on the Aerodynamic Characteristics of Several 12-Percent-Thick Wings Having 35° of Sweepback and Various Amounts of Camber. NACA RM A50K27, 1951. (U)

8. Boyd, J. W., and Peterson, V. L.: Static Stability and Control of Canard Configurations at Mach Numbers from 0.7 to 2.22 – Longitudinal Characteristics of a Triangular Wing and Canard. NACA RM A57J15, 1958. (U)

9. Palazzo, E. B., and Spearman, M. L.: Static Longitudinal and Lateral Stability and Control Characteristics of a Model of a 35° Swept-Wing Airplane at a Mach Number of 1.41. NACA RM L54G08, 1955. (U)

10. Cooper, M., and Sevier, J. R., Jr.: Effects of a Series of Inboard Plan-Form Modifications on the Longitudinal Characteristics of Two 47° Sweptback Wings of Aspect Ratio 3.5, Taper Ratio 0.2, and Different Thickness Distributions at Mach Numbers of 1.61 and 2.01. NACA RM L53E07a, 1953. (U)

11. Wetzel, B. E.: Effect of Taper Ratio on Lift, Drag, and Pitching-Moment Characteristics of Thin Wings of Aspect Ratio 3 with 53.1° Sweepback of Leading Edge at Subsonic and Supersonic Speeds. NACA RM A54J20, 1955. (U)

TABLE 4.3.3.2-A
SUBSONIC WING-BODY DRAG DUE TO LIFT OF STRAIGHT-TAPERED WINGS
METHOD 1
DATA SUMMARY AND SUBSTANTIATION
NO TWIST OR CAMBER

Ref	A	λ	Λ_{LE} (deg)	NACA Airfoil	$R_{\ell_{MAC}} \times 10^{-6}$	M	α	C_{D_L} Calc.	C_{D_L} Test	ΔC_{D_L}
3	3.0	0	53.1	0003-63	5.9	0.25	4	0.010	0.010	0
							8	0.052	0.045	0.007
							12	0.124	0.114	0.010
							14	0.164	0.156	0.008
							16	0.213	0.203	0.010
					4.8	0.61	4	0.011	0.012	−0.001
							8	0.053	0.052	0.001
							10	0.084	0.084	0
							12	0.125	0.125	0
	2.0	0	63.4	0003-63	3.0	0.81	4	0.009	0.012	−0.003
							8	0.050	0.060	−0.010
							12	0.116	0.130	−0.014
							14	0.168	0.184	−0.016
							16	0.224	0.243	−0.019
	4.0	0	45.0	biconvex t/c=0.03	9.1	0.25	4	0.010	0.010	0
							8	0.057	0.053	0.004
							12	0.128	0.121	0.007
							14	0.177	0.170	0.007
					4.2	0.61	4	0.012	0.015	−0.003
							8	0.061	0.061	0
							10	0.097	0.097	0
							12	0.136	0.139	−0.003
	2.0	0	63.4	0005-63	3.0	0.40	4	0.008	0.008	0
							8	0.038	0.038	0
							12	0.093	0.089	0.004
							14	0.130	0.127	0.003
							16	0.182	0.178	0.004
					8.0	0.25	4	0.006	0.006	0
							8	0.034	0.025	0.009
							12	0.095	0.080	0.015
							14	0.135	0.117	0.018
							16	0.186	0.166	0.020
				0008-63	3.0	0.40	4	0.006	0.008	−0.002
							8	0.028	0.026	0.002
							12	0.084	0.066	0.018
							14	0.130	0.100	0.030
							16	0.181	0.139	0.042
						0.60	4	0.006	0.006	0
							8	0.028	0.028	0
							12	0.084	0.080	0.004
							14	0.129	0.120	0.009
							16	0.182	0.170	0.012
						0.80	4	0.006	0.008	−0.002
							8	0.036	0.036	0
							12	0.108	0.102	0.006
							14	0.149	0.142	0.007
							16	0.198	0.190	0.008
		0.333	45.0	biconvex t/c=0.03	4.8	0.61	4	0.012	0.012	0
							8	0.056	0.055	0.001
							10	0.088	0.088	0
							12	0.129	0.132	−0.003
							14	0.169	0.171	−0.002

TABLE 4.3.3.2-A (CONTD)

Ref	A	λ	Λ_{LE} (deg)	NACA Airfoil	$R\varrho_{MAC} \times 10^{-6}$	M	α	C_{D_L} Calc.	C_{D_L} Test	ΔC_{D_L}
3	3.08	0.388	19.1	biconvex t/c=0.03	3.8	0.61	4	0.014	0.013	0.001
							8	0.066	0.066	0
							12	0.153	0.153	0
							14	0.196	0.196	0
							16	0.231	0.217	0.014
						0.71	4	0.014	0.014	0
							8	0.068	0.068	0
							12	0.150	0.152	−0.002
							14	0.179	0.183	−0.004
							16	0.213	0.223	−0.010
6	2.0	0.600	48.4	65A006	4.53	0.60	4	0.006	0.006	0
							8	0.035	0.039	−0.004
							12	0.099	0.114	−0.015
							14	0.141	0.166	−0.025
							16	0.190	0.220	−0.030
					5.46	0.80	4	0.009	0.008	0.001
							8	0.043	0.045	−0.002
							12	0.122	0.129	−0.007
							14	0.162	0.167	−0.005
							16	0.198	0.202	−0.004
	4.0	0.600	46.7	65A006	2.78	0.60	4	0.007	0.007	0
							8	0.047	0.043	0.004
							12	0.128	0.138	−0.010
							14	0.171	0.182	−0.011
							16	0.222	0.234	−0.012
					3.35	0.80	4	0.010	0.010	0
							8	0.061	0.059	0.002
							12	0.145	0.133	0.012
							14	0.191	0.176	0.015
							16	0.221	0.214	0.007
	.0	0.600	46.2	65A006	2.39	0.70	4	0.007	0.007	0
							8	0.058	0.045	0.013
							12	0.129	0.118	0.011
							14	0.159	0.167	−0.008
							16	0.177	0.215	−0.038
7	5.14	0.713	36.2	65_1A012	2.0	0.40	4	0.004	0.005	−0.001
							8	0.040	0.019	0.021
							12	0.121	0.090	0.031
							14	0.170	0.148	0.022
							16	0.240	0.194	0.046
						0.80	4	0.008	0.007	0.001
							8	0.060	0.051	0.009
							10	0.106	0.100	0.006
							12	0.150	0.150	0
							14	0.175	0.175	0

$|\Delta C_{D_L}|_{av} = 0.008$

TABLE 4.3.3.2-B
TRANSONIC WING-BODY DRAG DUE TO LIFT OF STRAIGHT-TAPERED WINGS
METHOD 1
DATA SUMMARY AND SUBSTANTIATION
NO TWIST OR CAMBER

Ref	A	λ	Λ_{LE} (deg)	NACA Airfoil	$R_{\ell_{MAC}} \times 10^{-6}$	M	α	C_{D_L} Calc.	C_{D_L} Test	ΔC_{D_L}
3	3.0	0	53.1	0003-63	1.9	0.92	4	0.013	0.017	−0.004
							6	0.036	0.041	−0.005
							8	0.066	0.070	−0.004
						1.2	4	0.010	0.015	−0.005
							8	0.055	0.067	−0.012
							12	0.128	0.150	−0.022
							14	0.177	0.199	−0.022
	3.08	0.388	19.1	biconvex t/c=0.03	1.4	1.2	4	0.020	0.019	0.001
							8	0.085	0.086	−0.001
							10	0.129	0.135	−0.006
							12	0.180	0.191	−0.011
							14	0.241	0.249	−0.008
	3.0	0.4	45.0	biconvex t/c=0.03	3.8	0.91	4	0.015	0.017	−0.002
							6	0.041	0.043	−0.002
							7	0.060	0.060	0
	2.0	0.333	45.0	biconvex t/c=0.03	1.9	0.93	4	0.017	0.014	0.003
							6	0.042	0.039	0.003
							8	0.073	0.071	0.002
						1.2	4	0.015	0.015	0
							6	0.036	0.037	−0.001
							8	0.067	0.069	−0.002
							10	0.103	0.109	−0.006
8	2.0	0	63.3	0003-63	1.84	1.0	4	0.012	0.017	−0.005
							6	0.027	0.032	−0.005
							8	0.061	0.063	−0.002
							10	0.103	0.098	0.005
						1.1	4	0.011	0.013	−0.002
							8	0.053	0.056	−0.003
							10	0.087	0.090	−0.003
							12	0.129	0.127	0.002
							14	0.184	0.180	0.004

$\left|\Delta C_{D_L}\right|_{av} = 0.005$

TABLE 4.3.3.2-C
SUPERSONIC WING-BODY DRAG DUE TO LIFT OF STRAIGHT-TAPERED WINGS
METHOD 1
DATA SUMMARY AND SUBSTANTIATION
NO TWIST OR CAMBER

Ref	A	λ	Λ_{LE} (deg)	NACA Airfoil	$R_{\ell_{MAC}} \times 10^{-6}$	M	α	C_{D_L} Calc.	C_{D_L} Test	ΔC_{D_L}
2	3.0	0.40	45.0	64A005	2.9	1.50	4	0.015	0.013	0.002
							8	0.058	0.053	0.005
							10	0.089	0.087	0.002
							12	0.126	0.120	0.006
							14	0.175	0.160	0.015
						1.90	4	0.018	0.011	0.007
							8	0.050	0.043	0.007
							10	0.075	0.065	0.010
							12	0.103	0.094	0.009
							14	0.138	0.128	0.010

TABLE 4.3.3.2-C (CONTD)

Ref	A	λ	Λ_{LE} (deg)	NACA Airfoil	$R_{\ell_{MAC}} \times 10^{-6}$	M	α	C_{D_L} Calc.	C_{D_L} Test	ΔC_{D_L}
9	4.0	0.50	38.1	65A006	1.96	1.41	4	0.018	0.016	0.002
				65A004			6	0.039	0.037	0.002
							8	0.066	0.064	0.002
							10	0.105	0.101	0.004
10	3.5	0.20	51.6	hexagonal	2.68	1.61	4	0.022	0.013	0.009
				t/c=0.06			6	0.044	0.029	0.015
							8	0.076	0.052	0.024
							10	0.119	0.081	0.038
						2.01	4	0.010	0.012	−0.002
							6	0.025	0.024	0.001
							8	0.050	0.048	0.002
11	3.0	0	53.1	0003-63	3.6	1.5	4	0.014	0.013	0.001
							8	0.053	0.055	−0.002
							10	0.081	0.082	−0.001
							12	0.113	0.120	−0.007
							14	0.160	0.157	0.003
						1.9	4	0.009	0.011	−0.002
							8	0.037	0.041	−0.004
							10	0.060	0.063	−0.003
							12	0.089	0.091	−0.002
							14	0.125	0.123	0.002
		0.20			3.1	1.5	4	0.017	0.015	0.002
							8	0.063	0.055	0.008
							10	0.096	0.088	0.008
							12	0.133	0.126	0.007
							14	0.180	0.157	0.023
						1.9	4	0.014	0.011	0.003
							8	0.048	0.043	0.005
							10	0.074	0.067	0.007
							12	0.105	0.093	0.012
							14	0.146	0.125	0.021
		0.40			2.9	1.5	4	0.016	0.014	0.002
							8	0.055	0.053	0.002
							10	0.083	0.080	0.003
							12	0.122	0.114	0.008
							14	0.178	0.153	0.025
						1.9	4	0.020	0.011	0.009
							8	0.055	0.043	0.012
							10	0.078	0.067	0.011
							12	0.108	0.092	0.016
							14	0.150	0.122	0.028
8	2.0	0	63.26	0003-63	1.84	1.3	4	0.008	0.010	−0.002
							8	0.044	0.046	−0.002
							10	0.072	0.078	−0.006
							12	0.104	0.109	−0.005
							14	0.150	0.153	−0.003
						1.9	4	0.007	0.008	−0.001
							8	0.030	0.034	−0.004
							10	0.050	0.052	−0.002
							12	0.073	0.072	0.001
							14	0.103	0.097	0.006

$|\Delta C_{D_L}|_{av} = 0.007$

TABLE 4.3.3.2-D
METHOD 1
REGRESSION COEFFICIENTS
M = 0.600

α	B_0	B_1	B_2	B_3	B_4	B_5
1	0.00045	0.00165	0.00026	−0.00069	0.00192	−0.00004
2	0.00353	0.00445	0.00042	−0.00109	−0.01622	−0.00029
3	0.01317	−0.00024	0.00013	−0.00266	−0.03562	−0.00043
4	0.02608	−0.00589	−0.00014	−0.00588	−0.05901	−0.00043
5	0.04109	−0.01099	0.00023	−0.00694	−0.14925	−0.00082
6	0.05140	−0.00482	0.00223	−0.01028	−0.24447	−0.00112
7	0.05749	0.00003	0.00539	−0.01129	−0.33547	−0.00137
8	0.07379	−0.00890	0.00734	−0.01049	−0.44144	−0.00175
9	0.09548	−0.03037	0.00885	−0.00781	−0.58794	−0.00170
10	0.12873	−0.05227	0.00855	−0.00826	−0.69952	−0.00295
11	0.15889	−0.07595	0.00833	−0.01261	−0.82886	−0.00220
12	0.18028	−0.07664	0.00745	−0.01593	−0.90625	−0.00181
13	0.21132	−0.11041	0.00433	−0.01859	−0.70087	−0.00001
14	0.25119	−0.14562	0.00092	−0.01361	−0.66342	0.00038
15	0.25845	−0.15418	0.00148	−0.00483	−0.69530	0.00152
16	0.28929	−0.18997	0.00143	−0.00886	−0.85331	0.00161
17	0.30498	−0.20240	−0.00196	0.02569	−0.65569	0.00096
18	0.31398	−0.22017	−0.00140	0.04032	−0.51782	0.00025

α	B_6	B_7	B_8	B_9	B_{10}	B_{11}
1	−0.00017	0.00079	−0.00243	0.00100	−0.00003	−0.00127
2	−0.00030	0.00434	−0.00817	0.00277	0.00001	−0.01298
3	−0.00047	0.00775	−0.02023	0.01039	−0.00038	−0.05350
4	−0.00068	0.01653	−0.04953	0.02785	−0.00165	−0.10679
5	−0.00121	0.02395	−0.05927	0.03084	−0.00222	−0.02883
6	−0.00168	0.04265	−0.11424	0.06512	−0.00275	0.19133
7	−0.00261	0.06777	−0.16815	0.09609	−0.00309	0.32420
8	−0.00330	0.09456	−0.23327	0.14239	−0.00204	0.77765
9	−0.00486	0.11723	−0.25173	0.14974	−0.00243	1.51741
10	−0.00487	0.14051	−0.28982	0.16952	−0.00215	2.27613
11	−0.00595	0.16340	−0.32756	0.18710	−0.00370	3.88429
12	−0.00386	0.19145	−0.42892	0.26626	−0.00202	4.34530
13	−0.00504	0.21710	−0.50195	0.30725	−0.00346	3.76319
14	−0.00566	0.22051	−0.50067	0.30752	−0.00086	3.48312
15	−0.00791	0.22128	−0.45958	0.28357	0.00040	4.43698
16	−0.01134	0.20554	−0.39035	0.25450	0.00294	6.01805
17	−0.00901	0.23888	−0.50267	0.32743	0.00370	4.60500
18	−0.00926	0.29613	−0.70455	0.49100	0.00020	4.00069

α	B_{12}	B_{13}	B_{14}	$B_{15} \times 10^{+6}$
1	0.02836	0.00293	−0.00471	−0.00004
2	0.05179	0.03795	−0.00819	−0.00022
3	0.07105	0.05725	−0.01192	−0.00033
4	0.08494	0.07442	−0.01580	−0.00036
5	0.09681	0.02204	−0.02255	−0.00049
6	0.11610	−0.10824	−0.03253	−0.00061
7	0.14943	−0.35912	−0.04761	−0.00049
8	0.19746	−0.49931	−0.06384	−0.00077
9	0.29222	−0.47586	−0.07863	−0.00067
10	0.34643	−0.52607	−0.09097	−0.00076
11	0.39755	−0.49629	−0.10051	0.00002
12	0.43743	−0.48216	−0.10223	0.00044
13	0.49084	−0.30237	−0.10159	0.00092
14	0.51916	−0.11923	−0.09866	0.00021
15	0.50871	−0.06195	−0.09704	0.00095
16	0.49258	0.00176	−0.10124	0.00083
17	0.49678	0.00645	−0.09760	0.00009
18	0.52715	−0.01712	−0.09182	0.00077

TABLE 4.3.3.2-D (CONTD)
METHOD 1
REGRESSION COEFFICIENTS
M = 0.700

α	B_0	B_1	B_2	B_3	B_4	B_5
1	–0.00007	0.00201	0.00022	–0.00135	–0.00725	0.00007
2	–0.00033	0.00463	0.00074	–0.00148	–0.03061	0.00012
3	0.00298	0.00816	0.00104	–0.00409	–0.05738	0.00022
4	0.00952	0.00977	0.00158	–0.00596	–0.10542	0.00024
5	0.01365	0.01690	0.00255	–0.00959	–0.16575	0.00060
6	0.02140	0.02569	0.00468	–0.01204	–0.21467	–0.00007
7	0.03280	0.03299	0.00753	–0.01552	–0.31023	–0.00068
8	0.04427	0.02903	0.01022	–0.01617	–0.41625	–0.00056
9	0.07156	0.01444	0.01163	–0.01605	–0.53882	–0.00079
10	0.11009	–0.02070	0.00879	–0.01748	–0.57938	–0.00131
11	0.13603	–0.04580	0.00794	–0.01852	–0.65951	–0.00053
12	0.09477	0.06299	0.01071	–0.01897	–0.54804	–0.00173
13	0.13093	0.02476	0.00847	–0.00460	–0.61551	–0.00301
14	0.15005	0.07016	0.00453	–0.02278	–0.26831	–0.00323
15	0.11178	0.13769	0.00500	0.00024	–0.01360	–0.00467
16	0.16474	0.10007	0.00168	–0.02076	0.23531	0.00169
17	0.27867	–0.01521	–0.00150	–0.03375	0.53500	0.00416
18	0.35631	–0.05496	–0.00269	–0.04285	0.32793	0.00590

α	B_6	B_7	B_8	B_9	B_{10}	B_{11}
1	–0.00001	0.00605	–0.01896	0.01137	0.00007	0.05663
2	–0.00038	0.01304	–0.03081	0.01730	–0.00037	0.17544
3	–0.00024	0.02194	–0.05995	0.03480	–0.00051	0.27522
4	–0.00071	0.03369	–0.08731	0.04965	–0.00072	0.35126
5	–0.00042	0.05308	–0.14787	0.08719	–0.00078	0.41736
6	–0.00069	0.07008	–0.19058	0.11191	–0.00074	0.21681
7	–0.00097	0.08932	–0.23841	0.13886	–0.00121	0.56157
8	–0.00254	0.13154	–0.33205	0.19557	0.00003	1.08763
9	–0.00512	0.16180	–0.37175	0.21318	0.00190	1.52565
10	–0.00517	0.19468	–0.43251	0.24542	0.00542	2.11903
11	–0.00530	0.19852	–0.43424	0.24919	0.00584	3.19374
12	0.00049	0.30677	–0.81576	0.52282	0.01558	2.42095
13	–0.00132	0.29722	–0.71510	0.45468	0.01598	2.83715
14	0.00483	0.22818	–0.52780	0.28270	0.02293	–0.19638
15	0.01013	0.30323	–0.81142	0.50265	0.02790	–2.43719
16	–0.00023	0.28821	–0.68001	0.35785	0.03395	–2.90182
17	–0.00071	0.26551	–1.03124	0.70318	0.02908	–7.14091
18	–0.00632	0.22175	–0.87165	0.58893	0.02677	–6.40790

α	B_{12}	B_{13}	B_{14}	$B_{15} \times 10^{+6}$
1	0.03248	0.02814	–0.00546	0.00012
2	0.04260	0.04867	–0.00974	0.00021
3	0.06622	0.06841	–0.01333	0.00028
4	0.09946	0.10427	–0.01888	0.00024
5	0.10760	0.01684	–0.02734	0.00043
6	0.14430	–0.12045	–0.04174	0.00035
7	0.18066	–0.27628	–0.05621	0.00015
8	0.24523	–0.46906	–0.07745	0.00034
9	0.33416	–0.43756	–0.09118	–0.00040
10	0.41420	–0.36868	–0.09857	–0.00051
11	0.45796	–0.33092	–0.10509	0.00037
12	0.45015	–0.14214	–0.08911	–0.00146
13	0.50671	–0.05438	–0.08978	–0.00174
14	0.28798	0.22777	–0.06876	–0.00277
15	0.26261	0.25419	–0.05078	–0.00464
16	0.31661	0.21182	–0.07109	–0.00514
17	0.20470	0.24062	–0.06928	–0.00801
18	0.27279	0.36714	–0.06778	–0.00899

TABLE 4.3.3.2-D (CONTD)
METHOD 1
REGRESSION COEFFICIENTS
M = 0.800

α	B_0	B_1	B_2	B_3	B_4	B_5
1	0.00221	−0.00144	−0.00009	−0.00073	−0.00797	0.00001
2	0.00338	−0.00302	0.00036	−0.00054	−0.04293	0.00016
3	0.01022	−0.00891	0.00044	−0.00118	−0.09171	0.00029
4	0.02014	−0.01193	0.00101	−0.00320	−0.16796	0.00031
5	0.03137	−0.01895	0.00175	−0.00608	−0.26045	0.00073
6	0.04483	−0.02209	0.00408	−0.00776	−0.38466	0.00035
7	0.05954	−0.02427	0.00622	−0.01036	−0.46785	−0.00004
8	0.08586	−0.04047	0.00675	−0.01503	−0.53205	0.00026
9	0.12288	−0.06032	0.00656	−0.01914	−0.61233	−0.00006
10	0.15902	−0.09484	0.00500	−0.01786	−0.67543	0.00000
11	0.19087	−0.12050	0.00370	−0.01996	−0.70864	0.00052
12	0.19993	−0.10093	0.00286	−0.00938	−0.80847	−0.00080
13	0.21762	−0.05888	0.00378	−0.01095	−0.87035	−0.00312
14	0.22825	−0.06174	0.00297	−0.00059	−0.75253	−0.00286
15	0.26345	−0.08437	−0.00007	0.01070	−0.72073	−0.00351
16	0.26728	−0.04519	0.00045	0.01068	−0.81612	−0.00314
17	0.26672	0.03024	0.00162	0.00616	−0.73124	−0.00435
18	0.38780	−0.06958	−0.00033	−0.04003	−0.00836	0.00680

α	B_6	B_7	B_8	B_9	B_{10}	B_{11}
1	−0.00011	0.00404	−0.00852	0.00366	−0.00020	0.04986
2	−0.00059	0.01149	−0.02119	0.01016	−0.00084	0.27904
3	−0.00081	0.01741	−0.03594	0.01916	−0.00120	0.48014
4	−0.00136	0.02455	−0.05123	0.02690	−0.00164	0.88190
5	−0.00160	0.03701	−0.08555	0.04712	−0.00185	1.46725
6	−0.00268	0.04932	−0.10395	0.05655	−0.00274	2.24272
7	−0.00275	0.06720	−0.13865	0.07161	−0.00361	2.52398
8	−0.00385	0.09758	−0.19441	0.09494	−0.00314	2.78528
9	−0.00533	0.13366	−0.27088	0.13617	−0.00244	3.34227
10	−0.00651	0.14191	−0.25370	0.11523	−0.00263	4.11935
11	−0.00645	0.12269	−0.19227	0.07658	−0.00338	4.86755
12	−0.00359	0.12092	−0.17696	0.07638	0.00149	5.29550
13	−0.00071	0.12946	−0.23012	0.11647	0.00542	4.41136
14	0.00082	0.11291	−0.19585	0.10526	0.00530	2.93353
15	0.00351	0.12110	−0.33286	0.23396	0.01239	1.94911
16	0.00615	0.17305	−0.52066	0.36192	0.01483	2.44009
17	0.00963	0.20127	−0.66993	0.46675	0.02226	1.45434
18	−0.01148	0.23079	−0.81556	0.53140	0.01939	−4.53597

α	B_{12}	B_{13}	B_{14}	$B_{15} \times 10^{+6}$
1	0.03464	0.03796	−0.00568	0.00011
2	0.05100	0.05301	−0.01138	0.00034
3	0.07937	0.08300	−0.01716	0.00055
4	0.10986	0.11608	−0.02432	0.00065
5	0.12995	0.04853	−0.03608	0.00101
6	0.17974	0.01871	−0.05082	0.00108
7	0.23537	−0.06230	−0.06341	0.00109
8	0.28989	−0.20397	−0.08062	0.00119
9	0.34386	−0.16500	−0.08937	0.00023
10	0.40218	−0.06673	−0.09428	0.00021
11	0.43511	0.01019	−0.09377	0.00072
12	0.44284	0.01175	−0.08753	−0.00022
13	0.39269	−0.55132	−0.08675	−0.00105
14	0.24896	0.03958	−0.07231	−0.00175
15	0.23602	−0.13912	−0.07000	−0.00357
16	0.21889	−0.40147	−0.08010	−0.00315
17	0.17675	−0.44420	−0.07856	−0.00488
18	0.35079	0.06490	−0.07221	−0.00986

TABLE 4.3.3.2-D (CONTD)
METHOD 1
REGRESSION COEFFICIENTS
M = 0.900

α	B_0	B_1	B_2	B_3	B_4	B_5
1	−0.00018	0.00149	0.00049	−0.00073	−0.01288	0.00002
2	0.00085	0.00228	0.00121	−0.00194	−0.03023	0.00020
3	0.00686	0.00006	0.00220	−0.00452	−0.09050	0.00033
4	0.01655	0.00152	0.00381	−0.00939	−0.16820	0.00044
5	0.03421	0.00025	0.00585	−0.01606	−0.31665	0.00011
6	0.05013	0.00707	0.00817	−0.02358	−0.40391	−0.00009
7	0.07780	−0.00719	0.00818	−0.02851	−0.48392	−0.00013
8	0.10210	−0.03657	0.00766	−0.02671	−0.49372	0.00080
9	0.14499	−0.06085	0.00615	−0.03327	−0.58207	0.00055
10	0.16459	−0.05228	0.00708	−0.03939	−0.57416	0.00041
11	0.17308	−0.01765	0.00635	−0.03038	−0.60311	−0.00147
12	0.24567	−0.01323	−0.00076	−0.04699	−0.52503	−0.00381
13	0.25980	−0.02503	−0.01431	−0.03221	0.02489	−0.00265
14	0.28659	−0.02031	−0.01516	−0.03412	−0.24196	−0.00242
15	0.35500	−0.10280	−0.03013	−0.00726	−0.15999	−0.00365
16	−0.02321	0.50911	0.05826	−0.07837	0.10819	0.00110
17	0.00224	0.41838	0.05118	−0.02457	−0.19688	−0.00106
18	−0.30160	0.86541	0.12481	−0.02627	−0.15727	−0.00442

α	B_6	B_7	B_8	B_9	B_{10}	B_{11}
1	−0.00029	0.00368	−0.00564	0.00171	−0.00034	0.15304
2	−0.00072	0.01144	−0.02520	0.01329	−0.00058	0.46101
3	−0.00119	0.01294	−0.02237	0.00728	−0.00094	1.09961
4	−0.00198	0.01829	−0.02715	0.00418	−0.00092	1.81146
5	−0.00250	0.03007	−0.05654	0.01904	−0.00117	3.06166
6	−0.00294	0.04804	−0.08597	0.02708	−0.00198	3.45630
7	−0.00267	0.07875	−0.15670	0.06535	−0.00157	3.48608
8	−0.00470	0.10510	−0.17727	0.06858	−0.00079	3.23396
9	−0.00499	0.12259	−0.20621	0.07849	−0.00095	3.85120
10	−0.00507	0.13288	−0.21749	0.07251	0.00073	3.69670
11	−0.00161	0.16048	−0.22384	0.05180	−0.00034	2.96357
12	0.00356	0.13104	−0.17885	−0.00130	0.00693	1.11615
13	0.00890	0.11813	−0.20085	0.01759	0.01678	−1.67578
14	0.00994	0.08859	−0.07871	−0.08308	0.02128	−0.12470
15	0.01574	0.11651	−0.16128	−0.00975	0.02559	−2.81231
16	0.00687	0.02378	0.11590	−0.29281	0.04029	−3.95931
17	0.00761	−0.07051	0.08506	1.29494	0.05010	−1.21388
18	0.00782	−0.17396	0.57898	0.55814	0.05542	−3.35470

α	B_{12}	B_{13}	B_{14}	$B_{15} \times 10^{+6}$
1	0.03891	0.09467	−0.00564	0.00009
2	0.07985	0.20140	−0.01169	0.00016
3	0.10833	0.27199	−0.01904	0.00040
4	0.14272	0.28821	−0.02860	0.00040
5	0.16786	0.18235	−0.04081	0.00046
6	0.19252	0.03040	−0.05024	0.00032
7	0.26545	0.11939	−0.05983	0.00022
8	0.31886	−0.00803	−0.06984	0.00025
9	0.35199	−0.03479	−0.07633	−0.00009
10	0.38080	−0.13176	−0.08018	−0.00031
11	0.40789	−0.30354	−0.07411	−0.00174
12	0.38815	−0.39060	−0.06307	−0.00512
13	0.30251	−0.36091	−0.04905	−0.00682
14	0.28643	−0.42389	−0.05155	−0.00616
15	0.25151	−0.54633	−0.03975	−0.00792
16	0.28255	−0.09940	−0.05434	−0.00888
17	0.27277	0.21319	−0.05330	−0.00839
18	0.32974	0.55880	−0.04722	−0.01182

TABLE 4.3.3.2-D (CONTD)
METHOD 1
REGRESSION COEFFICIENTS
M = 0.950

α	B_0	B_1	B_2	B_3	B_4	B_5
1	−0.00838	0.01178	0.00121	0.00009	0.00809	−0.00005
2	−0.00357	0.00752	0.00193	−0.00002	−0.05533	0.00001
3	0.00810	0.00508	0.00244	−0.00514	−0.09663	0.00006
4	0.03190	−0.00520	0.00165	−0.01368	−0.15750	0.00036
5	0.05470	−0.00974	0.00215	−0.02267	−0.22959	0.00049
6	0.08580	−0.02069	0.00170	−0.03115	−0.37571	0.00084
7	0.11675	−0.03737	0.00250	−0.03773	−0.50555	0.00100
8	0.14670	−0.04756	0.00030	−0.04832	−0.40434	0.00248
9	0.18449	−0.07402	−0.00266	−0.05180	−0.01091	0.00153
10	0.19113	−0.02070	0.00791	−0.06569	−0.60252	0.00152
11	0.22544	0.02716	0.01117	−0.09426	−0.87604	0.00286

α	B_6	B_7	B_8	B_9	B_{10}	B_{11}
1	−0.00025	−0.00078	0.01625	−0.01505	0.00018	0.12846
2	−0.00070	0.00316	0.02724	−0.02814	−0.00030	0.98002
3	0.00008	0.00303	0.01796	−0.02569	−0.00131	1.49493
4	0.00201	0.01412	−0.04312	0.01461	−0.00291	2.11918
5	0.00291	0.01358	−0.04992	0.01207	−0.00344	2.24598
6	0.00382	0.02640	−0.08947	0.03485	−0.00382	3.11378
7	0.00222	0.02453	−0.04389	−0.01608	−0.00198	4.23658
8	0.00404	0.01225	−0.04267	−0.01428	−0.00337	3.55768
9	0.00426	−0.00656	0.03526	−0.08574	−0.00147	−0.81326
10	0.00052	0.02266	0.03270	−0.11326	−0.00128	3.94893
11	0.00030	0.00033	0.12082	−0.20285	−0.00459	7.53037

α	B_{12}	B_{13}	B_{14}	$B_{15} \times 10^{+6}$
1	0.11372	0.26412	−0.00790	0.00011
2	0.12969	0.38083	−0.01354	−0.00028
3	0.16049	0.36673	−0.02110	−0.00072
4	0.13857	0.14239	−0.03305	−0.00143
5	0.13531	0.05344	−0.04690	−0.00172
6	0.28422	0.62238	−0.06146	−0.00241
7	0.33755	0.64386	−0.07750	−0.00263
8	0.46401	1.49135	−0.08695	−0.00337
9	0.78061	2.53411	−0.10360	−0.00386
10	0.48502	0.10404	−0.09913	−0.00361
11	0.43784	0.31377	−0.10616	−0.00522

TABLE 4.3.3.2-D (CONTD)
METHOD 1
REGRESSION COEFFICIENTS
M = 1.000

α	B_0	B_1	B_2	B_3	B_4	B_5
1	−0.00184	−0.00510	−0.00023	0.00191	0.03683	0.00037
2	0.00039	0.00326	0.00184	−0.00236	−0.11220	0.00046
3	−0.05094	0.09969	0.01520	−0.01431	−0.17369	0.00029
4	−0.11879	0.29136	0.04005	−0.05546	−0.94287	0.00031
5	−0.02635	0.14202	0.02414	−0.04156	−0.84098	0.00055
6	−0.06161	0.24704	0.03977	−0.06338	−1.21329	0.00049
7	−0.51857	1.09040	0.14419	−0.15946	−1.51798	−0.00163
8	−0.41208	0.95781	0.12733	−0.15441	−1.45667	−0.00103
9	−0.54877	1.19553	0.15925	−0.17971	−1.07918	−0.00208
10	−1.12307	2.34028	0.28663	−0.32300	−1.47035	−0.00457
11	−1.88393	2.80793	0.39284	−0.17471	4.11060	0.00066
12	−3.71327	6.39571	0.88455	−0.64685	−7.92697	0.00000

α	B_6	B_7	B_8	B_9	B_{10}	B_{11}
1	−0.00042	−0.00431	0.03435	−0.03837	0.00017	−0.32067
2	−0.00063	0.02795	−0.10548	0.11581	−0.00009	1.43644
3	−0.00086	0.05446	−0.23999	0.24547	−0.00045	1.83557
4	−0.00097	0.16868	−0.87339	0.95296	−0.00023	12.40156
5	−0.00112	0.13169	−0.61505	0.66843	0.00069	9.69120
6	−0.00123	0.18757	−0.91157	0.99576	−0.00101	13.90155
7	0.00503	0.48849	−2.82813	3.13791	−0.00809	14.80998
8	0.00425	0.48904	−2.79021	3.11841	−0.00832	13.65930
9	0.00586	0.47045	−2.83951	3.18905	−0.00556	8.54019
10	0.01387	1.11512	−6.47644	7.23240	−0.02132	14.09991
11	−0.00727	−1.38447	5.79307	−6.58945	−0.00979	−49.73547
12	−0.00495	1.72879	−7.81054	8.85635	−0.08292	43.19402

α	B_{12}	B_{13}	B_{14}	$B_{15} \times 10^{+6}$
1	−0.02364	0.11396	−0.00713	0.00017
2	0.12498	−0.00827	−0.01494	−0.00004
3	0.14708	−0.41706	−0.02709	0.00015
4	1.05810	−1.47681	−0.04821	−0.00010
5	0.76958	−1.14098	−0.06112	−0.00073
6	0.94294	−1.81063	−0.07002	−0.00083
7	3.24042	3.22464	−0.05688	−0.00211
8	2.89318	2.79437	−0.07367	−0.00250
9	4.30224	6.63418	−0.07343	−0.00203
10	8.16605	12.54916	−0.04314	−0.00417
11	−6.18641	15.14346	0.00058	−0.00022
12	6.25554	16.75446	0.35531	0.00127

TABLE 4.3.3.2-D (CONTD)
METHOD 1
REGRESSION COEFFICIENTS
M = 1.100

α	B_0	B_1	B_2	B_3	B_4	B_5
1	−0.04484	0.08372	0.00940	−0.00817	−0.04487	−0.00010
2	−0.04355	0.09444	0.01029	−0.01400	−0.03926	−0.00006
3	−0.03818	0.10749	0.01176	−0.01903	−0.13134	−0.00036
4	−0.06102	0.16158	0.01869	−0.02982	−0.14335	−0.00010
5	−0.04984	0.18025	0.02032	−0.03960	−0.21009	−0.00026
6	−0.03717	0.20704	0.02251	−0.05545	−0.36705	0.00009
7	−0.08362	0.32672	0.03894	−0.07228	−0.58530	−0.00065
8	−0.18809	0.43881	0.05636	−0.06272	−0.54914	0.00034
9	−0.16553	0.43886	0.05666	−0.07680	−0.46356	0.00229
10	−0.27549	0.59413	0.08484	−0.07664	−0.30332	−0.00097
11	−0.29751	0.66053	0.09320	−0.07554	−0.40645	−0.00235
12	−0.29560	0.73732	0.10393	−0.09837	−0.59564	−0.00164
13	−0.34429	0.87460	0.12440	−0.12202	−0.66147	−0.00237
14	0.17848	0.28522	0.02090	−0.14298	0.56890	−0.00414
15	0.53359	−0.32241	−0.06227	−0.07706	1.53930	−0.00261

α	B_6	B_7	B_8	B_9	B_{10}	B_{11}
1	−0.00083	0.03295	−0.15500	0.16983	−0.00164	0.82746
2	−0.00051	0.02717	−0.11801	0.12194	−0.00174	0.88339
3	−0.00098	0.04605	−0.19072	0.21743	−0.00164	1.67764
4	−0.00129	0.04320	−0.18755	0.22187	−0.00101	2.18522
5	−0.00125	0.09835	−0.42457	0.47771	−0.00091	2.80951
6	−0.00171	0.09902	−0.45321	0.55087	0.00099	4.98784
7	−0.00311	0.17055	−0.79734	0.96443	0.00293	6.25124
8	0.00066	0.10552	−0.29838	0.25776	0.00349	5.58307
9	−0.00065	0.12365	−0.35773	0.28341	0.00473	5.89547
10	−0.00037	0.04642	0.05276	−0.21425	0.01034	2.61690
11	−0.00004	0.06654	0.09562	−0.29549	0.00938	2.41419
12	−0.00302	0.18490	−0.45240	0.26825	0.00698	3.69788
13	−0.00304	0.18917	−0.50258	0.27871	0.00968	3.72855
14	0.01223	−0.01709	0.42603	−1.46168	0.01947	−4.76428
15	0.02637	−0.26299	2.21540	−4.14095	0.02659	−14.41504

α	B_{12}	B_{13}	B_{14}	$B_{15} \times 10^{+6}$
1	0.02607	−0.02705	−0.01003	−0.00003
2	0.05290	0.00332	−0.01502	0.00010
3	0.08191	0.05082	−0.02014	−0.00013
4	0.10961	0.04423	−0.02851	0.00019
5	0.13773	0.03226	−0.03272	−0.00033
6	0.15323	−0.07582	−0.04362	−0.00004
7	0.18095	−0.05587	−0.05040	−0.00065
8	0.20404	−0.22864	−0.05851	0.00162
9	0.22347	−0.35035	−0.07051	0.00174
10	0.26634	−0.28726	−0.07333	0.00219
11	0.26552	−0.32247	−0.07404	0.00224
12	0.26718	−0.38297	−0.07983	0.00126
13	0.27717	−0.32919	−0.08411	0.00081
14	0.18642	−0.06096	−0.04441	−0.00357
15	0.23323	0.06531	0.01127	−0.00447

TABLE 4.3.3.2-D (CONTD)
METHOD 1
REGRESSION COEFFICIENTS
M = 1.200

α	B_0	B_1	B_2	B_3	B_4	B_5
1	−0.00629	−0.00384	0.00036	0.00199	0.08753	0.00062
2	−0.01132	0.01013	0.00209	−0.00207	0.11552	0.00063
3	−0.01203	0.02211	0.00350	−0.00806	0.16420	0.00065
4	−0.01206	0.03319	0.00473	−0.01526	0.25095	0.00110
5	−0.02330	0.07276	0.01135	−0.02196	0.14635	0.00072
6	−0.01091	0.07268	0.01255	−0.02780	0.13904	0.00107
7	−0.01717	0.12154	0.02004	−0.03729	−0.00996	0.00014
8	−0.00842	0.15381	0.02466	−0.05047	−0.15838	−0.00012
9	−0.03652	0.22732	0.03691	−0.06119	−0.19927	−0.00114
10	0.09571	0.07832	0.01571	−0.06356	−0.23286	−0.00067
11	0.15972	0.01584	0.01023	−0.06640	−0.28670	−0.00091
12	0.12048	0.13091	0.02415	−0.07384	−0.18197	−0.00249
13	−0.03809	0.43572	0.06381	−0.10453	−0.43468	−0.00246
14	−0.11557	0.63985	0.08428	−0.12262	−0.48088	−0.00327
15	−1.28236	2.60841	0.32970	−0.29107	−0.11267	−0.00158

α	B_6	B_7	B_8	B_9	B_{10}	B_{11}
1	−0.00080	0.00609	0.00409	−0.00586	−0.00122	−0.11648
2	−0.00049	0.00324	0.01675	−0.02070	−0.00128	−0.20069
3	0.00031	−0.00122	0.02598	−0.03330	−0.00115	−0.40599
4	0.00101	0.00664	−0.00919	−0.01439	−0.00104	−0.49071
5	0.00005	0.01615	−0.02405	−0.01345	−0.00075	0.03910
6	−0.00012	0.02910	−0.06189	0.00746	−0.00100	0.24032
7	−0.00057	0.04242	−0.10277	0.02792	0.00014	0.92401
8	−0.00206	−0.02183	0.29348	−0.51237	0.00193	2.70883
9	−0.00289	−0.06161	0.56545	−0.91636	0.00456	3.31566
10	−0.00229	−0.06868	0.70933	−1.18044	0.00520	3.65242
11	−0.00206	−0.11603	1.05318	−1.75138	0.00531	4.08376
12	−0.00695	0.04728	0.18852	−0.46850	0.00759	2.22800
13	−0.00794	0.03489	0.17526	−0.50592	0.00558	6.71935
14	−0.00674	0.14918	−0.57903	0.61631	0.00038	5.64320
15	−0.01478	2.42693	−17.16211	27.39923	−0.01586	1.34910

α	B_{12}	B_{13}	B_{14}	$B_{15} \times 10^{+6}$
1	0.06357	0.06844	−0.00754	0.00020
2	0.07738	0.04564	−0.01260	0.00037
3	0.06695	−0.04451	−0.01749	0.00060
4	0.06682	−0.15000	−0.02362	0.00084
5	0.05120	−0.29811	−0.02926	0.00082
6	0.05617	−0.41686	−0.03565	0.00098
7	0.06405	−0.48130	−0.04083	0.00076
8	0.00266	−0.71579	−0.05045	0.00109
9	−0.04614	−0.98680	−0.05984	0.00117
10	−0.11013	−1.29176	−0.06452	0.00122
11	−0.16349	−1.54903	−0.07158	0.00157
12	−0.07644	−1.77188	−0.08773	0.00029
13	−0.25184	−2.00624	−0.10028	0.00047
14	−0.23828	−2.04665	−0.10330	0.00022
15	0.51026	3.57818	−0.12676	−0.00872

TABLE 4.3.3.2-D (CONTD)
METHOD 1
REGRESSION COEFFICIENTS
M = 1.300

α	B_0	B_1	B_2	B_3	B_4	B_5
1	0.01073	−0.01651	−0.00239	−0.00130	0.03077	0.00032
2	0.01124	−0.01236	−0.00186	−0.00349	0.06002	0.00025
3	0.01222	−0.00992	−0.00090	−0.00610	0.09056	0.00054
4	0.01289	0.00091	0.00109	−0.00977	0.13145	0.00014
5	0.01732	0.00436	0.00258	−0.01275	0.18255	0.00037
6	0.04046	−0.00836	0.00183	−0.01702	0.20021	0.00010
7	0.03964	0.01740	0.00620	−0.02283	0.22781	−0.00059
8	0.03812	0.04382	0.01016	−0.03103	0.25309	0.00026
9	0.12317	−0.00959	0.00143	−0.04214	0.14197	−0.00374
10	0.14136	−0.00742	0.00110	−0.05227	0.27808	−0.00146
11	0.07022	0.06183	0.01130	−0.04890	0.50921	0.00200
12	0.08746	0.09711	0.01424	−0.05404	0.28856	−0.00129
13	0.37881	−0.20159	−0.03400	−0.07169	−0.38882	−0.00079
14	0.35522	−0.11761	−0.03078	−0.07623	0.13295	0.00246
15	−0.71802	1.47949	0.21882	−0.13860	0.37682	0.00262

α	B_6	B_7	B_8	B_9	B_{10}	B_{11}
1	0.00074	0.00224	−0.01367	0.00902	−0.00037	−0.08973
2	0.00113	0.01025	−0.04063	0.02565	−0.00071	−0.17503
3	0.00111	0.02331	−0.08208	0.05267	−0.00086	−0.26347
4	0.00155	0.03354	−0.11671	0.07414	−0.00092	−0.33645
5	0.00126	0.07141	−0.24091	0.15987	−0.00110	−0.60188
6	0.00147	0.09155	−0.31135	0.20772	−0.00097	−0.71345
7	0.00216	0.11071	−0.38611	0.25792	−0.00076	−1.05681
8	0.00142	0.18615	−0.76108	0.74001	−0.00013	−1.35729
9	0.00681	0.09964	−0.30165	−0.00252	0.00032	0.05106
10	0.00536	0.16930	−0.54852	0.20149	0.00133	−1.39210
11	0.00871	0.21573	−0.34730	−0.55274	0.00252	−3.93809
12	0.01268	0.19176	−0.22055	−0.71886	0.00238	−2.50095
13	0.01891	0.25610	−0.61300	−0.34549	0.00206	4.39566
14	0.01283	0.57924	−2.91125	3.62863	−0.00003	−3.12316
15	−0.05784	1.30330	−9.95914	18.12476	0.00216	−0.97701

α	B_{12}	B_{13}	B_{14}	$B_{15} \times 10^{+6}$
1	0.01334	−0.06052	−0.00463	0.00028
2	0.02758	−0.12623	−0.00965	0.00034
3	0.02390	−0.25254	−0.01479	0.00045
4	0.00935	−0.41783	−0.02001	0.00036
5	−0.00116	−0.68714	−0.02647	0.00021
6	−0.00696	−0.90402	−0.03292	0.00002
7	0.13956	−0.51697	−0.03541	−0.00031
8	0.17097	−0.59970	−0.04157	−0.00041
9	0.17897	−0.58601	−0.04958	−0.00024
10	0.20709	−0.69765	−0.05311	−0.00056
11	0.23022	−1.12538	−0.05796	0.00077
12	0.22683	−1.17960	−0.06484	0.00127
13	0.08343	−1.80161	−0.08567	0.00253
14	0.33804	−0.57097	−0.06865	0.00025
15	0.35827	2.28471	−0.09056	−0.01175

TABLE 4.3.3.2-D (CONTD)
METHOD 1
REGRESSION COEFFICIENTS
M = 1.400

α	B_0	B_1	B_2	B_3	B_4	B_5
1	0.00157	−0.00557	−0.00067	−0.00067	0.04543	0.00020
2	0.00283	−0.00385	−0.00035	−0.00231	0.08027	0.00020
3	0.00580	−0.00543	0.00011	−0.00436	0.13016	0.00044
4	0.01126	−0.00755	0.00060	−0.00607	0.16445	0.00036
5	0.01710	−0.00602	0.00147	−0.00887	0.21080	0.00052
6	0.03541	−0.01819	0.00101	−0.01140	0.22765	0.00043
7	0.04051	−0.00700	0.00376	−0.01602	0.24154	0.00042
8	0.04478	−0.00232	0.00583	−0.01817	0.34976	0.00084
9	0.07564	−0.00509	0.00509	−0.02763	0.20858	0.00099
10	0.08951	0.00473	0.00632	−0.03430	0.16744	0.00120
11	0.11793	−0.00028	0.00502	−0.04128	0.18050	0.00162
12	0.08874	0.08143	0.01520	−0.04933	0.21049	0.00090
13	0.26017	−0.12899	−0.01372	−0.04668	0.12047	0.00000
14	0.06149	0.12399	0.01598	−0.02868	0.40721	−0.00173
15	0.32684	−0.00669	−0.00231	−0.09153	0.13368	−0.00016

α	B_6	B_7	B_8	B_9	B_{10}	B_{11}
1	0.00049	−0.00040	0.00088	−0.00206	−0.00018	−0.21101
2	0.00065	0.00556	−0.01723	0.00889	−0.00065	−0.31472
3	0.00066	0.01074	−0.03276	0.01790	−0.00112	−0.52483
4	0.00095	0.01416	−0.04143	0.02282	−0.00151	−0.61570
5	0.00092	0.03055	−0.09043	0.05429	−0.00172	−0.91572
6	0.00083	0.04136	−0.12409	0.07650	−0.00188	−1.06178
7	0.00059	0.06188	−0.19356	0.12308	−0.00183	−1.29615
8	0.00034	0.09682	−0.30521	0.20226	−0.00202	−2.30528
9	0.00104	0.19819	−0.85614	0.92464	−0.00193	−1.16990
10	0.00204	0.22722	−0.95835	1.01882	−0.00219	−0.83807
11	0.00182	0.27365	−1.15352	1.24001	−0.00241	−0.99790
12	0.00170	0.32167	−1.34443	1.47775	−0.00156	−1.42727
13	0.00886	0.13442	0.06467	−1.04149	−0.00131	−0.91704
14	0.01785	−0.02692	0.81494	−1.76098	−0.00915	−5.61367
15	−0.01151	0.26982	−1.48732	2.19990	0.00757	0.06241

α	B_{12}	B_{13}	B_{14}	$B_{15} \times 10^{+6}$
1	0.01591	−0.05851	−0.00435	0.00024
2	0.02992	−0.13305	−0.00929	0.00030
3	0.04719	−0.17722	−0.01392	0.00043
4	0.04159	−0.29398	−0.01873	0.00062
5	0.04397	−0.43206	−0.02376	0.00065
6	0.06035	−0.53017	−0.02925	0.00071
7	0.16772	−0.29734	−0.03314	0.00062
8	0.21498	−0.26741	−0.03588	0.00037
9	0.24629	−0.29801	−0.04400	0.00029
10	0.25079	−0.45710	−0.05218	0.00082
11	0.23820	−0.66717	−0.05883	0.00091
12	0.22909	−0.91669	−0.06660	0.00074
13	0.16346	−1.43306	−0.07209	0.00208
14	0.22960	−0.52901	−0.04924	0.00550
15	0.14657	−0.55797	−0.06595	−0.00540

TABLE 4.3.3.2-D (CONTD)
METHOD 1
REGRESSION COEFFICIENTS
M = 1.500

α	B_0	B_1	B_2	B_3	B_4	B_5
1	0.00028	−0.00531	−0.00047	0.00083	0.01860	0.00016
2	0.00572	−0.01091	−0.00099	0.00044	0.04745	0.00011
3	0.00691	−0.00879	−0.00019	−0.00178	0.10149	0.00033
4	0.02023	−0.02725	−0.00172	−0.00011	0.10141	0.00023
5	0.02641	−0.01846	−0.00020	−0.00592	0.18507	0.00036
6	0.04958	−0.05108	−0.00283	−0.00226	0.13830	0.00036
7	0.06259	−0.04729	−0.00172	−0.00838	0.16567	0.00038
8	0.07827	−0.04638	−0.00111	−0.01498	0.25049	0.00072
9	0.09523	−0.04553	−0.00034	−0.02197	0.31504	0.00126
10	0.10838	−0.04623	0.00092	−0.02505	0.38815	0.00207
11	0.11457	−0.02888	0.00335	−0.03059	0.48120	0.00267
12	0.15792	−0.05294	−0.00049	−0.03716	0.53228	0.00291
13	0.21437	−0.12313	−0.00797	−0.02976	0.59260	0.00220
14	0.06391	0.09522	0.01730	−0.03031	0.62570	0.00079
15	0.32106	−0.07231	−0.00820	−0.07269	0.22147	0.00030
16	103.09483	−130.05203	−23.01212	−0.12115	1.41383	−0.26344
17	75.90837	−96.81050	−17.28999	0.43793	2.46481	−0.20733

α	B_6	B_7	B_8	B_9	B_{10}	B_{11}
1	0.00041	0.00447	−0.01491	0.01125	−0.00042	−0.04700
2	0.00054	0.00779	−0.02110	0.01391	−0.00111	−0.12996
3	0.00058	0.01793	−0.05555	0.03640	−0.00135	−0.44197
4	0.00112	0.02610	−0.08192	0.05726	−0.00260	−0.28129
5	0.00045	0.04744	−0.14930	0.09895	−0.00205	−1.02289
6	0.00102	0.06170	−0.19775	0.13913	−0.00390	−0.58817
7	0.00070	0.07877	−0.25819	0.17831	−0.00358	−0.77266
8	0.00035	0.11264	−0.37444	0.25663	−0.00328	−1.41942
9	−0.00007	0.15081	−0.50534	0.34530	−0.00271	−2.00938
10	−0.00133	0.23586	−0.98431	1.05085	−0.00333	−3.04438
11	−0.00223	0.26174	−1.02835	1.04236	−0.00439	−4.08522
12	−0.00240	0.24543	−0.82995	0.65777	−0.00453	−4.59546
13	−0.00054	0.18633	−0.30029	−0.24104	−0.00544	−5.99071
14	0.01018	0.00806	0.60273	−1.42956	−0.01247	−7.48227
15	−0.00483	0.16214	−0.49650	0.31938	0.00032	−2.96651
16	5.07326	−141.25533	589.65942	−677.16602	−1.35118	−13.47584
17	3.99498	−108.87743	472.99951	−562.11035	−1.13367	−21.36497

α	B_{12}	B_{13}	B_{14}	$B_{15} \times 10^{+6}$
1	0.02767	−0.03146	−0.00443	0.00025
2	0.03932	−0.12355	−0.00939	0.00033
3	0.07609	−0.12497	−0.01370	0.00032
4	0.06646	−0.26070	−0.01820	0.00072
5	0.08017	−0.40137	−0.02307	0.00033
6	0.10356	−0.43001	−0.02758	0.00091
7	0.15294	−0.41352	−0.03275	0.00083
8	0.18420	−0.45614	−0.03651	0.00041
9	0.22163	−0.48580	−0.04082	0.00006
10	0.28647	−0.43662	−0.04560	−0.00007
11	0.30032	−0.57579	−0.04976	−0.00002
12	0.30269	−0.67818	−0.05251	−0.00015
13	0.30106	−0.96184	−0.05740	0.00054
14	0.31863	−0.32660	−0.04391	0.00445
15	0.26122	−0.41801	−0.05250	−0.00274
16	144.72121	390.29077	0.37379	1.40259
17	121.12621	271.07422	0.28761	1.14584

TABLE 4.3.3.2-D (CONTD)
METHOD 1
REGRESSION COEFFICIENTS
M = 2.000

α	B_0	B_1	B_2	B_3	B_4	B_5
1	0.02739	−0.04233	−0.00606	0.00381	−0.02875	0.00029
2	0.07553	−0.11930	−0.01586	0.01171	−0.07630	0.00056
3	0.07364	−0.11607	−0.01476	0.01119	−0.05201	0.00056
4	0.08820	−0.13065	−0.01690	0.01067	−0.04046	0.00073
5	0.10524	−0.15034	−0.01915	0.01121	−0.00600	0.00085
6	0.11737	−0.15989	−0.02016	0.01074	0.00851	0.00097
7	0.13005	−0.16403	−0.02019	0.00823	0.01741	0.00097
8	0.15887	−0.19848	−0.02321	0.00928	0.01671	0.00114
9	0.19314	−0.22421	−0.02756	0.00788	0.04264	0.00100
10	0.21766	−0.23029	−0.02967	0.00394	0.06635	0.00087
11	0.22138	−0.22948	−0.02480	0.00030	0.03912	0.00094
12	0.27413	−0.27002	−0.03168	−0.00152	−0.02566	0.00089
13	0.29047	−0.25721	−0.03340	−0.00232	0.04553	0.00036
14	0.37017	−0.34377	−0.04454	0.00100	0.04507	0.00075
15	0.56237	−0.47765	−0.06868	−0.02981	−0.19184	−0.00103

α	B_6	B_7	B_8	B_9	B_{10}	B_{11}
1	−0.00045	0.04098	−0.23030	0.38557	−0.00046	0.26480
2	−0.00166	0.09261	−0.56299	1.03211	−0.00012	1.13879
3	−0.00137	0.09665	−0.57350	1.02931	−0.00037	1.01436
4	−0.00139	0.11595	−0.64778	1.10953	−0.00082	0.92580
5	−0.00176	0.13154	−0.70979	1.19218	−0.00132	0.78751
6	−0.00200	0.15482	−0.81082	1.31452	−0.00148	0.65558
7	−0.00212	0.17280	−0.89271	1.41543	−0.00208	0.51476
8	−0.00186	0.17449	−0.83012	1.25395	−0.00413	0.17723
9	−0.00236	0.21284	−0.99934	1.47842	−0.00507	−0.04647
10	−0.00321	0.25793	−1.23851	1.83802	−0.00493	0.08167
11	−0.00250	0.22251	−1.00127	1.40514	−0.00436	−0.00866
12	−0.00398	0.28785	−1.30884	1.85827	−0.00494	0.42450
13	−0.00477	0.36357	−1.63001	2.31215	−0.00656	−0.45700
14	−0.00421	0.28733	−1.07968	1.39936	−0.01287	−0.91426
15	−0.00647	0.13657	−0.18101	−0.06424	−0.00363	2.27686

α	B_{12}	B_{13}	B_{14}	$B_{15} \times 10^{+6}$
1	0.01276	−0.14413	−0.00677	0.00026
2	−0.00739	−0.45431	−0.01837	0.00048
3	0.01489	−0.45917	−0.02103	0.00058
4	0.03859	−0.56613	−0.02521	0.00076
5	0.04974	−0.57770	−0.02809	0.00079
6	0.05515	−0.65604	−0.03121	0.00090
7	0.08463	−0.64573	−0.03368	0.00094
8	0.11120	−0.74441	−0.03771	0.00152
9	0.13302	−0.83799	−0.04221	0.00141
10	0.14411	−0.94664	−0.04835	0.00113
11	0.17336	−0.91347	−0.05040	0.00154
12	0.17794	−1.16748	−0.06059	0.00159
13	0.19870	−1.30091	−0.06413	0.00117
14	0.21462	−1.31872	−0.06397	0.00160
15	0.10918	−1.62533	−0.06664	−0.00145

TABLE 4.3.3.2-D (CONTD)
METHOD 1
REGRESSION COEFFICIENTS
M = 2.500

α	B_0	B_1	B_2	B_3	B_4	B_5
1	0.00478	−0.01228	−0.00200	0.00178	0.02268	0.00042
2	−0.00290	0.00255	0.00032	−0.00094	0.00174	0.00052
3	−0.00643	0.01813	0.00254	−0.00548	−0.04823	0.00057
4	0.03039	−0.01018	−0.00289	−0.00806	−0.06663	0.00035
5	0.18151	−0.13661	−0.02839	−0.01167	−0.17355	−0.00194
6	0.10365	−0.04753	−0.01221	−0.01596	−0.10382	−0.00109
7	0.05376	−0.01156	−0.00259	−0.01308	−0.03618	0.00015
8	0.09862	−0.04772	−0.00967	−0.01519	−0.07924	0.00002
9	0.15347	−0.09079	−0.01754	−0.01811	−0.11204	−0.00043
10	0.23161	−0.14988	−0.02798	−0.02334	−0.18635	−0.00097
11	0.21702	−0.12739	−0.02026	−0.03322	−0.19810	−0.00056
12	0.24585	−0.14100	−0.02160	−0.03754	−0.15242	−0.00033
13	0.36687	−0.35416	−0.04882	−0.00576	0.35939	0.00081
14	0.20578	−0.24662	−0.02417	0.02798	0.61627	0.00130
15	0.38159	−0.28580	−0.03447	−0.03879	0.01325	−0.00040

α	B_6	B_7	B_8	B_9	B_{10}	B_{11}
1	0.00046	0.03499	−0.19529	0.30678	−0.00252	−0.31168
2	0.00030	0.01727	−0.04537	−0.01635	−0.00044	−0.44534
3	−0.00034	0.00483	0.08492	−0.31595	0.00307	−0.62776
4	−0.00130	0.01234	0.06025	−0.23702	0.00223	−0.95984
5	−0.00438	0.03798	−0.18556	0.57011	−0.00334	−0.15262
6	−0.00305	0.01707	0.04987	−0.11416	−0.00016	−1.03480
7	−0.00178	0.04656	−0.03574	−0.22868	0.00149	−1.98522
8	−0.00242	0.06384	−0.12008	−0.03324	0.00061	−1.46935
9	−0.00345	0.08977	−0.20825	0.09932	−0.00032	−2.02305
10	−0.00545	0.11321	−0.25012	0.18655	−0.00271	−2.29838
11	−0.00359	−0.02825	0.54326	−1.28762	0.00672	−0.67739
12	−0.00346	−0.02755	0.58868	−1.43130	0.00327	−0.88390
13	0.00062	−0.00716	0.50164	−1.02755	−0.01386	−4.00934
14	0.00750	−0.02177	0.82050	−1.68213	−0.01220	−7.39198
15	−0.00074	−0.32694	2.67639	−4.90278	0.00633	−2.65221

α	B_{12}	B_{13}	B_{14}	$B_{15} \times 10^{+6}$
1	0.04574	0.10784	−0.00198	0.00046
2	0.06010	0.09237	−0.00325	0.00042
3	0.06792	0.01173	−0.00551	0.00035
4	0.08604	−0.08550	−0.00935	0.00010
5	0.01677	−0.58262	−0.01818	−0.00145
6	0.09659	−0.35116	−0.01834	−0.00077
7	0.15009	−0.24464	−0.01898	0.00026
8	0.12706	−0.38722	−0.02282	0.00019
9	0.18927	−0.41734	−0.02724	0.00013
10	0.19130	−0.72356	−0.03387	−0.00038
11	0.14314	−0.66563	−0.03354	−0.00065
12	0.14943	−0.75084	−0.03504	−0.00105
13	0.14865	−0.84247	−0.02897	−0.00132
14	0.16566	−0.72137	−0.01595	0.00093
15	0.11597	−1.18691	−0.03044	−0.00194

4.4 WING-WING COMBINATIONS AT ANGLE OF ATTACK (WING FLOW FIELDS)

4.4.1 WING-WING COMBINATIONS AT ANGLE OF ATTACK

This section presents methods of estimating the properties of wing flow fields. The subsonic methods include the effects of flow direction (downwash) and dynamic-pressure ratio. The supersonic methods include the effects of downwash, dynamic-pressure ratio, and Mach number.

A. SUBSONIC

Downwash*

The downwash behind a wing in subsonic flow is a consequence of the wing-trailing-vortex system. The trailing-vortex system behind a swept wing is shown in Sketch (a). A vortex sheet is shed by the lifting wing, and the sheet is deflected downward by the bound or lifting vortex and the tip vortices, which comprise the vortex system. In general, the sheet is not flat, but the curvature near the wing midspan is usually relatively small. This is particularly true of straight wings of reasonably large aspect ratio, for which the central portion of the vortex sheet is extremely flat. Wings with considerable trailing-edge sweepback produce a vortex sheet that is bowed upward near the plane of symmetry.

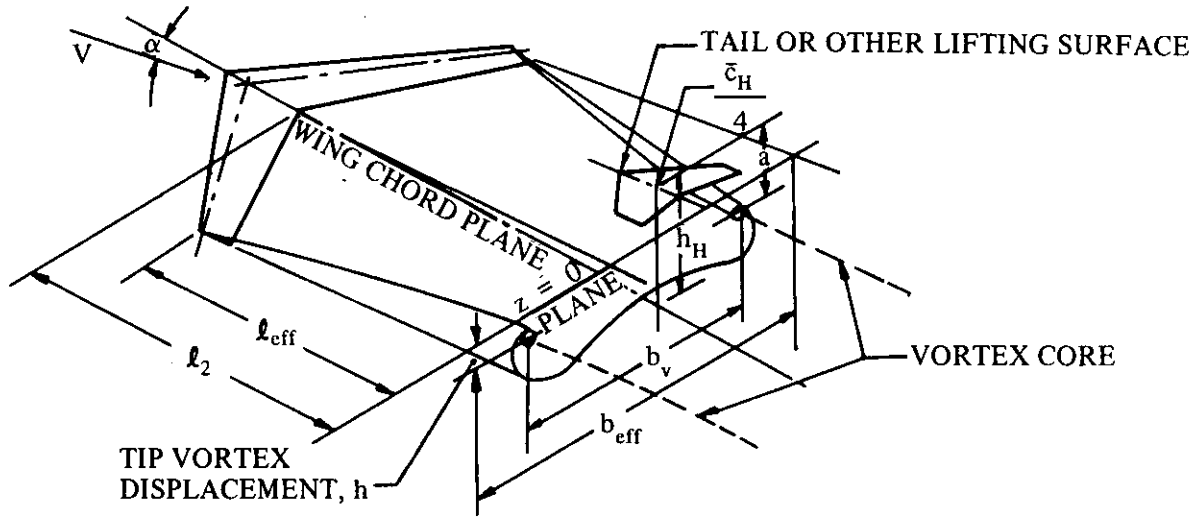

SKETCH (a)

The tip vortices do not experience a vertical displacement as great as the displacement of the central portion of the vortex sheet. In general, they trail back comparatively close to the streamwise direction.

*This general discussion is essentially quoted from Reference 1.

Furthermore, as the vortex system proceeds downstream, the tip vortices tend to move inboard. Also, with increasing distance behind the wing, the trailing-sheet vorticity tends to be transferred to the tip vortices. The transfer of vorticity and inboard movement of the tip vortices takes place in such a fashion that the lateral center of gravity of the vorticity remains at a fixed spanwise location. When all of the vorticity is transferred from the sheet to the trailing vortices, the vortex system is considered to be fully rolled up, and, in a nonviscous fluid, the vortex system then extends unchanged to infinity.

Ahead of the longitudinal station for complete rollup, the spanwise downwash distribution is dependent upon the spanwise lift distribution of the wing. However, when the rollup is complete, the downwash angles for all wings of equal lift and equal effective span are identical. It is evident that the shape of the vortex sheet has a significant influence on the downwash experienced by a tail located in the flow field of a wing and that the tail location relative to the trailing vortices is very important. Since the tip vortices are somewhat above the vortex sheet, the downwash above the sheet is somewhat greater than the downwash beneath the sheet.

The tip vortices spring from the wing tips at angles of attack for which the flow is unseparated. However, wings with high sweepback angles tend to stall at the tips, and in many instances the tip vortices originate well inboard of the wing tip at high angles of attack. This phenomenon has a significant influence on the downwash.

The previous discussion has been concerned with wings that behave in a somewhat conventional manner at high angles of attack. Certain thin, highly swept wings have a significantly different flow pattern in the higher angle-of-attack range. These wings are characterized by a leading-edge separation vortex that lies above the surface of the wing. From its inception near the plane of symmetry, it moves outboard in the approximate direction of the wing leading edge and is finally shed in a streamwise direction near the wing tip. Reference 2 shows some interesting studies of the separation vortex. It is clear that the existence of this vortex has an important influence on the downwash.

For very low-aspect-ratio configurations or for canard configurations, the tip vortex from the forward panel may impinge directly on the aft surface. Reference 3 contains a method (presented as Method 3 herein) of estimating the lift acting on the aft panel for this type of configuration. The method assumes that the trailing vortices are shed at a spanwise station corresponding to the center of vorticity of the isolated panel. The vortex pair is then assumed to remain at this spacing for longitudinal distances at least beyond the aft panel. This spacing is also assumed to be constant as a function of angle of attack. In the vertical plane the vortex pair is assumed to trail in the free-stream direction. These assumptions are shown in Reference 3 to be not only convenient, but reasonable in the light of experimental data. With the position of the vortices determined and their strength calculated from the lift of the forward panel, the integrated lift on the aft panel can be computed by means of strip theory. Because the theoretical vortex contains infinite velocities at its center, the method gives erroneous answers where the vortices trail very close to the aft panel. In reality the cores of the vortices revolve as solid bodies with zero tangential velocity at their centers.

Downwash Due to Flap Deflection

The downwash behind a wing is substantially modified by the deflection of trailing-edge flaps. This deflection creates an increase in the spanwise loading on the wing that increases the strength of the wing-trailing-vortex system. Consequently, the increased strength of the wing-trailing vortex produces an increase in the downwash angle.

At present, no theoretical methods exist that lend themselves to hand calculation for predicting the variation in downwash angle due to flap deflection. However, empirical curves are presented for estimating the variation in downwash angle due to deflection of plain or slotted flaps at small angles of attack at low subsonic speeds. The correlation parameters used to generate these curves are presented in Reference 4. The curve for slotted flaps is based on data from single- and double-slotted flap data.

Upwash

Upwash ahead of the wing is induced by the wing vortex system in a manner similar to that for downwash. A knowledge of flow fields beneath and ahead of a wing is sometimes required for the determination of forces and moments on nacelles or external stores or for the determination of inflow velocities into propellers of jet-engine intakes. Reference 3 contains charts for determining upwash about any straight-tapered swept or unswept wing. Because of their volume, these charts have not been included in the Datcom. Reference 5 contains a limited treatment for unswept wings only.

Dynamic-Pressure Ratio

The effectiveness of a lifting surface is directly proportional to the average dynamic pressure acting over that surface. A surface operating in the wake of an upstream surface therefore experiences a loss in effectiveness because of the reduced dynamic pressure. The decrease in dynamic pressure is caused by the loss of flow energy in the form of friction and separation drag of the forward surface; the greater the drag, the greater the pressure loss.

The wake, usually thin and intense at or near the trailing edge, spreads and decays with increasing distance downstream in such a manner that the integrated momentum across the wake at any station is constant. This type of wake, which is due to viscous effects, occurs at all speeds.

DATCOM METHODS

Subsonic Downwash

Three methods are presented below for estimating downwash characteristics. The first method is somewhat laborious, but enables the complete downwash curve to be estimated. The second method is accurate and expedient to use, but predicts only the downwash gradient. The third method is applicable only for configurations where the span of the forward surface is approximately equal to or less than that of the aft surface. Tables 4.4.1-A and -B present a data summary and substantiation for Methods 1 and 2,respectively, using the same test data.

Method 1

This method for estimating the downwash behind straight-tapered lifting wings at subsonic speeds is taken from Reference 1. The method is applicable to configurations in which the span of the wing is at least 1.5 times as large as that of the horizontal tail ($b/b_H \geqslant 1.5$). The basic approach is as follows (see Sketch (a)):

1. Determine the downwash in the plane of symmetry at the height of the vortex cores and at the longitudinal station of the quarter-chord point of the horizontal-tail mean aerodynamic chord.

2. Correct this value for the horizontal-tail height above or below the trailing vortices.

3. Evaluate the effect of horizontal-tail span by relating the average downwash at the tail to the downwash determined in the second step.

The downwash gradient $\frac{\partial \epsilon}{\partial \alpha}$ at the trailing edge of a wing is unity. The value at a distance infinitely far downstream is given by (Reference 6) as

$$\left(\frac{\partial \epsilon}{\partial \alpha}\right)_{\infty} = \frac{2\ (57.3)}{\pi A}\ C_{L_\alpha} \qquad 4.4.1\text{-a}$$

If these two values are known, the downwash gradient for any intermediate longitudinal position can be found by means of lifting-line theory.

For straight wings that have tip stall or thin swept wings that shed the leading-edge vortices inboard of the wing tips, the effective wing aspect ratio is considerably less than the geometric aspect ratio. An effective aspect ratio based on induced-drag considerations has been determined for these wings.

The maximum downwash at the plane of symmetry occurs at the intersection of the plane of symmetry with the plane containing the tip vortices. The ratio of the downwash at the plane of symmetry at a height a above or below this intersection to the downwash at the height of the vortex cores $\frac{\epsilon}{\epsilon_v}$ is given by

$$\frac{\epsilon}{\epsilon_v} = \frac{1}{1 + \left(\frac{2a}{b_v}\right)^2} \qquad 4.4.1\text{-b}$$

where b_v is the span of the wing-tip vortices at the quarter-chord point of the horizontal-tail MAC, and a is the height determined by means of Equation 4.4.1-c or 4.4.1-d (see Sketch (a)).

Because of the spanwise variation of downwash, the effective downwash acting on a horizontal tail is different from that at the plane of symmetry. A correction for tail-span effect is presented from Reference 1; it is based on the assumption that the vortices are essentially rolled up at the longitudinal tail station. This is a valid assumption except for cases where the core of the vortex approaches the surface of the tail. It should be noted that the vortex rolls up in a shorter distance as the angle of attack is increased. This is fortunate, because downwash effects become increasingly important at the higher angles of attack.

The subsonic downwash is obtained from the procedure outlined in the following steps:

Step 1. The effective wing aspect ratio A_{eff} and the effective wing span b_{eff} are obtained from Figure 4.4.1-66 as a function of the wing angle-of-attack parameter $\frac{\alpha - \alpha_0}{\alpha_{C_{L_{max}}} - \alpha_0}$. α is the selected wing angle of attack and α_0 and $\alpha_{C_{L_{max}}}$ may be estimated from Sections 4.1.3.1 and 4.1.3.4, respectively.

Step 2. The downwash gradient $\left(\frac{\partial \epsilon}{\partial \alpha}\right)_v$ in the plane of symmetry at the height of the vortex core is obtained for any longitudinal station, e.g., the quarter-chord point of the MAC of the horizontal tail, from Figure 4.4.1-67. This figure is entered with $2\frac{\ell_2}{b}$ and A_{eff}, where ℓ_2 is the distance measured parallel to the wing root chord, between the aft end of the wing root chord and the quarter-chord point of the MAC of the horizontal tail (see Sketch (a)).

Step 3. Determine the vertical position of the vortex core (see Sketch (a)). This depends upon the type of wing flow separation as determined from Figure 4.4.1-68a.

For trailing-edge separation

$$a = h_H - \ell_{eff}\left(\alpha - \frac{0.41\,C_L}{\pi\,A_{eff}}\right) - \frac{b_{eff}}{2}\tan\,\Gamma \qquad 4.4.1\text{-c}$$

For leading-edge separation

$$a = h_H - (\ell_2 + \ell_3)\left(\alpha - \frac{0.41\,C_L}{\pi\,A_{eff}}\right) - \frac{b_{eff}}{2}\tan\,\Gamma \qquad 4.4.1\text{-d}$$

where

C_L is the wing-alone lift coefficient obtained from test data or estimated by using the straight-tapered-wing method of Paragraph A of Section 4.1.3.3.

a is the distance from the quarter-chord point of the MAC of the horizontal tail to the plane of the tip vortex cores, positive for the horizontal tail MAC above the plane of the tip vortex cores.

h_H is the height of the horizontal-tail MAC quarter-chord point above or below the plane of the wing root chord, measured in the plane of symmetry and normal to the extended wing root chord, positive for the horizontal tail MAC above the plane of the wing root chord.

ℓ_{eff} is the distance measured parallel to the wing root chord, between the effective wing-tip quarter-chord point and the horizontal-tail MAC quarter-chord point.

ℓ_3 is the distance measured parallel to the plane of symmetry, between the forward end of the wing MAC and the aft end of the wing root chord, and ℓ_2 is defined in Step 2. In both Equations 4.4.1-c and 4.4.1-d, α is in radians, and the values of ℓ_{eff}, ℓ_2, and ℓ_3 are positive.

Step 4. Determine the span of the vortices at the longitudinal location of the quarter-chord point of the horizontal-tail MAC by

$$b_v = b_{eff} - \left(b_{eff} - b_{v_{ru}}\right)\left(\frac{2\ell_{eff}}{b\xi_{ru}}\right)^{1/2} \qquad 4.4.1\text{-e}$$

where

$$b_{v_{ru}} = [0.78 + 0.10\,(\lambda - 0.4) + 0.003\,\Lambda_{c/4}]\,b_{eff} \quad (\Lambda_{c/4} \text{ in degrees}) \qquad 4.4.1\text{-f}$$

$$\xi_{ru} = \frac{0.56\,A}{C_L}$$

Step 5. By using the parameters calculated in the above steps, obtain the average downwash gradient acting on the tail $\left(\frac{\partial \bar{\epsilon}}{\partial \alpha}\right)$ from Figure 4.4.1-68b.

Step 6. The procedures of Steps 1 through 5 are for low speeds. For higher subsonic Mach numbers the downwash gradient is given by

$$\left(\frac{\partial \bar{\epsilon}}{\partial \alpha}\right)_M = \left(\frac{\partial \bar{\epsilon}}{\partial \alpha}\right)_{\substack{\text{low} \\ \text{speed}}} \frac{\left(\frac{dC_L}{d\alpha}\right)_M}{\left(\frac{dC_L}{d\alpha}\right)_{\substack{\text{low} \\ \text{speed}}}} \qquad 4.4.1\text{-g}$$

where

$\left(\frac{\partial \bar{\epsilon}}{\partial \alpha}\right)_{\substack{\text{low} \\ \text{speed}}}$ is obtained by using Steps 1 through 5.

$\left(\frac{dC_L}{d\alpha}\right)_M$ and $\left(\frac{dC_L}{d\alpha}\right)_{\substack{\text{low} \\ \text{speed}}}$ are given by the straight-tapered wing methods of Paragraph A of Sections 4.1.3.2 or 4.1.3.3, depending upon the Mach number and angle of attack.

Step 7. Determine the average downwash acting on the horizontal tail by integrating the average downwash gradient from Step 5 or 6, i.e.,

$$\bar{\epsilon} = \int_{\alpha_0}^{\alpha} \frac{\partial \bar{\epsilon}}{\partial \alpha}\, d\alpha$$

A sample problem illustrating the use of this method is presented on Pages 4.4.1-12 through 4.4.1-16. The method will predict the downwash angles at the horizontal tail with accuracy acceptable for preliminary-design purposes for most configurations. However, since the effect of tail span has been determined under the assumption that the vortices are essentially rolled up at the tail location, caution should be used in applying the method if the tail length is short and the tail plane is near the location of the vortex core height.

Not enough test data are available to substantiate the validity of the compressibility correction given by Equation 4.4.1-g.

Method 2

An empirical method for estimating the downwash gradient behind straight-tapered wings at subsonic speeds is taken from Reference 7. The method is restricted to the angle-of-attack range over which the variation of downwash angle is a linear function of angle of attack.

The average low-speed downwash gradient at the horizontal tail is given by

$$\frac{\partial \bar{\epsilon}}{\partial \alpha} = 4.44 \left[K_A K_\lambda K_H (\cos \Lambda_{c/4})^{1/2} \right]^{1.19} \qquad 4.4.1\text{-h}$$

where K_A, K_λ, and K_H are wing-aspect-ratio, wing-taper-ratio, and horizontal-tail-location factors obtained from Figures 4.4.1-69a, 4.4.1-69b, and 4.4.1-70, respectively. In Figure 4.4.1-70, ℓ_H is the distance measured parallel to the wing root chord, between the wing MAC quarter-chord point and the quarter-chord point of the MAC of the horizontal tail, and h_H is the position of the quarter-chord point of the horizontal tail MAC relative to the plane of the wing root chord as defined in Method 1.

At higher subsonic speeds the effect of compressibility is approximated by

$$\left(\frac{\partial \bar{\epsilon}}{\partial \alpha}\right)_M = \left(\frac{\partial \bar{\epsilon}}{\partial \alpha}\right)_{\substack{\text{low} \\ \text{speed}}} \frac{\left(C_{L_\alpha}\right)_M}{\left(C_{L_\alpha}\right)_{\substack{\text{low} \\ \text{speed}}}} \qquad 4.4.1\text{-i}$$

where

$\left(\frac{\partial \bar{\epsilon}}{\partial \alpha}\right)_{\substack{\text{low} \\ \text{speed}}}$ is obtained using Equation 4.4.1-h.

$\left(C_{L_\alpha}\right)_{\substack{\text{low} \\ \text{speed}}}$ and $\left(C_{L_\alpha}\right)_M$ are the wing lift-curve slopes at the appropriate Mach numbers, obtained by using the straight-tapered-wing method of Paragraph A of Section 4.1.3.2.

A comparison of low-speed test data with $\partial\epsilon/\partial\alpha$ calculated by this method is presented as Table 4.4.1-B. The ranges of geometric parameters of the test data are:

$$2.00 \leqslant A \leqslant 8.00$$

$$0 \leqslant \lambda \leqslant 1.625$$

$$3.4 \leqslant \Lambda_{c/4} \leqslant 56.5$$

$$-0.177 \leqslant \frac{2\,h_H}{b} \leqslant 0.537$$

$$0.78 \leqslant \frac{2\,\ell_H}{b} \leqslant 2.44$$

$$0.280 \leqslant \frac{b_H}{b} \leqslant 0.800$$

Since the tail-span effect has not been explicitly included in this method, the authority of the method outside the limits $0.280 \leqslant \frac{b_H}{b} \leqslant 0.800$ is unknown.

Not enough test data are available to substantiate the validity of the compressibility correction given by Equation 4.4.1-i.

Method 3

For configurations in which the span of the forward surface is approximately equal to or less than that of the aft surface, the following method, taken from Reference 3, is recommended.

Step 1. The spatial position of the trailing vortices is first determined relative to the aft surface. The lateral spacing is determined from Figure 4.4.1-71 as a function of the exposed forward-surface planform geometry. This spacing is invariant with longitudinal distance and angle of attack. The vertical position is determined by assuming that the vortex springs from the trailing edge at the previously determined lateral position and trails in the free-stream direction. The pertinent vertical dimension is the distance between the quarter-chord point of the MAC of the aft surface and the vortex as determined above.

Step 2. The vortex interference factor $I_{v_{W'(W'')}}$ is obtained from Figures 4.3.1.3-7a through 4.3.1.3-7ℓ as a function of the lateral and vertical vortex positions, determined in Step 1 above, and the geometry of the aft panel. (The primed notation refers to the forward panel and the double-primed notation refers to the aft panel.)

Step 3. The vortex interference factor so determined is used in Sections 4.5.1.1 and 4.5.1.2 to obtain the lift generated on the aft surface for complete wing-body-tail combinations.

The use of the sample problem on Page 4.4.1-16 as a guide is essential in applying this method.

Subsonic Downwash Due to Flap Deflection

The method for estimating the change in downwash due to deflection of plain or slotted flaps is based on the empirical curves presented in Figure 4.4.1-72. Tables 4.4.1-C and -D present a data summary and substantiation of the test data used to generate these empirical curves. The user is advised to exercise caution when evaluating a configuration with different geometric parameters from those appearing in Table 4.4.1-C.

To utilize Figure 4.4.1-72, the user obtains a value for $\frac{\Delta\epsilon\ A[b_f/(b/2)]}{\Delta C_L}$ based on the flap type and the ratio of tail height above the wing-chord plane to wing semispan $\frac{h_H}{b/2}$. The change in downwash angle $\Delta\epsilon$ is then

obtained by

$$\Delta\epsilon = \left\{\frac{\Delta\epsilon\ A[b_f/(b/2)]}{\Delta C_L}\right\} \frac{\Delta C_L}{A[b_f/(b/2)]}$$

where

A is the wing aspect ratio.

$\frac{b_f}{b/2}$ is the ratio of flap span of one wing to wing semispan.

ΔC_L is the lift increment due to flap deflection obtained from test data or Section 6.1.4.1.

$b/2$ is the wing semispan.

h_H is the tail height above the wing-chord plane, positive up.

Subsonic Upwash

The upwash gradient $\frac{\partial \epsilon_u}{\partial \alpha}$ in the plane of symmetry of an unswept wing is presented as a function of the wing aspect ratio in Figure 4.4.1-73. This chart is from Reference 5.

In Reference 3, the flow characteristics beneath a wing are calculated by assuming the wing to be represented by a multiple arrangement (both chordwise and spanwise) of horseshoe vortices and accounting for the effects of wing thickness distribution by using the appropriate singularity distribution in conjunction with simple sweep theory. The calculative procedures, together with the required design charts, are presented in Reference 3. Also presented are comparisons between detailed experimental flow fields around swept and unswept wing-fuselage combinations and wing-alone flow fields calculated by this method. The calculated results are qualitatively correct in all cases investigated.

Subsonic Dynamic-Pressure Ratio

This method for estimating the dynamic-pressure q/q_∞ at subsonic speeds and in the linear angle-of-attack range is based on the method presented in Reference 8, which relates the dynamic-pressure ratio to the drag coefficient of the wing. The method gives values of q/q_∞ at the plane of symmetry only. Actually, considerable variations in q/q_∞ can occur in both the spanwise and longitudinal directions. Sketches (b) and (c) show typical spanwise and longitudinal variations, respectively, of dynamic-pressure ratio for a straight wing and a 60° sweptback wing (from Reference 9). In general these data indicate that stronger spanwise deviations result when the wing is swept back, and stronger longitudinal deviations result when the wing is unswept.

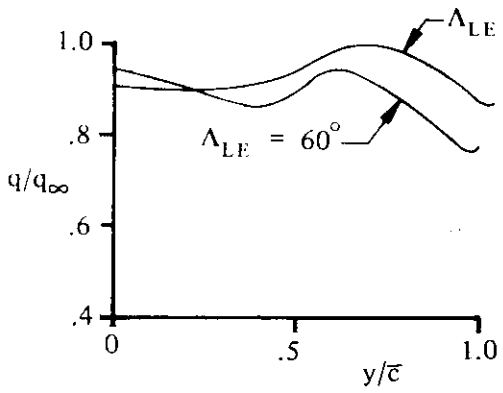

SKETCH (b)

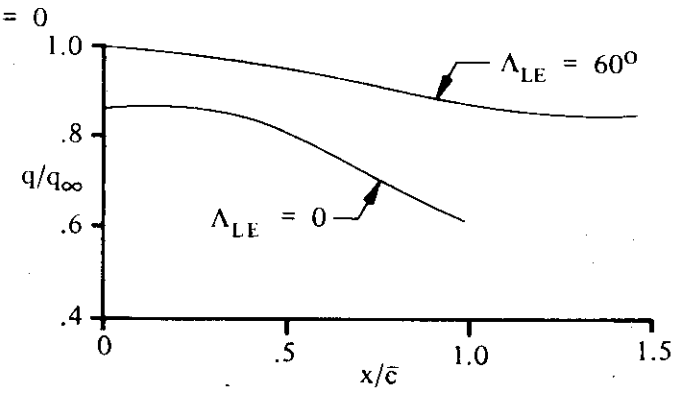

SKETCH (c)

In the linear angle-of-attack range, the ratio of the dynamic pressure in the plane of symmetry at some distance x aft of the wing-root-chord trailing edge to the free-stream dynamic pressure q/q_∞ is obtained from the procedure outlined in the following steps:

Step 1. Calculate the half-width of the wing wake by

$$\frac{z_w}{\bar{c}} = 0.68 \sqrt{C_{D_0}\left(\frac{x}{\bar{c}} + 0.15\right)} \qquad 4.4.1\text{-j}$$

where

x is the longitudinal distance measured along the wake center line from the wing-root-chord trailing edge, positive aft.

z_w is the half-width of the wake at any position x.

C_{D_0} is the wing zero-lift drag coefficient obtained from Paragraph A of Section 4.1.5.1.

Step 2. Calculate the downwash in the plane of symmetry at the vortex sheet (assumed to be the same location as the wake center line) by

$$\epsilon = \frac{1.62\, C_L}{\pi A} \text{ (radians)} \qquad 4.4.1\text{-k}$$

Step 3. Determine the vertical distance z from the vortex sheet to the point of interest (usually the quarter-chord point of the MAC of the horizontal tail) by

$$z = x \tan(\gamma + \epsilon - \alpha) \qquad 4.4.1\text{-}\ell$$

where γ is defined in Sketch (d).

Step 4. Determine the dynamic-pressure-loss ratio at the wake center $\left(\frac{\Delta q}{q}\right)_o$ by the empirical relation

$$\left(\frac{\Delta q}{q}\right)_o = \frac{2.42\,(C_{D_0})^{1/2}}{\frac{x}{\bar{c}} + 0.30} \qquad 4.4.1\text{-m}$$

Step 5. Determine the dynamic-pressure-loss ratio for points not on the wake center line by

$$\frac{\Delta q}{q} = \left(\frac{\Delta q}{q}\right)_o \cos^2\left(\frac{\pi}{2}\,\frac{z}{z_w}\right) \qquad 4.4.1\text{-n}$$

where $\left(\frac{\pi}{2}\,\frac{z}{z_w}\right)$ is expressed in radians.

Step 6. Determine the dynamic-pressure ratio in the plane of symmetry at an arbitrary distance x aft of the wing-root-chord trailing edge by

$$\frac{q}{q_\infty} = 1 - \frac{\Delta q}{q} \qquad 4.4.1\text{-o}$$

Note, that if the distance from the vortex sheet to the point of interest is equal to or greater than the wing wake half-width, the dynamic-pressure ratio at the point of interest is unity, i.e., $q/q_\infty = 1.0$ for $z/z_w \geqslant 1.0$.

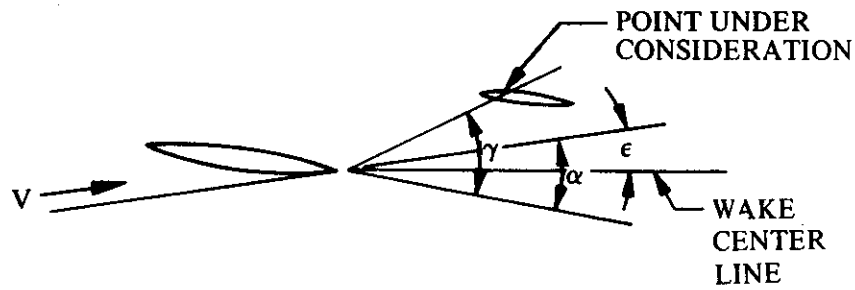

SKETCH (d)

A comparison of test data with dynamic-pressure ratios calculated by this method is given in Table 4.4.1-E.

Sample Problems

1. Subsonic Downwash (Method 1)

Given: The wing-body-tail configuration of Reference 20.

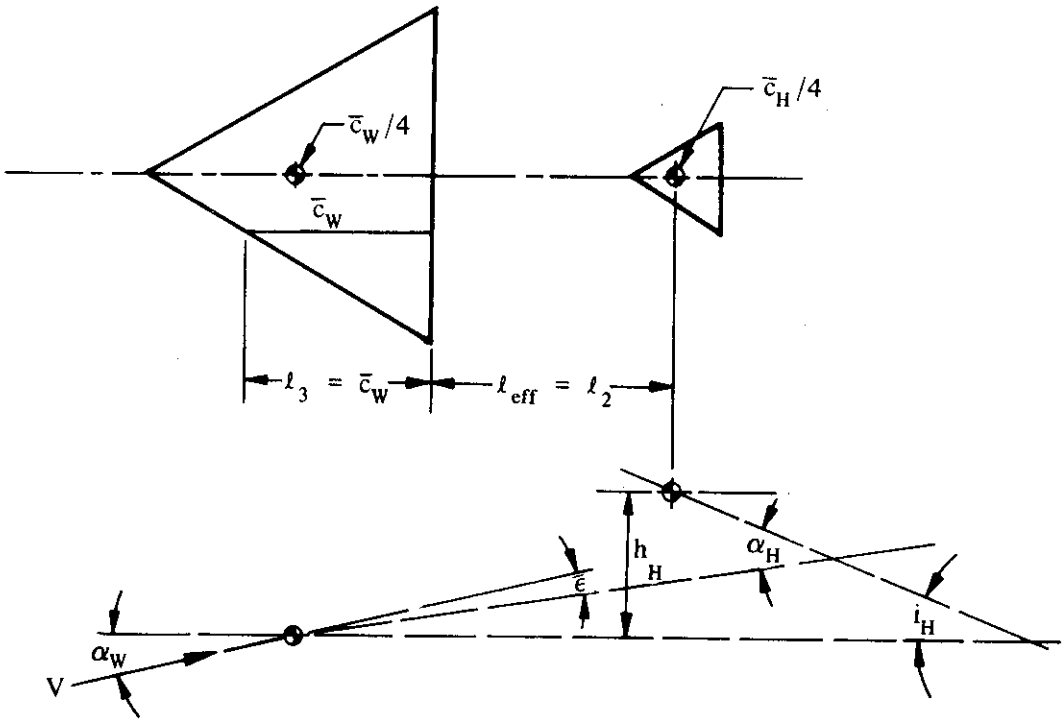

Wing Characteristics:

$A = 2.31 \quad \lambda = 0$

$\Lambda_{c/4} = 52.4^o \quad i_W = 0$

$\Gamma = 0 \quad b = 36.5$ in.

$\bar{c} = 21.1$ in.

NACA $65_{(06)}$–006.5 (free-stream direction)

Horizontal-Tail Characteristics:

$b_H = 11.53$ in. $\qquad h_H = 15.88$ in.

Additional Characteristics:

$\ell_3 = \bar{c}_W$ (delta wing) $\quad \ell_2 = 26.28$ in. $\quad \ell_{eff} = \ell_2$ (delta wing)

Low speed (M = 0.17)

$(\alpha_0)_W = 0 \qquad \left(\alpha_{C_{L_{max}}}\right)_W = 33^o$

α	4^o	8^o	12^o	16^o	20^o	24^o	28^o
C_L	0.15	0.315	0.48	0.655	0.825	0.975	1.115

} (wing-alone test data from Reference 20)

Compute:

The final calculations are presented in table form on Page 4.4.1-15. Many of the quantities listed below appear as columns in the table.

Determine the effective wing aspect ratio and the effective wing span.

$$\frac{\alpha - \alpha_0}{\alpha_{C_{L_{max}}} - \alpha_0} = \frac{\alpha - 0}{33.0 - 0} = \frac{\alpha}{33.0}$$

$\frac{A_{eff}}{A}$

$\frac{b_{eff}}{b}$

} (Figure 4.4.1-66)

Determine the downwash gradient in the plane of symmetry at the height of the vortex core.

$$\frac{2\ell_2}{b} = \frac{2(26.28)}{36.5} = 1.44$$

$\left(\frac{\partial \epsilon}{\partial \alpha}\right)_v$ (Figure 4.4.1-67)

Determine the vertical position of the vortex core.

$\Delta y = 1.28\%\, c$ (Figure 2.2.1-8)

Leading-edge separation is predominant (Figure 4.4.1-68a); therefore

$$a = h_H - (\ell_2 + \ell_3)\left(\alpha - \frac{0.41\ C_L}{\pi\ A_{eff}}\right) - \frac{b_{eff}}{2}\tan\Gamma \quad \text{(Equation 4.4.1-d)}$$

$$= 15.88 - (26.28 + 21.10)\left(\alpha - \frac{0.41\ C_L}{\pi\ A_{eff}}\right) - 0$$

$$= 15.88 - 47.38\left(\alpha - \frac{0.41\ C_L}{\pi\ A_{eff}}\right)$$

Determine the span of the vortices at the longitudinal location of the quarter-chord point of the tail MAC.

$$b_{v_{ru}} = [0.78 + 0.10\ (\lambda - 0.4) + 0.003\ \Lambda_{c/4}]\ b_{eff} \quad \text{(Equation 4.4.1-f)}$$

$$= [0.78 + 0.10\ (0 - 0.4) + 0.003\ (52.4)]\ b_{eff}$$

$$= 0.897\ b_{eff}$$

$$\xi_{ru} = \frac{0.56\ A}{C_L} = \frac{(0.56)\ (2.31)}{C_L} = \frac{1.294}{C_L}$$

$$b_v = b_{eff} - (b_{eff} - b_{v_{ru}})\left(\frac{2\ell_{eff}}{b\ \xi_{ru}}\right)^{1/2} \quad \text{(Equation 4.4.1-e)}$$

$$= b_{eff} - (b_{eff} - b_{v_{ru}})\left(\frac{1.44}{\xi_{ru}}\right)^{1/2}$$

Determine the average downwash gradient acting on the tail.

$$\left(\frac{\partial\bar{\epsilon}}{\partial\alpha}\right) \Big/ \left(\frac{\partial\epsilon}{\partial\alpha}\right)_v = f\left(\frac{2a}{b_v}, \frac{b_H}{b_v}\right) \quad \text{(Figure 4.4.1-68b)}$$

Solution:

① α (deg)	② $\frac{\alpha-\alpha_0}{\alpha_{C_{L_{max}}}-\alpha_0}$ ①/33.0	③ $\frac{A_{eff}}{A}$ (Fig. 4.4.1-66)	④ $\frac{b_{eff}}{b}$ (Fig. 4.4.1-66)	⑤ A_{eff} 2.31③	⑥ b_{eff} (in.) 36.5④	⑦ $(\partial\epsilon/\partial\alpha)_v$ (Fig. 4.4.1-67)	⑧ C_L Test Values
4	0.121	1.00	1.00	2.31	36.5	0.590	0.150
8	0.242	↓	↓	↓	↓	↓	0.315
12	0.364	↓	↓	↓	↓	↓	0.480
16	0.485	0.975	0.988	2.25	36.1	0.600	0.655
20	0.606	0.875	0.933	2.02	34.1	0.640	0.825
24	0.727	0.780	0.877	1.80	32.0	0.670	0.975
28	0.848	0.680	0.809	1.57	29.5	0.730	1.115

⑨ α (deg)	$\frac{0.41\,C_L}{\pi A_{eff}}$ $\frac{0.41\,⑧}{\pi\,⑤}$	⑩ a (Eq. 4.4.1-d) $15.88-47.38\left(\frac{①}{57.3}-⑨\right)$	⑪ ξ_{ru} $\frac{1.294}{⑧}$	⑫ $b_{v_{ru}}$ (Eq. 4.4.1-f) 0.897⑥	⑬ b_v (Eq. 4.4.1-e) $⑥-\lvert⑥-⑫\rvert\left(\frac{1.44}{⑪}\right)^{1/2}$
4	0.0085	12.97	8.627	32.7	34.9
8	0.0178	10.11	4.108	↓	34.3
12	0.0271	7.24	2.696	↓	33.7
16	0.0380	4.45	1.976	32.4	32.9
20	0.0533	1.87	1.568	30.6	30.7
24	0.0707	− 0.61	1.327	28.7	28.6
28	0.0927	− 2.88	1.161	26.5	26.2

α (deg)	⑭ $\frac{2a}{b_v}$ 2⑩/⑬	⑮ $\frac{b_H}{b_v}$ 11.53/⑬	⑯ $\left(\frac{\partial\bar{\epsilon}}{\partial\alpha}\right)\Big/\left(\frac{\partial\epsilon}{\partial\alpha}\right)_v$ (Fig. 4.4.1-68b)	⑰ $\frac{\partial\bar{\epsilon}}{\partial\alpha}$ ⑦⑯	⑱ $\int_0^{\alpha}{}^{\bar{\epsilon}}$ ⑰ $d\alpha$
4	0.743	0.330	0.65	0.3835	1.44
8	0.590	0.336	0.73	0.4307	3.06
12	0.430	0.342	0.82	0.4838	4.88
16	0.271	0.350	0.92	0.552	6.92
20	0.122	0.376	0.99	0.6336	9.28
24	−0.043	0.403	1.04	0.6935	11.96
28	−0.220	0.440	0.95	0.6968	14.76

The calculated results are compared with test values from Reference 20 in Sketch (e).

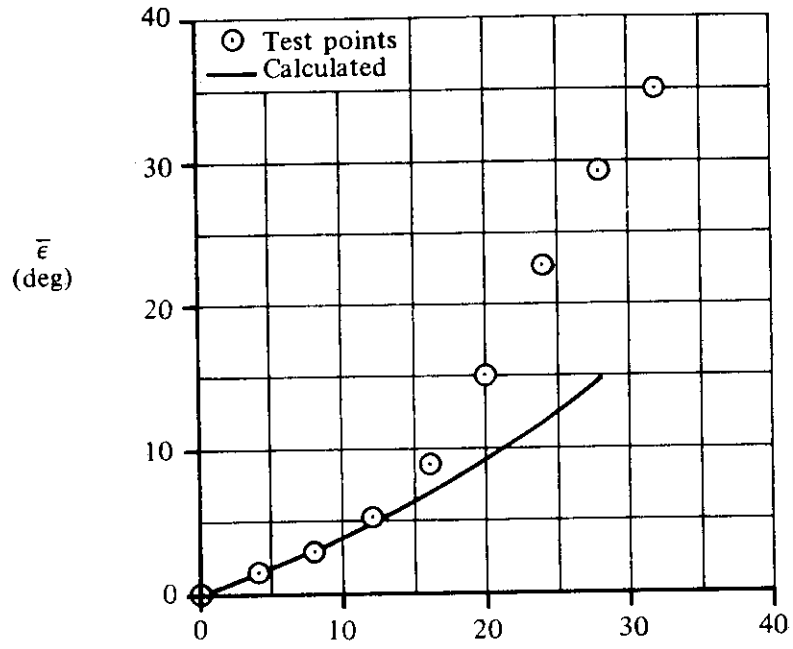

SKETCH (e)

2. Subsonic Downwash (Method 2)

Given: The wing-body-tail configuration of Reference 20. This is the same configuration as Sample Problem 1 above.

Wing Characteristics:

$A = 2.31$ $\lambda = 0$ $\Lambda_{c/4} = 52.4^{o}$ $i_W = 0$ $\Gamma = 0$

$b = 36.5$ in. NACA $65_{(06)}$–006.5 (free-stream direction)

Horizontal-Tail Characteristics:

$h_H = 15.88$ in.

Additional Characteristics:

$\ell_H = 31.57$ in. Low speed ($M = 0.17$)

Compute:

$$\frac{2h_H}{b} = \frac{2(15.88)}{36.5} = 0.870$$

$$\frac{2\ell_H}{b} = \frac{2(31.57)}{36.5} = 1.73$$

$K_A = 0.240$ (Figure 4.4.1-69a)

$K_\lambda = 1.43$ (Figure 4.4.1-69b)

$K_H = 0.470$ (Figure 4.4.1-70)

Solution:

$$\frac{\partial \bar{\epsilon}}{\partial \alpha} = 4.44 \left[K_A \, K_\lambda \, K_H \, (\cos \Lambda_{c/4})^{1/2} \right]^{1.19} \quad \text{(Equation 4.4.1-h)}$$

$$= 4.44 \left[(0.240)\,(1.43)\,(0.470)\,(\cos 52.4^o)^{1/2} \right]^{1.19}$$

$$= 4.44\,(0.126)^{1.19}$$

$$= 0.377$$

The calculated value compares with a test value of 0.330 from Reference 20.

3. Subsonic Downwash (Method 3)

Given: The same configuration as that of Sample Problem 2 of Paragraph A of Section 4.5.1.1.

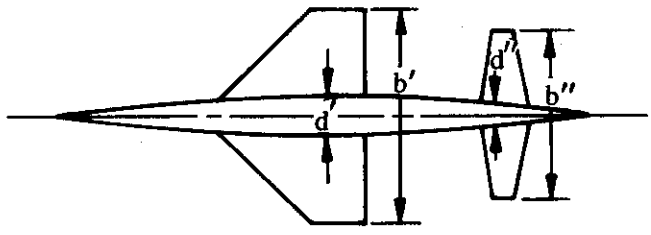

Wing Characteristics:

$A_e' = 1.80$ $\lambda_e' = 0.378$ $b'/2 = 141.42$ in. $d'/2 = 26.94$ in.

$\Lambda_{TE} = 0$

Horizontal-Tail Characteristics:

$\lambda_e'' = 0.515$ $\quad b''/2 = 110.64$ in. $\quad d''/2 = 22.08$ in.

Additional Characteristics:

Low speed (M = 0.13); $\beta = 0.9915$

x = 165.6 in. (distance from the wing trailing edge to the quarter-chord point of the horizontal-tail MAC)

Compute:

Determine the lateral spacing of the trailing vortices at station x.

$\beta A_e' = (0.9915)(1.80) = 1.785$

$\dfrac{b_v'/2 - d'/2}{b'/2 - d'/2} = 0.785$ (Figure 4.4.1-71c)

$b'/2 - d'/2 = 141.42 - 26.94 = 114.48$ in.

$b_v'/2 - d'/2 = (0.785)(114.48) = 89.87$ in.

$b_v'/2 = 89.87$ in. $+ d'/2 = 116.81$ in.

$b_v''/2 = b_v'/2 = 116.81$ in. (The method assumes that the lateral spacing of trailing vortices is invariant with longitudinal distance and angle of attack.)

$\dfrac{b_v''/2}{b''/2} = \dfrac{116.81}{110.64} = 1.056$ (This value is used in place of $\dfrac{y_o}{b_w/2}$ in Figure 4.3.1.3-7.)

Determine the vertical position of the trailing vortices.

$h_v = x \tan\alpha = 165.6 \tan\alpha$ (see table below) (The method assumes the vortex springs from the wing trailing edge and trails in the free-stream direction.)

The ratio $\dfrac{h_v}{b''/2}$ is used in place of $\dfrac{z_o}{b_w/2}$ in Figure 4.3.1.3-7.

$\dfrac{d''/2}{b''/2} = \dfrac{22.08}{110.64} = 0.200$ (This value is used in place of $\dfrac{r}{b_w/2}$ in Figure 4.3.1.3-7.)

Solution:

α (deg)	h_v $165.6 \tan\alpha$ (in.)	$\frac{h_v}{b''/2}$	$I_{v_{W'(W'')}}$ Fig. 4.3.1.3-7 @ λ_e'', $\frac{b_v''/2}{b''/2}$ and $\frac{h_v}{b''/2}$
0	0	0	−3.0
5	14.49	0.131	−2.5
10	29.20	0.264	−2.0
15	44.37	0.401	−1.68
20	60.27	0.545	−1.40
23	70.29	0.635	−1.27
26	80.77	0.730	−1.15

The interference factor $I_{v_{W'(W'')}}$ at $\alpha =$ 0 is used in Sample Problem 2 of Paragraph A of Section 4.5.1.1 to obtain the effect on total airplane lift, of the wing trailing vortices on the horizontal tail.

4. Subsonic Downwash Due to Flap Deflection

Given: The wing-body-tail configuration of Reference 31

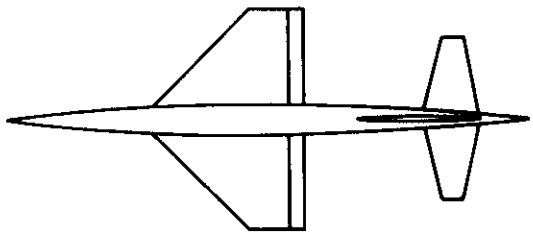

Wing Characteristics:

A = 2.0 b = 23.56 ft ΔC_L = 0.57 (test data)

Inboard flap station η_i = 0.191 Outboard flap station η_o = 1.00

Slotted trailing-edge flaps $\delta_f = 40^o$

Tail Characteristic:

$h_H = 0$

Compute:

$$\frac{h_H}{b/2} = \frac{0}{(23.56/2)} = 0$$

$$\frac{b_f}{b/2} = \eta_o \quad \eta_i$$

$$= 1.00 \quad 0.191 = 0.809$$

$$\left\{\frac{\Delta\epsilon\, A[b_f/(b/2)]}{\Delta C_L}\right\} = 28.5 \quad \text{(Figure 4.4.1-72)}$$

Solution:

$$\Delta\epsilon = \left\{\frac{\Delta\epsilon\, A[b_f/(b/2)]}{\Delta C_L}\right\} \frac{\Delta C_L}{A[b_f/(b/2)]}$$

$$= (28.5)\ \frac{0.57}{(2.0)\,(0.809)}$$

$$= 10.04^\circ$$

This compares with a test value of 8.8° from Reference 31.

5. Subsonic Dynamic-Pressure Ratio

Given: A wing-tail configuration of Reference 9

Wing Characteristics:

$A = 6.0 \quad \lambda = 1.0 \quad \bar{c} = 10.0$ in. $\quad S_W = 600$ sq in. $\quad S_{wet} = 1200$ sq in.

NACA 0015 airfoil (x_t @ 0.30c)

Additional Characteristics:

x = 20.0 in. (survey station location, aft of wing trailing edge)

Low speed $\quad R_\ell = 0.62 \times 10^6$ (based on $\bar{c}$) $\quad \gamma = 0$

Smooth surface (assume k = 0) $\quad S_{ref} = S_W = 600$ sq in.

α	0	1°	2°	3°	4°	6°	8°
C_L	−.01	.055	.115	.175	.240	.360	.485

(test data from Reference 9)

Compute:

Determine the half-width of the wake.

$\ell/k = \infty$; read C_f at given R_ℓ

$C_f = 0.00487$ (Figure 4.1.5.1-26)

$\left[1 + L\left(\frac{t}{c}\right) + 100\left(\frac{t}{c}\right)^4\right] = 1.225$ (figure 4.1.5.1-28a, for L = 1.2)

$\cos \Lambda_{(t/c)_{max}} = \cos 0 = 1.0$

$R_{L.S.} = 1.07$ (Figure 4.1.5.1-28b)

$\frac{S_{wet}}{S_{ref}} = \frac{1200}{600} = 2.0$

$C_{D_0} = C_f \left[1 + L\left(\frac{t}{c}\right) + 100\left(\frac{t}{c}\right)^4\right] R_{L.S.} \frac{S_{wet}}{S_{ref}}$ (Equation 4.1.5.1-a)

$= (0.00487)(1.225)(1.07)(2.0)$

$= 0.0128$

$x/\bar{c} = 20.0/10.0 = 2.0$

$\frac{z_w}{\bar{c}} = 0.68 \sqrt{C_{D_0}\left(\frac{x}{\bar{c}} + 0.15\right)}$ (Equation 4.4.1-j)

$= 0.68 \sqrt{(0.0128)(2.15)}$

$= 0.113$

Determine the downwash in the plane of symmetry at the vortex sheet.

$\epsilon = \frac{1.62\, C_L}{\pi A}$ (Equation 4.4.1-k)

$= \frac{1.62\, C_L}{\pi 6.0} = 0.0859\, C_L$ (radians)

$= 4.92\, C_L$ (degrees) (see calculation table below)

Determine the vertical distance z from the vortex sheet to the point of interest.

$z = x \tan(\gamma + \epsilon - \alpha)$ (Equation 4.4.1-ℓ)

$= 20.0 \tan(0 + \epsilon - \alpha) = 20.0 \tan(\epsilon - \alpha)$ (see calculation table below)

Determine the dynamic-pressure-loss ratio at the wake center.

$$\left(\frac{\Delta q}{q}\right)_o = \frac{2.42\left(C_{D_0}\right)^{1/2}}{\frac{x}{\bar{c}} + 0.30} \qquad \text{(Equation 4.4.1-m)}$$

$$= \frac{2.42(0.0128)^{1/2}}{2.0 + 0.30} = 0.119$$

Determine the dynamic-pressure-loss ratio for points not on the wake center line.

$$\frac{\Delta q}{q} = \left(\frac{\Delta q}{q}\right)_o \cos^2\left(\frac{\pi}{2}\,\frac{z}{z_w}\right) \qquad \text{(Equation 4.4.1-n)}$$

$$= 0.119\ \cos^2\left(\frac{\pi}{2}\,\frac{z}{1.13}\,\frac{57.3}{1}\right)$$

$$= 0.119\ \cos^2\ (79.65\ z) \qquad \text{(see calculation table below)}$$

Solution:

The dynamic-pressure ratio in the plane of symmetry at a distance x = 20.0 in. aft of the wing-root-chord trailing edge is

$$\frac{q}{q_\infty} = 1 - \frac{\Delta q}{q} \qquad \text{(Equation 4.4.1-o)} \qquad \text{(see calculation table below)}$$

①	②	③	④	⑤	⑥	⑦
α (deg)	C_L test values	ϵ (deg) (Eq. 4.4.1-k) 4.92 ②	$\frac{z}{z_w}$ (Eq. 4.4.1-l) 20 tan (③ − ①)	$\cos^2\left(\frac{\pi}{2}\frac{z}{z_w}\right)$ ($\cos^2$ (79.65 ④)	$\frac{\Delta q}{q}$ (Eq. 4.4.1-n) 0.119 ⑤	$\frac{q}{q_\infty}$ (Eq.4.4.1-o) 1 − ⑥
0	−0.01	−0.049	−0.0172	0.9994	0.119	0.881
1	0.055	0.271	−0.2544	0.8800	0.105	0.895
2	0.115	0.566	−0.5008	0.5887	0.0701	0.930
3	0.175	0.861	−0.7470	0.1576	0.0307	0.969
4	0.240	1.181	−0.9848	0.0402	0.0048	0.995
6	0.360	1.771	−1.4790	–	–	1.00*
8	0.485	2.386	−1.9660	–	–	1.00*

* $q/q_\infty = 1.0$ when $z/z_w \geq 1.0$.

The calculated results are compared with test values from Reference 9 in Table 4.4.1-E. (This is the second configuration given in Table 4.4.1-E.)

B. TRANSONIC

Downwash

In general, the downwash gradient is proportional to the lift-curve slope. The transonic lift-curve-slope characteristics are discussed in detail in Section 4.1.3.2. The following discussion summarizes these transonic characteristics.

For thin, low-aspect-ratio wings the downwash gradient varies smoothly with Mach number. The typical variation is similar to the lift-curve-slope variation for Type "B" wings shown on Page 4.1.3.2-13. For thick, high-aspect-ratio wings at low angles of attack the variation is like that of Type "A" wings (shown on the same page), but at high angles of attack the downwash-gradient variation of these wings is smooth.

The erratic behavior of the thicker wings at low angles of attack is frequently accentuated by shock-induced boundary-layer separation, which can cause significant changes in the span-load characteristics and hence in the downwash distribution behind a wing.

No design charts for the transonic range are presented, because so few flow surveys are available.

Dynamic-Pressure Ratio

No method has been suggested in the literature for estimating the dynamic-pressure ratio at transonic speeds. Furthermore, few data measuring this parameter are known to exist. The method suggested herein is therefore tentative.

DATCOM METHODS

Transonic Downwash

No accurate method is available for the prediction of transonic downwash characteristics. It is suggested that values be approximated by assuming that the downwash gradient is proportional to the lift-curve slope as given in Section 4.1.3.2 for low angles of attack and in Section 4.1.3.3 for high angles of attack.

Transonic Dynamic-Pressure Ratio

For estimating the transonic dynamic-pressure ratio, it is suggested that the method presented in Paragraph A above be applied, with the appropriate zero-lift drag values from Section 4.1.5.1 (excluding wave drag).

C. SUPERSONIC

Downwash

At supersonic speeds downwash is caused by two factors. First, the region behind the trailing-edge shock or expansion wave is distorted by the wing vortex system in a manner similar to that which occurs at subsonic speeds. Because of the variation in span load, a vortex sheet is shed that rolls up with increasing downstream distance from the surface. Tip vortices similar to their subsonic counterparts are also present. At the supersonic Mach numbers, however, the entire flow field is swept back and isolated regions of

influence may exist over certain portions of the wing surface and in the flow field behind it. For instance, regions not affected by the wing tip are generally present. For a rectangular wing such a region can be treated in a two-dimensional manner, i.e., no lateral variation of downwash exists.

Secondly, a change in flow direction occurs in the flow region between the leading- and trailing-edge shock or expansion waves. Since this region of the flow field does not "see" the wing vortex system, numerical values of downwash can be calculated by applying shock-expansion theory. In order to simplify the calculations, it is standard practice to perform the calculations with wing-root geometry and to assume two-dimensional flow. For cases in which the vehicle component (i.e., horizontal tail) immersed in the wing flow field has less span than the wing, this latter assumption is justified. For cases in which the aft component is large compared to the forward component (i.e., a wing following a canard surface), this assumption is not justified, because of the significant spanwise downwash variations associated with the wing tips. Behind the trailing-edge shock or expansion wave the downwash due to these compressibility effects is zero.

Dynamic-Pressure Ratio

Variations in the dynamic-pressure ratio exist throughout the field of influence of a wing in supersonic flight. A thin viscous wake exists behind the wing, with characteristics quite similar to its subsonic counterpart (see Paragraph A above). In addition, the nonviscous flow region behind the leading-edge shock or expansion wave also exhibits dynamic-pressure-ratio variations due to compressibility effects. The application of shock-expansion theory has been shown to yield a reasonable approximation for the dynamic-pressure ratio in the nonviscous portion of the flow field.

The existence of the trailing-edge shock wave on the upper surface can cause a significant boundary-layer-separation region under conditions of low Reynolds number and/or large angles of attack (see Sketch (f)). This region of separation creates a wide wake near the trailing edge that is not predicted by the method presented herein.

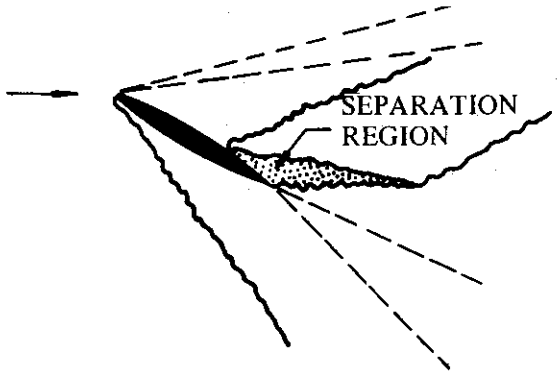

SKETCH (f)

Mach Number Effects

The local Mach number between the leading- and trailing-edge shock or expansion waves can vary significantly from the free-stream value. Expansion fields increase the Mach number, and compression fields decrease the Mach number. Vehicle components immersed in these flow fields exhibit different aerodynamic characteristics because of the varying Mach number. This is illustrated in Sketch (g) for a double wedge airfoil.

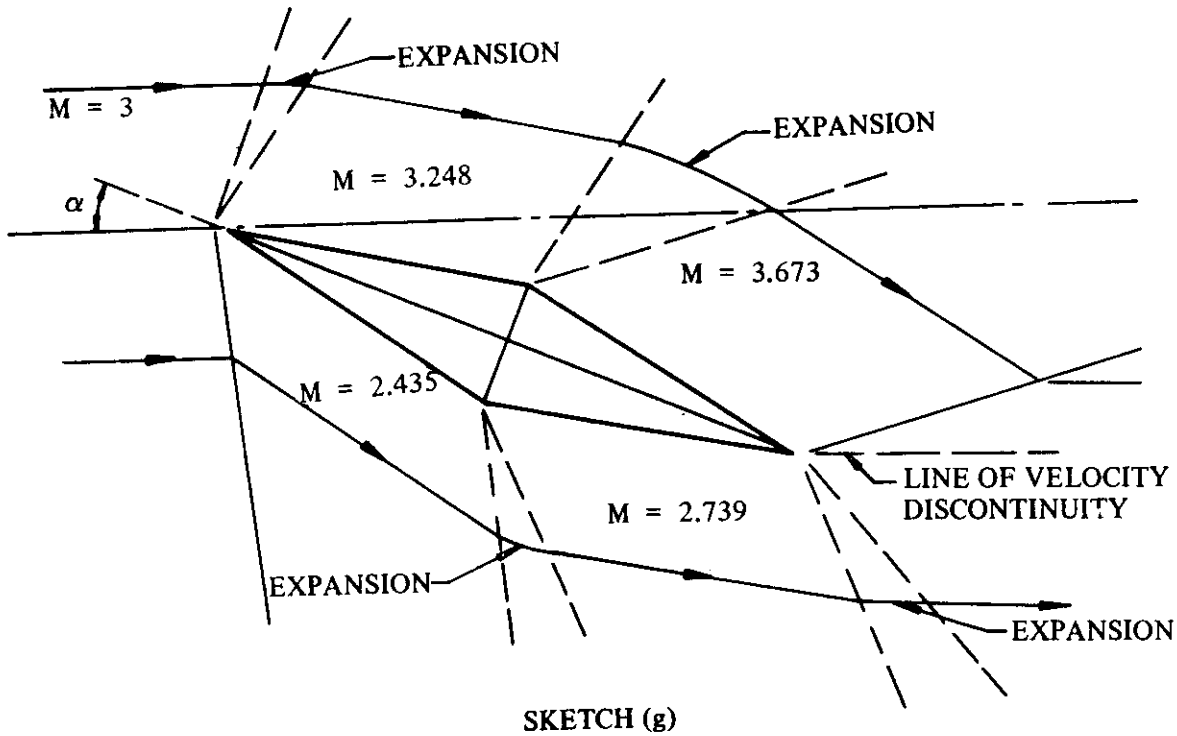

SKETCH (g)

Lumped Parameter

At least one author(Reference10) has treated the flow field at supersonic speeds by combining the effects of downwash, dynamic-pressure ratio, and Mach number into a single lumped parameter. This approach gives valid values for determining the effect of the wing shock-expansion field on stabilizer effectiveness but cannot give the isolated effects. In the Datcom, this analysis is presented in Section 4.5.1.2.

DATCOM METHODS

Supersonic Downwash

Method 1

The downwash behind a straight-tapered wing for either subsonic or supersonic leading and trailing edges can be approximated by the theoretical method presented in Reference 11. The basic theory uses a system of 20 swept unit horseshoe vortices placed along the load line of the wing (assumed to be the midchord line in the Datcom). The vortices are then weighted by the span-load variation. The integrated contribution of each bound and each trailing vortex is then determined as a function of the spatial coordinates and presented in either table or chart form.

For computing downwash in the plane of symmetry, tables have been prepared based on the downwash due to the system of swept unit horseshoe vortices.

For computing the spanwise variation of downwash, design charts have been prepared based on an approximation of the downwash due to the system of swept unit horseshoe vortices. The swept lifting line

has been approximated with semi-infinite unswept horseshoe vortices. Although this approximation does not predict the exact magnitude of the spanwise variation in downwash, it has been applied in an effort to simplify the final solution and to allow design charts to be presented in lieu of lengthy calculation tables. By using this approach, the calculated level of the spanwise downwash variation is adjusted, if necessary, to the value at the plane of symmetry obtained using the tables.

This method is presented in the Datcom because of its wide range of applicability, even though the tables and design charts of Reference 11 have not been reproduced. However, the basic equations are presented for use in the event that the reference is not available to the user. The span loading of the particular wing being considered must be known. At the present time this information must be obtained from sources other than the Datcom, for instance Reference 12.

The derivative $\frac{\partial \epsilon}{\partial \alpha}$ at a particular point (x, y, z) in the flow field not close to the trailing edge of the wing is obtained by means of the equation

$$\frac{\partial \epsilon}{\partial \alpha} = -\frac{w}{V_\infty \alpha} \qquad 4.4.1\text{-p}$$

For points on the plane of symmetry

$$-w = 2\sum_{i=o}^{n_2} \frac{\Gamma_{y_{i+1}} - \Gamma_{y_{i-1}}}{b/2} F_w(|y_{i,o}|) + \frac{\Gamma_o}{b/2} F_{w,o} \qquad 4.4.1\text{-q}$$

For points not on the plane of symmetry (spanwise downwash)

$$-w = -\sum_{i=n_1}^{o} \frac{\Gamma_{y_{i+1}} - \Gamma_{y_{i-1}}}{b/2} F_w(Y_{i,o}) + \sum_{i=o}^{i=n_2} \frac{\Gamma_{y_{i+1}} - \Gamma_{y_{i-1}}}{b/2} F_w(Y_{i,o}) \qquad 4.4.1\text{-r}$$

The functions $F_w(|y_{i,o}|)$, $F_w(Y_{i,o})$, and $F_{w,o}$ are presented in Reference 11 as Table II, Figure 6, and Table III, respectively, and are expressed mathematically by

$$F_w(|y_{i,o}|) = \frac{-|y_{i,o}|X_{i,o}^3 + X_{i,o}(z_o^2 - y_{i,o}^2) + \beta m^2 |y_{i,o}| X_{i,o}(|y_{i,o}|^2 + 2z_o^2) + \beta m^2 |y_{i,o}|(z_o^2 + |y_{i,o}|^2)}{4\pi\sqrt{X_{i,o}^2 - \beta^2 m^2 (|y_{i,o}|^2 + z_o^2)}\,[(|y_{i,o}|X_{i,o} + z_o^2 + |y_{i,o}|^2)^2 + z_o^2(X_{i,o}^2 - \beta^2 m^2 |y_{i,o}|^2 - \beta^2 m^2 z_o^2)]}$$

4.4.1-s

$$F_w(Y_{i,o}) = \frac{Y_{i,o}\bar{X}_i^3 - Y_{i,o}\bar{X}_i(Y_{i,o}^2 + 2z_o^2)}{4\pi\sqrt{\bar{X}_i^2 - Y_{i,o}^2 - z_o^2}\,(\bar{X}_i^2 - z_o^2)(Y_{i,o}^2 + z_o^2)} \qquad 4.4.1\text{-t}$$

$$F_{w,o} = \frac{x_o}{\pi\sqrt{x_o^2 - \beta^2 m^2 z_o^2}\,[x_o^2 + z_o^2(1 - \beta^2 m^2)]} \qquad 4.4.1\text{-u}$$

Definitions applying to this method are given as follows (symbolism used for this method is identical with that of Reference 11).

V_∞ = free-stream velocity.

α = angle of attack in radians.

x,y,z = standard rectangular Cartesian coordinates with the origin at the 50-percent-chord point of the root section.

x_i, y_i = standard rectangular Cartesian coordinates of the inboard corners of the horseshoe vortices.

$$x_o = \frac{mx}{b/2}$$

$$x_{i,o} = \pm \frac{mx_i}{b/2} = \pm y_{i,o}$$

$$X_{i,o} = x_o - x_{i,o} = x_o \pm y_{i,o} = \frac{mX_i}{b/2}$$

$$\bar{X}_i = \bar{x} \pm \frac{y_{i,o}}{\beta m}$$

$$\bar{x} = \frac{x}{\beta b/2} \left(= \frac{x_o}{\beta m} \text{ for swept lifting line} \right)$$

$$y_o = \frac{y}{b/2}$$

$$y_{i,o} = \frac{y_i}{b/2}$$

$$Y_{i,o} = y_o - y_{i,o} = \frac{Y_i}{b/2}$$

$$z_o = \frac{z}{b/2}$$

i = variable index used in summation, designating a particular horseshoe vortex. Values of i from o to n_1 are associated with negative values of y_i and values from o to n_2 with positive values of y_i.

m = slope of lifting line ($\cot|\Lambda_{c/2}|$)

n_1, n_2 = value of i at left- and right-hand wing tips of a swept wing, looking from trailing edge to leading edge.

Γ_y = value of circulation at any spanwise station. If the load distribution is given in terms of the section lift coefficient, the circulation is determined by the equation

$$\Gamma_y = 1/2\ c_\ell V c$$

where c is the local chord.

Γ_o = circulation at $y_i = 0$

The suggested method of adjusting the calculated spanwise downwash given by Equation 4.4.1-r is to translate the curve of calculated spanwise downwash so that the value at the plane of symmetry ($y_o = 0$) is made to coincide with that computed by using Equation 4.4.1-q. This approach is illustrated in the sample problem on Page 4.4.1-35.

For locations near the wing trailing edge, lifting-line theory does not give adequate answers and a more precise determination must be made. An exact equation is given in Reference 13 for determining this value, which involves the local angle of attack and the perturbation velocity at the trailing edge.

The effects of vortex-sheet displacement and distortion have not been included in this method, although this effect may be approximated by the theory of Reference 14. (See Steps 1 and 2 of Method 2 that follows.) The displacement of the vortex sheet at the center line is determined, and it is assumed that this displacement is constant for all lateral stations. Therefore, the effects of vortex-sheet displacement and distortion are approximated by calculating a new z_o value to be used in this method. In using the design charts associated with Method 2, it should be noted that the origin of the spatial coordinates is located at the wing apex rather than at the 50-percent-chord point of the root section as for this method.

Method 2

Supersonic downwash for straight-tapered wings with supersonic leading edges ($\beta \cot \Lambda_{LE} > 1$) and supersonic trailing edges ($\beta \cot \Lambda_{TE} > 1$) may be computed by means of the charts presented in Reference 14. (It should be noted that Figures 4.4.1-76a and -76d from Reference 14 have been expanded somewhat, based on available test data. In addition, Figure 4.4.1-76e has been obtained semiempirically by using Figure 4.4.1-76d as a basis and should be applied with caution.) The charts, based on lifting-line theory, are derived for flat-plate wings and include a correction for the displacement and distortion of the trailing vortex sheet. The lifting line is assumed to be at $\Lambda_{c/2}$ for the rectangular and trapezoidal wings and at $\Lambda_{3c/4}$ for the triangular wings. Near the sonic-leading-edge condition, the lift of a finite-thickness wing is significantly less than the values for flat-plate wings (see Section 4.1.3.2). The downwash gradient $\partial\bar{\epsilon}/\partial\alpha$ may be corrected to account for wing thickness effects as indicated in the procedure below. Table 4.4.1-F presents a data summary and substantiation. The limited number of test points presented precludes substantiation of this method over other than very limited ranges of planform and flow parameters.

The derivative $\frac{\partial\bar{\epsilon}}{\partial\alpha}$ for wings with supersonic leading and trailing edges is obtained by the following procedure:

Step 1. For the Mach number under consideration, the coordinates of the point where the downwash is desired are reduced to the parameters $\frac{2x}{\beta b}$, $\frac{2y}{b}$, and $\frac{2z}{b}$ measured from an origin at the apex of the wing (x, y, and z are positive in the conventional sense and refer to wind axes).

Step 2. The effects of displacement and distortion of the vortex sheet are accounted for by determining the displacement of the sheet at the center line and assuming that this displacement is constant for all lateral stations (see Reference 14). The vertical displacement 2h/b of the vortex sheet at the center line is obtained from Figure 4.4.1-74 (derived from Reference 8). This value is added to the parameter $\frac{2z}{b}$ from Step 1 to obtain the effective value of the height parameter relative to the displaced vortex. This effective parameter is designated $\left(\frac{2z}{b}\right)_{eff}$

Step 3. For the values of $\frac{2x}{\beta b}$, $\frac{2y}{b}$, and $\left(\frac{2z}{b}\right)_{eff}$, the derivative $\frac{\partial \bar{\epsilon}}{\partial \alpha}$ is obtained from Figures 4.4.1-76a through 4.4.1-76e, depending upon the appropriate wing planform geometry. This value is valid for finite-thickness wings except near the sonic-leading-edge condition, where an additional correction is required.

Step 4. For near-sonic-leading-edge conditions, the value of $\frac{\partial \bar{\epsilon}}{\partial \alpha}$ obtained from Step 3 is multiplied by the thickness correction factor from Figure 4.1.3.2-60.

Step 5. For moderate angles of attack below wing stall, where the nonlinear lift becomes important, the downwash gradient determined from Step 3 can be approximately corrected by the equation

$$\frac{\partial \bar{\epsilon}}{\partial \alpha} = \frac{(C_{N_\alpha})_{4.1.3.3}}{(C_{N_\alpha})_{4.1.3.2}} \left(\frac{\partial \bar{\epsilon}}{\partial \alpha}\right)_{\text{step 3}} \qquad \text{4.4.1-v}$$

where

$(C_{N_\alpha})_{4.1.3.3}$ is the local normal-force-curve slope from Paragraph C of Section 4.1.3.3 for the angle of attack under consideration. It is $(C_{N_\alpha})_{4.1.3.2}$ corrected for thickness effects.

$(C_{N_\alpha})_{4.1.3.2}$ is the normal-force-curve slope at zero angle of attack from the straight-tapered-wing method of Paragraph C of Section 4.1.3.2, excluding the thickness correction factor of Figure 4.1.3.2-60.

$\left(\frac{\partial \epsilon}{\partial \alpha}\right)_{\text{step 3}}$ is the downwash gradient from Step 3.

Step 6. The average downwash over the span of a horizontal tail is obtained by computing the downwash at several spanwise locations and computing an average value.

Step 5 should be used with caution. Nonlinear lift (which is characteristic of low-aspect-ratio configurations) is caused by strong vortices that generally move inboard with increasing angle of attack and may have a spanwise spacing comparable to that of the downstream surfaces.

For those configurations that do not satisfy the supersonic leading- and trailing-edge condition, an approximation (used in Digital Datcom) for the downwash gradient may be obtained by using Equation 4.4.1-k, i.e.,

$$\epsilon = \frac{1.62\, C_L}{\pi A} \quad \text{(radians)}$$

From this equation a relationship is obtained for ϵ as a function of angle of attack. Plotting the curve from this relationship enables the user to obtain a value for $\partial\epsilon/\partial\alpha$ at a specific angle of attack. However, this approximation should be used with caution since it has not been substantiated in the supersonic speed regime.

Method 3

For low-aspect-ratio or canard configurations the vortex pair from the forward surface interacts more directly with the aft surface and the following method from Reference3 is applicable.

Step 1. The spatial position of the trailing vortices is first determined relative to the aft surface. The lateral spacing is determined from Figure 4.4.1-80 as a function of the exposed forward-surface planform geometry. This spacing is invariant with longitudinal distance and angle of attack. The vertical position is determined by assuming that the vortex springs from the trailing edge at the previously determined lateral position and trails in the free-stream direction. The pertinent vertical dimension is the distance between the quarter-chord point of the MAC of the aft surface and the vortex as determined above.

Step 2. The vortex interference factor $I_{v_{W'(W'')}}$ is obtained from Figures 4.3.1.3-7a through 4.3.1.3-7ℓ as a function of the lateral and vertical vortex positions, determined in Step 1, and the geometry of the aft panel. (The primed notation refers to the forward panel and the double-primed notation refers to the aft panel.)

Step 3. The vortex interference factor so determined is used in Sections 4.5.1.1 and 4.5.1.2 to obtain the lift generated on the aft surface for complete wing-body-tail combinations.

This method is similar to Method 3 for estimating subsonic downwash in paragraph A. The use of the subsonic sample problem on Page 4.4.1-17 as a guide is essential in applying this method.

Supersonic Dynamic-Pressure Ratio

The dynamic-pressure ratio at supersonic speeds is estimated separately for the nonviscous and viscous flow regions. The nonviscous flow region is approximated by the flow emanating from the wing in the absence of separation, and bound by shock or expansion waves. The viscous flow region is considered to be the viscous wake behind a wing, with attached flow in the vicinity of the trailing edge.

Nonviscous Flow Field

The dynamic-pressure ratio in the nonviscous flow field of a wing is estimated by means of shock-expansion theory. Application of this technique assumes that the flow field is two-dimensional. For a rectangular wing, the region outside the influence of the tips is two-dimensional. Therefore, the method applied to rectangular wings will, in general, predict the experimental trends and even the magnitude of the flow-field quantities with fair accuracy, except in the region influenced by the tip or in the viscous wake. For some rectangular wings of high effective aspect ratio (βA), the greater portion of the flow field can be predicted reasonably well by shock-expansion theory.

Strictly speaking, this method can not be applied to sweptback wings, since the large portion of the flow field of such wings will not be two-dimensional. However, the method might furnish a good approximation to the dynamic-pressure-ratio variations, because the theory does account for the presence of shock and expansion waves. In Reference 15 the method has been applied to a triangular wing with supersonic leading edges, and the dynamic-pressure ratio was predicted fairly accurately except in the viscous flow region. No comparison of calculated results with experimental data has been made for wings with subsonic leading edges.

The theory as applied herein allows calculation of the dynamic-pressure ratio on an arbitrarily selected survey plane located downstream from the wing. The geometric relationship between points on this plane and points on the airfoil from which the disturbance originates is illustrated in Sketch (h). It is assumed that disturbances emanating from a point on the wing (x ' – z 'plane)

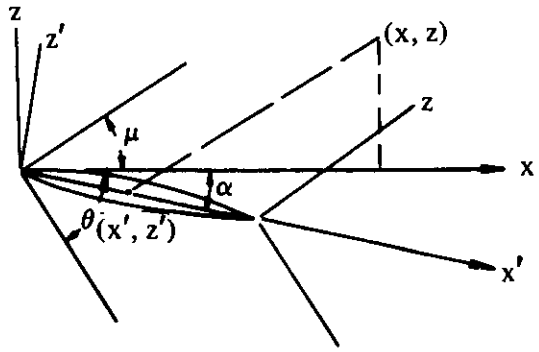

SKETCH (h)

proceed downstream at the theoretical Mach angle μ for surfaces with an initial expansion angle, and at the shock angle θ for surfaces with an initial compression angle. It is further assumed that the dynamic-pressure ratio at some point (x, y) on the survey plane is the same as that at the corresponding point (x', y') on the airfoil surface.

The basic approach is as follows:

1. For a given airfoil and flow condition determine the points (x, y) in the flow field at the survey plane corresponding to the points (x′, y′) on the airfoil from which the disturbance is assumed to originate.

2. By using shock-expansion theory, determine the dynamic-pressure ratio at point (x, y) in the flow field which is assumed to be the same as that at corresponding point (x′, y′).

In applying shock-expansion theory the flows on the upper and lower airfoil surfaces can be treated separately. The type of flow (either expansion or compression) at a given point is governed by the sign of the flow-deflection angle at that point.

If the flow-deflection angle is positive, the flow expands isentropically and the characteristics of the flow are given by Prandtl-Meyer expansion relations. If the flow quantities are known at one point, the values at any second point can be calculated by identifying the change in the flow angle between the two points.

If the flow-deflection angle is negative, the flow is compressed and the flow characteristics are given by oblique-shock-wave relations. The Datcom presents a design chart showing the variation of shock angle with flow-deflection angle for various upstream Mach numbers. In addition, since flow through weak shock waves is nearly isentropic, compressions through small angles may also be calculated by regarding them as reversed Prandtl-Meyer expansions.

Although expansion and compression waves proceed at different angles and therefore interact, this simplified method does in some cases give a good approximation of the dynamic-pressure ratio. The accuracy of the method deteriorates as the wing thickness and/or distance of the survey plane aft of the wing increase.

The following steps outline the procedure to be followed for determining the supersonic dynamic-pressure ratio in the nonviscous flow field. The use of the sample problem on Page 4.4.1-41 as a guide is essential in applying this procedure.

Step 1. For a given airfoil and flow condition, determine the flow-deflection angles on the upper and lower airfoil surfaces at the leading edge.

For an airfoil at a positive angle of attack the flow-deflection angle at the leading edge is given by:

For the upper airfoil surface

$$\delta'_{LE} = \alpha - \delta_{LE_{upper}}$$

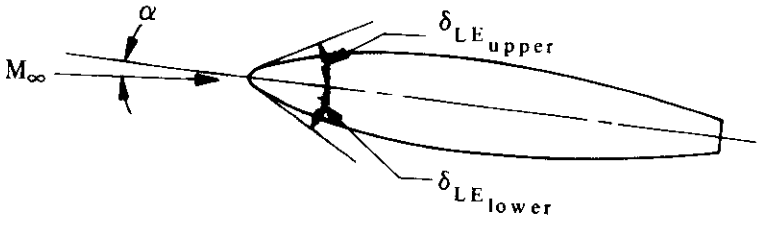

For the lower airfoil surface

$$\delta'_{LE} = -\alpha - \delta_{LE_{lower}}$$

where the δ' values are the flow-deflection angles and the δ values are the slopes of the airfoil surface with respect to the chord plane x′.

If δ'_{LE} is positive the surface has an initial expansion angle. If δ'_{LE} is negative the surface has an initial compression angle.

Step 2. Determine the points (x , z) in the flow field corresponding to the points (x′ , z′) on the airfoil from which the disturbance is assumed to have originated.

For surfaces with an initial expansion angle

$$z = \frac{-x' + x\cos\alpha - \dfrac{x\sin\alpha}{\tan(\mu+\alpha)}}{\sin\alpha + \dfrac{\cos\alpha}{\tan(\mu+\alpha)}} \qquad \text{4.4.1-w}$$

where

x' is an arbitrarily chosen point on the airfoil chord plane, positive aft of the leading edge.

x is the location of the arbitrarily chosen survey plane on the x-axis, positive aft of the leading edge.

α is the angle of attack in degrees.

μ is the Mach angle, $\mu = \sin^{-1}\dfrac{1}{M_\infty}$.

For surfaces with initial compression angles

$$z = \frac{-x' + x\cos\alpha - \dfrac{x\sin\alpha}{\tan(\alpha-\theta)}}{\sin\alpha + \dfrac{\cos\alpha}{\tan(\alpha-\theta)}} \qquad \text{4.4.1-x}$$

where x', x, and α are defined above and θ is the shock-wave angle obtained as a function of the free-stream Mach number and the flow-deflection angle from Figure 4.4.1-81.

Equations 4.4.1-w and 4.4.1-x are based on the assumption that the disturbance originates from a point located on the airfoil chord. Therefore, $z' = 0$.

Step 3. Determine the dynamic-pressure ratio at point (x , z) – which is assumed to be the same as that at corresponding point (x′, z′).

For expansion fields (positive flow-deflection angles) the procedure is as follows:

a. Using the Mach number upstream of a point M_{n-1}, enter Figure 4.4.1-82 and obtain ν_{n-1}, the Prandtl-Meyer angle (angle through which the supersonic stream is turned to expand from $M = 1$ to $M > 1$). n refers to an individual point.

b. Determine $\Delta\nu_n$, the change in flow-deflection angle between two points. In expanding from the free stream to a point downstream of the leading edge, $\Delta\nu_n = \alpha - \delta_{LE}$. On the airfoil surface $\Delta\nu_n$ is simply the change in surface slope between two points; i.e., $\Delta\nu_n = \delta_{n-1} - \delta_n$.

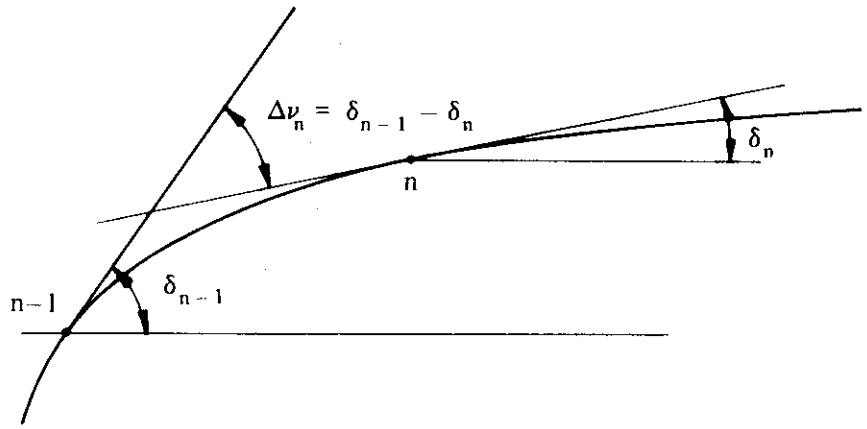

c. Determine the new Prandtl-Meyer angle at point n by $\nu_n = \nu_{n-1} + \Delta\nu_n$

d. Enter Figure 4.4.1-82 with ν_n and read M_n.

e. Using M_{n-1} (upstream Mach number) and M_n (Mach number at point in question), enter Figure 4.4.1-82 and read the ratio of dynamic pressure to total pressure q/p_t at the respective Mach numbers. Then

$$\frac{q_n}{q_\infty} = \frac{(q/p_t)_n}{(q/p_t)_{n-1}} \quad \frac{q_{n-1}}{q_\infty} \qquad 4.4.1\text{-y}$$

For compression fields (negative flow-deflection angles) the procedure is as follows:

The dynamic-pressure ratio following an oblique shock is given by

$$\frac{q_n}{q_{n-1}} = \frac{60}{M_{n-1}^2} \quad \frac{(1 + 0.2\, M_{n-1}^2)^{7/2}}{(5 + M_{n-1}^2 \sin^2\theta)^{5/2}} \qquad 4.4.1\text{-z}$$

where n refers to an individual point and

M_{n-1} is the Mach number upstream of the shock.

θ is the shock-wave angle obtained as a function of the upstream Mach number M_{n-1} and the flow-deflection angle δ 'at the point in question.

The Mach number behind an oblique shock is given by

$$M_n = \left[\frac{M_{n-1}^2 \sin^2\theta + 5}{7\, M_{n-1}^2 \sin^2\theta - 1}\right]^{1/2} \quad \frac{1}{\sin(\theta + \delta')} \qquad 4.4.1\text{-aa}$$

where M_{n-1}, θ, and δ are defined under Equation 4.4.1-z.

At the airfoil trailing edge the flow over both the upper and lower surfaces of the airfoil returns to nearly free-stream flow. If the Mach number at the trailing edge is greater than the free-stream Mach number, the flow is compressed through a shock wave θ_{TE} corresponding to the Mach number at the trailing edge, and the flow-deflection angle $\delta' = -\alpha + \delta_{TE}$. If the Mach number at the trailing edge is less than the free-stream Mach number, the flow is expanded through the angle $\Delta\nu_{TE} = \alpha + \delta_{TE}$.

This procedure is best applied by starting with the leading edge. The sample problem on Page 4.4.1-41 illustrates the procedure.

Viscous Flow Field

No known method exists in the literature for estimating the dynamic-pressure ratio in the viscous wake of a wing at supersonic speeds. Because of the similarity of this part of the flow field to the corresponding viscous wake at subsonic speeds, it is recommended that the method presented for determining the subsonic dynamic-pressure ratio in Paragraph A be applied at supersonic Mach numbers. In using this method the appropriate value of C_{D_0} must be obtained from Paragraph C of Section 4.1.5.1.

It should be noted that the x- and z-distances used in this method are measured from different origins from those used in the method for the nonviscous flow field. In this method x is measured from the wing-root trailing edge and z is measured from the wake center line.

Mach Number Effects

No explicit method is presented in the Datcom for determining the Mach number field about an airfoil. However Reference 16 explains and illustrates a calculation process. Compressibility tables such as those of Reference 17 can be of great help in estimating compressible-flow properties.

Sample Problems

1. Supersonic Downwash (Method 1)

Given:

The sample problem presented in Reference 11. The calculation procedure is illustrated by showing calculations for one Mach number and two points in the flow field, one in the plane of symmetry ($y_o = 0$) and one outside the plane of symmetry at $y_o = 0.15$. The points for which the downwash calculations are given are both located at longitudinal position $x_o = 2.2$ and vertical position $z_o = 0$.

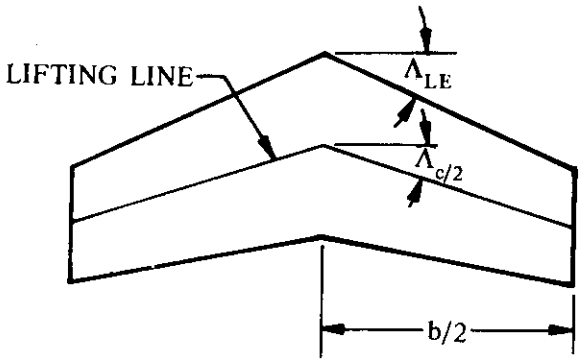

$A = 3.57$ $\lambda = 0.565$

$\Lambda_{LE} = 38.8^{o}$ $\Lambda_{c/2} = \Lambda_{\text{lifting line}} = 33^{o}$

$m_o = \cot \Lambda_{LE} = 1.244$

$m = \cot \Lambda_{c/2} = 1.54$

$M = 1.64$; $\beta = 1.30$

The following span-load distribution from Reference 12 at a constant angle of attack as f(A, λ, M, Λ_{LE}).

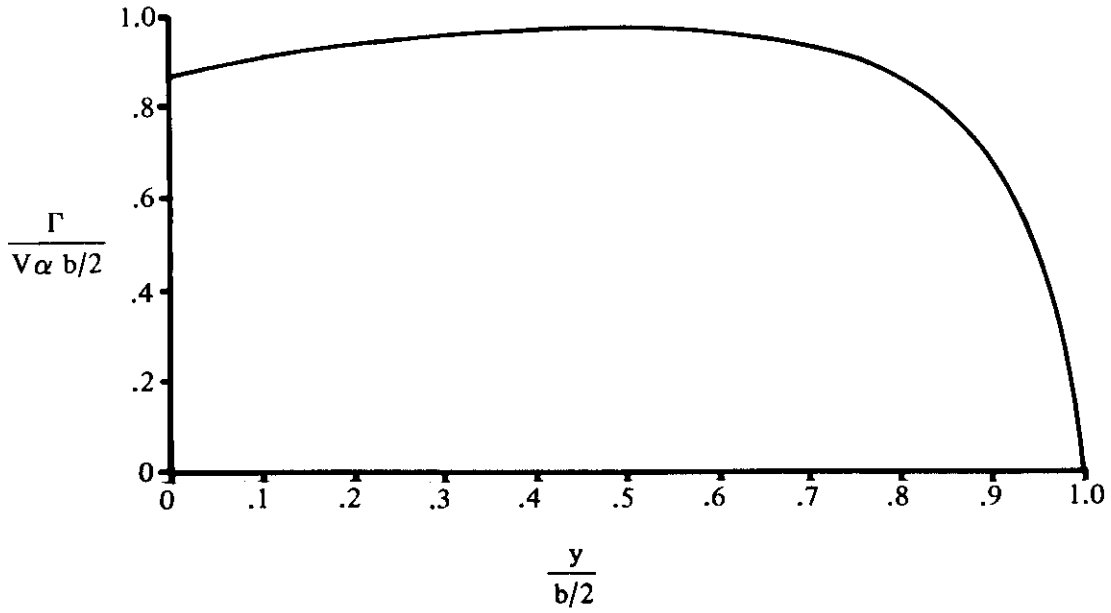

Compute: Plane of Symmetry

Determine the downwash gradient in the plane of symmetry ($y_o = 0$) at $z_o = 0$, $x_o = 2.2$.

$$-w = 2\sum_{i=o}^{n_2} \frac{\Gamma_{y_{i+1}} - \Gamma_{y_{i-1}}}{b/2} F_w\,(|y_{i,o}|) + \frac{\Gamma_o}{b/2} F_{w,o}$$

(Equation 4.4.1-q)

(see calculation table below)

Solution: , Plane of Symmetry

$$\frac{\partial \epsilon}{\partial \alpha} = -\frac{w}{V_\infty \alpha} \quad \text{(Equation 4.4.1-p)}$$

①	②	③	④	⑤	⑥	⑦
$y_{i,o}$ Spanwise location of trailing vortices	$\frac{\Gamma y_i}{V\alpha b/2}$ Circulation strength at $y_{i,o}$ (given)	$\frac{\Gamma y_{i+1} - \Gamma y_{i-1}}{V\alpha b/2}$ Incremental circulation strength	$F_w\ (\lvert y_{i,o} \rvert)$ From Equation 4.4.1-s or Table II of Reference 11	③ × ④	$F_{w,o}$ From Equation 4.4.1-u or Table III of Reference 11	$\frac{\partial \epsilon}{\partial \alpha} =$ 2Σ ⑤ + ⑥ $\frac{\Gamma_o}{V\alpha b/2}$
0	0.868	0	....	....	0.144686	−0.11184
0.05	0.890	0.043	−1.553695	−0.0668089		
0.10	0.911	0.034	−0.756150	−0.0257091		
0.15	0.924	0.023	−0.489023	−0.0112475		
0.20	0.934	0.018	−0.354408	−0.0063793		
0.25	0.942	0.020	−0.272706	−0.0054541		
0.30	0.954	0.018	−0.217364	−0.0039126		
0.35	0.960	0.012	−0.176978	−0.0021237		
0.40	0.966	0.010	−0.145812	−0.0014581		
0.45	0.970	0.003	−0.120639	−0.0003619		
0.50	0.969	−0.002	−0.099455	+0.0001989		
0.55	0.968	−0.012	−0.080882	0.0009706		
0.60	0.957	−0.018	−0.063801	0.0011484		
0.65	0.950	−0.020	−0.046973	0.0009395		
0.70	0.937	−0.048	−0.027827	0.0013357		
0.75	0.902	−0.075	0	0		
0.80	0.862	−0.102	0	0		
0.85	0.800	−0.179	0	0		
0.90	0.682	−0.345	0	0		
0.95	0.455	−0.683	0	0		
1.00	0	−0.455	0	0		

$\Sigma = -0.1188621$

Compute: Outside the Plane of Symmetry

Determine the downwash gradient outside the plane of symmetry at $y_o = 0.15$, $z_o = 0$, $x_o = 2.2$

$$-w = -\sum_{i=n_1}^{o} \frac{\Gamma_{y_{i+1}} - \Gamma_{y_{i-1}}}{b/2} F_w\ (Y_{i,o}) + \sum_{i=o}^{i=n_2} \frac{\Gamma_{y_{i+1}} - \Gamma_{y_{i-1}}}{b/2} F_w\ (Y_{i,o}) \quad \text{(Equation 4.4.1-r)}$$

(see calculation table below)

Solution: Outside the Plane of Symmetry

$$\frac{\partial \epsilon}{\partial \alpha} = -\frac{w}{V_\infty \alpha} \quad \text{(Equation 4.4.1-p)}$$

① $y_{i,o}$ Spanwise location of trailing vortices (L.H. panel)	② $Y_{i,o} = y_o - y_{i,o} = 0.15 - ①$ (L.H. panel)	③ $\overline{X}_i = \frac{x_o}{\beta m} + \frac{y_{i,o}}{\beta m} = 1.1 + \frac{①}{2}$	④ $F_w(Y_{i,o})$ From Equation 4.4.1-t or Fig. 6 of Ref. 11	⑤ $\frac{\Gamma_{y_{i+1}} + \Gamma_{y_{i-1}}}{V \alpha b/2}$ Incremental circulation strength	⑥ ④ × ⑤	⑦ $y_{i,o}$ Spanwise location of trailing vortices (R.H. panel)	⑧ $Y_{i,o} = y_o - y_{i,o} = 0.15 - ⑦$ (R.H. panel)	⑨ $F_w(Y_{i,o})$ From Equation 4.4.1-t or Fig. 6 of Ref. 11	⑩ ⑤ × ⑨	⑪ $\frac{\partial \epsilon}{\partial \alpha} = \Sigma$ ⑩ $= \Sigma \epsilon_6$
−1.0	1.15	0.6	0	−0.455	0	1.0	−0.85	0	0	0.003
−0.95	1.10	0.625	0	−0.683	0	0.95	−0.80	0	0	
−0.90	1.05	0.650	0	−0.345	0	0.90	−0.75	0	0	
−0.85	1.00	0.675	0	−0.179	0	0.85	−0.70	0	0	
−0.80	0.95	0.700	0	−0.102	0	0.80	−0.65	−0.045	0.004590	
−0.75	0.90	0.725	0	−0.075	0	0.75	−0.60	−0.074	0.005550	
−0.70	0.85	0.750	0	−0.048	0	0.70	−0.55	−0.098	0.004704	
−0.65	0.80	0.775	0	−0.020	0	0.65	−0.50	−0.118	0.002360	
−0.60	0.75	0.800	0.036	−0.018	−0.000648	0.60	−0.45	−0.146	0.002628	
−0.55	0.70	0.825	0.060	−0.012	−0.000720	0.55	−0.40	−0.173	0.002076	
−0.50	0.65	0.850	0.078	−0.002	−0.000156	0.50	−0.35	−0.207	0.000414	
−0.45	0.60	0.875	0.097	0.003	0.000291	0.45	−0.30	−0.248	−0.000744	
−0.40	0.55	0.900	0.114	0.010	0.001140	0.40	−0.25	−0.307	−0.003070	
−0.35	0.50	0.925	0.133	0.012	0.001596	0.35	−0.20	−0.388	−0.004656	
−0.30	0.45	0.950	0.156	0.018	0.002808	0.30	−0.15	−0.523	−0.009414	
−0.25	0.40	0.975	0.181	0.020	0.003620	0.25	−0.10	−0.793	−0.015860	
−0.20	0.35	1.000	0.213	0.018	0.003834	0.20	−0.05	−1.590	−0.028620	
−0.15	0.30	1.025	0.254	0.023	0.005842	0.15	0	.....	.....	
−0.10	0.25	1.050	0.312	0.034	0.010608	0.10	0.05	1.591	0.054094	
−0.05	0.20	1.075	0.391	0.043	0.016813	0.05	0.10	0.794	0.034142	
0	0.15	1.100	0.526	0	0	0	0.15	0.526	0	
					$\Sigma = 0.04503$				$\Sigma = 0.04819$	

Additional results are presented in Reference 11 for the variation of $\partial\epsilon/\partial\alpha$ in the plane of symmetry with Mach number and longitudinal position. These results are shown in Sketch(i).

SKETCH (i)

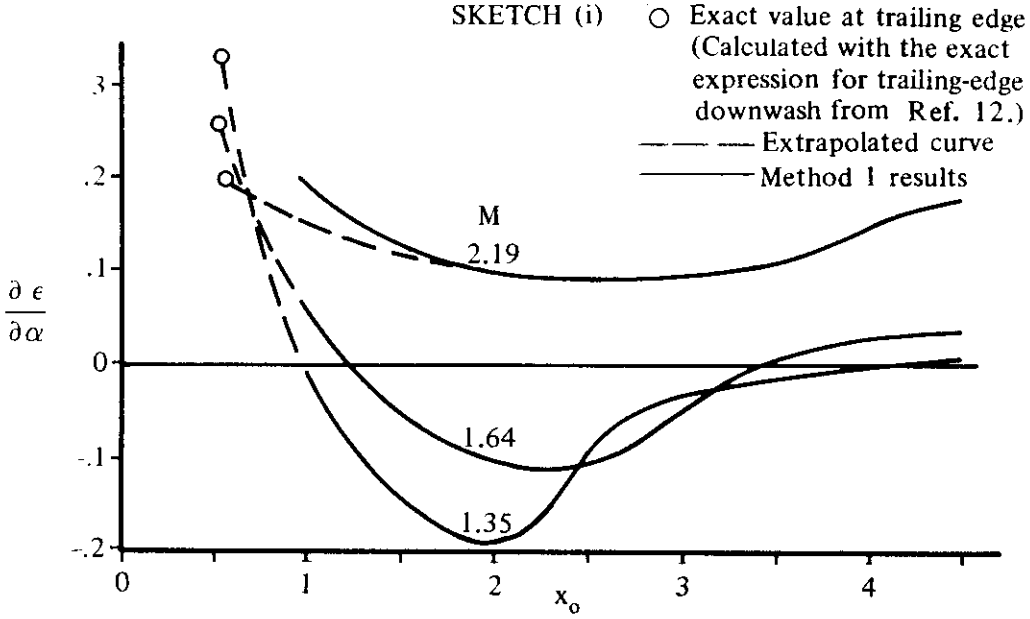

The inaccuracies in Method 1 near the trailing edge are not too apparent except for the M = 2.19 curve. As was pointed out previously (Page 4.4.1-28), these inaccuracies may be minimized by determining the exact value at the trailing edge.

Additional results from Reference 11 for the spanwise variation of downwash are shown in Sketch(j). The spanwise variation of downwash at $x_o = 2.2$ and $z_o = 0$, calculated by Equation 4.4.1-r, is shown by the solid curve. This curve is then translated so that the value at $y_o = 0$ coincides with that calculated using Equation 4.4.1-q. The translated values shown by the dashed curve agree reasonably well with values calculated by the more exact method, which uses the swept vortex equation of Reference 11.

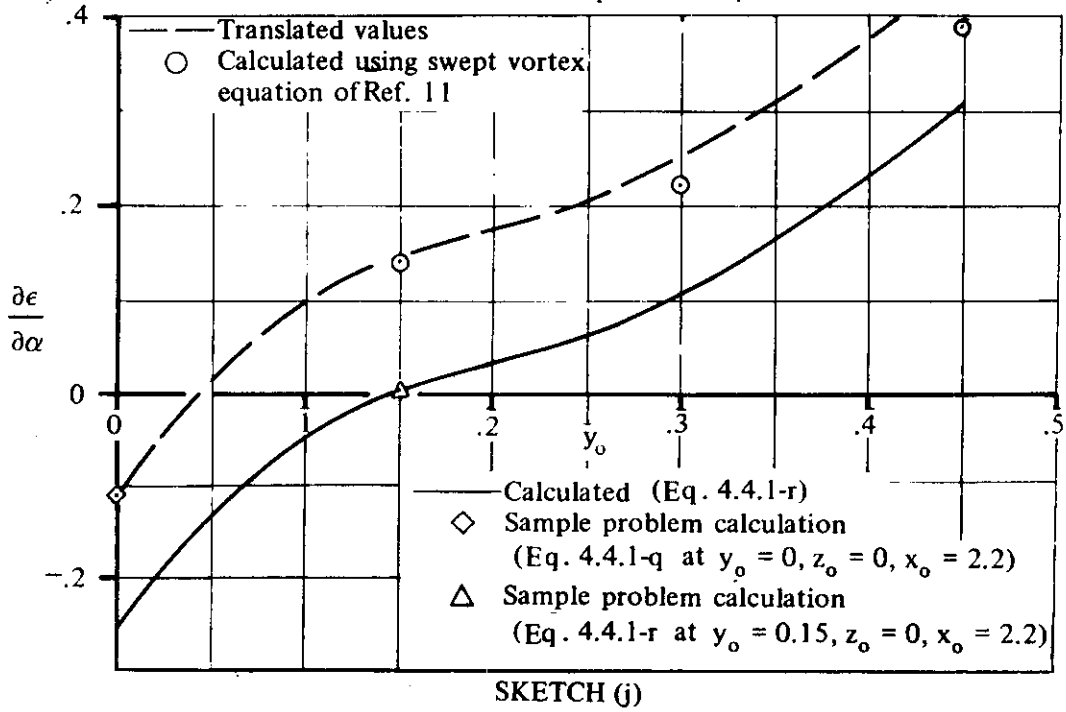

SKETCH (j)

2. Supersonic Downwash (Method 2)

Given: A rectangular wing.

Wing Characteristics:

$A = 2.31$ $b = 10.0$ ft $\lambda = 1.0$ $c = 4.33$ ft

Coordinates of Quarter-Chord of Tail MAC:

$x = 15.0$ ft $y = 1.50$ ft $z = 1.0$ ft

Additional Characteristics:

$M = 2.0$; $\beta = 1.732$ $\alpha = 4^{o} = 0.07$ rad

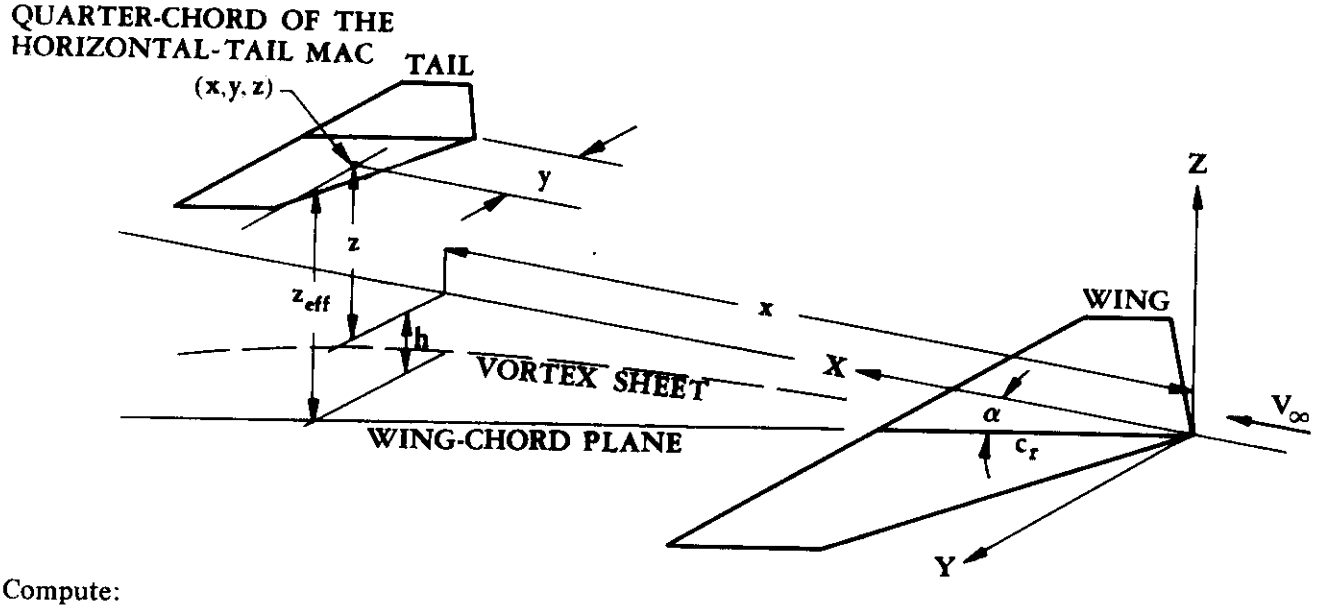

Compute:

$$\frac{2x}{\beta b} = \frac{(2)(15)}{(1.732)(10)} = 1.73$$

$$\frac{2y}{b} = \frac{(2)(1.5)}{10} = 0.30$$

$$\frac{2z}{b} = \frac{(2)(1)}{10} = 0.20$$

$$\beta A = (1.732)(2.31) = 4.0$$

$$\frac{2h}{\alpha \beta b} = 0.64$$ (Figure 4.4.1-74d)

$$\left(\frac{2z}{b}\right)_{eff} = \left(\frac{2z}{b}\right) + \left(\frac{2h}{\alpha\beta b}\right)\alpha\beta$$

$$= 0.20 + (0.64)\,(0.07)\,(1.732)$$

$$= 0.28$$

Solution:

$\frac{\partial\bar{\epsilon}}{\partial\alpha}$ is obtained from Figure 4.4.1-76 as $f\left[\frac{2x}{\beta b}, \left(\frac{2z}{b}\right)_{eff}, \frac{2y}{b}, \beta A\right]$

$$\frac{\partial\bar{\epsilon}}{\partial\alpha} = 0.270$$

3. Supersonic Dynamic-Pressure Ratio

Given: The rectangular wing of Reference 15

Wing Characteristics:

$A = 2.0$ $\quad b_W = 8.0$ in. $\quad c_r = \bar{c} = 4.0$ in.

$\Lambda_{c/4} = 0$ $\quad S_W = S_{ref} = 32.0$ in.

Additional Characteristics:

$M_\infty = 2.46;\ \beta = 2.25$ $\quad R_\ell = 1.04 \times 10^6$ (based on $\bar{c}$)

Smooth surface (assume $k = 0$) $\quad$ Survey plane at $x = 6.4$ in.

$\alpha = 6^o$ $\quad C_L = 0.159$ (test value)

Symmetrical airfoil with following characteristics:

Point	x' (in.)	δ (surface slope) (deg)
1 (LE)	0	5.1
2	0.80	3.4
3	1.60	1.0
4	2.40	−0.5
5	3.20	−1.7
6 (TE)	4.00	−2.6

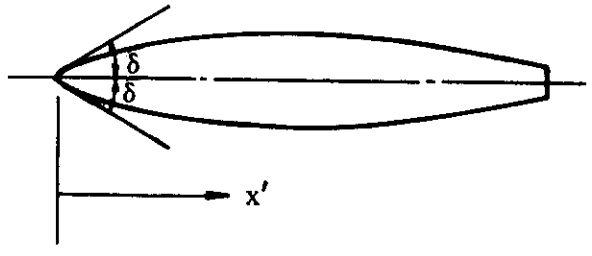

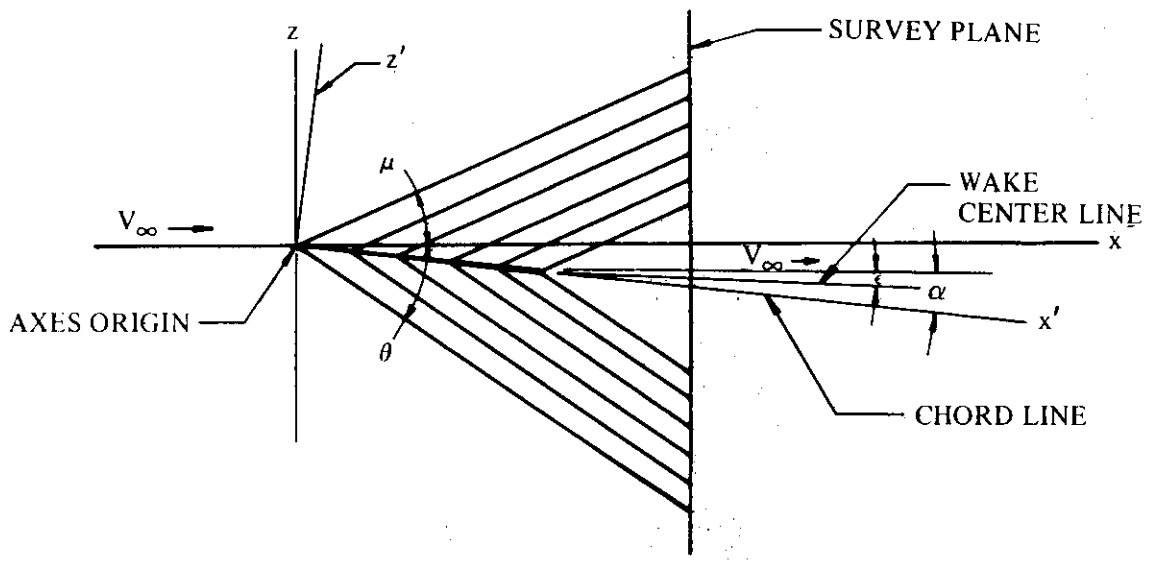

Outside Wake Portion (nonviscous flow field)

Compute:

Determine the flow-deflection angles at the leading edge.

Upper surface

$$\delta'_{LE} = \alpha - \delta_{LE_{upper}} = 6^{o} - 5.1^{o} = 0.9^{o} \text{ (expansion)}$$

Lower surface

$$\delta'_{LE} = -\alpha - \delta_{LE_{lower}} = -6^{o} - 5.1^{o} = -11.1^{o} \text{ (compression)}$$

Determine the values of z on the survey plane (located at x = 6.4 in. from the airfoil leading edge) corresponding to x ' values of 0, 0.8, 1.6, 2.4, 3.2, and 4.0 (points 1 - 6).

Upper surface (initial expansion angle)

$$\mu = \sin^{-1}\frac{1}{M_{\infty}} = \sin^{-1}\frac{1}{2.46} = 24^{o}$$

$$z = \frac{-x' + x\cos\alpha - \dfrac{x\sin\alpha}{\tan(\mu+\alpha)}}{\sin\alpha + \dfrac{\cos\alpha}{\tan(\mu+\alpha)}} \quad \text{(Equation 4.4.1-w)}$$

$$= \frac{-x' + (6.4)\cos 6^o - \dfrac{(6.4)\sin 6^o}{\tan (24^o + 6^o)}}{\sin 6^o + \dfrac{\cos 6^o}{\tan (24^o + 6^o)}} = \frac{-x'(6.4)(0.9945) - \dfrac{(6.4)(0.1045)}{0.5774}}{0.1045 + \dfrac{0.9945}{0.5774}}$$

$$= 0.5473\, x' + 2.85$$

	x' (in.)	z (in.)	$\frac{z}{b_w/2}$
LE	0	2.850	0.713
	0.8	2.412	0.603
	1.6	1.974	0.494
	2.4	1.536	0.384
	3.2	1.098	0.275
TE	4.0	0.660	0.165

Lower surface (initial compression angle)

$\theta = 33.5^o$ (Figure 4.4.1-81 at $M_\infty = 2.46$ and $\delta' = -11.1^o$)

$$z = \frac{-x' + x\cos\alpha - \dfrac{x\sin\alpha}{\tan(\alpha - \theta)}}{\sin\alpha + \dfrac{\cos\alpha}{\tan(\alpha - \theta)}} \qquad \text{(Equation 4.4.1-x)}$$

$$= \frac{-x' + (6.4)\cos 6^o - \dfrac{(6.4)\sin 6^o}{\tan (6^o - 33.5^o)}}{\sin 6^o + \dfrac{\cos 6^o}{\tan (6^o - 33.5^o)}} = \frac{-x' + (6.4)(0.9945) - \dfrac{(6.4)(0.1045)}{-0.5206}}{0.1045 + \dfrac{0.9945}{-0.5206}}$$

$$= 0.554\, x' - 4.236$$

	x' (in.)	z (in.)	$\frac{z}{b_w/2}$
LE	0	−4.236	−1.059
	0.8	−3.793	−0.948
	1.6	−3.350	−0.838
	2.4	−2.906	−0.727
	3.2	−2.463	−0.616
TE	4.0	−2.020	−0.505

Determine q/q_∞ at points (x,z) on the survey plane corresponding to points (x',z') on the airfoil.

Upper surface

Point 1 (x' = 0)

$M_\infty = 2.46$

$\Delta\nu_1 = \alpha - \delta_1 = 6^o - 5.1^o = 0.9^o$ (expansion)

$\nu_\infty = 38.2^o$ (Figure 4.4.1-82 at M_∞)

$\nu_1 = \nu_\infty + \Delta\nu_1 = 38.2^o + 0.9^o = 39.1^o$

$M_1 = 2.50$ (Figure 4.4.1-82 at ν_1)

$\left(q/p_t\right)_\infty = 0.264$ (Figure 4.4.1-82 at M_∞)

$\left(q/p_t\right)_1 = 0.256$ (Figure 4.4.1-82 at M_1)

$q_1/q_\infty = \left(q/p_t\right)_1 / \left(q/p_t\right)_\infty = 0.256/0.264 = 0.970$

Point 2 (x' = 0.8 in.)

$\Delta\nu_2 = \delta_1 - \delta_2 = 5.1^o - 3.4^o = 1.7^o$ (expansion)

$\nu_2 = \nu_1 + \Delta\nu_2 = 39.1^o + 1.7^o = 40.8^o$

$M_2 = 2.57$ (Figure 4.4.1-82 at ν_2)

$\left(q/p_t\right)_2 = 0.243$ (Figure 4.4.1-82 at M_2)

$$\frac{q_n}{q_\infty} = \frac{\left(q/p_t\right)_n}{\left(q/p_t\right)_{n-1}} \frac{q_{n-1}}{q_\infty}$$ (Equation 4.4.1-y)

$$\frac{q_2}{q_\infty} = \frac{\left(q/p_t\right)_2}{\left(q/p_t\right)_1} \frac{q_1}{q_\infty} = \frac{0.243}{0.256}(0.970) = 0.921$$

Point 3 (x′ = 1.6 in.)

$$\Delta\nu_3 = \delta_2 - \delta_3 = 3.4^o - 1.0^o = 2.4^o \text{ (expansion)}$$

$$\nu_3 = \nu_2 + \Delta\nu_3 = 40.8^o + 2.4^o = 43.2^o$$

$$M_3 = 2.68 \quad \text{(Figure 4.4.1-82 at } \nu_3\text{)}$$

$$\left(q/p_t\right)_3 = 0.223 \quad \text{(Figure 4.4.1-82 at } M_3\text{)}$$

$$\frac{q_3}{q_\infty} = \frac{\left(q/p_t\right)_3}{\left(q/p_t\right)_2}\ \frac{q_2}{q_\infty} = \frac{0.223}{0.243}(0.921) = 0.845 \quad \text{(Equation 4.4.1-y)}$$

Point 4 (x′ = 2.4 in.)

$$\Delta\nu_4 = \delta_3 - \delta_4 = 1.0^o - (-0.5^o) = 1.5^o \text{ (expansion)}$$

$$\nu_4 = \nu_3 + \Delta\nu_4 = 43.2^o + 1.5^o = 44.7^o$$

$$M_4 = 2.75 \quad \text{(Figure 4.4.1-82 at } \nu_4\text{)}$$

$$\left(q/p_t\right)_4 = 0.211 \quad \text{(Figure 4.4.1-82 at } M_4\text{)}$$

$$\frac{q_4}{q_\infty} = \frac{\left(q/p_t\right)_4}{\left(q/p_t\right)_3}\ \frac{q_3}{q_\infty} = \frac{0.211}{0.223}(0.845) = 0.800 \quad \text{(Equation 4.4.1-y)}$$

Point 5 (x′ = 3.2 in.)

$$\Delta\nu_5 = \delta_4 - \delta_5 = -0.5^o - (-1.7^o) = 1.2^o \text{ (expansion)}$$

$$\nu_5 = \nu_4 + \Delta\nu_5 = 44.7^o + 1.2^o = 45.9^o$$

$$M_5 = 2.81 \quad \text{(Figure 4.4.1-82 at } \nu_5\text{)}$$

$$\left(q/p_t\right)_5 = 0.201 \quad \text{(Figure 4.4.1-82 at } M_5\text{)}$$

$$\frac{q_5}{q_\infty} = \frac{\left(q/p_t\right)_5}{\left(q/p_t\right)_4}\ \frac{q_4}{q_\infty} = \frac{0.201}{0.211}(0.800) = 0.762 \quad \text{(Equation 4.4.1-y)}$$

Point 6 (x = 4.0 in.)

$$\Delta\nu_6 = \delta_5 - \delta_6 = -1.7^\circ - (-2.6^\circ) = 0.9^\circ \text{ (expansion)}$$

$$\nu_6 = \nu_5 + \Delta\nu_6 = 45.9^\circ + 0.9^\circ = 46.8^\circ$$

$$M_6 = 2.85 \quad \text{(Figure 4.4.1-82 at } \nu_6\text{)}$$

$$\left(q/p_t\right)_6 = 0.194 \quad \text{(Figure 4.4.1-82 at } M_6\text{)}$$

$$\frac{q_6}{q_\infty} = \frac{\left(q/p_t\right)_6}{\left(q/p_t\right)_5}\frac{q_5}{q_\infty} = \frac{0.194}{0.201}(0.762) = 0.735 \quad \text{(Equation 4.4.1-y)}$$

Return to free-stream flow at TE (x = 4.0 in.)

Since $M_6 > M_\infty$, the flow is compressed by turning through an oblique shock at the upper surface trailing edge.

$$\delta' = -\alpha + \delta_{TE} = -6^\circ + (-2.6^\circ) = -8.6^\circ$$

$$\theta = 27.2^\circ \quad \text{(Figure 4.4.1-81 at } M_6 = 2.85 \text{ and } \delta' = -8.6^\circ\text{)}$$

$$\theta + \delta = 27.2^\circ - 8.6^\circ = 18.6^\circ$$

$$M_n = \left[\frac{M_{n-1}^2 \sin^2\theta + 5}{7 M_{n-1}^2 \sin^2\theta - 1}\right]^{1/2} \frac{1}{\sin(\theta + \delta')} \quad \text{(Equation 4.4.1-aa)}$$

$$M_7 = \left[\frac{M_6^2 \sin^2\theta + 5}{7 M_6^2 \sin^2\theta - 1}\right]^{1/2} \frac{1}{\sin(\theta + \delta')}$$

$$= \left[\frac{(2.85)^2 (\sin^2 27.2^\circ) + 5}{7(2.85)^2 (\sin^2 27.2^\circ) - 1}\right] \frac{1}{\sin(18.6^\circ)} = 2.46$$

$$\frac{q_n}{q_{n-1}} = \frac{60}{M_{n-1}^2} \frac{\left(1 + 0.2 M_{n-1}^2\right)^{7/2}}{\left(5 + M_{n-1}^2 \sin^2\theta\right)^{5/2}} \quad \text{(Equation 4.4.1-z)}$$

$$\frac{q_7}{q_6} = \frac{60}{M_6^2} \frac{\left(1 + 0.2\ M_6^2\right)^{7/2}}{\left(5 + M_6^2 \sin^2 \theta\right)^{5/2}} = \frac{60}{(2.85)^2} \frac{\left[1 + 0.2(2.85)^2\right]^{7/2}}{\left[5 + (2.85)^2 \left(\sin^2 27.2\right)\right]^{5/2}}$$

$$= \frac{60}{(2.85)^2} \frac{29.28}{116.0} = 1.86$$

$$\frac{q_7}{q_\infty} = \frac{q_7}{q_6} \frac{q_6}{q_\infty} = (1.86)\ (0.735) = 1.367$$

Lower surface

Point 1 ($x' = 0$)

$\Delta\nu_1 = \delta' = \alpha - \delta_{LE} = -6^o - 5.1^o = -11.1^o$ (compression)

$\theta = 33.5^o$ (Figure 4.4.1-81 at $M_\infty = 2.46$ and $\delta' = -11.1^o$)

$$\frac{q_n}{q_{n-1}} = \frac{60}{M_{n-1}^2} \frac{\left(1 + 0.2\ M_{n-1}^2\right)^{7/2}}{\left(5 + M_{n-1}^2 \sin^2 \theta\right)^{5/2}}$$ (Equation 4.4.1-z)

$$\frac{q_1}{q_\infty} = \frac{60}{M_\infty^2} \frac{\left(1 + 0.2\ M_\infty^2\right)^{7/2}}{\left(5 + M_\infty^2 \sin^2 \theta\right)^{5/2}} = \frac{60}{(2.46)^2} \frac{\left[1 + 0.2(2.46)^2\right]^{7/2}}{\left[5 + (2.46)^2\ (\sin^2 33.5^o)\right]^{5/2}}$$

$$= \frac{60}{(2.46)^2} \frac{16.06}{122.5} = 1.300$$

$$M_n = \left[\frac{M_{n-1}^2 \sin^2 \theta + 5}{7\ M_{n-1}^2 \sin^2 \theta - 1}\right]^{1/2} \frac{1}{\sin(\theta + \delta')}$$ (Equation 4.4.1-aa)

$$M_1 = \left[\frac{M_\infty^2 \sin^2 \theta + 5}{7\ M_\infty^2 \sin^2 \theta - 1}\right]^{1/2} \frac{1}{\sin(\theta + \delta')}$$

$$= \left[\frac{(2.46)^2\ (\sin^2 33.5^o) + 5}{7(2.46)^2\ (\sin^2 33.5^o) - 1}\right]^{1/2} \frac{1}{\sin\left[33.5^o + (-11.1^o)\right]}$$

$$= (0.758)\ (2.621) = 1.987$$

$\nu_1 = 26.0^o$ (Figure 4.4.1-82 at M_1)

$$\left(q/p_t\right)_1 = 0.360 \quad \text{(Figure 4.4.1-82 at } M_1\text{)}$$

Point 2 ($x' = 0.8$ in.)

$$\Delta\nu_2 = \delta_1 - \delta_2 = 5.1^o - 3.4^o = 1.7^o \text{ (expansion)}$$

$$\nu_2 = \nu_1 + \Delta\nu_2 = 26.0^o + 1.7^o = 27.7^o$$

$$M_2 = 2.05 \quad \text{(Figure 4.4.1-82 at } \nu_2\text{)}$$

$$\left(q/p_t\right)_2 = 0.348 \quad \text{(Figure 4.4.1-82 at } M_2\text{)}$$

$$\frac{q_2}{q_\infty} = \frac{\left(q/p_t\right)_2}{\left(q/p_t\right)_1}\frac{q_1}{q_\infty} = \frac{0.348}{0.360}(1.300) = 1.256 \quad \text{(Equation 4.4.1-y)}$$

Point 3 ($x' = 1.6$ in.)

$$\Delta\nu_3 = \delta_2 - \delta_3 = 3.4^o - 1.0^o = 2.4^o \text{ (expansion)}$$

$$\nu_3 = \nu_2 + \Delta\nu_3 = 27.7^o + 2.4^o = 30.1^o$$

$$M_3 = 2.14 \quad \text{(Figure 4.4.1-82 at } \nu_3\text{)}$$

$$\left(q/p_t\right)_3 = 0.329 \quad \text{(Figure 4.4.1-82 at } M_3\text{)}$$

$$\frac{q_3}{q_\infty} = \frac{\left(q/p_t\right)_3}{\left(q/p_t\right)_2}\frac{q_2}{q_\infty} = \frac{0.329}{0.348}(1.256) = 1.187 \quad \text{(Equation 4.4.1-y)}$$

Point 4 ($x' = 2.4$ in.)

$$\Delta\nu_4 = \delta_3 - \delta_4 = 1.0^o - (-0.5^o) = 1.5^o \text{ (expansion)}$$

$$\nu_4 = \nu_3 + \Delta\nu_4 = 30.1^o + 1.5^o = 31.6^o$$

$$M_4 = 2.20 \quad \text{(Figure 4.4.1-82 at } \nu_4\text{)}$$

$$\left(q/p_t\right)_4 = 0.317 \quad \text{(Figure 4.4.1-82 at } M_4\text{)}$$

$$\frac{q_4}{q_\infty} = \frac{\left(q/p_t\right)_4}{\left(q/p_t\right)_3}\frac{q_3}{q_\infty} = \frac{0.317}{0.329}(1.187) = 1.141 \quad \text{(Equation 4.4.1-y)}$$

Point 5 (x′ = 3.2 in.)

$$\Delta\nu_5 = \delta_4 - \delta_5 = -0.5^\circ - (-1.7)^\circ = 1.2^\circ \text{ (expansion)}$$

$$\nu_5 = \nu_4 + \Delta\nu_5 = 31.6^\circ + 1.2^\circ = 32.8^\circ$$

$$M_5 = 2.24 \quad \text{(Figure 4.4.1-82 at } \nu_5\text{)}$$

$$\left(q/p_t\right)_5 = 0.308 \quad \text{(Figure 4.4.1-82 at } M_5\text{)}$$

$$\frac{q_5}{q_\infty} = \frac{\left(q/p_t\right)_5}{\left(q/p_t\right)_4}\frac{q_4}{q_\infty} = \frac{0.308}{0.317}(1.141) = 1.109 \quad \text{(Equation 4.4.1-y)}$$

Point 6 (x′ = 4.0 in.)

$$\Delta\nu_6 = \delta_5 - \delta_6 = -1.7^\circ - (-2.6)^\circ = 0.9^\circ \text{ (expansion)}$$

$$\nu_6 = \nu_5 + \Delta\nu_6 = 32.8^\circ + 0.9^\circ = 33.7^\circ$$

$$M_6 = 2.28 \quad \text{(Figure 4.4.1-82 at } \nu_6\text{)}$$

$$\left(q/p_t\right)_6 = 0.300 \quad \text{(Figure 4.4.1-82 at } M_6\text{)}$$

$$\frac{q_6}{q_\infty} = \frac{\left(q/p_t\right)_6}{\left(q/p_t\right)_5}\frac{q_5}{q_\infty} = \frac{0.300}{0.308}(1.109) = 1.080 \quad \text{(Equation 4.4.1-y)}$$

Return to free-stream flow at TE (x = 4.0 in.)

Since $M_6 < M_\infty$, the flow is expanded at the lower surface trailing edge

$$\Delta\nu_7 = \Delta\nu_{TE} = \alpha + \delta_{TE} = 6^\circ + (-2.6^\circ) = 3.4^\circ$$

$$\nu_7 = \nu_6 + \Delta\nu_7 = 33.7^\circ + 3.4^\circ = 37.1^\circ$$

$$M_7 = 2.41 \quad \text{(Figure 4.4.1-82 at } \nu_7\text{)}$$

$$\left(q/p_t\right)_7 = 0.274 \quad \text{(Figure 4.4.1-82 at } M_7\text{)}$$

$$\frac{q_7}{q_\infty} = \frac{\left(q/p_t\right)_7}{\left(q/p_t\right)_6}\frac{q_6}{q_\infty} = \frac{0.274}{0.300}(1.080) = 0.986 \quad \text{(Equation 4.4.1-y)}$$

The results for q/q_∞ calculated above for the nonviscous flow field are compared with test data in Figure 4.4.1-83. A summary of the above calculations is presented in the following table.

① Surface	② Point	③ x′ (in.)	④ $\frac{z}{b_w/2}$	⑤ δ (deg)	⑥ $\frac{\Delta\nu}{④_{n-1} - ④}$ (deg)	⑦ ν $⑤ + ⑥_{n-1}$ (deg)	⑧ M (Fig 4.4.1-82)	⑨ q/p_t (Fig 4.4.1-82)	⑩ $\frac{(q/p_t)_n}{(q/p_t)_{n-1}}$ $⑨/⑨_{n-1}$	⑪ $\frac{q}{q_\infty}$ $⑨\ ⑩_{n-1}$
Upper	∞	0	0.713			38.2	2.46	0.264		1.0
	1(LE)	0	0.713	5.1	0.9	39.1	2.50	0.256	0.970	0.970
	2	0.8	0.603	3.4	1.7	40.8	2.57	0.243	0.949	0.921
	3	1.6	0.494	1.0	2.4	43.2	2.68	0.223	0.918	0.845
	4	2.4	0.384	−0.5	1.5	44.7	2.75	0.211	0.946	0.800
	5	3.2	0.275	−1.7	1.2	45.9	2.81	0.201	0.953	0.762
	6(TE)	4.0	0.165	−2.6	0.9	46.8	2.85	0.194	0.965	0.735
	7	4.0	0.165		−8.6		2.46			1.367
Lower	∞	0	−1.059				2.46			1.0
	1(LE)	0	−1.059	5.1		26.0	1.987	0.360		1.300
	2	0.8	−0.948	3.4	1.7	27.7	2.05	0.348	0.966	1.256
	3	1.6	−0.838	1.0	2.4	30.1	2.14	0.329	0.946	1.187
	4	2.4	−0.727	−0.5	1.5	31.6	2.20	0.317	0.963	1.141
	5	3.2	−0.616	−1.7	1.2	32.8	2.24	0.308	0.972	1.109
	6(TE)	4.0	−0.505	−2.6	0.9	33.7	2.28	0.300	0.974	1.080
	7	4.0	−0.505		3.4	37.1	2.41	0.274	0.913	0.986

Inside-Wake Portion (viscous flow field)

Compute:

Determine the half-width of the viscous wake at the survey plane.

Skin-friction drag coefficient

$\ell/k = \infty$; read C_f at give R_ℓ

$C_f = 0.00305$ (Figure 4.1.5.1-26)

Wave-drag coefficient

$\beta \cot \Lambda_{LE_{bw}} = 2.25 \cot (0) > 1$; leading edge is supersonic

$K = 16/3$ (Table, Page 4.1.5.1-16)

$$C_{D_w} = \frac{K}{\beta} \left(\frac{t}{c}\right)^2_{eff} \frac{S_{bw}}{S_{ref}} \quad \text{(Equation 4.1.5.1-k)}$$

$$= \frac{16}{3(2.25)} (0.05)^2 \frac{32.0}{32.0} = 0.00593$$

Zero-lift drag coefficient

$$C_{D_0} = C_{D_f} + C_{D_w} \quad \text{(Equation 4.1.5.1-h)}$$

$$= 0.00305 + 0.00593$$

$$= 0.00898$$

$$\frac{x}{\bar{c}} = \frac{6.4 - 4.0}{4.0} = 0.60 \quad \text{(x measured from wing-root-chord trailing edge)}$$

$$\frac{z_W}{\bar{c}} = 0.68 \sqrt{C_{D_0}\left(\frac{x}{\bar{c}} + 0.15\right)} \quad \text{(Equation 4.4.1-j)}$$

$$= 0.68 \sqrt{0.00898\ (0.60 + 0.15)}$$

$$= 0.0558$$

$$z_W = (0.0558)(\bar{c}) = (0.0558)(4) = 0.223 \text{ in.}$$

Determine the downwash in the plane of symmetry at the vortex sheet (wake center line).

$$\epsilon = \frac{1.62\, C_L}{\pi A} \quad \text{(Equation 4.4.1-k)}$$

$$= \frac{(1.62)(0.159)}{\pi\, 2.0}$$

$$= 0.041 \text{ rad} = 2.35 \text{ deg}$$

Calculate the vertical location, measured from the x-axis, of the intersection of the wake center line and the survey plane.

Distance of origin O below x-axis $= -[4 \sin\alpha + (6.4 - 3.97) \sin\epsilon] = -0.518$ in. In determining the dynamic-pressure ratio in the viscous region, this location is taken as the origin of the vertical distance from the wake center line to the points of interest on the survey plane.

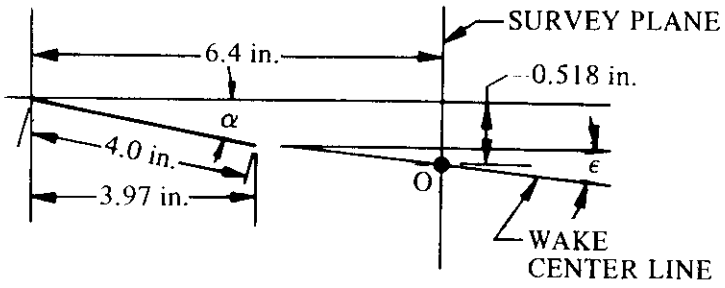

The points in the viscous wake at which the dynamic-pressure ratios are to be calculated are arbitrarily selected. For this example the following points are selected:

$z = 0$	wake center line
$z = \pm 0.08$	within the wake
$z = \pm 0.16$	within the wake
$z = \pm 0.223$	at the edges of the wake

Determine the dynamic-pressure-loss ratio at the wake center.

$$\left(\frac{\Delta q}{q}\right)_o = \frac{2.42\,(C_{D_0})^{1/2}}{\frac{x}{c} + 0.30} \quad \text{(Equation 4.4.1-m)}$$

$$= \frac{(2.42)\,(0.00898)^{1/2}}{0.60 + 0.30} = 0.255$$

Determine the dynamic-pressure-loss ratio for points not on the wake center line.

$$\frac{\Delta q}{q} = \left(\frac{\Delta q}{q}\right)_o \cos^2\left(\frac{\pi}{2}\,\frac{z}{z_w}\right) \quad \text{(Equation 4.4.1-n)}$$

$$= 0.255 \cos^2\left(\frac{\pi}{2}\,\frac{z}{z_w}\right) \text{ (see calculation table below)}$$

Solution: Viscous flow field

$$\frac{q}{q_\infty} = 1 - \frac{\Delta q}{q} \quad \text{(Equation 4.4.1-o) (see calculation table below)}$$

①	②	③	④	⑤
z (in.) (measured from origin O)	$\frac{z}{z_W}$ ① /0.223	$\frac{\pi}{2}\frac{z}{z_W}$ (rad)	$\Delta q/q$ (Eq. 4.4.1-n) $0.255 \cos^2$ ③	q/q_∞ (Eq. 4.4.1-o) 1 - ④
-0.223	-1.0	$-\pi/2$	0	1.00
0.160	-0.717	-1.127	0.047	0.953
-0.080	-0.359	-0.564	0.182	0.818
0	0	0	0.255	0.745
0.080	0.359	0.564	0.182	0.818
0.160	0.717	1.127	0.047	0.953
0.223	1.0	$\pi/2$	0	1.00

The calculated results for both the nonviscous and viscous flow fields are compared with test data in Figure 4.4.1-83. The results are plotted as a function of $\frac{z}{b_W/2}$, where z is measured from the x-axis. The wake center is at $\frac{z}{b_W/2} = \frac{-0.518}{4.0} = -0.1295$.

REFERENCES

1. Decker, J. L.: Prediction of Downwash at Various Angles of Attack for Arbitrary Tail Locations. Aeronautical Engineering Review, Vol. 15, No. 8, 1956. (U)

2. Lange, R. H., and Fink, M. P.: Studies of the Flow Field Behind a Large Scale 47.5° Sweptback Wing Having Circular-Arc Airfoil Sections and Equipped With Drooped-Nose and Plain Flaps. NACA RM L51L12, 1952. (U)

3. Pitts, W., Nielsen, J., and Kaattari, G.: Lift and Center of Pressure of Wing-Body-Tail Combinations at Subsonic, Transonic, and Supersonic Speeds. NACA TR1307, 1957. (U)

4. Neely, R. H., and Griner, R. F.: Summary and Analysis of Horizontal-Tail Contribution to Longitudinal Stability of Swept-Wing Airplanes at Low Speeds. NASA TR R-49, 1959. (U)

5. Ribner, H. S.: Notes on the Propeller Slipstream in Relation to Stability. NACA WR L-25, 1944. (U)

6. Glauert, H.: The Elements of Airfoil and Airscrew Theory. Cambridge University Press, Cambridge, Great Britain, 1948. (U)

7. Sanders, K. L.: An Empirical Method for the Estimation of Downwash. Ryan Rpt. No. 29254-2A, 1967. (U)

8. Silverstein, A., and Katzoff, S.: Design Charts for Predicting Downwash Angles and Wake Characteristics Behind Plain and Flapped Wings. NACA TR 648, 1939. (U)

9. Hoggard, H. P., Jr., and Hagerman, J. R.: Downwash and Wake Behind Untapered Wings of Various Aspect Ratios and Angles of Sweep. NACA TN 1703, 1948. (U)

10. Nielsen, J. N.: The Effects of Body Vortices and the Wing Shock-Expansion Field on the Pitch-Up Characteristics of Supersonic Airplanes. NACA RM A57L23, 1958. (U)

11. Bobbitt, P. J.: Tables for the Rapid Estimation of Downwash and Sidewash Behind Wings Performing Various Motions at Supersonic Speeds. NASA Memo 2-20-59L, 1959. (U)

12. Martin, J. C., and Jeffreys, I.: Span Load Distributions Resulting from Angle of Attack, Rolling, and Pitching for Tapered Sweptback Wings with Streamwise Tips — Supersonic Leading and Trailing Edges. NACA TN 2643, 1952. (U)

13. Martin, J. C.: The Calculation of Downwash Behind Wings of Arbitrary Plan Form at Supersonic Speeds. NACA TN 2135, 1950. (U)

14. Huefeli, R. C., Mirels, H., and Cummings, J. L.: Charts for Estimating Downwash Behind Rectangular, Trapezoidal, and Triangular Wings at Supersonic Speeds. NACA TN 2141, 1950. (U)

15. Centolanzi, F. J.: Measured and Theoretical Flow Fields Behind a Rectangular and a Triangular Wing Up to High Angles of Attack at a Mach Number of 2.46. NASA TN D-92, 1959. (U)

16. Schaaf, S. A., and Talbot, L.: Handbook of Supersonic Aerodynamics, Section 6, Two-Dimensional Airfoils. NAVORD Report 1488 (Vol. 3), June 1957. (U)

17. Ames Research Staff: Equations, Tables, and Charts for Compressible Flow. NACA TR 1135, 1953. (U)

18. Purser, P. E., Spearman, M. L., and Bates, W. R.: Preliminary Investigation at Low Speed of Downwash Characteristics of Small-Scale Sweptback Wings. NACA TN 1378, 1947. (U)

19. Anderson, A. E.: An Investigation at Low Speed of a Large-Scale Triangular Wing of Aspect Ratio Two. – The Effect of Airfoil Section Modifications and the Determination of the Wake Downwash. NACA RM A7H28, 1947. (U)

20. Jaquet, B. M.: Effects of Horizontal Tail Position, Area, and Aspect Ratio on Low-Speed Static Longitudinal Stability and Control Characteristics of a 60° Triangular-Wing Model Having Various Triangular All-Movable Horizontal Tails. NACA RM L51I06, 1951. (U)

21. Griner, R. F., and Foster, G. V.: Low-Speed Longitudinal and Wake Air-Flow Characteristics at a Reynolds Number of 6.0×10^6 of a 52° Sweptback Wing Equipped With Various Spans of Leading-Edge and Trailing-Edge Flaps, a Fuselage, and a Horizontal Tail at Various Vertical Positions. NACA RM L50K29, 1951. (U)

22. Salmi, R. J., and Jacques, W. A.: Effect of Vertical Location of a Horizontal Tail on the Static Longitudinal Stability Characteristics of a 45° Sweptback-Wing-Fuselage Combination of Aspect Ratio 8 at a Reynolds Number of 4.0×10^6. NACA RM L51J08, 1952. (U)

23. Hadaway, W. M., and Cancro, P. A.: Low-Speed Longitudinal Characteristics of Two Unswept Wings of Hexagonal Airfoil Sections Having Aspect Ratios of 2.5 and 4.0 With Fuselage and Horizontal Tail Located at Various Vertical Positions. NACA RM L53H14a, 1953. (U)

24. Foster, G. V., Mollenberg, E. F., and Woods, R. L.: Low-Speed Longitudinal Characteristics of an Unswept Hexagonal Wing With and Without a Fuselage and a Horizontal Tail Located at Various Positions at Reynolds Numbers From 2.8×10^6 to 7.6×10^6. NACA RM L52L11b, 1953. (U)

25. Ross, J. G., et al: Wind-Tunnel Tests on a 90° Apex Delta Wing of Variable Aspect Ratio (Sweepback 36.8°). ARC CP 83, 1952. (U)

26. Foster, G. V.: Longitudinal Stability and Wake-Flow Characteristics of a Twisted and Cambered Wing-Fuselage Combination of 45° Sweepback and Aspect Ratio 8 With a Horizontal Tail and Stall-Control Devices at a Reynolds Number of 4.0×10^6. NACA RM L53D08, 1953. (U)

27. Foster, G. V., and Griner, R. F.: Low-Speed Longitudinal and Wake Air-Flow Characteristics at a Reynolds Number of 5.5×10^6 of a Circular-Arc 52° Sweptback Wing With a Fuselage and a Horizontal Tail at Various Vertical Positions. NACA RM L51C30, 1951. (U)

28. Spooner, S. H., and Martina, A. P.: Longitudinal Stability Characteristics of a 42° Sweptback Wing and Tail Combination at a Reynolds Number of 6.8×10^6. NACA RM L8E12, 1948. (U)

29. Woods, R. L., and Spooner, S. H.: Effects of High-Lift and Stall-Control Devices, Fuselage, and Horizontal Tail on a Wing Swept Back 42° at the Leading Edge and Having Symmetrical Circular-Arc Airfoil Sections at a Reynolds Number of 6.9×10^6. NACA RM L9B11, 1949. (U)

30. Graham, D., and Koenig, D. G.: Tests in the Ames 40- by 80-Foot Wind Tunnel of an Airplane Configuration With an Aspect Ratio 4 Triangular Wing and an All-Movable Horizontal Tail – Longitudinal Characteristics. NACA RM A51H10a, 1951. (U)

31. Franks, R. W.: Tests in the Ames 40- by 80-Foot Wind Tunnel of Two Airplane Models Having Aspect Ratio 2 Trapezoidal Wings of Taper Ratios 0.33 and 0.20. NACA RM A52L16, 1953. (U)

32. Graham, D., and Koenig, D. B.: Tests in the Ames 40- by 80-Foot Wind Tunnel of an Airplane Configuration With an Aspect Ratio 2 Triangular Wing and an All-Movable Horizontal Tail – Longitudinal Characteristics. NACA RM A51B21, 1951. (U)

33. Salmi, R. J.: Horizontal-Tail Effectiveness and Downwash Surveys for Two 47.7° Sweptback Wing-Fuselage Combinations With Aspect Ratios of 5.1 and 6.0 at a Reynolds Number of 6.0×10^6. NACA RM L50K06, 1951. (U)

34. Franks, R. W.: Tests in the Ames 40- by 80-Foot Wind Tunnel of an Airplane Model With an Aspect Ratio 4 Triangular Wing and an All-Movable Horizontal Tail – High-Lift Devices and Lateral Controls. NACA RM A52K13, 1953. (U)

35. Goodson, K. W., and Few, A. G., Jr.: Low-Speed Static Longitudinal and Lateral Stability Characteristics of a Model with Leading-Edge Chord-Extensions Incorporated on a 40° Sweptback Circular-Arc Wing of Aspect Ratio 4 and Taper Ratio 0.50. NACA RM L52I18, 1952. (U)

36. Schuldenfrei, M., Comisarow, P., and Goodson, K. W.: Stability and Control Characteristics of a Complete Airplane Model Having a Wing With Quarter-Chord Line Swept Back 40°, Aspect Ratio 2.50, and Taper Ratio 0.42. NACA TN 2482, 1951. (U)

37. Weil, J., Sleeman, W. C., and Byrnes, A. L., Jr.: Investigation of the Effects of Wing and Tail Modifications on the Low-Speed Stability Characteristics of a Model Having a Thin 40° Swept Wing of Aspect Ratio 3.5. NACA RM L53C09, 1953. (U)

38. Perkins, E. W., and Canning, T. N.: Investigation of Downwash and Wake Characteristics at a Mach Number of 1.53. I – Rectangular Wing. NACA RM A8L16, 1949. (U)

39. Spearman, M. L., and Hilton, J. H., Jr.: An Investigation of a Supersonic Aircraft Configuration Having a Tapered Wing with Circular-Arc Sections and 40° Sweepback. Static Longitudinal Stability and Control Characteristics at a Mach Number of 1.59. NACA RM L50E12, 1950. (U)

40. Spearman, M. L.: An Investigation of a Supersonic Aircraft Configuration Having a Tapered Wing with Circular-Arc Sections and 40° Sweepback. Static Longitudinal Stability and Control Characteristics at a Mach Number of 1.40. NACA RM L9L08, 1950. (U)

41. Grant, F. C., and Gapcynski, J. P.: An Investigation of a Supersonic Aircraft Configuration Having a Tapered Wing with Circular-Arc Sections and 40° Sweepback. Estimated Downwash Angles Derived from Pressure Measurements on the Tail at Mach Numbers of 1.40 and 1.59. NACA RM L51L17, 1952. (U)

42. Ellis, M. C., Jr., and Grigsby, C. E.: Aerodynamic Investigation at Mach Number of 1.92 of a Rectangular Wing and Tail and Body Configuration and Its Components. NACA RM L9L28a, 1950. (U)

43. Grigsby, C. E.: An Investigation at Mach Numbers of 1.62 and 1.93 of the Lift Effectiveness and Integrated Downwash Characteristics of Several In-Line Missile Configurations Having Equal-Span Wings and Tails. NACA RM L52A02, 1952. (U)

44. Adamson, D., and Boatright, W. B.: Investigation of Downwash, Sidewash, and Mach Number Distribution Behind a Rectangular Wing at a Mach Number of 2.41. NACA RM L50G12, 1950. (U)

45. Boatright, W. B.: An Analysis of Pressure Studies and Experimental and Theoretical Downwash and Sidewash Behind Five Pointed-Tip Wings at Supersonic Speeds. NACA RM L54B10, 1954. (U)

TABLE 4.4.1-A

SUBSONIC DOWNWASH GRADIENT BEHIND STRAIGHT-TAPERED WINGS
METHOD 1

DATA SUMMARY AND SUBSTANTIATION

Ref.	A	λ	$\Lambda_{c/4}$ (deg)	$\frac{b_H}{b}$	$\frac{2\ell_H}{b}$	$\frac{2h_H}{b}$	$\partial\bar{\epsilon}/\partial\alpha$ Calc. ($\alpha = 0$)	$\partial\bar{\epsilon}/\partial\alpha$ Test	$\lvert\Delta\bar{\epsilon}\rvert$ Average Error (deg)
18	4.00	1.00	40.0	0.50	1.00	0.18	0.518	0.400	0.8
					1.50		0.491	0.335	0.6
	2.50	1.00	40.0	0.80	1.60	0.29	0.619	0.520	1.0
					2.40		0.600	0.465	1.0
				0.50	1.50		0.600	0.440	1.8
						0.03	0.720	0.510	1.0
					2.30	0.29	0.583	0.360	2.1
						0.03	0.695	0.400	0.8
	3.00	1.625	37.5	0.50	1.36	0.43	0.465	0.300	0.9
						0.21	0.550	0.400	0.6
						0.03	0.620	0.420	0.7
					1.91	0.43	0.451	0.270	0.7
						0.22	0.528	0.320	1.1
						0.04	0.596	0.400	0.3
19	2.00	0	56.5	0.378	1.64	0	0.730	0.710	1.0
					1.96		0.686	0.660	0.5
					2.28		0.658	0.630	0.7
20	2.31	0	52.4	0.316	1.73	0.870	0.363	0.330	0.6
						0.290	0.586	0.570	0.1
						−0.060	0.657	0.720	0.6
21	2.88	0.625	50.0	0.48	1.229	0.504	0.446	0.390	0.7
						0.196	0.554	0.500	0.8
						−0.074	0.588	0.500	4.3
22	8.0	0.45	45.0	0.282	0.785	−0.060	0.317	0.375	1.3
						0.140	0.310	0.310	2.4
						0.300	0.284	0.238	1.9
23	4.00	0.625	3.4	0.50	1.66	−0.177	0.472	0.390	2.5
						0.177	0.558	0.490	2.1
						0.400	0.472	0.380	1.0
24	2.50	0.625	5.3	0.50	1.63	−0.177	0.839	0.600	3.9
						0.177	0.831	0.600	2.2
						0.400	0.646	0.550	1.0
					2.44	0.177	0.730	0.600	0.8
						0.400	0.620	0.440	2.7

TABLE 4.4.1-A (CONTD)

Ref.	A	λ	$\Lambda_{c/4}$ (deg)	$\frac{b_H}{b}$	$\frac{2\ell_H}{b}$	$\frac{2h_H}{b}$	$\partial\bar{\epsilon}/\partial\alpha$ Calc. ($\alpha = 0$)	$\partial\bar{\epsilon}/\partial\alpha$ Test	$\lvert\Delta\bar{\epsilon}\rvert$ Average Error (deg)
25	2.30	0.25	36.8	0.35	1.37	0	0.800	0.770	0.3
						0.223	0.720	0.645	0.4
						0.450	0.614	0.500	0.5
	3.00	0.14	36.8	0.30	1.17	0.200	0.663	0.615	0.3
					0.78	0.388	0.840	0.560	1.2
						0.200	0.786	0.660	0.7
26	8.00	0.45	45.0	0.28	0.767	0.300	0.285	0.310	2.1
						0.140	0.308	0.285	4.3
						−0.060	0.516	0.320	1.7
27	2.84	0.616	50.0	0.48	1.229	0.442	0.453	0.380	1.9
						0.136	0.570	0.500	2.1
						−0.132	0.580	0.500	3.1
28	4.00	0.625	40.0	0.40	1.018	−0.060	0.520	0.500	3.8
						0.160	0.525	0.500	3.7
						0.420	0.443	0.410	4.0
29	3.94	0.625	40.0	0.40	1.033	−0.011	0.512	0.475	1.7
						0.211	0.560	0.400	2.0
						0.339	0.525	0.410	2.2
30	4.00	0	36.9	0.52	1.275	0	0.640	0.560	0.3
						0.360	0.551	0.430	1.3
31	2.00	0.33	36.9	0.78	1.95	0	1.034	0.760	1.4
				0.67		0.537	0.727	0.510	0.5
32	2.00	0	56.3	0.74	1.80	0	0.870	0.660	0.7
				0.63		0.254	0.635	0.660	0.7
						0.506	0.500	0.500	0.7
33	5.10	0.383	45.0	0.366	0.928	0.382	0.379	0.331	0.2
						−0.053	0.455	0.437	2.8
	6.00	0.313		0.328	0.800	0.343	0.353	0.312	0.7
						−0.048	0.355	0.410	1.6

Average $\lvert\Delta\bar{\epsilon}\rvert$ = 1.45

TABLE 4.4.1-B

SUBSONIC DOWNWASH GRADIENT BEHIND STRAIGHT-TAPERED WINGS
METHOD 2

DATA SUMMARY AND SUBSTANTIATION

Ref.	A	λ	$\Lambda_{c/4}$ (deg)	$\frac{b_H}{b}$	$\frac{2\ell_H}{b}$	$\frac{2h_H}{b}$	$\partial\bar{\epsilon}/\partial\alpha$ Calc.	$\partial\bar{\epsilon}/\partial\alpha$ Test	e Percent Error
18	4.00	1.00	40.0	0.50	1.00	0.18	0.386	0.400	− 3.5
					1.50		0.326	0.335	− 2.7
	2.50	1.00	40.0	0.80	1.60	0.29	0.439	0.520	−15.6
					2.40		0.377	0.465	−18.9
				0.50	1.50		0.451	0.440	2.5
						0.03	0.537	0.510	5.3
					2.30	0.29	0.382	0.360	6.1
						0.03	0.451	0.400	12.8
	3.00	1.625	37.5	0.50	1.36	0.43	0.263	0.300	−12.3
						0.21	0.338	0.400	−15.5
						0.03	0.377	0.420	−10.2
					1.91	0.43	0.229	0.270	−15.2
						0.22	0.266	0.320	−16.9
						0.04	0.297	0.400	−25.8
19	2.00	0	56.5	0.378	1.64	0	0.790	0.710	11.3
					1.96		0.737	0.660	11.7
					2.28		0.693	0.630	10.0
20	2.31	0	52.4	0.316	1.73	0.870	0.377	0.330	12.5
						0.290	0.595	0.570	4.4
						−0.060	0.702	0.720	− 2.5
21	2.88	0.625	50.0	0.48	1.229	0.504	0.400	0.390	2.6
						0.196	0.497	0.500	− 0.6
						−0.074	0.539	0.500	7.8
22	8.0	0.45	45.0	0.282	0.785	−0.060	0.324	0.375	−13.6
						0.140	0.310	0.310	0
						0.300	0.275	0.238	15.5
23	4.00	0.625	3.4	0.50	1.66	−0.177	0.446	0.390	14.3
						0.177	0.446	0.490	− 9.0
						0.400	0.382	0.380	0.5
24	2.50	0.625	5.3	0.50	1.63	−0.177	0.664	0.600	10.7
						0.177	0.664	0.600	10.7
						0.400	0.566	0.550	2.9
					2.44	0.177	0.559	0.600	− 6.8
						0.400	0.482	0.440	9.5

TABLE 4.4.1-8 (CONTD)

Ref.	A	λ	$\Lambda_{c/4}$ (deg)	$\frac{b_H}{b}$	$\frac{2\ell_H}{b}$	$\frac{2h_H}{b}$	$\partial\bar{\epsilon}/\partial\alpha$ Calc.	$\partial\bar{\epsilon}/\partial\alpha$ Test	e Percent Error
25	2.30	0.25	36.8	0.35	1.37	0	0.875	0.770	13.6
						0.223	0.764	0.645	18.4
						0.450	0.648	0.500	29.6
	3.00	0.14	36.8	0.30	1.17	0.200	0.693	0.615	12.7
					0.78	0.388	0.710	0.560	26.8
						0.200	0.813	0.660	23.2
26	8.00	0.45	45.0	0.28	0.767	0.300	0.280	0.310	− 9.7
						0.140	0.313	0.285	9.8
						−0.060	0.329	0.320	2.8
27	2.84	0.616	50.0	0.48	1.229	0.442	0.417	0.380	9.7
						0.136	0.515	0.500	3.0
						−0.132	0.515	0.500	3.0
28	4.00	0.625	40.0	0.40	1.018	−0.060	0.497	0.500	− 0.6
						0.160	0.470	0.500	− 6.0
						0.420	0.389	0.410	− 5.1
29	3.94	0.625	40.0	0.40	1.033	−0.011	0.526	0.475	10.7
						0.211	0.463	0.400	15.8
						0.339	0.429	0.410	4.6
30	4.00	0	36.9	0.52	1.275	0	0.622	0.560	11.1
						0.360	0.488	0.430	13.5
31	2.00	0.33	36.9	0.78	1.95	0	0.804	0.760	5.8
				0.67		0.537	0.559	0.510	9.6
32	2.00	0	56.3	0.74	1.80	0	0.764	0.660	13.0
				0.63		0.254	0.648	0.660	− 1.8
						0.506	0.539	0.500	7.8
33	5.10	0.383	45.0	0.366	0.928	0.382	0.335	0.331	7.3
						−0.053	0.439	0.437	0.5
	6.00	0.313		0.328	0.800	0.343	0.346	0.312	10.9
						−0.048	0.417	0.410	1.7

Average Error = $\frac{\Sigma \mid e \mid}{n}$ = 9.7%

TABLE 4.4.1-C
SUBSONIC CHANGE IN DOWNWASH ANGLE DUE TO SLOTTED-FLAP DEFLECTION
DATA SUMMARY AND SUBSTANTIATION

Ref.	A	$\Lambda_{c/4}$ (deg)	b_f/b	$\frac{h_H}{b/2}$	ΔC_L	δ_f (deg)	$\Delta\epsilon_{calc.}$	$\Delta\epsilon_{test}$	$\Delta\epsilon_{test} - \Delta\epsilon_{calc.}$
31	2.0	36.9	0.809	0	0.57	40	9.93	8.8	−1.13
↓	2.0	45.0	0.778	0	0.55	40	9.97	8.7	−1.27
33	5.1	45.4	0.288	0.382	0.44	40	3.55	2.5	−1.05
↓	5.1	45.4	0.288	−0.053	0.42	40	9.49	6.5	−3.0
↓	6.0	45.4	0.35	0.343	0.55	40	3.30	3.3	0
↓	6.0	45.4	0.35	−0.048	0.57	40	8.88	5.5	−3.38
34	4.0	36.9	0.539	0	0.61	40	7.98	8.4	0.42
Unpub. data	6.8	35.0	0.524	0.0862	1.01	50	6.22	3.6	−2.62
↓	6.8	35.0	0.524	0.0862	0.63	25	3.88	2.3	−1.58
↓	8.5	24.0	0.547	0.466	1.23	50	2.80	2.8	0
↓	8.7	24.5	0.522	0.441	1.08	50	2.59	3.3	0.71
↓	7.0	30.6	0.475	0.093	0.84	50	5.46	5.3	−0.16
↓	7.5	30.6	0.456	0.089	0.84	50	5.34	6.0	0.66
↓	7.8	−0.5	0.467	0.071	0.96	40	6.06	4.9	−1.16
↓	6.2	2.7	0.403	0.157	0.67	40	4.88	5.1	0.22
↓	9.4	2.0	0.503	0.085	0.62	30	2.89	2.9	0.01
↓	9.4	2.0	0.503	0.088	1.16	50	5.35	4.9	−0.45
↓	12.1	−0.6	0.517	0.033	0.73	25	2.88	3.2	0.32
↓	12.1	−0.6	0.517	0.033	1.50	50	5.92	6.3	0.38
↓	6.25	2.0	0.529	0.28	0.39	20	1.66	2.2	0.54
↓	6.25	2.0	0.529	0.28	0.71	40	3.03	4.0	0.97

TABLE 4.4.1-D
SUBSONIC CHANGE IN DOWNWASH ANGLE DUE TO PLANE FLAP DEFLECTION
DATA SUMMARY AND SUBSTANTIATION

Ref.	A	$\Lambda_{c/4}$ (deg)	b_f/b	h_H b/2	ΔC_L	δ_f (deg)	$\Delta\epsilon_{calc.}$	$\Delta\epsilon_{test}$	$\Delta\epsilon_{test} - \Delta\epsilon_{calc.}$
23	4.0	3.4	0.393	0.40	0.33	50	1.89	3.0	1.11
↓	↓	↓	↓	0.177	↓	↓	2.85	3.1	0.25
↓	↓	↓	↓	−0.177	↓	↓	6.02	6.3	0.28
↓	2.5	5.3	0.35	0.40	0.26	↓	2.67	2.6	−0.07
↓	↓	↓	↓	0.177	↓	↓	4.04	3.9	−0.14
↓	↓	↓	↓	−0.177	↓	↓	8.53	8.3	−0.23
35	4.0	40	0.496	0.246	0.39	50	2.29	2.4	0.11
24	2.5	6.4	0.35	0.4	0.28	50	2.88	2.9	0.02
↓	↓	↓	0.75	0.4	0.47	↓	2.26	3.5	1.24
36	2.5	40	0.814	0.322	0.28	50	1.37	1.2	−0.17
↓	↓	↓	↓	↓	0.25	↓	1.22	1.2	−0.02
37	3.5	40	0.363	0.36	0.315	40	2.33	2.4	0.07

TABLE 4.4.1-E

SUBSONIC DYNAMIC-PRESSURE RATIO

DATA SUMMARY AND SUBSTANTIATION

Ref	A	Λ_{LE} (deg)	λ	$\frac{x}{c}$	$\frac{z}{c}$	α (deg)	q/q_∞ Calc.	q/q_∞ Test	e Percent Error
9	3.0	0	1.0	2.0	0	0	0.88	0.90	−2.2
	↓	↓	↓	↓	↓	1	0.89	0.92	−3.3
						2	0.92	0.94	−2.1
						3	0.95	0.95	0
						4	0.98	0.96	2.1
	↓	↓	↓	↓	↓	6	1.00	0.96	4.2
	6.0	0	1.0	2.0	0	0	0.88	0.87	1.1
	↓	↓	↓	↓	↓	1	0.89	0.89	0
						2	0.93	0.92	1.1
						3	0.97	0.93	4.3
						4	0.99	0.95	4.2
	↓	↓	↓	↓	↓	6	1.00	0.97	3.1
	6.0	0	1.0	2.0	0.28	6	1.00	0.97	3.1
	↓	↓	↓	↓	↓	8	0.98	0.96	2.1
						10	0.91	0.93	−2.2
	4.5	30.0	1.0	2.0	0	0	0.88	0.96	−8.3
	↓	↓	↓	↓	↓	1	0.89	0.96	−7.3
						2	0.92	0.95	−3.2
						3	0.95	0.95	0
						4	0.98	0.94	4.3
	↓	↓	↓	↓	↓	6	1.00	0.98	2.0
	5.2	30.0	1.0	2.0	0	0	0.88	0.95	−7.4
	↓	↓	↓	↓	↓	1	0.89	0.94	−5.3
						2	0.92	0.94	−2.1
						3	0.96	0.94	2.1
						4	0.99	0.94	5.3
					↓	6	1.00	0.96	4.2
					0.28	6	1.00	1.01	−1.0
					↓	8	0.996	1.02	−2.4
						10	0.94	1.02	−7.8
↓	↓	↓	↓	↓	↓	12	0.88	1.01	−13.0

TABLE 4.4.1-E (CONTD)

Ref.	A	Λ_{LE} (deg)	λ	$\frac{x}{\bar{c}}$	$\frac{z}{\bar{c}}$	α (deg)	q/q_∞ Calc.	q/q_∞ Test	e Percent Error
9	1.5	60.0	1.0	2.0	0	0	0.89	0.95	−6.3
						1	0.895	0.95	−5.8
						2	0.91	0.95	−4.2
						3	0.93	0.94	−1.1
						4	0.96	0.94	2.1
						6	0.99	0.97	2.1
						8	1.00	1.00	0
	3.0	60.0	1.0	3.0	0	0	0.92	0.92	0
						1	0.93	0.93	0
						2	0.96	0.95	1.1
						3	0.99	0.97	2.1
						4	1.00	0.99	1.0
2	3.5	47.5	0.5	1.213	0	0	0.85	–	–
						1	0.86	–	–
						2	0.89	–	–
						3	0.93	0.86	8.1
						4	0.96	0.88	9.1
						6	1.00	0.92	8.7
5	4.01	42.0	0.625	1.814	0.25	8	1.00	1.00	0
						10	0.98	1.00	−2.0
						12	0.95	1.00	−5.0
						13.1	0.91	1.00	−9.0
						14	0.90	0.98	−8.2
6	4.00	42.0	0.5	2.504	0	0	0.93	0.94	−1.1
						1	0.94	0.95	−1.1
						2	0.97	0.96	1.0
						3	0.98	0.96	2.1
						4	1.00	0.97	3.1

$$\text{Average Error} = \frac{\Sigma|e|}{n} = 3.5\%$$

TABLE 4.4.1-F
SUPERSONIC DOWNWASH GRADIENT BEHIND STRAIGHT-TAPERED WINGS
METHOD 2
DATA SUMMARY AND SUBSTANTIATION

Ref.	A	λ	Λ_{LE} (deg)	$\frac{2x}{b}$	$\frac{2y}{b}$	$\frac{2z}{b}$	$\partial\bar{\epsilon}/\partial\alpha$ Calc.	$\partial\bar{\epsilon}/\partial\alpha$ Test	$\Delta\partial\bar{\epsilon}/\partial\alpha$
38	3.5	1.0	0	1.72	0.10	0.20	0.23	0.26	−0.03
				↓	0.30	↓	0.26	0.38	−0.12
				1.72	0.10	0.40	0.14	0.14	0
				↓	0.30	↓	0.16	0.12	0.04
				2.52	0.10	0.20	0.31	0.35	−0.04
				↓	0.30	↓	0.35	0.39	−0.04
39	4.0	0.5	42.7	1.39	0.176	0.22	0.20	0.18	0.02
40	4.0	0.5	42.7	1.39	0.176	0.22	0.18	0.214	−0.034
41	4.0	0.5	42.7	1.39	0.176	0.206	0.20	0.244	−0.044
	↓	↓	↓	1.38	↓	0.013	0.24	0.325	−0.085
	4.0	0.5	42.7	1.39	0.176	0.206	0.24	0.21	0.03
	↓	↓	↓	↓	↓	0.11	0.28	0.32	−0.04
42	4.0	1.0	0	1.85	0.25	0.35	0	0.06	−0.06
↓	↓	↓	↓	↓	↓	0.175	0.04	0	0.04
↓	↓	↓	↓	1.55	↓	↓	0	−0.02	0.02
43	3.11	1.0	0	2.73	0.333	0	0.28	0.14	0.14
↓	↓	↓	↓	↓	↓	↓	0.38	0.30	0.08
44	2.34	1.0	0	2.13	0.286	0	0.06	0.08	−0.02
↓	↓	↓	↓	↓	↓	↓	0.03	0.07	−0.04
↓	↓	↓	↓	2.98	↓	0.309	0.14	0.12	0.02
↓	↓	↓	↓	↓	↓	0	0.22	0.14	0.08
↓	↓	↓	↓	↓	↓	−0.309	0.14	0.13	0.01
↓	↓	↓	↓	↓	↓	0.309	0.17	0.085	0.085
↓	↓	↓	↓	↓	↓	0	0.21	0.145	0.065
↓	↓	↓	↓	↓	↓	−0.309	0.17	0.14	0.03
↓	↓	↓	↓	↓	↓	−0.10	0.215	0.145	0.07
45	3.36	0	50	3.0	0.4	0.134	0.40	0.40	0
↓	↓	↓	↓	↓	0.6	↓	0.32	0.32	0
↓	↓	↓	↓	↓	0.8	↓	0.22	0.14	0.08
↓	↓	↓	↓	↓	0.4	−0.089	0.43	0.32	0.11
↓	↓	↓	↓	↓	↓	−0.315	0.29	0.24	0.05
↓	↓	↓	↓	↓	0.6	↓	0.21	0.17	0.04
↓	↓	↓	↓	↓	0.8	↓	0.10	−0.07	0.17

TABLE 4.4.1-F (CONTD)

Ref.	A	λ	Λ_{LE} (deg)	2x/b	2y/b	2z/b	$\partial\bar{\epsilon}/\partial\alpha$ Calc.	$\partial\bar{\epsilon}/\partial\alpha$ Test	$\Delta\partial\bar{\epsilon}/\partial\alpha$
45	3.36	0	50	3.0	0.4	0.346	0.26	0.29	−0.03
						0.130	0.40	0.39	0.01
						−0.093	0.44	0.40	0.04
						−0.317	0.27	0.29	−0.02
					0.35	0.394	0.03	0.08	−0.05
					0.4		0	0.08	−0.08
					0.35	−0.049	0.27	0.29	−0.02
					0.4		0.24	0.24	0
					0.6		0.14	0.13	0.01
					0.8		0.05	0	0.05
					0.35	−0.345	0.05	0.10	−0.05
	2.04	0	63	3.0	0.4	0.386	0.23	0.22	0.01
					0.6		0.14	0.10	0.04
					0.8		0.03	−0.02	0.05
					0.4	−0.049	0.46	0.52	−0.06
					0.6		0.36	0.36	0
					0.8		0.26	0.25	0.01
				4.9	0.275	0.386	0.33	0.28	0.05
						−0.103	0.52	0.42	0.10
						−0.348	0.35	0.28	0.07
Average $\lvert\Delta\partial\bar{\epsilon}/\partial\alpha\rvert$ = 0.045									

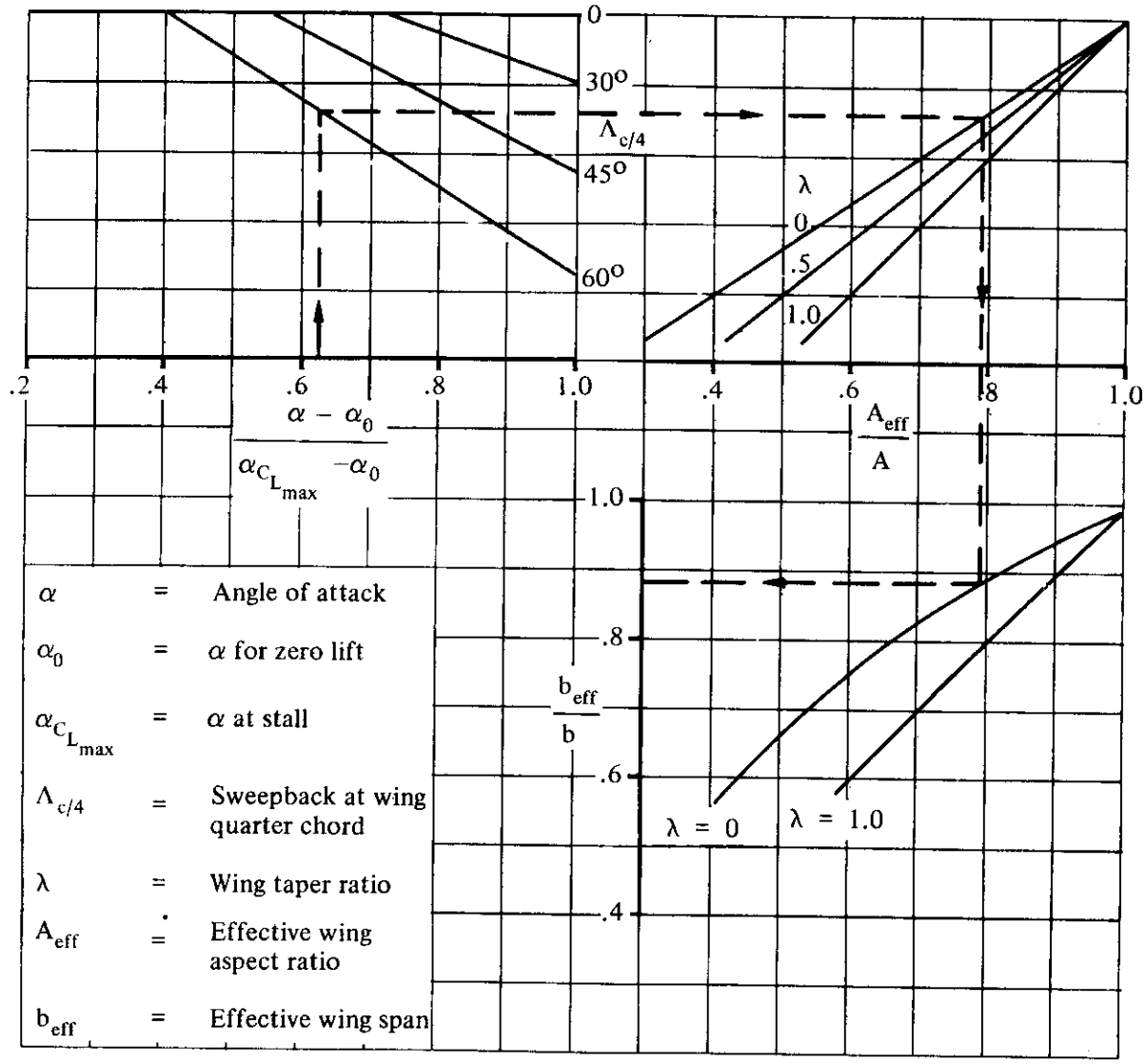

FIGURE 4.4.1-66 EFFECTIVE WING ASPECT RATIO AND SPAN – LOW SPEEDS

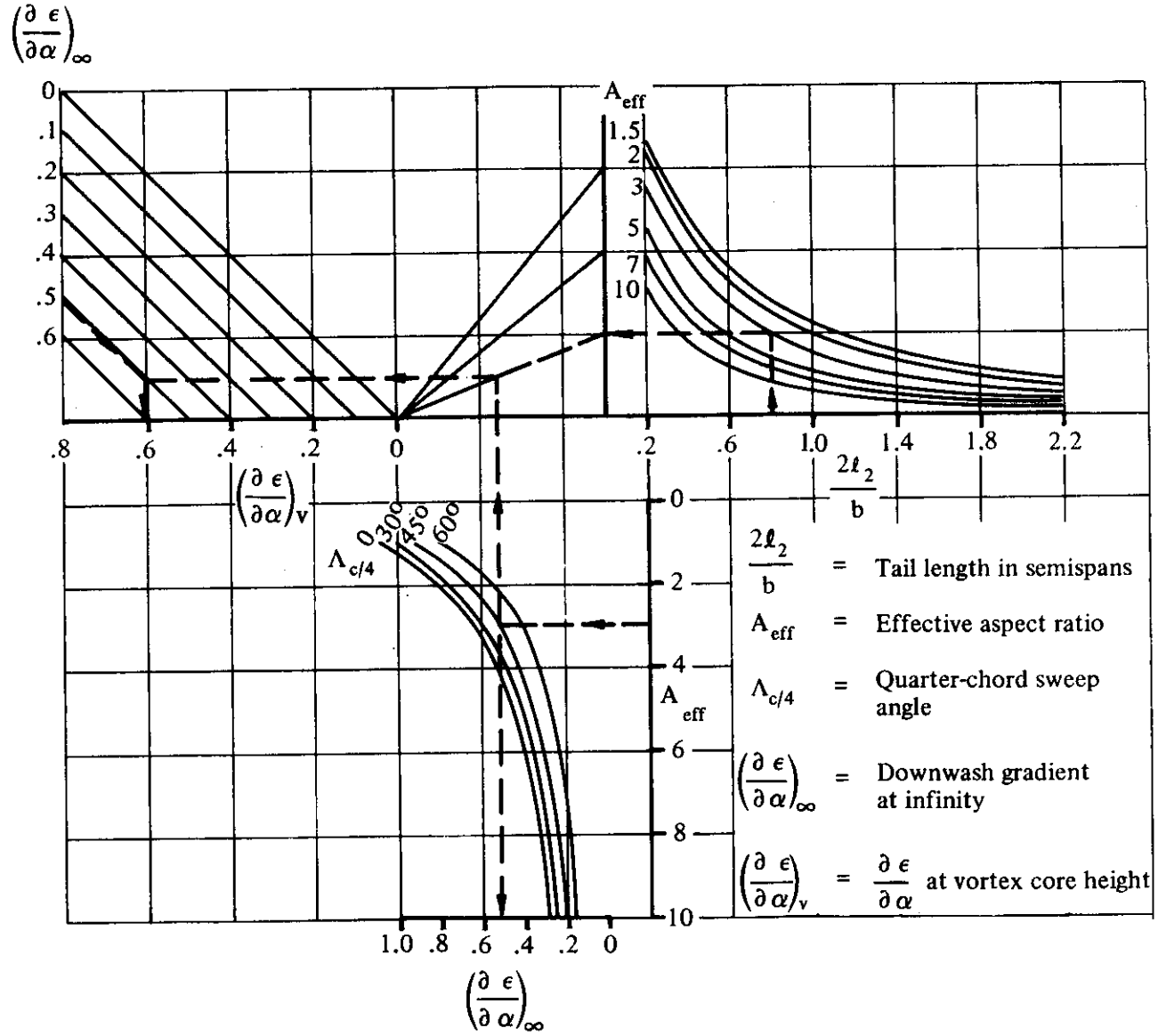

FIGURE 4.4.1-67 DOWNWASH AT THE PLANE OF SYMMETRY AND HEIGHT OF VORTEX CORE – LOW SPEEDS

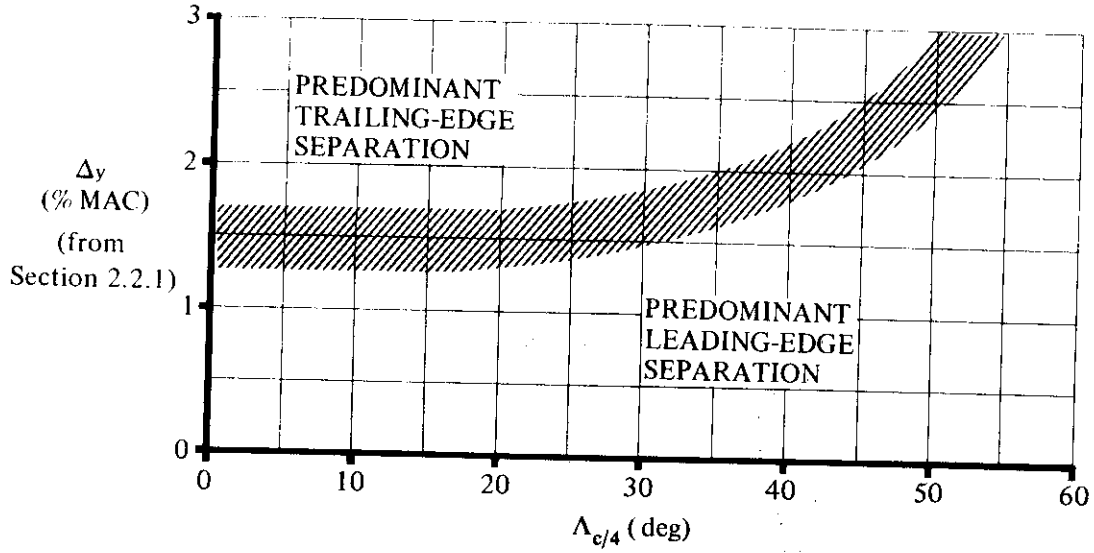

FIGURE 4.4.1-68a TYPE OF FLOW SEPARATION AS A FUNCTION OF AIRFOIL AND WING SWEEP – SUBSONIC SPEEDS

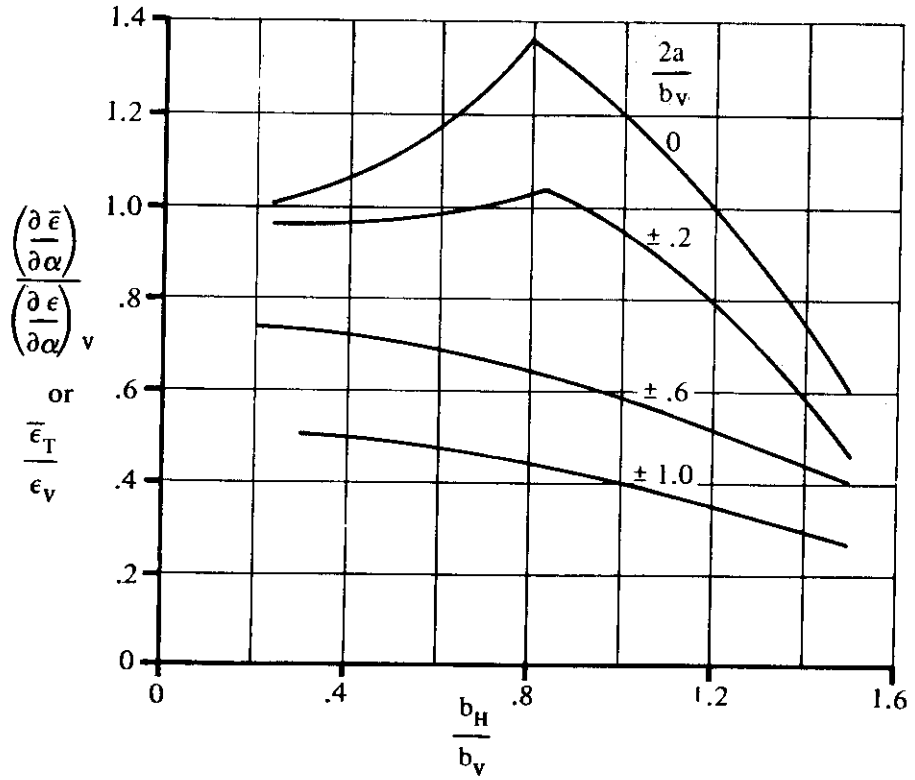

FIGURE 4.4.1-68b AVERAGE DOWNWASH ACTING ON AFT LIFTING SURFACE – LOW SPEEDS

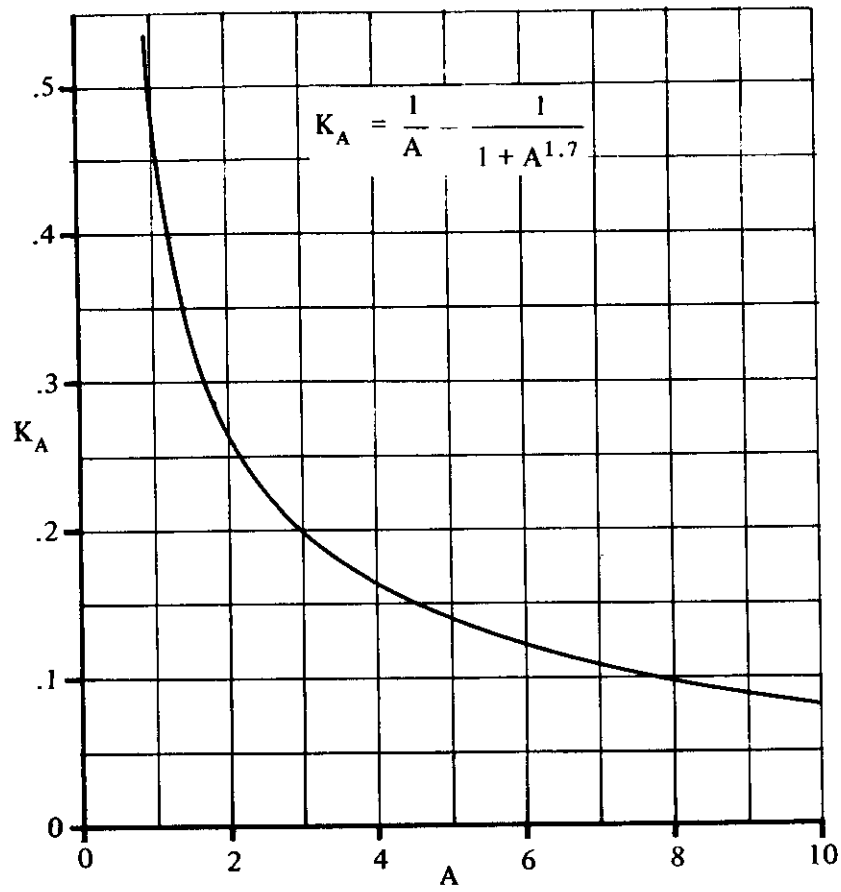

FIGURE 4.4.1-69a WING ASPECT-RATIO FACTOR – METHOD 2

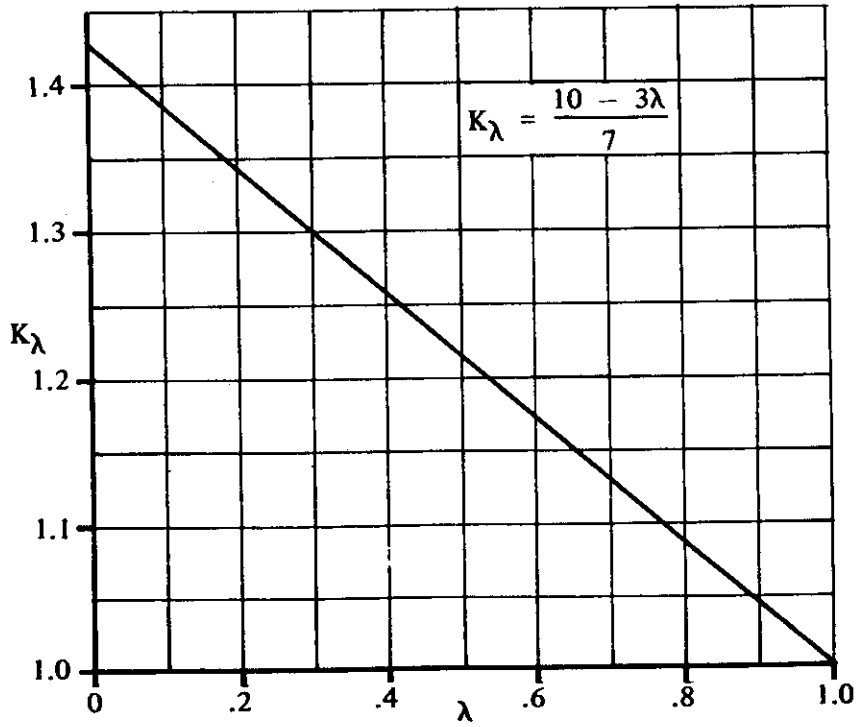

FIGURE 4.4.1-69b WING TAPER-RATIO FACTOR – METHOD 2

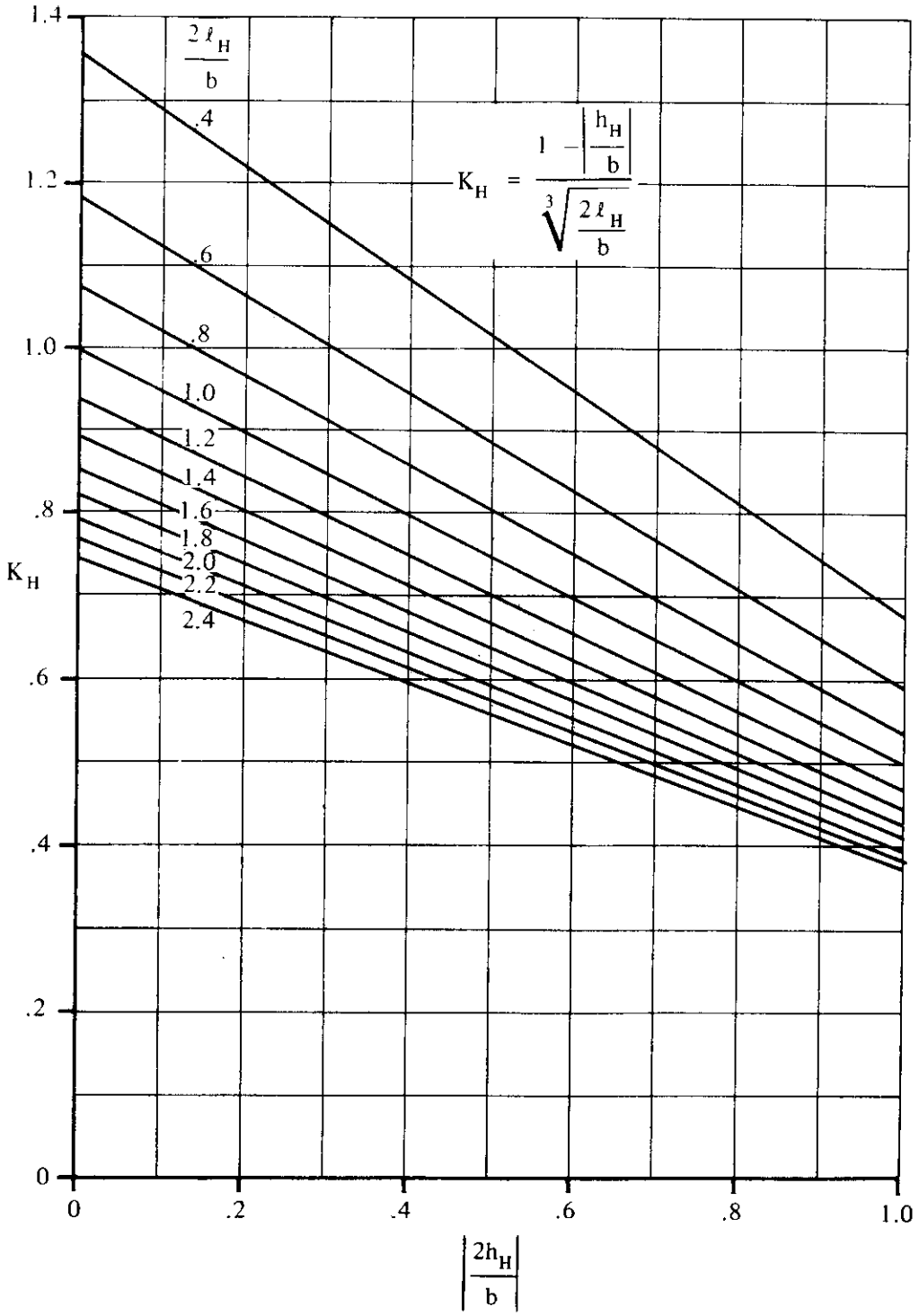

FIGURE 4.4.1-70 HORIZONTAL-TAIL-LOCATION FACTOR – METHOD 2

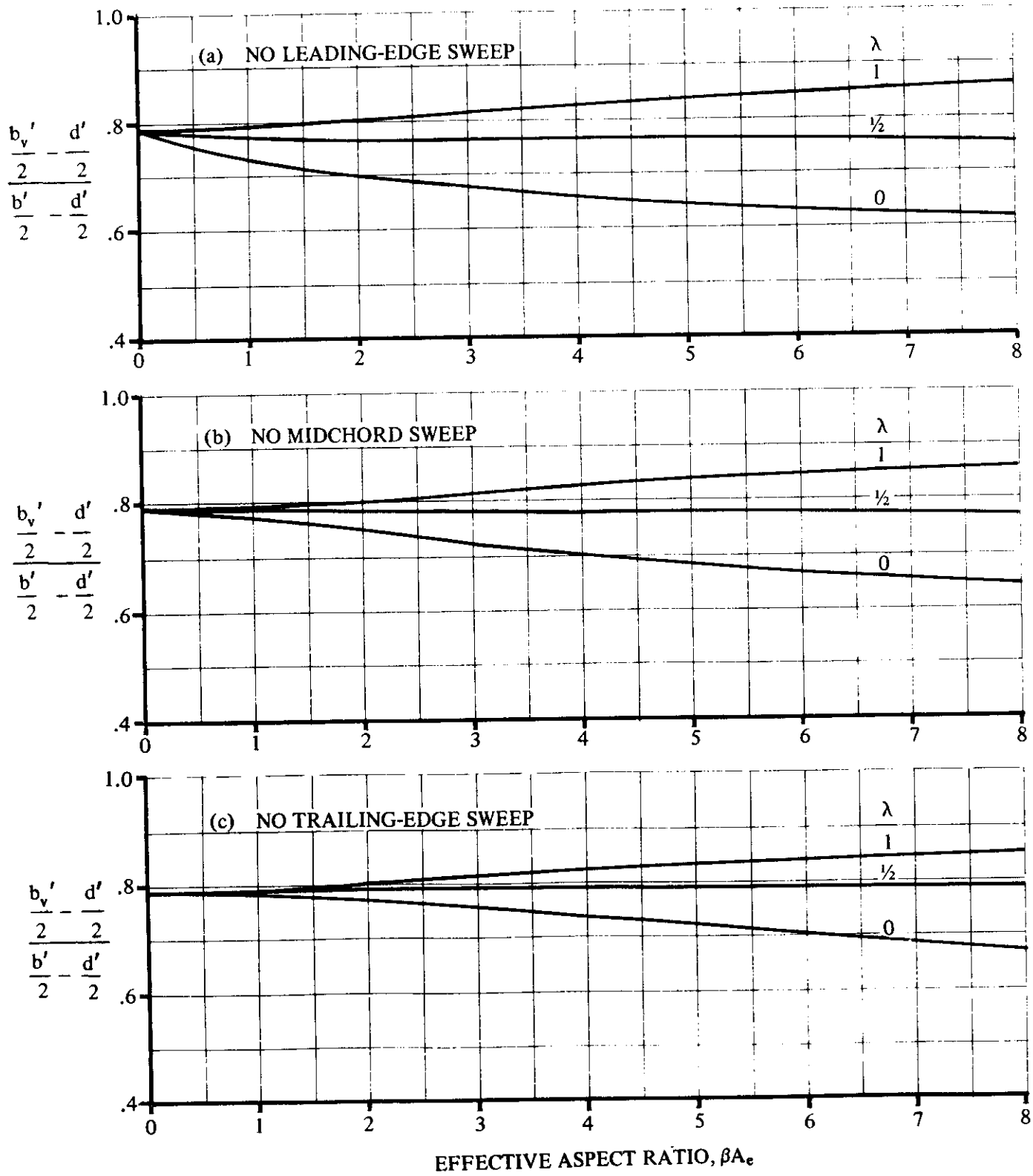

FIGURE 4.4.1-71 WING-VORTEX LATERAL POSITIONS AT SUBSONIC SPEEDS

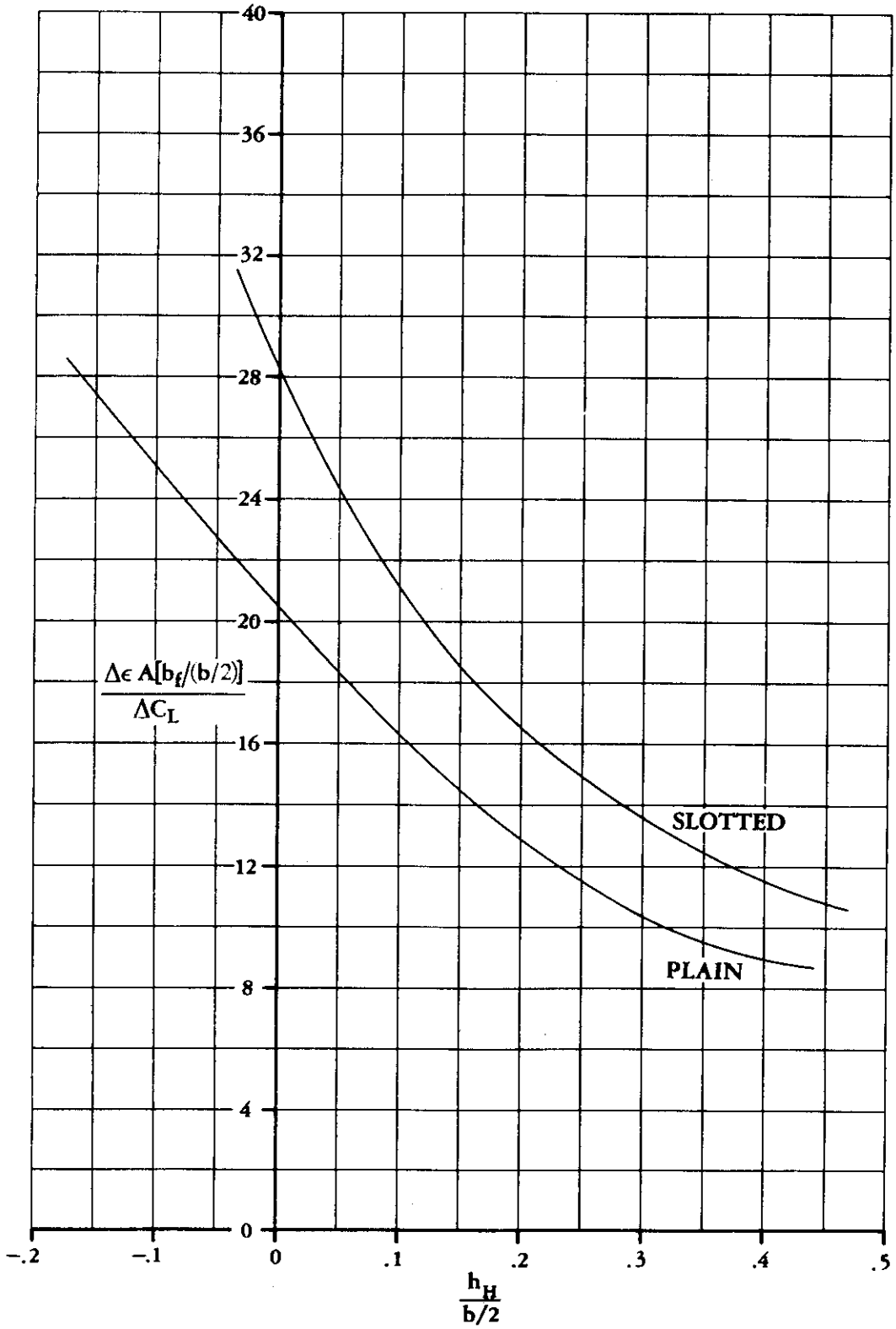

FIGURE 4.4.1-72 DOWNWASH INCREMENT DUE TO FLAPS

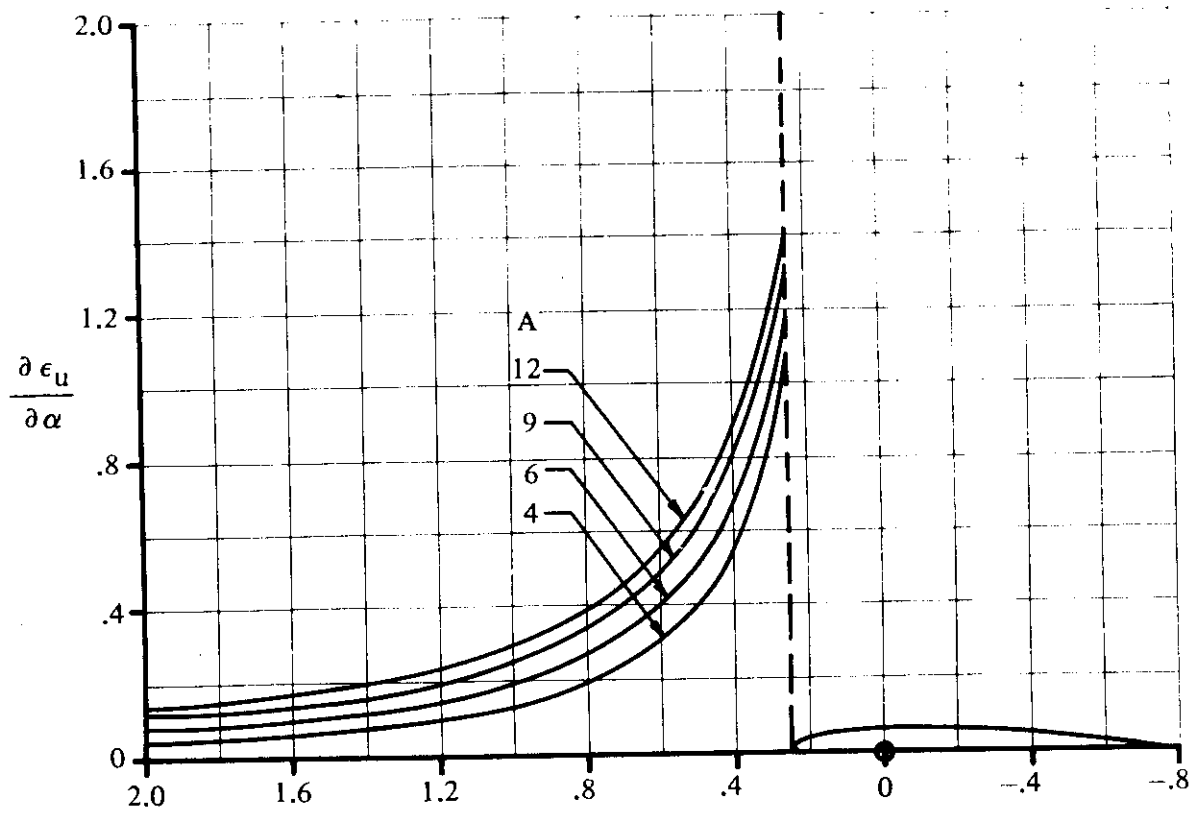

FIGURE 4.4.1-73 UPWASH GRADIENT AT PLANE OF SYMMETRY FOR UNSWEPT WINGS

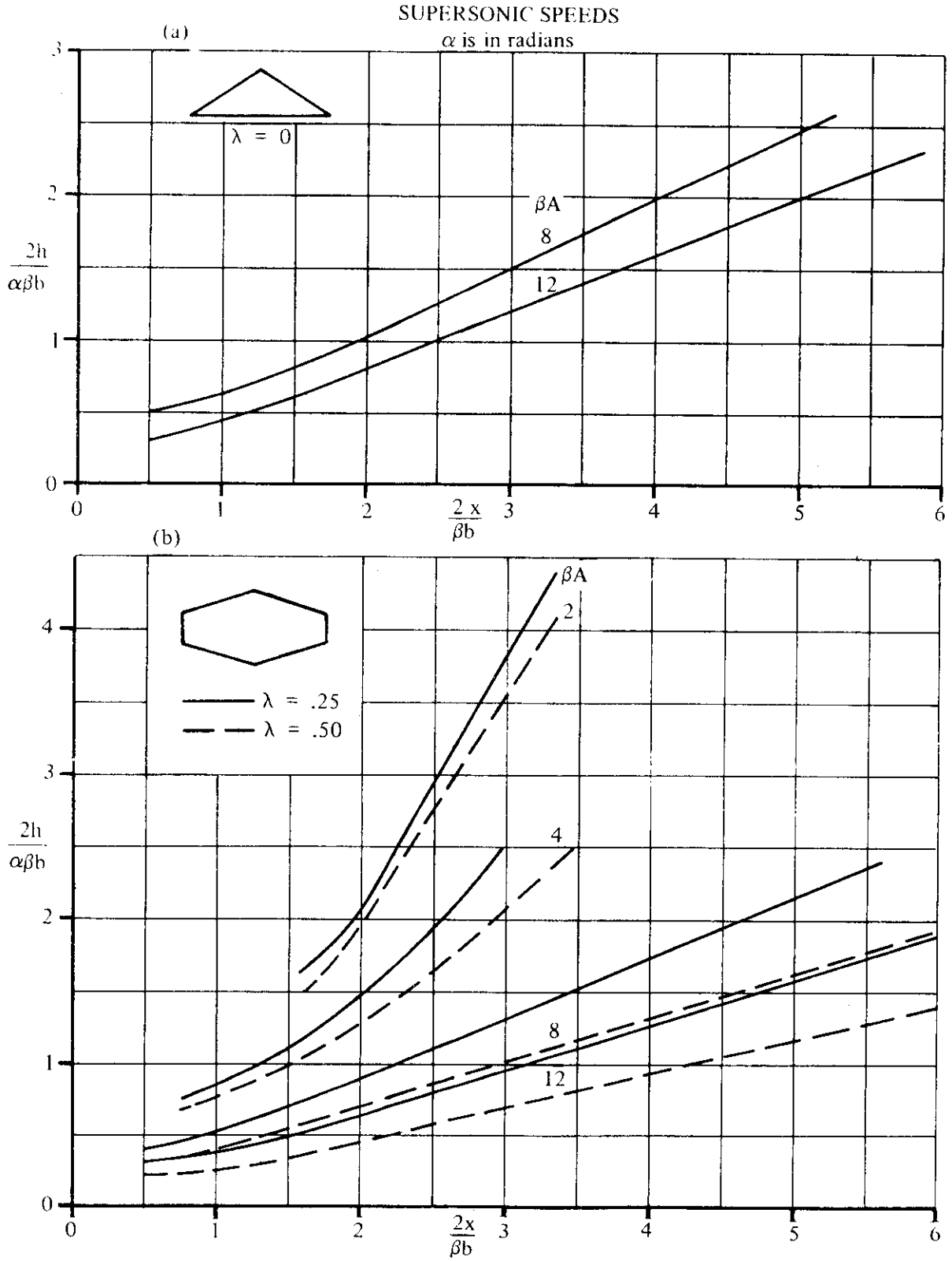

FIGURE 4.4.1-74 DOWNWARD DISPLACEMENT OF VORTEX CORE BELOW Z = 0 PLANE

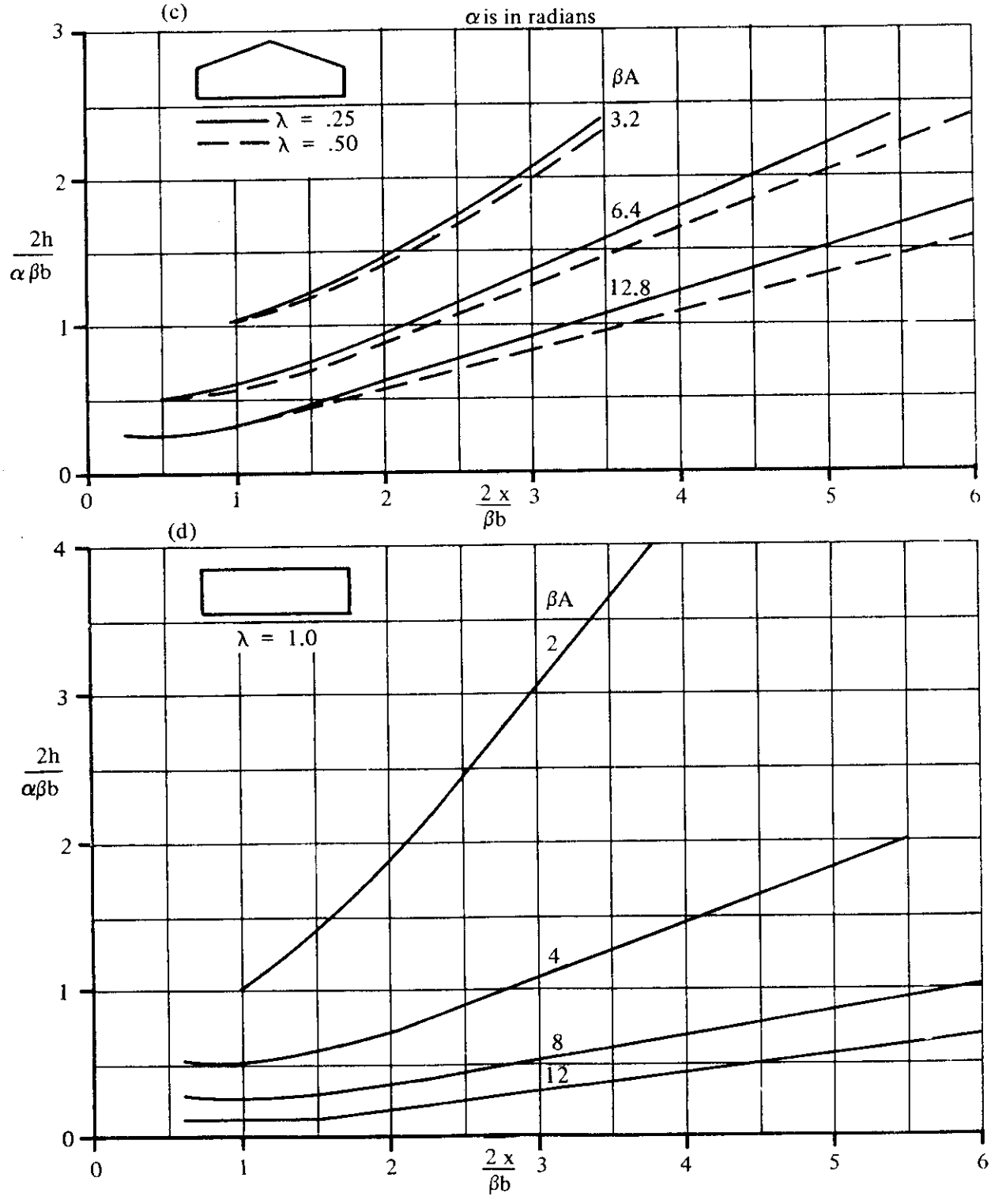

FIGURE 4.4.1-74 (CONTD)

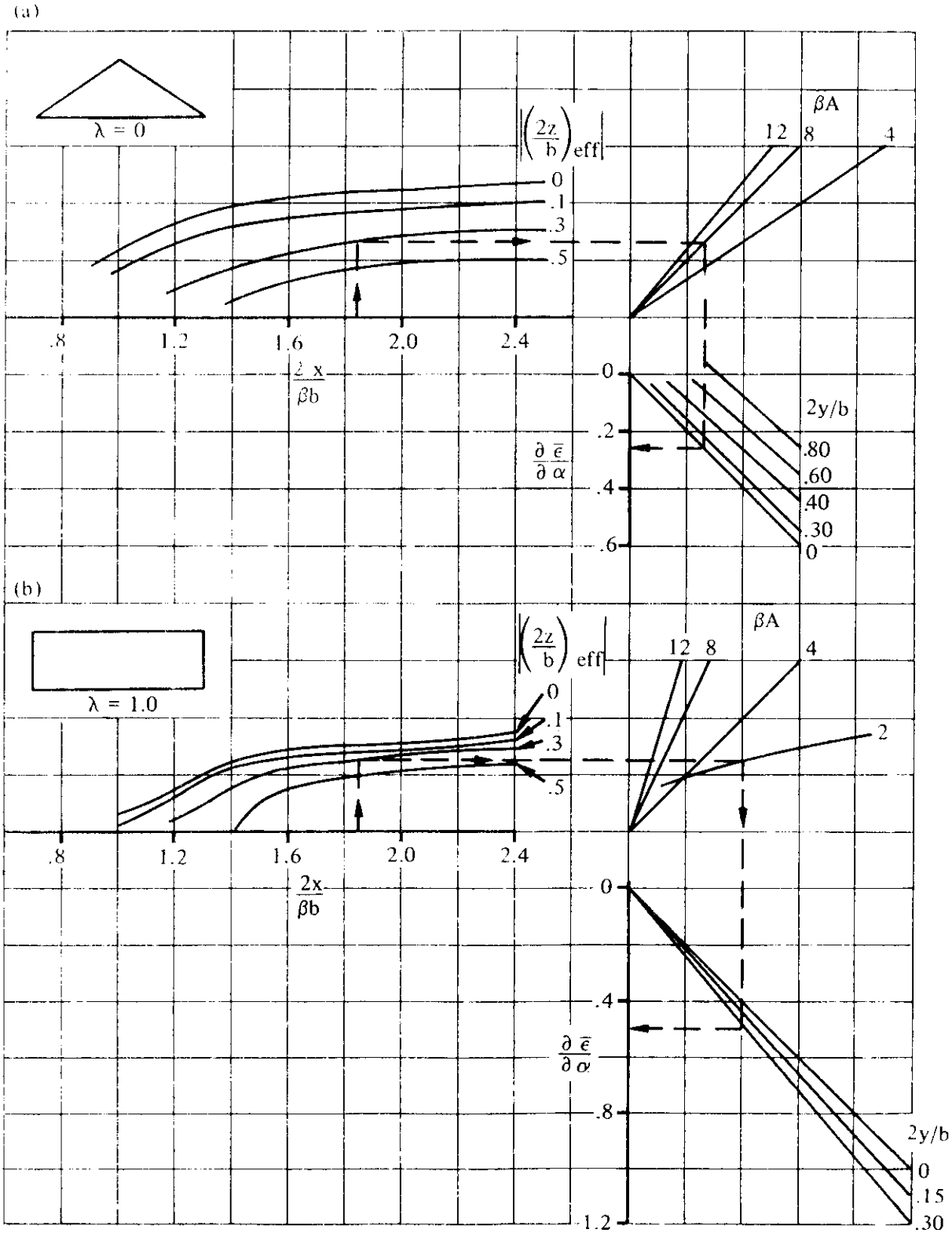

FIGURE 4.4.1-76 DOWNWASH AT SUPERSONIC SPEEDS

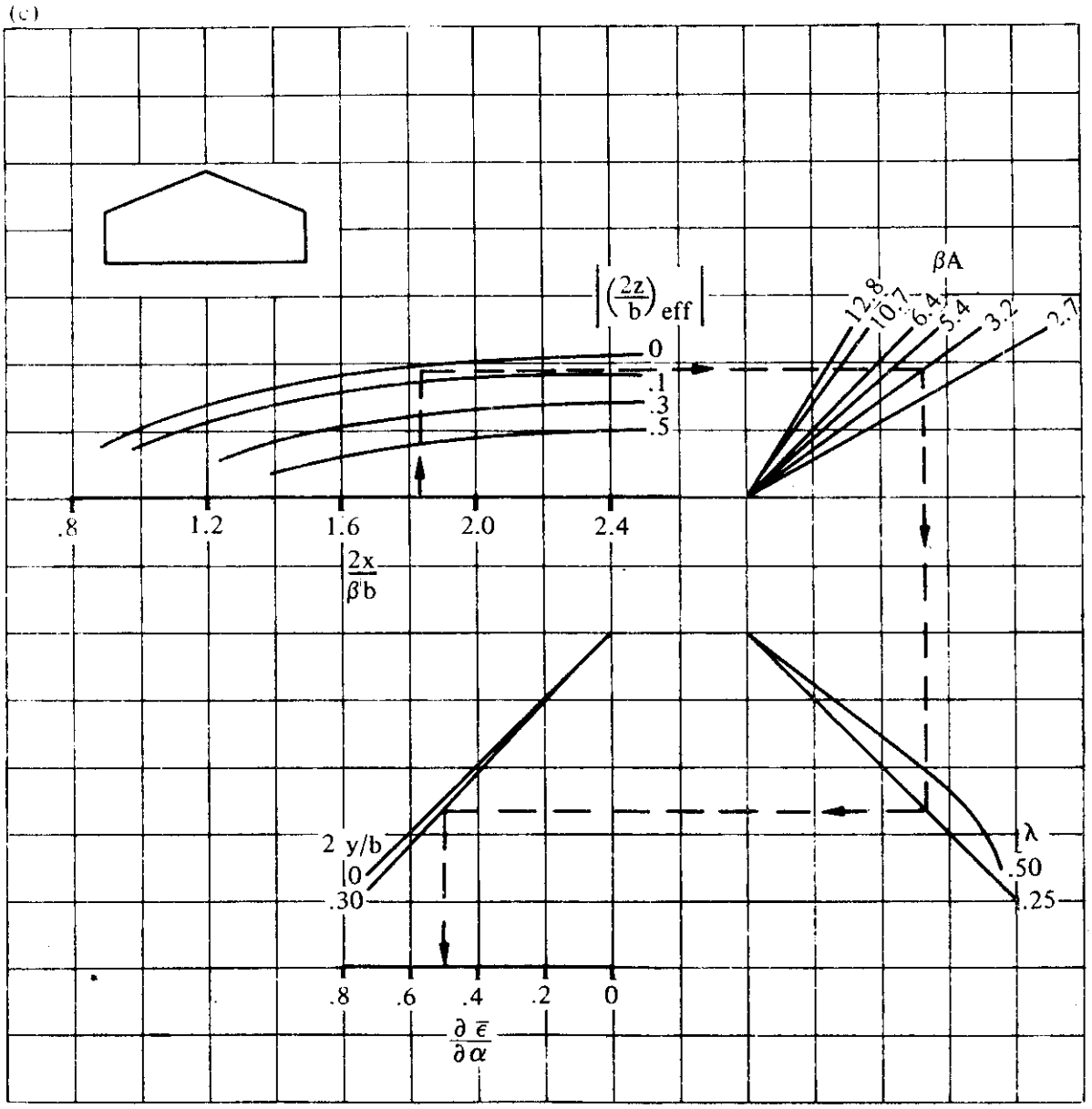

FIGURE 4.4.1-76 (CONTD)

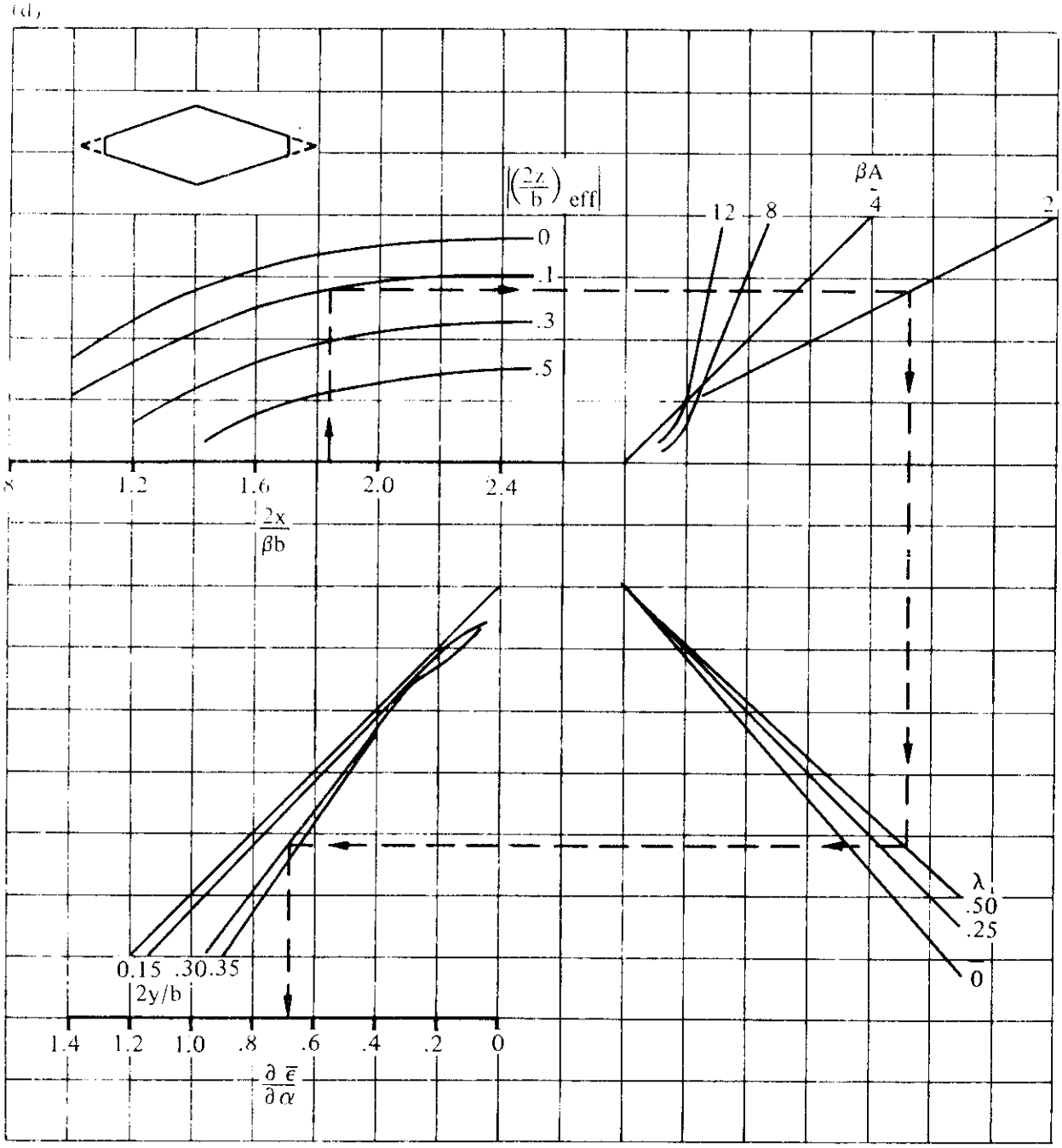

FIGURE 4.4.1-76 (CONTD)

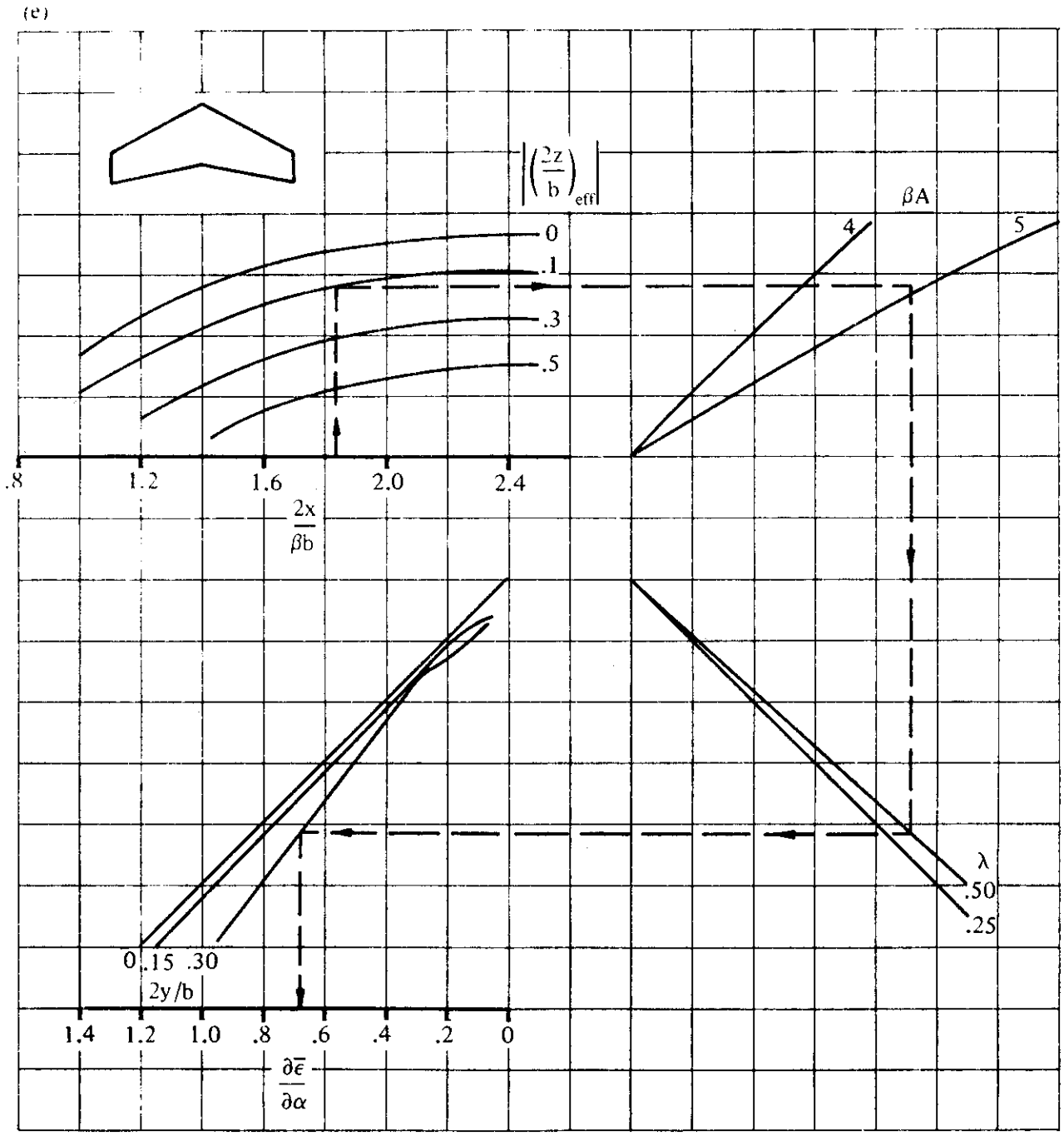

FIGURE 4.4.1-76 (CONTD)

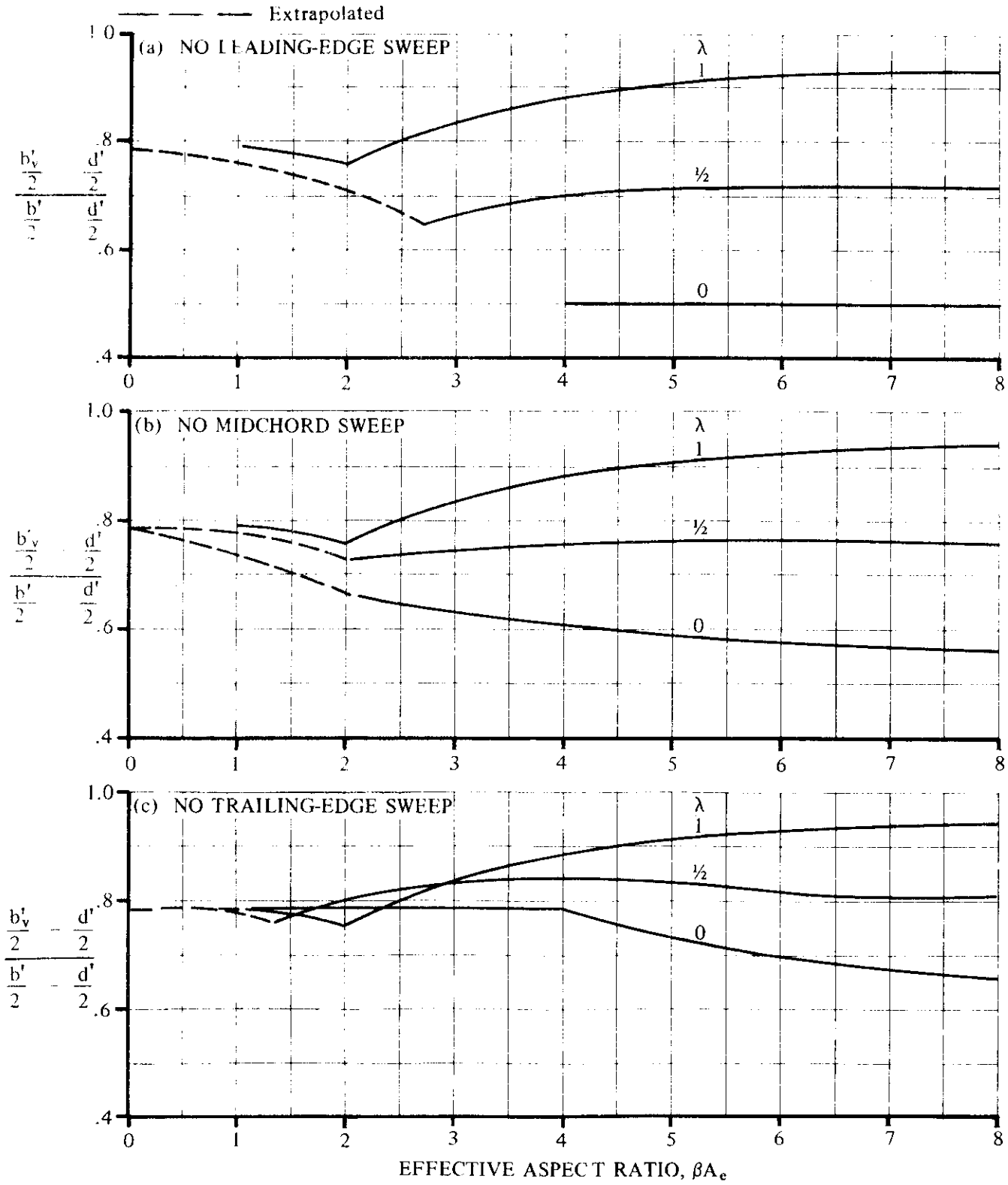

FIGURE 4.4.1-80 WING VORTEX LATERAL POSITION AT SUPERSONIC SPEEDS

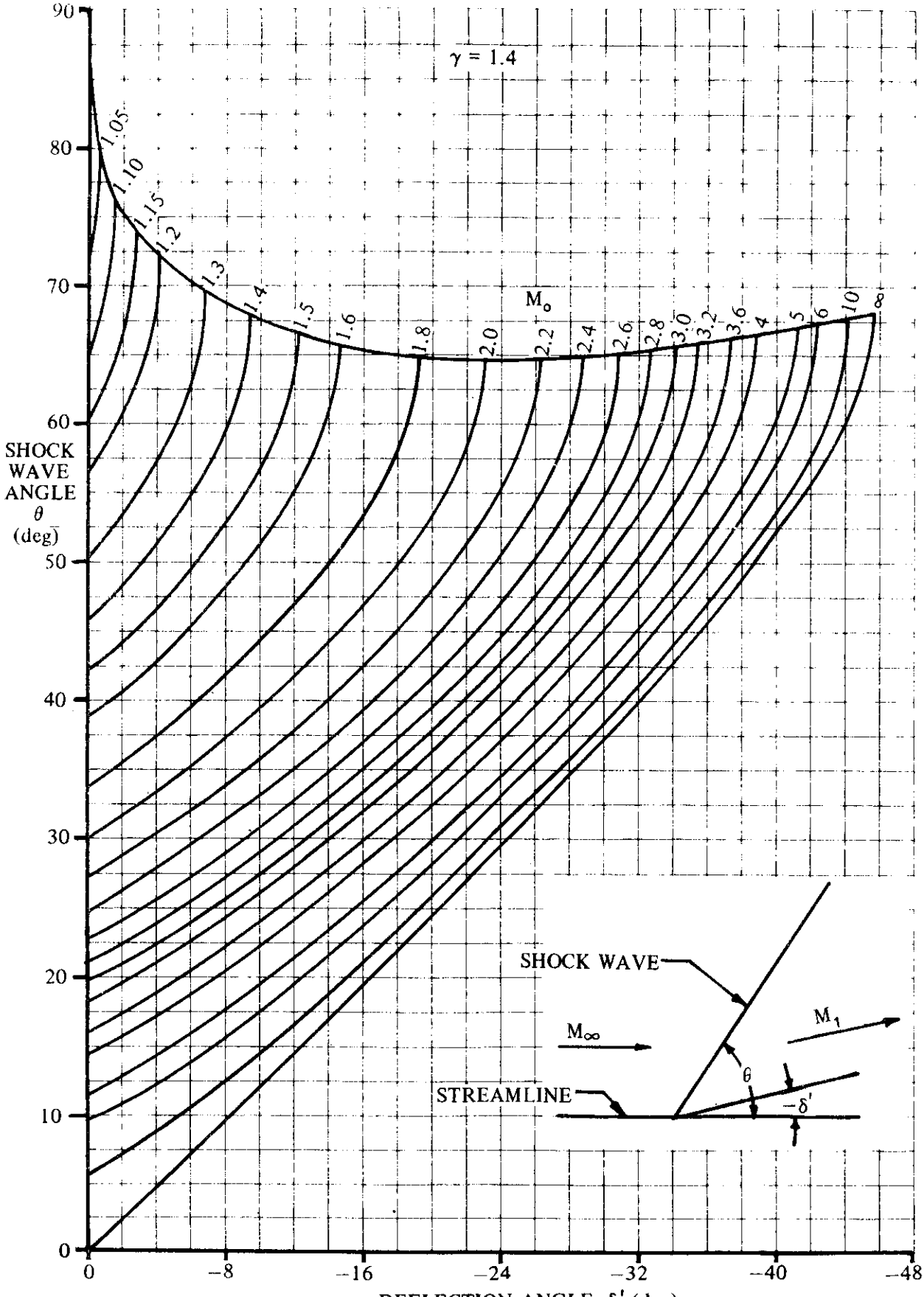

FIGURE 4.4.1-81 SHOCK ANGLE FOR TWO-DIMENSIONAL WEDGE

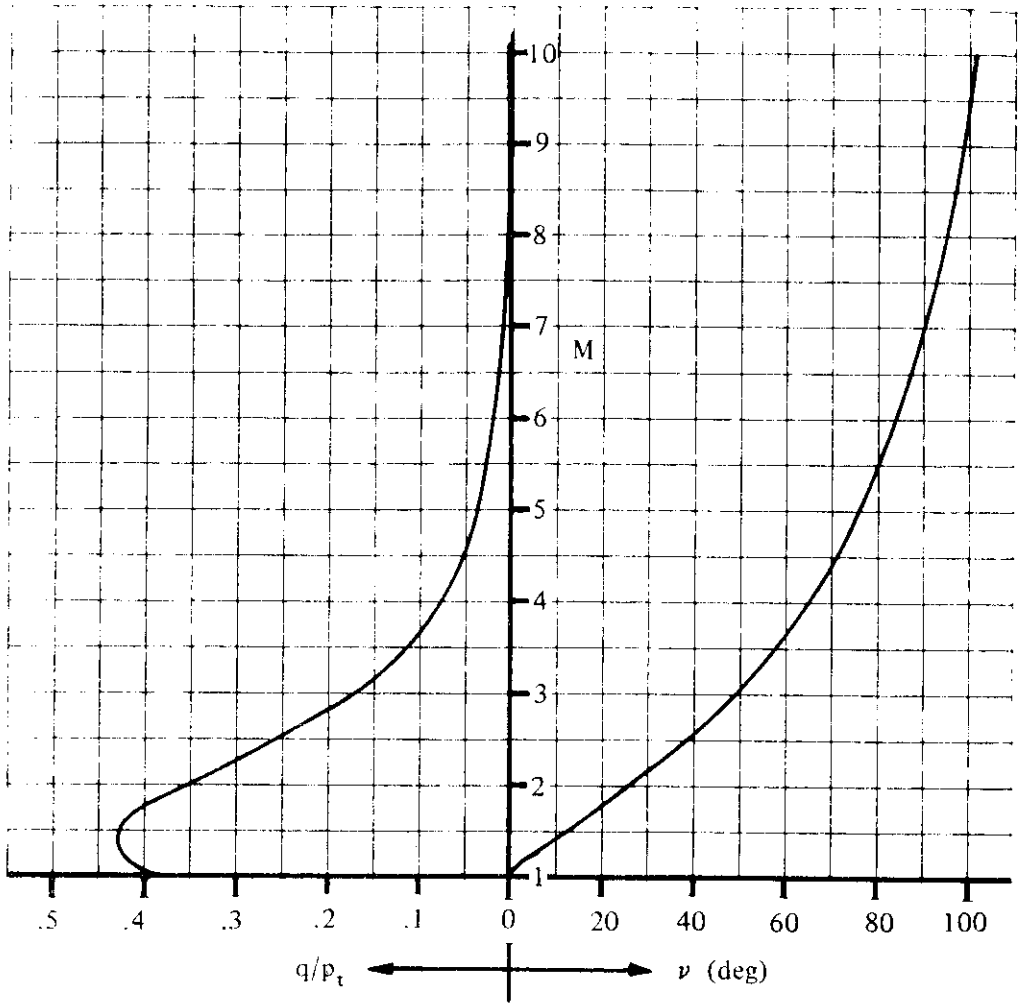

FIGURE 4.4.1-82 DYNAMIC-PRESSURE RATIO AND MACH NUMBER FOR PRANDTL-MEYER EXPANSION

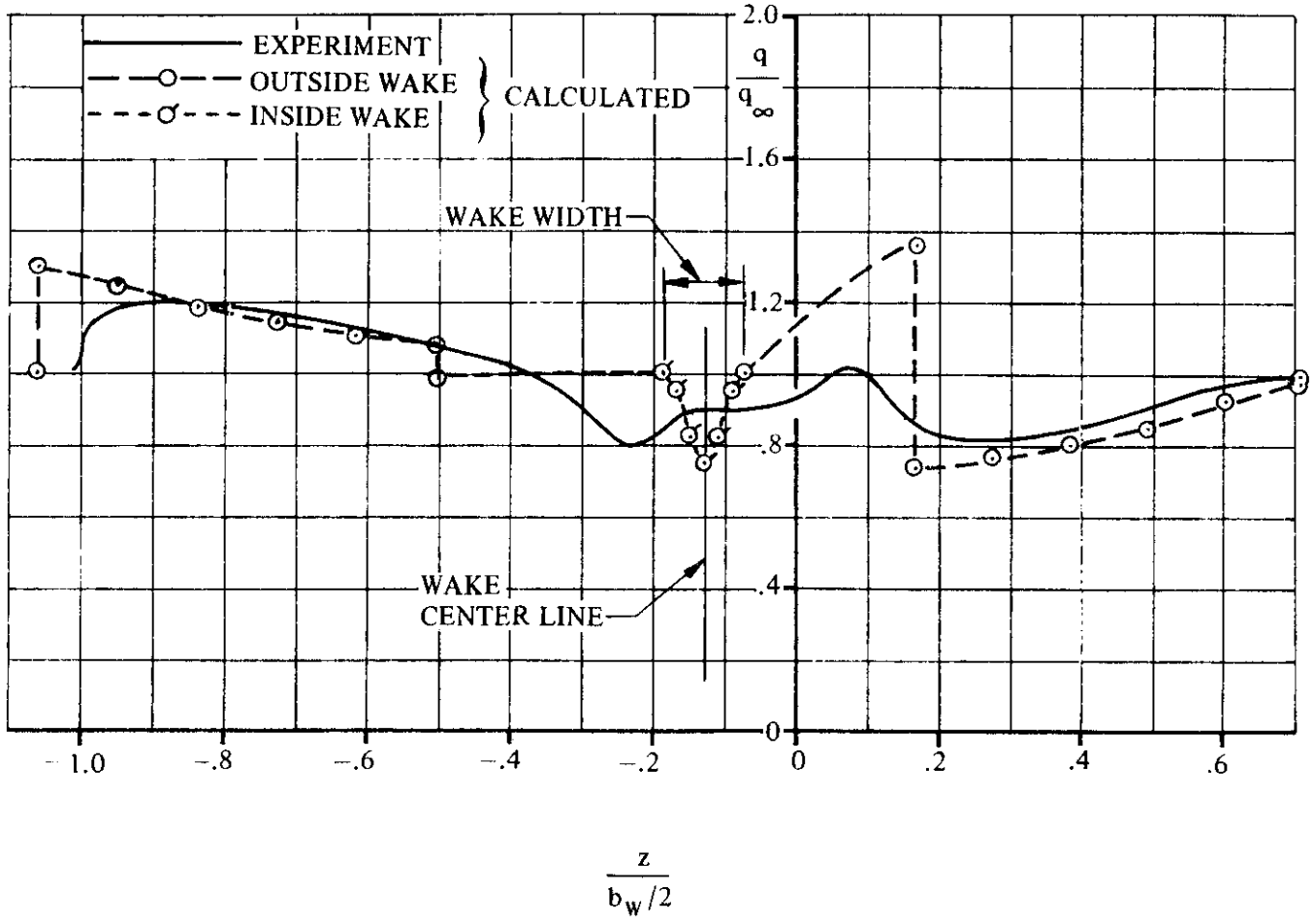

FIGURE 4.4.1-83 SUPERSONIC SAMPLE PROBLEM RESULTS

4.5 WING-BODY-TAIL COMBINATIONS AT ANGLE OF ATTACK
4.5.1 WING-BODY-TAIL LIFT

4.5.1.1 WING-BODY-TAIL LIFT-CURVE SLOPE

The information contained in this section is for the estimation of the lift-curve slope of wing-body-tail combinations at low angles of attack. In general, it consists of a synthesis of material presented in other sections, although some new information is presented.

The lift-curve slope of typical high-aspect-ratio subsonic aircraft is quite linear up to angles of attack approaching the stall. The lift of the panels is actually linear with angle of attack while the body lift varies as the square of the angle of attack. However, for angles of attack below the stall, the body contribution is small enough so that the lift characteristic of the combination is still sensibly linear. In fact, first-order estimates of lift-curve slope frequently neglect the lift of the body.

When the forward surface has a considerably larger span than the aft surface, the tip vortices shed from the forward panels lie outboard of the aft panels. As a consequence, the integrated effect of the downwash over the aft panel decreases the effectiveness of the aft panel in a linear fashion, and hence the lift-curve slope of the combination still remains linear. This effect is quite constant until the forward panel begins to exhibit flow separation, which distorts the span loading and/or the effective planform. For these types of configurations it is also necessary to assume that the vortex is not fully rolled up (see Paragraph A of Section 4.4.1), and the actual distance between the two surfaces must be taken into account.

When the span of the forward surface is approximately equal to or less than that of the aft surface, the vortex shed from the forward surface interacts directly with the aft surface, generally causing nonlinear lift characteristics at relatively low angle of attack.

A. SUBSONIC

Several methods of estimating the subsonic lift-curve slope of a wing-body-tail combination are available in the Datcom. Two of these methods are presented, differing only in their treatment of the effect of the flow field of the forward surface on the aft surface.

DATCOM METHODS

Method 1

For configurations in which the span of the forward surface is large compared to that of the aft surface, the following approach can be used. For purposes of the Datcom this method is to be used when the ratio of forward- to aft-surface span is 1.5 or greater. The lift-curve slope is given by the equation

$$C_{L_\alpha} = (C_{L_\alpha})'_e [K_N + K_{W(B)} + K_{B(W)}]' \frac{S_e'}{S'} + (C_{L_\alpha})''_e [K_{W(B)} + K_{B(W)}]'' \left(1 - \frac{\partial \bar{\epsilon}}{\partial \alpha}\right) \frac{q''}{q_\infty} \frac{S''}{S'} \frac{S_e''}{S''} \qquad \text{4.5.1.1-a}$$

where

C_{L_α} is the desired lift-curve slope of the wing-body-tail combination.

$(C_{L_\alpha})'_e$ and $(C_{L_\alpha})''_e$ are the lift-curve slopes of the exposed forward and aft surfaces, respectively, from Section 4.1.3.2. (See Section 4.3.1.2 for the definition of exposed surfaces.)

$[K_N + K_{W(B)} + K_{B(W)}]'$ and $[K_{W(B)} + K_{B(W)}]''$ are the appropriate wing-body interference factors from Section 4.3.1.2 for the forward and aft surfaces, respectively.

$\frac{\partial \bar{\epsilon}}{\partial \alpha}$ is the downwash gradient averaged over the aft surface, from Section 4.4.1.

$\frac{q''}{q_\infty}$ is the average dynamic-pressure ratio acting on the aft surface, from Section 4.4.1.

$\frac{S_e'}{S'}$ and $\frac{S_e''}{S''}$ are the ratios of the exposed to gross planform areas of the fore and aft surfaces, respectively.

$\frac{S''}{S'}$ is the ratio of aft to forward gross planform areas.

Equation 4.5.1.1-a is valid only where the aerodynamic parameters are linear. Specifically, the equation is valid for high-aspect-ratio, unswept configurations up to angles of attack approaching the stall. For low-aspect-ratio or swept wings, the applicable angle-of-attack range is considerably less, depending upon the degree of accuracy desired.

Method 2

For configurations in which the spans of the forward and aft surfaces are approximately equal or in which the span of the forward surface is less than that of the aft surface, the following procedure is recommended. The lift-curve slope of the combination is given by the equation

$$C_{L_\alpha} = (C_{L_\alpha})'_e [K_N + K_{W(B)} + K_{B(W)}]' \frac{S_e'}{S'} + (C_{L_\alpha})''_e [K_{W(B)} + K_{B(W)}]'' \frac{q''}{q_\infty} \frac{S''}{S'} \frac{S_e''}{S''} + (C_{L_\alpha})_{W''(v)} \qquad 4.5.1.1\text{-b}$$

where

$$(C_{L_\alpha})_{W''(v)} = \frac{(C_{L_\alpha})'_e \frac{S_e'}{S'} (C_{L_\alpha})''_e \frac{q''}{q_\infty} K_{W(B)}' I_{v_{W'(W'')}} \left(\frac{b''}{2} - \frac{d''}{2}\right)}{2\pi A'_e \left(\frac{b_e'}{2} - \frac{d'}{2}\right)}$$

The parameters in the first two terms on the right-hand side are the same as in equation 4.5.1.1-a. The last term represents the effect of the forward-surface vortices on the aft surface. To obtain the contribution of the last term to the lift-curve slope, refer to Method 3 of Paragraph A in Section 4.4.1. The quantities $(C_{L_\alpha})'_e$ and $(C_{L_\alpha})''_e$ of the last term must be expressed in radians. If the result of this term is desired per degree, the conversion must be applied after the term is evaluated.

Sample Problems

1. Method 1

Given:

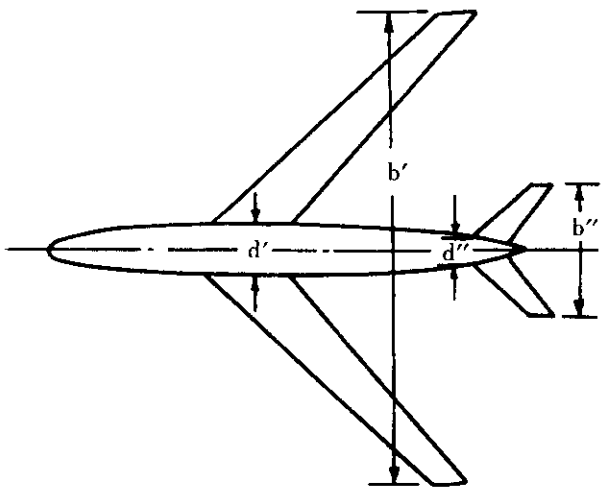

Wing Characteristics:

Total Panel			Exposed Panel
$A' = 8$	$\lambda' = 0.45$		$A'_e = 7.61$
$\Lambda'_{LE} = 46.3$	$\Lambda'_{c/4} = 45°$	$\Lambda'_{c/2} = 43.6°$	$\lambda'_e = 0.470$
$i' = 0$	$\Gamma' = 0$		

NACA 63A012 airfoil section

$\alpha'_l = 0$

Horizontal-Tail Characteristics:

Total Panel			Exposed Panel
$A'' = 4$	$\lambda'' = 0.45$		$A''_e = 3.45$
$\Lambda''_{LE} = 47.6°$	$\Lambda''_{c/4} = 45°$	$\Lambda''_{c/2} = 42.2°$	$\lambda''_e = 0.507$
$i'' = 0$	$\gamma = -3.6°$		

NACA 63A012 airfoil section

The following ratios, based on total panel dimensions:

$\frac{b'}{b''} = 3.536$	$\frac{b'}{d'} = 10.0$	$\frac{b''}{d''} = 4.9$
$\frac{2\ell_a}{b'} = 0.954$	$\frac{\ell_3}{b'} = -0.054$	$\frac{\ell_{eff}}{b'} = 0.120$
$\frac{h_H}{b'} = -0.03$	$\frac{x}{c'} = 3.64$	

The following area ratios:

$\frac{S'_e}{S'} = 0.896$	$\frac{S''_e}{S''} = 0.735$	$\frac{S''}{S'} = 0.160$
$\frac{S_{N_{ref}}}{S'_e} = 0.0701$		

Additional characteristics:

$M = 0.19$	$R = 4 \times 10^6$
$\beta = 0.9818$	smooth surfaces

Note: The above parameters are defined in the sections used to calculate C_{L_α}.

Compute:

Step 1. Lift-curve slopes for the exposed wing and exposed horizontal-tail panels.

Exposed wing panel (Section 4.1.3.2)

$c_{\ell_\alpha} = 6.30$ per rad (Section 4.1.1.2) $\qquad \kappa = \frac{c\ell_\alpha}{2\pi} = 1.0$

$$\frac{A'_e}{K}\left[\beta^2 + \tan^2 \Lambda'_{c/2}\right]^{1/2} = 10.41$$

$\frac{(C_{L_\alpha})'_e}{A'_e} = 0.500$ per rad (Figure 4.1.3.2-49)

$(C_{L_\alpha})'_e = 0.0664$ per deg

Exposed horizontal-tail panel (Section 4.1.3.2)

$c\ell_\alpha = 6.30$ per rad (Section 4.1.1.2) $\qquad \kappa = \frac{c\ell_\alpha}{2\pi} = 1.0$

$\frac{A''_e}{\kappa}[\beta^2 + \tan^2 \Lambda''_{c/2}]^{1/2} = 4.610$

$\frac{(C_{L_\alpha})''_e}{A''_e} = 0.900$ per rad (Figure 4.1.3.2-49)

$(C_{L_\alpha})''_e = 0.0542$ per deg

Step 2. Wing-body and tail-body interference factors (Section 4.3.1.2)

Wing-body

$(C_{L_\alpha})_N = 2.0$ per rad

$K'_N = \frac{(C_{L_\alpha})_N}{(C_{L_\alpha})'_e}\frac{S_{N_{ref}}}{S'_e} = .037$

$K_{W(B)}' = 1.08$, $K_{B(W)}' = .14$ } Figure 4.3.1.2-10 for $\frac{d'}{b'} = .10$

$[K_N + K_{W(B)} + K_{B(W)}]' = 1.257$

Horizontal-tail-body

$K_{W(B)}'' = 1.170$, $K_{B(W)}'' = .290$ } Figure 4.3.1.2-10 for $\frac{d''}{b''} = .204$

$[K_{W(B)} + K_{B(W)}]'' = 1.460$

Step 3. Downwash parameter (Section 4.4.1)

Obtain value at $\alpha = 0°$

$C_L = 0$ $\qquad \frac{\alpha - \alpha_o}{\alpha_{C_{L_{max}}} - \alpha_o} = 0$

$\frac{A'_{eff}}{A'} = 1.0$, $\frac{b'_{eff}}{b'} = 1.0$ } Figure 4.4.1-66

$A'_{eff} = 8$ $\qquad \left(\frac{\partial \epsilon}{\partial \alpha}\right)_\infty = .23$, $\left(\frac{\partial \epsilon}{\partial \alpha}\right)_v = .3$ } Figure 4.4.1-67

$\Delta y = 2.65$ (Section 2.2.1)

Type of flow separation: trailing-edge separation is predominant (Figure 4.4.1-68a)

$$\frac{a}{b'} = \frac{h_H}{b'} - \frac{\ell_{eff}}{b'}\left(\alpha - \frac{0.41\ C_L}{\pi A'_{eff}}\right) - \frac{b'_{eff}}{2b'}\tan\Gamma^v \quad \text{(Equation 4.4.1-c)}$$

$$\frac{a}{b'} = -0.03$$

$$\frac{b_v}{b'} = \frac{b_{eff}}{b'} \quad (\text{at } C_L = 0)$$

$$\frac{b_H}{b_v} = \frac{b''}{b_v} = \frac{b''}{b'}\frac{b'}{b_v} = 0.283$$

$$\frac{2a}{b_v} = 2\frac{a}{b'}\frac{b'}{b_v} = -0.06$$

$$\frac{\left(\frac{\partial \bar{\epsilon}}{\partial \alpha}\right)_v}{\left(\frac{\partial \epsilon}{\partial \alpha}\right)_v} = 1.0 \quad \text{(Figure 4.4.1-68b)}$$

$$\frac{\partial \bar{\epsilon}}{\partial \alpha} = \frac{\left(\frac{\partial \bar{\epsilon}}{\partial \alpha}\right)_v}{\left(\frac{\partial \epsilon}{\partial \alpha}\right)_v}\left(\frac{\partial \epsilon}{\partial \alpha}\right)_v = 0.30$$

$$\left(1 - \frac{\partial \epsilon}{\partial \alpha}\right) = 0.70$$

Step 4. Dynamic-pressure ratio at the horizontal tail (Section 4.4.1)

Obtain value at $\alpha = 0°$

$$\epsilon = 0$$

$$(\gamma + \epsilon - \alpha) = -3.6°$$

$$\frac{z}{\bar{c}'} = \frac{x}{\bar{c}'}\tan(\gamma + \epsilon - \alpha) = -0.229 \quad \text{(Equation 4.4.1-l)}$$

$C_f = 0.00350$ (Figure 4.1.5.1-26)

$$C_{D_0} = C_f\left[1 + L\left(\frac{t}{c}\right) + 100\left(\frac{t}{c}\right)^4\right]R_{L.S.}\frac{S_{wet}}{S_{ref}} \quad \text{(Equation 4.1.5.1-a)}$$

$$= 0.0088$$

$$\frac{z_w}{\bar{c}'} = .68\sqrt{C_{D_0}\left(\frac{x}{\bar{c}'} + .15\right)} = .124 \quad \text{(Equation 4.4.1-j)}$$

$$\frac{z}{z_w} = \frac{z/\bar{c}'}{z_w/\bar{c}'} = -1.85$$

Since $\left|\frac{z}{z_w}\right| \geq 1.0$, $\frac{q''}{q_\infty} = 1.0$

Step 5. Solution for C_{L_α} of wing-body-tail combination

$$C_{L_\alpha} = (C_{L_\alpha})'_e\left[K_N + K_{W(B)} + K_{B(W)}\right]'\frac{S'_e}{S'} + (C_{L_\alpha})''_e\left[K_{W(B)} + K_{B(W)}\right]''\left(1 - \frac{\partial \epsilon}{\partial \alpha}\right)\frac{q''}{q_\infty}\frac{S''}{S'}\frac{S_e''}{S''}$$

(Equation 4.5.1.1-a)

$C_{L_\alpha} = 0.0748 + 0.0065$

$C_{L_\alpha} = 0.0813$ per deg

2. Method 2

Given:

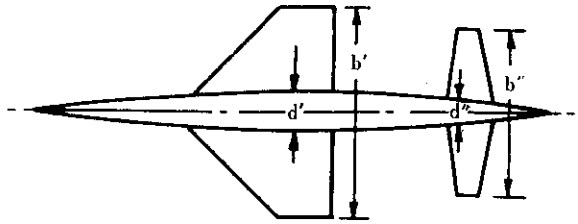

Wing Characteristics:

	Total Panel		Exposed Panel
$A' = 2$	$\lambda' = 0.33$		$A'_e = 1.80$
$\Lambda'_{LE} = 45°$	$\Lambda'_{c/4} = 36.8°$	$\Lambda'_{c/2} = 26.45°$	$\lambda'_e = 0.378$
$i' = 0$	$\Gamma' = 0$		
NACA 0005 airfoil section			
$\alpha_0 = 0$			

Horizontal-Tail Characteristics:

	Total Panel		Exposed Panel
$A'' = 4.4$	$\lambda'' = 0.46$		$A''_e = 3.82$
$\Lambda''_{LE} = 9.46°$	$\Lambda''_{c/4} = 4.74°$	$\Lambda''_{c/2} = 0$	$\lambda''_e = 0.515$
$i'' = 0$	$\gamma = 0$		
NACA 0005 airfoil section			

The following ratios, based on total panel dimensions:

$\frac{b'}{b''} = 1.278$ $\quad \frac{b'}{d'} = 5.25$ $\quad \frac{b''}{d''} = 5.01$

$\frac{x}{c'} = 1.080$

The following area ratios:

$\frac{S_e'}{S'} = 0.730$ $\quad \frac{S_e''}{S''} = 0.741$ $\quad \frac{S''}{S'} = 0.277$

$\frac{S_{Nref}}{S_e'} = 0.0781$

Additional characteristics:

$M = 0.13$ $\quad R_l = 11.4 \times 10^6$

$\beta = 0.9915$ $\quad$ smooth surface

Compute:

The calculation procedures of Method 2 that are similar to those of Method 1 are not listed in detail here. See sample problem 1 for a detailed presentation.

Step 1. Lift-curve slopes for the exposed wing and exposed horizontal-tail panels (Section 4.1.3.2)

$(C_{L_\alpha})_e' = 0.0405$ per deg

$(C_{L_\alpha})_e'' = 0.0667$ per deg

Step 2. Wing-body and tail-body interference factors (Section 4.3.1.2)

Wing-body

$K_N' = 0.067$ $\quad K_{W(B)}' = 1.16$ $\quad K_{B(W)}' = 0.27$

Tail-body

$K_{W(B)}'' = 1.17$ $\quad K_{B(W)}'' = 0.28$

Step 3. Dynamic-pressure ratio at the horizontal tail (Section 4.4.1)

Obtain at $\alpha = 0$

$$\frac{q''}{q_\infty} = 0.859$$

Step 4. Lift-curve slope of tail section due to wing vortices

$$(C_{L_\alpha})_e' \frac{S_e'}{S'} = .0405\ (.730) = 0.0296 \text{ per deg}$$

$$= 1.696 \text{ per rad}$$

$$(C_{L_\alpha})_e'' \frac{q''}{q_\infty} = .0667\ (.859) = 0.0574 \text{ per deg}$$

$$= 3.28 \text{ per rad}$$

$K_{W(B)}' = 1.16$ $\quad A_e'' = 3.82$

Tail interference factor, $I_{v_{W'(W'')}}$, at $\alpha = 0$

$I_{v_{W'(W'')}} = -3.0$ (sample problem 3, paragraph A, Section 4.4.1)

$\left.\begin{aligned} \frac{b''}{2} - \frac{d''}{2} &= 88.56 \text{ in.} \\ \frac{b_v'}{2} - \frac{d'}{2} &= 89.87 \text{ in.} \end{aligned}\right\}$ also from above sample problem

$$(C_{L_\alpha})_{W''(v)} = \frac{(C_{L_\alpha})_e' \frac{S_e'}{S'} (C_{L_\alpha})_e'' \frac{q''}{q_\infty} K_{W(B)}' I_{v_{W'(W'')}} \left(\frac{b''}{2} - \frac{d''}{2}\right)}{2\pi A_e'' \left(\frac{b_v'}{2} - \frac{d'}{2}\right)}$$

$$= \frac{1.696\ (3.280)\ (1.16)\ (-3.0)\ (88.56)}{2\pi\ (3.82)\ (89.87)}$$

$$= -0.794 \text{ per rad}$$

$$= -0.0139 \text{ per deg}$$

Step 5. Solution for C_{L_α} of wing-body-tail combination

$$C_{L_\alpha} = (C_{L_\alpha})_e' [K_N + K_{W(B)} + K_{B(W)}]' \frac{S_e'}{S'}$$

$$+ (C_{L_\alpha})_e'' [K_{W(B)} + K_{B(W)}]'' \frac{q''}{q_\infty} \frac{S''}{S'} \frac{S_e''}{S''}$$

$$+ (C_{L_\alpha})_{W''(v)}$$

In the above equation the first term represents the wing contribution, including interference effects, and the last two terms represent the tail contribution, including interference effects.

$$C_{L_\alpha} = .0405\ (1.497)\ (.730) + .0667\ (1.450)\ (.859)\ (.277)\ (.741) + (-.0139)$$

$$= 0.0443 + 0.0171 - 0.0139$$

$$= \underset{\text{(wing)}}{0.0443} + \underset{\text{(tail)}}{0.0032}$$

$$C_{L_\alpha} = 0.0475 \text{ per deg}$$

B. TRANSONIC

The estimation of transonic characteristics is one of the nebulous topics of aerodynamics. Variations in the lift-curve slope with Mach number for wing-body-tail configurations at transonic speeds are determined primarily by the wing characteristics, since body characteristics do not change significantly with Mach number. Also the lift-curve slope (at low angles of attack) of the body is generally small compared to that of the lifting surfaces, so that again the low-angle-of-attack lift characteristics can be approximated by the lift of the panels alone. Refinements can be made by applying theoretically derived wing-body interference parameters such as those presented in Section 4.3.1.2, but the improvement in accuracy is questionable.

DATCOM METHOD

It is recommended that the methods presented in Paragraph A above be applied directly to the transonic speed regime. Care should be taken to estimate the lift-curve slope of the isolated lifting panels at the proper Mach number. The interference factors should be obtained from Paragraph C, Section 4.3.1.2.

C. SUPERSONIC

The procedure for estimating the supersonic lift-curve slope of a wing-body-tail combination is essentially identical to that at subsonic speeds. Several methods are presented that depend upon the general arrangement of the configuration.

DATCOM METHODS

Method 1

For configuration in which the forward surface has a span at least 1.5 times the aft-surface span, the lift-curve slope of the configuration can be estimated by using equation 4.5.1.1-a of paragraph A above. Two methods of estimating the interference "K" factors in this equation are presented in Section 4.3.1.2. Two methods of determining the downwash gradient for this type of configuration at supersonic speeds are presented as Methods 1 and 2 in Section 4.4.1.

Method 2

For configurations in which the span of the forward surface is approximately equal to or less than that of the aft surface, equation 4.5.1.1-b of paragraph A is used. For this type of configuration, the trailing vortices of the forward surface strongly interact with the aft surface, and a special accounting must be taken of this situation. Method 3 of Section 4.4.1. which estimates the contribution of this interaction to aft-panel lift, should therefore be used to evaluate the last term of equation 4.5.1.1-b.

4.5.1.2 WING-BODY-TAIL LIFT IN THE NONLINEAR ANGLE-OF-ATTACK RANGE

The lift of wing-body-tail combinations in the nonlinear angle-of-attack range depends primarily on the characteristics of the isolated components. Although little is known about the mutual aerodynamic interference effects in this range, certain reasonable assumptions can be made. First, the wing lift carryover onto the body and the effect of the body upwash on the wing lift are similar in nature to those of the low-angle-of-attack case. These effects, calculated for low angles of attack by slender-body theory, are presented in Section 4.3.1.2.

The effects of the shed vortices are somewhat more involved. For high-aspect-ratio, unswept subsonic configurations, the flow remains attached over the lifting panels up to angles of attack approaching the stall. For this angle-of-attack range, the aerodynamic lift characteristics are linear and the methods of the previous section are adequate. During the stalling process the flow may separate in an infinite variety of ways – depending upon the details of the wing design – each producing a different flow behind the surface and hence a different lift contribution from the aft panel. At present the stalling range of angles of attack is not covered in the Datcom. It can be assumed that above the stall angle of the forward panel the flow from the forward surface does not interact with the aft surface if the aft surface is not directly in the wake, i.e., $\frac{\partial \epsilon}{\partial \alpha} = 0$. For the purposes of the Datcom the wake of a stalled wing can be taken to be bounded by the lines emanating from the leading and trailing edges of the forward surface in the streamwise direction. For aft panels lying within this stall region, the aft-panel contribution to lift is taken to be zero.

For swept and/or low-aspect-ratio configurations, the trailing vortices are shed at progressively more inboard stations as the angle of attack is increased. The effect appears in the downwash field and hence in the lift generated by the aft panel.

The bodies of these configurations lift in a continuous fashion as a function of angle of attack and do not stall in the normal sense. The nonlinear cross-flow contribution to body lift is sizable at the higher angles (near and beyond stall) and should not be neglected. This cross-flow lift is caused by a pair of body vortices that can also strongly affect the lift contributions from the panels. These effects have been accounted for in the Datcom.

A. SUBSONIC

DATCOM METHOD

The lift of a wing-body-tail combination can be estimated at subsonic speeds by using the following equations*:

$$\text{For } \frac{b'}{b''} \geqq 1.5: \quad C_N = \left\{ (C'_{N_1})'_{\alpha} [K_N + K_{W(B)} + K_{B(W)}]' + (C'_{N_2})'_{\alpha} [k_{W(B)} + k_{B(W)}]' \right\} \frac{S'_e}{S'}$$

$$+ \left\{ (C'_{N_1})''_{\alpha} [K_{W(B)} + K_{B(W)}]'' + (C'_{N_2})''_{\alpha} [k_{W(B)} + k_{(B)W}]'' \right\} \frac{q''}{q_\infty} \frac{S''_e}{S'}$$

$$+ I_{v_{B(W')}} \left(\frac{\Gamma}{2\pi a V_r} \right)' \frac{r'}{b_W'/2} \left| \frac{q'}{q_\infty} (C_{L_\alpha})' \alpha' + I_{v_{B(W'')}} \left(\frac{\Gamma}{2\pi a V_r} \right)'' \frac{r''}{b_W''/2} \frac{S''}{S'} \frac{q''}{q_\infty} (C_{L_\alpha})'' \alpha'' \right.$$

4.5.1.2-a

*Note: The limits suggested for b'/b" are quite flexible, depending upon the configuration details and the degree of accuracy desired.

For $\frac{b'}{b''} < 1.5$:

$$C_N = \left\{(C'_{N_1})'_e[K_N + K_{W(B)} + K_{B(W)}]' + (C'_{N_2})'_e\,[k_{W(B)} + k_{B(W)}]'\right\}\frac{S'_e}{S'}$$

$$+ \left\{(C'_{N_1})''_e[\,K_{W(B)} + K_{B(W)}]'' + (C'_{N_2})''_e\,[k_{W(B)} + k_{B(W)}]''\right\}\frac{q''}{q_\infty}\frac{S''_e}{S'}$$

$$+ \frac{(C_{L_\alpha})'_e\frac{S'_e}{S'}\,(C_{L_\alpha})''_e\frac{q''}{q_\infty}K_{W(B)}\,'\,\alpha\,I_{v_{W'(W'')}}\left(\frac{b''}{2} - \frac{d''}{2}\right)}{2\pi A''_e\left(\frac{b'_v}{2} - \frac{d'}{2}\right)\cos\alpha}$$

$$+ I_{v_{B(W')}}\left(\frac{\Gamma}{2\pi a\,Vr}\right)'\frac{r'}{b_{W'}/2}\left|\frac{q'}{q_\infty}\,(C_{L_\alpha})'\,\alpha' + I_{vB(W'')}\left(\frac{\Gamma}{2\pi a\,Vr}\right)''\frac{r''}{b_{W''}/2}\,\frac{S''}{S'}\,\frac{q''}{q_\infty}(C_{L_\alpha})''\,\alpha''\right.$$

4.5.1.2-b

where the primed quantities refer to the forward panel, the double-primed quantities refer to the aft panel, and the subscript e refers to the exposed panel.

$(C'_{N_1})'_e$ is the pseudonormal-force coefficient of the exposed forward panel calculated at the wing angle $\alpha - \alpha'_0$ where α is the angle of attack of the body reference line and α'_0 is the angle, negative in sign, measured from the wing chord line at the MAC to the wing zero-lift line. The value of $(C'_{N_1})'_e$ is obtained from Section 4.1.3.3. (See Section 4.3.1.2 for the definition of exposed panels.)

$(C'_{N_2})'_e$ is the pseudonormal-force coefficient of the exposed forward panel calculated at the wing angle of incidence i' from Section 4.1.3.3. $\left[(C'_{N_2})'_e = 0 \text{ for } i' = 0.\right]$

$(C'_{N_1})''_e$ is the pseudonormal-force coefficient of the exposed aft panel calculated from Section 4.1.3.3 at the angle $\alpha - \epsilon$ for $\frac{b'}{b''} \geq 1.5$ and at α for $\frac{b'}{b''} < 1.5$. The downwash angle ϵ is obtained from Section 4.4.1.

$(C'_{N_2})''_e$ is the pseudonormal-force coefficient of the exposed aft panel calculated from Section 4.1.3.3 at the aft-surface incidence angle i''. $\left[(C'_{N_2})''_e = 0 \text{ for } i'' = 0.\right]$

$(C_{L_\alpha})'_e$ and $(C_{L_\alpha})''_e$ are the lift-curve slopes of the exposed forward and aft panels, respectively, from Section 4.1.3.2.

$(C_{L_\alpha})'$ and $(C_{L_\alpha})''$ are the lift-curve slopes of the forward and aft panels, respectively, from Section 4.1.3.2.

K_N, $K_{W(B)}$, $K_{B(W)}$, $k_{W(B)}$, and $k_{B(W)}$ are the aerodynamic interference factors from Section 4.3.1.2.

$\left[\frac{\Gamma_B}{2\pi\,Vr\alpha}\right]'$ and $\left[\frac{\Gamma_B}{2\pi Vr\alpha}\right]''$ are nondimensional vortex strenths obtained from Section 4.3.1.3.

$I_{v_{B(W')}}$, $I_{v_{B(W'')}}$, and $I_{v_{W'(W'')}}$ are the vortex interference factors between vehicle components. The values

$I_{v_{B(W')}}$ and $I_{v_{B(W'')}}$ are obtained from Section 4.3.1.3 and $I_{v_{W'(W'')}}$ is obtained from Section 4.4.1.

$\frac{r'}{b'}$ and $\frac{r''}{b''}$ are the ratios of the body radii at the midpoint of the exposed root chord to the total spans of the forward and aft panels, respectively.

α'' is the angle of attack of the aft panel, $\alpha - \epsilon + i''$, where ϵ is obtained from Section 4.4.1.

b'_v is the lateral position of the forward-surface vortex from Section 4.4.1.

$\frac{q''}{q_\infty}$ is the dynamic-pressure ratio due to the forward panel acting on the aft panel. This value is obtained from Section 4.4.1. The value of $\frac{q}{q_\infty}$ is almost always taken to be 1.0.

For configurations in which the body is relatively small compared to the span of the panels, the terms involving $I_{v_{B(W')}}$ and $I_{v_{B(W'')}}$ in equations 4.5.1.2-a and 4.5.1.2-b can be neglected. For purposes of the Datcom these terms are neglected when $b'/(2r)$ or $b''/(2r) \geq 3.0$ (care should be taken to evaluate the coefficients at the proper angles of attack and incidence).

Sample Problems

1. The span of the forward panel is large compared to that of the aft panel ($b'/b'' \geq 1.5$).

Given: Configuration of sample problem 1, paragraph A, Section 4.5.1.1.

Compute:

Step 1. $(C'_{N_1})'_e$ and $(C'_{N_2})'_e$ (Section 4.1.3.3)

From sample problem 1, paragraph A, Section 4.5.1.1

$a'_0 = 0$ $\qquad (C_{L_\alpha})'_e = 0.0664$ per deg $= 3.805$ per rad

$\Delta y = 2.65$

Obtain $(C_{L_{max}})'_e$ and $(\alpha_{C_{L_{max}}})'_e$ (Section 4.1.3.4)

Test for method most applicable

$C_1 = 0.32$ (figure 4.1.3.4-24b)

$$\frac{4}{(C_1 + 1)\cos \Lambda'_{LE}} = 4.386$$

Since $A'_e = 7.61 > 4.386$, use high-aspect-ratio method

$\left(\frac{C_{L_{max}}}{c\ell_{max}}\right)'_e = 0.68$ (figure 4.1.3.4-21a)

$(c\ell_{max})'_e = 1.45$ (Section 4.1.1.4)

$(\Delta C_{L_{max}})'_e = 0$ (figure 4.1.3.4-22)

$(\Delta\alpha_{C_{L_{max}}})'_e = 5.7°$ (figure 4.1.3.4-21b)

$$(C_{L_{max}})'_e = \left[\left(\frac{C_{L_{max}}}{c\ell_{max}}\right) c\ell_{max} + \Delta C_{L_{max}}\right]'_e = 0.986 \quad \text{(equation 4.1.3.4-d)}$$

$$(\alpha_{C_{L_{max}}})'_e = \left[\frac{C_{L_{max}}}{C_{L_\alpha}} + \alpha_0 + \Delta\alpha_{C_{L_{max}}}\right]'_e = 20.5° \quad \text{(equation 4.1.3.4-e)}$$

Obtain $(\alpha^*)'$ (Section 4.1.1)

$(\alpha^*)' = 10°$

Construct curve of $(C_L)'_e$ vs α

$(C_L)'_e = (C_{L_\alpha})'_e \alpha$ for α's below $(\alpha^*)'$

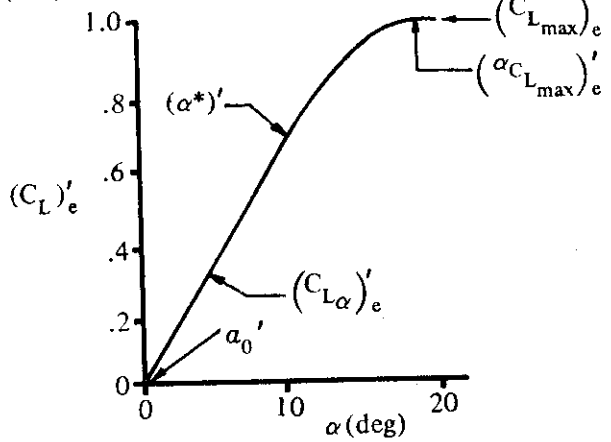

From constructed curve, obtain $(C_{N_1})'_e$, substituting the wing angle $\alpha - \alpha_0'$ for α.

$\alpha - \alpha_0' = \alpha - 0 = \alpha$

① α deg	② $\alpha - \alpha_0'$ deg	③ $(C_L)'_e$ at ②	④ $(C_{N_1})'_e = (C_L)'_e/\cos$ ②
0	0	0	0
5	5	.332	.333
10	10	.664	.674
15	15	.915	.947
20.5	20.5	.986	1.053

$(C_{N_2})'_e = 0$, since $i' = 0$

Step 2. Downwash angle at horizontal tail (Section 4.4.1). Sample problem 1, paragraph A, Section 4.5.1.1, has the procedure briefly outlined and sample problem 1, paragraph A, Section 4.4.1, is a detailed example.

The final result is shown below.

α deg	ϵ deg	$\alpha - \epsilon$ deg
0	0	0
5	1.5	3.5
10	2.9	7.1
15	4.9	10.1
20.5	8.0	12.5

Step 3. $(C'_{N_1})''_e$ and $(C'_{N_2})''_e$ (Section 4.1.3.3)

Test for method most applicable (Section 4.1.3.4)

$C_1 = 0.32$ (figure 4.1.3.4-24b)

$$\frac{4}{(C_1 + 1)\cos \Lambda''_{LE}} = 4.494; \quad \frac{3}{(C_1 + 1)\cos \Lambda''_{LE}} = 3.370$$

$A''_e = 3.45$, which lies between the above limits.

Borderline case: use low-aspect-ratio method

$(C_{N_\alpha})''_e = (C_{L_\alpha})''_e = 0.0542$ per deg $= 3.106$ per rad (sample problem 1, paragraph A, Section 4.5.1.1)

Obtain $(C_{L_{max}})''_e$ and $(\alpha_{C_{L_{max}}})''_e$

$$(C_1 + 1)\frac{A''_e}{\beta}\cos \Lambda''_{LE} = 3.13$$

$$\left[(C_{L_{max}})_{base}\right]''_e = 0.80 \text{ (figure 4.1.3.4-23a)}$$

$C_2 = 1.05$ (figure 4.1.3.4-24b)

$(C_2 + 1)\, A''_e \tan \Lambda''_{LE} = 7.75$

$(\Delta C_{L_{max}})''_e = 0.22$ (figure 4.1.3.4-24a)

$$\left[(\alpha_{C_{L_{max}}})_{base}\right]''_e = 22° \text{ (figure 4.1.3.4-25a)}$$

$(\Delta\alpha_{C_{L_{max}}})''_e = 4°$ (figure 4.1.3.4-25b)

$(C_{L_{max}})''_e = \left[(C_{L_{max}})_{base} + \Delta C_{L_{max}}\right]''_e = 1.02$ (equation 4.1.3.4-g)

$(\alpha_{C_{L_{max}}})''_e = \left[(\alpha_{C_{L_{max}}})_{base} + \Delta\alpha_{C_{L_{max}}}\right]''_e = 26°$ (equation 4.1.3.4-h)

Obtain $\left[(C_{N_{\alpha\alpha}})_{ref}\right]''_e$

$$\left[C_{N'} @ C_{L_{max}}\right]''_e = \left(\frac{C_{L_{max}}}{\cos \alpha_{C_{L_{max}}}}\right)''_e = 1.13$$

$$\left[(C_{N_{\alpha\alpha}})_{ref}\right]''_e = \frac{\left[C_{N'} @ C_{L_{max}}\right]''_e - (C_{N_\alpha})''_e \frac{\sin 2\alpha}{2}}{\sin \alpha \,|\sin \alpha|} = -0.292 \text{ (equation 4.1.3.3-b, } (C_{N_\alpha})''_e \text{ in rad)}$$

where $\alpha = (\alpha_{C_{L_{max}}})''_e$

Obtain J

$$J = 0.3\,(C_1 + 1)\frac{A''_e}{\beta}\cos \Lambda''_{LE}\left\{(C_1 + 1)\,(C_2 + 1) - \left[\frac{(C_2 + 1)\, A''_e \tan \Lambda''_{LE}}{7}\right]^3\right\} = 1.27$$

Calculate $(C'_{N_1})''_e$ vs α'' (equation 4.1.3.3-a)

① α'' deg	② $\frac{\tan \alpha''}{\tan (\alpha_{C_{L_{max}}})''_e}$	③ $(\Delta C_{N_{\alpha\alpha}})''_e$ figure 4.1.3.3-55a	④ $(C_{N_{\alpha\alpha}})''_e = \left[(C_{N_{\alpha\alpha}})_{ref} + \Delta C_{N_{\alpha\alpha}}\right]''_e$	⑤ $(C_{N_{\alpha\alpha}})''_e \sin^2\alpha''$ $= ④ \sin^2\alpha''$	⑥ $(C_{N_\alpha})''_e \frac{\sin 2\alpha''}{2}$ $= 3.106 \frac{\sin 2\alpha''}{2}$	⑦ $(C'_{N_1})''_e$ $= ⑤ + ⑥$
5	.179	1.85	1.558	0.0118	.269	0.281
10	.361	1.85	1.558	0.0468	.531	0.578
15	.550	1.50	1.208	0.081	.777	0.858
20.5	.767	0.75	0.458	0.056	1.019	1.075

Plot $(C'_{N_1})''_e$ vs α and read values at $\alpha \quad \epsilon$ (since $b'/b'' > 1.5$)

α deg	α'' $(\alpha - \epsilon)$	$(C'_{N_1})''_e$
5	3.5	0.195
10	7.1	0.408
15	10.1	0.583
20.5	12.5	0.720

$(C'_{N_2})''_e = 0$, since $i'' = 0$

Step 4. Wing-body and tail-body interference factors (Section 4.3.1.2)

From sample problem 1, paragraph A, Section 4.5.1.1

$[K_N + K_{W(B)} + K_{B(W)}]' = 1.257$

$[K_{W(B)} + K_{B(W)}]'' = 1.460$

Step 5. Dynamic pressure at horizontal tail (Section 4.4.1)

Sample problem 1, paragraph A, Section 4.5.1.1, has the procedure briefly outlined and sample problem 4, paragraph A, Section 4.4.1, is a detailed example.

The final result is shown below.

$\frac{q''}{q_\infty} = 1.0$ for all α's

(since $\left|\frac{z}{z_W}\right| > 1.0$ for all α's)

Step 6. Vortices effect (Section 4.3.1.3)

$$\frac{b'}{d'} = 10 \qquad \frac{b''}{d''} = 4.9$$

Since these ratios are both greater than 3.0, the vortices effect can be neglected.

$I_{v_{B(W')}} = I_{v_{B(W'')}} = 0$

Step 7. Solution for C_N vs α

$$C_N = \left\{(C'_{N_1})'_e [K_N + K_{W(B)} + K_{B(W)}]' + (C'_{N_2})'_e [k_{W(B)} + k_{B(W)}]'\right\} \frac{S_e'}{S'}$$
$$+ \left\{(C'_{N_1})''_e [K_{W(B)} + K_{B(W)}]'' + (C'_{N_2})''_e [k_{W(B)} + k_{B(W)}]''\right\} \frac{q''}{q_\infty} \frac{S_e''}{S'}$$

(equation 4.5.1.2-a simplified)

$C_N = (C'_{N_1})'_e (1.257) (.896) + (C'_{N_1})''_e (1.460) (1.0) (.118)$

$= 1.126 (C'_{N_1})'_e + .1723 (C'_{N_1})''_e$

①	②	③	④	⑤	⑥
α deg	$(C'_{N_1})'_e$	$(C'_{N_1})''_e$	$1.126 (C'_{N_1})'_e$	$.1723 (C'_{N_1})''_e$	$C_N = ④ + ⑤$
0	0	0	0	0	0
5	0.333	0.195	0.375	0.0336	0.4086
10	0.674	0.408	0.759	0.0705	0.8295
15	0.947	0.583	1.066	0.1000	1.166
20.5	1.053	0.720	1.186	0.1240	1.310

2. The span of the forward panel is approximately equal to or less than the span of the aft panel ($b'/b'' < 1.5$).

Given: Configuration of sample problem 2, paragraph A, Section 4.5.1.1.

Compute:

The calculation procedures of sample problem 2 that are similar to those of sample problem 1 are not listed in detail here.

Step 1. $(C'_{N_1})'_e$ and $(C'_{N_2})'_e$ (Section 4.1.3.3)

The low-aspect-ratio method is used to calculate $(C'_{N_1})'_e$.

$(C_{L_{max}})'_e = 0.935$ $\qquad$ $(\alpha_{C_{L_{max}}})'_e = 26.0°$

$(C_{N_\alpha})'_e = 0.0405$ per deg $= 2.32$ per rad $\qquad$ $[(C_{N_{\alpha\alpha}})_{ref}]'_e = 0.655$ per rad

$J = 1.60$ $\qquad$ $[C'_N @ C_{L_{max}}]'_e = 1.04$

$$(C'_{N_1})'_e = (C_{N_\alpha})'_e \frac{\sin 2\alpha}{2} + (C_{N_{\alpha\alpha}})'_e \sin\alpha \,|\sin\alpha| \quad \text{(equation 4.1.3.3-a)}$$

①	②	③	④	⑤	⑥	⑦
α deg	$\frac{\tan\alpha}{\tan(\alpha_{C_{L_{max}}})'_e}$	$(\Delta C_{N_{\alpha\alpha}})'_e$ figure 4.1.3.3-55a	$(C_{N_{\alpha\alpha}})'_e = [(C_{N_{\alpha\alpha}})_{ref} + \Delta C_{N_{\alpha\alpha}}]'_e$	$(C_{N_{\alpha\alpha}})'_e \sin^2\alpha$	$(C_{N_\alpha})'_e \frac{\sin 2\alpha}{2}$	$(C'_{N_1})'_e = ② + ⑥$
5	.179	2.10	2.755	.021	.202	.223
10	.361	2.10	2.755	.083	.397	.480
15	.549	1.80	2.455	.164	.580	.744
20	.746	1.00	1.655	.194	.746	.940
23	.870	.50	1.155	.176	.835	1.011
26	1.0	0	.655	.126	.914	1.040

$(C'_{N_2})'_e = 0$, since $i' = 0$

Step 2. $(C'_{N_1})''_e$ and $(C'_{N_2})''_e$ (Section 4.1.3.4)

Since $\frac{b'}{b''} < 1.5$, evaluate $(C'_{N_1})''_e$ at α.

From low-aspect-ratio method, the following is obtained.

$(C_{L_{max}})''_e = 0.705$ $\qquad$ $(\alpha_{C_{L_{max}}})''_e = 14.5°$

Since $(\alpha_{C_{L_{max}}})''_e$ is considerably lower than $(\alpha_{C_{L_{max}}})'_e$, the solution for $(C'_{N_1})''_e$ must include both below-stall and above-stall calculations. The final result is listed below.

α deg	$(C'_{N_1})''_e$
5	.330
10	.625
15	.749
20	.738
23	.767
26	.824

Because of the limitation of the method, the accuracy deteriorates at high angles of attack. Calculate the remaining portion of the solution at $\alpha \leqq 20°$.

$(C'_{N_2})''_e = 0$, since $i'' = 0$

Step 3. Wing-body and tail-body interference factors (Section 4.3.1.2)

From sample problem 2, paragraph A, Section 4.5.1.1

$[K_N + K_{W(B)} + K_{B(W)}]' = 1.497$

$[K_{W(B)} + K_{(B)W}]'' = 1.450$

Step 4. Dynamic pressures at horizontal tail

From the methods of Section 4.4.1 the following is obtained.

α deg	$\frac{q''}{q_\infty}$
0	.859
5	.937
10	.999
15	1.0
20	1.0

Step 5. Vortices effect

$$\frac{b'}{d'} = 5.25 \qquad \frac{b''}{d''} = 5.01$$

Since these ratios are both greater than 3.0, the terms involving $I_{v_{B(W')}}$ and $I_{v_{B(W'')}}$ can be neglected.

Calculate lift of tail due to wing vortices.

From sample problem 2, paragraph A, Section 4.5.1.1

$$(C_{L_\alpha})'_e \frac{S_e'}{S'} = 1.696 \text{ per rad}$$

$$(C_{L_\alpha})''_e \frac{q''}{q_\infty} = 3.28 \text{ per rad (at } \alpha = 0)$$

Therefore $(C_{L_\alpha})''_e \frac{q''}{q_\infty} = 3.82 \frac{q''}{q_\infty}$ per rad

$K_{W(B)'} = 1.16$

$$\frac{\frac{b''}{2} - \frac{d''}{2}}{2\pi A''_e \left(\frac{b_v'}{2} - \frac{d'}{2}\right)} = 0.04106$$

$$C_{L_{W''(v)}} = \frac{(C_{L_\alpha})'_e \frac{S_e'}{S'} (C_{L_\alpha})''_e \frac{q''}{q_\infty} K_{W(B)'} \alpha I_{v_{W'(W'')}} \left(\frac{b''}{2} - \frac{d''}{2}\right)}{2\pi A''_e \left(\frac{b_v'}{2} - \frac{d'}{2}\right)}$$

$$= 1.696 \left(3.82 \frac{q''}{q_\infty}\right) (1.16)\ (0.04106)\ \alpha I_{v_{W'(W'')}}$$

$$= 0.308 \frac{q''}{q_\infty} \alpha I_{v_{W'(W'')}} \quad (\alpha \text{ in radians})$$

The variation of $I_{v_{W'(W'')}}$ with α has been calculated in sample problem 3, paragraph A, Section 4.4.1 and is not repeated here.

①	②	③	④	⑤
α deg	α rad	$I_{v_{W'(W'')}}$	$C_{L_{W''(v)}} = 0.308 \frac{q''}{q_\infty} ② ③$	$C_{N_{W''(v)}} = ④/\cos\alpha$
0	0	−3.0	0	0
5	0.08725	−2.5	−0.063	−0.063
10	0.1745	−2.0	−0.108	−0.110
15	0.2618	−1.68	−0.135	−0.140
20	0.3490	−1.40	−0.150	−0.160

Step 6. Solution for C_N vs α

$$C_N = \left\{(C_{N_1})'_e [K_N + K_{W(B)} + K_{B(W)}]' + (C'_{N_2})'_e [k_{W(B)} + k_{B(W}]' \right\} \frac{S_e'}{S'}$$

$$+ \left\{(C'_{N_1})''_e [K_{W(B)} + K_{B(W)}]'' + (C'_{N_2})''_e [k_{W(B)} + k_{B(W)}]'' \right\} \frac{q''}{q_\infty} \frac{S_e''}{S'}$$

$$+ C_{N_{W''(v)}} \quad \text{(equation 4.5.1.2-b simplified)}$$

Substituting the constants gives

$$C_N = (C'_{N_1})'_e (1.497)\ (.730) + (C'_{N_1})''_e (1.450) \frac{q''}{q_\infty} (.205) + C_{N_{W''(v)}}$$

$$= 1.093\ (C'_{N_1})'_e + .2973\ (C'_{N_1})''_e \frac{q''}{q_\infty} + C_{N_{W''(v)}}$$

①	②	③	④	⑤	⑥	⑦	⑧
α deg	$(C'_{N_1})'_e$	$(C'_{N_1})''_e$	$\frac{q''}{q_\infty}$	$1.093\ (C'_{N_1})'_e$	$.2973\ (C'_{N_1})''_e \frac{q''}{q_\infty}$	$C_{N_{W''(v)}}$	C_N ⑤ + ⑥ + ⑦
0	0	0	.859	0	0	0	0
5	.223	.330	.937	.244	.092	−0.063	0.265
10	.480	.625	.999	.525	.186	−0.110	0.601
15	.744	.749	1.0	.813	.223	−0.140	0.896
20	.940	.738	1.0	1.027	.219	−0.160	1.086

B. TRANSONIC

At present it is not possible to predict the aerodynamic characteristics of wing-body-tail combinations in the nonlinear angle-of-attack range. However, it is anticipated that the interference effects can be large.

DATCOM METHOD

It is recommended that the equations presented in paragraph A above be applied throughout the transonic speed range. Care should be exercised to evaluate the various terms of these equations at the proper Mach number. The interference k factors are most accurate for slender configurations. The vortex

terms $I_{v_{B(W')}}$, etc., are thought to be quite valid. But the characteristics of the isolated panels and the downwash cannot be determined as accurately.

C. SUPERSONIC

At supersonic speeds the direct influence of the wing shock-expansion field on the horizontal tail must be considered, as well as the effects of wing vortices and body vortices considered in the subsonic method of paragraph A. The introductory discussion pertaining to body-vortex and wing-vortex effects applies equally as well at subsonic and supersonic speeds.

In cases for which the wing shock-expansion effects are important, account can be taken of the downwash angle, dynamic pressure, and Mach number at the tail by direct application of shock-expansion theory. It is assumed that the flow in the region of the horizontal tail is the two-dimensional shock-expansion field radiating from the exposed root chord of the wing (see sketch (a)). Any effects of wing-body interference or wing section in distorting the shock-expansion field are neglected. This assumption is valid only if the span of the forward surface is greater than the span of the aft surface; i.e., $b' > b''$.

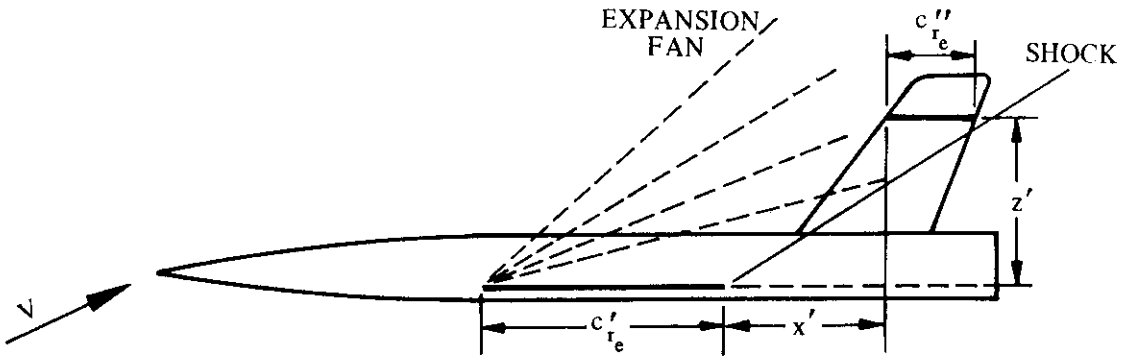

SKETCH (a)

The tail in sketch (a) is in a high downwash field so that the flow at the tail is nearly parallel to the tail chord. As the angle of attack is increased, the tail will move downward with respect to the trailing-edge shock wave, out of the shock-expansion field and into a region of lower downwash. If the tail were initially above the expansion fan from the wing leading edge, an increase in angle of attack would move the tail into the shock-expansion field and, consequently, into a region of increased downwash. It is seen then that the wing shock-expansion field can cause either an increase or a decrease in the tail download in contrast to body vortices and wing vortices, which cause only an increase in tail download.

DATCOM METHOD

The lift of a wing-body-tail combination in the nonlinear angle-of-attack range at supersonic speeds is approximated by using the subsonic method (paragraph A) minus the second term on the right-hand side of the equation,which accounts for the horizontal tail effects, plus an additional term to account for the direct influence of the wing shock-expansion field on the horizontal tail. The influence of the shock-expansion field may be evaluated only for configurations with $b' > b''$. Furthermore, the shock-expansion term presented in the Datcom is applicable only to configurations with neither wing nor tail incidence. In using the method of paragraph A, care should be taken to evaluate all parameters at the proper Mach number.

It should be noted that if the tail is in the wing shock-expansion field, it cannot "see" the wing trailing vortices. In this case, the contribution of the wing-vortex interference (third term of equation 4.5.1.2-b) is

neglected. If, however, the tail is behind the wing shock-expansion field, it can "see" the wing trailing vortices and the wing-vortex interference should be considered rather than the shock-expansion field.

The shock-expansion term for configurations with neither wing nor tail incidence, taken from reference 1*, is

$$\left(\Delta C_L\right)_{SE} = \eta_\alpha \frac{S''}{S'} \alpha C_{L_\alpha}'' \qquad 4.5.1.2\text{-c}$$

where all terms except η_α are defined in the subsonic paragraph.

η_α is a "lumped" angle-of-attack effectiveness parameter obtained from figures 4.5.1.2-13a through 4.5.1.2-13p for combinations of angle of attack of 5°, 10°, 15°, and 20° and Mach numbers of 2, 3, 4, and 5. η_α accounts for the change in dynamic pressure at the tail, the change in the tail lift-curve slope, and the downwash at the tail, and is defined as

$$\eta_\alpha = \frac{q''}{q_\infty}\left(1 - \frac{\epsilon}{\alpha}\right)\frac{\left(C_{L_\alpha}''\right)_{M_H}}{\left(C_{L_\alpha}''\right)_{M_\infty}}$$

where

$\left(C_{L_\alpha}''\right)_{M_H}$ is the lift-curve slope of the horizontal tail operating at the local Mach number of the flow in the region of the horizontal tail.

$\left(C_{L_\alpha}''\right)_{M_\infty}$ is the lift-curve slope of the isolated horizontal tail at the free-stream Mach number.

The procedure for using figure 4.5.1.2-13 is as follows:

Step 1. Determine the exposed-wing root chord c_{r_e}' and the exposed-tail root chord c_{r_e}''.

Step 2. Determine the longitudinal distance x' from the trailing edge of the exposed-wing root chord to the leading edge of the exposed-tail root chord, positive for the leading edge of the exposed-tail root chord aft of the trailing edge of the exposed-wing root chord (see sketch (a)).

Step 3. Determine the vertical distance z', measured normal to the longitudinal axis, between the exposed-wing root chord and the exposed-tail root chord, positive for the tail plane above the wing plane (see sketch (a)).

Step 4. Calculate x'/c_{r_e}' and z'/c_{r_e}', and by using these parameters locate the exposed-tail root chord c_{r_e}'' in the proper influence zone of the shock-expansion field of figure 4.5.1.2-13.

*In reference 1, the case of a configuration with tail incidence is analyzed. The shock-expansion term is given by

$$(\Delta C_L)_{SE} = C_{L_\alpha}'' \alpha \frac{S''}{S'}\left(\eta_\alpha + \frac{i_W}{\alpha_W}\eta_\delta\right)$$

where η_δ is the tail-incidence effectiveness parameter. Unfortunately, no design charts are available for determining η_δ.

Step 5. The exposed-tail root chord will be divided into several segments by the shock-expansion field. It is assumed that the average value of η_α in the various influence zones is uniform over the tail area within that zone. The average value of η_α in each zone is then multiplied by the ratio of the tail area in that zone to the total exposed tail area S_e'' to obtain a weighted value in each zone.

Step 6. Sum the weighted values of η_α to obtain the total "lumped" effectiveness parameter η_α.

Step 7. Interpolation for angle of attack and/or Mach number may be necessary. If so, a three-point interpolation for α should be made using weighted values of η_α. Two points are sufficient for Mach number interpolation.

For a specified initial Mach number there is a maximum value of the angle of attack for which there exists an oblique-shock solution. Or, conversely, for a specified angle of attack there is a minimum initial Mach number for which there is an oblique-shock solution. The relation between Mach number and angle of attack, below which no solutions for η_α may be obtained, is indicated in sketch (b).

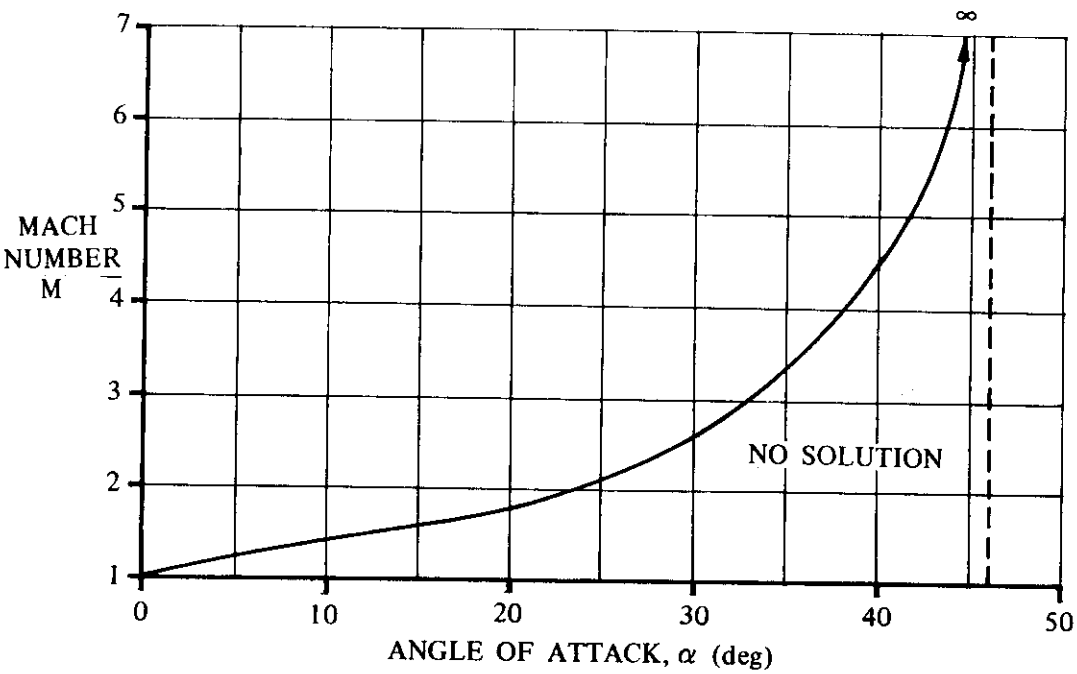

SKETCH (b)

REFERENCES

1. Nielsen, J. N.: The Effect of Body Vortices and the Wing Shock-Expansion Field on the Pitch-Up Characteristics of Supersonic Airplanes. NACA RM A57L23, 1958. (U)

2. Ames Research Staff: Equations, Tables, and Charts for Compressible Flow. NACA TR 1135, 1953. (U)

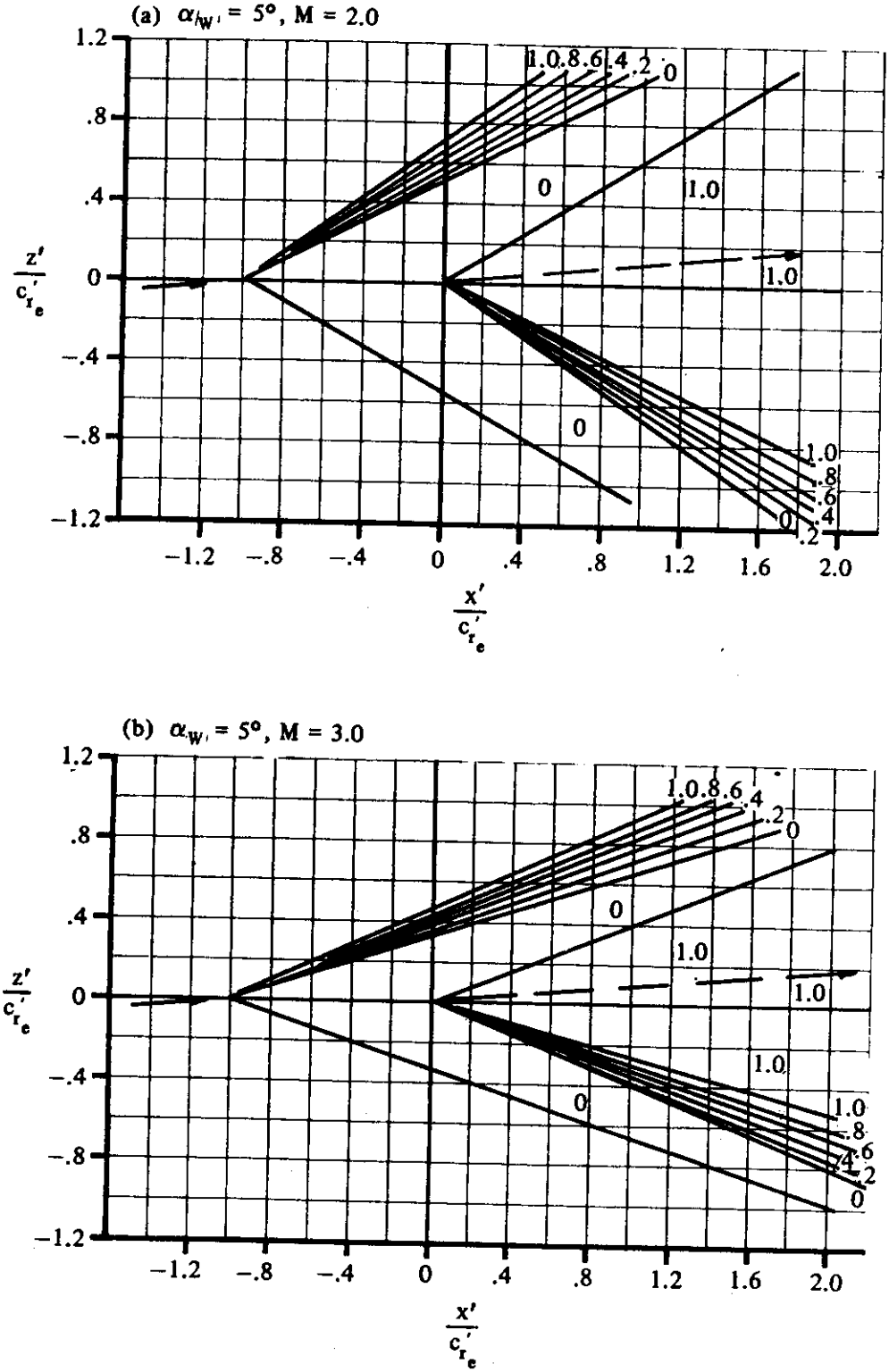

FIGURE 4.5.1.2-13 TAIL-EFFECTIVENESS PARAMETER, η_α

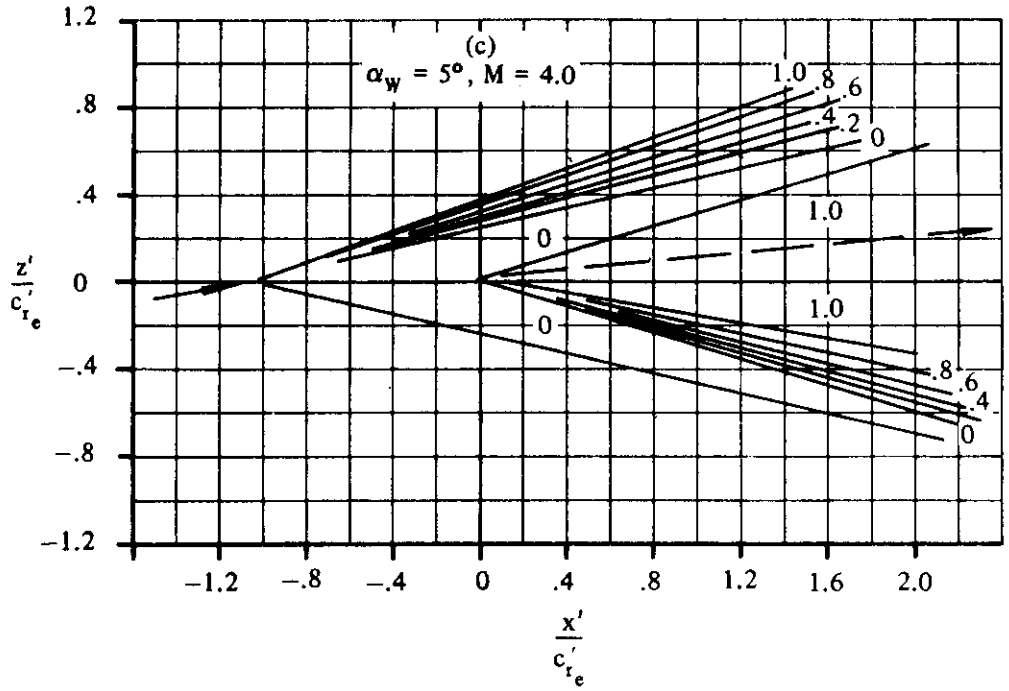

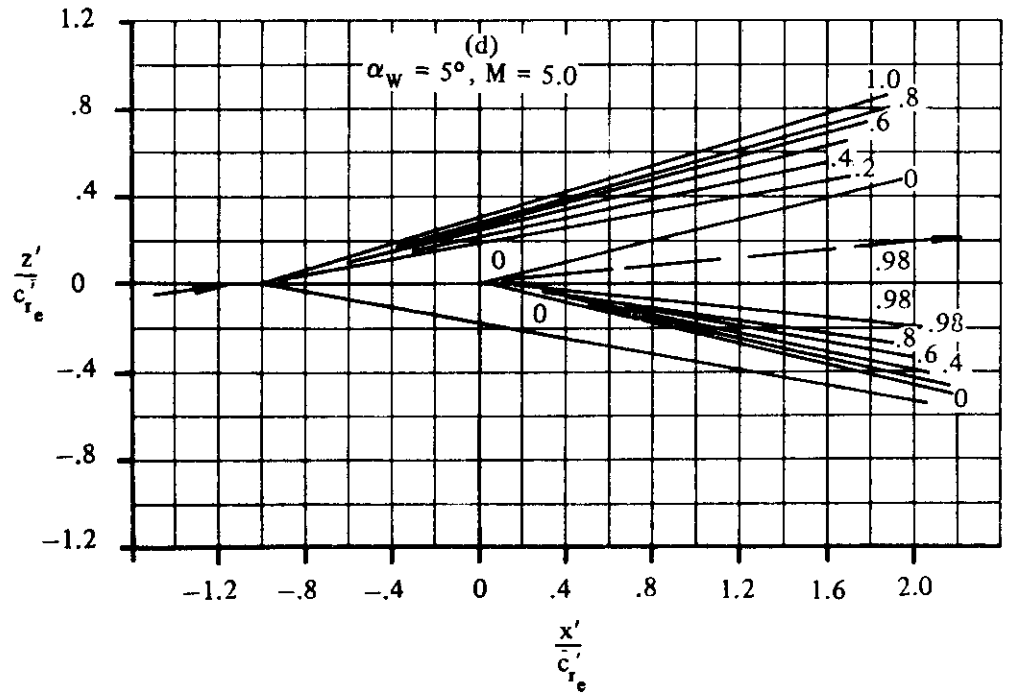

FIGURE 4.5.1.2-13 TAIL-EFFECTIVENESS PARAMETER, η_α (CONTD)

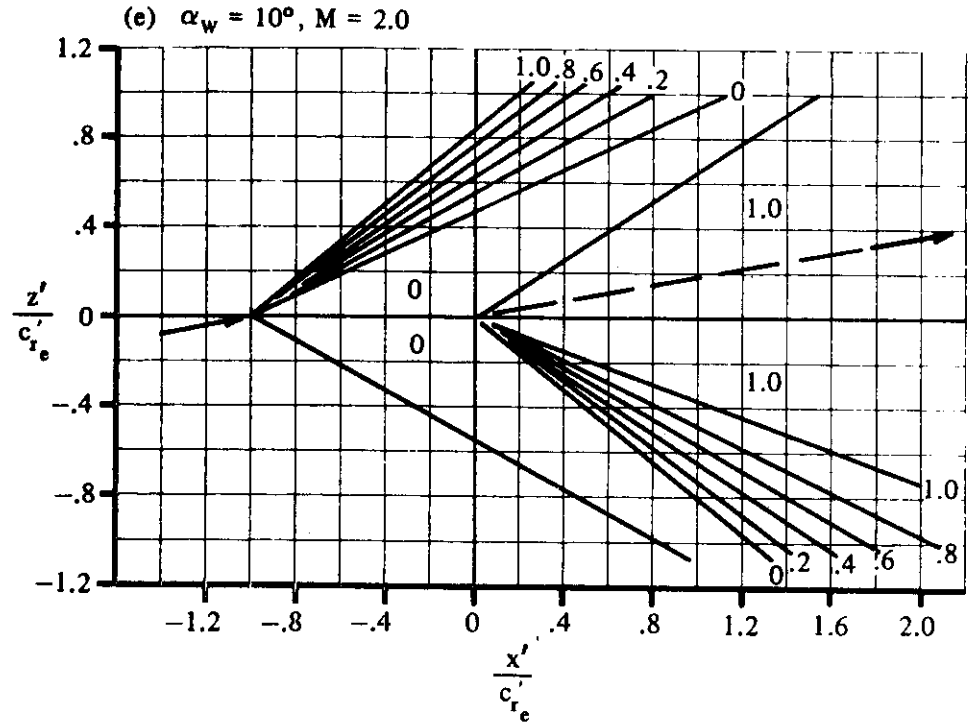

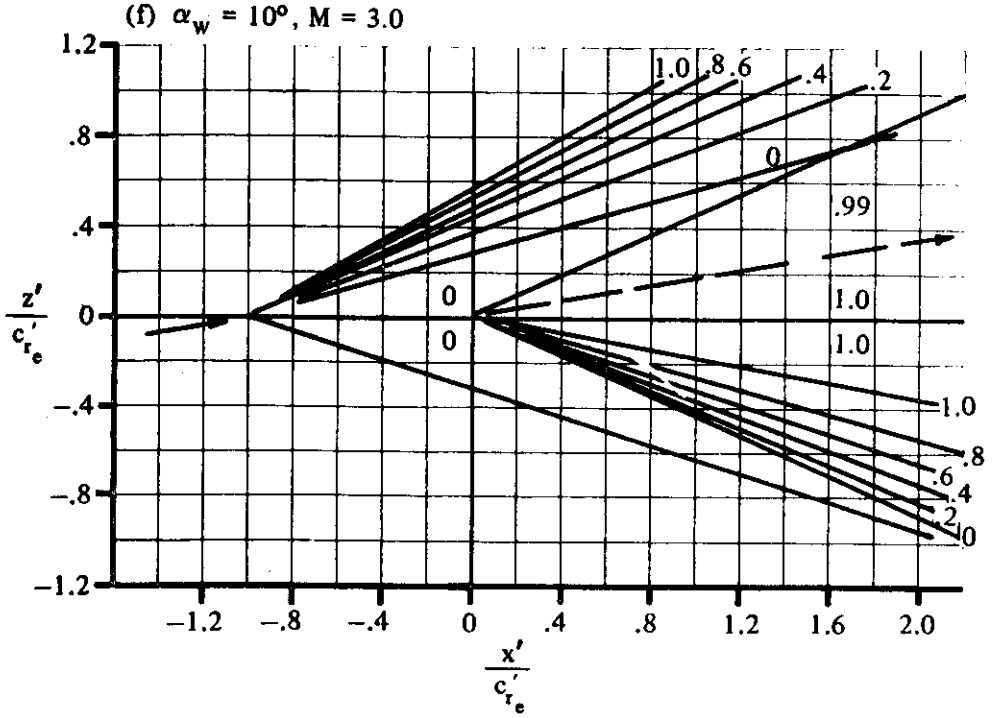

FIGURE 4.5.1.2-13 (CONTD)

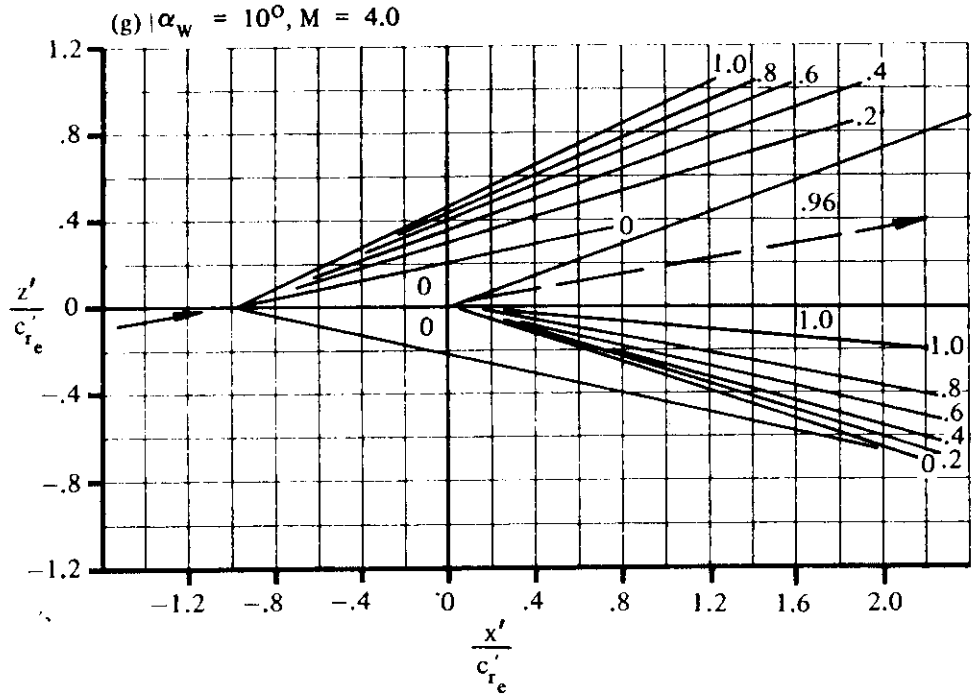

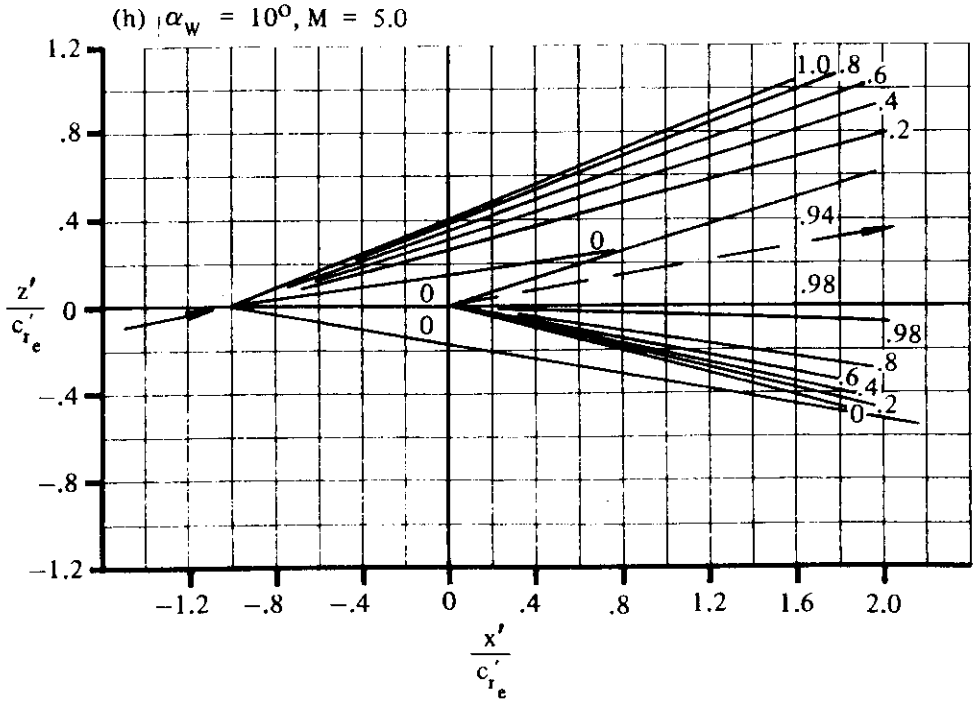

FIGURE 4.5.1.2-13 (CONTD)

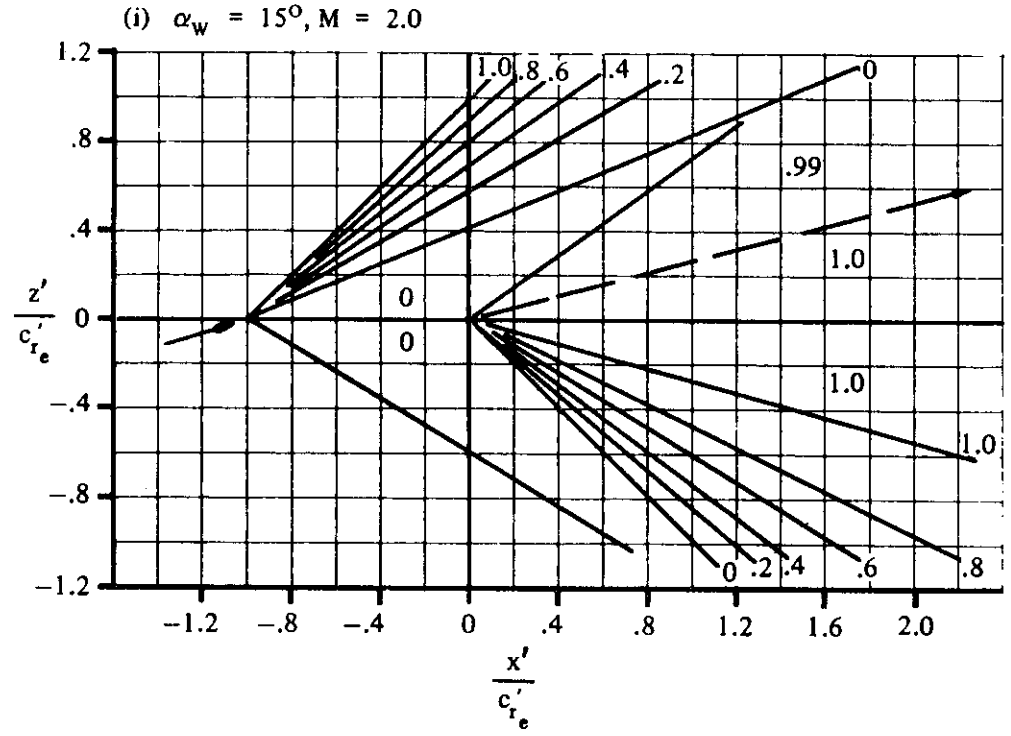

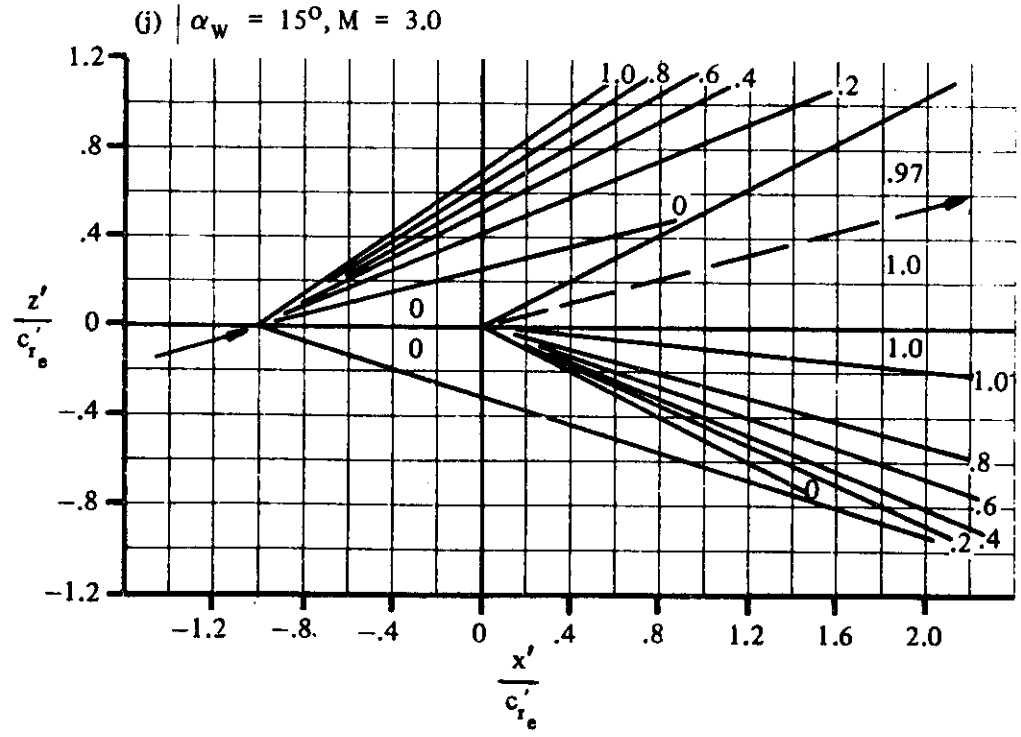

FIGURE 4.5.1.2-13 (CONTD)

(k) $\alpha_w = 15^o$, M = 4.0

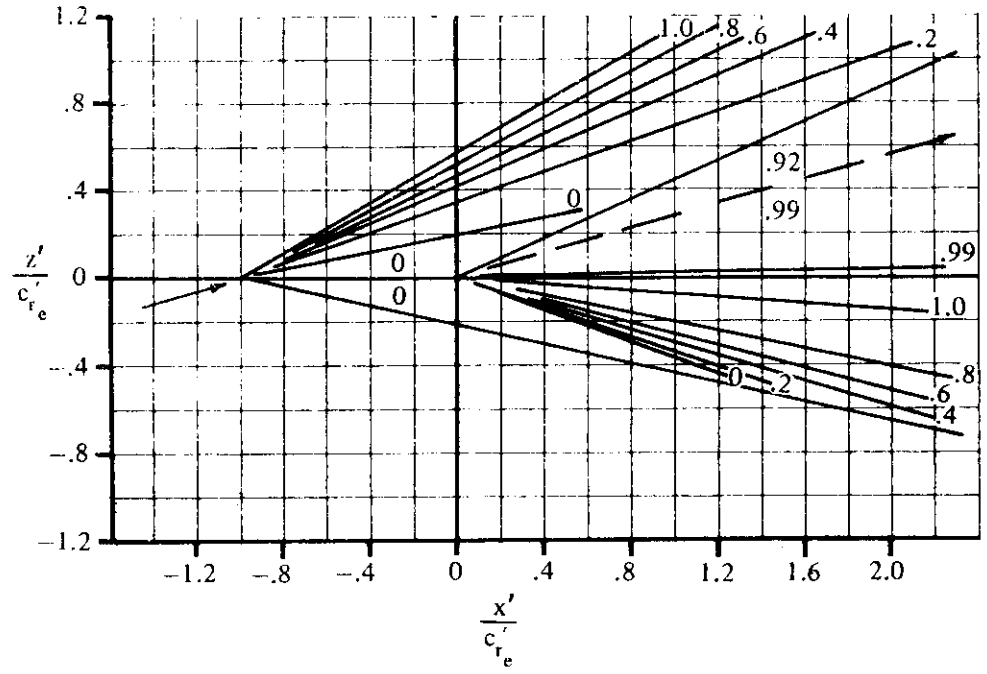

(ℓ) $\alpha_w = 15^o$, M = 5.0

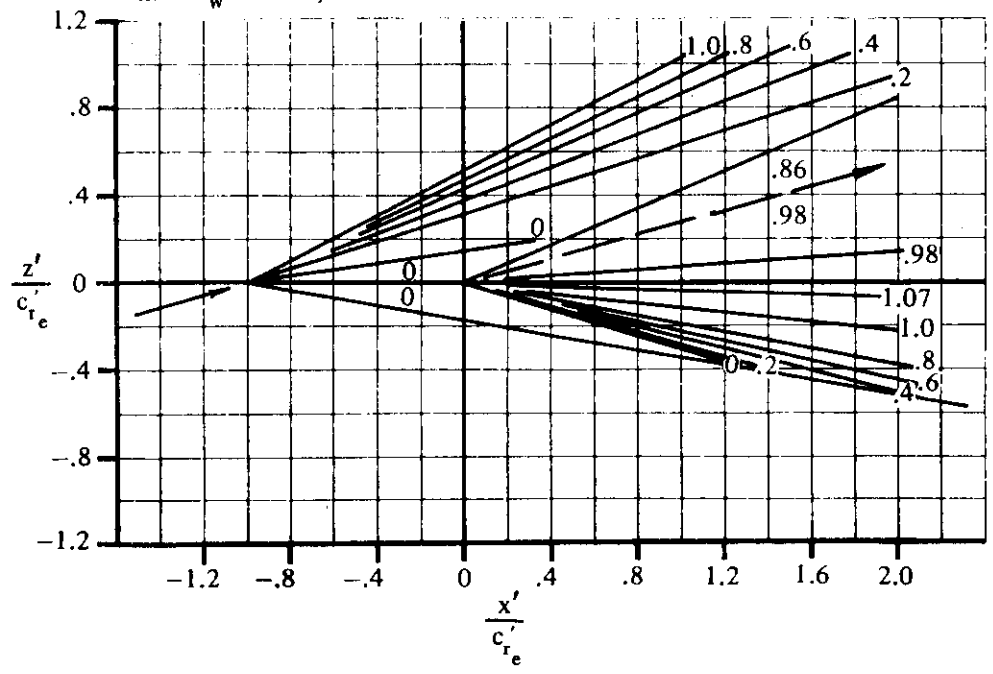

FIGURE 4.5.1.2-13 (CONTD)

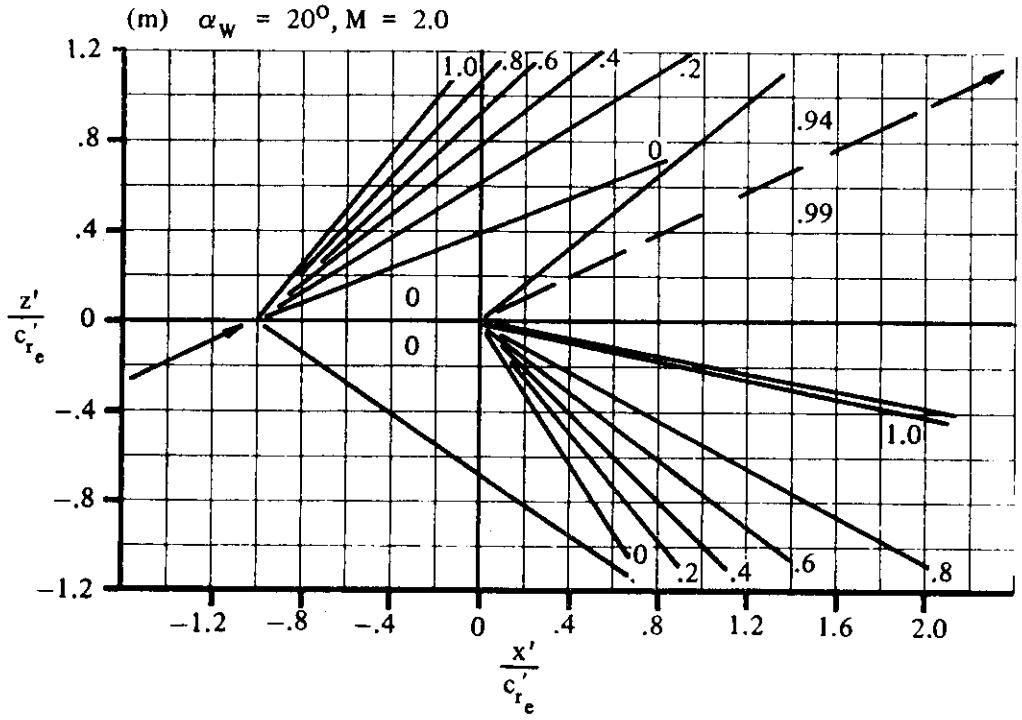

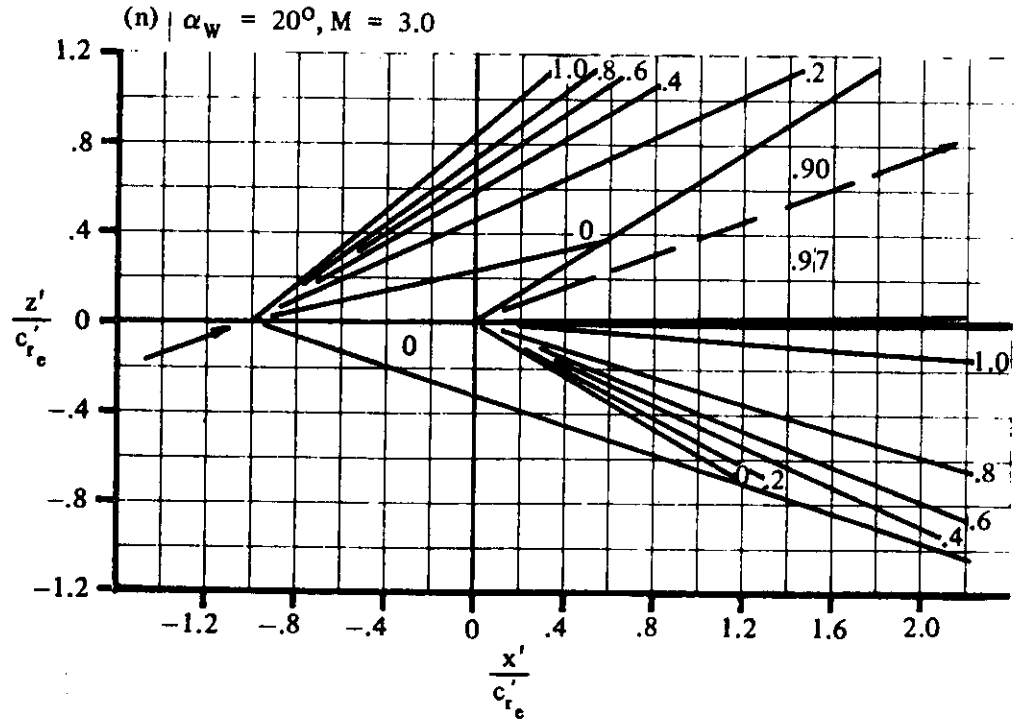

FIGURE 4.5.1.2-13 (CONTD)

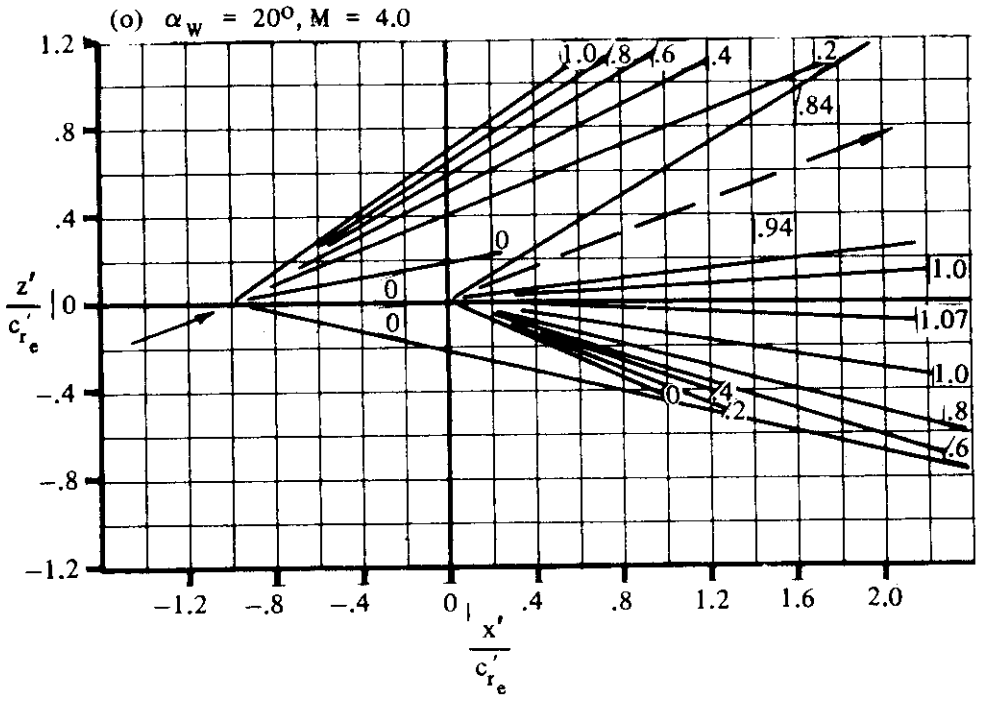

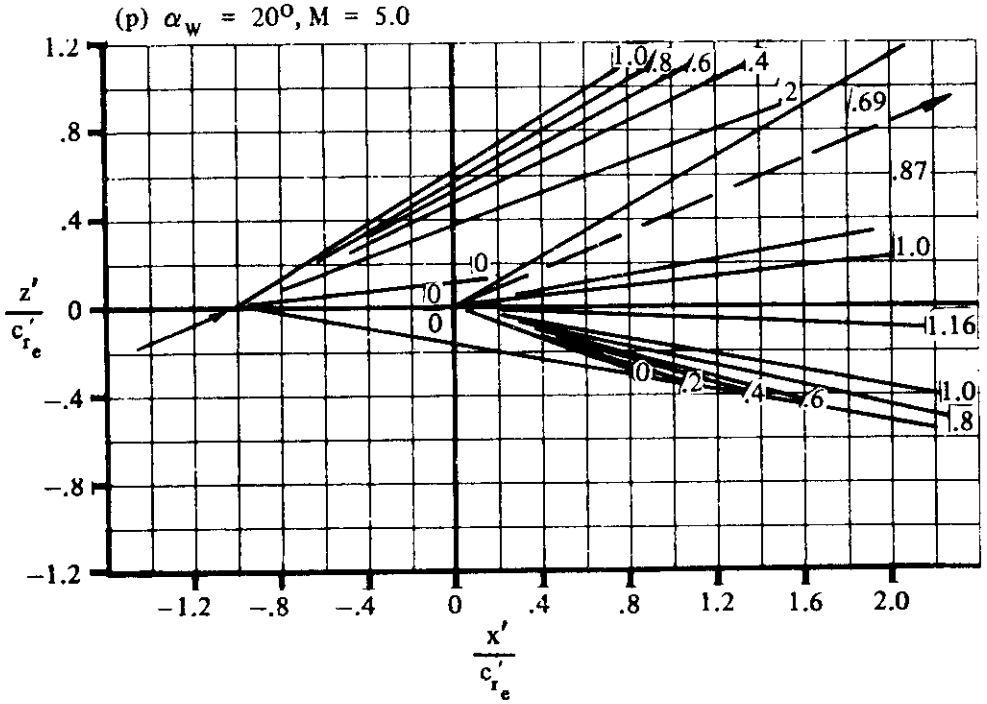

FIGURE 4.5.1.2-13 (CONTD)

4.5.1.3 WING-BODY-TAIL MAXIMUM LIFT

In this section a general method applicable to all speed regimes is presented for estimating the usable or trimmed maximum lift coefficient for a wing-body-tail configuration with no high-lift devices. The wing-body-tail maximum lift is assumed to occur at the wing-body angle of attack for maximum lift.

The effective tail-body lift component is a direct result of the wing-body pitching moment that must be trimmed. Most conventional clean-wing tail-off configurations exhibit a positive pitching moment at stall, therefore requiring a positive tail lift, which generates a balancing negative pitching moment.

The contribution of the tail lift is only as accurate as the wing-body pitching-moment estimate at stall. Unfortunately, many configurations exhibit nonlinear pitching-moment characteristics at or before stall that effectively prohibit an accurate analytical estimate of the pitching moment at stall. For this reason, it is highly desirable to have pitching-moment test data for the particular configuration or for a similar configuration.

DATCOM METHOD

The wing-body-tail angle of attack at maximum lift is assumed to be identical to the wing-body angle of attack at maximum lift from Section 4.3.1.4.

The following method is based on the wing-body maximum lift plus the tail-body lift that is required to trim the vehicle at $(\alpha_{C_{L_{max}}})_{WB}$. The wing-body-tail maximum lift, based on the wing area S_W and neglecting the vertical-tail drag, is determined by

$$C_{L_{max}} = (C_{L_{max}})_{WB} + C_{L_{H(WBV)}} \qquad 4.5.1.3\text{-a}$$

where

$(C_{L_{max}})_{WB}$ is the wing-body maximum lift from test data or Section 4.3.1.4 at the appropriate speed, based on S_W.

$C_{L_{H(WBV)}}$ is the horizontal-tail lift at $(\alpha_{C_{L_{max}}} - \epsilon)$ in the presence of the wing-body, and vertical tail, based on the wing area S_W. The value of this term is determined from considering the horizontal-tail forces that affect the vehicle pitching moment.

The tail lift can be evaluated using one of the three equations that are presented below. The first equation is complete; whereas, the second and third equations are simplifications of the first equation.

$$C_{L_{H(WBV)}} = \frac{\left(C_{m_{WB}}\right)_{\alpha_{C_{L_{max}}}} + C_{D_H} \cos\left(\alpha_{C_{L_{max}}} - \epsilon\right) \frac{z_H}{\bar{c}} - C_{D_H} \sin\left(\alpha_{C_{L_{max}}} - \epsilon\right) \frac{\ell''}{\bar{c}} + C_{m_{H(WBV)}}}{\cos\left(\alpha_{C_{L_{max}}} - \epsilon\right) \frac{\ell''}{\bar{c}} + \sin\left(\alpha_{C_{L_{max}}} - \epsilon\right) \frac{z_H}{\bar{c}}}$$

4.5.1.3-b

where

$\left(C_{m_{WB}}\right)_{\alpha_{C_{L_{max}}}}$ is the wing-body pitching moment at the stall angle of attack based on $S_W \bar{c}_W$ with respect to $\bar{c}_W/4$, obtained from test data for the particular configuration. If no test data are available, it is suggested that an approximation be made by using the methods of Sections 4.1.4.2, 4.1.4.3, and 4.3.2.2 in conjunction with test data on a similar configuration.

C_{D_H} is the horizontal-tail-body drag at $\left(\alpha_{C_{L_{max}}} - \epsilon\right)$ based on S_W, obtained from test data or the appropriate methods of Sections 4.3.3.1 and 4.3.3.2.

$\alpha_{C_{L_{max}}}$ is the wing-body angle of attack at stall, obtained from test data or from the appropriate method of Section 4.3.1.4.

ϵ is the wing downwash at the horizontal tail, obtained from test data or the appropriate method of Section 4.4.1.

$\frac{z_H}{\bar{c}}$ is the ratio of the height of the quarter-chord point of the horizontal-tail MAC above the quarter-chord point of the wing MAC, to the wing MAC. The height is measured perpendicular to the longitudinal axis and is positive for the horizontal tail above the wing (see Sketch (a)).

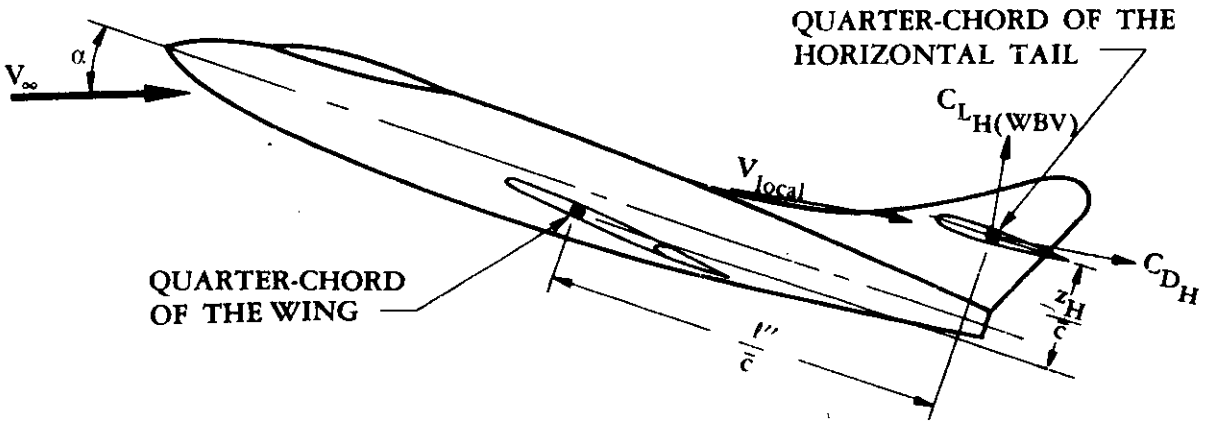

SKETCH (a)

$\frac{\ell''}{\bar{c}}$ is the ratio of the distance from the quarter-chord point of the wing MAC to the quarter-chord point of the horizontal panel MAC (measured parallel to the longitudinal axis), to the wing MAC (see Sketch (a)).

$C_{m_{H(WBV)}}$ is the horizontal-tail pitching moment at $\left(\alpha_{C_{L_{max}}} - \epsilon\right)$ based on $S_W \bar{c}_W$ with respect to the quarter-chord point of the horizontal-tail MAC obtained from test data. If no test data are available, it is suggested that an approximation be made by using the methods from Sections 4.1.4.2, 4.1.4.3, and 4.3.2.2 in conjunction with test data on a similar configuration. However, for horizontal tails with symmetrical airfoil sections, this term can be neglected.

For those configurations where the horizontal-tail drag is very small in comparison with the wing-body pitching moment, the drag terms of Equation 4.5.1.3-b can be omitted. In addition, since most horizontal tails have symmetrical airfoil sections, the $C_{m_{H(WBV)}}$ term can also be omitted. Thus Equation 4.5.1.3-b can be written as

$$C_{L_{H(WBV)}} = \frac{\left(C_{m_{WB}}\right)_{\alpha_{C_{L_{max}}}}}{\cos\left(\alpha_{C_{L_{max}}} - \epsilon\right)\frac{\ell''}{\bar{c}} + \sin\left(\alpha_{C_{L_{max}}} - \epsilon\right)\frac{z_H}{\bar{c}}} \qquad 4.5.1.3\text{-c}$$

If the small-angle approximation can be justified for $\left(\alpha_{C_{L_{max}}} - \epsilon\right)$, the above can be further simplified to yield

$$C_{L_{H(WBV)}} = \frac{\left(C_{m_{WB}}\right)_{\alpha_{C_{L_{max}}}}}{\frac{\ell''}{\bar{c}}} \qquad 4.5.1.3\text{-d}$$

No substantiation is presented because of the lack of test data on wing-body-tail configurations.

Sample Problem

Given:

$\left(C_{L_{max}}\right)_{WB} = 1.0$ $\quad \alpha_{C_{L_{max}}} = 16.5^{o}$ $\quad \epsilon = 9.2^{o}$ $\quad \left(C_{m_{WB}}\right)_{\alpha_{C_{L_{max}}}} = 0.10$

$C_{D_H} = 0.02$ $\quad C_{m_{H(WBV)}} = 0$ $\quad \frac{\ell''}{\bar{c}} = 2.75$ $\quad \frac{z_H}{\bar{c}} = 1.23$

Compute:

$$C_{L_{H(WBV)}} = \frac{\left(C_{m_{WB}}\right)_{\alpha_{C_{L_{max}}}} + C_{D_H} \cos\left(\alpha_{C_{L_{max}}} - \epsilon\right) \frac{z_H}{\bar{c}} - C_{D_H} \sin\left(\alpha_{C_{L_{max}}} - \epsilon\right) \frac{\ell''}{\bar{c}} + C_{m_{H(WBV)}}}{\cos\left(\alpha_{C_{L_{max}}} - \epsilon\right) \frac{\ell''}{\bar{c}} + \sin\left(\alpha_{C_{L_{max}}} - \epsilon\right) \frac{z_H}{\bar{c}}}$$

(Equation 4.5.1.3-b)

$$= \frac{0.10 + 0.02 \cos (16.5^{o} - 9.2^{o}) (1.23) - 0.06 \sin (16.5^{o} - 9.2^{o}) (2.75) + 0}{\cos (16.5^{o} - 9.2^{o}) (2.75) + \sin (16.5^{o} - 9.2^{o}) (1.23)}$$

$$= \frac{0.10 + (0.02) (0.9919) (1.23) - (0.06) (0.1271) (2.75)}{(0.9919) (2.75) + (0.1271) (1.23)}$$

$$= \frac{0.1034}{2.884}$$

$$= 0.0359$$

Solution:

$$C_{L_{max}} = (C_{L_{max}})_{WB} + C_{L_{H(WBV)}} \quad \text{(Equation 4.5.1.3-a)}$$

$$= 1.0 + 0.036$$

$$= 1.036$$

4.5.2 WING-BODY-TAIL PITCHING MOMENT

4.5.2.1 WING-BODY-TAIL PITCHING-MOMENT-CURVE SLOPE

Pitching-moment-estimation methods are inherently less accurate than those for lift, since pitching moment is dependent primarily on load distribution, while lift depends primarily on gross forces. Many of the comments on lift given in Section 4.5.1.1 are also applicable to this Section.

A. SUBSONIC

DATCOM METHODS

Two methods are presented, differing in their treatment of the effect of the forward-surface flow field on the aft surface.

Method 1 ($b'/b'' \geq 1.5$)

For configurations in which the span of the forward surface is large compared to that of the aft surface, the following approach can be used. This method is to be used when the ratio of the forward- to the aft-surface span is 1.5 or greater. The complete equation for the pitching-moment-curve slope C_{m_α} of a wing-body-tail configuration based on the gross area and MAC of the forward panel and an arbitrary center-of-gravity position is given by

$$C_{m_\alpha} = -\frac{x_{cg} - x'}{\bar{c}'}\left[\left\{-(C_L)' + (C_{D_\alpha})'\right\}\sin\alpha + \left\{(C_{L_\alpha})' + (C_D)'\right\}\cos\alpha\right]$$

$$-\frac{z_{cg} - z'}{\bar{c}'}\left[\left\{(C_{L_\alpha})' + (C_D)'\right\}\sin\alpha + \left\{(C_L)' - (C_{D_\alpha})'\right\}\cos\alpha\right]$$

$$-\frac{x_{cg} - x''}{\bar{c}''}\left[\left\{-(C_L)'' + (C_{D_\alpha})''\right\}\sin(\alpha - \epsilon) + \left\{(C_{L_\alpha})'' + (C_D)''\right\}\cos(\alpha - \epsilon)\right]\frac{q''}{q_\infty}\frac{S''}{S'}\frac{\bar{c}''}{\bar{c}'}\left(1 - \frac{\partial\epsilon}{\partial\alpha}\right)$$

$$-\frac{z_{cg} - z''}{\bar{c}''}\left[\left\{(C_{L_\alpha})'' + (C_D)''\right\}\sin(\alpha - \epsilon) + \left\{(C_L)'' - (C_{D_\alpha})''\right\}\cos(\alpha - \epsilon)\right]\frac{q''}{q_\infty}\frac{S''}{S'}\frac{\bar{c}''}{\bar{c}'}\left(1 - \frac{\partial\epsilon}{\partial\alpha}\right)$$

where

geometric parameters are defined in figure 4.5.2.1-7 (note that g', g'', and l'' are always positive)

primed quantities pertain to the forward panel

double-primed quantities pertain to the aft panel

the lift and drag terms below are calculated by the methods of Sections 4.3.1.2 and 4.3.3.2, respectively

$(C_L)'$ and $(C_D)'$ are the complete lift and drag coefficients of the forward panel and body, including wing-body interference. The coefficients are evaluated at the angle $\alpha - \alpha_o + i'$.

$(C_{L_\alpha})'$ and $(C_{D_\alpha})'$ are the complete lift-curve and drag-curve slopes of the forward panel and body including interferences.

$(C_L)''$ and $(C_D)''$ are the lift and drag coefficients of the aft panel evaluated at the tail angle of attack $\alpha'' = \alpha - \epsilon + i''$. These coefficients include wing-body interferences.

$(C_{L_\alpha})''$ and $(C_{D_\alpha})''$ are the lift-curve and drag-curve slopes of the aft panel including wing-body interference effects.

ϵ and $\frac{\partial\epsilon}{\partial\alpha}$ are the downwash angle and downwash gradient, respectively, from Section 4.4.1

α'' is the angle of attack of the aft panel, $\alpha - \epsilon + i''$, where ϵ is the average downwash angle (Section 4.4.1) acting on the aft panel evaluated at the forward-panel angle of attack $\alpha - \alpha_o + i'$

$$\frac{x_{cg} - x'}{\bar{c}'} = \frac{x_{cg}}{\bar{c}'} + \left(\frac{x_{ac}'}{c_r'}\right)\left(\frac{c_r'}{\bar{c}'}\right) - \frac{g'}{\bar{c}'} - .25 \qquad \text{4.5.2.1-b}$$

$$\frac{x_{cg} - x''}{\bar{c}''} = \frac{l''}{\bar{c}''} + \frac{x_{cg}}{\bar{c}''} + \left(\frac{x_{ac}''}{c_r''}\right)\left(\frac{c_r''}{\bar{c}''}\right) - \frac{g''}{\bar{c}''} - .25 \qquad \text{4.5.2.1-c}$$

$x'_{a.c.}$ is the aerodynamic center of the forward panel obtained from Section 4.3.2.2 (referred to the forward-panel apex and based on exposed panel geometry)

$x''_{a.c.}$ is the aerodynamic center of the aft panel obtained from Section 4.3.2.2 (referred to the aft-panel apex and based on exposed panel geometry)

For most configurations the terms involving z_{cg} are negligible, and frequently the drag terms are small enough to be negligible. If, in addition, the usual approximations for small angle of attack are made, equation 4.5.2.1-a can be simplified to give

$$C_{m_\alpha} = -\frac{x_{cg} - x'}{\bar{c}'}(C_{L_\alpha})' - \frac{x_{cg} - x''}{\bar{c}''}(C_{L_\alpha})''\frac{q''}{q_\infty}\frac{S''}{S'}\frac{\bar{c}''}{\bar{c}'}\left(1 - \frac{\partial\epsilon}{\partial\alpha}\right) \qquad 4.5.2.1\text{-d}$$

which can be written as

$$C_{m_\alpha} = -\frac{x_{cg} - x'}{\bar{c}'}[K_N + K_{B(W)} + K_{W(B)}]'(C_{L_\alpha})'_e\frac{S_e'}{S'}$$

$$-\frac{x_{cg} - x''}{\bar{c}''}[K_{B(W)} + K_{W(B)}]''(C_{L_\alpha})''_e\left(1 - \frac{\partial\epsilon}{\partial\alpha}\right)\frac{q''}{q_\infty}\frac{S_e''}{S'}\frac{S''}{S'}\frac{\bar{c}''}{\bar{c}'} \qquad 4.5.2.1\text{-d}'$$

where

$$\frac{x_{cg} - x'}{\bar{c}'} = \frac{x_{cg}}{\bar{c}'} + \left(\frac{x_{ac}'}{c_r'}\right)\left(\frac{c_r'}{\bar{c}'}\right) - \frac{g'}{\bar{c}'} - .25 \quad \text{(equation 4.5.2.1-b)}$$

$$\frac{x_{cg} - x''}{\bar{c}''} = \frac{\ell''}{\bar{c}''} + \frac{x_{cg}}{\bar{c}''} \qquad 4.5.2.1\text{-e}$$

and the remaining terms are defined in Section 4.5.1.1.

Method 2 $(b'/b'') < 1.5$

For configurations in which the span of the forward surface is approximately equal to or less than that of the aft surface, the vortex shed from the forward surface interacts directly with the aft surface and the resulting interference effects must be accounted for in the tail terms. This method is to be used when the ratio of the forward- to the aft-surface span is less than 1.5. The contribution of this interference effect to the drag coefficient is not given in literature. However, by making the assumptions that led to equation 4.5.2.1-d, a simplified expression for the pitching-moment-curve slope of a complete wing-body-tail configuration based on the gross area and MAC of the forward panel and an arbitrary center-of-gravity position is:

$$C_{m_\alpha} = -\frac{x_{cg} - x'}{\bar{c}'}(C_{L_\alpha})' - \frac{x_{cg} - x''}{\bar{c}''}\left(\frac{\bar{c}''}{\bar{c}'}\right)\left[(C_{L_\alpha})''\frac{S''}{S'}\frac{q''}{q_\infty} + (C_{L_\alpha})_{W''(v)}\right] \qquad 4.5.2.1\text{-f}$$

Equation 4.5.2.1-f can be written as

$$C_{m_\alpha} = -\frac{x_{cg} - x'}{\bar{c}'}[K_N + K_{(B)W} + K_{W(B)}]'(C_{L_\alpha})'_e\frac{S_e'}{S'}$$

$$-\frac{x_{cg} - x''}{\bar{c}''}\left(\frac{\bar{c}''}{\bar{c}'}\right)\left\{[K_{W(B)} + K_{B(W)}]''(C_{L_\alpha})''_e\frac{S_e''}{S''}\frac{S''}{S'}\frac{q''}{q_\infty} + (C_{L_\alpha})_{W''(v)}\right\} \qquad 4.5.2.1\text{-f}'$$

where

$\frac{x_{cg} - x'}{\bar{c}'}$ is given by equation 4.5.2.1-b

$\frac{x_{cg} - x''}{\bar{c}''}$ is given by equation 4.5.2.1-e

$(C_{L_\alpha})_{W''(v)}$ is the effect of the forward-surface vortices on the aft surface as defined in Section 4.5.1.1 and the remaining terms are defined in Section 4.5.1.1.

Sample Problems

1. Method 1 ($b'/b'' \geq 1.5$)

Given:

Configuration of sample problem 1, paragraph A, Section 4.5.1.1. Additional characteristics are based on total-panel dimensions.

c.g. at $\frac{\bar{c}'}{4}$

$\frac{c_r'}{\bar{c}'} = 1.316$ $\qquad$ $\frac{\bar{c}''}{\bar{c}'} = 0.566$

$\frac{g'}{\bar{c}'} = 1.745$ $\qquad$ $\frac{\ell''}{\bar{c}''} = 5.30$

$\left(\frac{x_{ac}}{c_r}\right)_N = -0.783$

$\left(\frac{x_{ac}}{c_r}\right)_{W(B)} = 1.650$ } From Section 4.3.2.2; functions of wing-body geometry

$\left(\frac{x_{ac}}{c_r}\right)_{B(W)} = 0.822$

Compute:

Step 1. $\frac{x_{ac}'}{c_r'}$

From Section 4.3.1.2:

$$(C_{L_\alpha})_N = K_{N'} (C_{L_\alpha})_e' \frac{S_e'}{S'}$$

$$(C_{L_\alpha})_{W(B)} = K_{W(B)'} (C_{L_\alpha})_e' \frac{S_e'}{S'}$$

$$(C_{L_\alpha})_{B(W)} = K_{B(W)'} (C_{L_\alpha})_e' \frac{S_e'}{S'}$$

The above parameters have been calculated in sample problem 1. paragraph A, Section 4.5.1.1.

$(C_{L_\alpha})_e' \frac{S_e'}{S'} = .0664\ (.896) = .0595$ per deg

$(C_{L_\alpha})_N = 0.037\ (.0595) = 0.0022$ per deg

$(C_{L_\alpha})_{W(B)} = 1.08\ (.0595) = 0.0643$ per deg

$(C_{L_\alpha})_{B(W)} = 0.14\ (.0595) = 0.0083$ per deg

From Section 4.3.2.2:

$$\frac{x_{ac}'}{c_r'} = \frac{\left(\frac{x_{ac}}{c_r}\right)_N (C_{L_\alpha})_N + \left(\frac{x_{ac}}{c_r}\right)_{W(B)} (C_{L_\alpha})_{W(B)} + \left(\frac{x_{ac}}{c_r}\right)_{B(W)} (C_{L_\alpha})_{B(W)}}{(C_{L_\alpha})_N + (C_{L_\alpha})_{W(B)} + (C_{L_\alpha})_{B(W)}} \quad \text{(equation 4.3.2.2-a)}$$

$$= \frac{.783\ (.0022) + 1.650\ (.0643) + .822\ (.0083)}{0.0022 + 0.0643 + 0.0083}$$

$$= 1.49$$

Step 2 $\frac{x_{cg} - x'}{\bar{c}'}$ and $\frac{x_{cg} - x''}{\bar{c}''}$

$\frac{x_{ac}}{\bar{c}'} = 0$

$\frac{x_{cg} - x'}{\bar{c}'} = \frac{x_{cg}}{\bar{c}'} + \left(\frac{x_{ac}'}{c_r'}\right)\left(\frac{c_r'}{\bar{c}'}\right) - \frac{g'}{\bar{c}'} - .25$ (equation 4.5.2.1-b)

$= 0 + 1.49\ (1.316) - 1.745 - .25$

$= -0.034$

$\frac{x_{cg} - x''}{\bar{c}''} = \frac{\ell''}{\bar{c}''} + \frac{x_{cg}}{\bar{c}''} = 5.30$ (equation 4.5.2.1-e)

Step 3. Solution for C_{m_α}

$(C_{L_\alpha})'$ and $(C_{L_\alpha})''$ have been calculated in sample problem 1, paragraph A, Section 4.5.1.1.

$(C_{L_\alpha})' = 0.0748$ per deg

$(C_{L_\alpha})'' \frac{q''}{q_\infty} \frac{S''}{S'}\left(1 - \frac{\partial \epsilon}{\partial \alpha}\right) = 0.0065$ per deg (this value includes wake and wash effects calculated in referenced problem)

$C_{m_\alpha} = -\frac{x_{cg} - x'}{\bar{c}'}(C_{L_\alpha})' - \frac{x_{cg} - x''}{\bar{c}''}(C_{L_\alpha})'' \frac{q''}{q_\infty} \frac{S''}{S'} \frac{\bar{c}''}{\bar{c}'}\left(1 - \frac{\partial \epsilon}{\partial \alpha}\right)$ (equation 4.5.2.1-d)

$= -(-.034)\ (.0748) - (5.30)\ (.566)\ (.0065)$

$= 0.0025 - 0.0195$

$= -0.0170$ per deg

2. Method 2 ($b'/b'' < 1.5$)

Given:

Configuration of sample problem 2, paragraph A, Section 4.5.1.1. Additional characteristics are based on total panel dimensions.

e.g. at $\frac{\bar{c}'}{4}$

$\frac{c_r'}{\bar{c}'} = 1.38 \quad \frac{\bar{c}''}{\bar{c}'} = 0.343 \quad \frac{g'}{\bar{c}'} = 0.389 \quad \frac{\ell''}{\bar{c}''} = 5.32$

$\left(\frac{x_{ac}}{c_r}\right)_N = -0.333$

$\left(\frac{x_{ac}}{c_r}\right)_{W(B)} = 0.526$

$\left(\frac{x_{ac}}{c_r}\right)_{B(W)} = 0.356$

} From Section 4.3.2.2; functions of wing-body geometry

Compute:

Step 1. $\frac{x_{ac}'}{c_r'}$:

From Section 4.3.1.2:

$$(C_{L_\alpha})_N = K_N' \, (C_{L_\alpha})_e' \, \frac{S_e'}{S'}$$

$$(C_{L_\alpha})_{W(B)} = K_{W(B)}' \, (C_{L_\alpha})_e' \, \frac{S_e'}{S'}$$

$$(C_{L_\alpha})_{B(W)} = K_{B(W)}' \, (C_{L_\alpha})_e' \, \frac{S_e'}{S'}$$

The above parameters have been calculated in sample problem 2, paragraph A, Section 4.5.1.1.

$$(C_{L_\alpha})_e' \, \frac{S_e'}{S'} = (0.0405) \; (0.730) = 0.0296 \text{ per deg}$$

$$(C_{L_\alpha})_N = (0.67) \; (0.0296) = 0.0198 \text{ per deg}$$

$$(C_{L_\alpha})_{W(B)} = (1.16) \; (0.0296) = 0.0343 \text{ per deg}$$

$$(C_{L_\alpha})_{B(W)} = (0.27) \; (0.0296) = 0.0080 \text{ per deg}$$

$$\frac{x_{ac}'}{c_r'} = \frac{\left(\frac{x_{ac}}{c_r}\right)_N (C_{L_\alpha})_N + \left(\frac{x_{ac}}{c_r}\right)_{W(B)} (C_{L_\alpha})_{W(B)} + \left(\frac{x_{ac}}{c_r}\right)_{B(W)} (C_{L_\alpha})_{B(W)}}{(C_{L_\alpha})_N + (C_{L_\alpha})_{W(B)} + (C_{L_\alpha})_{B(W)}} \quad \text{(equation 4.3.2.2-a)}$$

$$= \frac{(-0.333) \; (0.0198) + (0.526) \; (0.0343) + (0.356) \; (0.0080)}{0.0198 + 0.0343 + 0.008}$$

$$= 0.230$$

Step 2. $\frac{x_{cg} - x'}{\bar{c}'}$ and $\frac{x_{cg} - x''}{\bar{c}''}$:

$$\frac{x_{cg}}{\bar{c}'} = 0$$

$$\frac{x_{cg} - x'}{\bar{c}'} = \frac{x_{cg}}{\bar{c}'} + \left(\frac{x_{ac}'}{c_r'}\right)\left(\frac{c_r'}{\bar{c}'}\right) - \frac{g'}{\bar{c}'} - .25 \quad \text{(equation 4.5.2.1-b)}$$

$$= 0 + (0.230) \; (1.38) - 0.389 - .25$$

$$= -0.3216$$

$$\frac{x_{cg} - x''}{\bar{c}''} = \frac{\ell''}{\bar{c}''} + \frac{x_{cg}}{\bar{c}''} \quad \text{(equation 4.5.2.1-e)}$$

$$= 5.32$$

Step 3. Solution for C_{m_α}:

$$C_{m_\alpha} = \frac{x_{cg} - x'}{\bar{c}'} [K_N + K_{W(B)} + K_{B(W)}]' \, (C_{L_\alpha})_e' \, \frac{S_e'}{S'}$$

$$- \frac{x_{cg} - x''}{\bar{c}''} \left(\frac{\bar{c}''}{\bar{c}'}\right) \left\{ [K_{W(B)} + K_{B(W)}]'' \, (C_{L_\alpha})_e'' \, \frac{S_e''}{S''} \, \frac{S''}{S'} \, \frac{q''}{q_\infty} + (C_{L_\alpha})_{W''(v)} \right\} \quad \text{(equation 4.5.2.1-f')}$$

Using the above results and the parameters calculated in sample problem 2, paragraph A, Section 4.5.1.1 gives

$$C_{m_\alpha} = -(-0.3216)\ (1.497)\ (0.0405)\ (0.730)$$
$$(5.32)\ (0.343)\ [(1.45)\ (0.0667)\ (0.741)\ (0.277)\ (0.859) + (-0.0139)]$$
$$= 0.0085 \text{ per deg}$$

B. TRANSONIC

At transonic speeds the mutual interferences that exist between components can have pronounced effects upon the pitching-moment characteristics of wing-body-tail combinations. The sensitivity of shock-wave position and strength to minor configuration changes and the common occurrence of shock-induced boundary-layer separation have significant effects on the pressure-loading variations and hence the pitching characteristics. At present the methods of predicting these effects are either nonexistent or oversimplified. The downwash from the forward panel is also difficult to evaluate for cases of mixed flow and/or separation over the forward panel.

DATCOM METHOD

It is recommended that the procedure outlined in paragraph A above be applied at transonic speeds.

C. SUPERSONIC

The information included in the Datcom accounts for most of the mutual interferences that occur between components at supersonic speeds. In particular, the wing-body interferences have been accounted for by the slender-body interference factors of Section 4.3.1.2. The wing-wing interference methods include the effects of the downwash field due to lift, the downwash due to the local compressible flow field, Mach number, and the local dynamic pressure.

DATCOM METHOD

The equations presented in paragraph A for estimating the pitching-moment-curve slope of wing-body-tail combinations are applicable to the supersonic speed regime.

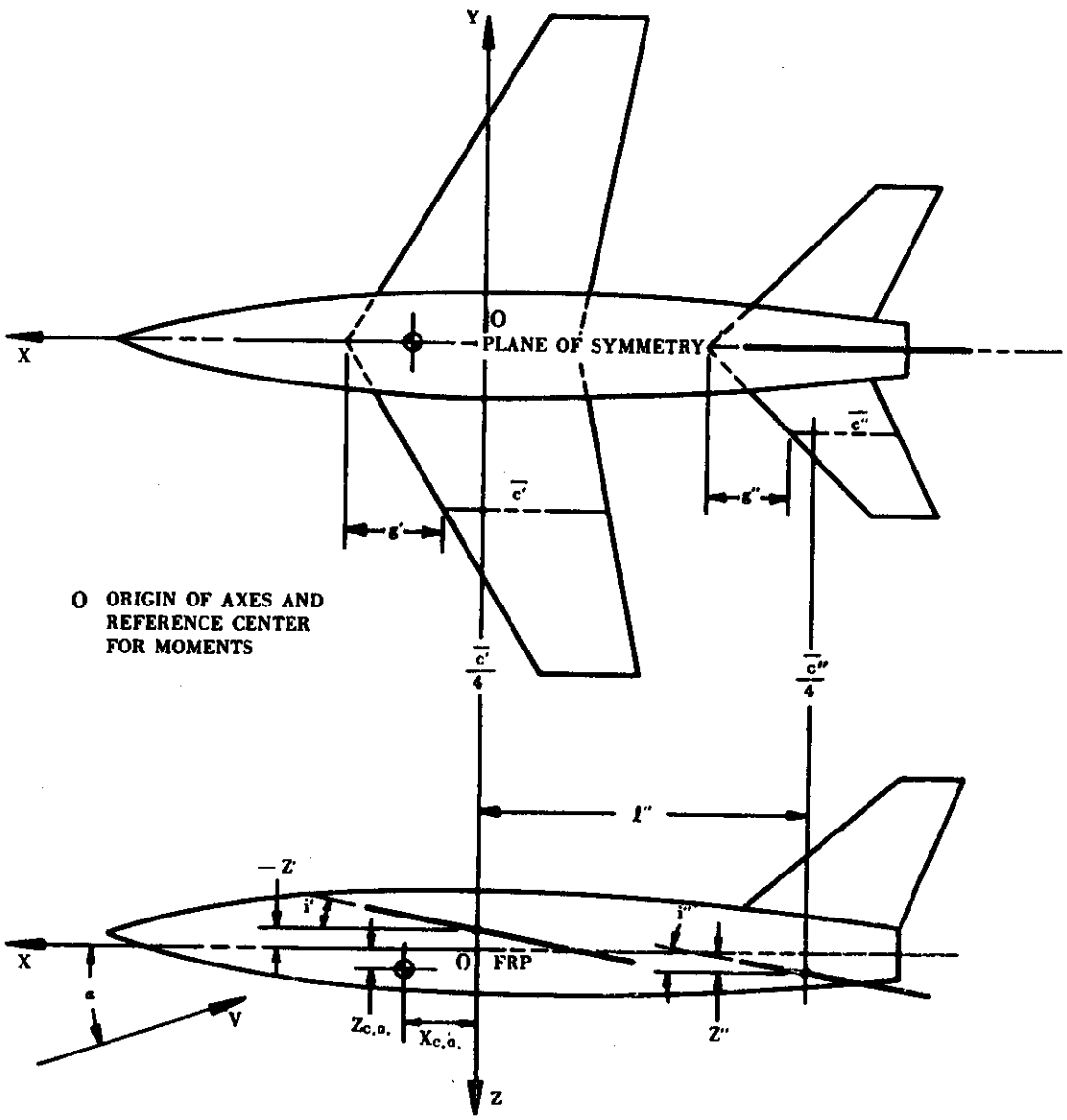

VEHICLE GEOMETRY FOR TAIL-LAST CONFIGURATIONS

Figure 4.5.2.1-7a VEHICLE GEOMETRIC PARAMETERS

Note: Z' and Z'' are measured from the FRP to the aerodynamic centers of the forward and aft surfaces, respectively.

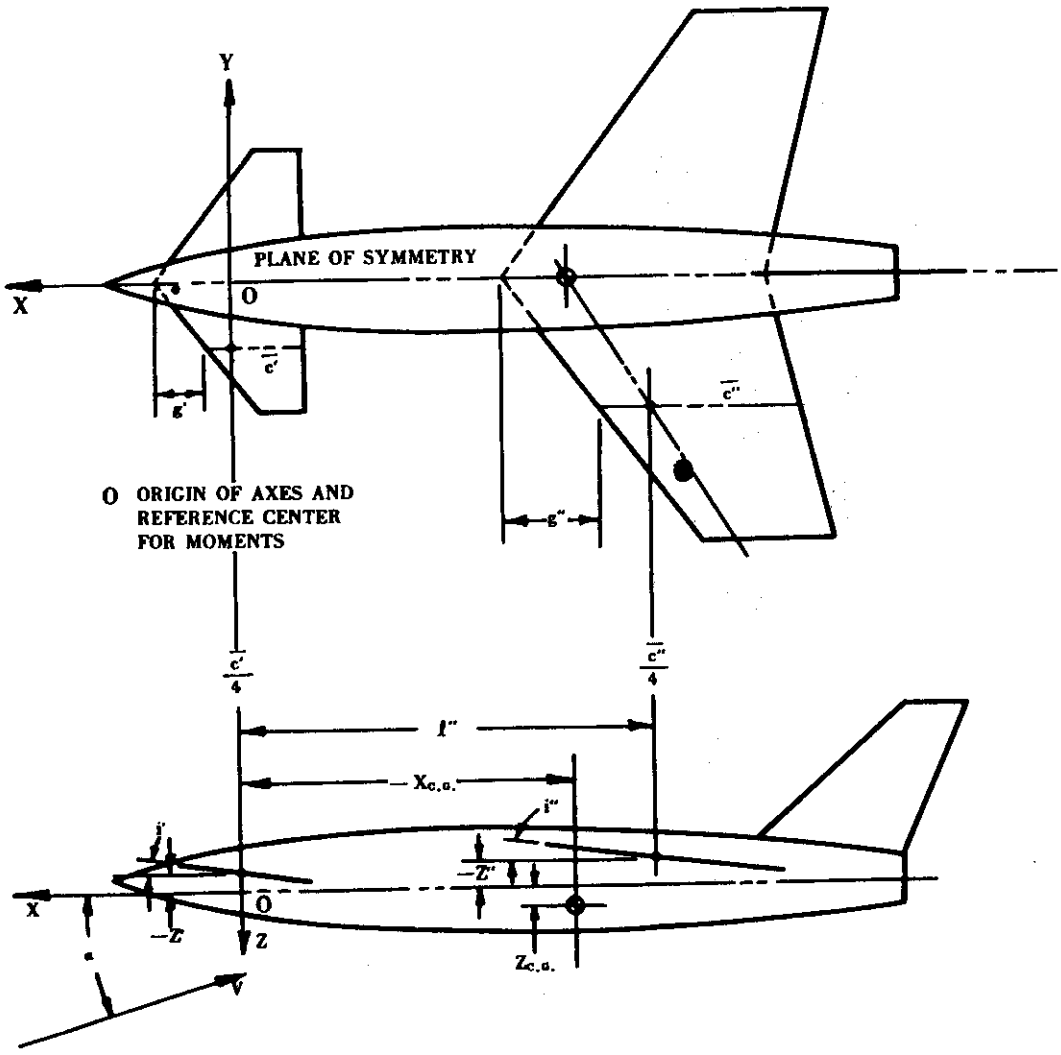

GEOMETRY FOR TAIL-FIRST CONFIGURATIONS

Figure 4.5.2.1-7b VEHICLE GEOMETRIC PARAMETERS (CONTD)

Note: Z' and Z" are measured from the FRP to the aerodynamic centers of the forward and aft surfaces, respectively.

4.5.3 WING-BODY-TAIL DRAG

4.5.3.1 WING-BODY-TAIL ZERO-LIFT DRAG

The information presented in this section is for estimating the zero-lift drag coefficient of complete configurations in the aerodynamically clean condition. In general it consists of a synthesis of material presented in other sections. The methods are presented for a tail-aft configuration. The procedures to be applied in treating canard configurations in the various speed regimes are noted.

The problem of estimating the zero-lift drag is one of accounting for the mutual interferences between components. The methods use basically the same approaches to account for mutual interferences at subsonic and supersonic speeds as those of paragraphs A and C, respectively, of Section 4.3.3.1 for determining wing-body zero-lift drag. The Datcom method at subsonic speeds consists of applying an interference correction factor to the skin-friction and pressure-drag contributions of the exposed wing and body, and treating the tail panels as exposed components. At supersonic speeds the zero-lift drag of the configuration is obtained by adding the drag contributions of the exposed lifting surfaces and the isolated body. A simple fairing technique is used to approximate the zero-lift drag rise through the transonic speed regime.

Discussions of the various applicable theories are given in Sections 4.1.5.1, 4.2.3.1, and 4.3.3.1 and are not repeated here.

It should be pointed out that the basic approach taken here is satisfactory for preliminary design stability studies and that no attempt is made to provide methods suitable for performance estimates.

A. SUBSONIC ($M \leq 0.70$)

The zero-lift drag of a wing-body-tail configuration is approximated by adding the wing-body zero-lift drag determined by the method of Section 4.3.3.1 and the drag contributions of the isolated tail panels determined by the method of Section 4.1.5.1. Although the method for determining the wing-body contribution includes interference correction factors based on experimental results for wing-body combinations, it should be pointed out that most of the bodies were conventional, ogive-cylinder combinations of high fineness ratio, and no detailed investigation has been made to evaluate body effects. The tail-body combination also produces interference drag, but no explicit correction factors are presented for this effect. Chapter VII of reference 1 discusses the interference drag produced by tail configurations at their junctions with the fuselage as well as in the corners formed by the intersection of horizontal and vertical tails. Tail-body interference is compensated for to some extent in the Datcom by assuming that the average dynamic-pressure ratio at the tail panels is unity.

The Datcom method is applicable to configurations employing the following two classes of wing planforms:

Straight-Tapered Wings (conventional, trapezoidal planforms)

Non-Straight-Tapered Wings

- Double-delta wings
- Cranked wings
- Curved (Gothic and ogee) wings

Non-straight-tapered wing geometric parameters are presented in Section 2.2.2.

DATCOM METHOD

The subsonic zero-lift drag coefficient of a complete configuration is approximated by

$$C_{D_0} = \left(C_{D_0}\right)_{WB} + \Sigma_p \left(C_{D_0}\right)_p \qquad 4.5.3.1\text{-a}$$

where the subscript p refers to the tail panels, and

$\left(C_{D_0}\right)_{WB}$ is the zero-lift drag coefficient of the wing-body configuration, based on the reference area, obtained from paragraph A of Section 4.3.3.1.

$\left(C_{D_0}\right)_p$ is the zero-lift drag coefficient of a tail panel, based on the exposed panel geometry and referred to the reference area, obtained from paragraph A of Section 4.1.5.1. Applied in this manner, equation 4.1.5.1-a is expressed as

$$\left(C_{D_0}\right)_p = (C_f)_p \left[1 + L\left(\frac{t}{c}\right) + 100\left(\frac{t}{c}\right)^4\right]_p (R_{L.S.})_p \frac{\left[(S_{wet})_p\right]_e}{S_{ref}}$$

where $\left[(S_{wet})_p\right]_e$ is the wetted area of the exposed panel. The Reynolds number used in determining the turbulent flat-plate skin-friction coefficient is based on the mean aerodynamic chord $(\bar{c}_p)_e$ of the exposed panel.

The method is applied to tail-forward configurations by applying the wing-body method of Section 4.3.3.1 to the primary lifting-surface-body combination and the method of Section 4.1.5.1 to the exposed forward panel.

Sample Problem

Given: A wing-body-tail configuration of reference 2, designated 53-series.

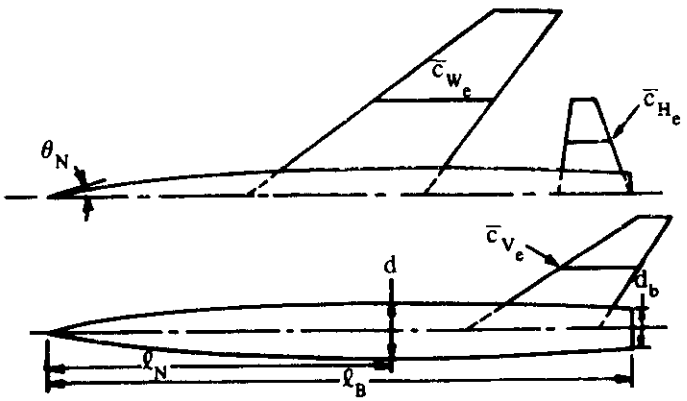

Wing Characteristics:

$A_W = 3.0$ $b_W = 10.80$ in. $\lambda_W = 0.40$ $S_W = S_{ref} = 38.89$ sq in.

$\Lambda_{LE_W} = 53.13^o$ $(\bar{c}_W)_e = 3.55$ in. $\left[(S_{wet})_W\right]_e = 62.86$ sq in.

$(t/c)_{av} = 0.044$ $(t/c)_{max}$ @ 0.30c $\Lambda_{(t/c)_{max}} = 49.3^o$

$$\frac{\left[(S_{wet})_W\right]_e}{S_{ref}} = 1.616$$

Horizontal-Tail Characteristics:

$A_H = 3.994$ $b_H = 5.56$ in. $\lambda_H = 0.334$ $\Lambda_{LE_H} = 8.53^o$

$(\bar{c}_H)_e = 1.296$ in. $\left[(S_{wet})_H\right]_e = 10.372$ sq in. $t/c = 0.03$

$(t/c)_{max}$ @ 0.30c $\Lambda_{(t/c)_{max}} = 0$ $\dfrac{\left[(S_{wet})_H\right]_e}{S_{ref}} = 0.2667$

Vertical-Tail Characteristics:

$A_V = 1.356$ $b_V = 3.294$ in. $\lambda_V = 0.275$ $\Lambda_{LE_V} = 56.55^o$

$(\bar{c}_V)_e = 2.305$ in. $\left[(S_{wet})_V\right]_e = 11.01$ sq in. $t/c = 0.03$

$(t/c)_{max}$ @ 0.30c $\Lambda_{(t/c)_{max}} = 45.3^o$ $\dfrac{\left[(S_{wet})_V\right]_e}{S_{ref}} = 0.2832$

Body Characteristics:

$\ell_B = 17.0$ in. $d = d_{max} = 1.588$ in. $d_b = 1.174$ in. $S_B = 1.083$ sq in.

$f = \ell_B/d = 10.70$ $d_b/d = 0.739$ $(S_S)_e = 23.63$ sq in. $\dfrac{(S_S)_e}{S_B} = 21.82$

$\dfrac{(S_S)_e}{S_{ref}} = 0.6076$ $\dfrac{S_B}{S_{ref}} = 0.0278$ Body ordinates: $r = 0.794\left[1 - \left(1 - \dfrac{2x}{19.833}\right)^2\right]^{3/4}$

The body is modified by a 1.369-inch cylindrical extension at $x = 12$.

Additional Characteristics:

$R_\ell = 0.393 \times 10^6$ per in. Polished metal surfaces (assume k = 0)

M = 0.4, 0.6, 0.7

Compute:

Step 1. Determine C_f for each component (Section 4.1.5.1) (For all components the admissible roughness $\ell/k = \infty$, and the skin-friction coefficient is obtained at the calculated R_ℓ)

Reynolds numbers

Wing: $R_\ell = (0.393 \times 10^6)(\bar{c}_W)_e = (0.393 \times 10^6)(3.55) = 1.395 \times 10^6$

Horizontal: $R_\ell = (0.393 \times 10^6)(\bar{c}_H)_e = (0.393 \times 10^6)(1.296) = 5.09 \times 10^5$

Vertical: $R_\ell = (0.393 \times 10^6)(\bar{c}_V)_e = (0.393 \times 10^6)(2.305) = 9.06 \times 10^5$

Body: $R_\ell = (0.393 \times 10^6)(\ell_B) = (0.393 \times 10^6)(17.0) = 6.68 \times 10^6$

Skin-friction coefficients as f(M) (figure 4.1.5.1-26)

M	$(C_f)_W$	$(C_f)_H$	$(C_f)_V$	$(C_f)_B$
0.4	0.00413	0.00495	0.00444	0.00315
0.6	0.00407	0.00488	0.00440	0.00310
0.7	0.00404	0.00484	0.00436	0.00308

Step 2. Determine the skin-friction and pressure-drag contributions of the components. (Sections 4.1.5.1 and 4.2.3.1)

Wing: $\left[1 + L\left(\frac{t}{c}\right) + 100\left(\frac{t}{c}\right)^4\right]_W = 1.05$ (figure 4.1.5.1-26a, for L = 1.2)

Horizontal: $\left[1 + L\left(\frac{t}{c}\right) + 100\left(\frac{t}{c}\right)^4\right]_H = 1.02$ (figure 4.1.5.1-26a, for L = 1.2)

Vertical: $\left[1 + L\left(\frac{t}{c}\right) + 100\left(\frac{t}{c}\right)^4\right]_V = 1.02$ (figure 4.1.5.1-26a, for L = 1.2)

Body: $$\left[1 + \frac{60}{(\ell_B/d)^3} + 0.0025\,\frac{\ell_B}{d}\right] = \left[1 + \frac{60}{(10.7)^3} + 0.0025\,(10.7)\right] = 1.0757$$

Step 3. Determine the lifting-surface correction factors. (Section 4.1.5.1)

Wing: $\cos \Lambda_{(t/c)_{max}} = 49.3^{o} = 0.6521$

Horizontal: $\cos \Lambda_{(t/c)_{max}} = \cos(0) = 1.00$

Vertical: $\cos \Lambda_{(t/c)_{max}} = \cos 45.3^{o} = 0.7034$

Lifting-surface correction factors as f(M) (figure 4.1.5.1-28b)

M	$(R_{L.S.})_W$	$(R_{L.S.})_H$	$(R_{L.S.})_V$
0.4	0.960	1.105	1.000
0.6	1.002	1.150	1.044
0.7	1.058	1.205	1.098

Step 4. Determine the wing-body interference correlation factor (figure 4.3.3.1-37

$R_{\ell_{fus}} = 6.68 \times 10^{6}$ (calculated above)

M	R_{WB}
0.40	1.028
0.60	0.988
0.70	0.963

Step 5. Determine the wing-body zero-lift drag exclusive of base drag. (Section 4.3.3.1)

$$\left(C_{D_0}\right)_{WB} - C_{D_b}\,\frac{S_B}{S_{ref}} = \left\{(C_f)_W \left[1 + L\left(\frac{t}{c}\right) + 100\left(\frac{t}{c}\right)^4\right]_W (R_{L.S.})_W \frac{\left[(S_{wet})_W\right]_e}{S_{ref}} + (C_f)_B \left[1 + \frac{60}{(\ell_B/d)^3} + 0.0025\,\frac{\ell_B}{d}\right]\frac{(S_S)_e}{S_{ref}}\right\} R_{WB} \quad \text{(equation 4.3.3.1-a)}$$

$$= \left\{(C_f)_W\,(1.05)\,(R_{L.S.})_W\,(1.616) + (C_f)_B\,(1.0757)\,(0.6076)\right\} R_{WB}$$

$$= \left\{(1.697)\,(C_f)_W\,(R_{L.S.})_W + (0.6536)\,(C_f)_B\right\} R_{WB}$$

①	②	③	④	⑤	⑥	⑦	⑧
M	$(C_f)_W$ step 1	$(R_{L.S.})_W$ step 3	(1.697) ② ③	$(C_f)_B$ step 1	(0.6536) ⑤	R_{WB} step 4	$(C_{D_0})_{WB} - C_{D_b} \frac{S_B}{S_{ref}}$ eq. 4.3.3.1-a (④ + ⑥) ⑦
0.4	0.00413	0.960	0.00673	0.00315	0.00206	1.028	0.00904
0.6	0.00407	1.002	0.00692	0.00310	0.00203	0.988	0.00884
0.7	0.00404	1.058	0.00725	0.00308	0.00201	0.963	0.00892

Step 6. Determine the base drag (based on S_B) (Section 4.2.3.1)

$$C_{D_b} = 0.029 \left(\frac{d_b}{d}\right)^3 \Big/ \sqrt{(C_{D_f})_b} = 0.0117 \Big/ \sqrt{(C_{D_f})_b} \quad \text{(equation 4.2.3.1-b)}$$

$$(C_{D_f})_b = (C_f)_B \left[1 + \frac{60}{(\ell_B/d)^3} + 0.0025 \frac{\ell_B}{d}\right] \frac{(S_S)_e}{S_B} = (C_f)_B (1.0757)(21.82) = (23.47)(C_f)_B$$

①	②	③	④	⑤
M	$(C_f)_B$ step 1	$(23.47)(C_f)_B$	$\sqrt{③}$	C_{D_b} eq. 4.2.3.1-b 0.0117/ ④
0.4	0.00315	0.0739	0.272	0.0430
0.6	0.00310	0.0728	0.270	0.0433
0.7	0.00308	0.0723	0.269	0.0435

Step 7. Determine the total wing-body zero-lift drag using equation 4.3.3.1-a.

①	②	③	④	⑤
M	$\left(C_{D_0}\right)_{WB} - C_{D_b}\frac{S_B}{S_{ref}}$ step 5, col. ⑧	C_{D_b} (based on S_B) step 6, col. ⑤	$C_{D_b}\frac{S_B}{S_{ref}}$ ③ (0.0278)	$\left(C_{D_0}\right)_{WB}$ (based on S_{ref}) ② + ④
0.4	0.00904	0.0430	0.00120	0.01024
0.6	0.00884	0.0433	0.00120	0.01004
0.7	0.00892	0.0435	0.00121	0.01013

Step 8. Determine the horizontal- and vertical-tail zero-lift drag contributions.

$$\left(C_{D_0}\right)_H = (C_f)_H \left[1 + L\left(\frac{t}{c}\right) + 100\left(\frac{t}{c}\right)^4\right]_H (R_{L.S.})_H \frac{\left[(S_{wet})_H\right]_e}{S_{ref}} \quad \text{(equation 4.1.5.1-a)}$$

$$= (C_f)_H\,(1.02)\,(R_{L.S.})_H\,(0.2667)$$

$$= (0.2720)\,(C_f)_H\,(R_{L.S.})_H$$

$$\left(C_{D_0}\right)_V = (C_f)_V \left[1 + L\left(\frac{t}{c}\right) + 100\left(\frac{t}{c}\right)^4\right]_V (R_{L.S.})_V \frac{\left[(S_{wet})_V\right]_e}{S_{ref}} \quad \text{(equation 4.1.5.1-a)}$$

$$= (C_f)_V\,(1.02)\,(R_{L.S.})_V\,(0.2832)$$

$$= (0.2889)\,(C_f)_V\,(R_{L.S.})_V$$

①	②	③	④	⑤	⑥	⑦
M	$(C_f)_H$ step 1	$(R_{L.S.})_H$ step 3	$\left(C_{D_0}\right)_H$ (based on S_{ref}) (0.2720) ② ③	$(C_f)_V$ step 1	$(R_{L.S.})_V$ step 3	$\left(C_{D_0}\right)_V$ (based on S_{ref}) (0.2889) ⑤ ⑥
0.4	0.00495	1.105	0.00149	0.00444	1.000	0.00128
0.6	0.00488	1.150	0.00153	0.00440	1.044	0.00133
0.7	0.00484	1.205	0.00159	0.00436	1.098	0.00138

Solution:

$$C_{D_0} = \left(C_{D_0}\right)_{WB} + \Sigma_p \left(C_{D_0}\right)_p \qquad \text{(equation 4.5.3.1-a)}$$

$$= \left(C_{D_0}\right)_{WB} + \left(C_{D_0}\right)_H + \left(C_{D_0}\right)_V$$

①	②	③	④	⑤
M	$\left(C_{D_0}\right)_{WB}$ step 7, col ⑤	$\left(C_{D_0}\right)_H$ step 8, col ④	$\left(C_{D_0}\right)_V$ step 8, col ⑦	C_{D_0} (based on S_{ref}) ② + ③ + ④
0.4	0.01024	0.00149	0.00128	0.0130
0.6	0.01004	0.00153	0.00133	0.0129
0.7	0.01013	0.00159	0.00138	0.0131

The calculated results are compared with test values from reference 2 in figure 4.5.3.1-18.

B. TRANSONIC ($0.7 \leq M \leq 1.1$)

Interference effects in the transonic range are generally greater than those in the subsonic range. This is due to the higher local velocities over the individual components and the greater propagation of the associated perturbations from their source. Furthermore, large supersonic flow regions often exist that contribute substantially to the wave drag. These effects may be accounted for by the application of the area-rule method, whereby the zero-lift drag of a wing-body-tail combination can be calculated as though the combination were a body of revolution with equivalent-area cross sections.

Application of the area-rule method for computation of transonic zero-lift drag is discussed in paragraph B of Section 4.3.3.1 and will not be repeated here. Since the method is quite tedious to compute by hand, automatic computing equipment is invariably used.

There is no general method available for determining the interference drag between components at transonic speeds. The method of approach used in Section 4.3.3.1 to determine transonic wing-body zero-lift drag could be extended to include the contributions of the tail panels in a manner similar to that used in paragraph A. However, such a method is considered to be unwarranted in view of the approximate nature of the results in conjunction with the labor required to apply the method.

The Datcom method has been selected for its ease of application. The degree of accuracy of the Datcom method should be equivalent to that using the build-up procedure discussed above.

DATCOM METHOD

An indication of the wing-body-tail zero-lift drag coefficient at transonic speeds may be obtained by the following procedure:

Step 1. Calculate the zero-lift drag coefficient over the subsonic and supersonic speed regimes by the methods of paragraphs A and C, respectively.

Step 2. Obtain the drag-divergence Mach number M_D from figure 4.5.3.1-19 as a function of wing geometry and general wing-body configuration.

Step 3. Obtain the zero-lift drag coefficient at M_D by

$$\left(C_{D_0}\right)_{M_D} = \left(C_{D_0}\right)_{M=0.7} + 0.002 \qquad \text{4.5.3.1-b}$$

Step 4. Using the information determined in steps 1 through 3 as a guide, construct the approximate zero-lift drag coefficient for the range of Mach numbers between 0.7 and 1.1. The C_{D_0} vs M curve is faired tangent to a line whose slope is $\partial C_D/\partial M = 0.10$ passing through $\left(C_{D_0}\right)_{M_D}$

Equation 4.5.3.1-b for determining $\left(C_{D_0}\right)_{M_D}$ is arbitrary, since for all configurations an initial drag rise at $M_I = 0.7$ is assumed, and the drag-rise increment $\Delta C_{D_0} = \left[\left(C_{D_0}\right)_{M_D} - \left(C_{D_0}\right)_{M_I}\right]$ is assumed to be 0.002. (See sketch (a)).

The method is applicable only to tail-aft configurations with straight-tapered wings.

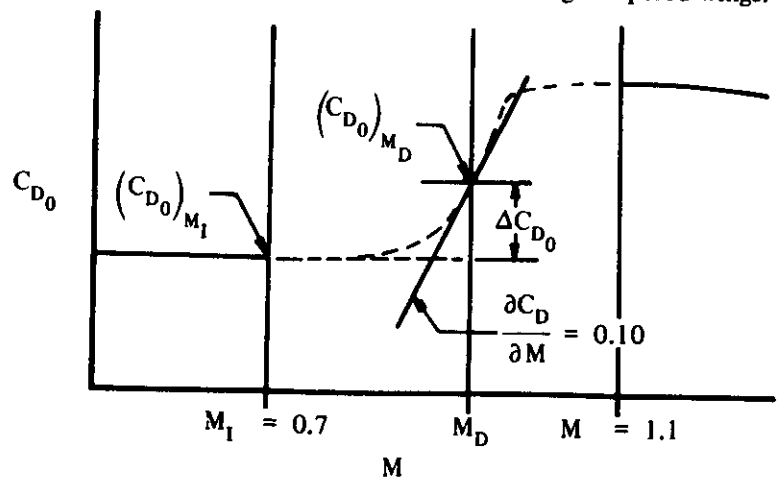

SKETCH (a)

Sample Problem

Given: The configuration of the sample problem of paragraph A. Some of the characteristics are repeated.

$A_W = 3.0 \quad \lambda_W = 0.40 \quad (\Lambda_{c/4})_W = 49.8^o$

$(t/c)_{av}$ = 0.044 Swept wing design without area rule

Compute:

M_D = 0.96 (figure 4.5.3.1-19)

$\left(C_{D_0}\right)_{M=0.7}$ = 0.0131 (sample problem, paragraph A)

$\left(C_{D_0}\right)_{M_D} = \left(C_{D_0}\right)_{M=0.7} + 0.002$ (equation 4.5.3.1-b)

$= 0.0131 + 0.002$

$= 0.0151$

The zero-lift drag coefficient is constructed for the range of Mach numbers between 0.7 and 1.1 in figure 4.5.3.1-18.

C. SUPERSONIC ($M \geq 1.1$)

The area-rule method, discussed in paragraph B of Section 4.3.3.1, has been adapted to supersonic speeds to allow the computation of the zero-lift drag of complete configurations at supersonic speeds. The resulting method, termed the "supersonic area rule" gives wave drag, including aerodynamic interferences, at a given Mach number.

Application of the "supersonic area rule" requires automatic computing equipment. A general discussion of the method and the steps required to prepare the machine input and to interpret the computed drag values are given in paragraph C of Section 4.3.3.1.

The method presented is essentially the same as that of paragraph A of this section. The zero-lift drag of exposed tail panels determined by the method of Section 4.1.5.1 is added to the wing-body zero-lift drag determined by the method of Section 4.3.3.1.

The Datcom method may be applied to configurations having the following classes of wing planforms:

Straight-Tapered Wings (conventional, trapezoidal planforms)

Non-Straight-Tapered Wings

- Double-delta wings
- Cranked wings
- Curved (Gothic and ogee) wings

Non-straight-tapered wing geometric parameters are presented in Section 2.2.2.

It is assumed that the average dynamic-pressure ratio at the tail panels is unity.

DATCOM METHOD

The supersonic zero-lift drag coefficient of a complete configuration is approximated by equation 4.5.3.1-a; i.e.,

$$C_{D_0} = \left(C_{D_0}\right)_{WB} + \Sigma_p \left(C_{D_0}\right)_p$$

where the subscript p refers to the tail panels, and

$\left(C_{D_0}\right)_{WB}$ is the zero-lift drag of the wing-body configuration, based on the reference area, obtained from paragraph C of Section 4.3.3.1.

$\left(C_{D_0}\right)_p$ is the zero-lift drag coefficient of a tail panel, based on the exposed panel geometry and referred to the reference area, obtained from paragraph C of Section 4.1.5.1. In applying this method the Reynolds numbers used in determining the turbulent flat-plate skin-friction coefficients are based on the mean aerodynamic chord $(\bar{c}_p)$ of the exposed panels, and the wetted areas are the exposed wetted areas of the panels $\left[(S_{wet})_p\right]_e$.

The method is applied to tail-forward configurations in the same manner as noted at the conclusion of paragraph A.

Sample Problem

Given: The configuration of the sample problem of paragraph A. Some of the characteristics are repeated.

Wing Characteristics:

$S_W = S_{ref} = 38.89$ sq in. $\quad (S_W)_e = 31.43$ sq in.

$\Lambda_{LE} = 53.13^o \quad (\bar{c}_W)_e = 3.55$ in. $\quad \left[(S_{wet})_W\right]_e = 62.86$ sq in.

$(t/c)_{av} = (t/c)_{eff} = 0.044 \quad \dfrac{(S_W)_e}{S_{ref}} = 0.808 \quad \dfrac{\left[(S_{wet})_W\right]_e}{S_{ref}} = 1.616$

Horizontal-Tail Characteristics:

$(S_H)_e = 5.186$ sq in. $\quad \left[(S_{wet})_H\right]_e = 10.372$ sq in.

$\Lambda_{LE_H} = 8.53^o \quad (\bar{c}_H)_e = 1.296$ in. $\quad t/c = (t/c)_{eff} = 0.03$

$\dfrac{(S_H)_e}{S_{ref}} = 0.1333 \quad \dfrac{\left[(S_{wet})_H\right]_e}{S_{ref}} = 0.2667$

Vertical-Tail Characteristics:

$(S_V)_e$ = 5.507 sq in. $\left[(S_{wet})_V\right]_e$ = 11.014 sq in.

Λ_{LE_V} = 56.55° $(\bar{c}_V)_e$ = 2.305 in. t/c = $(t/c)_{eff}$ = 0.03

$\frac{(S_V)_e}{S_{ref}}$ = 0.1416 $\frac{\left[(S_{wet})_V\right]_e}{S_{ref}}$ = 0.2832

Body Characteristics:

ℓ_B = 17.0 in. d = d_{max} = 1.588 in. d_b = 1.174 in. S_B = 1.083 sq in.

ℓ_A = 7.0 in. ℓ_N = 10.0 in. $f_A = \ell_A/d$ = 4.408 $f_N = \ell_N/d$ = 6.297

θ_N = 17° $(S_S)_e$ = 23.63 sq in. $\frac{(S_S)_e}{S_{ref}}$ = 0.6076 $\frac{S_B}{S_{ref}}$ = 0.0278

$\frac{(S_S)_e}{S_B}$ = 21.82

Additional Characteristics:

$R_\ell \simeq 0.250 \times 10^6$ per in. Polished metal surface (assume k = 0)

M	1.10	1.20	1.30	1.40
β	0.458	0.663	0.831	0.980

Biconvex airfoils

Compute:

Step 1. Determine C_f for each component (Section 4.1.5.1) (For all components the admissible roughness $\ell/k = \infty$, and the skin-friction coefficient is obtained at the calculated R_ℓ.)

Reynolds number

Wing: $R_\ell = (0.250 \times 10^6)(\bar{c}_W)_e = (0.250 \times 10^6)(3.55) = 8.875 \times 10^5$

Horizontal: $R_\ell = (0.250 \times 10^6)(\bar{c}_H)_e = (0.250 \times 10^6)(1.296) = 3.24 \times 10^5$

Vertical: $R_\ell = (0.250 \times 10^6)(\bar{c}_V)_e = (0.250 \times 10^6)(2.305) = 5.76 \times 10^5$

Body: $R_\ell = (0.250 \times 10^6)(\ell_B) = (0.250 \times 10^6)(17.0) = 4.25 \times 10^6$

Skin-friction coefficients (figure 4.1.5.1-26)

M	$(C_f)_W$	$(C_f)_H$	$(C_f)_V$	$(C_f)_B$
1.10	0.00417	0.00503	0.00450	0.00317
1.20	0.00411	0.00498	0.00443	0.00312
1.30	0.00404	0.00490	0.00436	0.00307
1.40	0.00397	0.00482	0.00429	0.00302

Step 2. Determine the skin-friction drag coefficients of the lifting surfaces, based on S_{ref}. (Section 4.3.3.1)

$$C_{D_f} = C_f \frac{(S_{wet})_e}{S_{ref}} \quad \text{(equation 4.3.3.1-f)}$$

Wing: $$\left(C_{D_f}\right)_W = (C_f)_W \frac{\left[(S_{wet})_W\right]_e}{S_{ref}} = 1.616\,(C_f)_W$$

Horizontal: $$\left(C_{D_f}\right)_H = (C_f)_H \frac{\left[(S_{wet})_H\right]_e}{S_{ref}} = 0.2667\,(C_f)_H$$

Vertical: $$\left(C_{D_f}\right)_V = (C_f)_V \frac{\left[(S_{wet})_V\right]_e}{S_{ref}} = 0.2832\,(C_f)_V$$

M	$\left(C_{D_f}\right)_W$	$\left(C_{D_f}\right)_H$	$\left(C_{D_f}\right)_V$
1.10	0.00674	0.00134	0.00127
1.20	0.00664	0.00133	0.00125
1.30	0.00653	0.00131	0.00123
1.40	0.00642	0.00129	0.00121

Step 3. Determine the wave-drag coefficients of the lifting surfaces, based on S_{ref}. (Section 4.3.3.1) (Since all lifting surfaces are conventional, straight-tapered planforms, the subscript bw used in Section 4.3.3.1 has been dropped.)

Wing:

$K = \frac{16}{3}$ (biconvex airfoil. See table, paragraph C, Section 4.1.5.1.)

$\beta \cot \Lambda_{LE_W} < 1.0$ for all M

$$\left(C_{D_w}\right)_W = K \cot \Lambda_{LE_W} \left(\frac{t}{c}\right)^2_{eff} \frac{(S_W)_e}{S_{ref}} \text{ (equation 4.3.3.1-i)}$$

$$= \frac{16}{3} \cot 53.13^o (0.044)^2 (0.808) = 0.00626$$

Horizontal

$K = \frac{16}{3}$ (biconvex airfoil)

$\beta \cot \Lambda_{LE_H} > 1.0$ for all M

$$\left(C_{D_w}\right)_H = \frac{K}{\beta} \left(\frac{t}{c}\right)^2_{eff} \frac{(S_H)_e}{S_{ref}} \text{ (equation 4.3.3.1-h)}$$

$$= \frac{16}{3\beta} (0.03)^2 (0.1333) = \frac{0.000640}{\beta}$$

M	1.10	1.20	1.30	1.40
β	0.458	0.663	0.831	0.980
$\left(C_{D_w}\right)_H$	0.00140	0.000965	0.000770	0.000653

Vertical

$K = \frac{16}{3}$ (biconvex airfoil)

$\beta \cot \Lambda_{LE_V} < 1.0$ for all M

$$\left(C_{D_w}\right)_V = K \cot \Lambda_{LE_V} \left(\frac{t}{c}\right)^2_{eff} \frac{(S_V)_e}{S_{ref}} \text{ (equation 4.3.3.1-i)}$$

$$= \frac{16}{3} \cot 56.55^o (0.03)^2 (0.1416) = 0.000449$$

Step 4. Determine the zero-lift drag of the lifting surfaces by combining the results of steps 2 and 3.

$$\left(C_{D_0}\right)_{\substack{\text{lifting} \\ \text{surface}}} = \left(C_{D_f} + C_{D_w}\right)_{\substack{\text{lifting} \\ \text{surface}}} \text{ (based on } S_{ref}\text{) (equation 4.3.3.1-e)}$$

	WING			HORIZONTAL			VERTICAL		
①	②	③	④	⑤	⑥	⑦	⑧	⑨	⑩
M	$(C_{D_f})_W$ step 2	$(C_{D_w})_W$ step 3	$(C_{D_0})_W$ ② + ③	$(C_{D_f})_H$ step 2	$(C_{D_w})_H$ step 3	$(C_{D_0})_H$ ⑤ + ⑥	$(C_{D_f})_V$ step 2	$(C_{D_w})_V$ step 3	$(C_{D_0})_V$ ⑧ + ⑨
1.10	0.00674	0.00626	0.01300	0.00134	0.00140	0.00274	0.00127	0.000449	0.00172
1.20	0.00664	↓	0.01290	0.00133	0.000965	0.00230	0.00125	↓	0.00170
1.30	0.00653		0.01279	0.00131	0.000770	0.00208	0.00123		0.00168
1.40	0.00642		0.01268	0.00129	0.000653	0.00194	0.00121		0.00166

Step 5. Determine the body zero-lift drag coefficient.

Skin-friction coefficient (see step 1)

Wave-drag coefficients (method 2, paragraph C, Section 4.2.3.1)

Forebody

$$f_N = 6.297$$

$$K_N = 1.012 \text{ (figure 4.2.3.1-63)}$$

$$\left[f_N{}^2 + \frac{1}{4}\right] K_N = \left[(6.297)^2 + \frac{1}{4}\right] (1.012) = 40.38$$

①	②	③	④	⑤
M	β	β/f_N ② /6.297	$C_{D_{N_2}}\left[f_N{}^2 + \frac{1}{4}\right]K_N$ fig. 4.2.3.1-61	$C_{D_{N_2}}$ ④ /40.38
1.10	0.458	0.073	1.130	0.0280
1.20	0.663	0.105	1.124	0.0278
1.30	0.831	0.132	1.112	0.0275
1.40	0.980	0.156	1.100	0.0272

Afterbody

$d_b/d = 0.739$; $f_A = 4.408$

①	②	③	④	⑤
M	β	β/f_A ② /4.408	$C_{D_A}(f_A)^2$ fig. 4.2.3.1-64	C_{D_A} ④ /19.43
1.10	0.458	0.104	0.297	0.0153
1.20	0.663	0.150	0.290	0.0149
1.30	0.831	0.189	0.265	0.0136
1.40	0.980	0.222	0.248	0.0128

Nose bluntness

$C_{D_{N_1}} = 0$ (no bluntness)

Afterbody interference-drag coefficient

$$\left(\frac{2\ell_A}{d}\right)^2 = \left[\frac{(2)\ (7.0)}{1.588}\right]^2 = 77.72; \frac{\ell_N}{\ell_A} = \frac{10.0}{7.0} = 1.429; \left(\frac{d_b}{d}\right)^2 = (0.739)^2 = 0.546$$

$C_{D_{A(NC)}}\left(\frac{2\ell_A}{d}\right)^2 = 0.350$ (figure 4.2.3.1-44a)

$C_{D_{A(NC)}} = (0.350)/(77.72) = 0.00450$

Base-drag coefficient

$f_A = 4.408$; $(d_b/d)^2 = (0.739)^2 = 0.546$

$C_{D_b} = -C_{p_b}\left(\frac{d_b}{d}\right)^2$ (equation 4.2.3.1-g)

① M	② C_{P_b} fig. 4.2.3.1-60, interpolated	③ C_{D_b} eq. 4.2.3.1-g ② (0.546)
1.10	-0.101	0.0551
1.20	-0.101	0.0551
1.30	-0.101	0.0551
1.40	-0.101	0.0551

$$\left(C_{D_0}\right)_B = (C_f)_B \frac{(S_S)_e}{S_B} + C_{D_{N_2}} + C_{D_A} + C_{D_{A(NC)}} + C_{D_{N_1}} + C_{D_b} \quad \text{(based on } S_B\text{)}$$

(equation 4.2.3.1-h)

① M	② $(C_f)_B$ step1	③ $(C_f)_B \frac{(S_S)_e}{S_B}$ ② (21.82)	④ $C_{D_{N_2}}$	⑤ C_{D_A}	⑥ $C_{D_{A(NC)}}$	⑦ $C_{D_{N_1}}$	⑧ C_{D_b}	⑨ $\left(C_{D_0}\right)_B$ eq. 4.2.3.1-h ③ + ④ + ⑤ + ⑥ + ⑦ + ⑧
1.1	0.00317	0.0692	0.0280	0.0153	0.00450	0	0.0551	0.1721
1.2	0.00312	0.0681	0.0278	0.0149	↓	0	↓	0.1704
1.3	0.00307	0.0670	0.0275	0.0136		0		0.1677
1.4	0.00302	0.0659	0.0272	0.0128		0		0.1655

Solution:

$$C_{D_0} = \left(C_{D_0}\right)_{WB} + \Sigma_p \left(C_{D_0}\right)_p \quad \text{(based on } S_{ref}\text{)} \quad \text{(equation 4.5.3.1-a)}$$

$$= \left(C_{D_0}\right)_W + \left(C_{D_0}\right)_B \frac{S_B}{S_{ref}} + \left(C_{D_0}\right)_H + \left(C_{D_0}\right)_V$$

①	②	③	④	⑤	⑥	⑦
M	$(C_{D_0})_W$ step 4	$(C_{D_0})_H$ step 4	$(C_{D_0})_V$ step 4	$(C_{D_0})_B$ step 5	$(C_{D_0})_B \frac{S_B}{S_{ref}}$ ⑤ (0.0278)	C_{D_0} eq. 4.5.3.1-a ② + ③ + ④ + ⑥
1.10	0.01300	0.00274	0.00172	0.1721	0.00478	0.02224
1.20	0.01290	0.00230	0.00170	0.1704	0.00474	0.02164
1.30	0.01279	0.00208	0.00168	0.1677	0.00466	0.02121
1.40	0.01268	0.00194	0.00166	0.1655	0.00460	0.02088

The calculated results are compared with test values from reference 2 in figure 4.5.3.1-18.

REFERENCES

1. Hoerner, S.F.: Fluid-Dynamic Drag. Published by Author, 1958. (U)

2. Wakefield, R.M.: Effects of Wing-Crank, Leading Edge Chord Extensions and Horizontal-Tail Height on the Longitudinal Stability of Swept-Wing Models at Mach Numbers From 0.6 to 1.4. NASA TM X-92, 1959. (U)

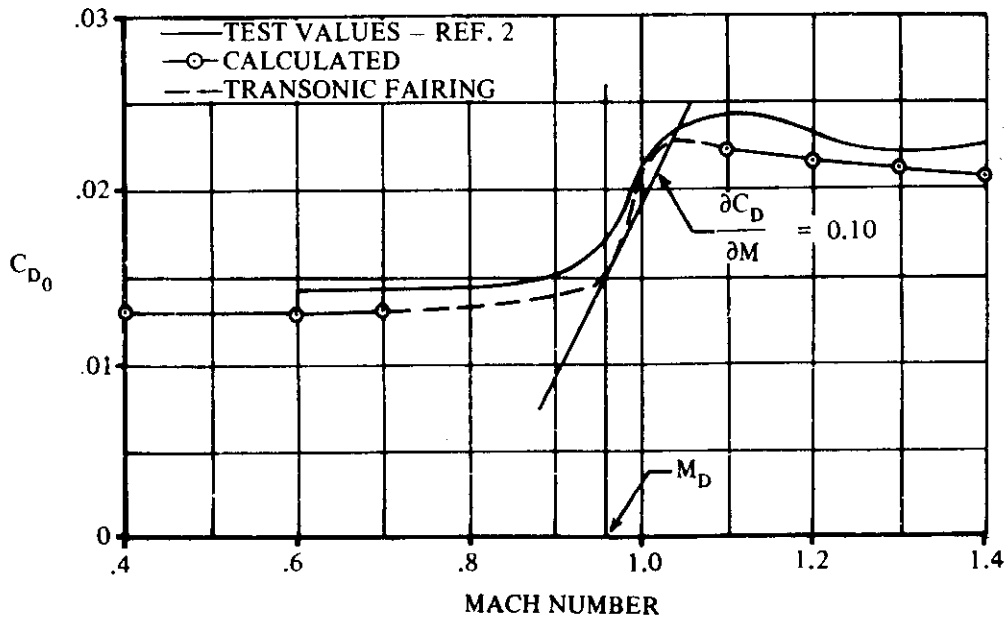

FIGURE 4.5.3.1-18 WING-BODY-TAIL ZERO-LIFT DRAG SUMMARY

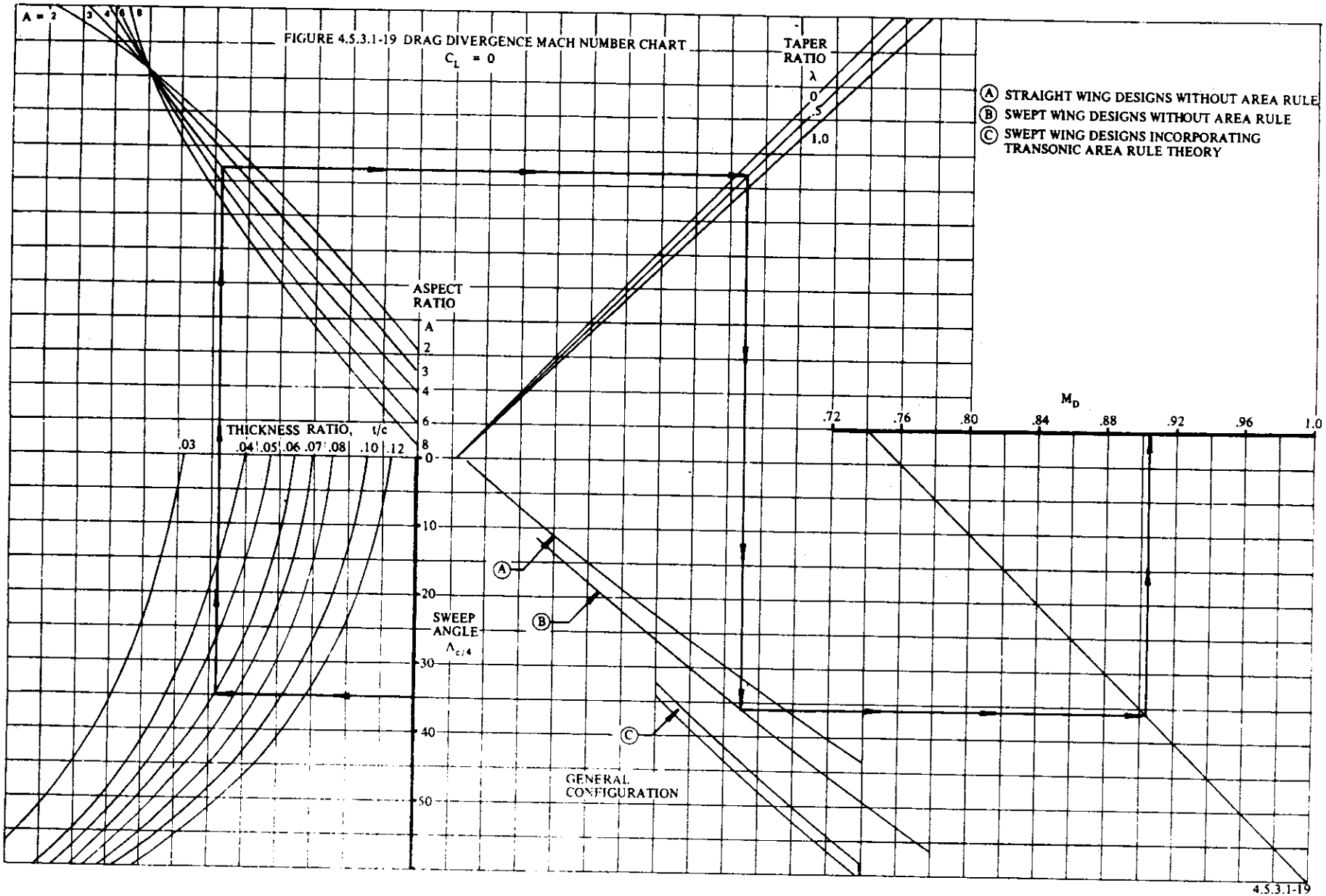
FIGURE 4.5.3.1-19 DRAG DIVERGENCE MACH NUMBER CHART
C_L = 0
TAPER RATIO λ
0
.5
1.0
A STRAIGHT WING DESIGNS WITHOUT AREA RULE
B SWEPT WING DESIGNS WITHOUT AREA RULE
C SWEPT WING DESIGNS INCORPORATING TRANSONIC AREA RULE THEORY
ASPECT RATIO
A
2
3
4
6
8
THICKNESS RATIO, t/c
.03
.04
.05
.06
.07
.08
.10
.12
0
10
20
30
40
50
SWEEP ANGLE $\Lambda_{c/4}$
M_D
.72
.76
.80
.84
.88
.92
.96
1.0
A
B
C
GENERAL CONFIGURATION
4.5.3.1-19

4.5.3.2 WING-BODY-TAIL DRAG AT ANGLE OF ATTACK

The information contained in this section is for estimating the drag coefficient of complete vehicle configurations at angle of attack.

The total vehicle drag at angle of attack consists of the following items:

1. wing-body zero-lift drag
2. wing-body induced drag
3. vertical stabilizer zero-lift drag
4. horizontal-stabilizer zero-lift drag
5. horizontal-stabilizer induced drag

The aerodynamic phenomena associated with, and methods for estimating Items 1-3 are presented in Sections 4.1.5.1, 4.3.3.1, 4.3.3.2, and 4.5.3.1 and are not repeated here.

A vehicle in non-maneuvering flight has the horizontal stabilizer or elevator deflected such that the sum of all moments about the vehicle center of gravity is zero. The pitching moment required to trim arises from the tail-lift and drag vectors and the position of these vectors with respect to the vehicle center of gravity. The method presented in this section is concerned primarily with the estimation of the drag increment resulting from the horizontal-stabilizer contribution required to trim the vehicle ($C_{m_{cg}} = 0$) at usable lift coefficients. A tail-aft configuration is assumed.

The equations pertinent to trim drag presented herein are applicable at all speeds. The method is restricted only by the limitations imposed upon the parameters in other sections of the Datcom. Of course, wing-body test values at the appropriate angle of attack are preferred.

DATCOM METHOD

All Speeds

The drag coefficient of a wing-body-tail configuration at angle of attack is given by

$$C_D = \left(C_{D_0}\right)_{WB} + \left(C_{D_0}\right)_V + \left(C_{D_i}\right)_{WB} + \Delta C_{D_{trim}} \qquad 4.5.3.2\text{-a}$$

where all coefficients are based on total wing area, and

$\left(C_{D_0}\right)_{WB}$ is the wing-body zero-lift drag coefficient obtained from Section 4.3.3.1.

$\left(C_{D_0}\right)_V$ is the vertical-stabilizer zero-lift drag coefficient obtained from Section 4.1.5.1 (see Section 4.5.3.1 for proper treatment of this term).

$\left(C_{D_i}\right)_{WB}$ is the induced drag coefficient of the wing-body combination obtained from Section 4.3.3.2.

$\Delta C_{D_{trim}}$ is the drag-coefficient increment between the drag coefficient of the complete vehicle in pitch equilibrium and the drag coefficient of the wing-body-vertical-tail configuration.

The trim-drag coefficient is given by

$$\Delta C_{D_{trim}} = \left(C_{D_H} \cos \epsilon_H + C_{L_H} \sin \epsilon_H\right) \frac{S_H}{S_W} \frac{q_H}{q_\infty} \qquad 4.5.3.2\text{-b}$$

where

C_{D_H} is the horizontal-stabilizer drag coefficient, based on total horizontal-stabilizer area and taken relative to the local-flow direction at the horizontal stabilizer.

C_{L_H} is the horizontal-stabilizer lift coefficient required to trim, based on total horizontal-stabilizer area and taken relative to the local-flow direction at the horizontal stabilizer.

ϵ_H is the average downwash angle at the horizontal stabilizer, obtained from Section 4.4.1.

S_H/S_W is the ratio of total horizontal-stabilizer area to total wing area.

q_H/q_∞ is the average dynamic-pressure ratio at the horizontal tail, obtained from Section 4.4.1.

The horizontal-stabilizer drag coefficient is given by

$$C_{D_H} = \left(C_{D_0}\right)_H + \left(C_{D_i}\right)_H \qquad 4.5.3.2\text{-c}$$

where

$\left(C_{D_0}\right)_H$ is the horizontal-stabilizer zero-lift drag coefficient obtained from Section 4.1.5.1 (see Section 4.5.3.1 for proper treatment of this term).

$\left(C_{D_i}\right)_H$ is the horizontal-stabilizer induced-drag coefficient given by

$$\left(C_{D_i}\right)_H = \frac{\left(C_{L_H}\right)^2}{\pi A_H e_H} \qquad 4.5.3.2\text{-d}$$

where

A_H is the geometric aspect ratio of the horizontal stabilizer.

e_H is Oswald's efficiency factor for induced drag of the horizontal tail. No method presently exists for determining this parameter. For purposes of the Datcom $e_H = 0.50$ for a horizontal stabilizer mounted on a body, and 0.70 for a horizontal stabilizer mounted on the vertical stabilizer.

The horizontal-stabilizer lift coefficient required to trim is given by

$$C_{L_H} = \frac{2\left[\dfrac{C_{m_{WB}}}{\cos(\Omega - \alpha + \epsilon_H)\ \dfrac{S_H}{S_W}\ \dfrac{q_H}{q_\infty}\ \dfrac{x_H}{\bar{c}_W}} + C_{D_{0_H}} \tan(\Omega - \alpha + \epsilon_H)\right]}{1 + \sqrt{1 - 4\left[\dfrac{\tan(\Omega - \alpha + \epsilon_H)}{\pi A_H e_H}\right]\left[\dfrac{C_{m_{WB}}}{\cos(\Omega - \alpha + \epsilon_H)\ \dfrac{S_H}{S_W}\ \dfrac{q_H}{q_\infty}\ \dfrac{x_H}{\bar{c}_W}} + C_{D_{0_H}} \tan(\Omega - \alpha + \epsilon_H)\right]}}$$

4.5.3.2-e

where

$(C_m)_{WB}$ is the wing-body pitching-moment coefficient given by

$$(C_m)_{WB} = (C_L)_{WB}\left(\frac{dC_m}{dC_L}\right)_{WB} + (C_{m_0})_{WB} \qquad 4.5.3.2\text{-f}$$

where

$\left(\dfrac{dC_m}{dC_L}\right)_{WB}$ is the wing-body pitching-moment-curve slope obtained from Section 4.3.2.2.

$(C_{m_0})_{WB}$ is the wing-body zero-lift pitching-moment coefficient. This parameter must be obtained from test data on a similar configuration or from Section 4.3.2.1.

$(C_L)_{WB}$ is the wing-body lift coefficient given by

$$(C_L)_{WB} = (C_{L_\alpha})_{WB}(\alpha - \alpha_0)_{WB} \qquad 4.5.3.2\text{-g}$$

where

$(C_{L_\alpha})_{WB}$ is the wing-body lift-curve slope, obtained from Section 4.3.1.2.

$(\alpha_0)_{WB}$ is the wing-body zero-lift angle of attack obtained from the wing-alone data of Section 4.1.3.1*.

α_{WB} is the wing-body angle of attack.

*Test data from a similar configuration should be used if available. Wing surface velocity is increased by the presence of the fuselage; therefore, when the fuselage is below the wing the lift is reduced and with the fuselage above the wing the lift will be increased. This effect is generally small unless wing-mounted bodies such as stores or nacelles are close to the fuselage or to each other.

x_H is the distance between the vehicle center of gravity and the quarter-chord point of the horizontal-stabilizer MAC (see Figure 4.5.3.2-4).

Ω is the angle defined by the intersection of x_H with the FRP (see Figure 4.5.3.2-4).

The drag increment due to longitudinally trimming a vehicle is used in conjunction with the lift increment required for trim to obtain points on the trimmed drag polar. The procedure used to obtain points on the trimmed drag polar is illustrated in Sketch (a).

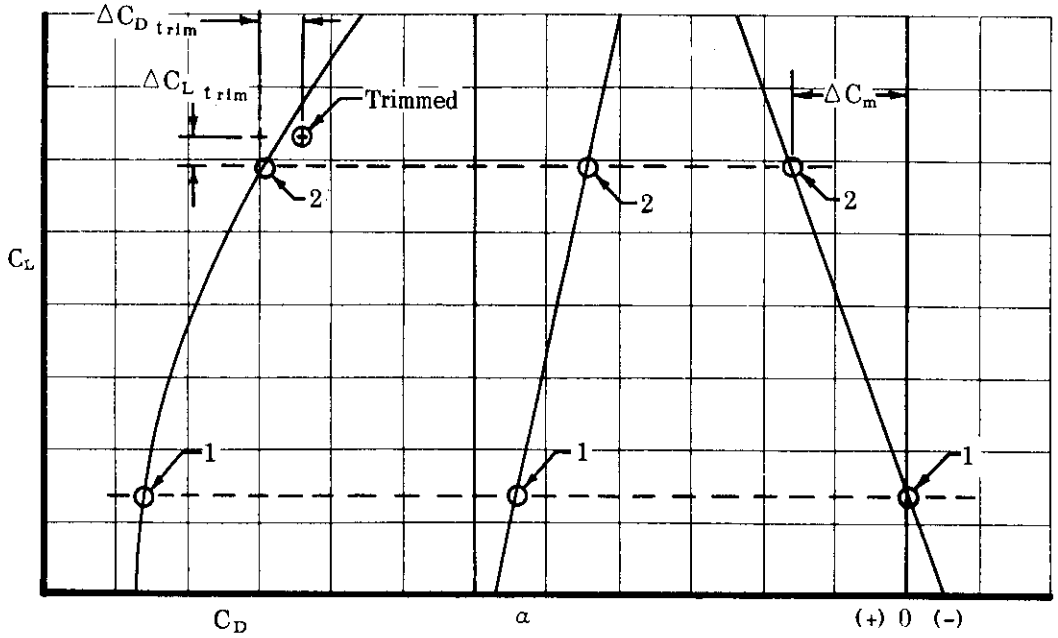

SKETCH (a)

Point 1 represents the horizontal tail-off trimmed condition ($C_{m_{WB}} = 0$). To trim the vehicle at Point 2 the drag polar is corrected for the horizontal-tail load required to apply ΔC_m. This tail load is (see Figure 4.5.3.2-5)

$$-\Delta C_m = -\Delta C_{D_{trim}} \frac{x_H}{\bar{c}_W} \sin(\Omega - \alpha) + \Delta C_{L_{trim}} \frac{x_H}{\bar{c}_W} \cos(\Omega - \alpha)$$

where the lift increment required to trim is

$$\Delta C_{L_{trim}} = \left(C_{L_H} \cos \epsilon_H - C_{D_H} \sin \epsilon_H\right) \frac{S_H}{S_W} \frac{q_H}{q_\infty}$$

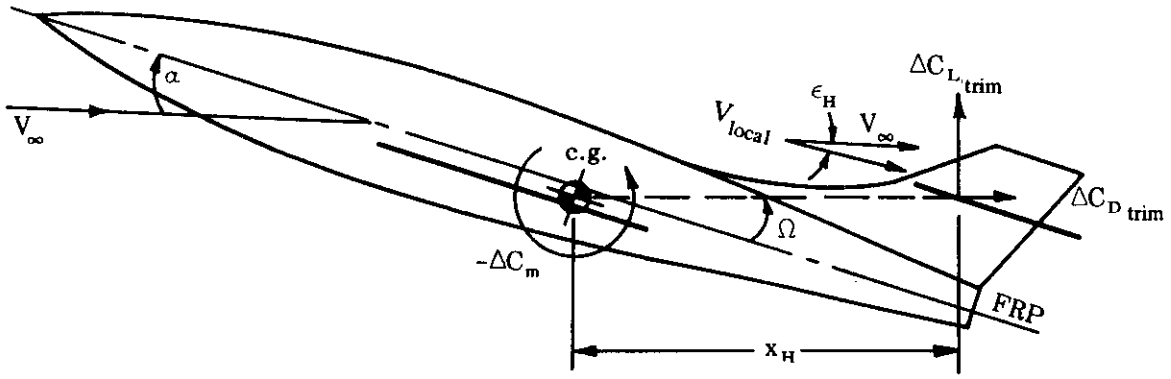

VIEW IN PLANE OF SYMMETRY

α = Airplane angle of attack (positive as shown)

x_H = Distance from c.g. to quarter-chord point of horizontal-stabilizer MAC

Ω = Angle defined by intersection of x_H with FRP (positive as shown with horizontal stabilizer above c.g.)

FIGURE 4.5.3.2-5 DEFINITION SKETCH FOR TRIM DRAG CALCULATIONS

4.6 POWER EFFECTS AT ANGLE OF ATTACK

The propulsion unit has many important influences upon the aerodynamic parameters of a vehicle, other than its main function of overcoming drag. The stability and control characteristics in particular can often be affected significantly by the effects of power.

This section presents methods for analyzing the power effects of jet- and propeller-propulsion units. In order to apply the Datcom methods, it is necessary to have experimental results for or to be able to estimate power-off lift and drag-force characteristics of the wing.

The power effects arising from propeller operation are frequently large enough to warrant consideration in preliminary analysis, especially in take-off and landing configurations. The propeller wash usually interacts with the flow around several of the airplane components, creating numerous separate effects that must be evaluated.

Propeller and propeller-wash characteristics are dependent upon several factors, such as blade shapes, fin effects, flow entrainment, and propeller rotating properties (dual rotating, counter rotating, etc.). These factors have prevented the formulation of a complete and accurate theoretical analysis. Consequently, propeller and propeller-wash effects are usually estimated by empirical methods.

The majority of the experimental data used to formulate the methods and design charts for propeller effects in this section were based on single-engine flaps-up configurations, because of a scarcity of adequate flaps-down data on single- or multiple-engine configurations. Consequently, the accuracy of the method for evaluating the power effects for flaps-down configurations is unknown. Methods are presented in Section 9.2 for evaluating the power effects of V/STOL-type aircraft configurations. For flaps-down configurations the methods of Section 9.2 should be used, since they will probably give a more accurate evaluation of the propeller power effects.

Although many of the power effects arising from propellers are undesirable, i.e., destabilizing, some are advantageous. For instance, large increases in maximum lift can be obtained from wing sections immersed in the propeller slipstream with the propeller operating at high-power conditions.

The power effects from jet-propelled aircraft are generally easy to analyze and have relatively minor effects on the stability and control characteristics of a vehicle. The increased simplicity is due to the elimination of the propeller and of the complex flow region of its slipstream on the wing, tail, and other surfaces. Jet-propelled aircraft are designed to keep the jet exhaust at a safe distance from the horizontal tail because of its extreme heat. Therefore, slipstream problems are minimized.

The Datcom methods presented in the following sections estimate the propeller effects at subsonic speeds and the jet effects at subsonic and supersonic speeds on the lift, drag, and pitching moments of a vehicle. By using the methods presented, a variety of vehicle and

power-plant configurations can be evaluated. These include conventional tail-aft aircraft and canard aircraft, having tractor, pusher, and single- and multiple-power plants. Positive- and negative-thrust and windmilling conditions for propellers are included. Reverse-thrust conditions that cause large interferences and flow separation cannot be evaluated by the methods presented in the following sections.

A general notation list and reference list are included in this section for all power-effects sections. Figures 4.6-12 and 4.6-13 indicate the geometric data required by the methods of these sections. Figure 4.6-12 specifically illustrates the geometric data required for calculating the wing area immersed in the slipstream.

NOTATION

SYMBOL	DEFINITION
A	aspect ratio
A_H	aspect ratio of horizontal tail
A_I	engine inlet duct area
A_i	effective aspect ratio of the immersed wing
a	inflow factor
b_H	span of horizontal tail, ft
b_i	span of immersed wing, ft
b_p	blade width, ft
C_1, C_2	constants for determining downwash
C_D	drag coefficient
C_{D_b}	base drag coefficient
C_{D_L}	drag-coefficient due to lift
C_{D_0}	zero-lift drag coefficient

SYMBOL	DEFINITION
ΔC_{D_0}	increment in zero-lift drag coefficient
$\left(\Delta C_{D_0}\right)_s$	increment in skin-friction drag caused by change in dynamic pressure
C_f	local skin-friction drag coefficient
C_L	lift coefficient
C_{L_P}	propeller lift coefficient
C_{L_W}	wing lift coefficient
$\left(\Delta C_L\right)_H$	change in lift coefficient due to horizontal tail
$\Delta C_{L_{max}}$	increment of maximum lift due to power effects
$\left(\Delta C_L\right)_{N_j}$	increment in lift due to the turning of the free-stream flow at the engine inlet
$\left(\Delta C_l\right)_{N_p}$	increment in lift due to propeller normal force
$\left(\Delta C_L\right)_q$	change in lift coefficient due to the change in slipstream dynamic pressure
$\left(\Delta C_L\right)_T$	increment in lift due to thrust
C_{L_α}	lift-curve slope of the power-off lift curve
$C_{L_{\alpha_H}}$	lift-curve slope of the horizontal tail
$\left(\Delta C_L\right)_{\Delta\alpha_w}$	increment in lift due to the upwash or downwash of the propeller flow field
$\left(\Delta C_L\right)_e$	increment in lift due to jet interference effects
C_m	pitching-moment coefficient

SYMBOL	DEFINITION
$\left(C_{m_0}\right)_i$	zero-lift pitching-moment coefficient of the components immersed in the slipstream
$\left(C_{m_0}\right)_{\text{area not immersed}}$	zero-lift pitching-moment coefficient of the area not immersed in the slipstream
$\left(C_{m_0}\right)_{\text{wing-body}}$	zero-lift pitching-moment coefficient of the wing-body combination
$\left(\Delta C_m\right)_H$	total change in pitching-moment coefficient of the horizontal tail
$\left(\Delta C_m\right)_L$	increment in pitching-moment coefficient due to the immersed-wing lift increments
$\left(\Delta C_m\right)_{N_p}$	increment in pitching-moment coefficient due to propeller normal force
$\left(\Delta C_m\right)_q$	increment in pitching-moment coefficient due to the change in slipstream dynamic pressure
$\left(\Delta C_m\right)_T$	increment in pitching-moment coefficient due to the offset of the thrust axis from the origin of the axes
$\left(\Delta C_{m_H}\right)_q$	increment in pitching-moment coefficient due to a change in the dynamic pressure on the horizontal tail
$\left(\Delta C_{m_H}\right)_\epsilon$	increment in pitching-moment coefficient due to a change in the downwash at the horizontal tail
C_{N_p}	propeller normal-force coefficient
$\left(C_{N_\alpha}\right)_p$	propeller normal-force derivative
$\left[\left(C_{N_\alpha}\right)_p\right]_{K_N=80.7}$	propeller normal-force derivative based on $K_N = 80.7$
c_i	average chord of immersed wing section
$\bar{c}$	mean aerodynamic chord, MAC

SYMBOL	DEFINITION
$\bar{c}_H$	mean aerodynamic chord of the horizontal tail
$\bar{c}_{\text{area not immersed}}$	mean aerodynamic chord of the wing area not immersed in the slipstream
f	propeller-inflow factor
h	altitude
i_H	incidence of the horizontal tail
i_T	incidence of the thrust axis
i_W	incidence of the wing
K	maximum-lift empirical constant
K_1	nacelle or fuselage empirical constant
K_D	propeller drag factor
K_N	empirical normal-force factor
ℓ_H	distance from axes origin to quarter-chord point on the mean aerodynamic chord of the horizontal tail
M_∞	free-stream Mach number
n	number of engines
n'	load factor
p	pressure
Δp	change in pressure
q	dynamic pressure
Δq	change in dynamic pressure

SYMBOL	DEFINITION
R_j	radius of jet orifice
R_j'	radius of equivalent jet orifice
R_p	propeller radius
S	reference area
S_{H_i}	area of portion of horizontal tail immersed in propeller slipstream
S_I	total surface area immersed in the slipstream
S_p	propeller disk area
S_W	wing area
S_{W_f}	wing planform area including and directly forward of flap area
T	thrust per engine
T_c'	thrust coefficient per engine
V	velocity
V_j	actual jet velocity
V_j'	equivalent jet velocity
W	weight
x_e'	longitudinal distance from the jet exit to the quarter-chord point of horizontal-tail mean aerodynamic chord
x_H'	longitudinal distance from jet-wake origin to quarter-chord point of horizontal-tail mean aerodynamic chord
x_I	longitudinal distance from quarter-chord point of wing mean aerodynamic chord to leading edge of engine inlet
x_j'	longitudinal distance from jet-wake origin to jet exit, usually considered to be 4.6 times the orifice exhaust radius

SYMBOL	DEFINITION
x_p	longitudinal distance from intersection of propeller plane with thrust axis and the quarter-chord point of the wing mean aerodynamic chord
x_w	longitudinal distance from moment-reference-center location to the aerodynamic center of the wing area immersed in the slipstream, positive for the aerodynamic center forward of the moment reference center.
y_T	spanwise distance from thrust axis to fuselage center line
z_H	vertical distance from X-axis to quarter-chord point of horizontal-tail mean aerodynamic chord
$z_{H_{eff}}$	vertical distance from quarter-chord point of horizontal-tail mean aerodynamic chord to the slipstream center line
z_{H_T}	vertical distance from propeller thrust axis to quarter-chord point of horizontal-tail mean aerodynamic chord
z_j'	vertical distance from jet thrust axis to quarter-chord point of horizontal-tail mean aerodynamic chord
z_s	vertical distance from X-axis to propeller-slipstream center line at the quarter-chord point of the wing mean aerodynamic chord
z_T	vertical distance from propeller thrust axis to coordinate origin
z_w	vertical distance from the quarter-chord point of the wing mean aerodynamic chord to the coordinate origin
α	angle of attack
α_0	angle of attack at zero lift
α_j	angle between thrust axis and direction of local velocity
α_p	angle between direction of local airstream and thrust axis
α_T	angle between thrust axis and direction of free stream
α_w	wing angle of attack
$\alpha_{C_{L_{max}}}$	angle of attack at maximum lift

SYMBOL	DEFINITION
β	propeller blade angle at 0.75 radius
ϵ_H	downwash at the quarter-chord point of the horizontal-tail mean aerodynamic chord
ϵ_p	downwash angle behind the propeller
ϵ_u	upwash angle ahead of wing
$\bar{\epsilon}$	effective downwash over the wing span
$\Delta\epsilon$	downwash increment
$\Delta\bar{\epsilon}$	mean-effective-downwash increment
$\frac{\Delta\bar{\epsilon}}{\Delta\epsilon}$	mean-effective-downwash ratio
$\frac{\partial\epsilon_p}{\partial\alpha_p}$	propeller-downwash gradient
$\frac{\partial\epsilon_u}{\partial\alpha}$	upwash gradient
λ_H	taper ratio of the horizontal tail
$\Lambda_{c/4}$	sweep angle of the wing quarter-chord
$\Lambda_{H_{c/4}}$	sweep angle of the horizontal-tail quarter-chord

SUBSCRIPTS

b	base conditions
H	horizontal tail
i	immersed in slipstream
L	lift
N	normal force

SYMBOL	DEFINITION
N_p	propeller normal force
s	slipstream conditions
T	thrust
W	wing
α	angle of attack
∞	free-stream conditions

REFERENCES

1. Abzug, M. J.: Effect of Jet and Rocket Operation on Static Longitudinal and Directional Stability. BuAer ADR Report M-35, 1945. (U)

2. Anon.: Flow Fields of Free Air Jets – A Report Bibliography. Defense Doc Center, DDC-ARB-41,247, 1965. (SRD) Title Unclassified

3. Anon.: Model C-133A Estimated Basic Stability and Control Data. Douglas Aircraft Co. Report LB-21984, 1956. (U)

4. Anon.: Preliminary Description of Method Used to Determine Slipstream Power Reduction Factor. Douglas Aircraft Co. Report DAC RR-1104, 1952. (U)

5. Anon.: Velocity Correlation Measurements in the Mixing Region of a Jet. AGARD 452, 1963. (U)

6. Bradbury, L. J. S., and Wood, M. N.: Static Pressure Distribution Around a Circular Jet Exhausting Normally From a Plane Wall Into an Airstream. ARC CP-822, 1964. (U)

7. Bressette, W. E.: Investigation of the Jet Effects on a Flat Surface Downstream of the Exit of a Simulated Turbojet Nacelle at a Free-Stream Mach Number of 2.02. NACA RM L54E05a, 1954. (U)

8. Carroll, R. L.: Aerodynamics of Powered Flight. John Wiley and Sons, New York, 1960. (U)

9. Charwat, A. F.: Investigation of the Flow and Drag Due to Supersonic Jets Discharging Upstream Into a Supersonic Flow. Rand Corp., P-2943, 1964. (U)

10. Church, R. M. W.: A Method for the Calculation of Force, Moment and Power Coefficients of Propellers in Forward Flight of Tilt Angles From 0 to 90 Degrees. Naval Ship Research and Development Center, TN AL-119, 1969. (U)

11. Cubbage, J. M., Jr.: Jet Effects on Base and Afterbody Pressures of a Cylindrical Afterbody at Transonic Speeds. NACA RM L56C21, 1956. (U)

12. Curry, T. B., Jr., and Crabill, N. L.: Rocket-Model Investigation of Lateral Stability Characteristics and Power Effects of a Jet-Engine Airplane Configuration with Tail Boom at Mach Numbers From 1.15 to 1.37. NASA TN D-638, 1961. (U)

13. Decker, J., et al: USAF Stability and Control Handbook. M-3671, 1956. (U)

14. Draper, J. W., and Kuhn, R. E.: Investigation of the Aerodynamic Characteristics of a Model Wing-Propeller Combination and of the Wing and Propeller Separately at Angles of Attack up to 90°. NACA TN 3304, 1954. (U)

15. Falanga, R. A., and Judd, J. H.: Flight Investigation of the Effect of Underwing Propulsive Jets on the Lift, Drag, and Longitudinal Stability of a Delta-Wing Configuration at Mach Numbers from 1.23 to 1.62. NACA RM L55I13, 1955. (U)

16. Falange, R. A., and Judd, J. H.: Low-Lift Flight Tests of Four-Engine Delta-Wing Configurations to Obtain Wing Pressure and Aerodynamic Coefficients Including Some Jet Effects From Mach Numbers 0.5 to 1.5. NASA TM X-282, 1960. (C) Title Unclassified

17. Faris, G.N.: Some Entrainment Properties of a Turbulent Axi-Symmetric Jet. Mississippi Univ. RR 39, 1963. (U)

18. Ferrari, C. Interference Between a Jet Issuing Laterally From a Body and the Enveloping Supersonic Stream. Johns Hopkins Univ., Bumblebee Report 286, 1959. (U)

19. Fink, M. P., Cocke, B. W., and Lipson, S.: A Wind-Tunnel Investigation of a 0.4-Scale Model of an Assault-Transport Airplane With Boundary-Layer Control Applied. NACA RM L55G26a, 1956. (U)

20. George, M., and Kisielowski, E.: Investigation of Propeller Slipstream Effects on Wing Performance. USAAVLABS TR-67-67, 1967. (U)

21. Goett, H. J., and Delaney, N. K.: Effect of Tilt of the Propeller Axis on the Longitudinal-Stability Characteristics of Single-Engine Airplanes. NACA A-59, 1944. (U)

22. Graham, E. W., et al: A Preliminary Theoretical Investigation of the Effects of Propeller Slipstream on Wing Lift. Douglas Aircraft Co. Report SM-14991, 1953. (U)

23. Greenwood, G. H.: An Investigation Into a Technique for Measuring Jet Interference Effects Using Free-Flight Models. ARC CP-969, 1966. (U)

24. Harries, M. H.: Pressure on Axisymmetric Base in Transonic or Supersonic Free Stream in the Presence of a Jet. Aero. Res. Inst. of Sweden FFA R-111, 1967. (U)

25. Jackson, B. G., and Crabill, N. L.: Free-Flight Investigation of Jet Effects at Low Supersonic Mach Numbers on a Fighter-Type Configuration Employing a Tail-Boom Assembly -- Longitudinal Stability and Trim. NACA RM L57F19, 1957. (U)

26. Johnson, H. S.: Wind-Tunnel Investigation of Effects of Tail Length on the Longitudinal and Lateral Stability Characteristics of a Single-Propeller Airplane Model. NACA TN 1766, 1948. (U)

27. Korst, H. H., Chow, W. L., and Zumwalt, G. W.: Research on Transonic and Supersonic Flow of a Real Fluid at Abrupt Increases in Cross Section. Univ. of Ill. ME Tech Report 39-2-5, 1959. (U)

28. Krase, W. H.: Thrust Deflection for Cruise. Rand Corp. Paper 3450, 1966. (U)

29. Lees, J. H., Davies, H., and Callen, C.: Wind Tunnel Tests on the Effect of Extreme Slipstream on Single and Twin-Engine Monoplanes with Split or Slotted Flaps. ARC R&M 1797, 1937. (U)

30. Peake, D. J.: The Pressures on a Surface Surrounding a Jet Issuing Normal to a Mainstream. NRCC Aero Report LR-410, 1964. (U)

31. Pitts, W. C., and Wiggins, L. E.: Axial-Force Reduction by Interference Between Jet and Neighboring Afterbody. NASA TN D-332, 1960. (U)

32. Ribner, H. S.: Field of Flow About a Jet and Effects of Jets on Stability of Jet-Propelled Airplanes. NACA WR L-213, 1946. (U)

33. Ribner, H. S.: Formulas for Propellers in Yaw and Charts of the Side-Force Derivative. NACA WR L-217, 1943. (U)

34. Ribner, H. S.: Notes on the Propeller and Slipstream in Relation to Stability. NACA WR L-25, 1944. (U)

35. Ribner, H. S.: Propellers in Yaw. NACA WR L-219, 1943. (U)

36. Ribner, H. S.: Proposal for a Propeller Side-Force Factor. NACA WR L-336, 1943. (U)

37. Ribner, H. S.,: A Transonic Propeller of Triangular Planform. NACA TN 1303, 1947. (U)

38. Rossiter, J. E., and Kurn, A. G.: Wind Tunnel Measurements of the Effect of a Jet on the Time Average and Unsteady Pressures on the Base of a Bluff Afterbody. ARC CP-[illegible], 1[illegible]5. (U)